INSTITUTO SUPERIOR TÉCNICO

BIANISOTROPICS 2000

8th International Conference on Electromagnetics of Complex Media

Proceedings

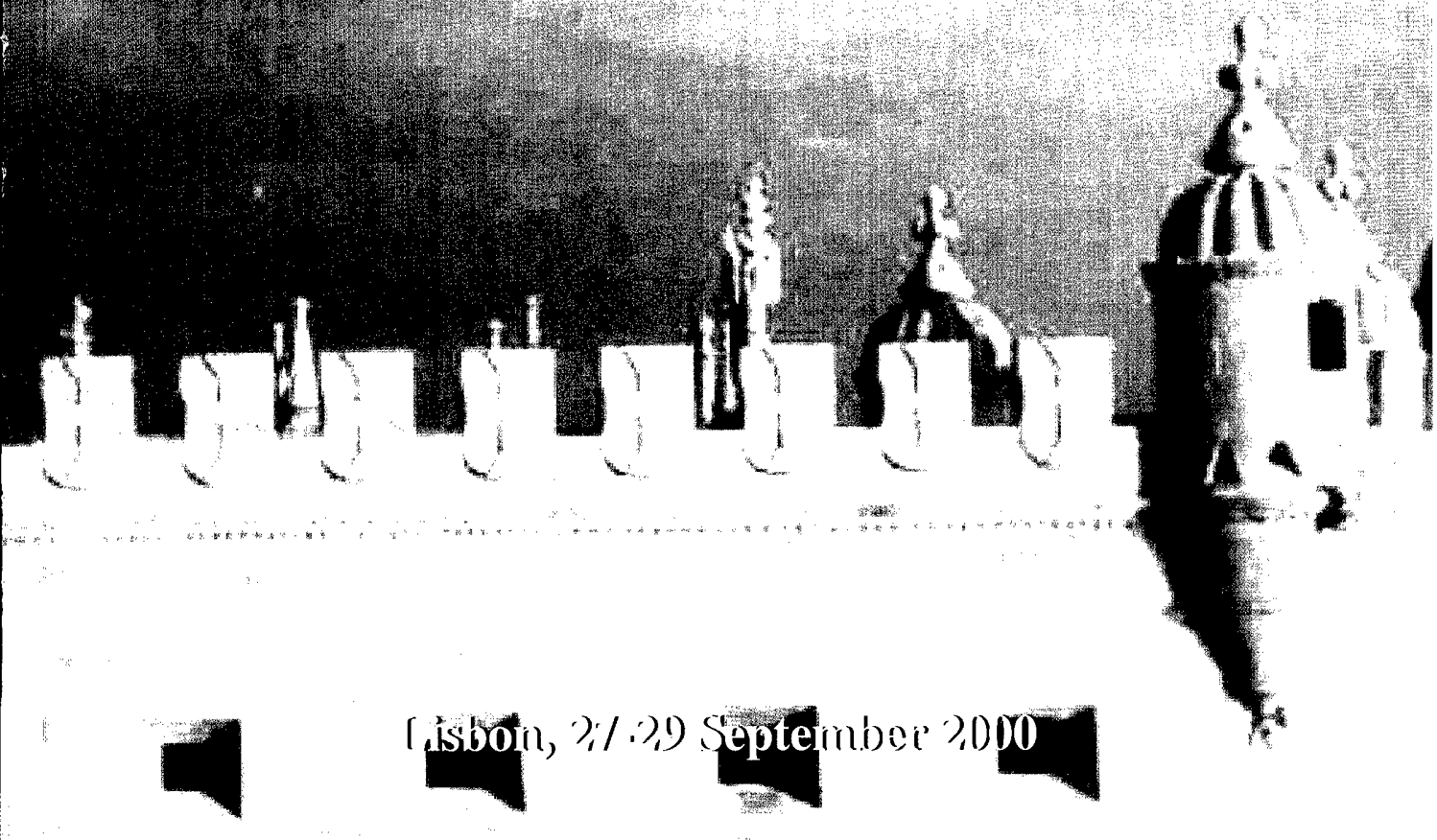

Lisbon, 27-29 September 2000

BIANISOTROPICS 2000

8th International Conference

on Electromagnetics of Complex Media

Lisbon, Portugal, 27–29 September 2000

Proceedings

Edited by

Afonso M. Barbosa and António L. Topa

Ficha Técnica

Título:
Proceedings of BIANISOTROPICS 2000

Projecto Gráfico:
Instituto de Telecomunicações – Pólo de Lisboa

1ª Edição:
Setembro de 2000

Tiragem:
150 Exemplares

Depósito Legal:
155561/00

ISBN:
972–98115–1–2

The edition of the Proceedings of BIANISOTROPICS 2000 has been partially supported by a grant from Fundação Calouste Gulbenkian - Lisboa

Contents

Preface

Welcome to Lisbon

It is my pleasure to welcome you to Instituto Superior Técnico, where BIANISOTROPICS 2000 takes place. I hope you enjoy your stay and take the opportunity to attend an exciting conference and visit a beautiful town.

BIANISOTROPICS 2000 is the eighth in a series of conferences devoted to Electromagnetics of Complex Media, the first one held in 1993, in Helsinki. This is a very unique meeting joining researchers with very different backgrounds actively contributing to new developments in this scientific discipline.

After the issue of a Call for Papers, in December 1999, a very positive reaction was registered: 101 regular contributions have been received and, after an external review, 96 have been considered adequate for presentation. Moreover, 9 invited contributions by leading experts in the field will complete an interesting technical program. By the printing deadline, a total of 93 full manuscripts have been received and are included in these Proceedings.

Following the format of last editions, the program includes oral sessions and poster presentations as well as a round table discussion on a selected topic.

Around 80 delegates from 20 countries are expected to attend the Conference.

I sincerely hope you may consider your participation in BIANISOTROPICS 2000 a rewarding experience.

Once again welcome and I wish you a pleasant stay in Lisbon.

Afonso M. Barbosa
Conference Organizer

Lisbon, September 2000

Acknowledgements

The organization of an event such as this one requires the collaboration of many individuals. During the past year I had the opportunity to listen to many opinions and comments of colleagues and friends. It is not possible to mention all of them.

However, I would like to mention a few persons whose support was essential:

- A. Sihvola (Helsinki) for the initial invitation to organize this meeting in Lisbon and for constant advice and encouragement;
- W. Weiglhofer (Glasgow) and A. Jacob (Braunschweig) who shared with me their expertise as organizers of Bianisotropics'97 and Bianisotropics'98 and provided many suggestions on organization and funding matters;
- S. Tretyakov (St. Petersburg) for many suggestions and collaboration in arrangements for FSU participants;
- A. Lakhtakia (State College), D. Jaggard (Philadelphia), S. Ström (Stockholm), J. P. Parneix (Bordeaux), I. Lindell (Helsinki), G. Slepyan (Minsk), F. Olyslager (Gent), H. Cory (Haifa), K. Whites (Lexington), C. Krowne (Washington), G. Kristensson (Lund), S. Tretyakov (St. Petersburg), A. Sihvola (Helsinki), R. Raab (Natal), for reviewing all abstracts;
- The members of the Organizing Committee and the Scientific Advisory Committee;
- W. R. Stone (IEEE AP Magazine, La Jolla) Mrs. I. Heleu (URSI, Gent) and the IEEE-EDS staff for their support in providing free advertising;
- A few members of the staff of Instituto Superior Técnico and Instituto de Telecomunicações directly involved in the organization of this event;

Last but not least, A. L. Topa, who shared with me the tasks of the Local Organizing Committee. His enthusiasm and permanent collaboration were essential to the success of this meeting.

Afonso M. Barbosa
Conference Organizer

Lisbon, September 2000

Organization

Conference Chairman

A. M. Barbosa	Instituto Superior Técnico	Portugal

Scientific Advisory Committee

A. Lakhtakia	Pennsylvania State University	USA
D. L. Jaggard	University of Pennsylvania	USA
S. Ström	Royal Institute of Technology	Sweden
G. Ya Slepyan	Belarus State University	Belarus
I. Lindell	Helsinki University of Technology	Finland
F. Olyslager	University of Ghent	Belgium
H. Cory	Technion-Israel Institute of Technology	Israel
G. Kristensson	Lund Institute of Technology	Sweden
K. W. Whites	University of Kentucky	USA
W. C. Chew	University of Illinois	USA
J. P. Parneix	PIOM	France
J. M. Arnold	University of Glasgow	Great Britain
C. Krowne	Naval Research Laboratory	USA

Organizing Committee

A. P. Vinogradov	Russian Academy of Sciences	Russia
U. B. Unrau	Technische Universität Braunschweig	Germany
I. Semchenko	Gomel State University	Belarus
J. H. Cloete	University of Stellenbosch	South Africa
N. Engheta	University of Pennsylvania	USA
A. Jacob	Technische Universität Braunschweig	Germany
A. H. Sihvola	Helsinki University of Technology	Finland
S. Tretyakov	St. Petersburg State Technical University	Russia
W. S. Weiglhofer	University of Glasgow	Great Britain

Local Organizaing Committee

A. M. Barbosa	Instituto Superior Técnico	Portugal
A. L. Topa	Instituto Superior Técnico	Portugal

Sponsors

The Conference Organizer is very grateful to several institutions and organizations that provided sponsorship to BIANISOTROPICS 2000.

Financial support was obtained from the following institutions:

- European Union, D. G. Information Technology (Brussels);
- U. S. Office of Naval Research (London);
- Fundação para a Ciência e a Tecnologia (Lisboa);
- Universidade Técnica de Lisboa;
- Fundação Calouste Gulbenkian (Lisboa);
- Fundação Luso–Americana para o Desenvolvimento (Lisboa);
- PT - Inovação, S. A. (Aveiro);
- IEEE - MTT, Region 8.

Other support was obtained from the following institutions and organizations:

- Instituto Superior Técnico (Lisboa);
- Instituto de Telecomunicações (Lisboa);
- IEEE – EDS (Electron Devices Society), for technical co-sponsorship;
- URSI (International Union of Radio Science), for Mode A sponsorship;

and also from:

- BPI, Banco Português de Investimento (Lisboa);
- ICEP, Investimentos, Comércio e Turismo de Portugal (Lisboa)

Session 1

Wednesday - September 27, 2000

09:50 - 10:50

Complex Media I

Waves and Fields: From Uniaxial to Biaxial Mediums, in Between and Beyond

W. S. Weiglhofer[1] and A. Lakhtakia[2]

[1] Department of Mathematics, University of Glasgow
University Gardens, Glasgow G12 8QW, Great Britain
Fax: + 44 - 141 - 330 4111; email: wsw@maths.gla.ac.uk

[2] CATMAS — Computational & Theoretical Materials Sciences Group
Department of Engineering Science and Mechanics, Pennsylvania State University
University Park, PA 16802–6812, USA

Abstract

First, a consistent perspective for the formulation of constitutive dyadics for biaxial mediums — for the anisotropic dielectric and the full bianisotropic cases — is provided. Then, the connection between the existence of closed–form, infinite–medium, dyadic Green functions and the factorization properties of certain scalar differential operators is explored by focusing on a special type of homogeneous, anisotropic, dielectric medium. Its anisotropy is of a higher degree of complexity than an uniaxial medium's but falls short of a fully biaxial medium's.

1. From Uniaxiality to Biaxiality

An anisotropic dielectric medium of the simplest type has a relative permittivity dyadic $\underline{\underline{\epsilon}}$ that is *uniaxial*. Stated as[1]

$$\underline{\underline{\epsilon}}_{uni} = \epsilon_a \, \underline{\underline{I}} + \epsilon_b \, \mathbf{u}\,\mathbf{u} \,, \tag{1}$$

it employs two complex–valued scalars (i.e., ϵ_a and ϵ_b) and one unit vector (i.e., $\mathbf{u}$) which is parallel to the sole distinguished axis of the medium [1]. Extending the structure of (1) to the permeability dyadic and the magnetoelectric dyadics as well, we arrive at a *uniaxial bianisotropic* medium [2].

Generalization from medium uniaxiality to *biaxiality* requires the introduction of a second distinguished axis. Recently, we [3] put forward a consistent approach to that issue for *biaxial bianisotropic mediums*, delineating their frequency–dependent constitutive relations as

$$\mathbf{D}(\mathbf{x}) = \epsilon_0 \, \underline{\underline{\epsilon}}_{bi} \cdot \mathbf{E}(\mathbf{x}) + (\sqrt{\epsilon_0/\mu_0}) \, \underline{\underline{\alpha}}_{bi} \cdot \mathbf{B}(\mathbf{x}) \,, \tag{2}$$

$$\mathbf{H}(\mathbf{x}) = (\sqrt{\epsilon_0/\mu_0}) \, \underline{\underline{\beta}}_{bi} \cdot \mathbf{E}(\mathbf{x}) + (1/\mu_0) \, \underline{\underline{\chi}}_{bi} \cdot \mathbf{B}(\mathbf{x}) \,. \tag{3}$$

Here, the four constitutive dyadics are given by

$$\underline{\underline{\epsilon}}_{bi} = \epsilon_a \, \underline{\underline{I}} + \epsilon_b \, (\mathbf{u}_m \, \mathbf{u}_n + \mathbf{u}_n \, \mathbf{u}_m) \,, \tag{4}$$

$$\underline{\underline{\alpha}}_{bi} = \alpha_a \, \underline{\underline{I}} + \alpha_b \, (\mathbf{u}_m \, \mathbf{u}_n + \mathbf{u}_n \, \mathbf{u}_m) \,, \tag{5}$$

[1] In this paper, vectors are in boldface; dyadics are underlined twice; $\mathbf{a} \cdot \mathbf{b} = \sum_i a_i b_i$; $\underline{\underline{A}} = \mathbf{a}\,\mathbf{b}$ is a dyad with elements $A_{ij} = a_i \, b_j$; $\underline{\underline{I}}$ is the unit dyadic and $\underline{\underline{0}}$ is the null dyadic; the superscript $^{-1}$ indicates inversion of dyadics and differential operators; while $\mathbf{x}$ and $\mathbf{x}'$ are the observation and the source points, respectively.

$$\underline{\underline{\beta}}_{bi} = \beta_a \underline{\underline{I}} + \beta_b \left(\mathbf{u}_m \mathbf{u}_n + \mathbf{u}_n \mathbf{u}_m \right) , \tag{6}$$

$$\underline{\underline{\chi}}_{bi} = \chi_a \underline{\underline{I}} + \chi_b \left(\mathbf{u}_m \mathbf{u}_n + \mathbf{u}_n \mathbf{u}_m \right) , \tag{7}$$

with $\mathbf{u}_m$ and $\mathbf{u}_n$ as two unit vectors that are, in general, neither parallel nor anti–parallel to each other. The simplification $\mathbf{u}_m = \pm \mathbf{u}_n$ leads us back to uniaxial bianisotropic mediums.

The two unit vectors in (4)–(7), and both corresponding distinguished axes [1], are common to all four constitutive dyadics. Furthermore, these dyadics contain eight complex–valued parameters: ϵ_a, ϵ_b, α_a, α_b, β_a, β_b, χ_a and χ_b, while the angle $\phi = \cos^{-1}(\mathbf{u}_m \cdot \mathbf{u}_n)$ is real–valued. Therefore, any biaxial bianisotropic medium is characterized by $8 \times 2 + 1 = 17$ real–valued constitutive scalars. A redundancy in this scheme is filtered out by the *Post constraint* [4]:

$$\text{Trace} \left(\underline{\underline{\alpha}}_{bi} - \underline{\underline{\beta}}_{bi} \right) = 0 \quad \Rightarrow \quad 3 \left(\alpha_a - \beta_a \right) + 2 \left(\alpha_b - \beta_b \right) \cos \phi = 0 . \tag{8}$$

Hence, (4)–(7) actually contain just 15 real–valued independent constitutive scalars. Furthermore, as presently defined, the biaxial bianisotropic medium is a *nonreciprocal* medium.

A *biaxial anisotropic* medium [1] arises as a special case when $\underline{\underline{\alpha}}_{bi} = \underline{\underline{\beta}}_{bi} \equiv \underline{\underline{0}}$ in (4)–(7). The biaxiality is thus purely in the dielectric–magnetic properties, and is described by 4 complex–valued constitutive parameters plus the real–valued angle ϕ. As the Post constraint (8) is then trivially fulfilled, a biaxial anisotropic medium is uniquely described by 9 real–valued constitutive scalars.

Perhaps the most attractive feature of the representation (4)–(7) is found in the possibility that one and the same orthogonal transformation is able to diagonalize all four constitutive dyadics. Full details about that feature, as well as a comprehensive study of electromagnetic wave propagation in biaxial bianisotropic mediums, are available elsewhere [3].

2. Dyadic Green Functions

The dyadic differential equation

$$\underline{\underline{L}}(\nabla) \cdot \underline{\underline{G}}(\mathbf{x}, \mathbf{x}') = \delta(\mathbf{x} - \mathbf{x}') \underline{\underline{I}} , \tag{9}$$

constitutes the standard field problem for the electric field phasor, with the $\exp(-i\omega t)$ time–dependence implicit throughout. The dyadic Green function (specifically, of the electric type) is denoted by $\underline{\underline{G}}(\mathbf{x}, \mathbf{x}')$, while $\delta(\mathbf{x} - \mathbf{x}')$ is the Dirac delta function. The specific form of the dyadic, second–order, differential operator $\underline{\underline{L}}(\nabla)$ depends on the type of medium being considered; see Ref. [5] for the relevant exposition of the general Green function technique.

For brevity's sake, we limit our attention here to *anisotropic dielectric* mediums, whose permeability dyadic equals $\underline{\underline{I}}$ and whose magnetoelectric dyadics equal $\underline{\underline{0}}$. A closed–form expression[2] for $\underline{\underline{G}}(\mathbf{x}, \mathbf{x}')$ for an uniaxial dielectric medium is available in textbooks [1], but none is known to exist for a biaxial dielectric medium. The latter is not surprising in view of some results pertaining to the so–called determinant operator of $\underline{\underline{L}}(\nabla)$.

An important step towards a closed–form solution is to determine whether the determinant operator

$$H_{det} = \underline{\underline{L}}(\nabla) \cdot \underline{\underline{L}}_{adj}(\nabla) = \underline{\underline{L}}_{adj}(\nabla) \cdot \underline{\underline{L}}(\nabla) , \tag{10}$$

can be factorized into a product of two second–order operators, the *adjoint* operator $\underline{\underline{L}}_{adj}(\nabla)$ in (10) being always of the fourth order by virtue of the structure of the Maxwell equations. It was

[2]The dyadic Green function should be expressible through simple mathematical functions which will most often be *scalar* Green functions of second–order Helmholtzian operators and derivatives as well as linear combinations thereof. It does not include representations in terms of integrals, because such representations can be trivially achieved with spatial Fourier transformations due to the linearity of (9).

first stated in Ref. [6] — see also Ref. [7] — that the determinant operator can be factorized only if the relative permittivity dyadic has the structure

$$\underline{\underline{\epsilon}}_{fact} = \lambda \underline{\underline{I}} + \mathbf{a}\mathbf{b}\,, \tag{11}$$

where λ is a scalar while $\mathbf{a}$ and $\mathbf{b}$ are vectors. Parenthetically, the formulas given in Refs. [6, 7] pertain to the more general anisotropic dielectric–magnetic mediums.

The form of $\underline{\underline{\epsilon}}_{fact}$ stated above is only *sufficient* but not necessary for factorization. Furthermore, the relation between factorization and the availability of closed–form solutions is not clear. In fact, closed–form expressions for dyadic Green functions could not be obtained, despite factorization, for certain types of *uniaxial bianisotropic* mediums, as was first observed in Ref. [8] and explored further in Refs. [9, 2].

3. More than Uniaxial — Not quite Biaxial

We now consider an anisotropic dielectric medium whose relative permittivity dyadic is

$$\underline{\underline{\epsilon}} = \epsilon_a \underline{\underline{I}} + \epsilon_b \, \mathbf{u}_m \, \mathbf{u}_n \,, \tag{12}$$

where $\mathbf{u}_m$ and $\mathbf{u}_n$ are distinct unit vectors. The right side of (12) is clearly equivalent in form to $\underline{\underline{\epsilon}}_{fact}$. In general, the chosen medium is not *reciprocal* as $\underline{\underline{\epsilon}}$ does not equal its transposed dyadic. The uniaxial medium defined through (1) appears as a specialization of (12) when $\mathbf{u}_m = \mathbf{u}_n$. However, (12) also has a connection to a biaxial structure: Upon decomposition of its right side into symmetric and skew–symmetric parts, (12) can be rewritten as

$$\underline{\underline{\epsilon}} = \epsilon_a \underline{\underline{I}} + \frac{\epsilon_b}{2} \left(\mathbf{u}_m \, \mathbf{u}_n + \mathbf{u}_n \, \mathbf{u}_m \right) + \frac{\epsilon_b}{2} \left(\mathbf{u}_m \, \mathbf{u}_n - \mathbf{u}_n \, \mathbf{u}_m \right) . \tag{13}$$

The first two terms on the right side of (13) have the exact biaxial structure of (4), whereas the last term has a typical *gyrotropic* form. Nevertheless, neither the biaxial dielectric nor the gyrotropic dielectric medium can be obtained from (13) as special cases — because the last two terms on the right side of (13) are far too intimately linked to allow those specializations.

For the medium characterized by (12), we obtain [10]

$$\underline{\underline{L}}_{adj}(\nabla) = H_m \, \underline{\underline{L}}_e(\nabla) - k^2 \tau \, (\nabla \times \mathbf{u}_n) \, (\nabla \times \mathbf{u}_m) \,, \tag{14}$$

$$H_{det} = -k^2 \left(1 + \tau \, \mathbf{u}_m \cdot \mathbf{u}_n\right) H_e \, H_m \,, \tag{15}$$

where $k^2 = \omega^2 \epsilon_0 \epsilon_a \mu_0$, the ratio $\tau = \epsilon_b / \epsilon_a$, and the dyadic operator

$$\underline{\underline{L}}_e(\nabla) = \nabla \nabla + k^2 \left(1 + \tau \, \mathbf{u}_m \cdot \mathbf{u}_n\right) \left(\underline{\underline{I}} - \frac{\tau}{1 + \tau \, \mathbf{u}_m \cdot \mathbf{u}_n} \, \mathbf{u}_m \, \mathbf{u}_n \right) . \tag{16}$$

Of the two scalar, second–order operators appearing in (14) and (15), $H_m = \nabla^2 + k^2$ is a standard Helmholtz operator due to the magnetic isotropy of the medium, but

$$H_e = \nabla^2 - \frac{\tau}{1 + \tau \, \mathbf{u}_m \cdot \mathbf{u}_n} \, (\nabla \times \mathbf{u}_m) \cdot (\nabla \times \mathbf{u}_n) + k^2 \,, \tag{17}$$

is only a Helmholtzian operator as it reflects the dielectric anisotropy of the medium. As anticipated for the chosen medium, it is apparent from (15) that H_{det} indeed factorizes as a product of two second–order operators [10].

Further manipulations then lead to the complete representation of $\underline{\underline{G}}(\mathbf{x}, \mathbf{x}')$ in the form

$$\underline{\underline{G}}(\mathbf{x}, \mathbf{x}') = \frac{1}{k^2 \left(1 + \tau \, \mathbf{u}_m \cdot \mathbf{u}_n\right)} \left[\underline{\underline{L}}_e(\nabla) g_e(\mathbf{x}, \mathbf{x}') + k^2 \tau \, \underline{\underline{M}}(\mathbf{x}, \mathbf{x}') \right] , \tag{18}$$

where the scalar Green function

$$g_e(\mathbf{x}, \mathbf{x}') = \frac{1}{\sqrt{a_x a_y a_z}} \frac{\exp[ikD(\mathbf{x}, \mathbf{x}')]}{4\pi D(\mathbf{x}, \mathbf{x}')}, \tag{19}$$

satisfies the differential equation $H_e\, g_e(\mathbf{x}, \mathbf{x}') = -\delta(\mathbf{x} - \mathbf{x}')$, and the structure of the modified distance function $D(\mathbf{x}, \mathbf{x}')$ (which also contains $a_{x,y,z}$) is detailed in Ref. [10].

What remains unknown in (18) is the dyadic function $\underline{\underline{M}}(\mathbf{x}, \mathbf{x}')$, for which the differential equation

$$H_e H_m\, \underline{\underline{M}}(\mathbf{x}, \mathbf{x}') = (\nabla \times \mathbf{u}_n)\, (\nabla \times \mathbf{u}_m)\, \delta(\mathbf{x} - \mathbf{x}'), \tag{20}$$

must be solved. As discussed elsewhere [10], no closed–form solution for $\underline{\underline{M}}(\mathbf{x}, \mathbf{x}')$ appears to emerge from (20).

The medium considered here is the most general type of anisotropic dielectric medium for which the determinant operator is the product of two scalar, second–order differential operators of the Helmholtzian type; yet no closed–form expression for $\underline{\underline{G}}(\mathbf{x}, \mathbf{x}')$ appears to exist for this medium! Thus, we conclude that

(i) while all currently known closed–form, infinite–medium dyadic Green functions are based on factorizable determinant operators, factorization is not a sufficient condition for the existence of closed–form, infinite–medium, dyadic Green functions; and

(ii) within the class of anisotropic dielectric mediums, the uniaxial dielectric medium (or any medium that can be reduced to such a medium by, for example, affine transformations) remains the most general medium for which a closed–form, infinite–medium, dyadic Green function has been derived.[3]

Acknowledgement
WSW holds a *RSE/SOEID Research Support Fellowship* of the *Royal Society of Edinburgh*.

References

[1] H. C. Chen, *Theory of Electromagnetic Waves*. Fairfax, VA: TechBooks, 1993.
[2] W. S. Weiglhofer, "Dyadic Green function for unbounded general uniaxial bianisotropic medium," *Int. J. Electron.* **77**, 105–115, 1994.
[3] W. S. Weiglhofer and A. Lakhtakia, "On electromagnetic waves in biaxial bianisotropic media," *Electromagnetics* **19**, 351–362, 1999.
[4] W. S. Weiglhofer and A. Lakhtakia, "The Post constraint revisited," *Arch. Elektron. Übertrag.* **52**, 276–279, 1998.
[5] W. S. Weiglhofer, "Frequency–dependent dyadic Green functions for bianisotropic media," in T.W. Barrett and D.M. Grimes (eds.) *Advanced Electromagnetism: Foundations, Theory, Applications*. Singapore: World Scientific, 1995, 376–389.
[6] I. V. Lindell, *Methods for Electromagnetic Field Analysis*. Oxford: Clarendon Press, 1992.
[7] I. V. Lindell and F. Olyslager, "Factorization of the Helmholtz determinant operator for anisotropic media," *Arch. Elektron. Übertrag.* **52**, 261–267, 1998.
[8] W. S. Weiglhofer and I. V. Lindell "Fields and potentials in general uniaxial bianisotropic media I. Axial sources," *Int. J. Appl. Electromagn. Materials* **4**, 211–220, 1994.
[9] W. S. Weiglhofer, "On factorization of differential operators and analytic solutions in electromagnetic theory", in *IEEE Int. Antennas Propag. Symp. Dig.*, Seattle, WA, USA, 1994, 1598–1601.
[10] W. S. Weiglhofer, "On the connection between factorization properties and closed–form solutions of certain linear, dyadic differential operators," *Department of Mathematics, University of Glasgow*, preprint 2000/06, March 2000.

[3] Closed–form dyadic Green functions have been found for more general types of anisotropic mediums. Yet, the price paid for a larger parameter space of constitutive parameters is that such formulas only become available when specific algebraic conditions between the parameters are fulfilled. Those conditions appear motivated purely by mathematical necessities and not based on any fundamental symmetry or some other property of the medium.

Additional Boundary Conditions for Spatially Dispersive Media

S. I. Maslovski[1] and S. A. Tretyakov[2]

[1] Radiophysics Department, St. Petersburg State Technical University
Polytekhnicheskaya 29, 195251 St. Petersburg, Russia
E-mail: stas@radio.stu.neva.ru

[2] Electromagnetics Laboratory, Helsinki University of Technology
P.O. Box 3000, FIN-02015 HUT, Finland
E-mail: sergei.tretyakov@hut.fi

Abstract

In this paper we give a review of the current state in the investigations of spatially dispersive media and, especially, of the problems involving interface boundaries between such media.

1. Introduction

Natural and artificial media are dispersive (though rather weakly sometimes). We know two types of dispersion: temporal dispersion and spatial dispersion. Temporal dispersion results in different electromagnetic properties of media at different frequencies. This phenomenon occurs due to inertiality and (or) resonance behaviour of the medium polarization response. The effects of temporal dispersion are well known and investigated. No specific knowledge of the electromagnetic properties of media boundaries is needed to account for temporal dispersion. Mathematically, dispersion of this kind is described by frequency dependence of the medium material parameters.

Spatial dispersion is often more complicated to study. One of the reasons of that is difficulty in studying interfaces between media. Here the medium response is spatially nonlocal. This fact results in more complicated material relations and the increased complexity gives us differential equations for the fields having higher order than the usual ones. Hence, to solve a boundary value problem for a spatially dispersive medium we should use some additional boundary conditions.

Most of the results for spatially dispersive media were obtained for materials with the first-order spatial dispersion called reciprocal bianisotropic media. The theory shows that for the first-order spatial dispersion we can find such a form of the constitutive relations that no additional boundary conditions are necessary. The problem of the additional boundary conditions has been considered in the literature (e.g., [1, 2, 3]), but no general method for obtaining additional boundary conditions is available. Moreover, this question still causes conceptual problems, see recent paper [5] where the very necessity of additional boundary conditions is negated.

2. Theoretical Description of Spatially Dispersive Media

From the point of view of macroscopic electrodynamics the spatial dispersion phenomenon can be described by two main approaches. The first one deals with integral operators and the second one uses spatial derivatives of the fields. These approaches mostly lead to similar results

especially when Fourier space-transformed field equations are used. In such a case the set of the Maxwell equations together with the material relations for a spatially dispersive medium is reduced to a dispersion equation from which the propagation factors of the medium eigenwaves can be found. Here the spatial dispersion shows itself by appearance of new dispersion branches of eigenwaves.

Till today there is some misunderstanding in the macroscopic theory of the constitutive relations and the boundary conditions for spatially dispersive media. Different authors use different forms of relations to describe media of the same type. In non-magnetic media all the polarization effects can be described only with the help of the averaged electric polarization current in the medium. Using this method (valid also as a model of higher-order dispersion effects), one writes

$$\mathbf{D}'(\omega,\mathbf{k}) = \overline{\overline{\varepsilon}}'(\omega,\mathbf{k})\cdot\mathbf{E}(\omega,\mathbf{k}), \qquad \mathbf{B}(\omega,\mathbf{k}) = \mu_0\mathbf{H}'(\omega,\mathbf{k}) \tag{1}$$

Here $\overline{\overline{\varepsilon}}'(\omega,\mathbf{k})$ takes into account magnetoelectric interaction and induced magnetism in the medium. On the other hand, phenomenologically considering non-magnetic media with first-order spatial dispersion, the relations can be written in a symmetric way with no explicit dependence on the wave vector:

$$\begin{aligned} \mathbf{D}(\omega) &= \overline{\overline{\varepsilon}}(\omega)\cdot\mathbf{E}(\omega) + \overline{\overline{\kappa}}(\omega)\cdot\mathbf{H}(\omega) \\ \mathbf{B}(\omega) &= -\overline{\overline{\kappa}}^{T}(\omega)\cdot\mathbf{E}(\omega) + \overline{\overline{\mu}}(\omega)\cdot\mathbf{H}(\omega) \end{aligned} \tag{2}$$

It is often asked: which form of the constitutive relations is "more correct": symmetric (2) or nonsymmetric (1)? The answer is that both are correct[1] but only with appropriate boundary conditions.

Indeed, if vectors $\mathbf{E}$ and $\mathbf{B}$ are considered as defined by the Lorentz force, then $\mathbf{D}$ and $\mathbf{H}$ should be considered as auxiliary vectors. It is known that there is some freedom in the definition of $\mathbf{D}$ and $\mathbf{H}$. The Maxwell equations do not change under the following transformation with an arbitrary differentiable vector $\mathbf{T}$:

$$\mathbf{D} = \mathbf{D}' + \nabla\times\mathbf{T}, \qquad \mathbf{H} = \mathbf{H}' + j\omega\mathbf{T} \tag{3}$$

It can be shown that if one properly finds the necessary form of vector $\mathbf{T}$, the two systems of the constitutive relations (1) and (2) can be converted one into the other.

We want to emphasize here that not only the constitutive relations change under transformation (3). The boundary conditions involving the auxiliary vectors should be transformed too. This fact is sometimes ignored and the same boundary conditions (the usual Maxwellian plus some additional phenomenological conditions if needed) are used together with different sets of the material relations of a medium. For media with weak spatial dispersion this problem is discussed in [4].

3. Boundary Conditions

From the above consideration one can see that the boundary conditions and the material relations are connected, i.e. for different approaches used to describe the response of a material the

[1]Sometimes in the literature relations (2) are "generalized" to include also dependence on the wave vector (or convolutions over space coordinate variables). Care should be exersised here because the cross terms in these relations already come from the Taylor expansion of a space convolution kernel. For modelling reciprocal media just one space convolution integral is enough to account for arbitrary spatial dispersion effects, as in (1). Note also that sometimes relations (2) are called *local* constitutive relations because they connect the field vectors at the same point in space. This can be misleading because these relations account for first-order spatial dispersion effects. In fact, first-order derivatives of the electric field are "hidden" here, as it is obvious from the Maxwell equations.

boundary conditions must be different. Following [2] we can write the boundary conditions for the tangential field components as

$$\mathbf{z}_0 \times (\mathbf{H}_2 - \mathbf{H}_1) = -j\omega \left\{ \int_{-\delta}^{-0} \Delta\mathbf{D}_1 \, dz + \int_{+0}^{+\delta} \Delta\mathbf{D}_2 \, dz \right\}, \qquad \mathbf{z}_0 \times (\mathbf{E}_2 - \mathbf{E}_1) = 0 \tag{4}$$

where $\mathbf{z}_0$ is the unit vector normal to the interface boundary directed from medium 1 to medium 2. Here the right-hand side of the relation for $\mathbf{H}$ represents the surface polarization current. This current can be calculated as follows. Authors of [2] propose to consider a model reflection problem. The problem assumes fast but continuous changing of the material parameters through the interface (we denote the character size of the transition region as δ). To solve such a problem no additional boundary conditions are necessary. One should make here some assumptions on how the medium parameters vary across the interface layer. If the problem is solved, we can then find the difference between the smooth and sharp interface models. In (4) that difference is represented by $\Delta\mathbf{D}_1$ and $\Delta\mathbf{D}_2$ which correspond to the first and the second media, respectively. More exactly, $\Delta\mathbf{D} = \mathbf{D}(z, \mathbf{E}) - \mathbf{D}^{(0)}(z, \mathbf{E}^{(0)})$ where $\mathbf{D}(z, \mathbf{E})$ is obtained from the smooth model and $\mathbf{D}^{(0)}(z, \mathbf{E}^{(0)})$ is given by the sharp model, i.e. by the constitutive relations supposed to be correct up to the interface boundary. It allows the authors of [2] to conclude that considering boundary value problems may lead to necessity in new material relations for the surface polarization current.

From the above consideration we see that the problem of boundary conditions is not so simple as it may seem at first sight. Even the relations corresponding to the usual Maxwellian boundary conditions happen to be much more complex in the spatially dispersive media. The difficulties become yet more significant when the number of the usual conditions is not enough and some additional relations should be used. How to find these additional conditions? How do they correlate with the material relations? May they be obtained from the field equations as the usual ones? There are many questions here.

There is a chapter in [1] devoted to the considered problem. The authors of [1] try to find a general form of the boundary conditions. This form includes a set of unknown coefficients which could be then somehow found for particular cases. They propose to use the following form:

$$\mathbf{D} + \overline{\overline{\Gamma}} \cdot \mathbf{E} = 0 \tag{5}$$

Such a condition gives three additional scalar equations for the amplitudes of waves. If the number of new waves in a medium is greater than three, then some relations with space derivatives of the fields are needed. Also, here some questions arise: how does dyadic $\overline{\overline{\Gamma}}$ depend on $\mathbf{k}$ and ω? And how to specify the form of $\overline{\overline{\Gamma}}$? The authors of [1] claim that in general only the microscopic theory can give answers to such questions. However, considering the situation in the vicinity of an isolated exciton resonance, the form of $\overline{\overline{\Gamma}}$ can be specified as shown in [1].

Semiconductor is an example of a spatially dispersive medium. The dispersion effects exist there, for instance, due to charge diffusion. Phenomena of this kind at microwaves are considered in [3]. In presence of diffusion the macroscopic medium induced current can be represented as

$$\mathbf{J} = \sigma\mathbf{E} - \epsilon D \nabla(\nabla \cdot \mathbf{E}) \tag{6}$$

where D is the diffusion coefficient. Eq. (6) can be considered as a material relation for media with second-order spatial dispersion. Here the order of dispersion means the highest order of spatial derivatives of field presented in the relation. Second-order dispersion may lead to new eigenwaves in the medium and it can be necessary to use some additional boundary conditions there.

Authors of [3] give special attention to the boundary condition problem. They use an approach based on the uniqueness requirement. New form of the material relation requires to repeat the standard uniqueness development with new terms. Considering the difference between two possible solutions and writing down the Poynting theorem for the difference fields $\mathbf{E}$ and $\mathbf{H}$ they obtain:

$$\mathrm{Re}\int_S \{\mathbf{E}\times\mathbf{H}^* - \epsilon D\mathbf{E}(\nabla\cdot\mathbf{E}^*)\}\cdot d\mathbf{S} + \int_V \left\{\sigma|\mathbf{E}|^2 + \epsilon D|\nabla\cdot\mathbf{E}|^2\right\} dV = 0 \tag{7}$$

From here one can see that some conditions on the normal component of the electric field or on the divergence of the electric field are required in addition to the usual boundary conditions. For a dielectric-semiconductor interface this condition reduces to vanishing of the normal component of the current $\mathbf{J}$ at the surface.

In a recent paper [5] entitled "Additional boundary conditions: an historical mistake" the author claims that no additional boundary conditions are needed at all. Let us consider his speculations in more details. The author starts from a scalar electric field wave equation

$$\frac{\partial^2 E(x,\omega)}{\partial x^2} + \frac{\omega^2}{c^2}\int_{-\infty}^{+\infty} dx'\epsilon(x-x',\omega)E(x',\omega) = s(x,\omega) \tag{8}$$

Here sources $s(x,\omega)$ represent equivalent polarization in the transition region (an interface between free space and the medium is under investigation) induced additionally to that already considered in ϵ. These equivalent sources replace free-space volume and sources there, as in Huygens' principle. Next, the author assumes that the transition layer is negligibly thin compared to the wavelengths of all eigenmodes in the medium, and comes to the conclusion that the reflection problem has a unique solution with no need for additional boundary conditions. However, the thickness of the transition layer is comparable to the inhomogeneity scale of the medium. For example, for interfaces with regular crystals, the layer has thickness of a few periods of the lattice (for the theory of transition layers see e.g. [6] and references therein). Thus, the assumption that the transition layer is negligibly thin is in fact equivalent to the assumption that spatial dispersion effects in the medium can be neglected (because the inhomogeneity scale is very small compared to the wavelength). Naturally, no additional boundary conditions are needed in this case.

4. Conclusion

We see how many problems arise when we start to consider boundaries between spatially dispersive media. This area of science is very prospective to study and we hope that in the near future a more complete and logical theory of the boundary problems for spatially dispersive media will be developed.

References

[1] V. M. Agranovich and V. L. Ginzburg, *Crystal Optics with Spatial Dispersion and Excitons* (2nd Ed.). New York: Springer, 1984.

[2] A. A. Golubkov and V. A. Makarov, "Boundary conditions for electromagnetic field on the surface of media with weak spatial dispersion", *Uspekhi Fizicheskikh Nauk*, 38, no. 3, pp. 325–332, 1995.

[3] W. A. Davis, C. M. Krowne, "The effects of drift and diffusion in semiconductors on plane wave interaction at interfaces," *IEEE Trans. Ant. Prop.*, vol. 36, no. 1, pp. 97–102, 1988.

[4] F. I. Fedorov, *Theory of Gyrotropy*, Minsk: Nauka i Tekhnika, 1976 (in Russian).

[5] K. Henneberger, "Additional boundary conditions: an historical mistake," *Phys. Rev. Lett.*, vol. 80, no. 13, pp. 2889–2892, 1998.

[6] C. R. Simovski, S. A. Tretyakov, A. H. Sihvola, and M. M. Popov, "On the surface effect in thin molecular or composite layers," *European Physical J. Applied Physics*, 9, no. 3, pp. 195-204, 2000.

The Application of Orthonormal Electromagnetic Beams to Characterizing Complex Media

G. N. Borzdov

Department of Theoretical Physics, Belarusian State University
Fr. Skaryny avenue 4, 220050 Minsk, Belarus
Fax: + 375-17-226 0530; email: borzdov@phys.bsu.unibel.by

Abstract

We present an approach to characterizing complex media, based on the use of new families of orthonormal electromagnetic beams. Each familly consists of orthonormal exact solutions of Maxwell's equations, which differ fundamentally from the well-known approximate solutions — the Hermite–Gaussian and Laguerre–Gaussian beams. A promising type of such orthonormal beams—beams defined by the spherical harmonics—is discussed. The proposed approach makes it possible to use beams focused into a small spot on the sample surface.

1. Introduction

The free–space techniques for characterizing complex media are based on the use of the plane–wave approximation of the incident beam. Computer modelling [1, 2, 3] of the free–space techniques [1, 2, 3, 4], based on the covariant impedance methods, has shown that these techniques make it possible to extract all material parameters of an anisotropic, chiral, or general bianisotropic medium, provided that the reflection and transmission coefficients of planar samples under normal and oblique incidence of plane harmonic waves are measured with sufficient accuracy. However, this requires a rather complicated measurement setup, and in many cases the plane–wave approximation of beams in use proves to be inadequate, especially for thick samples.

The technique presented in Refs. [5, 6] makes it possible to compose a set of orthonormal beams in a complex medium or free space, normalized to the energy flux through a given plane. They can be used to generalize the free–space techniques [1, 2, 3, 4] for characterizing complex media, developed for the case of plane incident waves, to the case of incident beams. A promising type of such orthonormal beams—beams defined by the spherical harmonics—is introduced in Ref. [7]. In this paper, we discuss the properties and applications of these beams in more detail.

2. Beams Defined by the Spherical Harmonics

In this paper, we consider electromagnetic fields in free space of the form [7]

$$\mathbf{W}_j^s(\mathbf{r},t) = e^{-i\omega t}\int_0^{2\pi} d\varphi \int_{\theta_1}^{\theta_2} e^{i\mathbf{r}\cdot\mathbf{k}(\theta,\varphi)} Y_j^s(\theta,\varphi)\nu(\theta,\varphi)\mathbf{W}(\theta,\varphi)\sin\theta d\theta. \tag{1}$$

They are defined by the spherical harmonics

$$Y_l^m(\theta,\varphi) = N_{lm} P_l^{|m|}(\cos\theta) e^{im\varphi}, \tag{2}$$

where

$$N_{lm} = \sqrt{\frac{(2l+1)(l-|m|)!}{4\pi(l+|m|)!}}, \tag{3}$$

and $P_l^m(\cos\theta)$ and $j_l(kr)$ are the spherical Legendre and Bessel functions. The spherical harmonics $Y_l^m(\theta,\varphi)$ satisfy the relations

$$\langle Y_l^m|Y_{l'}^{m'}\rangle \equiv \int_0^{2\pi} d\varphi \int_0^{\pi} Y_l^{m*}(\theta,\varphi) Y_{l'}^{m'}(\theta,\varphi)\sin\theta d\theta = \delta_{ll'}\delta_{mm'}. \tag{4}$$

Hence, for the beams under consideration (see also Ref. [8]), $\mathcal{B}_u$ is a unit sphere ($\mathcal{B}_u = S^2$), the beam manifold $\mathcal{B} \subset \mathcal{B}_u$ is its zone with $\theta \in [\theta_1, \theta_2]$ and $\varphi \in [0, 2\pi]$; and $d\mathcal{B} = \sin\theta d\theta d\varphi$.

To compose electromagnetic beams in free space, it is convinient to set $\mathbf{W} = \mathrm{col}(\mathbf{E}, \mathbf{B}) = \mathrm{col}(\mathbf{E}, \mathbf{H})$. For a time–harmonic field, the component $S_3 = \mathbf{e}_3 \cdot \mathbf{S}$ of the time average Poynting vector $\mathbf{S}$ can be written as

$$S_3 = \frac{c}{16\pi}\mathbf{e}_3 \cdot (\mathbf{E}^* \times \mathbf{H} + \mathbf{E} \times \mathbf{H}^*) = \mathbf{W}^\dagger Q \mathbf{W}, \tag{5}$$

where

$$Q = \frac{c}{16\pi}\begin{pmatrix} 0 & \mathbf{e}_1 \otimes \mathbf{e}_2 - \mathbf{e}_2 \otimes \mathbf{e}_1 \\ \mathbf{e}_2 \otimes \mathbf{e}_1 - \mathbf{e}_1 \otimes \mathbf{e}_2 & 0 \end{pmatrix}, \tag{6}$$

and $\otimes$ is the tensor product. Therefore, for the electromagnetic beams $\mathbf{W}_j^s$, the condition $\langle \mathbf{W}_j^s|Q|\mathbf{W}_j^s\rangle = N_Q$ is in fact the normalization to the beam energy flux N_Q through the plane σ_0 normal to $\mathbf{q} = \mathbf{e}_3$:

$$\langle \mathbf{W}_j^s|Q|\mathbf{W}_j^s\rangle = \int_{\sigma_0} S_3 d\sigma_0 = N_Q. \tag{7}$$

Each family of the fields under consideration is described by functions which have integral expansions in plane waves with wave normals lying in the same given solid angle Ω. In particular, one can set the angular spectrum of plane waves by

$$\hat{\mathbf{k}} = \hat{\mathbf{k}}(\theta,\varphi) \equiv \hat{\mathbf{k}}[\theta'(\theta,\varphi), \varphi'(\theta,\varphi)], \tag{8}$$

where

$$\hat{\mathbf{k}} = \mathbf{k}/k = \sin\theta'(\mathbf{e}_1\cos\varphi' + \mathbf{e}_2\sin\varphi') + \mathbf{e}_3\cos\theta'. \tag{9}$$

In this paper, we restrict our consideration to beams with

$$\theta' = \kappa_0\theta, \quad \varphi' = \varphi, \tag{10}$$

where κ_0 is some real parameter; $0 < \kappa_0 \leq 1$. Correspondingly, to set the beam base, it is convinient to use the radial, the meridional, and the azimuthal basis vectors

$$\mathbf{e}_r(\theta',\varphi) = \sin\theta'(\mathbf{e}_1\cos\varphi + \mathbf{e}_2\sin\varphi) + \mathbf{e}_3\cos\theta', \tag{11}$$

$$\mathbf{e}_{\theta'}(\theta',\varphi) = \cos\theta'(\mathbf{e}_1\cos\varphi + \mathbf{e}_2\sin\varphi) - \mathbf{e}_3\sin\theta', \tag{12}$$

$$\mathbf{e}_\varphi(\varphi) = -\mathbf{e}_1\sin\varphi + \mathbf{e}_2\cos\varphi. \tag{13}$$

Let us set two amplitude functions by

$$\mathbf{W}(\theta,\varphi) \equiv \begin{pmatrix} \mathbf{E} \\ \mathbf{B} \end{pmatrix} = \begin{pmatrix} \mathbf{e}_{\theta'} \\ \mathbf{e}_\varphi \end{pmatrix}, \tag{14}$$

$$\mathbf{W}(\theta,\varphi) \equiv \begin{pmatrix} \mathbf{E} \\ \mathbf{B} \end{pmatrix} = \begin{pmatrix} \mathbf{e}_\varphi \\ -\mathbf{e}_{\theta'} \end{pmatrix}. \tag{15}$$

Since the beams with the amplitude function $\mathbf{W}$ [Eq. (14)] are composed from plane waves with the meridional orientation of $\mathbf{E}$ and the azimuthal orientation of $\mathbf{B}$, they will be referred to as E_M beams or B_A beams. Similarly, the amplitude function $\mathbf{W}$ [Eq. (15)] results in E_A beams or B_M beams. The field vectors of E_M and E_A beams are related by the duality transformation $\mathbf{E} \to \mathbf{B}$, $\mathbf{B} \to -\mathbf{E}$.

3. Orthonormal Beams

Let us first consider orthonormal beams with the angular spectrum $\Omega = 2\pi$, i.e., the superpositions of eigenwaves propagating into a given halfspace. To this end, let us set $\theta_1 = 0$ and $\theta_2 = \pi/2$ in Eq. (1), and $\kappa_0 = 1$ in Eq. (10). In this case, the amplitude functions $\mathbf{W}(\theta, \varphi)$ for E_M and E_A beams are given by Eqs. (14) and (15) with $\theta' = \theta$, and the orthonormalizing function $\nu = \nu(\theta, \varphi)$ reduces to a constant [5]. The beam manifold $\mathcal{B} = S_N^2$ is the northern hemisphere S_N^2 of the unit sphere S^2. This results in two different sets of orthonormal beams defined by the spherical harmonics Y_j^s with even and odd j, respectively. However, it is of value to have a complete system of orthonormal beams $\mathbf{W}_j^s$ defined by the whole set of spherical harmonics Y_j^s, for which $\langle \mathbf{W}_j^s | Q | \mathbf{W}_{j'}^{s'} \rangle = 0$, if at least one of the three conditions is met: $j' \neq j$, $s' \neq s$, or the beams have the alternative polarization states (E_M and E_A beams).

To this end, let us set the beam base of time–harmonic electromagnetic E_M beams $\mathbf{W}_j^s$ [Eq. (1)] by Eqs. (9) and (10)–(15) with $\theta_1 = 0$, $\theta_2 = \pi$, and $\kappa_0 \leq 1/2$. In this case, the beam manifold is the unit sphere ($\mathcal{B} = S^2$), the angular spectrum $\Omega \leq 2\pi$, and the orthonormalizing function has the form

$$\nu(\theta) = \frac{2}{\lambda} \sqrt{\frac{2\pi\kappa_0 N_Q \sin(\kappa_0 \theta)}{c \sin\theta}}. \tag{16}$$

These E_M beams also can be expanded into a series as described in Ref. [5]. As before, E_M and E_A beams are related by the duality transformation.

The smaller is κ_0, the smaller is the angular spectrum Ω, i.e., the more collimated is a beam. Conversely, if $\kappa_0 = 1/2$, i.e., $\Omega = 2\pi$, the beam becomes highly localized and has an energy distribution in the core region similar to the beams presented in Refs. [5, 6, 7]. When $s \neq 0$ and $\kappa = 1/2$, or $\kappa \approx 1/2$, these beams resemble electromagnetic tornadoes with spiral energy fluxes and pronounced core regions.

The general time–harmonic beam with two–dimensional beam manifold $\mathcal{B}$ can be written as

$$\mathbf{W}(\mathbf{r}, t) = e^{-i\omega t} \int_{\mathcal{B}} e^{i\mathbf{r}\cdot\mathbf{k}(b)} \nu(b) u(b) \mathbf{W}(b) d\mathcal{B}, \tag{17}$$

where $u : \mathcal{B} \to C^1$ is a complex scalar function on $\mathcal{B}$. Let (u_n) be an orthonormal base of complex functions on $\mathcal{B}$. Then, the function u can be expanded into a series as

$$u(b) = \sum_n c_n u_n(b), \tag{18}$$

where $c_n = \langle u_m | u \rangle$. By applying the approach described in Refs. [5, 8], we obtain an expansion of $\mathbf{W}$ (17) into a series of orthonormal beams $\mathbf{W}_n$ as

$$\mathbf{W} = \sum_n c_n \mathbf{W}_n. \tag{19}$$

It is essential that the coefficients c_n can be extracted from the beam $\mathbf{W}$ as follows:

$$c_n = \frac{1}{N_Q} \langle \mathbf{W}_n | Q | \mathbf{W} \rangle. \tag{20}$$

What is even more important they are measurable values provided that there exists a source of orthonormal beams $\mathbf{W}_n$. As it is shown in Refs. [5, 7], $\mathcal{I} = \langle \mathbf{W} | Q | \mathbf{W} \rangle$ is the energy flux through the plane σ_0 in the case of time–harmonic beams with two–dimensional manifold $\mathcal{B}$. Each of the complex coefficients c_n of the beam $\mathbf{W}$ (19) can be calculated from the results of three measurements [5, 7].

4. Conclusion

The presented approach to characterizing complex media is based on the use of new families of orthonormal electromagnetic beams. Each familly consists of orthonormal exact solutions of Maxwell's equations, which differ fundamentally from the well–known approximate solutions —the Hermite–Gaussian and Laguerre–Gaussian beams. By using these solutions, the results obtained in Refs. [1, 2, 3, 4] for the case of plane incident waves are generalized to the case of time–harmonic beams obliquely incident onto a general bianisotropic slab. To this end, the fields of incident, reflected, and transmitted waves are expanded into series of orthonormal vector functions. The obtained solutions make it possible to calculate the complex scalar coefficients of these series. It is shown that these coefficients are measurable values, and the corresponding measurement scheme is suggested. Assuming that they are given or measured, it is possible to reconstruct the reflection and transmission coefficients of the slab for partial incident plane waves and then, using the techniques presented in Refs. [1, 2, 3, 4], to extract the whole set of material parameters. One can use various families of orthonormal beams, in particular, the family of beams defined by the spherical harmonics. Results of numerical analysis of the latter and peculiarities of its possible application to characterizing various complex media will be reported orally.

The proposed approach makes it possible to use beams with wide angular spectrum, focused into a small spot on the sample surface. Usage of well focused beams eliminates the need to work in an anechoic enviroment.

References

[1] G. N. Borzdov, "Free space measurement techniques for characterizing anisotropic, chiral and bianisotropic media," in *Proc. Bianisotropics'98*, Braunschweig, Germany, pp. 261–264, June 1998.

[2] G. N. Borzdov, "An optimization of free space measurement schemes for characterizing complex media," in *Proc. Bianisotropics'98*, Braunschweig, Germany, pp. 301–304, June 1998.

[3] G. N. Borzdov, "On the measurement of material parameters of a general bianisotropic medium," in *Proc. PIERS'98*, Nantes, France, p. 516, July 1998.

[4] G. N. Borzdov, "Inverse problem of reflection and transmission for a bianisotropic medium," in *Advances in Complex Electromagnetic Materials* (A. Priou *et al.*, eds). Dordrecht: Kluwer, pp. 71–84, 1997.

[5] G. N. Borzdov, "Plane–wave superpositions defined by orthonormal scalar functions on two– and three–dimensional manifolds," *Phys. Rev. E*, vol.61, no. 4, pp. 4462–4478, April 2000.

[6] G. N. Borzdov, "New types of electromagnetic beams in complex media and free space," in *Abstracts of Millennium Conference on Antennas & Propagation AP2000*, Davos, Switzerland, Vol. II – Propagation, p. 228, April 2000.

[7] G. N. Borzdov, "Electromagnetic beams defined by the spherical harmonics with applications to characterizing complex media," in *Abstracts of Millennium Conference on Antennas & Propagation AP2000*, Davos, Switzerland, ol. II – Propagation, p. 229, April 2000.

[8] G. N. Borzdov, "New types of orthonormal electromagnetic beams in complex media and free space," in *Proc. Bianisotropics 2000*, Lisbon, Portugal, pp. 55–58, September 2000. .

Session 2

Wednesday - September 27, 2000

11:10 - 12:40

Complex Materials: Theory

On the Problem of Constitutive Parameter of Composite Materials

A. P. Vinogradov[1] and I. I. Skidanov[2]

[1] Institute for Theoretical and Applied Electromagnetism, Russian Academy of Sciences Izhorskaya 13/19, 127412, Moscow, Russia Tel: 7 095 484 26 44, Fax: 7 095 484 26 33, E-mail: vinogr@vinogr.msk.ru

[2] Department for Problems in Physics and Energetics, Moscow Physical and Technological Institute, Dolgoprudnyi, Russia, email: ins@aport.ru

Abstract

A comparison analysis of the Landau-Lifshitz and Casimir forms of the Maxwell equations in condensed media is made. It is shown that the Casimir form comprises sufficient information of the system to solve any electromagnetic problem whereas the Landau-Lifshitz form demands an additional constitutive equation for surface current. It is shown that the main difference in these forms is that the Casimir form being free from seeming spatial dispersion gives more adequate description of effects of spatial dispersion.

1. Introduction

The manufacturing of advanced artificial materials (chiral, percolation and etc.) challenges the researcher to develop an adequate description of the phenomena observed in these materials. The new theory must account for multipole interaction and effects of retardation. The theories of this a kind were well developed for serving phenomena in crystal or dilute systems [1], [2]. Unfortunately, they confine themselves to consideration of weak effects and deal in frame of perturbation theory. In frame of these theories one does not bother his head with strong definitions of involved quantities and concepts. Today we cannot permit ourselves to deal in such a manner. Here we review the existing forms of constitutive equations in the light of their predictions.

2. Constitutive Equations in Forms Suggested by Landau–Lifshitz and by Casimir

In the case of spatial dispersion Landau and Lifshitz [3], [4], [5] suggested including all the induced currents into definition of polarization

$$\frac{\partial \vec{P}^{LL}}{\partial t} = \vec{j} \tag{1}$$

avoiding introduction of magnetization. The most general form of linear constitutive equation looks as:

$$D_i^{LL} = \int_0^\infty d\tau \int d^3r' \varepsilon_{ij}^{LL}\left(\vec{r}, \vec{r}', \tau\right) E_j\left(\vec{r}', t-\tau\right) \tag{2}$$

where $D_i^{LL} = E_i + 4\pi P_i^{LL}$, E_i, and P_i^{LL} are macroscopic values of electrical induction, electrical field and electrical polarization. The frequency domain Maxwell equations together with this constitution equation could be written as:

$$i\omega\vec{B} = c\left[\nabla \times \vec{E}\right], \qquad -i\omega\vec{D}^{LL} = c\left[\nabla \times \vec{B}\right] \tag{3}$$

$$\left(\nabla \cdot \vec{B}\right) = 0, \qquad \left(\nabla \cdot \vec{D}^{LL}\right) = 0, \tag{4}$$

$$D_i^{LL} = \int d^3r' \varepsilon_{ij}^{LL}\left(\vec{r}, \vec{r}', \omega\right) E_j\left(\vec{r}', \omega\right), \tag{5}$$

$$\varepsilon_{ij}^{LL}\left(\vec{r}, \vec{r}', \omega\right) = \int_0^\infty d\tau \exp\left(i\omega\tau\right) \varepsilon_{ij}^{LL}\left(\vec{r}, \vec{r}', \tau\right) \tag{6}$$

The kernel in (5) decreases with increase of the distance $\vec{\rho} = \vec{r} - \vec{r}'$. If both the dimension a of an inclusion and the mean distance d between the inclusions are small in terms of the wavelength λ then the kernel radius in (5) is also small (the case of weak spatial dispersion). In this case we can expand the field under integral, in the Taylor series. The relation (5) can be rewritten as:

$$\begin{aligned} D_i^{LL}\left(\omega, \vec{r}\right) &= \widehat{\varepsilon}_{ij}^{LL}\left(\omega, \vec{r}\right) E_j\left(\omega, \vec{r}\right) = \\ &\left(\begin{array}{c} \varepsilon_{ij}^{LL(0)}\left(\omega, \vec{r}\right) + \\ \varepsilon_{ijk}^{LL(1)}\left(\omega, \vec{r}\right) \nabla_k + \varepsilon_{ijkl}^{LL(2)}\left(\omega, \vec{r}\right) \nabla_k \nabla_l + \ldots \end{array} \right) E_j\left(\omega, \vec{r}\right) \end{aligned} \tag{7}$$

where $\varepsilon^{LL(n)}$ are frequency dependent tensors. If during homogenization we separate mean current, eddy current, and saddle current we arrive at the Casimir form of constitutive equations based on the following representation of the macroscopic current ([6])

$$\vec{j} = \frac{\partial \overrightarrow{P^C}}{\partial t} - c\left(\nabla \cdot \frac{\partial \widehat{Q}}{\partial t}\right) + c\left[\nabla \times \vec{M}\right] \tag{8}$$

here $\vec{P}$, and $\widehat{Q}$, are the densities of electric dipole and electric quadrupole moments, $\vec{M}$ is the density of magnetic dipole moment. The next step is introduction of the magnetic field H and magnetic permeability μ^C:

$$\vec{H} = \vec{B} - 4\pi\vec{M}, \qquad B_i = \mu_{ij}^C H_j \tag{9}$$

And redefine electrical displacement [7], [6], [8]:

$$D_i^C = E_i + 4\pi P_i^C - 4\pi\nabla \cdot \widehat{Q} \tag{10}$$

The current representation (9) implies nonlocal relation of the moment densities to macroscopic field which results in nonlocal constitutive equations

$$D_i^C = \int d^3r' \varepsilon_{ij}^C\left(\vec{r}, \vec{r}', \omega\right) E_j\left(\vec{r}', \omega\right), \qquad B_i = \int d^3r' \mu_{ij}^C\left(\vec{r}, \vec{r}', \omega\right) H_j\left(\vec{r}', \omega\right) \tag{11}$$

Likewise in (7) we can write (11)

$$\begin{aligned} D_i^C\left(\omega, \vec{r}\right) &= \widehat{\varepsilon}_{ij}^C\left(\omega, \vec{r}\right) E_j\left(\omega, \vec{r}\right) = \\ &\left(\begin{array}{c} \varepsilon_{ij}^{C(0)}\left(\omega, \vec{r}\right) + \\ \varepsilon_{ijk}^{C(1)}\left(\omega, \vec{r}\right) \nabla_k + \varepsilon_{ijkl}^{C(2)}\left(\omega, \vec{r}\right) \nabla_k \nabla_l + \ldots \end{array} \right) E_j\left(\omega, \vec{r}\right) \end{aligned} \tag{12}$$

$$\begin{aligned} B_i\left(\omega, \vec{r}\right) &= \widehat{\mu}_{ij}^C\left(\omega, \vec{r}\right) E_j\left(\omega, \vec{r}\right) = \\ &\left(\begin{array}{c} \mu_{ij}^{C(0)}\left(\omega, \vec{r}\right) + \\ \mu_{ijk}^{C(1)}\left(\omega, \vec{r}\right) \nabla_k + \mu_{ijkl}^{C(2)}\left(\omega, \vec{r}\right) \nabla_k \nabla_l + \ldots \end{array} \right) E_j\left(\omega, \vec{r}\right) \end{aligned} \tag{13}$$

The Landau-Lifshitz and Casimir constitutive equations must explain and forecast the same phenomena. In other word there should be an equivalence relation between the tensor in (7) and the tensors in (12) and (13). It is suitable to write the relation for spatial Fourier transforms:

$$\varepsilon_{ij}^{LL}\left(\omega,\overrightarrow{k}\right)=\varepsilon_{ij}^{C}\left(\omega,\overrightarrow{k}\right)+\left(\frac{c}{\omega}\right)^{2}\left\{e_{ikl}e_{jnm}k_{k}k_{n}\left[\left(\mu_{lm}^{C}\right)^{-1}-\delta_{lm}\right]\right\} \tag{14}$$

The last relation is often treated as a condition of equivalence of two forms of constitutive equations. Really, one can reconstruct $\varepsilon_{ij}^{LL}\left(\omega,\overrightarrow{k}\right)$ from ε_{ij}^{C} and μ_{lm}^{C}, but it is impossible to solve the inverse problem of reconstruction ε_{ij}^{C} and μ_{lm}^{C} from ε_{ij}^{LL}. To make the latter problem solvable it often suggested that ε_{ij}^{C} and, μ_{lm}^{C} are scalars whereas ε_{ij}^{C} is a tensor. The last assumption seems to be unjustified. Moreover we loose a series of phenomena. For example, the existence of magnetic longitudinal waves can not be described. If ε_{ij}^{C} and μ_{lm}^{C} are tensors they have the form:

$$\varepsilon_{lm}^{C} = \varepsilon^{Ctr}\left(\omega,k\right)\left(\delta_{lm}-\frac{k_{l}k_{m}}{k^{2}}\right)+\varepsilon^{Cl}\left(\omega,k\right)\frac{k_{l}k_{m}}{k^{2}}, \tag{15}$$

$$\mu_{lm}^{C} = \mu^{Ctr}\left(\omega,k\right)\left(\delta_{lm}-\frac{k_{l}k_{m}}{k^{2}}\right)+\mu^{Cl}\left(\omega,k\right)\frac{k_{l}k_{m}}{k^{2}} \tag{16}$$

It is obvious that along with electrical longitudinal waves there may be magnetic longitudinal waves with μ^{Cl}, $\left(\overrightarrow{k}\cdot\overrightarrow{H}\right)\neq 0$. The examples are stratified medium and composite loaded with be-helix structures. The waves existing in both media are of evanescent. They cannot propagate through the infinite system but the may be generated on the boundaries. The irreversibility of (14) and the existence of the magnetic longitudinal waves means that the Casimir constitutive equations comprise more information of the system.

3. The Physical Sense of the Fields Governed by the Material Maxwell Equations and the Boundary Conditions

In order to understand the reason of incompleteness of the Landau-Lifshitz form we have to consider the problem of the boundary conditions. Dealing with bounded body demands a procedure of sewing together the solution of the Maxwell equation outside and inside the body because just on the boundary the Maxwell equations are not valid. If the dispersion equation

$$k^{2}=\left(\frac{\omega}{c}\right)^{2}\varepsilon^{Ctr}\left(\omega,k\right)\mu^{Ctr}\left(\omega,k\right),\qquad\left(\overrightarrow{k}\cdot\overrightarrow{H}\right)=0,\qquad\left(\overrightarrow{k}\cdot\overrightarrow{E}\right)=0 \tag{17}$$

has only one solution for k^2 the common Maxwell boundary conditions are enough. These conditions come about from the assumption that we deal with the same fields inside and outside the medium. In other words the physical sense of the fields $\overrightarrow{E}$ and $\overrightarrow{H}$ should be the same in vacuum and inside the medium. Saying about the physical sense of the fields implies that there must be determined a method of measuring these fields. By now almost all authors proceed from the Rosenfeld Ansatz. Rosenfeld [9] suggested determining the fields investigating the motion a small probe particle with charge e. Rosenfeld assumed that this particle moves under the Lorentz force

$$\overrightarrow{F}=e\overrightarrow{E}+e\left[v\times\overrightarrow{B}\right] \tag{18}$$

where $\overrightarrow{E}$ and $\overrightarrow{B}$ are just the fields staying in the Maxwell equations. "The fields are taken to be the primitive fields" [10]. The fields $\overrightarrow{D}$ and $\overrightarrow{H}$ are often considered being of secondary kind

or induction fields [10]. Indeed, one can introduce a new field $\overrightarrow{Q}$ and redefine the fields $\overrightarrow{D}$ and $\overrightarrow{H}$ [11].

$$\overrightarrow{D'} = \overrightarrow{D} + \mathrm{curl}\overrightarrow{Q}, \qquad \overrightarrow{H'} = \overrightarrow{H} + \frac{1}{\mathrm{c}}\frac{\partial}{\partial \mathrm{t}}\overrightarrow{Q} \tag{19}$$

The fields $\overrightarrow{D'}$ and also $\overrightarrow{H'}$ satisfy the Maxwell equations. In particular choosing $\overrightarrow{H'} = \overrightarrow{B}$ we can pass from the Casimir to Landau-Lifshitz form [11]. Unfortunately, this scheme ceases being so attracting if we remember that even in absence of the fields a charged particle moving through the matter looses energy polarizing the surrounding medium. There is another way to determine the fields. This way is tightly connected with boundary conditions. Temporarily forgetting that we deal with heterogeneous media let us recall that the field inside the anisotropically shaped cavity is equal to $\overrightarrow{E}$ $(\overrightarrow{H})$ if the cavity is elongated along the force lines and is equal to $\overrightarrow{D}$ $(\overrightarrow{B})$ if the cavity is flattened along the corresponding direction. This property is a consequence of the Maxwell boundary conditions. Thus if we assume that the Maxwell boundary conditions are valid we have the method of measuring all the fields involved in our problem. There is neither freedom nor uncertainty in definition of any field. Introduction of any auxiliary vector field $\overrightarrow{Q}$ results in changing the boundary conditions.

There are some indications that it is the Casimir form that is accompanied with the Maxwell boundary conditions. First of all along the surface separating two media may flow a surface current that is due to difference in eddy currents induced in different media. Another constitutive equation relating this current to fields should be added to. Thus the Landau-Lifshitz form is incomplete while describing edge effects including the evanescent waves. The suggestion that the Casimir form should be supplemented with the Maxwell boundary conditions means that ε_{ij}^{C} and μ_{lm}^{C} comprise information not only of the wavenumber but also of the impedance. This fact accounts for the irreversibility of (14).

4. Chiral (Optically Active) Media

It is worth emphasizing that really the problem exists if the effects of spatial dispersion are important. If it is not the case the situation becomes trivial. Indeed, the Landau-Lifshitz form produces seeming spatial dispersion. The relation (7) reduces in this case to

$$\overrightarrow{D} = \varepsilon(\omega)\overrightarrow{E} + \xi(\omega)\left[\overrightarrow{k} \times \left[\overrightarrow{k} \times \overrightarrow{E}\right]\right] \tag{20}$$

Employing $e_{ijk}k_jE_k = -(\omega/c)B_i$ we arrive at the usual Casimir form with scalar permeability $\mu = 1/(1 + i\omega\xi(\omega)/c)$. This seeming spatial dispersion may be a source of some troubles. Let us consider the phenomenon of chirality. It is well known that the chirality is the effect of first order in (ka), where is a characteristic dimension of the inclusion and k is the wavenumber. Nevertheless truncating the series (7) and (12), (13) at the same order in (ka) may lead to different consequences. As we shall see the reason of the disagreement is neglect of the seeming spatial dispersion. In the Landau-Lifshitz form the constitutive equations looks as

$$\overrightarrow{D^{LL}} = \varepsilon\overrightarrow{E} + \gamma\mathrm{curl}\overrightarrow{E} \tag{21}$$

where γ is a pseudo-scalar. The constitutive equation predicts rotation of the plane of polarization during propagation. Beside this, the theory employed together with the Maxwell boundary conditions predicts that in the case of normally incident, linearly polarized wave the reflected wave is elliptically polarized. Moreover, the main axis of the polarization ellipse is azimuth rotated (effect of optical activity on reflection). Such a behavior is an attribute of non-reciprocal medium. On the other hand the chiral system made of reciprocal elements should be reciprocal. The authors of [12] suppose that this behavior is connected with existence of transition layer

near the boundary surface. Indeed the boundary breaks the translation invariance. The kernel in (5) depends not only on difference of spatial variables but also on position of the point of observation. As a consequence there appear an additional term in the constitutive equation:

$$\overrightarrow{D^{LL}} = \varepsilon \overrightarrow{E} + \gamma \mathrm{curl} \overrightarrow{E} + \left[\mathrm{grad}\gamma \times \overrightarrow{E}\right] \tag{22}$$

The boundary conditions obtained by the usual way change too [12]

$$E_{t1} - E_{t2} = 0, \qquad B_{2t} - B_{1t} = \frac{\gamma}{c}\frac{\partial E_t}{\partial t} \tag{23}$$

The angle of main axis rotation changes his sign but the main result remains: the reflected wave is elliptically polarized. In the problem there appear a vector gradγ. The situation seems to remain the situation in ferromagnetic and antiferromagnetic where the rotation of polarization on reflection is a well known effect. Indeed, in ferromagnetic there is the vector of magnetization $\overrightarrow{M}$ and in antiferromagnetic there is the vector $\overrightarrow{L}$ which is equal to the difference of magnetizations of sublattices. The key moment is that in the last cases the vectors are axial whereas gradγ is a polar vector. Thus we cannot anticipate the appearance of nonreciprocity. To rest the theory in [13] the constitutive equation was generalized:

$$\overrightarrow{D^{LL}} = \varepsilon \overrightarrow{E} + \gamma_1 \mathrm{curl} \overrightarrow{E} + \left[\mathrm{grad}\gamma_2 \times \overrightarrow{E}\right] \tag{24}$$

Where it is assumed that $\gamma_1 = 2\gamma_2$. This relation between the quantities were determined from continuity of the Pointing vector and strange assumption that $\left[\overrightarrow{E} \times \partial\overrightarrow{E}/\partial t\right] \neq 0$. This corrects the boundary conditions so that the effect of optical activity on reflection disappears. All these troubles can be avoided if we deal with Casimir (in our case Born-Fedorov) constitutive equations. There is no effect of optical activity on reflection neither in uniform medium nor while taking into account a transition layer [11]. The background of complexity in boundary conditions appears due to incorrect treatment of derivatives in (7). Dealing with effects of spatial dispersion we must remember that there are two scales in the problem. The first one is the inclusion dimension a . The second scale is the wavelength. Thus coefficients staying in (7) in front of derivatives depend on both scales but only those depending on a contribute in the corresponding term of perturbation theory. The part depending on λ should be rewritten employing the Maxwell equation, relating the first derivatives of $\overrightarrow{E}$ to $\overrightarrow{B}$. In so doing we should take into consideration the term with third order derivative. This term produces the term $\gamma \mathrm{curl}\overrightarrow{B}$ in the Born-Fedorov constitutive equations.

5. Conclusion

Thus the Casimir form of the constitutive equations is more complete in comparison with the Landau-Lifshitz form. The Casimir form produces not only wavevector but also the impedance of the material, whereas the Landau-Lifshitz form demands introduction of additional constitutive equation for the surface current [15]. This additional constitutive equation usually appears as modification of the boundary conditions.

Acknowledgement
This work was supported in part by the Russian Foundation for Basic Research, grants No. 00-15-97570 and No. 99-02-16564.

References

[1] L. D. Barron, *Molecular Light Scattering and Pptical Activity.* Cambridge: Cambridge University Press, 1982.

[2] E. B. Graham, J. Pierrus, and R. E. Raab, *J.Phys. B*, vol. 25, pp. 4673-4684, 1992; R. E. Raab and J. H. Cloete, *JEWA*, vol. 8, pp. 1073-1089, 1994; E. B. Graham and R. E. Raab, *J. Opt. Soc. Am.*, vol. 6, pp. 1239-1248, 1996.

[3] L. D. Landau, E. M. Lifshitz, and L. P. Pitaevskii, *Electrodynamics of Continuous Media* (2nd Ed.). Oxford: Butterworth Heinemann, 1995.

[4] V. M. Agranovich and V. L. Ginzburg, *Spatial Dispersion in Crystal Optics and the Theory of Excitons*, Monographs and Texts in Physics and Astronomy, Vol. XIII. New York: Interscience, 1966.

[5] V. P. Silin and A. A. Rukhadze *Electromagnetic Properties of Plasma and Plasma-Like Media.* Moscow: GosAtomIzdat, 1961 (in Russian).

[6] A. P. Vinogradov and A. V. Aivazian, *Phys. Rev E*, vol. 60, pp. 987-993, 1999.

[7] J. E. Sipe and J. Van Kranendonk, *Phys. Rev. A* , vol. 9, p. 1806, 1974; *Can. J. Phys.*, vol. 53, p. 2095, 1975; G. Russakoff, *Am. J. Phys.*, vol. 38, p. 1188, 1970.

[8] J. D. Jackson *Classical Electrodynamics* (2nd Ed.). Singapore: John Wiley, 1990.

[9] L. Rosenfeld, *Theory of Electrons.* Amsterdam: North-Holland Pub. Company, 1951

[10] W. S. Weiglhofer, *J. Phys. A*, vol. 27, pp. L871-874, 1994.

[11] F. I. Fedorov, *Theory of Girotropy.* Minsk: Nauka i Tekhnika, 1976 (in Russian).

[12] A. R. Bungay, Yu. P. Svirko, and N.I. Zheludev, *Phys. Rev.B*, vol. 47, No. 18, pp. 11730-11735, 1993.

[13] Valkov A. Yu., V. P. Romanov, and A. N. Shalaginov, *Opt. i Spectr.*, vol. 69, pp. 635-639, 1990 (in Russian).

[14] B. V. Bokut and A. N. Serdyukov, *Zh. Prikl. Spectr.*, vol. 20, pp. 677-681, 1974; B. V. Bokut, A. N. Serdyukov, and F. I. Fedorov, *Opt. i Spectr.*, vol. 37, pp. 288-293, 1974 (in Russian).

[15] G. A. Smolenskii, R. V. Pisarev, and I. G. Sinii, *Uspekhi Fiz. Nauk*, vol.116, pp. 231-242, 1975 (im Russian).

Homogenization Formalisms for Nonlinear Particulate Composite Mediums

A. Lakhtakia[1], M. N. Lakhtakia[2] and W. S. Weiglhofer[3]

[1] CATMAS — Computational & Theoretical Materials Sciences Group
Department of Engineering Science and Mechanics, Pennsylvania State University
University Park, PA 16802–6812, USA
Tel: +1 814 863 4319; Fax: +1 814 863 7967; email: AXL4@psu.edu

[2] 1811 Red Lion Drive, State College, PA 16801–3012, USA

[3] Department of Mathematics, University of Glasgow
University Gardens, Glasgow G12 8QW, Great Britain

Abstract

The Maxwell Garnett (MG) and the Bruggeman (Br) formalisms are extended to homogenize *nonlinear*, two–component, composite mediums. The chosen material topology is ellipsoidal and weak nonlinearity is assumed. The MG formalism is illustrated by a case in which both component materials are bianisotropic, but only the inclusion component is nonlinear. Both component materials are isotropic dielectric in the following case, but only one has an intensity–dependent permittivity scalar; and the Br formalism is applied to show that the homogenized composite medium is anisotropic and has cubically nonlinear dielectric properties. Enhancement of nonlinearity emerges as a significant possibility.

1. Introduction

The Maxwell Garnett (MG) and the Bruggeman (Br) formalisms for the homogenization of linear composite mediums formed by randomly dispersing electrically small, bianisotropic, ellipsoidal inclusions in bianisotropic host materials can be extended to composite mediums comprising nonlinear materials. We illustrate this extension with an example for each formalism. The nonlinearity is assumed as weak and, therefore, perturbatively tractable.

In the first example, both component materials are bianisotropic, but only the inclusion material is nonlinear. The effective constitutive properties of the homogenized composite medium (HCM) are estimated using the MG formalism. The linear and nonlinear properties of the HCM are estimated separately in consequence of two assumptions: the nonlinearity of the inclusion material is weak, and the composite medium is dilute [1].

In the second example, both component materials are isotropic dielectric, but just one of them has an intensity–dependent permittivity scalar. Application of the Br formalism shows that the HCM is anisotropic and has cubically nonlinear dielectric properties. The anisotropy of nonlinearity can be considerably different from the anisotropy of the linearity; and the possibility of nonlinearity enhancement exists [2].

2. Nonlinear Bianisotropic Composite Medium

Consider a countably infinite number of identical, electrically small, ellipsoidal inclusions that are similarly oriented but randomly embedded in a host material. Each inclusion has a volume

v; the number density of inclusions is denoted by N; while $f = Nv$, $0 \le f \le 1$, is the volumetric proportion of the inclusion medium. Typically, $f < 0.2$ for the MG formalism to yield adequate results. The inclusions are described by a shape dyadic which is real symmetric with positive eigenvalues [3].

The use of 6–vectors and 6×6 dyadics is very convenient for bianisotropic mediums as it permits a compact notation. In this notation, the constitutive properties of the host material are expressed as

$$\underline{\mathbf{G}}(\omega) = \begin{pmatrix} \underline{\underline{\epsilon}}^h(\omega) & \underline{\underline{\xi}}^h(\omega) \\ \underline{\underline{\zeta}}^h(\omega) & \underline{\underline{\mu}}^h(\omega) \end{pmatrix} \cdot \underline{\mathbf{F}}(\omega) = \underline{\underline{\mathbf{C}}}^h(\omega) \cdot \underline{\mathbf{F}}(\omega)\,, \tag{1}$$

where the 6–vectors $\underline{\mathbf{F}}(\omega) = [\underline{E}(\omega), \underline{H}(\omega)]^T$ and $\underline{\mathbf{G}}(\omega) = [\underline{D}(\omega), \underline{B}(\omega)]^T$, the superscript T denoting the transpose.

With the 6×6 constitutive dyadic of free space denoted by $\underline{\underline{\mathbf{C}}}^v$ (which contains ϵ_0 and μ_0), the linear and the nonlinear constitutive properties of the inclusion material are best expressed through the 6–vector $\underline{\mathbf{Q}}(\omega) = [\underline{P}(\omega), \underline{M}(\omega)]^T = \underline{\mathbf{G}}(\omega) - \underline{\underline{\mathbf{C}}}^v \cdot \underline{\mathbf{F}}(\omega)$, which contains both the polarization field $\underline{P}(\omega)$ and the magnetization field $\underline{M}(\omega)$. This 6–vector is split into linear and nonlinear parts as $\underline{\mathbf{Q}}(\omega) = \underline{\mathbf{Q}}^\ell(\omega) + \underline{\mathbf{Q}}^{nl}(\omega)$. Its linear part $\underline{\mathbf{Q}}^\ell(\omega)$ obeys the constitutive relation $\underline{\mathbf{Q}}^\ell(\omega) = \left[\underline{\underline{\mathbf{C}}}^{in}(\omega) - \underline{\underline{\mathbf{C}}}^v\right] \cdot \underline{\mathbf{F}}(\omega)$, with $\underline{\underline{\mathbf{C}}}^{in}(\omega)$ analogous to $\underline{\underline{\mathbf{C}}}^h(\omega)$.

The nonlinear properties of the inclusion material are described as follows: Let $\mathcal{W} = \{\omega_1, \omega_2, \omega_3, \ldots, \omega_M\}$ be a set of $M > 1$ angular frequencies, there being no requirement that all members of $\mathcal{W}$ be distinct. Suppose there exists an ensemble of M fields $\underline{\mathbf{F}}(\omega_m)$, $(1 \le m \le M)$. Then the simultaneous action of this ensemble of fields in the inclusion material gives rise to the nonlinear part of $\underline{\mathbf{Q}}(\omega)$ at $\omega = \omega^{nl}$. The j–th element of this 6–vector is given by

$$Q_j^{nl}(\omega^{nl}) = \sum_{j_1=1}^{6} \sum_{j_2=1}^{6} \cdots \sum_{j_m=1}^{6} \cdots \sum_{j_M=1}^{6} \left\{ \chi^{nl}_{jj_1j_2\ldots j_m\ldots j_M}(\omega^{nl}; \mathcal{W}) \prod_{n=1}^{M} F_{j_n}(\omega_n) \right\}, \quad 1 \le j \le 6\,, \tag{2}$$

where $\chi^{nl}_{jj_1j_2\ldots j_m\ldots j_M}(\omega^{nl}; \mathcal{W})$ represents the nonlinear susceptibilities of the inclusion material. The angular frequency ω^{nl} is simply related to all members of $\mathcal{W}$ as $\omega^{nl} = a_1\,\omega_1 + a_2\,\omega_2 + \ldots + a_M\,\omega_M$, with $a_m = \pm 1$, $(1 \le m \le M)$; furthermore, ω^{nl} may or or may not lie in $\mathcal{W}$. When $a_n = -1$, $F_{j_n}(\omega_n)$ must be replaced by its complex conjugate on the right side of (2) and in subsequent derivative expressions.

Details of the implementation of the MG formalism to homogenize the described composite medium were given elsewhere [1]. In summary, the constitutive relation of the HCM is given by

$$\underline{\mathbf{G}}(\omega) = \underline{\underline{\mathbf{C}}}^{MG}(\omega) \cdot \underline{\mathbf{F}}(\omega) + s(\omega, \omega^{nl})\, \underline{\mathbf{Q}}^{nls}(\omega)\,, \quad \omega \in \left(\mathcal{W} \cup \left\{\omega^{nl}\right\}\right), \tag{3}$$

where the switching function $s(\omega, \omega^{nl})$ equals unity when both of its arguments are the same, but is null–valued otherwise. Expressions for $\underline{\underline{\mathbf{C}}}^{MG}(\omega)$ have been available for about three years [3], and need not be reproduced here. The nonlinear source polarization–magnetization field is expressed through [1]

$$\underline{\mathbf{Q}}^{nls}(\omega^{nl}) = \left\{ \underline{\underline{\mathbf{I}}} - i\omega^{nl} \left[\underline{\underline{\mathbf{I}}} - i\omega^{nl} f \underline{\underline{\tilde{\mathbf{D}}}}^{in/h}(\omega^{nl}) \cdot \underline{\underline{\mathbf{a}}}^{in/h}(\omega^{nl}) \right]^{-1} \cdot \underline{\underline{\tilde{\mathbf{D}}}}^{in/h}(\omega^{nl}) \right\} \cdot \underline{\mathbf{Q}}^{nl}_{eff}(\omega^{nl})\,, \tag{4}$$

where

$$\begin{aligned} \left(Q^{nl}_{eff}\right)_j(\omega^{nl}) \;=\; f \sum_{j_1=1}^{6} \sum_{j_2=1}^{6} \cdots \sum_{j_m=1}^{6} \cdots \sum_{j_M=1}^{6} \Bigg\{ & \chi^{nl}_{jj_1j_2\ldots j_m\ldots j_M}(\omega^{nl}; \mathcal{W}) \\ & \prod_{n=1}^{M} \left[\left(\underline{\underline{\mathbf{Y}}}^{in/MG}(\omega_n) \cdot \underline{\mathbf{F}}(\omega_n) \right)_{j_n} \right] \Bigg\}, \quad 1 \le j \le 6\,. \end{aligned} \tag{5}$$

In these expressions, the 6×6 dyadics

$$\underline{\underline{\mathbf{a}}}^{in/h}(\omega) = \left[\underline{\underline{\mathbf{C}}}^{in}(\omega) - \underline{\underline{\mathbf{C}}}^{h}(\omega)\right] \cdot \underline{\underline{\mathbf{Y}}}^{in/h}(\omega)\,, \tag{6}$$

$$\underline{\underline{\mathbf{Y}}}^{in/p}(\omega) = \left\{\underline{\underline{\mathbf{I}}} + i\omega\,\underline{\underline{\mathbf{D}}}^{in/p}(\omega) \cdot \left[\underline{\underline{\mathbf{C}}}^{in}(\omega) - \underline{\underline{\mathbf{C}}}^{p}(\omega)\right]\right\}^{-1}, \quad p = h,\, MG, \tag{7}$$

while $\underline{\underline{\mathbf{D}}}^{in/p}$ (resp. $\underline{\underline{\tilde{\mathbf{D}}}}^{in/p}$) is the 6×6 depolarization dyadic of an ellipsoidal (resp. spherical) exclusion region in a linear medium with $\underline{\underline{\mathbf{C}}}^{p}$ as its constitutive dyadic [3].

The presented formalism is general in that it can be used to examine harmonic generation, parametric oscillation, self-focusing, stimulated Raman scattering, and a multitude of nonlinear phenomenons. It also updates and extends our previous work on the MG formalism for complex nonlinear composite mediums [4, 5].

3. Anisotropic Dielectric Composite Medium with Intensity–Dependent Permittivity Dyadic

Next, we implement the Br formulation for homogenizing a mixture of two dielectric materials. For the sake of illustration, here only one component material is assumed to be nonlinear: it possesses an intensity–dependent permittivity scalar. Accordingly, $\underline{\underline{\epsilon}}^{h} = \epsilon^{h}\,\underline{\underline{I}}$, $\underline{\underline{\epsilon}}^{in} = \epsilon^{in}\underline{\underline{I}} = \left(\epsilon_{\ell}^{in} + \epsilon_{nl}^{in}|\underline{E}|^2\right)\underline{\underline{I}}$, $\underline{\underline{\mu}}^{h} = \underline{\underline{\mu}}^{in} = \mu_0\underline{\underline{I}}$, and the remaining components of $\underline{\underline{\mathbf{C}}}^{h}$ and $\underline{\underline{\mathbf{C}}}^{in}$ are null–valued. The ω–dependences are not explicitly identified, as both the linear and the nonlinear fields vibrate at the same frequency. Both component materials are assumed to have parallel ellipsoidal topologies. As both component materials are treated in the same manner in the Br formalism, the labels *in* and *h* lose the meanings they have for the MG formalism, and the results are valid *prima facie* for $f \in [0,\, 1]$.

The Br formalism requires the solution of the dyadic equation [3]

$$f\left(\epsilon^{in}\,\underline{\underline{I}} - \underline{\underline{\epsilon}}^{Br}\right) \cdot \left(\underline{\underline{X}}^{in/Br}\right)^{-1} + (1-f)\left(\epsilon^{h}\,\underline{\underline{I}} - \underline{\underline{\epsilon}}^{Br}\right) \cdot \left(\underline{\underline{X}}^{h/Br}\right)^{-1} = \underline{\underline{0}}, \tag{8}$$

where

$$\underline{\underline{X}}^{in/Br} = \underline{\underline{I}} + i\omega\,\underline{\underline{D}}^{in/Br} \cdot \left(\epsilon^{in}\,\underline{\underline{I}} - \underline{\underline{\epsilon}}^{Br}\right) \tag{9}$$

and $\underline{\underline{X}}^{h/Br}$ is defined similarly; while $\underline{\underline{D}}^{in/Br}$ and $\underline{\underline{D}}^{h/Br}$ are 3×3 depolarization dyadics.

The HCM is anisotropic, and the Br formalism predicts its permittivity dyadic as [3, 2]

$$\underline{\underline{\epsilon}}^{Br} = \epsilon_x^{Br}\,\underline{u}_x\underline{u}_x + \epsilon_y^{Br}\,\underline{u}_y\underline{u}_y + \epsilon_z^{Br}\,\underline{u}_z\underline{u}_z\,. \tag{10}$$

A perturbative treatment permits the *ansatz* $\underline{\underline{\epsilon}}^{Br} \simeq \underline{\underline{\epsilon}}_{\ell}^{Br} + \underline{\underline{\epsilon}}_{nl}^{Br}\left|\underline{E}\right|^2$, consistently with our assumption that the nonlinearity of ϵ^{in} is weak; hence,

$$\epsilon_x^{Br} \simeq \epsilon_{x_\ell}^{Br} + \epsilon_{x_{nl}}^{Br}\left|\underline{E}\right|^2, \quad \epsilon_y^{Br} \simeq \epsilon_{y_\ell}^{Br} + \epsilon_{y_{nl}}^{Br}\left|\underline{E}\right|^2, \quad \epsilon_z^{Br} \simeq \epsilon_{z_\ell}^{Br} + \epsilon_{z_{nl}}^{Br}\left|\underline{E}\right|^2. \tag{11}$$

Therefore, the Taylor expansions

$$\underline{\underline{D}}^{p/Br} \simeq \underline{\underline{D}}_{\ell}^{p/Br} + \underline{\underline{D}}_{nl}^{p/Br}\left|\underline{E}\right|^2, \quad p = in,\, h\,, \tag{12}$$

emerge. Expressions for $\underline{\underline{D}}_{nl}^{p/Br}$ are available in Ref. [2]. Accordingly,

$$\underline{\underline{X}}^{p/Br} \simeq \underline{\underline{X}}_{\ell}^{p/Br} + \underline{\underline{X}}_{nl}^{p/Br}\left|\underline{E}^{Br}\right|^2, \quad p = in,\, h\,, \tag{13}$$

where

$$\underline{\underline{X}}_{\ell}^{in/Br} = \underline{\underline{I}} + i\omega\, \underline{\underline{D}}_{\ell}^{in/Br} \cdot \left(\epsilon_{\ell}^{in}\, \underline{\underline{I}} - \underline{\underline{\epsilon}}_{\ell}^{Br} \right) , \tag{14}$$

$$\underline{\underline{X}}_{\ell}^{h/Br} = \underline{\underline{I}} + i\omega\, \underline{\underline{D}}_{\ell}^{h/Br} \cdot \left(\epsilon^{h}\, \underline{\underline{I}} - \underline{\underline{\epsilon}}_{\ell}^{Br} \right) , \tag{15}$$

$$\underline{\underline{X}}_{nl}^{in/Br} = i\omega \left[\underline{\underline{D}}_{\ell}^{in/Br} \cdot \left(g\, \epsilon_{nl}^{in}\, \underline{\underline{I}} - \underline{\underline{\epsilon}}_{nl}^{Br} \right) + \underline{\underline{D}}_{nl}^{in/Br} \cdot \left(\epsilon_{\ell}^{in}\, \underline{\underline{I}} - \underline{\underline{\epsilon}}_{\ell}^{Br} \right) \right] , \tag{16}$$

$$\underline{\underline{X}}_{nl}^{h/Br} = i\omega \left[- \underline{\underline{D}}_{\ell}^{h/Br} \cdot \underline{\underline{\epsilon}}_{nl}^{Br} + \underline{\underline{D}}_{nl}^{h/Br} \cdot \left(\epsilon^{h}\, \underline{\underline{I}} - \underline{\underline{\epsilon}}_{\ell}^{Br} \right) \right] . \tag{17}$$

The local field factor g is estimated, as a first approximation, as $g \simeq (1/9)|\text{trace}\left\{ \underline{\underline{Y}}_{\ell}^{in/Br} \right\}|^2$ where $\underline{\underline{Y}}_{\ell}^{in/Br} = \left(\underline{\underline{X}}_{\ell}^{in/Br} \right)^{-1}$ [2].

With the foregoing developments, the nonlinear dyadic equation (8) separates into two parts [2]: (i) $\underline{\underline{\epsilon}}_{\ell}^{Br}$ is the solution of

$$\underline{\underline{\epsilon}}_{\ell}^{Br} = \left[f\, \underline{\underline{X}}_{\ell}^{h/Br} + (1-f)\, \underline{\underline{X}}_{\ell}^{in/Br} \right]^{-1} \cdot \left[f \epsilon_{\ell}^{in}\, \underline{\underline{X}}_{\ell}^{h/Br} + (1-f) \epsilon^{h}\, \underline{\underline{X}}_{\ell}^{in/Br} \right] , \tag{18}$$

while (ii) $\underline{\underline{\epsilon}}_{nl}^{Br}$ has to obtained from

$$\begin{aligned} \underline{\underline{\epsilon}}_{nl}^{Br} \;=\; & \left[f\, \underline{\underline{X}}_{\ell}^{h/Br} + (1-f)\, \underline{\underline{X}}_{\ell}^{in/Br} \right]^{-1} \cdot \left[f g \epsilon_{nl}^{in}\, \underline{\underline{X}}_{\ell}^{h/Br} + \right. \\ & \left. f(\epsilon_{\ell}^{in}\, \underline{\underline{I}} - \underline{\underline{\epsilon}}_{\ell}^{Br}) \cdot \underline{\underline{X}}_{nl}^{h/Br} + (1-f)(\epsilon^{h}\, \underline{\underline{I}} - \underline{\underline{\epsilon}}_{\ell}^{Br}) \cdot \underline{\underline{X}}_{nl}^{in/Br} \right] . \end{aligned} \tag{19}$$

These two equations were solved iteratively on a computer. The obtained numerical results allowed us to conclude the following [2]:

(i) The anisotropy of nonlinearity can be considerably different from the anisotropy of the linearity in the chosen HCM.

(ii) Enhancement of nonlinearity over that of the inclusion material is possible, the enhancement being anisotropic too.

In closing, we note that the algorithm developed can be easily generalized when *both* component materials have intensity–dependent permittivity scalars.

Acknowledgement
WSW holds a *RSE/SOEID Research Support Fellowship* of the *Royal Society of Edinburgh* for the year 2000.

References

[1] A. Lakhtakia and W. S. Weiglhofer, "Maxwell Garnett formalism for weakly nonlinear, bianisotropic, dilute, particulate composite mediums," *Int. J. Electron.*, 2000 (at press).

[2] M. N. Lakhtakia and A. Lakhtakia, "Anisotropic composite materials with intensity–dependent permittivity tensor: Bruggeman approach," *Electromagnetics*, 2000 (accepted for publication).

[3] W. S. Weiglhofer, A. Lakhtakia, and B. Michel, "Maxwell Garnett and Bruggeman formalisms for a particulate composite with bianisotropic host medium," *Microw. Opt. Technol. Lett.* **15**, 263–266, 1997; erratum: **22**, 221, 1999.

[4] A. Lakhtakia and W. S. Weiglhofer, "Maxwell Garnett approach for nonlinear dilute particulate composites with bi–isotropic host media," *Int. J. Electron.* **80**, 665–676, 1996.

[5] A. Lakhtakia and W. S. Weiglhofer, "Maxwell Garnett approach for cubically nonlinear, gyrotropic, composite media," *Int. J. Electron.* **84**, 285–294, 1998.

The Incremental and Differential Maxwell Garnett Formalisms for Bianisotropic Composites

B. Michel[1], A. Lakhtakia[2], W.S. Weiglhofer[3], and T.G. Mackay[3]

[1] Scientific Consulting, Kirchenstraße 13, D–90537 Feucht–Moosbach, Germany
Fax: +49 9128 727812; email: BEST.Michel@t-online.de

[2] CATMAS, Department of Engineering Science and Mechanics
Pennsylvania State University, University Park, PA 16802–6812, USA

[3] Department of Mathematics, University of Glasgow
University Gardens, Glasgow G12 8QW, Great Britain

Abstract

We present two approaches to homogenize bianisotropic particulate composite mediums: (i) the Incremental Maxwell Garnett (IMG) formalism, in which the composite medium is built incrementally by adding the inclusions in N discrete steps to the host medium; and (ii) the Differential Maxwell Garnett (DMG) formalism, which is obtained from the IMG in the limit $N \to \infty$. Both formalisms are applicable to arbitrary inclusion concentration and are well–suited for computational purposes. Application of both formalisms is exemplified here by numerical results for a uniaxial dielectric composite medium and a chiroferrite.

1. Introduction

Discrete random mediums — comprising electrically small particles of a certain material dispersed randomly in some host medium — have been considered in the electromagnetics literature for about two centuries as homogeneous material continuums. Several homogenization formalisms exist to connect the electromagnetic response properties of a homogenized composite medium (HCM) to those of the constituent material phases; see Ref. [1] for a selection of milestone papers about this topic.

Perhaps the most widely used homogenization formalism is the Maxwell Garnett (MG) formalism. It was recently set up for bianisotropic composite mediums containing ellipsoidal inclusions [2], [3], covering thereby a large domain of electromagnetic applications in the materials sciences. One drawback of the MG formalism is that it can be used only for dilute composite mediums.

Our present work illustrates and enlarges upon an earlier report [4] on overcoming this handicap of the MG formalism. The so–called Incremental Maxwell Garnett (IMG) formalism is applicable to dense composite mediums. It has an iterative flavour, being based on the repeated use of the MG formalism for certain *intermediate* dilute composite mediums. Furthermore, we show that the IMG formalism leads to a Differential Maxwell Garnett (DMG) formalism that is based on the numerical solution of a system of differential equations. Details of the IMG/DMG formalisms shall be published shortly elsewhere [5]. A more general survey of homogenization formalisms for bianisotropic composite mediums is given in Ref. [6]; see also Ref. [7].

2. Theory

Suppose that identical, similarly oriented, electrically small inclusions made of a medium labelled b are randomly dispersed in a host medium labelled a. The volumetric proportions of the constituent material phases are denoted by f_a and $f_\mathrm{b} = 1 - f_\mathrm{a}$. Both mediums are linear and bianisotropic, their frequency–domain constitutive relations being specified as [3], [4]:

$$\left(\begin{array}{c} \underline{D} \\ \underline{B} \end{array} \right) = \underline{\underline{\mathbf{C}}}^{\alpha} \cdot \left(\begin{array}{c} \underline{E} \\ \underline{H} \end{array} \right) , \qquad (\alpha = \mathrm{a},\, \mathrm{b}) . \tag{1}$$

The 6×6 constitutive dyadic $\underline{\underline{\mathbf{C}}}^{\alpha}$ is composed of 3 × 3 dyadics in the following way:

$$\underline{\underline{\mathbf{C}}}^{\alpha} = \left(\begin{array}{cc} \underline{\underline{\epsilon}}^{\alpha} & \underline{\underline{\xi}}^{\alpha} \\ \underline{\underline{\zeta}}^{\alpha} & \underline{\underline{\mu}}^{\alpha} \end{array} \right) , \qquad (\alpha = \mathrm{a},\, \mathrm{b}) , \tag{2}$$

where $\underline{\underline{\epsilon}}^{\alpha}$ and $\underline{\underline{\mu}}^{\alpha}$ are the permittivity and permeability dyadics, respectively, whereas $\underline{\underline{\xi}}^{\alpha}$ and $\underline{\underline{\zeta}}^{\alpha}$ are the two magnetoelectric dyadics. An $\exp(-i\omega t)$ time–dependence is implicit in this work, ω being the angular frequency.

We define the 6×6 polarizability dyadic

$$\underline{\underline{\mathbf{a}}}^{\alpha' \,\mathrm{in}\, \alpha} = \left(\underline{\underline{\mathbf{C}}}^{\alpha'} - \underline{\underline{\mathbf{C}}}^{\alpha} \right) \cdot \left[\underline{\underline{\mathbf{I}}} + i\omega \underline{\underline{\mathbf{D}}}^{\alpha} \cdot \left(\underline{\underline{\mathbf{C}}}^{\alpha'} - \underline{\underline{\mathbf{C}}}^{\alpha} \right) \right]^{-1} \tag{3}$$

of an electrically small ellipsoid of medium α' embedded *in* medium α, where $\underline{\underline{\mathbf{I}}}$ is the 6×6 identity dyadic. In the general case of a bianisotropic medium, the 6×6 depolarization dyadic $\underline{\underline{\mathbf{D}}}^{\alpha}$ can be computed by numerical two–dimensional integration, and in many important cases even analytically [6].

The MG estimate $\underline{\underline{\mathbf{C}}}^{\mathrm{MG}}$ of the constitutive dyadic of the HCM is given by [2]

$$\underline{\underline{\mathbf{C}}}^{\mathrm{MG}}(\underline{\underline{\mathbf{C}}}^{\mathrm{a}}, \underline{\underline{\mathbf{C}}}^{\mathrm{b}}, f_\mathrm{b}) = \underline{\underline{\mathbf{C}}}^{\mathrm{a}} + f_\mathrm{b}\, \underline{\underline{\mathbf{a}}}^{\mathrm{b\,in\,a}} \cdot \left(\underline{\underline{\mathbf{I}}} - i\omega f_\mathrm{b} \underline{\underline{\tilde{\mathbf{D}}}}^{\mathrm{a}} \cdot \underline{\underline{\mathbf{a}}}^{\mathrm{b\,in\,a}} \right)^{-1} , \tag{4}$$

where $\underline{\underline{\tilde{\mathbf{D}}}}^{\alpha}$ is related to $\underline{\underline{\mathbf{D}}}^{\alpha}$ and the functional dependencies of $\underline{\underline{\mathbf{C}}}^{\mathrm{MG}}$ are identified explicitly.

In the *IMG formalism*, the actual composite medium is built *incrementally* by adding the inclusions not all at once, but in N stages. After each increment, the composite medium is homogenized using the MG formalism. In this fashion, the following iterative scheme emerges

$$\underline{\underline{\mathbf{C}}}^{(0)} = \underline{\underline{\mathbf{C}}}^{\mathrm{a}}, \qquad \underline{\underline{\mathbf{C}}}^{(\mathrm{n}+1)} = \underline{\underline{\mathbf{C}}}^{\mathrm{MG}}(\underline{\underline{\mathbf{C}}}^{(\mathrm{n})}, \underline{\underline{\mathbf{C}}}^{\mathrm{b}}, \delta_\mathrm{b}), \qquad (n = 0,\, 1,\, 2, \ldots) . \tag{5}$$

In order to terminate the iterative scheme in N stages, we fix the incremental proportion

$$\delta_\mathrm{b} = 1 - (1 - f_\mathrm{b})^{1/N} . \tag{6}$$

As the final result of the iteration, we obtain the IMG estimate $\underline{\underline{\mathbf{C}}}^{\mathrm{IMG}} = \underline{\underline{\mathbf{C}}}^{(\mathrm{N})}$.

The *DMG formalism* arises from the IMG formalism in the limit $N \to \infty$. The difference equation (5) is then converted into the ordinary differential equation

$$\frac{\partial}{\partial \eta} \underline{\underline{\mathbf{C}}}(\eta) = \frac{1}{1 - \eta} \underline{\underline{\mathbf{a}}}^{\mathrm{b\,in}\,\eta} , \tag{7}$$

with initial value $\underline{\underline{\mathbf{C}}}(0) = \underline{\underline{\mathbf{C}}}^{\mathrm{a}}$. The DMG estimate is then given by

$$\underline{\underline{\mathbf{C}}}^{\mathrm{DMG}} = \underline{\underline{\mathbf{C}}}(f_\mathrm{b}) . \tag{8}$$

3. Numerical Results and Discussion

Two independent numerical implementations of the IMG and DMG formalisms were set up by us. Both codes produced identical results in all cases tested. The number of iteration steps for the IMG formalism is finite, because N is finite, and therefore no convergence problems can arise so long as an adequately large value of N is used [4]. For implementing the DMG formalism, one can rely on well–tested algorithms in numerical libraries so that no numerical problems are to be expected either. Thus, the IMG and DMG implementations are more robust than the implementation of the Bruggeman (Br) formalism.

We now illustrate the IMG and DMG formalisms in relation to the MG and Br formalisms and begin with the simple case of a composite medium consisting of a uniaxial dielectric host medium with spherical isotropic dielectric inclusions. That is,

$$\underline{\underline{\epsilon}}^{\,a} = \epsilon_0 \left(\underline{\underline{I}} + 3\,\underline{u}\,\underline{u} \right) , \quad \underline{\underline{\epsilon}}^{\,b} = 10\,\epsilon_0\,\underline{\underline{I}}; \quad \underline{\underline{\mu}}^{\,a,b} = \mu_0\,\underline{\underline{I}}, \quad \underline{\underline{\xi}}^{\,a,b} = \underline{\underline{\zeta}}^{\,a,b} = \underline{\underline{0}}, \tag{9}$$

where ϵ_0 and μ_0 are the permittivity and permeability of free space, $\underline{u}$ is a unit vector parallel to the optical axis of the uniaxial medium, and $\underline{\underline{I}}$ is the 3×3 unit dyadic. The calculated nonzero components of the permittivity dyadic

$$\underline{\underline{\epsilon}}^{\,HCM} = \epsilon_0 \left[\epsilon^{HCM}\,\underline{\underline{I}} + \left(\epsilon_u^{HCM} - \epsilon^{HCM} \right) \underline{u}\,\underline{u} \right] , \tag{10}$$

are plotted as functions of f_b in Figure 1; trivially, $\underline{\underline{\mu}}^{\,HCM} = \mu_0\,\underline{\underline{I}}$, $\underline{\underline{\xi}}^{\,HCM} = \underline{\underline{\zeta}}^{\,HCM} = \underline{\underline{0}}$. The order of the IMG calculations was set to $N = 5$ to keep the differences with the DMG appreciable on the graphs presented. Both the DMG and IMG estimates are bounded by the MG and the Br estimates for $0 \leq f_b \leq 1$.

We now consider a fully bianisotropic composite medium, *viz.*, a chiroferrite conceptualized as a random deposition of electrically small, isotropic chiral spheres in a ferrite host. The constitutive dyadics are denoted as

$$\underline{\underline{\tau}}^{\,\alpha} = \tau_0 \left[\tau^\alpha\,\underline{\underline{I}} - i\tau_g^\alpha\,\underline{u} \times \underline{\underline{I}} + (\tau_u^\alpha - \tau^\alpha)\,\underline{u}\,\underline{u} \right] , \tag{11}$$
$$(\tau = \epsilon,\, \xi,\, \zeta,\, \mu; \quad \alpha = \text{a, b, MG, Br, IMG, DMG});$$

and we chose the following parameter values: $\epsilon_u^a = \epsilon^a = 5$, $\epsilon_g^a = 0$, $\underline{\underline{\xi}}^{\,a} = \underline{\underline{\zeta}}^{\,a} = \underline{\underline{0}}$, $\mu_u^a = \mu^a = 1.1$, $\mu_g^a = 1.3$ for medium a; and $\epsilon_u^b = \epsilon^b = 4$, $\epsilon_g^b = 0$, $\underline{\underline{\zeta}}^{\,b} = -\underline{\underline{\xi}}^{\,b}$, $\xi_u^b = \xi^b = 1$, $\xi_g^b = 0$, $\mu_u^b = \mu^b = 1.5$, $\mu_g^b = 0$ for medium b. Estimates of the three nonzero scalar components of the constitutive dyadics $\underline{\underline{\epsilon}}^{\,HCM}$, $\underline{\underline{\xi}}^{\,HCM}$, and $\underline{\underline{\mu}}^{\,HCM}$, are plotted as functions of f_b in Figure 2. Results for $\underline{\underline{\zeta}}^{\,HCM}$ are not displayed since $\underline{\underline{\xi}}^{\,HCM} = -\underline{\underline{\zeta}}^{\,HCM}$ follows numerically from all four formalisms.

Clearly, the differences between the predictions of the homogenization formalisms studied here are relatively small. The simplicity and robustness of the numerical implementation is then a clear advantage for the Incremental/Differential Maxwell Garnett formalisms over the Bruggeman formalism.

Acknowledgement

W. S. Weiglhofer is the holder of a *RSE/SOEID Research Support Fellowship* of the *Royal Society of Edinburgh*. The work of T. G. Mackay is supported by the *Carnegie Trust for the Universities of Scotland*.

References

[1] A. Lakhtakia (Ed.), *Selected Papers on Linear Optical Composite Materials.* (SPIE: Bellingham, WA, USA, 1996).

[2] W. S. Weiglhofer, A. Lakhtakia, and B. Michel, "Maxwell Garnett and Bruggeman formalisms for a particulate composite with bianisotropic host medium," *Microw. Opt. Technol. Lett.*, vol. 15, 263—266, 1997; erratum: **22**, 221, 1999.

[3] B. Michel, A. Lakhtakia, and W. S. Weiglhofer, "Homogenization of linear bianisotropic particulate composite media — Numerical studies," *Int. J. Appl. Electromag. Mech.*, vol. 9, 167–178, 1998; erratums: **10**, 537–538, 1999.

[4] A. Lakhtakia, "Incremental Maxwell Garnett formalism for homogenizing particulate composite media," *Microw. Opt. Technol. Lett.*, vol. 17, 276–279, 1998.

[5] B. Michel, A. Lakhtakia, W. S. Weiglhofer, and T. G. Mackay, "Incremental and differential Maxwell Garnett formalisms for bianisotropic composites," *Comp. Sci. Technol.*, 2000 at press.

[6] B. Michel, "Recent developments in the homogenization of linear bianisotropic composite materials," in O.N. Singh and A. Lakhtakia (Eds.), *Electromagnetic Fields in Unconventional Materials and Structures.* Wiley: New York, pp. 39–82, 2000.

[7] T. G. Mackay and W. S. Weiglhofer, "Numerical homogenization studies of biaxial bianisotropic composite materials," *Proc. Bianisotropics 2000*, A. M. Barbosa and A. L. Topa (Eds.), Lisbon, Portugal, pp. 237–240, 2000.

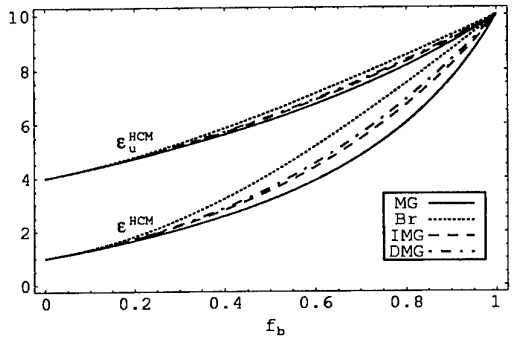

Figure 1: Relative permittivity scalars of a uniaxial dielectric composite as functions of the inclusion volumetric proportion f_b.

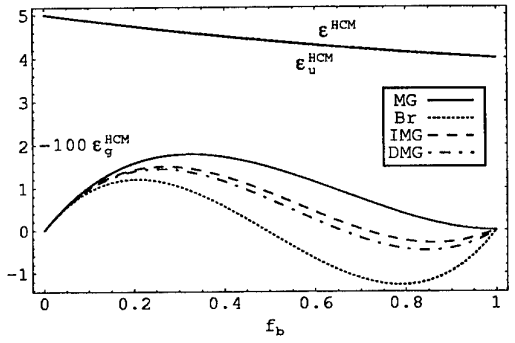

Figure 2a: Constitutive parameters ϵ^{HCM}, ϵ_u^{HCM}, ϵ_g^{HCM} of a chiroferrite HCM as functions of the inclusion volumetric proportion f_b.

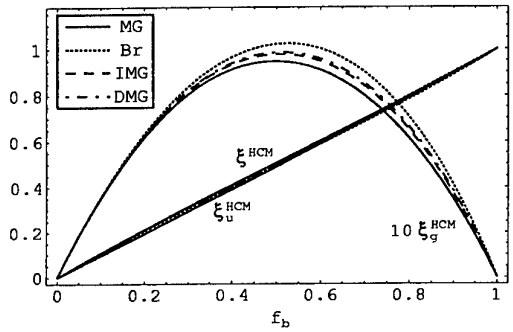

Figure 2b: Constitutive parameters ξ^{HCM}, ξ_u^{HCM}, ξ_g^{HCM} of a chiroferrite HCM as functions of the inclusion volumetric proportion f_b.

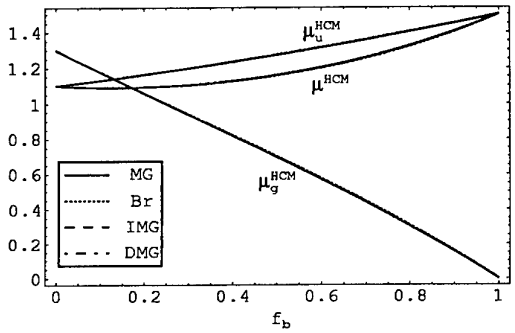

Figure 2c: Constitutive parameters μ^{HCM}, μ_u^{HCM}, μ_g^{HCM} of a chiroferrite HCM as functions of the inclusion volumetric proportion f_b.

Strong–Property–Fluctuation Theory for Homogenization of Bianisotropic Composites

T. G. Mackay[1], A. Lakhtakia[2], and W. S. Weiglhofer[1]

[1] Department of Mathematics, University of Glasgow
University Gardens, Glasgow G12 8QW, Great Britain
Fax: + 44 141 330 4111; email: tm@maths.gla.ac.uk

[2] CATMAS — Computational & Theoretical Materials Sciences Group
Department of Engineering Science and Mechanics, Pennsylvania State University
University Park, PA 16802–6812, USA

Abstract

The strong–property–fluctuation theory (SPFT) is developed for the homogenization of bianisotropic composites with two constituent material phases. A bianisotropic comparison medium is introduced as an initial ansatz in the perturbative process resulting in the SPFT estimate of the constitutive properties of the homogenized medium. Analytic results are presented for ellipsoidal topology, and under the bilocal and long–wavelength approximations.

1. Introduction

Many homogenization approaches — exemplified by the Maxwell Garnett and the Bruggeman formalisms, and their variants — are limited through their simplistic treatments of the distributional statistics of the constituent material phases [?]. A notable exception is the strong–property–fluctuation theory (SPFT), which provides a method to determine both local and nonlocal constitutive properties of composites while allowing for a sophisticated handling of the distributional statistics [?]. The theory has already been developed for isotropic dielectric [?], anisotropic dielectric [?], as well as chiral–in–chiral composites [?]. We present here a generalization of the theory to bianisotropic mediums; further details are reported elsewhere [?].

2. SPFT Preliminaries

We begin with the constitutive relations of a nonhomogeneous bianisotropic medium[1]

$$\underline{D}(\underline{r}) = \underline{\underline{\epsilon}}(\underline{r}) \cdot \underline{E}(\underline{r}) + \underline{\underline{\xi}}(\underline{r}) \cdot \underline{H}(\underline{r}), \qquad \underline{B}(\underline{r}) = \underline{\underline{\zeta}}(\underline{r}) \cdot \underline{E}(\underline{r}) + \underline{\underline{\mu}}(\underline{r}) \cdot \underline{H}(\underline{r}), \tag{1}$$

where $\underline{\underline{\epsilon}}(\underline{r})$ and $\underline{\underline{\mu}}(\underline{r})$ are the permittivity and permeability dyadics, respectively, and $\underline{\underline{\xi}}(\underline{r})$ and $\underline{\underline{\zeta}}(\underline{r})$ are the magnetoelectric dyadics. Substituting (??) into the source–free Maxwell curl postulates, we obtain the dyadic differential equation

$$\underline{\underline{\mathbf{L}}}(\nabla) \cdot \underline{\mathbf{F}}(\underline{r}) = -i\omega \underline{\underline{\mathbf{K}}}(\underline{r}) \cdot \underline{\mathbf{F}}(\underline{r}), \tag{2}$$

[1] Whereas 3–vectors (6–vectors) are in normal (bold) face and underlined, 3 × 3 dyadics (6 × 6 dyadics) are in normal (bold) face and underlined twice. The adjoint, determinant and inverse of the dyadic $\underline{\underline{\mathbf{Q}}}$ are denoted by adj($\underline{\underline{\mathbf{Q}}}$), det $\underline{\underline{\mathbf{Q}}}$ and $\underline{\underline{\mathbf{Q}}}^{-1}$, respectively.

where

$$\underline{\underline{\mathbf{L}}}(\nabla) = \left[\begin{array}{cc} \underline{\underline{0}} & \nabla \times \underline{\underline{I}} \\ -\nabla \times \underline{\underline{I}} & \underline{\underline{0}} \end{array} \right], \qquad \underline{\underline{\mathbf{K}}}(\underline{r}) = \left[\begin{array}{cc} \underline{\underline{\epsilon}}(\underline{r}) & \underline{\underline{\xi}}(\underline{r}), \\ \underline{\underline{\zeta}}(\underline{r}) & \underline{\underline{\mu}}(\underline{r}) \end{array} \right], \qquad \underline{\mathbf{F}}(\underline{r}) = \left[\begin{array}{c} \underline{E}(\underline{r}) \\ \underline{H}(\underline{r}) \end{array} \right], \tag{3}$$

with $\underline{\underline{I}}$ denoting the 3×3 unit dyadic.

Equation (??) is specialized to a two–phase composite mixed at the microscopic (but not molecular) length scale, each constituent material phase taken to be bianisotropic as follows: All space is divided into disjoint parts V_a and V_b such that

$$\underline{\underline{\epsilon}}(\underline{r}) = \underline{\underline{\epsilon}}_p, \quad \underline{\underline{\xi}}(\underline{r}) = \underline{\underline{\xi}}_p, \quad \underline{\underline{\zeta}}(\underline{r}) = \underline{\underline{\zeta}}_p, \quad \underline{\underline{\mu}}(\underline{r}) = \underline{\underline{\mu}}_p \quad \Rightarrow \quad \underline{\underline{\mathbf{K}}}(\underline{r}) = \underline{\underline{\mathbf{K}}}_p, \qquad \underline{r} \in V_p. \tag{4}$$

We introduce the characteristic function $\theta_p(\underline{r})$, defined as

$$\theta_p(\underline{r}) = 1, \qquad \underline{r} \in V_p; \qquad\qquad \theta_p(\underline{r}) = 0, \qquad \underline{r} \notin V_p. \tag{5}$$

The complete statistical information about the composite is contained in $\theta_p(\underline{r})$. On average, the composite is assumed to be homogeneous.

The concept of ensemble–averaging, i.e., averaging over a large number of different samples of the two–phase composite, is central to the SPFT. With ensemble–averages denoted by $\langle\ \rangle$, the nth moment of $\theta_p(\underline{r})$ is the expectation value $\langle \theta_p(\underline{r}_1) \ldots \theta_p \underline{r}_n) \rangle$, which represents the probability for $\underline{r}_1, \ldots, \underline{r}_n$ being inside V_p. The first moment for the phase p is its volume fraction $f_p = \langle \theta_p(\underline{r}) \rangle$. Only f_p, $(p = a, b)$ appear in the Maxwell Garnett and the Bruggeman formalisms, which thus contain minimal statistical information about the composite. A more detailed description is provided by the second moment $\langle \theta_a(\underline{r}) \theta_a(\underline{r}') \rangle$ of $\theta_a(\underline{r})$, or, equivalently, by the second *cumulant* or *covariance*

$$\tau(\underline{R}) = \langle \theta_a(\underline{r}) \theta_a(\underline{r}') \rangle - \langle \theta_a(\underline{r}) \rangle \langle \theta_a(\underline{r}') \rangle = \langle \theta_b(\underline{r}) \theta_b(\underline{r}') \rangle - \langle \theta_b(\underline{r}) \rangle \langle \theta_b(\underline{r}') \rangle, \tag{6}$$

where $\underline{R} = \underline{r} - \underline{r}'$. If the composite is disordered, it is usually possible to define a correlation length L such that $\tau(\underline{R})$ is negligible for $|\underline{R}| \gg L$; i.e., on scales larger than L, the composite may be considered homogeneous.

The formulation of SPFT requires the introduction of a bianisotropic comparison medium (BCM), which allows an approximate treatment of electromagnetic fields in $V_a \cup V_b$. This is a homogeneous medium, characterized by the constitutive dyadic $\underline{\underline{\mathbf{K}}}_{BCM}$, which serves as the preliminary ansatz for the SPFT and may be chosen as the result of implementing the Bruggeman formalism [?]. The corresponding dyadic Green function $\underline{\underline{\mathbf{G}}}_{BCM}(\underline{r} - \underline{r}')$ satisfies the differential equation

$$\left[\underline{\underline{\mathbf{L}}}(\nabla) + i\omega \underline{\underline{\mathbf{K}}}_{BCM} \right] \cdot \underline{\underline{\mathbf{G}}}_{BCM}(\underline{r} - \underline{r}') = \underline{\underline{\mathbf{I}}}\, \delta(\underline{r} - \underline{r}'), \tag{7}$$

where $\underline{\underline{\mathbf{I}}}$ is the unit 6×6 dyadic and $\delta(\underline{r} - \underline{r}')$ is the Dirac delta function. The singular behaviour of $\underline{\underline{\mathbf{G}}}_{BCM}(\underline{r} - \underline{r}')$ in the limit $\underline{r} \to \underline{r}'$ can be accommodated through

$$\underline{\underline{\mathbf{G}}}_{BCM}(\underline{R}) = \mathcal{P} \underline{\underline{\mathbf{G}}}_{BCM}(\underline{R}) + \underline{\underline{\mathbf{D}}}\, \delta(\underline{R}) \tag{8}$$

where $\mathcal{P}$ is the principal value operation excluding a certain infinitesimal region centred on $\underline{R} = \underline{0}$ and the corresponding depolarization dyadic $\underline{\underline{\mathbf{D}}}$ of the specified region in the BCM [?] is fixed at a later stage in the analysis.

In the SPFT, $\underline{\underline{\mathbf{K}}}_{BCM}$ is refined in a perturbative manner in order to estimate the constitutive dyadic $\underline{\underline{\mathbf{K}}}_{Dy}(\underline{R})$ of the nonlocal effective medium arising from the homogenization of the material phases a and b. However, when the principal electromagnetic wavelengths are much larger than

the correlation length L, a *macroscopic* description of the composite as a homogeneous local continuum is possible. In this long–wavelength regime, $\underline{\underline{\mathbf{K}}}_{Dy}(\underline{R}) \equiv \underline{\underline{\mathbf{K}}}_{Dy0}$, where

$$\underline{\underline{\mathbf{K}}}_{Dy0} = \underline{\underline{\mathbf{K}}}_{BCM} - \frac{1}{i\omega}\left(\underline{\underline{\mathbf{I}}} + \underline{\underline{\tilde{\Sigma}}}_0 \cdot \underline{\underline{\mathbf{D}}}\right)^{-1} \cdot \underline{\underline{\tilde{\Sigma}}}_0 ; \qquad \underline{\underline{\tilde{\Sigma}}}_0 = \int \underline{\underline{\Sigma}}(\underline{R})\, d^3\underline{R}. \tag{9}$$

The *mass operator* $\underline{\underline{\Sigma}}(\underline{R})$ consists of an infinite series of terms involving $\mathcal{P}\underline{\underline{\mathbf{G}}}_{BCM}(\underline{R})$. The lowest–order non–trivial result emerges from the *bilocal approximation*; thus,

$$\underline{\underline{\tilde{\Sigma}}}_0 = \left(\underline{\underline{\chi}}_a - \underline{\underline{\chi}}_b\right) \cdot \left[\mathcal{P}\int \tau(\underline{R})\, \underline{\underline{\mathbf{G}}}_{BCM}(\underline{R}) d^3\underline{R}\right] \cdot \left(\underline{\underline{\chi}}_a - \underline{\underline{\chi}}_b\right), \tag{10}$$

where

$$\underline{\underline{\chi}}_p = -i\omega\left[\underline{\underline{\mathbf{K}}}_p - \underline{\underline{\mathbf{K}}}_{BCM}\right] \cdot \left[\underline{\underline{\mathbf{I}}} + i\omega\underline{\underline{\mathbf{D}}} \cdot \left(\underline{\underline{\mathbf{K}}}_p - \underline{\underline{\mathbf{K}}}_{BCM}\right)\right]^{-1}, \qquad (p = a, b). \tag{11}$$

An explicit expression for $\underline{\underline{\mathbf{G}}}_{BCM}(\underline{R})$ cannot be written down, but (??) yields its Fourier transform as

$$\underline{\underline{\tilde{\mathbf{G}}}}_{BCM}(\underline{q}) = \frac{1}{i\omega}\frac{\mathrm{adj}\left(\underline{\underline{\tilde{\mathbf{A}}}}_{BCM}(\underline{q})\right)}{\det \underline{\underline{\tilde{\mathbf{A}}}}_{BCM}(\underline{q})}; \qquad \underline{\underline{\tilde{\mathbf{A}}}}_{BCM}(\underline{q}) = \begin{bmatrix} \underline{\underline{0}} & (\underline{q}/\omega)\times\underline{\underline{\mathbf{I}}} \\ -(\underline{q}/\omega)\times\underline{\underline{\mathbf{I}}} & \underline{\underline{0}} \end{bmatrix} + \underline{\underline{\mathbf{K}}}_{BCM}, \tag{12}$$

where $\underline{q}$ is the spatial frequency vector. Significantly, $\underline{\underline{\tilde{\mathbf{G}}}}_{BCM}(\underline{q})$ may be partitioned as [?]

$$\underline{\underline{\tilde{\mathbf{G}}}}_{BCM}(\underline{q}) = \underline{\underline{\tilde{\mathbf{G}}}}^{0}_{BCM}(\underline{q}) + \underline{\underline{\tilde{\mathbf{G}}}}^{\infty}_{BCM}(\hat{\underline{q}}), \qquad \underline{\underline{\tilde{\mathbf{G}}}}^{\infty}_{BCM}(\hat{\underline{q}}) = \lim_{q\to\infty} \underline{\underline{\tilde{\mathbf{G}}}}_{BCM}(\underline{q}). \tag{13}$$

Let V_η^e be an ellipsoidal region, centred at the origin of our coordinate system, of size determined by the linear measure η. We imagine that both constituent phases are distributed as conformal ellipsoids of surfaces parameterized by $\underline{R}_e(\theta,\phi) = \eta\underline{\underline{U}} \cdot \hat{\underline{R}}(\theta,\phi)$, where $\hat{\underline{R}}(\theta,\phi)$ is the radial unit vector depending on the spherical polar coordinates θ and ϕ, and $\underline{\underline{U}}$ is a real–valued dyadic of full rank. We determine $\underline{\underline{\mathbf{D}}}$ as the depolarization dyadic associated with the exclusion region of shape $\underline{\underline{U}}$ [?] and choose the covariance $\tau(\underline{R})$ to reflect the ellipsoidal topology relating to $\underline{\underline{\mathbf{D}}}$; accordingly,

$$\tau(\underline{R}) = f_a f_b, \qquad \underline{R} \in V_L^e; \qquad\qquad \tau(\underline{R}) = 0, \qquad \underline{R} \notin V_L^e. \tag{14}$$

Thus, the principal value integral in (??) becomes

$$\mathcal{P}\int \tau(\underline{R})\, \underline{\underline{\mathbf{G}}}_{BCM}(\underline{R})\, d^3\underline{R} = \\ \frac{f_a f_b}{2\pi^2}\int_{\phi=0}^{2\pi}\int_{\theta=0}^{\pi}\int_{v=0}^{\infty} \underline{\underline{\tilde{\mathbf{G}}}}^{0}_{BCM}(\underline{\underline{U}}^{-1}\cdot\underline{v})\left(\frac{\sin vL}{v} - L\cos vL\right)\sin\theta\, dv\, d\theta\, d\phi \tag{15}$$

where $\underline{v}$ is a dummy vector variable.

3. Implementation for Biaxial Bianisotropic Mediums

In order to illustrate the implementation of the long–wavelength approximation in the bilocal SPFT framework, we consider a two–phase composite for which both constituent phases belong

to the general class of reciprocal biaxial bianisotropic mediums. The constitutive dyadics of the constituent phases are taken to have the diagonal forms

$$\underline{\underline{\epsilon}}_p = \mathrm{diag}(\epsilon_x^p, \epsilon_y^p, \epsilon_z^p), \quad \underline{\underline{\xi}}_p = \mathrm{diag}(\xi_x^p, \xi_y^p, \xi_z^p) = -\underline{\underline{\zeta}}_p, \quad \underline{\underline{\mu}}_p = \mathrm{diag}(\mu_x^p, \mu_y^p, \mu_z^p), \quad (p = a, b), \quad (16)$$

where all diagonal entries are complex–valued. For simplicity, we choose a spherical particulate topology for the constituent phases, i.e., $\underline{\underline{U}} = \underline{\underline{I}}$. The integration with respect to v in (??) may be performed by means of residue calculus, exploiting symmetries in the integrand along the way: Introducing

$$\underline{\underline{\mathbf{N}}}(\underline{v}) = \frac{\mathrm{adj}\left(\underline{\underline{\tilde{\mathbf{A}}}}_{BCM}(\underline{v})\right) \; - \; \det\left(\underline{\underline{\tilde{\mathbf{A}}}}_{BCM}(\underline{v})\right) \underline{\underline{\tilde{\mathbf{G}}}}^{\infty}_{BCM}(\hat{\underline{v}})}{(\hat{\underline{v}} \cdot \underline{\underline{\epsilon}}_{BCM} \cdot \hat{\underline{v}})(\hat{\underline{v}} \cdot \underline{\underline{\mu}}_{BCM} \cdot \hat{\underline{v}}) + (\hat{\underline{v}} \cdot \underline{\underline{\xi}}_{BCM} \cdot \hat{\underline{v}})(\hat{\underline{v}} \cdot \underline{\underline{\xi}}_{BCM} \cdot \hat{\underline{v}})}, \quad (17)$$

we find that

$$\int_{\phi=0}^{2\pi} \int_{\theta=0}^{\pi} \int_{v=0}^{\infty} \underline{\underline{\tilde{\mathbf{G}}}}^{0}_{BCM}(\underline{v}) \left(\frac{\sin vL}{v} - L\cos vL \right) \sin\theta \, dv \, d\theta \, d\phi = \frac{\pi\omega^3}{4i} \int_{\phi=0}^{2\pi} \int_{\theta=0}^{\pi} \left\{ \frac{1}{\kappa_+ - \kappa_-} \right.$$
$$\left. \times \left[\frac{\mathrm{e}^{iLv}}{v^2} (1 - iLv) \left(\underline{\underline{\mathbf{N}}}(\underline{v}) + \underline{\underline{\mathbf{N}}}(-\underline{v}) \right) \right]_{v=\sqrt{\kappa_-}}^{v=\sqrt{\kappa_+}} + \frac{2\,\underline{\underline{\mathbf{N}}}(\underline{0})}{\kappa_+ \, \kappa_-} \right\} \sin\theta \, d\theta \, d\phi, \quad (18)$$

where $\kappa_\pm$ are the v^2 roots of $\det \underline{\underline{\tilde{\mathbf{A}}}}_{BCM}(\underline{v})$ and are assumed to be distinct.

4. Concluding Remarks

The constitutive dyadic $\underline{\underline{\mathbf{K}}}_{Dy0}$ is fully specified through (??), (??), (??), (??) and (??). The surface integral representation (??) requires numerical evaluation, in general; a selection of results is presented in [?]. These calculations reveal a biaxial bianisotropic composite structure which includes scattering losses, and is therefore attenuative even when the constituent material phases are nondissipative.

Acknowledgements
The work of TGM is supported by the *Carnegie Trust for the Universities of Scotland*. WSW is the holder of a *RSE/SOEID Research Support Fellowship* of the *Royal Society of Edinburgh*.

References

[1] A. Lakhtakia, "On direct and indirect scattering approaches for the homogenization of particulate composites", *Microw. Opt. Technol. Lett.*, vol. 25, pp. 53–56, 2000.

[2] L. Tsang and J. A. Kong, "Scattering of electromagnetic waves from random media with strong permittivity fluctuations," *Radio Sci.*, vol. 16, pp. 303–320, 1981.

[3] N. P. Zhuck, "Strong–fluctuation theory for a mean electromagnetic field in a statistically homogeneous random medium with arbitrary anisotropy of electrical and statistical properties," *Phys. Rev. B*, vol. 50, pp. 15636–15645, 1994.

[4] B. Michel and A. Lakhtakia, "Strong–property–fluctuation theory for homogenizing chiral particulate composites," *Phys. Rev. E*, vol. 51, pp. 5701–5707, 1995.

[5] T. G. Mackay, A. Lakhtakia and W. S. Weiglhofer, "Strong–property–fluctuation theory for homogenization of bianisotropic composites. Part I: Formulation," *Department of Mathematics, University of Glasgow*, preprint 2000/17, June 2000.

[6] B. Michel and W. S. Weiglhofer, "Pointwise singularity of dyadic Green function in a general bianisotropic medium," *Arch. Elektron. Übertrag.*, vol. 51, pp. 219–223, 1997; Erratum, vol. 52, p. 31, 1998.

Session 3

Wednesday - September 27, 2000

14:00 - 15:00

Composite Materials: Numerical Studies and Experiments

Numerical Studies of Nonlinear Composites

A. O. Pinchuk

Institute of Surface Chemistry
National Academy of Science of Ukraine
Kyiv, Nauki av., 31, Ukraine, 03022
Fax: (380) 44 264 04 46, e-mail: onmf@serv.biph.kiev.ua

Abstract

Bistable behavior of nonlinear composite structures with spherical metallic inclusions embedded in a weakly nonlinear dielectric host as well as coated spherical particles with a metallic core and a nonlinear dielectric shell have been theoretically studied using variational approach. A metal fraction of spherical inclusions causes a surface plasmon resonance. The dielectric permittivity of the nonlinear host depends on the intensity of the local electric field. It is shown that the bistable behavior can be achieved by adjusting the physical parameters of the constitutive materials.

1. Introduction

Recently, considerable attention has been devoted to composite nonlinear materials due to their potential uses as materials for optical devices [1-4]. Particularly, they can be exploited as materials for real time holographic and bistable memory devices, optical correlator devices, thresholding devices etc. The composite media with the optical bistable behavior have a particular interest as materials for optical devices. In this work the composite structures with Al spherical particles embedded in the nonlinear dielectric host as well as composite spherical particles with Al core and nonlinear dielectric shell were studied with respect to their bistable behavior based on the recently developed variational approach [1] for such media.

2. Theory

Let us consider the composite structure with the metallic spheres embedded in a weakly nonlinear dielectric host. The metallic spheres are described by the frequency dependent but field independent dielectric permittivity $\varepsilon^i(\omega)=\varepsilon'+i\varepsilon''$ while the host medium is described by the frequency independent but field dependent dielectric permittivity $\varepsilon^h(\vec{E})=\varepsilon_0+\chi|\vec{E}|^2$ Suppose that the concentration of the metallic inclusions is rather small, so we can neglect the interactions between them and the inclusions are small as compared with the wavelength of the incident electromagnetic waves (electrostatic approximation). Using variational approach [1] one can obtain the equation for the normalized field intensity t in the composite structure

$$f(t)\equiv t^3-2\mu t^2+t=\alpha \qquad (1)$$

where

$$t \equiv \left|B^2\right| \frac{8\chi E_0^2}{5\left|\varepsilon^i + 2\varepsilon_0\right|} \; ; \quad \mu \equiv -\frac{\mathrm{Re}\left(\varepsilon^i + 2\varepsilon_0\right)}{\left|\varepsilon^i + 2\varepsilon_0\right|} \; ; \quad \alpha \equiv \frac{8\chi E_0^2 \left|\varepsilon^i - \varepsilon_0\right|^2}{5\left|\varepsilon^i + 2\varepsilon_0^2\right|^3}$$

$$|\mu| < 1; \quad t > 0 . \tag{2}$$

B is the complex variational parameter, $\vec{E}_0$ is the averaged electric field in the composite medium. The bistable regime in the composite structure can be achieved if the Eq. (1) has two (three) solutions for real t. It always has at least one real solution. In order for it to have three solutions, μ and α must satisfy the additional inequalities

$$\mu \geq \sqrt{3}/2 \; , \; \alpha_- \geq \alpha \geq \alpha_+ \; , \; \alpha_\pm = f(t_\pm) \tag{3}$$

where $t_\pm$ are the positions of the maximum or minimum of $f(t)$ respectively.

$$t_\pm = \frac{1}{3}\left\{2\mu \pm \left(4\mu^2 - 3\right)^{1/2}\right\} \tag{4}$$

The quantity $\left|\varepsilon^i + 2\varepsilon_0\right|$ measures how far the composite structure is from a resonant condition, where it vanishes.

Consider the next particular composite structure with the composite spheres which consist of a metallic core, characterized by the same dielectric permittivity $\varepsilon^i(\omega)$, and a concentric dielectric spherical shell having the dielectric permittivity $\varepsilon^h(\vec{E})$. Using the same variational approach [1] one can obtain the following parameters for the equations (1), which correspond to the coated sphere model

$$t \equiv \left|B^2\right| \frac{\chi E_0^2 \left(5p^3 + 52p^2 + 16p + 8\right)}{5\left|\varepsilon^i + 2\varepsilon_0 - p\left(\varepsilon^i - \varepsilon_0\right)\right|} \tag{5}$$

$$\mu \equiv -\frac{\mathrm{Re}\left[\varepsilon^i + 2\varepsilon_0 - p\left(\varepsilon^i - \varepsilon_0\right)\right]}{\left|\varepsilon^i + 2\varepsilon_0 - p\left(\varepsilon^i - \varepsilon_0\right)\right|} \tag{6}$$

$$\alpha \equiv \frac{\chi E_0^2 \left(5p^3 + 52p^2 + 16p + 8\right)\left|\varepsilon^i - \varepsilon_0\right|^2}{5\left|\varepsilon^i + 2\varepsilon_0 - p\left(\varepsilon^i - \varepsilon_0\right)\right|^3} \tag{7}$$

where $p = \left(r^c / r^s\right)^3$ is the core to shell radius ratio of the composite sphere.

The complex dielectric permittivity for the metallic spheres can be described by the classical Drude free-electron model or by the Drude model in combination with the Lorentz oscillator for the bound - electrons[2]

$$\varepsilon^i(\omega) = \varepsilon_0\left(1 - \frac{\omega_{pf}^2}{\omega^2 + i\omega\gamma_f} + \frac{\omega_{pb}^2}{\omega_0^2 - \omega^2 + i\omega\gamma_b}\right) \tag{8}$$

with

$$\omega_{pf,b}^2 = {}^{N_{f,b}e^2}\!/_{\varepsilon_0 m_0}$$

where ω_{pf}, ω_{pb} are the plasma frequencies for the free and bound electrons respectively, ${}^{1}\!/_{\gamma_{f,b}} \equiv \tau_{f,b}$ is the free- and bound - electron scattering time, $N_{f,b}$ in the free- and bound - electron density, e, m_0 are the electron charge and mass respectively.

3. Numerical Results

As have been mentioned above the bistable regime in the nonlinear composite structure can be achieved at the conditions expressed by inequalities (2,3). Several types of composite structures with different metallic inclusions (Al, Au, Ag) have been examined as the possible candidates for composite media. The dispersive parameters for the Drude models of the dielectric permittivity were taken from the literature [2]. In this work the bistable regime was studied for the composite structure with Al spherical inclusions described by Drude free- electron model. The following parameters were employed for the dielectric permittivity of aluminium particles $\omega_{pf} = 2.28\times10^{16}\,\mathrm{sec}^{-1}$, $\tau_f = 6.9\,\mathrm{fsec}$. The nonlinear dielectric host was chosen as a doped glass so as to enhance its cubic nonlinearity coefficient $\chi = 10^{-8}$. As can be seen from Fig. 1 the bistable regime in the particular composite structure can be achieved at the frequency $\omega \approx 7.5\times10^{15}$ rad/sec . In this case we have $\mu = 0.895$, $t_+ = 0.742$, $t_- = 0.449$, $\alpha_+ = 0.167$, $\alpha_- = 0.179$, $\chi\left|\vec{E}_0\right|^2 = 4.6\times10^{-5}$, $B = 68$ and the required field intensity to produce the bistable regime $I = (c/4\pi)\left|\vec{E}_0\right|^2 \approx 10^6\, W/cm^2$. On the Fig. 2 one can see the similar analysis for the coated sphere with Al core and the nonlinear dielectric shell. For the coated sphere there is an additional adjustable parameter p which allows to tune the bistable regime to the desired range. The parameters used in this case are the same as in the previous model with the additional $p = 0.4$. The corresponding frequency of bistability $\omega \approx 5.45\times10^{15}$ rad/sec.

4. Conclusion

In this work the bistable regime was studied for the particular composite structures with Al small spherical particles embedded in the nonlinear dielectric host, as well as for the composite coated sphere with Al core and the nonlinear dielectric shell. It is shown that the bistable behavior can be achieved by adjusting the physical parameters of the constitutive materials.

References

[1] D. Bergman, O. Levy, and D. Stroud, "Theory of optical bistability in a weakly nonlinear composite medium," *Phys. Rev. B.*, vol. 49, no. 1, pp. 129-134, January 1994.

[2] A. E. Neeves and M. H. Birnoim, "Composite structures for the enhancement of nonlinear-optical susceptibility," *J. Opt. Soc. Am. B.*, vol. 6, no. 4, pp. 787-796, April 1989.

[3] H. M. Gibbs, *Optical Bistability: Controlling Light with Light*. Orlando: H. B. Jovanovich Publisher, 1985.

[4] X. Zhang and D. Stroud, "Numerical studies of the nonlinear properties of composites," *Phys. Rev. B.*, vol. 49, no. 2, pp. 944-955, January 1994.

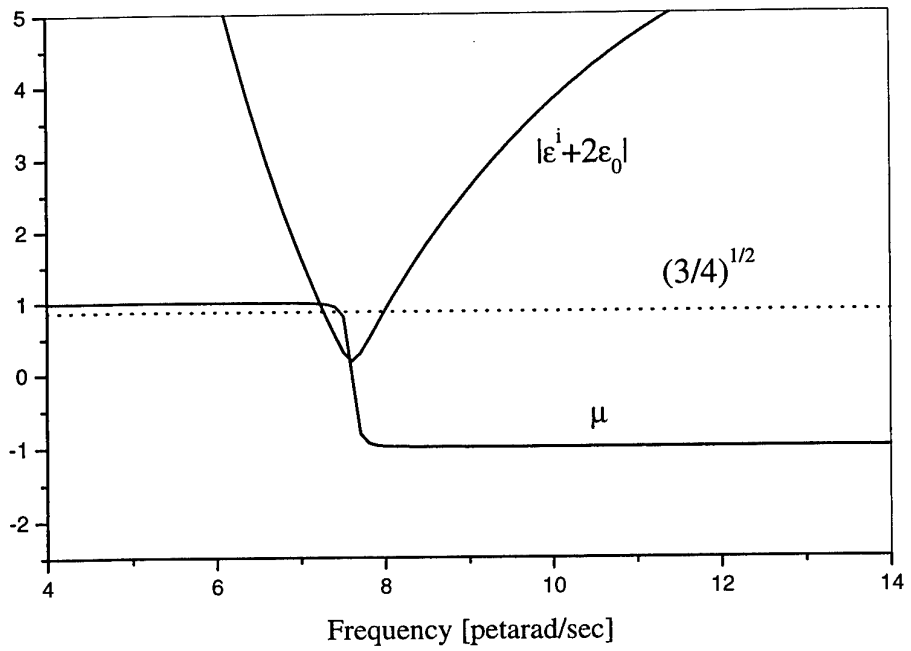

Fig. 1 The bistable regime in the nonlinear composite structure with spherical Al inclusions.

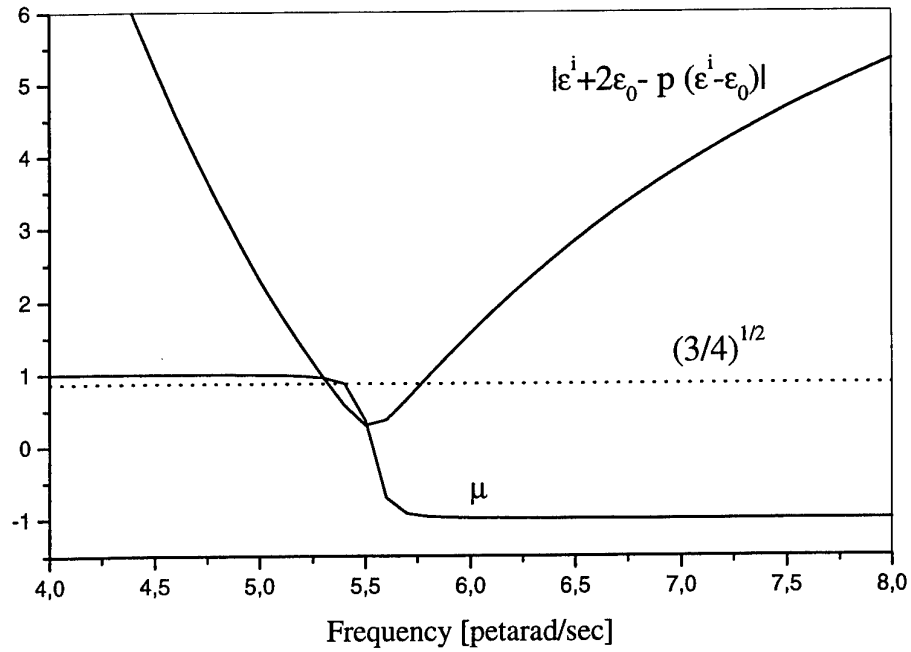

Fig. 2 The bistable regime in the nonlinear composite structure with the coated Al spherical inclusions.

Numerical Computation of the Effective Quasistatic Permittivity for Isotropic Lattices of Complex Shaped Inclusions

Keith W. Whites and Feng Wu

Department of Electrical Engineering, University of Kentucky
453 Anderson Hall, Lexington, KY 40506-0046 United States of America
Fax: + 1 - 859 - 257 - 3092; email: whites@engr.uky.edu

Abstract

A technique is presented for the accurate computation of the effective quasistatic permittivity of lattices containing particles with potentially complicated shape. This technique is based on the moment method for the computation of the electric dipole moments of the dielectric or conducting particles. Through proper homogenization of the lattice, a simple formula for the effective permittivity is given in terms of these particle dipole moments. Verification data is presented for lattices of dielectric spheres obtained with the *T*-matrix method. Results are shown for lattices of dielectric cubes. Mutual interaction between the edges and corners of such a lattice combine to reduce the effective permittivity to values near the lower Hashin-Shtrikman bound.

1. Introduction

The computation of the effective material constants for lattices of particles has in the past been restricted primarily to inclusions of canonical shape. For example, Rayleigh's approximate analysis considered round cylinders and spheres [1] and McPhedran, McKenzie and Derrick considered cubic lattices of spheres [2, 3]. Additionally, our recent work has produced solutions for multiphase lattices of spheres and round cylinders [4, 5]. One exception to this canonical shape rule is the work of Sareni, *et al.* who considered lattices of rods and disks, among other shaped particles [6, 7].

The objectives of this work are twofold. First, we present a methodology for the computation of the effective quasistatic permittivity for lattices of complex shaped particles. That is, particles with edges, corners or other complicated surface features such as those present on cubes (in 3-D lattices) and square cylinders (in 2-D lattices). This methodology is based on the moment method (MM) wherein a set of electric potential integral equations is solved for the infinite lattice and the electric dipole moments of the particles are computed. By properly homogenizing this lattice, we obtain an accurate effective permittivity that properly captures the scattering by the particles and their interactions.

The second primary objective of this work is to investigate the effect of the inclusion shape on the resulting effective permittivity. For example, to investigate the edge effects and the mutual interaction between particles with sharply defined edges and the resulting effective permittivity.

2. Integral Equation Solution for the Dipole Moments

The first step in the computation of the effective quasistatic permittivity for lattices of complex shaped particles is the accurate determination of the electric dipole moments of the particles when the lattice is illuminated by a uniform (but otherwise arbitrary) electric field. We have chosen to use the

MM for these calculations since the particles may not be of canonical shape. Following the surface equivalence theorem, exterior and interior equivalent problems are constructed using equivalent single (ρ_s) and double (τ) layers of charge density [8, 9]. Shown in Fig. 1, for example, is a portion of the original lattice as well as the exterior and interior equivalent problems.

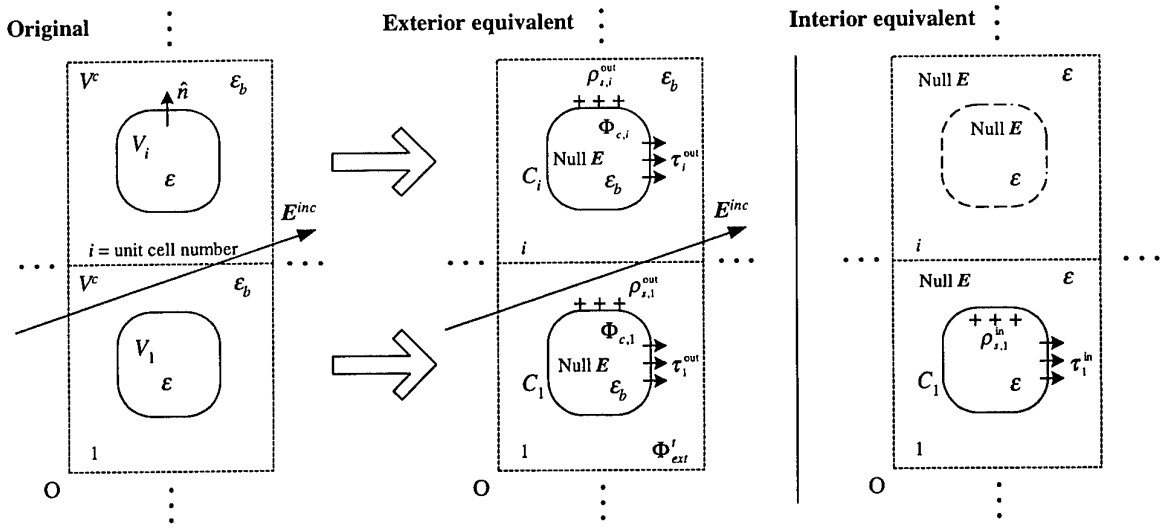

Figure 1 Geometry of the original and exterior equivalent scattering problems.

The scattered scalar potentials produced by these two types of equivalent sources are

$$\Phi_1(\boldsymbol{r}|\varepsilon,\rho_s)=\frac{1}{4\pi\varepsilon}\oiint_S\frac{\rho_s}{R}ds' \tag{1}$$

$$\Phi_2(\boldsymbol{r}|\varepsilon,\boldsymbol{\tau})=\frac{1}{4\pi\varepsilon}\oiint_S\boldsymbol{\tau}\cdot\nabla'(\frac{1}{R})ds' \tag{2}$$

In our MM solution to this lattice problem, we expand the two types of charge in sets of coincident constant basis functions

$$\rho_s=\sum_{n=1}^{N}\alpha_n T_n(\boldsymbol{r}') \tag{3}$$

$$\boldsymbol{\tau}=\sum_{n=1}^{N}\hat{n}\beta_n T_n(\boldsymbol{r}') \tag{4}$$

where T_n is the n^{th} flat triangular patch on the surface of the scatterer.

Using a simple point matching scheme and enforcing the proper boundary conditions in the exterior and interior equivalent problems [9], the following set of integral equations can be formed

$$-\frac{1}{4\pi\varepsilon_b}\sum_{n=1}^{N}\alpha_n\left(\sum_{i=1}^{\infty}\iint_{S_n}\frac{1}{R_{mn}}ds'\right)-\frac{1}{4\pi\varepsilon_b}\sum_{n=1}^{N}\beta_n\left(\sum_{i=1}^{\infty}\iint_{S_n}\hat{n}\cdot\nabla'(\frac{1}{R_{mn}})ds'\right)-\Phi_{c,1}=\Phi^{inc}(\boldsymbol{r}_1) \tag{5}$$

$$-\frac{1}{4\pi\varepsilon}\sum_{n=1}^{N}\alpha_n\left(\iint_{S_n}\frac{1}{R_{mn}}ds'\right)-\frac{1}{4\pi\varepsilon_b}\sum_{n=1}^{N}\beta_n\left(\iint_{S_n}\hat{n}\cdot\nabla'(\frac{1}{R_{mn}})ds'\right)=0 \tag{6}$$

where the i summation is over all particles in the lattice and $\Phi_{c,1}$ is the constant and unknown potential of particle 1. The double layer of surface charge we are solving for has zero average value over the surface so we add the constraint

$$\sum_{n=1}^{N}\beta_n A_n=0 \tag{7}$$

In matrix form, Eqns. (5) through (7) can be expressed as

$$\begin{bmatrix} [Z_{11}]_{N\times N} & [Z_{12}]_{N\times N} & [1]_{N\times 1} \\ [Z_{21}]_{N\times N} & [Z_{22}]_{N\times N} & [0]_{N\times 1} \\ [0]_{1\times N} & [A_n]_{1\times N} & 0 \end{bmatrix} \begin{pmatrix} [\alpha]_{N\times 1} \\ [\beta]_{N\times 1} \\ -\Phi_{c,1} \end{pmatrix} = \begin{pmatrix} [\Phi^{inc}(\boldsymbol{r}_1)]_{N\times 1} \\ [0]_{N\times 1} \\ 0 \end{pmatrix} \tag{8}$$

Once the matrix equation in (8) has been solved, the electric dipole moments of the particles can be computed as

$$\boldsymbol{p} = \iint_{C_i} (\rho_s \boldsymbol{\rho}' + \boldsymbol{\tau}) ds' \tag{9}$$

In the case of isotropic lattices, the effective permittivity can be determined using the simple and accurate expression [4, 10]

$$\varepsilon_{r,eff} = 1 + 3\frac{p/(3\varepsilon_0 E^{inc} V_c)}{1 - p/(3\varepsilon_0 E^{inc} V_c)} \tag{10}$$

We reiterate that after following the methodology presented in this section, this $\varepsilon_{r,\text{eff}}$ properly accounts for all scattering from (and mutual interactions between) particles that have possibly very complicated shape. A similar procedure has been developed for conducting 3-D particles as well as dielectric and conducting complex shaped 2-D cylinders [9, 11].

3. Results

In order to verify the accuracy of this technique, the effective permittivity of a simple cubic (SC) lattice of dielectric spheres with $\varepsilon_r = 40$ was computed for varying volume fraction f. These results are shown in Fig. 2. This $\varepsilon_{r,\text{eff}}$ compares well with $\varepsilon_{r,\text{eff}}$ computed using our T-matrix solution [4]. These two results deviate by no more than 1% even at ultra-high volume fractions ($f > 0.5$).

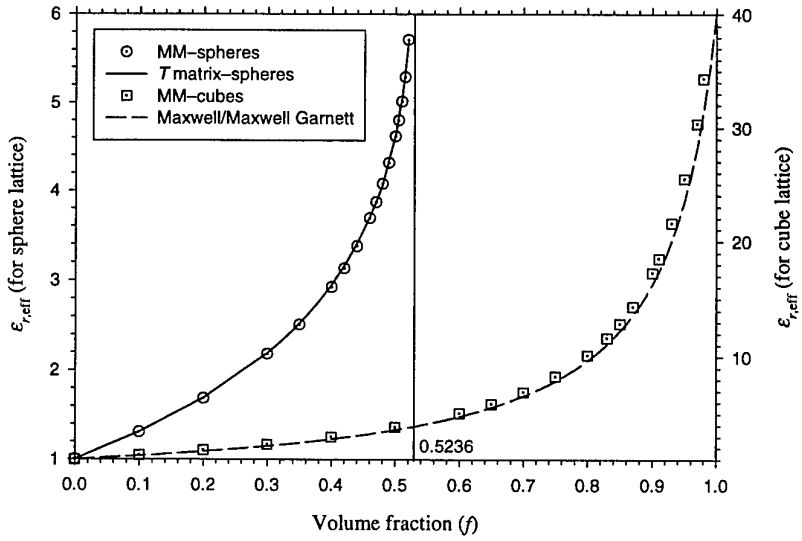

Figure 2 Computed $\varepsilon_{r,\text{eff}}$ for SC lattices of dielectric spheres and dielectric cubes. In both cases the particles have ε_r=40. Notice that the two vertical axes have different scales.

Also shown in Fig. 2 is $\varepsilon_{r,\text{eff}}$ for a SC lattice of dielectric cubes with $\varepsilon_r = 40$. Unlike the sphere lattice, the maximal volume fraction for this lattice is 1. For most of these MM cube results, 1304 flat triangular cells where used to discretize the cubes and 27 unit cells where used to truncate the infinite lattice sums for the numerical calculations. For volume fractions $f > 0.95$, however, it was necessary to increase both the discretization and the number of unit cells (1890 and 125, respectively) to achieve less than 1% variation in the electric dipole moment of the dielectric cube.

While there is no accurate analytically based formula with which to compare these results for the lattice of dielectric cubes, we alternatively present the Maxwell/Maxwell Garnett (MG) predictions [12, Arts. 314 and 430]. Interestingly, it is apparent that the MM results for the cubes and the MG predictions are quite close (up to approximately 9% variation at $f = 0.98$). Even closer agreement has been observed for conducting square 2-D cylinders where the maximum variation is less than 0.4% at $f = 0.99$ [11].

The close agreement between the cube and MG results in Fig. 2 may appear at first glance to be the result of little mutual coupling between the cubes at high volume fraction. However, our investigations have shown that this is not the case [11]. Instead, the close agreement in these dielectric cube results (and other similarly shaped particles shown elsewhere [9, 11]) is likely the result of the large mutual interaction between the edges and corners of the particles. Interestingly, such interactions produce a reduction in the polarization of the particles with respect to the isolated case. Consequently, the effective permittivity of the lattice is reduced almost to the theoretically minimal amounts predicted by the lower bound of Hashin and Shtrikman [13, 14].

Acknowledgement

This work was supported by the National Science Foundation through the Faculty Early Career Development (CAREER) Award ECS-9624486.

References

[1] L. Rayleigh, "On the influence of obstacles arranged in rectangular order upon the properties of a medium," *Philosophy Magazine*, vol. 34, pp. 481-502, 1892.

[2] R. C. McPhedran and D. R. McKenzie, "The conductivity of lattices of spheres: I. The simple cubic lattice," *Proc. R. Soc. Lond.*, vol. A. 359, pp. 45-63, 1978.

[3] D. R. McKenzie, R. C. McPhedran and G. H. Derrick, "The conductivity of lattices of spheres: II. The body centred and face centred cubic lattices," *Proc. R. Soc. Lond.*, vol. A. 362, pp. 211-232, 1978.

[4] K. W. Whites, "Permittivity of a multiphase and isotropic lattice of spheres at low frequency," *J. Appl. Phys.*, vol. 88, no. 4, to appear, 2000.

[5] F. Wu and K. W. Whites, "Computation of static permittivity for a multiphase system of cylinders," *Electromagn.*, accepted for publication.

[6] B. Sareni, L. Krähenbühl, A. Beroual and C. Brosseau, "Effective dielectric constant of periodic composite materials," *J. Appl. Phys.*, vol. 80, no. 3, pp. 1688-1696, 1996.

[7] B. Sareni, L. Krähenbühl, A. Beroual, A. Nicolas and C. Brosseau, "A boundary integral equation method for the calculation of the effective permittivity of periodic composites," *IEEE Trans. Magn.*, vol. 33, no. 2, pp. 1580-1583, 1997.

[8] K. W. Whites and F. Wu, "Computing the effective permittivity for a mixture of spherical particles," in *Bianisotropics'98 7th International Conference on Complex Media*, Braunschweig, Germany, June 3-6, 1998, pp. 285-288.

[9] F. Wu and K. W. Whites, "Quasi-static effective permittivity of periodic composites containing complex shaped dielectric particles," *IEEE Trans. Antennas Propagat.*, submitted.

[10] K. W. Whites, "Static permittivity of a multiphase system of spheres," in *IEEE Antennas and Propagation Society International Symposium Digest*, Orlando, FL, July 11-16, 1999, pp. 1934-1937.

[11] K. W. Whites and F. Wu, "Shape effects on the computation of the effective permittivity of periodic composite materials," *IEEE Microwave Guided Wave Lett.*, submitted.

[12] J. C. Maxwell, *A Treatise on Electricity and Magnetism*. New York: Dover, third ed., 1954.

[13] Z. Hashin and S. Shtrikman, "A variational approach to the theory of the effective magnetic permeability of multiphase materials," *J. Appl. Phys.*, vol. 33, no. 10, pp. 3125-3131, 1962.

[14] A. Sihvola, *Electromagnetic Mixing Formulas and Applications*. London: IEE, 1999.

Reconstruction of the Constitutive Parameters for Composite Media Using Kramers - Kronig Analysis

A. O. Pinchuk

Institute of Surface Chemistry
National Academy of Science of Ukraine
Kyiv, Nauki av., 31, Ukraine, 03022
Fax: (380) 44 264 04 46, e-mail: onmf@serv.biph.kiev.ua

Abstract

An alternative method of determining of the constitutive dispersion parameters for composite media is discussed. It is assumed, that the constitutive materials of composite media are characterized by the complex dielectric permittivity. Furthermore, we consider the composite media with small inclusions as compared with the wavelength of that range for which the dispersion parameters are determined. We have used the experimental reflectance spectra of the composite media from which the effective complex optical refractive index and effective complex dielectric permittivity were determined.

1. Introduction

Last time considerable attention has been devoted on the inverse problem of determining the constitutive parameters of complex media [1-3]. Sometimes using of general methods for determining the constitutive parameters of such media, e.g. solutions of biological macromolecules in aqueous media, is restricted by strong absorption of water outside the transparent ranges. To overcome this problem an alternative method of Kramers-Kroning analysis of the experimental spectra can be applied [3]. In this work, the effective optical functions $\tilde{n}$ and $\tilde{k}$, were obtained using Kramers-Kroning analysis from the experimental reflectance spectra of the composite medium. The real and imaginary parts of the effective complex dielectric permittivity $\tilde{\varepsilon}$ were calculated using the effective optical functions.

2. Theory

The complex reflection amplitude of a normal incident electromagnetic wave, used in the Kramers-Kronig analysis, is defined as follows [1]

$$\tilde{R}^{1/2} = \frac{(\tilde{n}-1)+i\tilde{k}}{(\tilde{n}+1)+i\tilde{k}} = R^{1/2}e^{i\varphi} \tag{1}$$

were R is the magnitude of the reflectance at the frequency ω. The phase φ is related to the reflectance by the dispersion equation, defined in the Kramers-Kronig analysis as follows

$$\varphi(\omega) = \frac{\omega}{\pi} P\int_0^{\infty} \frac{\ln R(\xi)}{\xi^2-\omega^2} d\xi - \pi \tag{2}$$

were P stands for the Cauchy principal value. The real and imaginary parts of the complex optical refractive index $\tilde{n}$ and $\tilde{k}$ are related to the reflectance amplitude and phase by the relations

$$\tilde{n} = \frac{1-R}{1+R+2R^{1/2}\cos\varphi}, \qquad \tilde{k} = \frac{-2R^{1/2}\sin\varphi}{1+R+2R^{1/2}\cos\varphi} \tag{3}$$

Using obtained complex refractive index we can calculate the real and imaginary parts of the effective dielectric permittivity of the composite medium $\tilde{\varepsilon}_1 = \tilde{n}^2 - \tilde{k}^2, \tilde{\varepsilon}_2 = 2\tilde{n}\tilde{k}$. Further, using the effective complex permittivity of the composite medium, we can obtain the complex dielectric permittivity of the constituents. For this purpose we can utilize one of the widely used approximations, such as Maxwell-Garnett or Bruggeman formalism

$$\tilde{\varepsilon}_{MG} = \varepsilon_h + 3f\varepsilon_h \frac{\varepsilon_i - \varepsilon_h}{(1-f)\varepsilon_i + (2+f)\varepsilon_h}, \quad f\frac{\varepsilon_i - \tilde{\varepsilon}_{BG}}{\varepsilon_i + 2\tilde{\varepsilon}_{BG}} + (1-f)\frac{\varepsilon_h - \tilde{\varepsilon}_{BG}}{\varepsilon_h + 2\tilde{\varepsilon}_{BG}} = 0 \tag{4}$$

were ε_i is the dielectric permittivity of the inclusions, ε_h is the dielectric permittivity of the host medium. Using known dielectric parameters of the host and the filling factor for the inclusions, we can reconstruct the dielectric permittivity for the inclusions, or using known dielectric permittivity of the inclusions and host medium we can determine the filling factor of the inclusions.

3. Numerical results

To demonstrate the validity of the above formalism the composite structure was considered in a mixture form of LiF small particles embedded in a KBr host. The optical constants for LiF particles correspond to the classical oscillator theory. The relevant real and imaginary parts of the complex dielectric permittivity have the following form

$$\varepsilon' = n^2 - k^2 = \varepsilon_\infty + \sum_j \frac{4\pi\rho_j\omega_j^2\left(\omega_j^2 - \omega^2\right)}{\left(\omega_j^2 - \omega^2\right)^2 + \left(\gamma_j\omega_j\right)^2}, \quad \varepsilon'' = 2nk = \sum_j \frac{4\pi\rho_j\omega_j^2\left(\gamma_j\omega_j\right)}{\left(\omega_j^2 - \omega^2\right)^2 + \left(\gamma_j\omega_j\right)^2} \tag{5}$$

The experimental reflectance spectra, taken from the literature [5], for the composite structure with filling factor $f = 0.2$ is shown on Fig.1. The calculated phase using Kramers-Kroning analysis is shown on same Fig.1. The effective optical constants of LiF-KCl composite, calculated using Kramers-Kroning, are shown on Fig.2. The experimental and restored effective complex dielectric permittivity for LiF-KCl composite are shown on Fig.3. Finaly, the restored real and imaginary parts of the complex dielectric permittivity of the inclusions are shown on Fig. 4.

4. Conclusion

The apparent conformity of restored complex effective dielectric permittivity with experimental curves proves the validity of above formalism. This rather simple procedure will be useful for spectroscopic investigation of complex media, e.g. in spectroscopic studying of biological macromolecules immersed in aqueous solutions with known dispersion properties.

References

[1] C. F. Bohren and D. R. Huffman, *Absorption and Scattering of Light by Small Particles,* New York, Wiley Publisher, 1983.

[2] Martin Norgren and Sailing He, "Reconstruction of the Constitutive Parameters for an Ω Material in a Rectangular Waveguide," *JEEE Trans. On Microwave Theory and Techniques*, vol. 43, no. 6, pp. 1315-1321, June 1995.

[3] J. M. Heller, R. N. Hamm, R. D. Bikhoff, and L. R. Painter, "Collective oscillation in liquid water," *The Journal of Chemical Physics*, vol. 60, no. 9, pp. 3483-3486, May 1974.

[4] J. R. Jasperse, A. Kahan, and J. N. Plendl, *Phys. Rev.* vol. 146 , pp. 526-542, 1966.

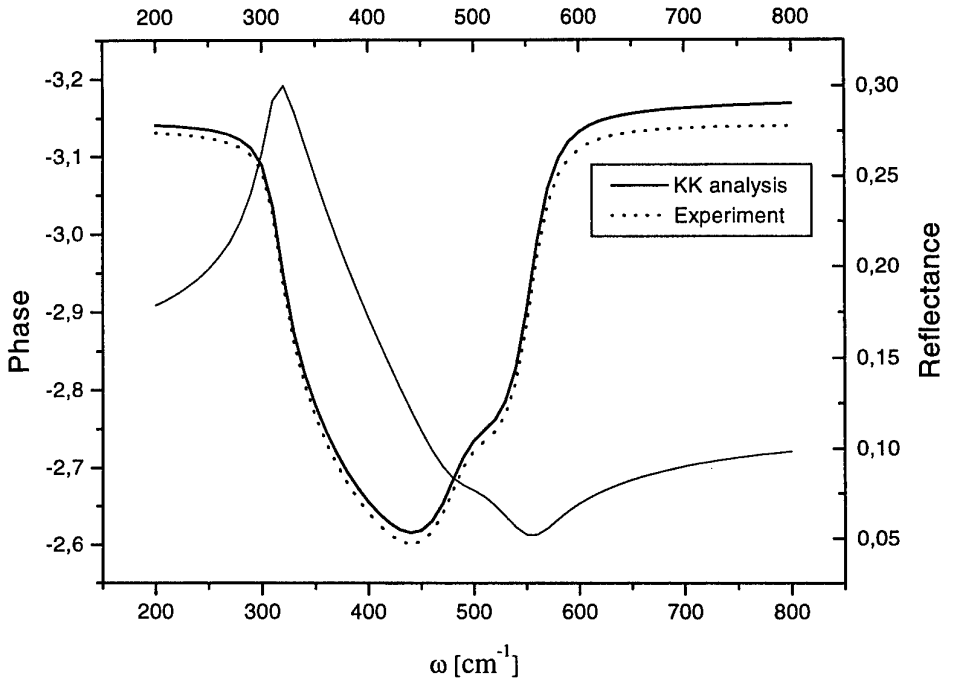

Fig. 1 Reflectance spectra and restored faze of reflected wave for LiF particles embedded in KBr host.

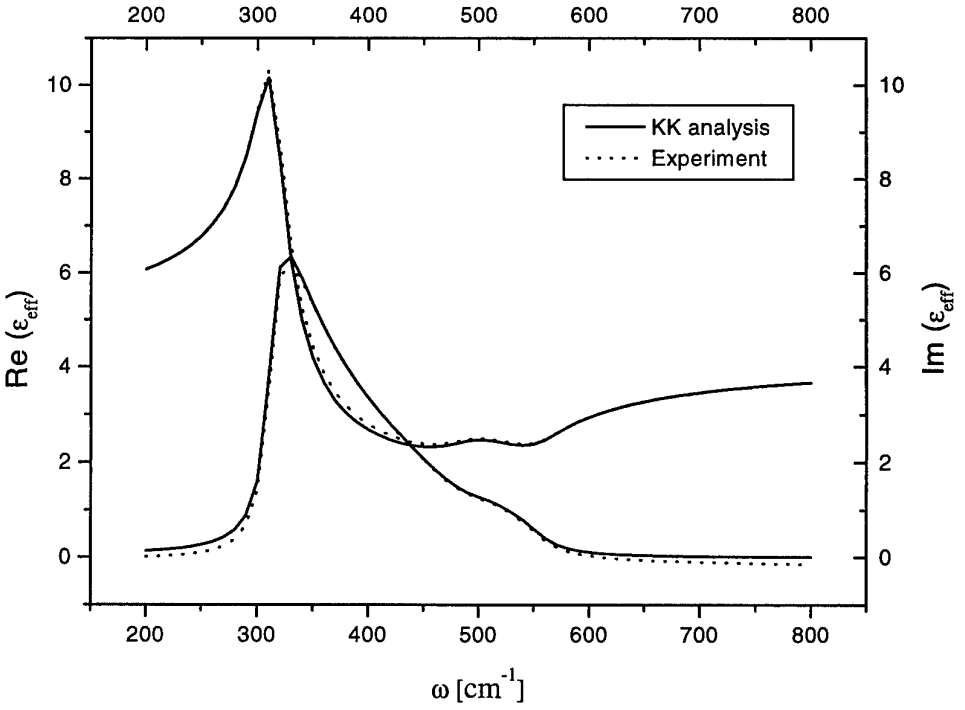

Fig. 2 Restored real and imaginary parts for the effective dielectric permittivity.

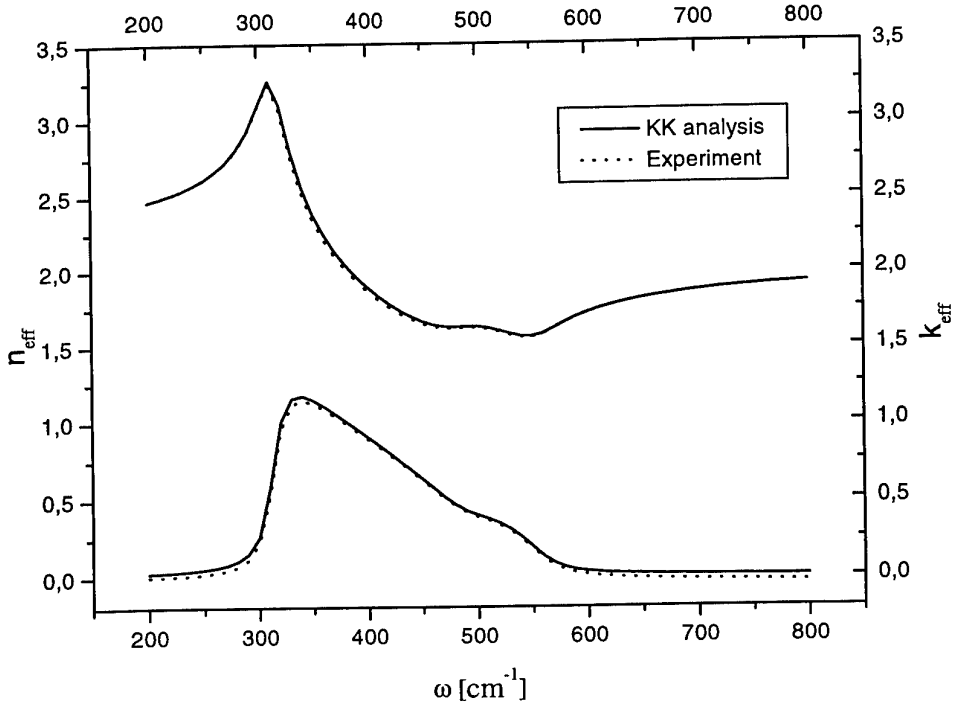

Fig. 3 Restored real and imaginary parts of the complex effective optical functions

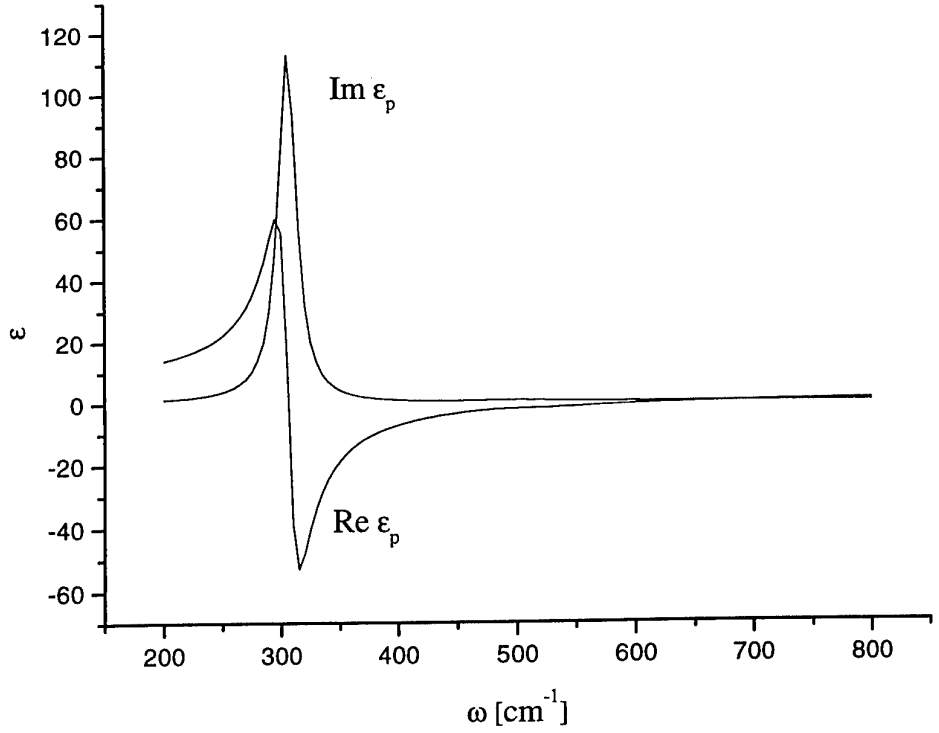

Fig. 4 Restored real and imaginary parts of the dielectric permittivity of the inclusions.

Poster Session I

Poster Session I

Wednesday - September 27, 2000

15:00 - 16:30

Surface Polaritons in the System of Ideal Metal – Dielectric Plate – Vacuum in the Constant Electric Field

N. A. Goncharuk[1] and D. A. Mamaluy[2]

[1] B. Verkin Institute for Low Temperature Physics & Engineering
47 Lenin Av., 61164 Kharkov, Ukraine
Fax: + 38–0572–33–55–93
E-mail: goncharuk@ilt.kharkov.ua

[2] E-mail: mamaluy@ilt.kharkov.ua or mamaluy@theochem.tu-muenchen.de

Abstract

The system of an ideal metal or superconductor – dielectric plate – vacuum or unpolarizable substance is considered in presence of the constant electric field directed normal to the plane of the plate. Dispersion relations for surface phonon polaritons of this system are derived and analyzed. These polaritons are induced by a dynamical magnetoelectric effect. It has been shown that in the case, when the plate thickness essentially exceeds the penetration depth of the surface polaritons, the approximation of a half-infinite (bulk) insulator satisfactory describes the polariton spectrum and the "switching over" effect is possible for a magnetoelectric wave: the variation of the electric field on the opposite one leads to "switching on" or "switching off" of the corresponding frequency branches. The dependence of the spectrum of surface phonon polaritons from the plate thickness is calculated numerically. The corresponding criterion of an existence of magnetoelectric waves in the dielectric plate has been found.

1. Introduction

A number of publications devotes to the influence of a dynamical magnetoelectric (ME) effect on the spectrum of surface phonon polaritons in an insulator. In these publications the «switching over» effect and the «rectification» one of surface polaritons at the change of direction of applied constant electric or magnetic fields.

We consider the system of an ideal metal (or superconductor) – dielectric plate – vacuum (or unpolarizable substance) in presence of a constant electric field directed normal to the plate. Dispersion relations for the spectrum of surface phonon polaritons are derived taking into account the dynamical ME effect influence. Restrictions for the plate thickness, when the «switching over» effect takes place, are analyzed. It is shown that in the case when the plate thickness essentially exceeds the penetration depth of surface polaritons the approximation of a half-infinite (bulk) insulator describes quite exact the polariton spectrum. While the dielectric plate thickness decreases, the «switching over» effect disappears. However, this effect can be kept down to the sufficient small plate thickness (depending on the value of the constant electric field). The dependence of the spectrum of surface polaritons on the plate thickness is calculated numerically. Analitical expressions for the dispersion law and the penetration depth of surface polaritons are obtained for small thicknesses.

2. Dispersion relations for the system of an Ideal Metal–Insulator–Vacuum

Let us consider an uniaxial non-magnetic insulator (z is an easy axis). It occupies the region of the space $0 < z < d$ and borders on ideal metal or superconductor $(z < 0)$ and vacuum or unpolarizable substance $(z > d)$, d is the insulator thickness. A constant electric field $\vec{E}_0$ is applied along the normal to the dielectric plate (i.e. along the z axis).

The linear responce of an insulator in the field of an electromagnetic wave with electric and magnetic components $\vec{e}, \vec{h}$ with taking into consideration of the dynamical ME effect has been obtained in [1]. Electric and magnetoelectric susceptibilities in the absence of damping and in the neglect of the space dispersion have been analyzed in works [2]–[6].

The electric ($\vec{d}$) induction of medium and the magnetic ($\vec{b}$) one are connected with electric and magnetic fields by means of the following relations

$$d_i = \varepsilon_{ik} e_k + \gamma_{ik} h_k, \quad b_i = \mu_{ik} h_i + \gamma^*_{ki} e_k \tag{1}$$

where $\varepsilon_{ik}, \mu_{ik}$ are the tensors of dielectric and magnetic permeabilities correspondingly, γ_{ik} is the tensor of magnetoelectric permeability. Components of the electric polarization of medium can be presented in the form:

$$P_i = \frac{1}{4\pi}\left((\varepsilon_{ik} - \delta_{ik}) e_k + \gamma_{ik} h_k\right) \tag{2}$$

where δ_{ik} is Kroneker symbol. In our case $\mu_{ik} = \delta_{ik}$ (non-magnetic insulator), and components of the electric and magnetoelectric permeabilities, which are not equal to zero, are determined by the following expressions:

$$\varepsilon_{xx} = \varepsilon_{yy} = \varepsilon_1 = \frac{\Omega_0^2 - \omega^2}{\omega_0^2 - \omega^2}, \ \varepsilon_{zz} = \varepsilon_3 = \frac{\Omega_e^2 - \omega^2}{\omega_e^2 - \omega^2}, \ \gamma_{xy} = \gamma^*_{yx} = -i\gamma, \ \gamma = \frac{4\pi\omega g P_0}{\omega_0^2 - \omega^2}. \tag{3}$$

Here P_0 is an equilibrium value of polarization. If the external constant electric field $E_0 = E_{0z}$ is applied to the insulator, then from the formula (2) we obtain $P_0 = P_{0z} = \frac{1}{4\pi}(\varepsilon_{zz} - 1)E_0$. In the case of ferroelectric, P_0 is spontaneous polarization; ω_0 is the excitation frequency of transverse components of the polarization P_x, P_y; ω_e is the excitation frequency of polarization along the easy axis z. Frequencies Ω_0, Ω_e are zeroes of dielectric permeabilities of transverse $(\varepsilon_{xx}, \varepsilon_{yy})$ and longitudinal (ε_{zz}) correspondingly. Besides, $g = e/mc$ is gyromagnetic ratio (e is the particle charge, m is the particle mass, c is the speed of light). An ionic polarizability is excited effectively in the IR region of the spectrum. Therefore, g is gyromagnetic retio for anion-cation pair. In the optic region of the spectrum where electronic polarizability prevails, g is gyromagnetic retio for an electron.

The Maxwell's equations for a wave that propagates along the x axis can be presented in the following way:

$$\frac{\partial}{\partial z} e_x + \frac{\omega}{c}\gamma e_x - i\left(k - \frac{\omega^2}{c^2 k}\varepsilon_3\right) e_z = 0, \ i\frac{\omega}{c}\varepsilon_1 e_x + \frac{\omega}{ck}\frac{\partial}{\partial z} e_z - \frac{\omega^2}{c^2 k}\gamma\varepsilon_3 e_z = 0, \ h_y = -\frac{\omega}{ck}\varepsilon_3 e_z \tag{4}$$

The solution of equations (4) in the insulator is sought in the form:

$$e_x = \left(A e^{-k_0 z} + B e^{k_0 z}\right) e^{i(kx - \omega t)}, \ e_z = \left(C e^{-k_0 z} + D e^{k_0 z}\right) e^{i(kx - \omega t)} \tag{5}$$

From the requirement of equality to zero of tangential components of an electric field at the boundary with an ideal metal (or superconductor) we obtain

$$A+B=0 \tag{6}$$

For the rest of amplitudes in the equation (5) the following expressions can be obtained when amplitude C is considered as independent one:

$$A=C\frac{\varepsilon_3\left(k_0+\frac{\omega}{c}\gamma\right)}{i\varepsilon_1 k},\ B=-A,\ D=C\frac{k_0+\frac{\omega}{c}\gamma}{k_0-\frac{\omega}{c}\gamma}. \tag{7}$$

The wave in vacuum is sought in the form

$$\tilde{e}_x=F\,\mathrm{e}^{-\tilde{k}_0 z}\mathrm{e}^{i(kx-\omega t)},\ \tilde{e}_z=G\,\mathrm{e}^{-\tilde{k}_0 z}\mathrm{e}^{i(kx-\omega t)} \tag{8}$$

Tangential components of an electric field and normal component of electric induction must be continuous at the boundary of the insulator with vacuum. Thus, such equalities must be implemented

$$e_x=\tilde{e}_x\big|_{z=d},\quad \varepsilon_3 e_z=\varepsilon_0\tilde{e}_z\big|_{z=d}. \tag{9}$$

Where ε_0 is dielectric constant of vacuum (then $\varepsilon_0=1$) or any unpolarizable substance in the considered frequency region. For amplitudes from equations (5) и (7) we obtain:

$$A\left(\mathrm{e}^{-k_0 d}-\mathrm{e}^{k_0 d}\right)=F\,\mathrm{e}^{-\tilde{k}_0 d},\ C\varepsilon_3\left(\mathrm{e}^{-k_0 d}-\frac{k_0 c+\omega\gamma}{k_0 c-\omega\gamma}\mathrm{e}^{k_0 d}\right)=G\varepsilon_0\,\mathrm{e}^{-\tilde{k}_0 d} \tag{10}$$

Solving the system of equations (4)–(10) we obtain finally for boundary conditions:

$$\left(k_0+\frac{\omega}{c}\gamma\right)\left(\mathrm{e}^{-2k_0 d}-1\right)\frac{\varepsilon_0}{\varepsilon_1}=\left(\mathrm{e}^{-2k_0 d}-\frac{k_0 c+\omega\gamma}{k_0 c-\omega\gamma}\right)\tilde{k}_0 \tag{11}$$

Besides, the following relation for nonzero solutions in the insulator must be implemented

$$\frac{\omega^2}{c^2}\varepsilon_1\varepsilon_3-k^2\varepsilon_1+\varepsilon_3\left(k_0^2-\frac{\omega^2}{c^2}\gamma^2\right)=0 \tag{12}$$

The analogous relation in vacuum

$$\frac{\omega^2}{c^2}\varepsilon_0-k^2+\tilde{k}_0^2=0 \tag{13}$$

must be realized when amplitudes F,G in (8) and (10) differ from zero.

The system of equations (11)–(13) determines the dispersion law of polaritons which propagate in the insulator parallel to the interface.

Let us analyze this system at $k_0 d>>1$ i.e. when the insulator thickness essentially exceeds the value of the penetration depth of the wave into the insulator. Then the equation (11) can be realized in two cases: $k_0 c=-\omega\gamma$ and $k_0 c\neq-\omega\gamma$, $\left(k_0-\frac{\omega}{c}\gamma\right)\varepsilon_0=\tilde{k}_0\varepsilon_1$.

In the first case we obtain the solution in the form of a wave which exists due to the dynamical ME effect. It is easy to see that equation (12) in this case will be $k^2=\frac{\omega^2}{c^2}\varepsilon_3$. From equation (7) one can see that from all amplitudes in the insulator A,B,C,D only the amplitude C is not equal to zero. Thus, the wave propagates along the boundary of ideal metal with insulator, and its amplitude exponentially damps deep into the insulator. From the equation (10) it follows that the amplitude F in vacuum is equal to zero, and the amplitude $G\to 0, k_0 d\to\infty$. Therefore, the equation (13) in this case does not exist. Further we will call this polariton wave as «magnetoelectric» one [3].

In the second case $\left(k_0 - \frac{\omega}{c}\gamma\right)\varepsilon_0 = \tilde{k}_0\varepsilon_1$ we have a common surface polariton wave at the boundary of the insulator with vacuum which exists in the frequency interval $[\omega_0, \omega_S]$, where $\omega_S^2 \approx \left(\Omega_e^2 + \omega_0^2\right)/2$ (see [7]). In [2] it has been shown that presence of the constant electric field (i.e. $\gamma \neq 0$) in this case leads to interesting effects whose quantities, however, are small since the dynamical ME effect is small too.

Hence, we can indicate the application limits of result of work [3]–[6] if we find the qualitative condition of existence of the «magnetoelectric» wave in the case of the finite plate thickness. The plate thickness of the insulator d must essentially exceeds the penetration depth into the insulator k_0^{-1}. From $k_0 d >> 1$, $ck_0 = -\omega\gamma$ and equality (3) we obtain:

$$d >> k_0^{-1} = \delta_{ME} = \frac{\omega_0^2 - \omega^2}{4\pi\omega^2 g P_0} c \tag{14}$$

The order of penetration depth of the «magnetoelectric» wave at values of constant electric field which is typical for the spontaneous polarization in the ferroelectric crystal $E_0 \sim P_0 \sim 10^4$ CGSE and optical frequencies ($\omega \sim 10^{14}$ sec^{-1}, $g \sim 10^7$) is $\delta_{ME} \sim 10^{-2}$ sm. Thus, for the relation of the condition $k_0 d >> 1$ the plate thickness of insulator must be greater or of the order of magnitude 1 mm. The numerical calculations of dispersion relations (11)–(13) performed by us confirm these qualitative results.

3. Conclusion

In the system of an ideal metal (or superconductor) – dielectric plate – vacuum (or any unpolarizable substance) surface polaritons propagate along the interface. For plate thicknesses d, which essentially exceed the characteristic penetration depth δ_{ME} (see (14)), the «magnetoelectric» wave propagates along the boundary of insulator with ideal metal (or superconductor). Thus, the condition $d >> \delta_{ME}$ shows the application limits of results of work [3]. At the optic frequencies and the value of the constant electric field $E_0 \sim 10^4$ CGSE the characteristic value is $\delta_{ME} \sim 10^{-2}$ sm. Therefore, for the experimental verification of the work [3] at the given value of the constant electric field (or at such value of the spontaneous polarization in the case of the ferroelectric) we can use the insulator layer with the thickness greater or of the order of magnitude 1 mm.

While the thickness of the dielectric plate decreases, the «magnetoelectric» wave destroys.

References

[1] I. E. Chupis, *Fiz. Nizk. Temp.*, vol. 23, p. 213, 1997; I. E. Chupis, *Ferroelectrics*, vol. 204, p. 173, 1997.

[2] I. E. Chupis and D. A. Mamaluy, *Fiz. Nizk. Temp.*, vol. 24, p. 1010, 1998 [English translation: *Low Temp. Phys.*, vol. 24, p. 762, 1998].

[3] I. E. Chupis and D. A. Mamaluy, *Pis'ma Zh. Eksp. Teor. Fiz.*, vol. 68, p. 876, 1998 [*JETP Letters*, vol. 68, p. 922, 1998].

[4] I. E. Chupis and D. A. Mamaluy, *Fiz. Nizk. Temp.*, vol. 25, p. 1112, 1999 [*Low Temp. Phys.*, vol. 25, p. 833, 1999].

[5] D. A. Mamaluy and I. E. Chupis, *Zh. Eksp. Teor. Fiz.*, vol. 117, p. 175, 2000 [*JETP*, vol. 117, p. 153, 2000].

[6] I. E. Chupis and D. A. Mamaluy, *J. Phys.: Condens. Matter*, vol. 12, p. 1413, 2000.

[7] V. M. Agranovich and D. L. Mills (Eds.), *Surface Polaritons*. North-Holland, Amsterdam, 1982.

New Types of Orthonormal Electromagnetic Beams in Complex Media and Free Space

G. N. Borzdov

Department of Theoretical Physics, Belarusian State University
Fr. Skaryny avenue 4, 220050 Minsk, Belarus
Fax: + 375–17–226 0530; email: borzdov@phys.bsu.unibel.by

Abstract

Vector plane–wave superpositions defined by a given set of orthonormal scalar functions on a two– or three–dimensional manifold are treated. We present a technique for composing orthonormal electromagnetic beams in complex media and free space. New families of exact time–harmonic solutions of the homogeneous Maxwell equations in linear media (isotropic, chiral, anisotropic, and bianisotropic) and free space, which describe orthonormal electromagnetic beams, are obtained.

1. Introduction

Properties of electromagnetic beams in composite and complex media (chiral, anisotropic, bianisotropic) are still investigated insufficiently. In some practical cases, for example, in characterizing complex media by free space techniques, the plane–wave approximation of incident beams proves to be inadequate. As in the case of conic refraction in biaxial crystals, in investigating possible physical phenomena caused by anomalous propagation in homogeneous [1, 2, 3, 4] and helicoidally nonhomogeneous [5, 6, 7] bianisotropic media, the plane–wave model of the incident beam is also inadequate. The most commonly used Hermite–Gaussian and Laguerre–Gaussian beams are mere the approximate solutions of Maxwell's equations in free space.

In Ref. [8], a novel technique for composing orthonormal electromagnetic beams and some other specific exact solutions of wave equations in linear media is suggested. By applying this technique, some new families of exact solutions of the homogeneous Maxwell equations for electromagnetic waves in isotropic media and free space are obtained in Refs. [8, 9, 10]. In this paper, we briefly outline the basic ideas of this technique and present its further applications.

2. Beam Manifold, Beam Base, and Beam State

Let (u_n) be a set of complex scalar functions $u_n : \mathcal{B}_u \to C^1$ on a real manifold $\mathcal{B}_u$, satisfying the orthogonality conditions

$$\langle u_m | u_n \rangle \equiv \int_{\mathcal{B}_u} u_m^*(b) u_n(b) d\mathcal{B} = \delta_{mn}, \tag{1}$$

where $d\mathcal{B}$ is the infinitesimal element of $\mathcal{B}_u$; u_m^* is the complex conjugate function to u_m, δ_{mn} is the Kronecker δ–function. Let us consider a plane–wave superposition (termed below the "beam" for brevity sake)

$$\begin{aligned} \mathbf{W}_n(\mathbf{x}) = & \int_{\mathcal{B}_u} e^{i\mathbf{x}\cdot\mathbf{K}(b)} u_n(b) \nu(b) \mathbf{W}(b) d\mathcal{B} \\ = & \int_{\mathcal{B}} e^{i\mathbf{x}\cdot\mathbf{K}(b)} u_n(b) \nu(b) \mathbf{W}(b) d\mathcal{B}, \end{aligned} \tag{2}$$

where $\mathcal{B} \subseteq \mathcal{B}_u$—beam manifold—is a subset of $\mathcal{B}_u$ with nonvanishing values of function $\mathbf{W}' = \nu(b)\mathbf{W}(b)$; $\mathbf{x}$ and $\mathbf{K}$ are the four–dimensional position and wave vectors. For electromagnetic waves, $\mathbf{W}$ can be any of the following quantities: the electric (magnetic) field vector $\mathbf{E}$ ($\mathbf{B}$), the four–dimensional field tensor F, or the six–dimensional vector $\mathrm{col}(\mathbf{E}, \mathbf{H})$. Functions $\mathbf{K} = \mathbf{K}(b)$ and $\mathbf{W} = \mathbf{W}(b)$ specify the set of plane harmonic waves involved in the beam (beam base), whereas a complex scalar function $\nu = \nu(b)$ specifies the beam state. The function $\mathbf{W}_n(\mathbf{x})$ is an exact solution of the linear field equations, provided that the integral in Eq. (2) exists.

The fields treated in this paper are composed of plane waves with factorized vector amplitudes $\mathbf{W}(b)\nu(b)u_n(b)d\mathcal{B}$, where each of the factors plays a specific part in determining the field structure. The normalized vector factor $\mathbf{W}(b)$ prescribes the polarization of the infinitesimal plane wave, whereas the scalar factors specify the intensity and the phase as follows. The function $\nu = \nu(b)$ is used mainly to obtain a set of orthonormal beams or to change the beam state [8]. In some special cases, it simply reduces to a normalizing constant factor. In the general case, the infinitesimal element $d\mathcal{B}$ depends on b, so that both u_n and $d\mathcal{B}$ act as weight functions defining the ratios in which plane waves with different propagation directions and polarization states are mixed in the beam $\mathbf{W}_n$. However, the distinctive features of $\mathbf{W}_n(\mathbf{x})$ as opposed to other beams are imprinted completely by the complex factor $u_n = u_n(b)$. This factorization is equally convenient both to set a unique wave pattern for each beam and to obtain the whole family of beams with a prescribed general property such as the orthonormality.

3. Time–Harmonic Orthonormal Beams

There are four key elements defining the properties of the presented beams: the set of complex scalar functions $u_n = u_n(b)$ on a real manifold $\mathcal{B}_u$, the beam manifold $\mathcal{B}$, the beam base functions $\mathbf{K} = \mathbf{K}(b)$ and $\mathbf{W} = \mathbf{W}(b)$, and the beam state function $\nu = \nu(b)$. By setting these elements in various ways, one can compose a multitude of normalized and orthonormal beams with very interesting properties [8, 9]. In particular, these elements can be set [8, 9] in such a way as to satisfy the orthonormality condition $s_{mn} \equiv \langle \mathbf{W}_m | Q | \mathbf{W}_n \rangle = N_Q \delta_{mn}$, where N_Q is some given scalar coefficient.

A time–harmonic beam of the form $\mathbf{W}_n$ [Eq. (2)] with a two–dimensional beam manifold $\mathcal{B}$, propagating in a homogeneous linear medium, can be written as

$$\mathbf{W}_n(\mathbf{r}, t) = e^{-i\omega t} \int_{\mathcal{B}} e^{i\mathbf{r}\cdot\mathbf{k}(b)} u_n(b)\nu(b)\mathbf{W}(b)d\mathcal{B}. \tag{3}$$

Let us introduce a scalar product

$$s_{mn} \equiv \langle \mathbf{W}_m | Q | \mathbf{W}_n \rangle = \int_{\sigma_0} \mathbf{W}_m^\dagger(\mathbf{r}, t) Q \mathbf{W}_n(\mathbf{r}, t) d\sigma_0, \tag{4}$$

where σ_0 is the plane with unit normal $\mathbf{q}$, passing through the point $\mathbf{r} = 0$, Q is some Hermitian operator, and $\mathbf{W}_m^\dagger(\mathbf{r}, t)$ is the Hermitian conjugate of $\mathbf{W}_m(\mathbf{r}, t)$. To compose orthonormal beams, it is convinient to set $\mathbf{W} = \mathrm{col}(\mathbf{E}, \mathbf{H})$, and

$$Q = \frac{c}{16\pi} \begin{pmatrix} 0 & -\mathbf{q}^\times \\ \mathbf{q}^\times & 0 \end{pmatrix}, \tag{5}$$

where $\mathbf{q}^\times$ is the antisymmetric tensor dual to $\mathbf{q}$ ($\mathbf{q}^\times \mathbf{E} = \mathbf{q} \times \mathbf{E}$). For a time–harmonic field, the normal component S_q of the time average Poynting vector $\mathbf{S}$ can be written as $S_q = \mathbf{q} \cdot \mathbf{S} = \mathbf{W}^\dagger Q \mathbf{W}$. Therefore, the condition $\langle \mathbf{W}_n | Q | \mathbf{W}_n \rangle = N_Q$ is in fact the normalization to the beam energy flux N_Q through the plane σ_0:

$$\langle \mathbf{W}_n | Q | \mathbf{W}_n \rangle = \int_{\sigma_0} S_q d\sigma_0 = N_Q. \tag{6}$$

We assume here that the tangential component $\mathbf{t}(b) = \mathbf{k}(b) - \mathbf{q}[\mathbf{q} \cdot \mathbf{k}(b)]$ of the wave vector $\mathbf{k}(b)$ is real for all $b \in \mathcal{B}$, and that the mapping $b \mapsto \mathbf{t}(b)$ is one-one (injective). It can be shown [8], that the beams $\mathbf{W}_n$ become orthonormal, if $\mathcal{B} = \mathcal{B}_u$, and the function $\nu(b)$ is given by

$$\nu(b) = \frac{1}{2\pi}\sqrt{\frac{N_Q J(b)}{g(b)\mathbf{W}^\dagger(b)Q\mathbf{W}(b)}}, \tag{7}$$

where $J(b) = D(t^j)/D(\xi^i)$ is the Jacobian determinant of the mapping $b \mapsto \mathbf{t}(b)$, calculated in terms of the local coordinate systems $(\xi^i,\ i = 1,2)$ on $\mathcal{B}$ and $(t^j,\ j = 1,2)$ on the t-plane, preserving the orientation $(J(b) > 0)$, and $d\mathcal{B} = g(b)d\xi^1 d\xi^2$. The expression under the square root in Eq. (7) has to be finite and positive almost everywhere, i.e., for all $b \in \mathcal{B}$ with the allowable exception of a set of measure zero in $\mathcal{B}$. This condition can be met with appropriately chosen beam manifold $\mathcal{B}$, operator Q, and normal $\mathbf{q}$. In some cases, when $\mathcal{B}$ is a proper subset of $\mathcal{B}_u$, i.e., $\mathcal{B} \neq \mathcal{B}_u$, the whole set of beams $\mathbf{W}_n$ [Eq. (3)] can not be orthonormalized; instead, its subset may be orthonormalized.

It is significant that the beam base functions $\mathbf{K} = \mathbf{K}(b)$ and $\mathbf{W} = \mathbf{W}(b)$, the beam state function $\nu = \nu(b)$, and the orthonormal functions $u_n = u_n(b)$ are defined on the same manifold $\mathcal{B}_u$. Therefore, the natural coordinates providing the coordinate representation of u_n, being used as integration variables, provide also the natural parametrization of the beams $\mathbf{W}_n(\mathbf{x})$ [Eq. (2)] or $\mathbf{W}_n(\mathbf{r}, t)$ [Eq. (3)]. In the case of beams defined by the spherical harmonics, treated in Refs. [8, 9, 10], $\mathcal{B}_u$ is a unit sphere. The polar angle θ and the azimuthal angle φ compose the natural coordinate system on it. These coordinates may coincide [8, 9] or be closely connected [10] with the spherical coordinates of the propagation direction, but this is by no means always the case. In particular, to compose the similar beams in a biaxially anisotropic medium, it is more advantageous to relate θ and φ with the biaxial coordinates [11]. These curvilinear coordinates yield the parametric representation of the wavevector surface, which makes possible to obviate the need for solving algebraic equations to describe this fourth order surface. They provide also a very convenient means for decription of field vectors of both eigenwaves and beams in biaxially anisotropic media.

If the beam $\mathbf{W}_n$ (3) consists of homogeneous eigenwaves, i.e., $\hat{\mathbf{k}}^*(b) = \hat{\mathbf{k}}(b)$ for all $b \in \mathcal{B}$, it may be of advantage to expand it into a series by using the Rayleigh formula

$$e^{i\mathbf{k}\cdot\mathbf{r}} = 4\pi \sum_{l=0}^{+\infty} i^l j_l(kr) \sum_{m=-l}^{l} Y_l^{m*}(\hat{\mathbf{k}}) Y_l^m(\hat{\mathbf{r}}) \ , \tag{8}$$

where $\hat{\mathbf{k}} = \mathbf{k}/k$, $\hat{\mathbf{r}} = \mathbf{r}/r$, and Y_l^m are the spherical harmonics. Substituting the expansion (8) into Eq. (3), we obtain

$$\mathbf{W}(\mathbf{r}, t) = e^{-i\omega t} \sum_{l=0}^{+\infty} i^l \sum_{m=-l}^{l} Y_l^m(\hat{\mathbf{r}}) \mathbf{W}_l^m(r) \ , \tag{9}$$

where

$$\mathbf{W}_l^m(r) = 4\pi \int_{\mathcal{B}} j_l(k(b)r) Y_l^{m*}(\hat{\mathbf{k}}(b)) \nu(b) u(b) \mathbf{W}(b) d\mathcal{B} \ . \tag{10}$$

Within the framework of this description, the beam is characterized by a set of radial vector functions $\mathbf{W}_l^m = \mathbf{W}_l^m(r)$. In an isotropic medium (achiral or chiral), these relations become

$$\mathbf{W}(\mathbf{r}, t) = e^{-i\omega t} \sum_{l=0}^{+\infty} i^l j_l(kr) \sum_{m=-l}^{l} Y_l^m(\hat{\mathbf{r}}) \mathbf{W}_l^m \ , \tag{11}$$

where the coordinate independent vector coefficients

$$\mathbf{W}_l^m = 4\pi \int_{\mathcal{B}} Y_l^{m*}(\hat{\mathbf{k}}(b))\nu(b)u(b)\mathbf{W}(b)d\mathcal{B} \tag{12}$$

completely characterize the beam.

4. Conclusion

New families of exact time–harmonic solutions of Maxwell's equations in homogeneous linear media (isotropic, chiral, anisotropic, and bianisotropic) and free space, which describe orthonormal electromagnetic beams, are obtained. Owing to the orthonormality conditions, these beams form convenient functional bases for more complex fields and provide a helpful technique for modelling the beams now in use and investigating their scattering and propagation in various media. The presented results form a basis for generalizing the wave–splitting technique developed in [12, 13] to the case of beams in plane–stratified media. They can be used for modelling of incident and scattered beams in investigating possible physical phenomena caused by anomalous propagation in homogeneous and helicoidally nonhomogeneous bianisotropic slabs.

In the poster presentation, we illustrate the obtained solutions by calculated spatial distributions of energy density, time average Poynting's vector, and local polarization parameters for a number of beams in complex media and free space.

References

[1] G. N. Borzdov, "Evolution operators of electromagnetic waves in crystals. I. Classification. Waves with cubic dependence of amplitude on coordinates," *Sov. Phys. Crystallogr.*, vol. 35, no. 3, pp. 313–316, June 1990.

[2] G. N. Borzdov, "Evolution operators of electromagnetic waves in crystals. II. Waves with linear dependence of amplitude on coordinates," *Sov. Phys. Crystallogr.*, vol. 35, no. 3, pp. 317–321, June 1990.

[3] G. N. Borzdov, "Evolution operators of electromagnetic waves in crystals. III. Waves with quadratic dependence of amplitude on coordinates," *Sov. Phys. Crystallogr.*, vol. 35, no. 3, pp. 322–325, June 1990.

[4] G. N. Borzdov, "Waves with linear, quadratic and cubic coordinate dependence of amplitude in crystals," *Pramana — J. Phys.*, vol. 46, no. 4, pp. 245–257, April 1996.

[5] A. Lakhtakia, "Anomalous axial propagation in helicoidal bianisotropic media," *Opt. Commun.*, vol. 157, pp. 193–201, December 1998.

[6] A. Lakhtakia, "On the possibility of anomalous axial propagation in highly dissipative dielectric TFHBMs," *J. Phys. D: Appl. Phys.*, vol. 31, pp. 235–239, 1998.

[7] A. Lakhtakia, "Anomalous axial propagation in a gyrotropic, locally uniaxial, dielectric, helicoidally nonhomogeneous medium," *Arch. Elektr. Über.*, vol. 53, no. 1, pp. 45–48, 1999.

[8] G. N. Borzdov, "Plane–wave superpositions defined by orthonormal scalar functions on two– and three–dimensional manifolds," *Phys. Rev. E*, vol.61, no. 4, pp. 4462–4478, April 2000.

[9] G. N. Borzdov, "New types of electromagnetic beams in complex media and free space," in *Abstracts of Millennium Conference on Antennas & Propagation AP2000*, Davos, Switzerland, April 2000, Vol. II – Propagation, p. 228.

[10] G. N. Borzdov, "Electromagnetic beams defined by the spherical harmonics with applications to characterizing complex media," in *Abstracts of Millennium Conference on Antennas & Propagation AP2000*, Davos, Switzerland, April 2000, Vol. II – Propagation, p. 229.

[11] G. N. Borzdov, "Orthogonal curvilinear coordinate systems on the wavevector surface in a transparent biaxial crystal," *Int. J. Appl. Electromagn. Mech.*, vol. 9, no. 2, pp. 143–156, April 1998.

[12] G. N. Borzdov, "Frequency–domain wave–splitting techniques for plane–stratified bianisotropic media," in *Proc. Bianisotropics'97*, Glasgow, Great Britain, June 1997, pp. 219–222.

[13] G. N. Borzdov, "Frequency domain wave splitting techniques for plane stratified bianisotropic media," *J. Math. Phys.*, vol.38, no. 12, pp. 6328–6366, December 1997.

Localized Electromagnetic Fields in Complex Media and Free Space

G. N. Borzdov

Department of Theoretical Physics, Belarusian State University
Fr. Skaryny avenue 4, 220050 Minsk, Belarus
Fax: + 375-17-226 0530; email: borzdov@phys.bsu.unibel.by

Abstract

The presented exact solutions of homogeneous Maxwell's equations in complex media and free space describe fields having a rather involved curl structure and a very small—about several wave lengthes of composing plane waves—and clearly defined core region with maximum intensity of field oscillations. In a given Lorentz frame L, a set of the obtained exact time-harmonic solutions of the free-space homogeneous Maxwell equations consists of three subsets—termed "storms", "whirls", and "tornadoes" for the sake of brevity—for which time average energy flux is identically zero at all points, azimuthal, and spiral, respectively. In any other Lorentz frame L', they will be observed as a kind of electromagnetic missiles moving without dispersing at speed $V < c$. The solutions which describe finite-energy evolving electromagnetic storms, whirls, tornadoes are also presented.

1. Introduction

In the beginning of eighties, Brittingham [1] proposed the problem of searching for specific electromagnetic waves—focus wave modes—having a three-dimensional pulse structure, being nondispersive for all time, and moving at light velocity in straight lines. A number of packet-like solutions have been presented [1, 2, 3]. However, it seems [3, 4, 5], finite-energy focus wave modes can not exist without sources. In 1985, Wu introduced [5] a conception of electromagnetic missiles moving at light velocity and having a very slow rate of decrease with distance. Because of these properties, such missiles have important possible applications [5].

In Ref. [6], vector plane-wave superpositions defined by a given set of orthonormal scalar functions on a two-dimensional or three-dimensional manifold—beam manifold $\mathcal{B}$—are treated. The proposed approach makes it possible to compose a set of orthonormal beams, normalized to either the energy flux through a given plane σ_0 with unit normal $\mathbf{q}$ (beams with two-dimensional $\mathcal{B}$) or to the total energy transmitted through this plane (beams with three-dimensional $\mathcal{B}$), as well as some other specific exact solutions of wave equations such as three-dimensional standing waves, moving and evolving whirls. This approach can be applied to any linear field, such as electromagnetic waves in free space, isotropic, anisotropic, and bianisotropic media, elastic waves in isotropic and anisotropic media, sound waves, etc. By way of illustration, some specific families of exact solutions of the homogeneous Maxwell equations, describing localized electromagnetic fields in free space, are obtained in Refs. [6, 7, 8]. In this paper, we present some new types of such localized electromagnetic fields in complex media and free space.

2. Time–Harmonic Localized Fields Defined by the Spherical Harmonics

In this paper, we treat time–harmonic electromagnetic fields in linear complex media or free space, defined by the spherical harmonics as

$$\mathbf{W}_j^s(\mathbf{r},t) = e^{-i\omega t}\int_0^{2\pi} d\varphi \int_{\theta_1}^{\theta_2} e^{i\mathbf{r}\cdot\mathbf{k}(\theta,\varphi)} Y_j^s(\theta,\varphi)\nu(\theta,\varphi)\mathbf{W}(\theta,\varphi)\sin\theta d\theta, \tag{1}$$

where $\mathbf{W} = \mathrm{col}(\mathbf{E},\mathbf{B})$ specifies the polarization of the eigenwave with the wave vector $\mathbf{k}$. To compose these beams, it is necessary first to calculate parameters of eigenwaves. The corresponding relations for electromagnetic waves in a general bianisotropic medium are presented in Ref. [6].

There are two main ways to set the beam base, i.e., to specify the functions $\mathbf{k} = \mathbf{k}(\theta,\varphi)$ and $\mathbf{W} = \mathbf{W}(\theta,\varphi)$. One can set first the unit wave normals of these eigenwaves by a function $\hat{\mathbf{k}} = \hat{\mathbf{k}}(\theta,\varphi)$. In particular, one can set the angular spectrum of plane waves by

$$\hat{\mathbf{k}} = \mathbf{k}/k = \sin\theta'(\mathbf{e}_1\cos\varphi + \mathbf{e}_2\sin\varphi) + \mathbf{e}_3\cos\theta, \tag{2}$$

where $\theta' = \kappa_0\theta$, and κ_0 is some real parameter. Then, one has to calculate the refractive indices $n_j(\theta,\varphi) = n_j(\hat{\mathbf{k}}(\theta,\varphi))$ of all isonormal waves and, by choosing some branch $n_j(\theta,\varphi)$, to specify the wave vector function $\mathbf{k}(b) = (\omega/c)n_j(\theta,\varphi)\hat{\mathbf{k}}(\theta,\varphi)$ and the amplitude function $\mathbf{W}(\theta,\varphi) = \mathrm{col}(\mathbf{E}(\theta,\varphi),\mathbf{B}(\theta,\varphi))$ as well. The alternative is to set first the tangenial components of wave vectors by a real vector function $\mathbf{t} = \mathbf{t}(\theta,\varphi)$. Then, the normal component $\xi_j(\theta,\varphi) = \xi_j(\mathbf{t}(\theta,\varphi))$ of $\mathbf{k}(\theta,\varphi) = \mathbf{t}(\theta,\varphi) + \xi_j(\theta,\varphi)\mathbf{q}$ is chosen from the roots of a quartic equation [6]. In addition to the parameters of eigenwaves themselves in the medium under study, there are three parameters defining the properties of the presented beams: θ_1, θ_2, and κ_0. By setting these parameters in various ways, one can compose various localized fields with very interesting properties. Let us illustrate this on the case of localized fields in free space.

In free space, the integral representations of the localized fields under consideration and the orthonormal beams, presented in Ref. [9], differ only by the values of the integration limits in Eq. (1). In both cases, there are beams with two independent polarization states—E_M and E_A beams.

Let us consider time–harmonic fields $\mathbf{W}_j^s$ [Eq. (1)] with $\theta_1 = 0$, $\pi/2 \le \theta_2 \le \pi$, and $\kappa_0 = 1$, i.e., with $\theta' = \theta$. These fields are composed of plane waves propagating in a solid angle $\Omega \in [2\pi, 4\pi]$. For the sake of simplicity, we assume that the beam state function $\nu = \nu(\theta,\varphi)$ reduces to a constant. A set of these exact time–harmonic solutions of the free-space homogeneous Maxwell equations consists of three subsets—termed "storms", "whirls", and "tornadoes" for brevity—for which time average energy flux is identically zero at all points, azimuthal, and spiral, respectively.

Let us first set $\theta_2 = \pi$. Then, the fields under consideration are composed from plane waves of all possible propagation directions, i.e., $\Omega = 4\pi$. They are in effect three–dimensional standing waves with rather involved structures of interrelated electric and magnetic fields. Beams with $s \neq 0$ are essentially electromagnetic whirls with azimuthal energy fluxes. For E_A and B_A electromagnetic storms, both of which are defined by the zonal spherical harmonics ($s = 0$), the time average Poynting vector $\mathbf{S}$ is vanishing at all points. The electric field vector $\mathbf{E}$ of E_A storms has the only—azimuthal—component, whereas the azimuthal component of the magnetic field vector $\mathbf{B}$ is everywhere zero. The opposite situation occurs with B_A storms.

The spherical harmonics with $s \neq 0$ define electromagnetic whirls for which the time average Poynting vector $\mathbf{S}$ has the only nonvanishing—azimuthal—component. This component, as well as the energy densities w_e and w_m of the electric $\mathbf{E}$ and magnetic $\mathbf{B}$ fields, is independent of the azimuthal angle ψ. The whirls with $j > s \ge 1$ have two major domains—above and below

the equatorial plane—with large energy fluxes. The whirls, defined by the sectorial harmonics ($j = s \geq 1$), have only one such domain, and the energy flux peaks in the equatorial plane.

Let us now consider time–harmonic fields $\mathbf{W}_j^s$ [Eq. (1)] with $\theta_1 = 0$, $\pi/2 < \theta_2 < \pi$, and $\kappa_0 = 1$, i.e., with $\theta' = \theta$, and $2\pi < \Omega < 4\pi$. As before, we assume that the beam state function $\nu = \nu(\theta, \varphi)$ reduces to a constant. In this case, the field also is highly localized, but the normal and the radial components of time average Poynting's vector $\mathbf{S}$ are not vanishing. As a result, lines of energy flux become spiral, provided that $s \neq 0$. We refer to such specific localized fields with spiral energy fluxes as electromagnetic tornadoes. Their lines of energy flux closely resemble spirals, and as θ_2 tends to π, the step of these spirals decreases. For the fields defined by the zonal spherical harmonics ($s = 0$), the lines of energy flux lie in meridional planes.

3. Evolving Storms, Whirls, and Tornadoes

Although, in many cases, the presented time–harmonic solutions may provide satisfactory models of real physical fields, more accurate models can be obtained by integrating these solutions with respect to frequency. In particular, some solutions which describe quasimonochromatic electromagnetic beams are obtained in Ref. [6].

Let us consider localized fields $\breve{\mathbf{W}}_j^s(\mathbf{r}, t)$ with three–dimensional beam manifold $\mathcal{B}_3 = \mathcal{B} \times [\omega_-, \omega_+]$, related with $\mathbf{W}_j^s(\mathbf{r}, t)$ [Eq. (1)] as

$$\breve{\mathbf{W}}_j^s(\mathbf{r}, t) = \frac{1}{2\Delta\omega} \int_{\omega_-}^{\omega_+} \mathbf{W}_j^s(\mathbf{r}, t) d\omega, \tag{3}$$

where $\Delta\omega = (\omega_+ - \omega_-)/2$. In the case of quasimonochromatic beams, $\Delta\omega \ll \omega$. For the beams under consideration, the amplitude function $\mathbf{W}(\theta, \varphi)$ is frequency independent. If the beam state function $\nu(\theta, \varphi)$ also is frequency independent, or its frequency dependence is negligibly small, we have

$$\begin{aligned} \breve{\mathbf{W}}_j^s(\mathbf{r}, t) = \quad & e^{-i\omega t} \int_0^{2\pi} d\varphi \int_{\theta_1}^{\theta_2} e^{i\mathbf{r}\cdot\mathbf{k}(\theta,\varphi)} Y_j^s(\theta, \varphi) j_0 \left[p_0 \left(\mathbf{r} \cdot \mathbf{k}(\theta, \varphi) - \omega t\right)\right] \\ & \times \nu(\theta, \varphi) \mathbf{W}(\theta, \varphi) \sin\theta d\theta, \end{aligned} \tag{4}$$

where $\omega = (\omega_+ + \omega_-)/2$ and $p_0 = \Delta\omega/\omega$. In free space, this field is composed of plane wave packets radially moving with the light velocity c.

Therefore, the field under considerarion is essentially an evolving whirl in the neighbourhood of the point $\mathbf{r} = 0$. It varies in intensity as different "peaks and valleys" reach the core region. At $-\pi/\Delta\omega < t < \pi/\Delta\omega$, the main peak passes through this region, and the whirl reaches its absolute maximum intensity at $t = 0$. At this moment, its field structure is very close to the structure of the corresponding time–harmonic whirl. In particular, lines of energy flux are circular for both whirls. At $-\pi/\Delta\omega < t < 0$ and $0 < t < \pi/\Delta\omega$, the energy flux lines of the evolving whirls are convergent and divergent, respectively.

On the whole, the evolution of the field can be described as follows. When $t \to \pm\infty$, the field tends to zero at all points $\mathbf{r}$. Therefore, the solution $\breve{\mathbf{W}}_j^s(\mathbf{r}, t)$ [Eq. (4)] describes initiation and evolution of a whirl, which originates at the infinity at $t = -\infty$ as infinitely small converging wave propagating with the light velocity c. At $t \ll -\pi/\Delta\omega$, there is a very small converging wave with maximum peak at the distance $r = -ct$. During all this time, there is also a weak whirl in the neighbourhood of the point $\mathbf{r} = 0$. It passes through maximums and minimums of activity, gradually gaining in intensity as t tends to zero.

The total field can be described as the superposition of converging and expanding waves with ever changing proportion. At $t > 0$, the whirl, still passing through maximums and minimums of activity, gradually transforms into expanding wave, which vanishes in the infinity as $t \to +\infty$.

It is significant that the evolving storms, whirls, and tornadoes have finite total energy.

4. Conclusion

In this paper, new families of exact solutions of the homogeneous Maxwell equations in complex media and free space, obtained on the basis of angular–spectrum representations, are presented. These families of solutions specify three–dimensionally localized electromagnetic fields having a rather involved curl structure and a very small—about several wave lengthes of composing plane waves—and clearly defined core region with maximum intensity of field oscillations. Outside of the core, the intensity of oscillations rapidly decrease in all directions. In complex media, these fields provide a unique global description of the medium under study, which is supplementary to the eigenwave description. Whereas each eigenwave specifies the properties of the medium for one particular direction of propagation, the field value of a three–dimensional standing wave in any point is defined by all eigenwaves. Moreover, even in free space such waves possess very interesting properties. In a given Lorentz frame L, a set of obtained time–harmonic free–space solutions consists of three subsets — termed "storms", "whirls", and "tornadoes" for brevity sake — for which time average energy flux is identically zero at all points, azimuthal, and spiral, respectively. In any other Lorentz frame L', they will be observed as a kind of electromagnetic missiles moving without dispersing at speed $V < c$. Solutions which describe, in the frame L, finite–energy quasi–monochromatic evolving electromagnetic storms, whirls, tornadoes, and correspondingly, in the frame L', various types of moving and evolving missiles, are also obtained. The intrinsic tensor technique in Minkowski space [10] provides a convenient means for investigating all these new types of waves. Their properties are illustrated in graphic form.

References

[1] J. N. Brittingham, "Focus waves modes in homogeneous Maxwell's equations: Transverse electric mode," *J. Appl. Phys.*, vol. 54, no. 3, pp. 1179–1189, March 1983.

[2] R. W. Ziolkowski, "Exact solutions of the wave equation with complex source locations," *J. Math. Phys.*, vol. 26, no.4, pp. 861–863, April 1985.

[3] A. Sezginer, "A general formulation of focus wave modes," *J. Appl. Phys.*, vol. 57, no. 3, pp. 678–683, February 1985.

[4] T. T. Wu and R. W. P. King, "Comment on "Focus waves modes in homogeneous Maxwell's equations: Transverse electric mode"," *J. Appl. Phys.*, vol. 56, no. 9, pp. 2587-2588, November 1984.

[5] T. T. Wu, "Electromagnetic missiles," *J. Appl. Phys.*, vol. 57, no. 7, pp. 2370–2373, April 1985.

[6] G. N. Borzdov, "Plane–wave superpositions defined by orthonormal scalar functions on two– and three–dimensional manifolds," *Phys. Rev. E*, vol.61, no. 4, pp. 4462–4478, April 2000.

[7] G. N. Borzdov, "New types of electromagnetic beams in complex media and free space," in *Abstracts of Millennium Conference on Antennas & Propagation AP2000*, Davos, Switzerland, April 2000, Vol. II – Propagation, p. 228.

[8] G. N. Borzdov, "Electromagnetic beams defined by the spherical harmonics with applications to characterizing complex media," in *Abstracts of Millennium Conference on Antennas & Propagation AP2000*, Davos, Switzerland, April 2000, Vol. II – Propagation, p. 229.

[9] G. N. Borzdov, "The application of orthonormal electromagnetic beams to characterizing complex media", this issue.

[10] G. N. Borzdov, "An intrinsic tensor technique in Minkowski space with applications to boundary value problems," *J. Math. Phys.*, vol. 34, no. 7, pp. 3162–3196, July 1993.

Point Sources of Magnetoelectric Fields

E.O. Kamenetskii

Department of Electrical Engineering - Physical Electronics
Faculty of Engineering, Tel-Aviv University, Tel Aviv 69978, Israel
Fax: +972-3-6423508; e-mail: kmnsk@eng.tau.ac.il

Abstract

In this paper, we show that the unified quasistatic magnetoelectric fields (QME fields) originated by point sources - the quasistatic magnetoelectric particles (QME particles) - can exist when symmetry properties of these fields are distinguished from that of the electromagnetic fields. The physical ground for QME particles can be found in small ferromagnetic resonators where short-wavelength (so-called magnetostatic) oscillations take place. The question about QME particles and fields arises in such a topical subject as artificial bianisotropic materials.

1. Introduction

The question about coupling of electric and magnetic polarizations arises in problems of artificial chiral and bianisotropic media [1,2]. It is supposed that there exists a possibility to describe properties of media with intrinsic coupling between the electric and magnetic polarizations by phenomenological constitutive relations with further use these constitutive relations in Maxwell's equations. Fundamental contradictions in such an approach can be perceived, however. Some of these contradictions concerning nonlocal properties of bianisotropic composites based on small helices and so-called omega-particles, we have recently discussed [3-5]. Is it possible to have artificial bianisotropic media with local properties? One can suppose that these composite materials should be based on *point* bianisotropic (magnetoelectric) particles that can be considered, by a simple model, as small coupled electric and magnetic dipoles. However, the question suggests itself: Can one consider (classical electrodynamically) two small, i.e. quasistatic (with sizes much less than the electromagnetic wavelength) coupled electric and magnetic dipoles as *point sources of the electromagnetic field*? To answer this question, the following aspects should be taken into account: (a) neither Lorentz nor Coulomb gauges [6] can be used to describe the fields of such particles and (b) mechanical interaction between two such particles cannot be described by the Lorentz force since potential energy of every particle is characterized not only by electric and magnetic energies, but also by energy of internal coupling between the electric and magnetic dipoles. Based on these aspects and also taking into account the fact that in a small region (much less than the electromagnetic wavelength) of sourceless free space a character of the unified field is physically undefined by the Maxwell equations, we should come to conclusion that *the unified quasistatic magnetoelectric fields (QME fields) originated by point sources - the quasistatic magnetoelectric particles (QME particles) - can exist when symmetry properties of these fields are distinguished from that of the electromagnetic fields.*

The physical ground for QME particles can, in particular, be found in small ferromagnetic resonant specimens where short-wavelength (so-called magnetostatic) oscillations take place [7]. In a case of small normally magnetized ferrite disks placed into a region of the uniform rf magnetic field, a long series of oscillating magnetostatic modes were observed experimentally [8,9]. Recently, we have shown that these oscillations can be characterized by a discrete spectrum

of energy levels [10]. The QME particles one can realize based on ferrite resonators with special-form surface electrodes. In this case, magnetostatic oscillations in a ferrite body are accompanied with short-wavelength surface-electric-charge oscillations on a metallic electrode [3,11]. Recently, the first experimental evidence for this magnetoelectric coupling in small ferrite resonators with special-form surface electrodes has been obtained [12,13].

2. Symmetry Properties of Ferrite QME Particles

Based on a semi-classical model, one can illustrate some symmetry properties of ferrite QME particles. These particles can conventionally be described as a pair of two coupled dipoles: an electric dipole with moment $\vec{p^e}$ and a magnetic dipole with moment $\vec{p^m}$. These two dipoles are mutually perpendicular and the bias magnetic field $\vec{H_0}$ is oriented perpendicular to the plane of $\vec{p^e}$, $\vec{p^m}$ vectors. So, one has a triple of mutually perpendicular vectors: $\vec{p^e}$, $\vec{p^m}$ and $\vec{H_0}$. As we discussed in [5], the PT invariance (the time-reversal operation T combined with the parity P) does not hold in this model of one polar ($\vec{p^e}$) and two axial ($\vec{p^m}$ and $\vec{H_0}$) vectors. But, the CPT invariance (when the charge conjugation C changes the sign of vector $\vec{p^e}$) takes place.

It should be clearly understood that in this our semi-classical model of a QME particle, the charge conjugation C does not mean interconversion of electrons and positions in the magnetic processes (of the atomic scales) in a ferrite. As an important fact, it is discussed in this paper that the problem of the charge conjugation has to be considered in connection with the *sign of energy eigenstates* of oscillations in a QME particle. To clarify the problem, we should analyze the "microscopic properties" of magnetostatic oscillations in ferrite QME particles.

3. Energy Eigenstates Magnetostatic Oscillations

The average magnetostatic energy of magnetostatic oscillations in a "pure" (without surface metallic electrodes) normally magnetized ferrite disk, having a small ratio of thickness h to radius a can be described as [10]:

$$\bar{W} = \frac{w\mu_0}{4} \int_s \left[X^{(\mathcal{D})} \left(\int_{-\infty}^{0} \psi\psi^* dz + \int_h^{\infty} \psi\psi^* dz \right) + \right.$$
$$\left. + X^{(F)} \int_0^h \psi\psi^* dz \right] ds \qquad (1)$$

where ψ is the magnetostatic potential, $X^{(\mathcal{D})}$ and $X^{(F)}$ are coefficients characterizing wave processes, respectively, in dielectric $\mathcal{D}$ ($z \leq 0$, $z \geq h$) and ferrite F ($0 \leq z \leq h$) regions. Coefficients X are found from the equations

$$-\frac{i}{X} \nabla_{\|}^2 \psi = \frac{\partial \psi}{\partial t} \qquad (2)$$

written for every region. Here $\nabla_{\|}^2$ is a longitudinal part of Laplace operator.

We suppose that in a ferrite disk resonator, magnetostatic potential ψ can be represented as [10]

$$\psi = \sum_{p,q} A_{pq}\, \tilde{\xi}_p\,(z)\; \tilde{\varphi}_q\,(\rho, \alpha) \qquad (3)$$

For "in-plane" resonant mode $\tilde{\varphi}_q$ (and p "thickness" mode), one has an operator equation for normalized energy of magnetosttic oscillations [10]

$$\hat{F}_{\perp} \tilde{\varphi}_q = E_{pq} \tilde{\varphi}_q \qquad (4)$$

Differential operator $\hat{F}_\perp$ is defined as

$$\hat{F}_\perp = g\frac{\mu_0}{4}\nabla_\perp^2 \tag{5}$$

where $\nabla_\perp^2$ is two-dimensional ("in-plane") Laplace operator, g is unit dimensional co-efficient. The property of energy orthonormality for magnetostatic oscillations is described as

$$(E_{pq} - E_{pq'}) \int_Q \tilde{\varphi}_q \tilde{\varphi}_{q'}^* ds = 0 \tag{6}$$

where Q is a square of "in-plane" cross section of an open ferrite disk including radius regions $Q_F(\rho \leq a)$ and $Q_{\mathcal{D}}(a \leq \rho < \infty)$.

4. Effect of the External Fields

We can write the Hamiltonian taking into account an interaction of the magnetoelectric particle with the exciting electric $\vec{\varepsilon}$ and magnetic $\vec{\mathcal{H}}$ fields. For a disk with unit thickness, the Hamiltonian has a form [14]

$$\hat{H} = \hat{F}_\perp + \hat{F}'_\perp + \frac{A}{b}\hat{\vec{l}}\hat{\vec{p^e}} + \mathcal{D}\hat{\vec{p^e}}\vec{\varepsilon} \tag{7}$$

where $\mathcal{D}$ is a constant that can be positive or negative, $\hat{F}'_\perp$ is the term of extra energy of the particle due to the external magnetic field.

Operator $\hat{F}'_\perp$ can be written as

$$\hat{F}'_\perp = \vec{\mathcal{H}}\hat{\vec{m}}_\perp \tag{8}$$

Here $\hat{\vec{m}}_\perp$ is the operator of the "in-plane" alternative magnetization. Operators $\hat{F}_\perp$ and $\hat{m}_\perp$ *do not commute* one with another. For a ferrite disk resonator placed in a tangential rf magnetic field, we have energy perturbations similar to those one has for atom placed in an external electric field (the Stark effect) [15]: the second-order effect of a split of energy levels in the external rf magnetic field. The energy split ΔE_n of energy level E_n is proportional to

$$\Delta E_n \sim \alpha_{ij}^{(n)} \mathcal{H}_i \mathcal{H}_j \tag{9}$$

where $\alpha_{ij}^{(n)}$ is the tensor of magnetic polarization ("in-plane") of a ferrite disk. For every energy level, an average magnetic moment of a ferrite disk is

$$(p^m)_i = \alpha_{ij}\mathcal{H}_j \tag{10}$$

Unlike the average magnetic moment, electric moments of a ferrite disk are not equal to zero in oscillation eigenstates. An interaction between the external rf electric field and a ferrite disk is similar to an interaction between the electrically neutral particles (neutron, atom) with ("magnetic") spin and external alternative magnetic field [15].

The particle can have potential energy in the external electric $\vec{\varepsilon}$ field. Similarly, the particle can possess potential energy in the external magnetic $\vec{\mathcal{H}}$ field. At the same time, because of the effect of internal magnetoelectric coupling, the particle should have potential energy in the combined $\vec{\varepsilon} + \vec{\mathcal{H}}$ field. The structure of this combined external $\vec{\varepsilon} + \vec{\mathcal{H}}$ field is not just a superposition of the $\vec{\varepsilon}$ and $\vec{\mathcal{H}}$ fields. It is clear that the $\vec{\varepsilon}$ and $\vec{\mathcal{H}}$ components of this (combined) field should be in a certain phase correlating to provide a maximum of potential energy. Because of this correlation we have to talk about the *unified* - quasistatic magnetoelectric

(QME) - field. If we suppose that potential energy due to the effect of magnetoelectric coupling is a small part of summarized potential energy that a particle has in separated $\vec{\varepsilon}$ and $\vec{\mathcal{H}}$ field, the total potential energy E_{total} can be represented as a sum of three components:

$$E_{total} = E_{\varepsilon} + E_{\mathcal{H}} + E' \,, \tag{11}$$

where E_{ε} is the potential energy of a particle due to external electric field, $E_{\mathcal{H}}$ is the potential energy of a particle due to external magnetic field, and E' is the potential energy due to a combined effect of action of two $\left(\vec{\varepsilon} \text{ and } \vec{\mathcal{H}}\right)$ fields

Conclusion

Based on "microscopic properties" of magnetostatic oscillations in ferrite disk resonators, we have shown, in this paper, that such resonators can be considered as QME particles: the point sources of unified QME fields. The symmetry properties of these fields are distinguished from that of the electromagnetic fields.

Magnetostatic oscillations in a ferrite disk resonator can be characterized by eigen angular momentum of magnetostaic oscillations with the so-called "electric spin" and the eigen electric moment. Similarly to neutrino (where spin is not separated from orbit moment), in our case, "electric spin" is also not separated from the angular momentum operator.

References

[1] A. Lakhtakia, *"Beltrami Fields in Chiral Media"*. Singapore: World Scientific 1994.
[2] I.V. Lindell, A.H. Sihvola, S.A. Tretyakov and A.J. Viitanen, *Electromagnetic Waves in Chiral and Bi-Isotropic Media.* Boston: Artech House, 1994.
[3] E.O. Kamenetskii, *Phys. Rev. E,*, vol. 57, p. 3563, 1998.
[4] E.O. Kamenetskii, *Phys. Rev. E,*, vol. 58, p. 7965, 1998.
[5] E.O. Kamenetskii, *Microw. Opt. Technol. Lett.*, vol. 19 vol. 6, p. 412, 1998.
[6] J.D. Jackson, *"Classical Electrodynamics"*, New York: Wiley, 1975.
[7] A.G. Gurevich and G.A. Melkov, *Magnetic Oscillations and Waves.* New York: CRC Press, 1996.
[8] J.F. Dillon, *J. Appl. Phys.*, vol. 31, p. 1605, 1960.
[9] T. Yukawa and K. Abe, *J. Appl. Phys.*, vol. 45, p. 3146, 1974.
[10] E.O. Kamenetskii, *Phys. Rev. E.*, submitted.
[11] E.O. Kamenetskii, *Microw. Opt. Technol. Lett.*, vol. 11, no. 2, p. 103, 1996.
[12] E.O. Kamenetskii, I. Awai and A.K. Saha, "Proceedings of the 29th European Microwave Conference", in *Microwave Engineering Europe*, Munich, Germany, 1999, pp. 40-43.
[13] E.O. Kamenetskii, I. Awai and A.K. Saha, *Microw. Opt. Technol. Lett.*, vol. 24, no. 1, p. 56, 2000.
[14] E.O. Kamemetskii. *Phys. Rev. E.*, submitted.
[15] L.D. Landau and E.M. Lifshitz, *Quantum Mechanics: Non-relativistic Theory.* Oxford: Pergamon 1977.

Quasistatic Magnetoelectric Particles: Experimental Investigation at Microwave Frequencies

A. K. Saha[1], E. O. Kamenetskii[2], and I. Awai[1]

[1] Department of Electrical & Electronic Engineering, Yamaguchi University, Tokiwadai 2-16-1, Ube Shi 755-8611, Japan, email: saha@emlab.eee.yamaguchi-u.ac.jp

[2] Department of Electrical Engineering-Physical Electronics, Tel-Aviv University Tel-Aviv-269978, Israel; email: kmntsk@eng.tau.ac.il

Abstract

The theoretical aspects of electrodynamics of bianisotropic media raised in recent publications may be considered as interesting as such but not very relevant as long as experimental validation, or at least some proof of principle is missing. New particulate bianisotropic composites – the magnetostatically controlled bianisotropic materials (MCBMs) - have been recently conceptualised. Recently, an experimental evidence for the magnetoelectric (ME) coupling in small straight-edge ferrite resonators with different -form surface metallizations has been observed experimentally. As the further extension of these investigations, experimental results of ME coupling in disk-type ferrite resonators are reported in this paper.

1. Introduction

New particulate bianisotropic composites based on ferrite ME particles – the MCBMs - have been recently conceptualised [1-2]. Different types of ferrite ME particles can be realized with the use of different forms of ferromagnetic resonant bodies and surface metallic electrodes. One of the main features of the YIG-film resonators is a very rich spectrum of magnetostatic (MS) oscillations. The straight-edge ferrite resonators have evident technological advantage in cutting as compared to the disk-form samples. At the same time, disk-form resonators have regular (with respect to magnitude and mutual spacing) spectrums of MS oscillations [3-4], when the spectrums of straight-edge samples are irregular [5]. In our previous experiments [6-8] with ME particles, based on straight-edge YIG-film resonators with different types of surface electrodes, we observed strong ME coupling. But characterization of the observed spectrums and an analysis of correlation between the MS and ME spectrums were hampered because of irregularity of pictures of MS oscillations in a straight-edge ferrite body. In this paper we show new experimental results of ME spectrums in disk-form ME particles with different types of surface metallic electrodes. Certain characterizations of the observed spectrums and important conclusions are made.

2. Experiment

A general view of a ferrite quasistatic ME particle is shown in Fig.1. We used a disk form (diameter = 5mm, thickness = 0.1mm) YIG film ($4\pi M_S$ = 1780 Gauss) resonator with two different types of surface metallic electrode. These two types of surface metallizations (one- dimensional, or wire-form and two-dimensional, elliptical form) are shown in Fig.2. ME particles were placed in different positions of a rectangular cavity (Fig.3), resonant in TE_{101} mode at 4.02 GHz. We observed rich spectrums of absorptions peaks. The experimental results with a wire type surface metallization are

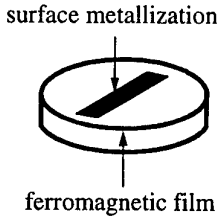

Fig.1 Suggested quasistatic ME particle

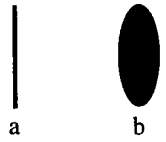

Fig.2 Two forms of surface metallizations (a) wire and (b) elliptical

shown in Fig. 4 and those with elliptical one are shown in Fig. 5. Position of the sample, type of metallization and orientation with respect to the y-axis (or, in other words, with respect to the E-field) are described in each figure.

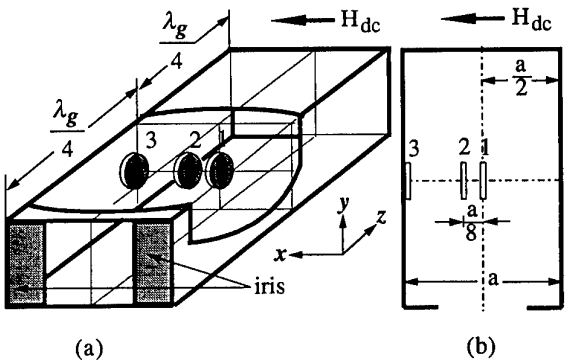

Fig.3 Experimental arrangement showing the positions of the ME particle in the cavity. (a) rough sketch, (b) top view

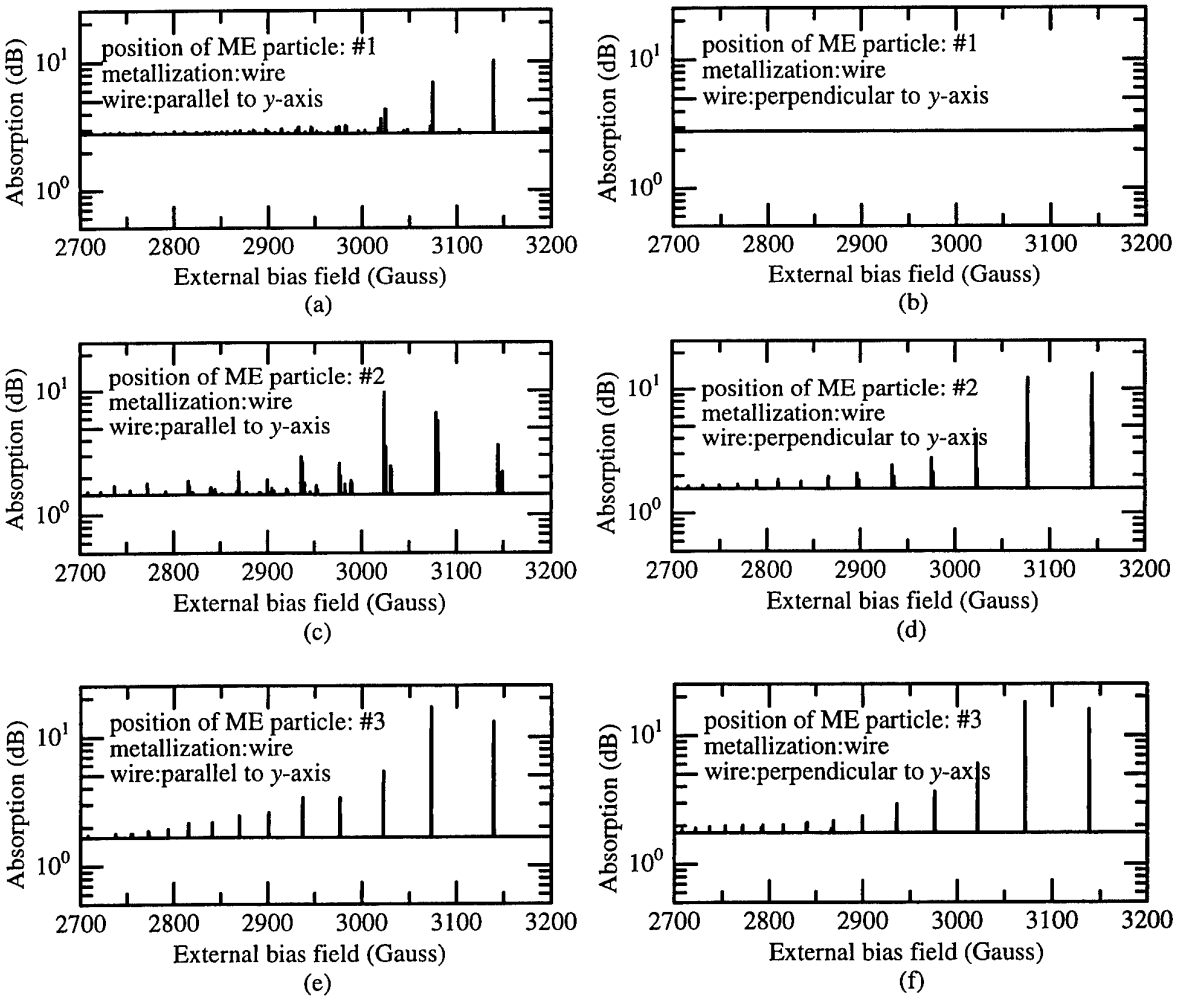

Fig. 4 Absorption spectrum of disk type YIG resonator with wire (length = 4mm and diameter= 0.1mm) type surface metallization.

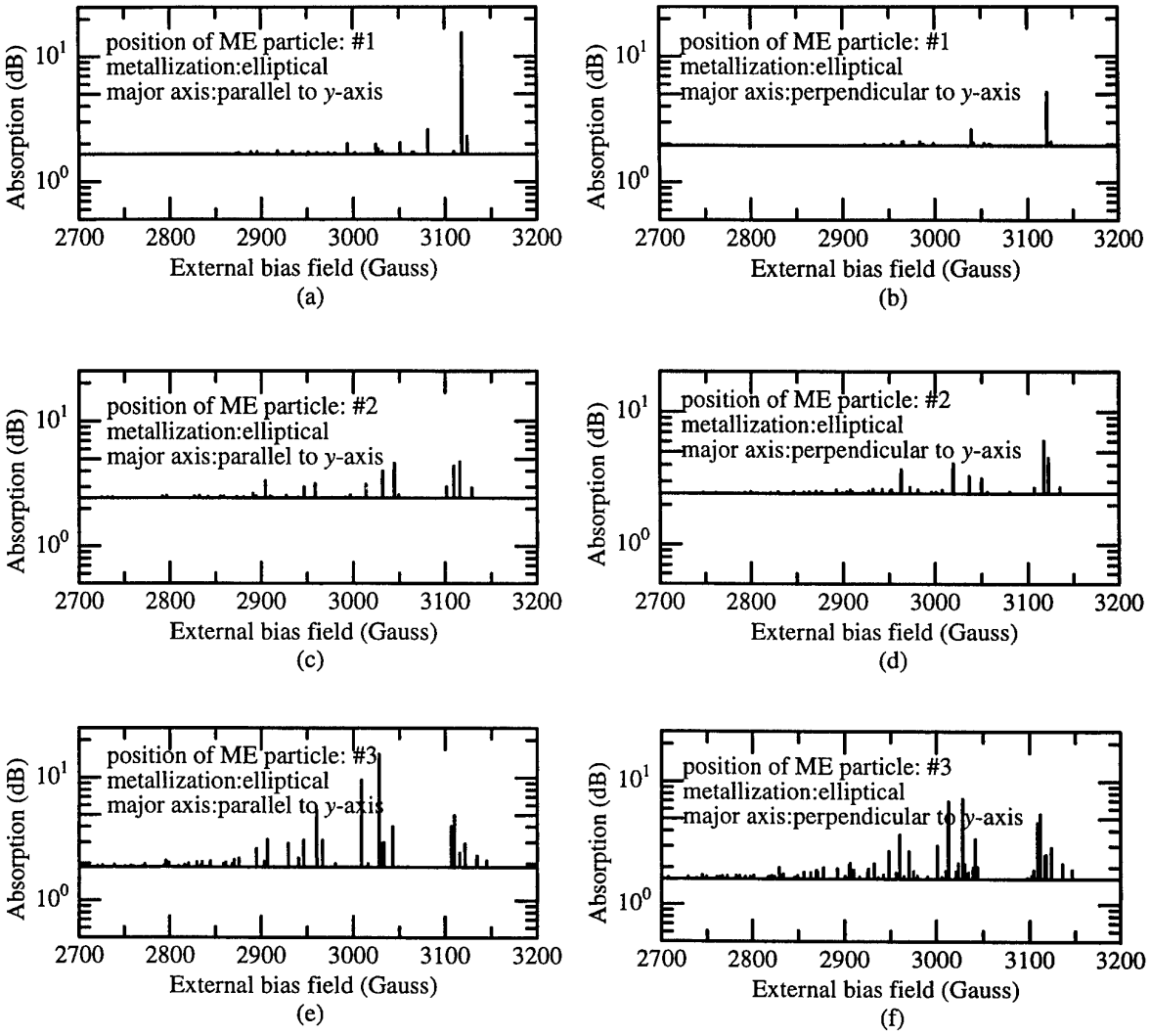

Fig. 5 Absorption spectrum of disk type YIG resonator with elliptic (major axis = 4mm and minor axis = 2mm) type surface metallization.

It is seen that zero levels of the absorption spectrums are different in each picture of Figs. 4 and 5. This is attributed to the fact of variation of the type and orientation of surface electrodes with respect to the *E*-field as well as positions of the ME particles in the cavity.

3. Discussion and Conclusion

A detailed analysis of absorption spectrums obtained for different types of ME particles and different types of the exciting fields leads us to a very important conclusion that only for ME particles based on disk-form ferrite resonators with wire-form surface electrodes, one has a spectrum of the unified ME oscillating modes. Since different types of the exciting fields produce the same oscillation spectrum, a system is characterized by a set of parameters with certain spectral properties. This fact gives us a possibility to represent a disk + wire ME particle as a particle characterized by two (electric and magnetic) moments and so find it as a particle most applicable for bianisotropic composites. Compared to a case of a wire-form metallization, where only linear surface electric currents are

possible, in two-dimensional metallizations different distributions of linear and circular (closed-loop) surface electric currents are possible. This fact gives different pictures of spectrums excited by the different-type external fields, as we can see in our experiment.

References

[1] E. O. Kamenetskii, "On the technology of making chiral and bianisotropic waveguides for microwave propagation," *Microw. Opt. Technol. Lett.*, Vol. 11 (2), pp. 103-107 (1996).

[2] E. O. Kamenetskii, "Theory of bianisotropic crystal lattices," *Phys. Rev. E*, Vol. 57, pp. 3563-3573 (1998).

[3] J .F. Dillon, Jr., "Magnetostatic modes in disks and rods," *J. Appl. Phys.*, Vol. 31, pp.1605-1614 (1960).

[4] T. Yukawa and K. Abe, "FMR spectrum of magnetostatic waves in a normally magnetized YIG disk," *J. Appl. Phys.*, Vol. 45, pp. 3146-3153 (1974).

[5] W. S. Ishak and K. W. Chang, "Tuneable microwave resonators using magnetostatic wave in YIG films," *IEEE Trans. Microw. Theory Techn.*, Vol. MTT-34, pp. 1383-1393 (1986).

[6] E. O. Kamenetskii, I. Awai, and A. K. Saha, "Experimental evidence for magnetoelectric coupling in a ferromagnetic resonator with a surface metallization," *Microw. Opt. Technol. Lett.*, 24 (1), pp. 56-60 (2000).

[7] E. O. Kamenetskii, I. Awai, and A. K. Saha, "Bianisotropic particles based on magnetostatic resonators: A way to realize microwave bianisotropic materials and devices," in *Proceedings of the 29th European Microwave Conference*, publ. Microwave Engineering Europe, Munich, Germany, 1999, Vol.1, pp.40-43.

[8] E. O. Kamenetskii, A. K. Saha, and I. Awai, "Microwave magnetoelectric effect in magnetostatic ferrite resonators: Role of surface electrode configuration," *IEEE Trans. Magn.* (accepted for publication).

Light Beams' Focusing in Biaxial Ferroelectrics

S.S.Girgel' and S.N.Kurilkina

Gomel State University
246699 Gomel, Belarus

Abstract

Among problems of modern optics the elaboration of the methods of formation and control by the space structure of light beams is of great importance. In the papers [1,2] it has been shown that the nonlens focusing and nondiffractional propagation of light, stipulated by the presence of concavity of wave vector surface, are possible near by optical axes of biaxial gyrotropic crystals. The application of external electric field leads to strengthening of concavity and then, increasing of focusing effect for slow waves near binormals [3]. But conducted consideration was limited by the case of the most symmetrical biaxial crystal, namely, orthorhombic one. At the same time many widely used gyrotropic biaxial crystals have lower symmetry. For example, their symmetry is of 2 or m class. Its description is very complex, but at the same time is of essential interest in the connection with enlargement of possibilities of controlling by parameters of optical radiation.

It is known that the big electrooptic effect takes place in ferroelectrics which have orientational spontaneous polarization in definite temperature range in the absence of external electric field. Characteristic peculiarity of given media is strong temperature dependence of optical and electrooptic properties which may be used for control by the focusing of optical radiation.

The aim of the paper is investigation of influence of electric and temperature fields on focusing properties of the lens created on the base of lower symmetrical ferroelectric crystal of 2 class.

1. Introduction

In this paper we analyze the peculiarities of wave vector surface near binormal of biaxial gyrotropic crystal of 2 class symmetry. It has been shown that the presence of gyrotropy leads to appearance of concavity on the wave vector surface for slow light wave and, hence, to possibility of focusing. It has been founded the conditions for this phenomenon. It has been analyzed the influence of temperature and electric field near Curie point on light beam focusing in ferroelectric crystals. It has been grounded that electrooptic interaction in ferroelectric lower symmetrical biaxial crystals may be used for creation of electro- and thermocontrolled crystalline lenses for which one can achieve slow thermochanges of focus length in wide range and fast changes of it by electric field. If the temperature is near Curie point the range of changes of focus length increases abruptly, but the aperture of proposed lenses decreases. By this, it is necessary to thermocontrol of crystalline model. Thus, while creating such elements you must conduct parameter optimization.

2. Peculiarities of Structure of Wave Vector Surface of Monoclinic Crystal near by Optical Axes

It is known [4] that the field of light radiation in the crystal in general case may be presented in the form:

$$\underline{E}(\underline{r},t) = \{(2\pi)^{-2} \int A(\underline{q})\,\underline{a}\, exp\, i[(\underline{r} - \underline{U}\,t)\underline{q} - \frac{1}{2} W\,\underline{q}\underline{q}\,t]\}x\ \ exp\, i(\underline{k}_o\,\underline{r} - \omega_o t), \tag{1}$$

Here $\underline{E}$ is the electric vector, A are amplitudes, $\underline{a}$ are polarization vector, $\underline{q} = \underline{k} - \underline{k}_0$; ω_0 and $\underline{k}_0$ are correspondently frequency and wave vector of "central" wave of the beam; $\underline{U} = \partial\omega / \partial\,\underline{k}$ is group velocity; $W = \partial\omega / \partial\,\underline{k}\ \partial\,\underline{k}$ is tensor of divergence of the group velocity which is connected with tensor of divergence of the wave vector surface. In the result of analysis of expression (1) it may be obtained that divergence of arbitrary light beam in the crystal is determined by eigenvalues of W tensor, namely: if $W_a > 0$, then, collimated beam in the medium is defocusing; if $W_a < 0$ it is focusing; by $W_a = 0$ it takes place nondiffractional propagation of radiation[4].

Let us consider the structure of wave vector surface in the case of propagation of light beams in the crystal of 2 class symmetry. For this let us analyze characteristic equation [5]

$$det\, L = 0, \tag{2}$$

where

$$L_{ie} = (\omega/c)^2 \delta_{ie} + \Gamma_{im}(a_{me} + i\delta_{mjl}G_j)$$

with $\Gamma_{im} = k_i k_m - k^2 \delta_{im}$ and where $G_j = \frac{\pi}{\lambda}\ g_{jm}\, k_m$ is gyration vector [6]; g_{jm} is gyration tensor ; $\underline{n}$ is wave normal; λ is light wavelength; δ_{ie}, δ_{imn} are Kroneker' and Levi- Chivita' symbols; a_{ml} is tensor of dielectric nonpermeability. Differentiating of characteristic equation (2) by components of wave vector $\underline{k}$ one may be obtained for the case of correct coincidence of beam's axis with optical axis:

$$W\underline{q}\underline{q} = (V^2/\omega)\, p_{\pm}\, q^2. \tag{3}$$

Here

$$p_{\pm} = (n_o^2/2)[a_1 + a_2 \pm a_o^2/G], \tag{4}$$

with

$$a_{3,1} = \{\, a_{11} + a_{33} \pm A^{1/2}\}/2\,, \tag{5a}$$

$$a_2 = a_{22}\,, \tag{5b}$$

$$A = [a_{11} - a_{33}]^2 + 4\, a_{13}^2, \tag{5c}$$

$$a_o = [(\, a_2 - a_3)\,(a_3 - a_1)\,)]^{1/2}\,, \tag{5d}$$

where $n_o^2 = V^2/c^2 = a_3 \pm G$; n_0 and V are correspondently refraction index and phase velocity of light wave in the direction of optical axis in gyrotropic crystal of 2 class symmetry; G is projection of gyration vector on optical axis; $q^2 = q_1^2 + q_2^2$. By this we consider that $a_2 > a_3 > a_1$ and plane of optical axes coincidences with (X_1X_2) crystallographic one. How it is evident, tensor W in the direction of optical axis has two equal eigenvalues: $W_{11} = W_{33} = W_\pm = (V^2/\omega)\, p_\pm$.

By influence of external electric field along ferroelectric axis X_2 dielectric constants are changed:

$$a_{ii}(E) = a_{ii} + r_{i2}E \tag{6a}$$

$$a_{13}(E) = a_{13} + r_{52}E\,, \tag{6b}$$

where r_{ij} are linear electrooptic coefficients. By this wave vector surface has deformation. Let's consider that the influence of external electric field is weak. By this, eigenvalues of tensor of derivative of group velocity may be determined from (3) by following changes: $a_{ij} \rightarrow a_{ij}(E)$, $A \rightarrow A(E)$. Then, how it follows from (3), by the case

$$a_1(E) + a_2(E) < a_o(E)^2/G, \tag{7}$$

eigenvalues of W tensor for slow waves are negative and, hence, in conformity with (1) focusing of slow light wave takes place. In conformity with [7-9] parameters of anisotropy and gyrotropy near Curie temperature in ferroelectric phase of crystal have essential temperature dependence. But correct analytical analysis of wave surface deformation by simultaneous influence of electric and temperature field near point of phase transition has essential difficulties. Let us estimate the focusing properties of ferroelectric crystals on the base of experimental data about physical constants of widely used crystal $NaNO_2$, for example, near Curie temperature.

How it follows from (3), decreasing of gyrotropy parameter G near Curie point Tc leads to strenthening of concavity of the wave vector surface for slow waves. Calculation that coefficient of thermostrenthening of concavity of wave vector surface $\Gamma = p_-(T) / p_-(T_n)$, where $T_n = 20$ °, for $NaNO_2$ by T=140^o achieves 1.3. Considered peculiarities of electrooptic interaction in lower symmetrical ferroelectric crystals may be used for creating of crystalline lenses. If divergent Gaussian beam falls into the crystal, in accordance with results of [2], the beam is focusing twice: into and out of the crystal on the distance $F_1 = -Z_1 n_o/p_-$ and $F_2 = -(Z_1 + Lp/n_o)$ from its entrance correspondently. Here Z_1 is distance from the weak point of entrance beam to crystal with the L length. Then, changes of focus length by variation of p_- are determined by correlations $F_1 = Z_1 n \Delta p / p_-^2$, $F_2 = L\Delta p_-^n/n$ and near Curie temperature may be great. For example, for $NaNO_2$ crystal $F_2 \sim 89$ cm by change of temperature from $T_n = 20$ ° to T=140^o and L=1 cm.

3. Conclusions

In this paper, it is shown that electrooptic interaction in ferroelectric lower symmetrical biaxial crystals may be used for creation of electro- and thermocontrolled crystalline lenses for which one can achieve slow thermochanges of focus length in wide range and fast changes of it by electric field. If the temperature is near Curie point the range of changes of focus length increases abruptly, but the aperture of proposed lenses decreases. By this, it is necessary to thermocontrol of crystalline model. Thus, while creating such elements you must conduct parameter optimization.

References

[1] A. G. Khatkevich and S. N. Kurilkina, *J. Appl. Spectrosc.*, Vol. 51, No. 6, p. 1005, 1989.
[2] A. M. Goncharenko, V. N. Belyi, S. N. Kurilkina S.N., *et al.*, *Opt. and Spectrosc.*, Vol. 78, No. 5, p. 872, 1995.
[3] V. N. Belyi,N. S. Kazak, S. N. Kurilkina, and N. A. Khili, *Opt. and Spectrosc.*, Vol. 83, No. 3, p. 393, 1997.
[4] A. G. Khatkevich and S. N. Kurilkina, *J. Appl. Spectrosc.*, Vol. 54, No. 5, p. 815, 1991.
[5] Ph. I. Phedorov, *Theory of Gyrotropy*. Mn., p. 468, 1976.
[6] Yu. I. Sirotin and M. P. Shaskol'skaya, *Principles of Crystallophysics*. M., p. 680, 1975.
[7] *Physics of Ferroelectric Phenomena,* G.A. Smosenskii (Ed.). M., p. 396, 1985.
[8] I. S. Rez, *Achievements of Physical Sciences*, Vol. 93, No. 4, p. 633, 1967.
[9] M.– J. Chern and R. A. Phillips, *J. Opt. Soc. Amer.*, Vol. 60, No. 9, p. 1230, 1970.
[10] M.–J. Chern and R. A. Phillips, *J. Appl. Phys.*, Vol. 43, No. 2, p. 496, 1972.

Resonant Magnon-Phonon Polaritons in a Ferrimagnet

I. E. Chupis and A. A. Mischenko

B.Verkin Institute for Low Temperature Physics &Engineering
National Academy of Sciences of Ukraine;47 Lenin Ave.,
61164 Kharkov, Ukraine; E-mail: chupis@ilt.kharkov.ua

Abstract

The influence of a dynamic magnetoelectric interaction on TE and TM polaritons in a ferrimagnet in IR region of the spectrum has been considered. Frequency dispersions of dielectric and magnetic tensors were taken into account. Spontaneous magnetization induces an electric gyrotropy in a ferrimagnet and the additional radiant TM mode. In the presence of a constant electric field the possibility of a resonant interaction and transformation of the TM polaritons into the TE one and vice versa was predicted.

1. Introduction

In a magnet with more than one magnetic sublattice the exchange spin mode may be in the same IR region of the spectrum where there is an optical phonon mode. In this case it is necessary to take into account the frequency dispersions of dielectric and magnetic tensors simultaneously. This situation was considered for polaritons in the cases when resonant (antiresonant) frequencies of dielectric and magnetic tensors are equal [1]. The appearance of the anomalous dispersion in the polariton spectrum was predicted.

We have considered the TE and the TM polaritons in a ferrimagnet in IR region of the spectrum in the cases of the different relations between the resonant and antiresonant frequencies of dielectric and magnetic tensors. The influence of a dynamic magnetoelectric (ME) interaction on TE and TM polaritons in a ferrimagnet was analyzed.

2. Energy and susceptibilities

For the example we consider a uniaxial ferrimagnet (z is an easy axis) with equilibrium antiparallel magnetic moments $\vec{M}_{10}, \vec{M}_{20}$ directed along z-axis, $M_{10} > M_{20}$. The density of the energy consists of a magnetic energy, electric dipole energy and the ME energy:

$$W = \Delta(\vec{M}_1\vec{M}_2) - \vec{h}(\vec{M}_1 + \vec{M}_2) + \frac{C_1}{2}P_z^2 + \frac{C_2}{2}(P_x^2 + P_y^2) - \vec{P}(\vec{E}_0 + \vec{e}) + \frac{1}{2\rho}\vec{\Pi}^2 + \frac{1}{c\rho}\vec{P}[\vec{\Pi}\times\vec{B}] \quad (1)$$

where $\vec{P}$ is the electric polarization, $\vec{\Pi}$ is the momentum density, $\vec{E}_0$ is a constant electric field, $\vec{e}$ and $\vec{h}$ are alternating electric and magnetic fields; $\rho = m/V_0$, m is the ion mass, V_0 is the volume of elementary cell; c is the velocity of light. Magnetic energy (two first terms) is written in exchange approximation, $\Delta > 0$ is the exchange constant. The last term in (1) is the dynamic ME energy [2].It is

the energy of the interaction of $\vec{P}$ with an effective electric field $E_{ef} = -(1/c)[\vec{v} \times \vec{B}]$ produced by the motion of charge e with velocity $\vec{v}$ in the media with magnetic induction $\vec{B} = \vec{h} + 4\pi(\vec{M}_1 + \vec{M}_2)$.

In the presence of a spontaneous magnetic moment $m = M_{10} - M_{20}$ the ME interaction induces the nondiagonal component of a dielectric tensor ε_{xy} and the precession of polarization around the direction of magnetic field. We obtain:

$$\varepsilon_{xx} = \varepsilon_{yy} = \varepsilon_1 = \frac{(\Omega_1^2 - \omega^2)(\Omega_2^2 - \omega^2)}{(\omega_1^2 - \omega^2)(\omega_2^2 - \omega^2)}, \quad \omega_{1,2} = \omega_t \mp \omega_m, \omega_m = 4\pi g m_0, g = e/mc,$$

$$\varepsilon_{xy} = i\varepsilon' = -\frac{i8\pi\omega\omega_m \overline{\omega}_0^2}{(\omega_1^2 - \omega^2)(\omega_2^2 - \omega^2)} \tag{2}$$

$$\varepsilon_{zz} = \varepsilon_2 = \frac{\Omega_e^2 - \omega^2}{\omega_e^2 - \omega^2}, \quad \Omega_e^2 = \omega_e^2 + 4\pi\omega_e^2$$

with

$$\Omega_{1,2}^2 = \omega_t^2 + 2\pi\overline{\omega}_0^2 + \omega_m^2 \mp 2\sqrt{\pi^2\overline{\omega}_0^4 + \omega_m^2(\omega_t^2 + 2\pi\overline{\omega}_0^2)}$$

$$\omega_t{}^2 = C_2\overline{\omega}_0^2, \omega_e^2 = C_1\overline{\omega}_0^2, \overline{\omega}_0^2 = e^2/mV_0$$

Here ω_e is the excitation frequency of P_z, and ω_t is the excitation frequency of the P_x, P_y in the absence of a spontaneous magnetization. In IR region of the spectrum the expressions for the components of a magnetic tensor are following

$$\mu_{xx} = \mu_{yy} = \mu \cong \frac{\Omega_0^2 - \omega^2}{\omega_0^2 - \omega^2}$$

$$\mu_{xy} = i\mu' \cong \frac{i\omega_f(\Omega^2 - \omega^2)}{\omega(\omega_0^2 - \omega^2)} \tag{3}$$

$$\mu_{zz} = 1$$

with

$$\Omega_0^2 = \omega_0^2 + 4\pi\Delta M_{10}M_{20}(g_1 - g_2)^2, \omega_0 = \Delta(g_2M_{10} - g_1M_{20})$$

$$\Omega^2 = 4\pi\Delta g_1 g_2 m_0^2 \omega_0 \omega_f^{-1}, \omega_f 4\pi(g_1M_{10} - g_2M_{20})$$

where ω_0 is the exchange frequency, $g_{1,2}$ is the gyromagnetic relations for electron magnetic moments. The gyromagnetic relation for ion $g << g_{1,2}$. We consider the exchange constant $\Delta >> 1$. Thus, we have that $\omega_m << \omega_f << \omega_0 \sim \omega_t$. The relations $\varepsilon'/\varepsilon_1 \sim 4\pi\omega_m/\omega_t << 1$, $|\mu'/\mu| \sim \omega_f/\omega_0 \sim 4\pi/\Delta << 1$.

In the presence of a constant electric field $\vec{E}_o$ directed along x-axis the ME susceptibilities X_{xy}^{em} and $X_{xx}^{em} << X_{xy}^{em}$ appear, where

$$X_{xy}^{em} = \frac{\partial P_x}{\partial h_y} \cong \frac{igE_0\omega}{C_1(\omega^2 - \omega_t^2)} = \frac{i}{4\pi}\gamma \tag{4}$$

3. Phonon and magnon polaritons

We solve the Maxwell equations for the ferrimagnet with the dielectric, magnetic and ME tensors (2-4) for waves propagating in the direction of the x-axis ($k = k_x$)

In the absence of a constant electric field ($X^{em} = 0$) the TE and TM polaritons are independent.

In TM polariton wave e_x, e_y and h_z are not zero. The spectrum is described by the relation (see Fig.1)

$$\begin{aligned} k^2 &= \omega^2 c^{-2}(\omega^2 - \tilde{\omega}_1^2)(\omega^2 - \tilde{\omega}_2^2)(\omega^2 - \Omega_1^2)^{-1}(\omega^2 - \Omega_2^2) \\ \tilde{\omega}_{1,2} &= \Omega_t \mp \omega_m, \Omega_t^2 = \omega_t^2 + 4\pi\overline{\omega}_0^2 \end{aligned} \tag{5}$$

The frequencies $\tilde{\omega}_2, \Omega_2, \tilde{\omega}_1$ are closed one to another because $(\tilde{\omega}_2 - \Omega_2) \sim (\Omega_2 - \tilde{\omega}_1) \sim \omega_m$. In the absence of a magnetization $\tilde{\omega}_2 = \tilde{\omega}_1 = \Omega_2$ and there are two modes of TM polaritons. Thus, the ME interaction adds the new mode. This mode is a radiant one because of the possibility of a resonance interaction of this mode with the electromagnetic mode $\omega = ck$ (see Fig. 1).

In the TE polariton wave, h_x, h_y and e_z are not zero. The dispersion relation is

$$k^2 = \omega^2 c^{-2}\varepsilon_2\mu^{-1}(\mu^2 - \mu'^2) \tag{6}$$

The spectrum consists of the three modes, which are similar to the shown one in figure 1. But these modes are not closed one to another. The value of the wave vector $k = 0$ if $\omega = \Omega_e$ and $\omega = \overline{\omega} = \Omega_0 + \omega_f(2\Omega_0^2)^{-1}(\Omega^2 - \Omega_0^2) \cong \Omega_0$. The wave vector $k \to \infty$ if $\omega = \Omega_0$ and $\omega = \omega_e$. The view of the polariton spectrum is the same as one in figure 1 but the disposition of the frequencies on the axis depends on the values of $\omega_e, \Omega_e, \omega_0$ and Ω_0. In the case when the phonon frequency ω_e is in the interval $[\omega_0, \Omega_0]$ the middle mode is the mode with anomaly dispersion. It exist in the interval $[\overline{\omega}, \Omega_0]$. So $\Omega_0 - \omega_0 \sim \omega_f$ in this case $\omega_e \cong \omega_0$.

4. Resonance of TE and TM polaritons

So the TM and TE modes belong to IR region of the spectrum the possibility of their crossover exists. For example, the intersection of the middle mode of the TE (TM) polaritons with another TM (TE) modes is possible. The exchange magnon frequency is often less than the mode of an optical phonon. Besides in a uniaxial crystal the value of ω_t is more than the value of ω_e. Then in the case when $\Omega_0 < \omega_e < \omega_1$ the crossover of the lower TM mode (Fig.1) with the middle TE mode is possible (the dashed curves in Fig. 2). Without a constant electric field the TE and TM modes do not interact.

In the presence of electric field $\vec{E}_0$ directed along the magnetization the interaction between the TE and TM polaritons appear due to the ME susceptibility (4). In the TM polaritons the fields h_x, h_y, e_z appear which are proportional to the small ME constant γ. So, we have

$$e_z = -\frac{\gamma[\varepsilon'\mu' + \mu(\varepsilon_1 - \nu^2)](\varepsilon')^{-1}}{\varepsilon_2(\mu^2 - \mu'^2) - \mu\nu^2} h_z, \quad \nu = ck/\omega \tag{7}$$

In the TE polariton excitations the weak fields e_x, e_y, h_z are induced by electric field. These additional fields are small far from the resonance of the modes. The resonance frequency ω_R is determined by the equation

$$\varepsilon_1\varepsilon_2\mu(\mu^2 - \mu'^2) = \varepsilon_1^2 - \varepsilon'^2 \tag{8}$$

Near the crossover the values of the additional fields in the modes increase (the dominator in (7) becomes a small) and the resonance interaction between the TE and TM polaritons takes place (Fig. 2). Thus, the resonance transformation of the TE(TM) polaritons into the TM (TE) one may be realized in the constant electric field.

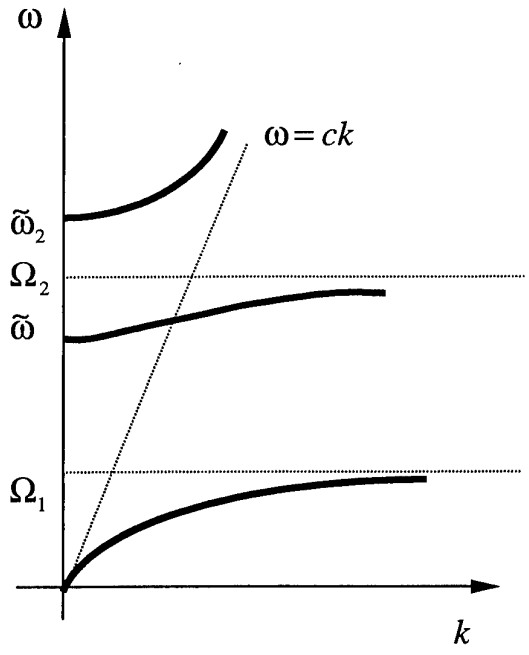

Fig. 1

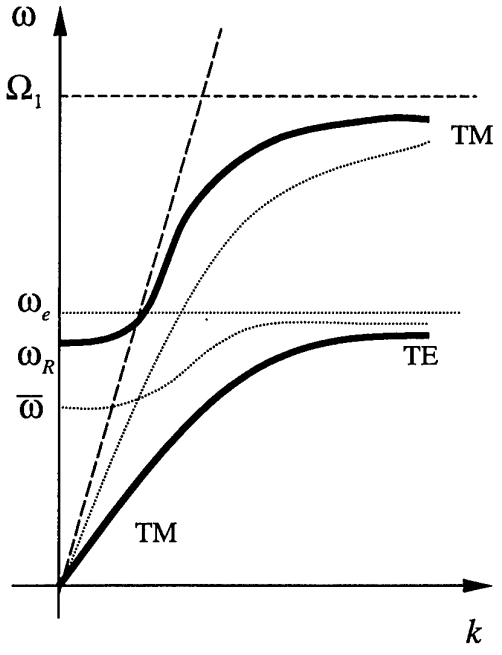

Fig. 2

References

[1] M. I. Kaganov, N. B. Pustyl'nik, and T. I. Schalaeva, *Usp. Fiz. Nauk, No.* 167, p. 191, 1997.
[2] I. E. Chupis, *Ferroelectrics*, No. 204, p. 173, 1997.

Charge-Carrier Drift Influence on the Electroacoustic Interactions in Piezoelectric Semiconductors with Induced Chiral Properties

S. A. Khakhomov

Department of General Physics, Gomel State University
Sovyetskaya Str. 104, 246019, Gomel, Belarus
Fax: + 3-75-232-576557; email: khakh@gsu.unibel.by

Abstract

Effects of charge-carrier drift on the electroacoustic interactions in piezoelectric semiconductors with spatial dispersion and induced chiral properties is studied. The wave numbers and ellipticities of eigenmodes of acoustic waves are found and effects of charge-carrier drift are investigated. Boundary-value problem for a slab under rotating electric field influence is solved.

1. Introduction

In the literature, electroacoustic interactions in media having dielectric and conducting properties are well known. A possibility to control acoustic wave polarization by electric field inducing artificial spiral anisotropy was shown by Belyi and Sevruk [1]. The availability of charge carriers in semiconductors allows to influence on the character of interaction of acoustic waves with external electric fields. Charge carriers interact with the electric field of waves in crystal. The character of interaction can be changed by external constant electric field with strength $\mathbf{E}'$. Under the action of this field, the electrons in a crystal start moving. Their averaged motion is described as electron drift with the velocity $\mathbf{v}_0 = -\mu\mathbf{E}'$, where μ is the electron mobility in the crystal. The objective of this study is to take into account a complex of various effects, i.e., the charge-carrier drift influence on the electroacoustic interaction in piezoelectric semiconductors with induced chiral properties and spatial dispersion. Below, we report the results of the study of electroacoustic interactions in piezoelectric semiconductors with spatial dispersion in rotating electric fields with due regard for the charge-carrier drift influence.

2. Theory and Discussion

Rotating bias electric field can be created by the electrodes which are placed on the wall of a waveguide [2]. The phase shift between the fields in electrode pairs is determined by the number of electrodes, and for the case two pairs of electrodes is $\frac{\pi}{2}$. We assume that the electric field rotates around the x axis and the incident wave propagates also along the same x axis. In practice, the change of the elastic constant of media under external electric field influence can reach 10 per cent. Acoustic properties of a semiconductor crystal (without a center of symmetry) which is placed into a rotating electric field can be described by the following constitutive relations taking into account spatial dispersion and piezoelectric effect [2]:

$$\sigma = c\gamma + b\frac{\partial\gamma}{\partial x} + g\mathbf{E}_0\varepsilon_0\varepsilon\mathbf{E}, \qquad \mathbf{D} = \varepsilon_0\varepsilon\mathbf{E} - \varepsilon_0\varepsilon g\mathbf{E}_0\gamma. \tag{1}$$

Here σ, γ, c, and b are tensors of tensions, deformations, elastic constants and acoustic gyration, respectively (scalar multiplication of tensors is implied). g is a tensor of rank four, $g\mathbf{E}_0$ is tensor of rank three, taking into account piezoelectric effect induced by the rotating electric field, ε_0 is the electric constant, ε is the relative permittivity of the medium. Electric field of propagating wave $\mathbf{E}$ consists of two components:

$$\mathbf{E} = \mathbf{E}_1 + \mathbf{E}', \tag{2}$$

where $\mathbf{E}_1$ is the longitudinal electric field created by piezoelectric effect, and $\mathbf{E}'$ is the external constant longitudinal electric field. $\mathbf{E}_0$ is the strength vector of the rotating electric field. The equation for the current density should contain terms that take into account the interaction of acoustic wave with external longitudinal electric field:

$$\mathbf{j} = -e(N_0 + n)(\mathbf{v}_0 + \mathbf{v}) \approx -eN_0 - eN_0\mathbf{v}_0 - en\mathbf{v}_0, \tag{3}$$

where n is the change in electron concentration induced by the acoustic wave, e is the unit charge. Electron velocity is $\mathbf{v}_0 + \mathbf{v}$, where $\mathbf{v}_0$ is velocity component due to the drift in bias electric field $\mathbf{E}'$, and N_0 is the equilibrium carrier concentration. In accordance to [2], the solution to the equation of elastic wave propagation is sought in the form of coupled plane monochromatic waves:

$$\mathbf{u} = [A_+\mathbf{n}_+e^{-i(\omega-\Omega)t} + A_-\mathbf{n}_-e^{-i(\omega+\Omega)t}]e^{ik(\omega)x} \tag{4}$$

having equal wavenumbers $k(\omega)$, different frequencies $\omega \pm \Omega$ and opposite circular polarizations described by vectors $\mathbf{n}_\pm = (\mathbf{y}_0 \mp i\mathbf{z}_0)/\sqrt{2}$, where $\mathbf{y}_0$ and $\mathbf{z}_0$ are the unit vectors of the Cartesian coordinate system. Here ω_0 is the incident acoustic wave frequency, Ω is the rotating electric field frequency, and $\omega = \omega_0 - \Omega$. As a result, we can arrive at the system of equations for the amplitudes which allows to determine the wavenumbers and ellipticities of eigenmodes. We have considered the case when on the crystal border $x = 0$ circularly polarized acoustic wave

$$\mathbf{u}_e = u_0\mathbf{n}_- \exp[-i\omega_0 t] \tag{5}$$

with frequency $\omega_0 \approx \Omega$ is incident. Displacement vector of this acoustic wave has the same rotation direction as the external electric field. This wave can interact in resonance with rotating electric field because its frequency is near to the rotation frequency of the anisotropy structure formed by the electric field. As a result of interaction of propagating wave with rotating electric field in crystal amplification of the transmitted wave and generation of reverse wave are possible [1, 2]. The displacement vectors of these waves on the crystal borders ($x = 0$ and $x = L$, L is the crystal thickness) can be described as follows:

$$\mathbf{u}_\tau = u_\tau\mathbf{n}_- \exp[-i\omega_0 t + ik_0 L], \quad \mathbf{u}_c = u_c\mathbf{n}_+ \exp[-i(\omega_0 - 2\Omega)t]. \tag{6}$$

Acoustic field in the crystal can be represented in the form of a superposition of two eigenmodes:

$$\mathbf{u} = \sum_{m=1}^{2} A_m \left(\mathbf{n}_-e^{-i\omega_0 t} + \xi_m^{-1}(\omega_0 - \Omega)\mathbf{n}_+e^{-i(\omega_0-2\Omega)t} \right) e^{ik_m(\omega_0-\Omega)x} \tag{7}$$

where $\xi_m = \frac{A_-}{A_+}$ is the ratio of the amplitudes of eigenwaves.

¿From the condition of continuity of the displacement vectors on the crystal borders we can obtain system of the following equations:

$$\sum_{m=1}^{2} A_m = u_0, \quad \sum_{m=1}^{2} A_m\xi_m^{-1}(\omega_0 - \Omega)e^{ik_m(\omega_0-\Omega)L} = 0,$$

$$\sum_{m=1}^{2} A_m e^{ik_m(\omega_0-\Omega)L} = u_\tau e^{ik_0 L}, \quad \sum_{m=1}^{2} A_m\xi_m^{-1}(\omega_0 - \Omega) = u_c. \tag{8}$$

The solution of this system allows to determine the amplitudes of reflected and transmitted acoustic waves.

3. Numerical results

Calculations have been made with the following values of parameters [2]: $m^* = 0.0145\ m_e$ (m_e is the electron mass), $\Omega = 10^9$ radn/s, $\nu = 10^{13}\ \mathrm{s}^{-1}$, $T = 300$ K, $c = 10^{11}\ \mathrm{N/m^2}$, $\rho = 5.7{\cdot}10^3\ \mathrm{kg/m^3}$, $\beta = 10^{-2}$, $b = 14.4$ N/m. The dependence of the wavenumbers of eigenmodes on the frequency is presented in Figure 1 (left). ¿From Figure 1(left) we can see that charge-carrier drift influence is displayed as a shift of diagrams. The dependence of the intensity of the transmitted waves normalized to the intensity of the incident waves (transmission coefficients) on the frequency is presented in Figure 1 (right). Analysis of numerical results leads us to the conclusion that charge-carrier drift influence can be a cause of a shift of the maximum of the transmission coefficients. The direction of the shift depends on the direction of carrier drift. When charge-carrier drift direction coincides with the incident wave propagation direction we can see an increase of the transmission coefficient. This effect can be explained by interaction of acoustic wave and electron "clouds". When charge-carrier drift direction is the opposite to the incident wave propagation direction we can see a shift of maxima of the transmission coefficient to the lower frequency region. The dependence of the intensity of the reflected waves as functions of the crystal thickness is presented in Figure 2 (left) in the logarithmic scale (the basis of logarithm is 10). When the crystal thickness L corresponds to the resonance condition [2], the reflection coefficients have periodic resonances. Spatial dispersion influence can be a cause of a decrease of the crystal thickness corresponding to maxima of the reflection coefficients. The influence of electron drift on the changing of the crystal thickness corresponding to maximum of reflection coefficients is much smaller than the spatial dispersion influence. Rotation of the polarization plane dependence on the incident wave frequency is presented in Figure 2 (right). The influence of charge-carrier drift exhibits as a change of the angle of rotation of the polarization plane in the case of resonant interaction. Charge-carrier drift influence leads to a shift of diagrams, and the relative change of the maximal rotation power can reach 2. Natural acoustic activity is comparable with the chiral properties of crystal induced by rotating electric fields.

4. Conclusion

Wave numbers and ellipticities of acoustic eigenmodes in semiconductors without a center of symmetry which are placed into rotating electric field have been found. So called *two-wave approximation* has been used to find the solution of the boundary-value problem. The transmission and reflection coefficients dependence on the incident wave frequency and crystal thickness have been studied. Found characteristics of transmitted and reflected waves have been compared with the results for semiconductors with spatial dispersion without charge-carrier drifts. The obtained results can be used for the design of devices that can rotate the polarization plane of ultrasound [3].

References

[1] V. N. Belyi, and B. B. Sevruk, "Control of polarization of acoustic waves by the electric field inducing spiral anisotropy," *Akust. Zhurnal*, vol. 57(2), pp. 157–161, 1983.

[2] I. V. Semchenko and S. A. Khakhomov, *Spatial Acoustic Waves in Crystals in the Rotating Electric Field.* Belaruskaya navuka, Minsk, 1998

[3] I. V. Semchenko, A. N. Serdyukov, S. A. Khakhomov, "The method and device for rotation of polarization plane of ultrasound waves," in *Patent of Russian Federation*, No 2123895, *Inventions*, No 36, Appl. 27.07.94, Publ. 27.12.98.

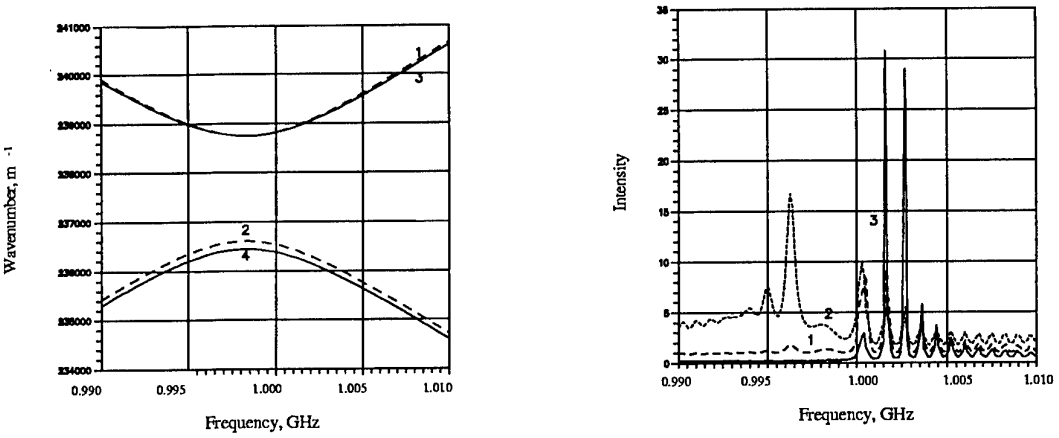

Figure 1: left)The wavenumbers of eigenmodes as functions of the frequency. Dashed lines (1 $-k_1$, 2 $-k_2$) correspond to the crystal without charge-carrier drifts, and solid lines (3 $-k_1$, 4 $-k_2$) correspond to the crystal with a charge-carrier drift; right) The intensity of the transmitted wave as a function of the frequency. 1 corresponds to the intensity of the transmitted wave without charge-carrier drift; 2 corresponds to the intensity of the transmitted wave taking into account charge-carrier drift ($v_0 = -10v_t$); 3 corresponds to the intensity of the transmitted wave taking into account charge-carrier drift ($v_0 = 10v_t$).

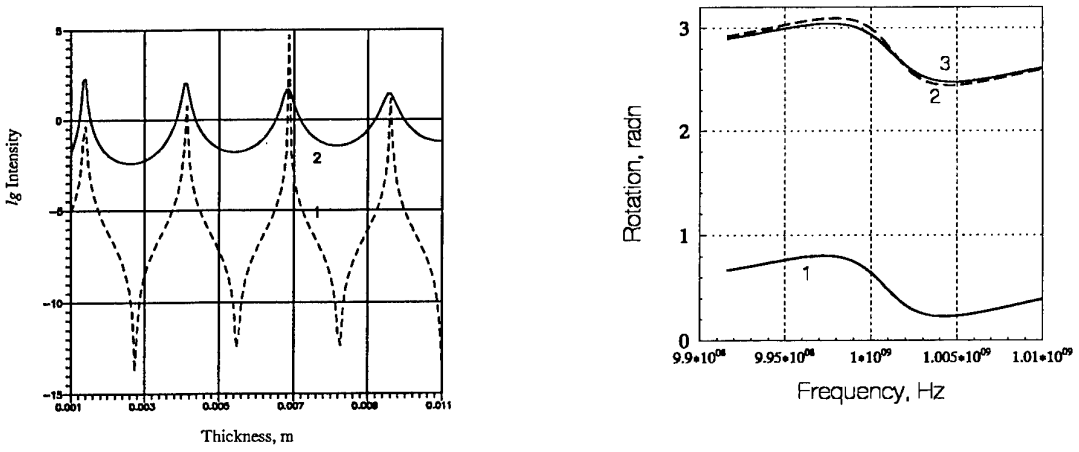

Figure 2: left) The intensity of the reflected waves as a function of the crystal thickness. 1 corresponds to the intensity of the reflected wave without charge-carrier drifts, and 2 corresponds to the intensity of the reflected wave taking into account charge-carrier drift ($v_0 = \pm 10v_t$); right) Rotation of the polarization plane dependence on the incident wave frequency ω: 1 corresponds to the crystal with the charge-carrier drift direction which is opposite to the incident wave propagation direction; 2 corresponds to the crystal with charge-carrier drift direction which coincides with the incident wave propagation direction; 3 corresponds to the crystal without charge-carrier drift.

Polarization State Transformation of Laser Beam Passing Through Quartz Crystals

I. T. Bodnar and M. P Anatska

Institute of Solid State and Semiconductors Physics of
National Academy of Belarus, P.Brovki str.17
220072, Belarus,
Fax: +351-172-84-08-88, E-mail: ivetta@ifttp.bas-net.by

Abstract

Periodical changing of laser beam polarization with initial polarization of 45°to the optical axis of quartz after its passing through quartz cube depends on crystallographic direction and turn angle of the cube. The resulting polarization is different for quartz with impurity of Co and without any impurity especially for direction parallel to the optical axis. Some peculiarities in the modulation pictures take place at initial polarization of laser beam + 45° or -45° to the optical axis of quartz. It is supposed that observed features in polarization of laser beam can be connected with anisotropy of crystal.

1. Introduction

Light polarization is very intricate area in optics. Polarization appearances are not quite the same for coherent and incoherent sources of light. It is known that many crystals change polarization of light, which passes through them. The study of these changing even for incoherent sources of light is very complicated problem. The use of lasers results in obtaining new information about interaction radiation and matter. We believe that the investigations of the state of polarization of laser beam after its passing through quartz single crystals are very interesting and useful not only for creation different optical devices but for obtaining new data about properties of crystals and coherent radiation.

According to Stocks [1] there are six basic states of polarization: horizontal linear polarization and vertical linear polarization, linear polarization under ± 45° and at last two kinds of elliptical polarization, right and left.. The polarization under angles ±45°to the optical axis is worthy the especial interest as far as it gives possibility to get almost 100% modulation of the laser beam intensity after its passing through the crystal and in dependence on the turn angle of the sample [2-4].

2. Experimental

The aim of the present work is to obtain the influence of Co impurity in quartz on the polarization of the laser beam passing through the quartz cube under various angles. The polarization of laser beam after passing through the crystal depends also on the initial polarization of laser beam (±45°) [1] that falls onto the sample and presence of impurity. Two kinds of quartz were measured: colorless quartz without impurity and slightly blue quartz with impurity of Co. The samples were prepared in form of cubes with high accuracy. One of the edges of cube was parallel to the optical axis of quartz. All measured single crystals were quite transparent and had high quality.

In our experiment the narrow laser beam was directed to the center of the quartz cube facet. The cube was placed between crossed polarizers on the table of goniometer. The sample can be rotated clockwise, counterclockwise, and also from position of normal incidence cloclwise (conditionally negative angles) and then counterclockwise (conditionally positive angles). The turn angle was measured with 5″ precision.

He-Ne was used as a source of light. The Bruster window of the laser tube was turned so that the laser beam was polarized under angle 45° to the optical axis of quartz.

3. Results and Discussion

It was obtained that the modulation of the laser beam intensity is connected with changing of the state polarization of light and takes place upon the sample rotation. During one period the polarization transforms from one linear polarization, for example -45°, to another linear polarization, +45°, passing through all forms of the elliptical polarization. Period of modulation depends on such factors as crystallographic direction, presence of impurity and initial polarization of laser beam.

The intensity modulation of laser beam after its passing through the cube made from colorless quartz in direction parallel to the optical axis at normal falling of the beam onto the cube face is shown in Fig. 1-a).

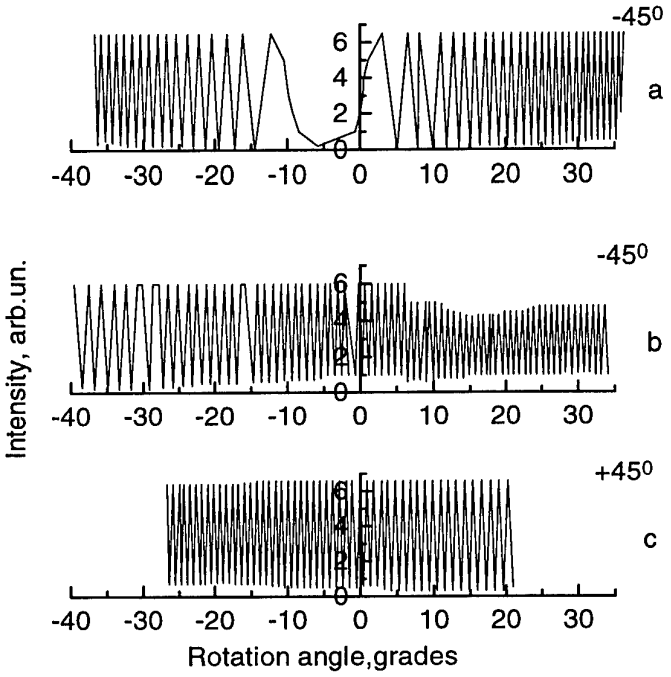

Fig. 1 Modulation pictures for laser beam passing normally to the optical axis for two kinds of quartz: a) Colorless quartz without impurity; b) and c) Belongs to two different samples with the same sizes which made from one piece of blue quartz with impurity of Co. Fig. 1-b) and 1-c) belong also to two different states of polarization of laser beam.

As one can see from the figure that the modulation period decreases to the side of the greater angles of falling and its minimum is equal ~ 50″, and its maximum value is equal ~ 3° without central part. The central part consists of two maximums with elliptical polarization and minimum between them with period ~ 15°. The polarization of next maximums and minimums corresponds to the linear polarization -45° and +45° accordingly.

The modulation period for blue quartz is changed in another way than for colorless quartz. The central part of each picture is wholly occupied with the small period (40 - 45″) maximums. One can say that central minimum with large period is absent for blue quartz. That is the difference between the modulation pictures for colorless quartz and blue quartz with impurity of Co. We would like to notice that transformation of the one linear polarization to another orthogonal one which is accompanied by the turn of electrical vector at 90°, takes place at the turn angle of the sample ~20-25″ when the period of modulation is equal to 40 -50″.

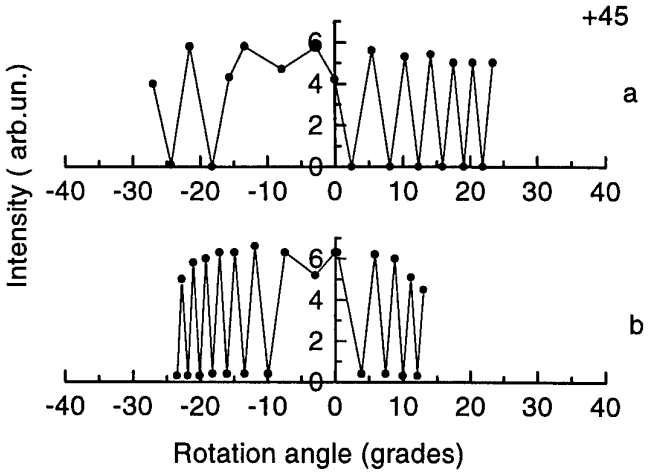

Fig. 2 The intensity modulation of laser beam after its passing through the two different pairs of parallel facets of cube made from blue quartz in direction perpendicular to the optical axis of quartz.

Fig. 1-b) and Fig. 1-c) differ with the different initial polarization of the laser beam what is falling onto the facet of crystal. The period of the intensity modulation decreases from conditionally negative angles towards the conditionally positive angles for the case depicted on Fig. 1-b) from 1,5° to ~ 30″. The same period increases from conditionally negative angles to conditionally positive ones for the second case with another initial polarization, Fig. 1-c).

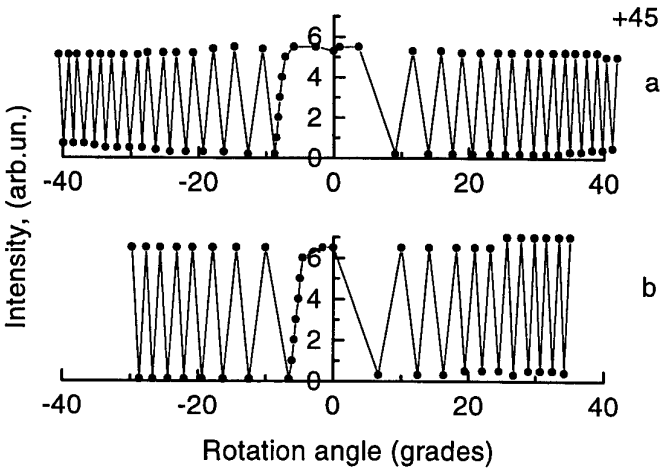

Fig. 3 The intensity modulation of laser beam after its passing through the two different pairs of parallel facets of cube made from colorless quartz in direction perpendicular to the optical axis of quartz.

Such modulation of intensity cannot be observed when the electrical vector of laser beam was parallel or perpendicular to the optical axis of quartz. It cannot be observed too when other non-laser sources of light are used, for example, mercury lamp.

As it is shown in Fig. 2 there is some difference between the two modulation pictures when laser beam passing in directions perpendicular to the optical axis for blue quartz. Here we can see central maximum with large period which is absent for the direction parallel to the optical axis for this sample and for this polarization shown in Fig. 1-c).

The difference between the two modulation pictures for the directions perpendicular to the optical axis is greater for blue quartz in comparison with colorless quartz for the same initial polarization. We believe that this difference is connected with anisotropy in atoms' location in lattice of quartz.

There is some difference between the modulation pictures obtained for some pair of parallel facets of one and the same sample but for different polarization of laser beam falling onto the facet of the cube. It can be difference in period of modulation, in the position of central part of the picture and in the intensity of radiation.

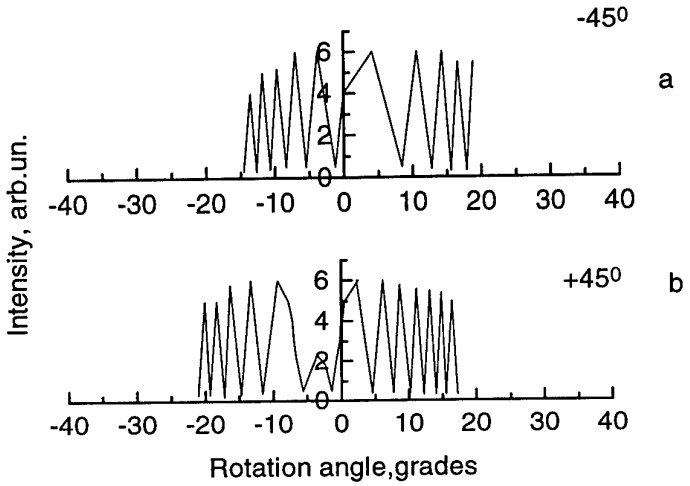

Fig. 4 The intensity modulation of laser beam after its passing through the cube made from blue quartz with impurity of Co in direction perpendicular to the optical axis for one and the same pair of facets but for different polarization of the falling beam.

4. Conclusions

Partly the picture of intensity modulation can be explained with interaction of the two orthogonal polarized waves, ordinary and extraordinary ones, which go the same way with different rates and amplitudes. This interaction depends on such parameters as birefringence, optical activity and the optical length of the light way. But it can be supposed that the main role in transformation of polarization of laser beam plays the features of structure of the measured crystals.

References

[1] R. E. Raab, *Proc. Bianisotropics' 98*, 7th International Conference on Complex Media 3-6 June 1998, pp. 29-34.

[2] I. T. Bodnar and A. K. Soika, *Opt. & Spectrosc.* (rus.), Vol. 69, pp. 197-199, 1990.

[3] I. T. Bodnar, *Proc. Bianisotropics' 98*, 7th International Conference on Complex Media, 3-6 June 1998, pp. 61-64.

[4] I. T.cBodnar, *Technical Digest*, 18th Congress of the International Commission for Optics, ICO XVIII, 2-6 August 1999, San Francisco, California, pp. 148-149.

Refractive Indices and Some Other Optical Properties of Synthetic Emerald: Temperature Dependence

I. T. Bodnar and G. L. Bychkov

Institute of Solid State and Semiconductors Physics of
National Academy of Sciences, P.Brovki str. 17,
220072 Minsk, Belarus.
Fax: +3755-172-84-08-88, E-mail: ivetta@ifttp.bas-net.by

Abstract

The temperature dependence of the refractive indices for ordinary and extraordinary rays of mercury spectrum three lines and laser line independently one from the other were measured in temperature interval 20-600°,C. It was obtained that the refractive indices increase along with the temperature growth and this dependence has quasilinear character. Emerald has quite low birefringence values that increases slightly along with the temperature growth and decreases with wavelength growth. The thermooptical coefficients for every wavelength were calculated. They have greater values for the extraordinary beams than for the ordinary ones. The dispersion curve for refractive indices was obtained.

1. Introduction

Emerald is a green beryl with the following chemical formula: $Be_3\ Al_2\ Si_6\ O_{18}$ with Cr impurity responsible for its green color. The crystal belongs to the hexagonal system and is optically positive. Si_6O_{18} rings form structure channels, which are parallel to unique axis. Octahedral positions occupied by Al in the beryl structure, may be substituted by Cr, Fe^{3+}, Fe^{2+}, Mg and Li; alcali and alcaline earth ions occupy the centers of Si_6O_{18} rings and water molecules lie centrally between the Si_6O_{18}. The limited amount of Cr is necessary for creation gem quality emerald (0,2 - 0,3%) [1].

The filling of the channels in the beryl structure with alcali ions and water molecules is the main cause of the variation in refractive index and density of natural beryl and emerald.

The increase of activity in the area on synthetic emerald appears to be due both to its utility as a gemstone and its reported use as a solid state maser crystal. Besides emerald can be used in low-noise microwave amplifiers as well as serve as the most effective laser medium in the range 450-600nm.

2. Crystal Growth

Single crystals of emerald were grown from flux melt [2] on oriented seeds in dynamical regime. Double system oxides of lead and vanadium was used as a flux. As numerous experiments on crystal growth in flux melt with correlation V_2O_5 / PbO from 8/2 to 2/8 showed, it is preferably to use solvents with the equal or slightly shifted to the side V_2O_5 ratio of oxides. The cuts of single crystals, grown by the method of spontaneous crystallization, parallel to the natural prism (1 0 $\bar{1}$ 0) and (1 1 $\bar{2}$ 0) faces and pinacoid (0 0 0 1) faces served as seeds. The seeds were arranged parallel each other in the planes oriented perpendicular to the flux melt surface and fixed to specially shaped platinum holders. Such configuration provides continuous washing of the growing crystal face and stirring of the melt at optimal rotation rate 30rs/min. The total area of the seed plates varied from 600mm^2 to

2000mm^2 depending on the crucible volume and the flux melt mass. The optimal experiment cycle lasted, in the average, for 3-4 months. The best single crystals grown in the experiment were almost perfect in terms of the optical parameters weighting as much as 150 carats.

3. Experimental

Refractive indices of the ordinary and extraordinary rays were measured during continuous heating or cooling of prisms cut out from crystals in such a way that the optic axis was parallel to the prism edge and the light beam propagated through the prism perpendicular to the optical axis. The size of prism was nearly 6x6x7x4mm, where 6 and 7mm was the sides of the triangular basis of prism and 4mm was its height. The least deviation method is used. He-Ne laser and a mercury lamp were sources of light. The temperature dependence of the refractive indices of mercury spectrum three lines and laser line independently one from the other was measured. The measurements were performed for the next wavelengths of mercury emission lines: violet, 4647Å; green, 5461Å; yellow, 5852Å and for laser line, 6328Å with a step 4°- 5° using a GS-5 goniometer-spectrometer. The heating (cooling) rate did not exceed 0,5K/min and the sample temperature was measured with a platinum-rhodium thermocouple with an accuracy of 0,1K.

4. Results

Temperature dependences of refractive indices for ordinary and extraordinary rays at different wavelenghts are shown in Fig. 1.

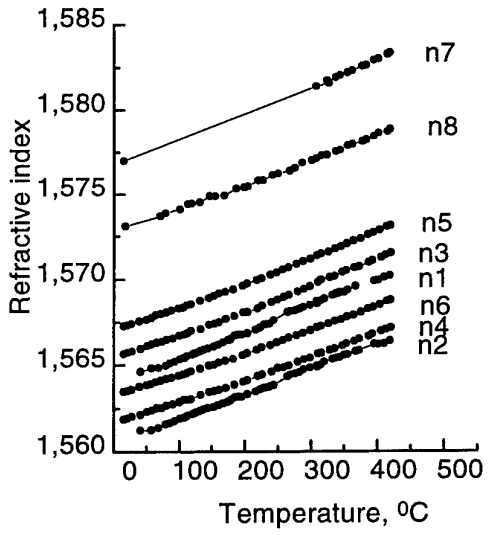

Fig. 1 Temperature dependence of refractive indices of ordinary and extraordinary rays for four different wavelengths. Curve n1 belongs to ordinary rays of red laser line, and curve n2 belongs to extraordinary rays of red laser line; curves n3, n5 and n7 reflect the temperature dependence of refractive indices of ordinary rays for green, yellow and violet lines of mercury spectrum, and curves n4, n6 and n8 are the temperature dependence of refractive indices of extraordinary rays for green, yellow and violet lines of mercury spectrum.

It is obtained that the refractive indices increase along with the temperature growth and this dependence has quasilinear character. Emerald possesses the following refractive indices at the room temperature: for $\lambda = 464,7nm$ $n_e = 1,5770$; $n_o = 1,5731$; for $\lambda = 546,1nm$ $n_e = 1,5673$; $n_o = 1,5635$; for $\lambda = 585,2nm$ $n_e = 1,565,6$; $n_o = 1,5619$; for $\lambda = 632,8nm$ $n_e = 1,5646$; $n_o = 1,5612$, where n_o and n_e - ordinary and extraordinary refractive indices.

We should note that emerald refractive indices just slightly change along with the temperature growth. The temperature dependence curves (images of collimator slit) for all the spectral lines are practically parallel. That means that the thermooptical coefficients are almost the same for all wave lengths of both ordinary and extraordinary rays. They are slightly greater for the extraordinary rays than for the ordinary ones, $1,45 - 1,5 \cdot 10^{-5}$ and $1,2 - 1,4 \cdot 10^{-5}$ accordingly.

Emerald has a very low birefringence value which does not change while temperature grows. Fig. 2 shows the graph of the temperature dependence of the birefringence.

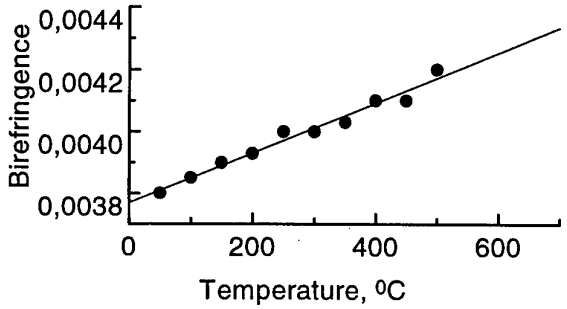

Fig. 2 Temperature dependence of birefringence (n_e-n_o) value, where n_o - refractive index of ordinary rays and n_e- refractive index of extraordinary rays.

The birefringence value does not practically change while the wave length increases, i.e. the birefringence dispersion is absent. At the time the dispersion for refractive indices appears normal because refractive indices decrease along with wave length incease, Fig. 3.

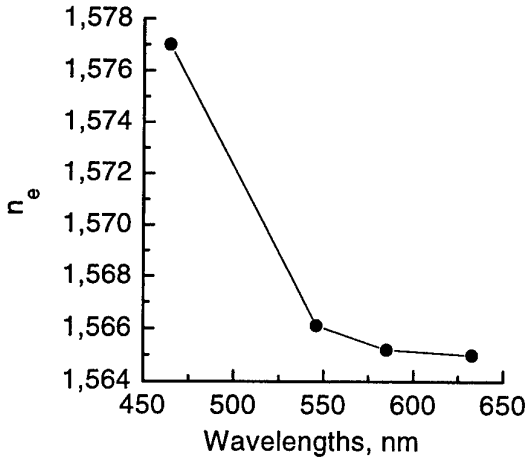

Fig. 3 Dispersion of the extraordinary rays refractive index.

5. Conclusion

We should note that emerald's behaviour is quite similar to one of the inert gases or noble metalls i.e. it does not practically interact with external medium if compared to other crystals such as ferroelectrics, nonlinear crystals, semiconductors and quartz. The slight increase of refractive indices monitored while temperature increases is likely to be caused by the thermal expansion of the lattice.

We believe the main particularity of this crystal is the absence of any particularities in the optical properties measured by us. We can consider that absence as the main positive attraction of emerald upon its employing in dirreferent optical devices as the sinthetical emerald is much cheaper than the natural one.

References

[1] E. M. Flanigen, D. W. Breck, N. R. Mumbach, and A. M. Taylor, "Characteristic of synthetic emeralds," *The American Mineralogist*, Vol. 52, May-June 1967.

[2] S. N. Barilo, G. L. Bychkov, L. A. Kurnevich, N. I. Leonuk, V. P. Mikhailov, S. V. Shiryaev, V. T. Koyava, and T. V. Smirniva, "Controlled crystallization of emerald from the fluxed melt," *Journal of Crystal Growth*, Vol. 198/199, pp. 716 - 722, 1999.

A New Method for Position Location in Random Media

F. A. Pujol, F. J. Ferrández, and J.M. García Chamizo

Departamento de Tecnología Informática y Computación, University of Alicante
P.O. Box 99, 03080 Alicante, Spain
Fax: + 34 96 590 3902; email: {fpujol, fjferran, juanma}@dtic.ua.es

Abstract

The development of wireless communication techniques has increased, as a consequence, the use of positioning systems. Concerning to this, GSM providers have predicted that position location will be an integrated service in the 3rd generation cellular phones. The techniques that are used by each one of the current positioning systems are well-known; they include time-difference-of-arrival measures, angle-of-arrival measures and power-of-arrival measures. In this paper we propose a new method, which is based on the transmission of several frames with different frequencies in order to determine the transmitter/receiver distance.

1. Introduction

Unlike wired communication systems that are static and easily characterized, radio channels are highly random, time varying and difficult to predict. The propagation path in a wireless communication system can vary in real-time from close range, stationary, line of sight to a heavily obstructed mobile path due to both moving and stationary objects [1]. Needless to say, although wireless communication systems share the radio channel as a common limiting factor, the channel can be extremely random in nature [2] and thus plays a major role in the design of many radio frequency communication systems.

One of the new uses of these systems is to provide accurate user position location (PL) information, and that is the reason why several different position location technologies have been developed in the last few years [3]. As it is well-known, the behavior of electromagnetic waves through random media is modified by several factors that appear in the environment [4]. If we know the limiting factors that restrict the propagation of the waves, the medium will be properly characterized and, as a result, a relationship between the propagation velocity and the frequency of transmission will be defined.

In this work, we propose a new method to determine the distance between the transmitter and the receiver by solving a system of non-linear equations, that depends on the physical model of the medium in which the wave is propagated. In Section 2, the theoretical basis of our method is described. Consequently, a system with a transmitter, a microscopic model of the channel and a receiver is simulated in *MATLAB*. The results are shown in Section 3. Finally, some conclusions are remarked in Section 4.

2. Previous Concepts of the Multi-Frequency Model

The propagation of electromagnetic waves depends on internal factors related to its nature and external factors that are characterized by means of the medium in which the wave is propagated. There are

many developments in this field: some measures of the GPS propagation principles can be found in [5], where reception delays due to atmospheric phenomena are estimated. Concerning to this, the ionospheric delays are considered in [6]. In both cases, the delays not only depend on the medium itself, but also on the signal frequency.

Taking into account these studies, a method which uses a multi-frequency technique, that is, the transmission of several frames with different frequencies, is proposed. Let us consider the general relationship:

$$v_i = g(w_i, k_1, \ldots, k_j) \tag{1}$$

where v_i is the propagation velocity and depends on the frequency, g is some function which must be determined, w_i is the frequency, and $k_1,\ldots,k_j$ are the factors related to the medium of propagation. From Eq. (1), the distance between the transmitter and the receiver can be estimated by using a system of non-linear equations [7]. These equations are obtained regarding these assumptions:

- If we suppose that a frame consisting of n frequencies is transmitted, then n equations like the following ones are obtained:

$$\begin{aligned} v_1 \cdot t_1 &= d \\ &\vdots \\ v_n \cdot t_n &= d \end{aligned} \tag{2}$$

  where $t_1,\ldots,t_n$ are the times of arrival for each frequency and d is the distance between the transmitter and the receiver.

- If the time difference of arrival for the different frequencies is calculated, c_i, then we will have $n-1$ equations, where the delay between each one of the frequencies is determined:

$$\begin{aligned} t_1 - t_2 &= c_1 \\ &\vdots \\ t_1 - t_n &= c_{n-1} \end{aligned} \tag{3}$$

- Finally, if we know the relationship between the velocities/frequencies, n equations like these ones can be found:

$$\begin{aligned} v_1 &= g(w_1, k_1, \ldots, k_j) \\ &\vdots \\ v_n &= g(w_n, k_1, \ldots, k_j) \end{aligned} \tag{4}$$

Therefore, the distance d, the n propagation velocities, the n times and the factors that represent the medium must be calculated. We have, then, a system with $3n-1$ equations and $2n+1+j$ unknown quantities, and, as a consequence, $n = j + 2$.

3. Position Location using the Multi-Frequency Model

In a common way, when the transmitter/receiver distance is found out, the equations system to determine the proper position of an object/person can be obtained as:

$$(X_i - R_x)^2 + (Y_i - R_y)^2 + (Z_i - R_z)^2 = d_i^{\,2} \tag{5}$$

where (R_x, R_y, R_z) is the receiver position, (X_i, Y_i, Z_i) are the n transmitters position, and d_i are the distances to each one of the n transmitters.

The parameters of the model that characterizes the medium can vary when the link conditions change. That is the reason why the positioning system will have to update the model in real-time. Following these requirements, a *MATLAB* simulation to calculate the distance in a satellite-earth link has been made. Considering the Drude-Lorentz's model for the ionosphere [8], we have:

$$k_r - 1 = \frac{w_p^2}{w_0^2 - w^2} \tag{6}$$

where k_r is the real part of the dielectric constant of the medium, w_p is the plasma frequency and w_0 is the natural frequency. If the refractive index is $n = \sqrt{k_r}$, the propagation velocity will be:

$$v = g(w, k_1, k_2) = \frac{c}{n} = \frac{c}{\sqrt{1 + \frac{w_p^2}{w_0^2 - w^2}}} \tag{7}$$

When a two-parameter model is used, the equations system will be:

$$\frac{c}{\sqrt{1 + \frac{k_1}{k_2 - w_i^2}}} \cdot t_i = d \tag{8}$$

where $i = 1,2,3,4$. The time differences can be calculated as:

$$\begin{aligned} t_1 - t_2 &= c_1 \\ t_1 - t_3 &= c_2 \\ t_1 - t_4 &= c_3 \end{aligned} \tag{9}$$

We see that the unknown quantities are $[t_1, t_2, t_3, t_4, k_1, k_2, d]$. As a result, we can deduce that the frames must be sent including four frequencies. We have to point out that we have used the Newton's method to solve the non-linear equations system. That is, the starting equations system is:

$$\begin{aligned} & f_1(x_1, x_2, x_3, x_4, x_5) = 0 \\ & \dots \qquad \Rightarrow \qquad \vec{F}(\vec{x}) = \begin{pmatrix} f_1(\vec{x}) \\ \vdots \\ f_7(\vec{x}) \end{pmatrix} = 0 \\ & f_7(x_1, x_2, x_3, x_4, x_5) = 0 \end{aligned} \tag{10}$$

Using the Taylor's expansion of Eq. (10), we obtain:

$$\vec{F}(\vec{x}) \approx \vec{F}(\vec{x}_0) + J(\vec{x}_0) \cdot (\vec{x} - \vec{x}_0) \tag{11}$$

where $J(\vec{x}_0)$ is the Jacobian matrix in the initial point $\vec{x}_0 = [t_{10}, t_{20}, t_{30}, t_{40}, k_{10}, k_{20}, d_0]$.

As a consequence, the following conditions must be considered:

1. A vector with some initial values for the variables of the system must be introduced.

2. After that, the Jacobian matrix $J(\vec{x}_{0(t-1)})$ for the current solution vector $\vec{x}_{0(t-1)}$ is calculated. The new solution vector is determined as:

$$\vec{x}_{ot} = \vec{x}_{0(t-1)} - J^{-1}(\vec{x}_{0(t-1)}) \cdot \vec{F}(\vec{x}_{0(t-1)}) \tag{12}$$

where $J^{-1}(\vec{x}_{0(t-1)})$ is the inverse matrix of $J(\vec{x}_{0(t-1)})$.

3. $\vec{x}_{0t}$ is replaced in $\vec{F}(\vec{x})$ and the error value is obtained. The variation of the error is revised to establish whether the solution is correct or not, and, then, if the algorithm is finished.

Table 1 shows the error in the calculation of the distance, for some different examples.

Distance	***500***	***1000***	***5000***
Two-parameter error	1.2 %	0.1 %	0.01 %

Table 1: Variation of the error and distance

4. Conclusion

In this paper we have explained a new method to reach a complete position location service. We have shown in a theoretical way that scattering phenomena can be used to estimate the transmitter/receiver distance in a radio frequency link. Moreover, any electromagnetic communication in which scattering appears could be considered in the same way. Some of the advantages of this system are, on the one hand, that there are no measures in absolute time and, on the other hand, that it is not necessary to synchronize the receiving antennas (see [7]).

As a future work, we propose to combine this method with a power-of-arrival one so as to avoid the wrong distance estimations. Finally, the design of the whole positioning system, hardware and software, will be considered as well.

References

[1] J. B. Anderson, T. S. Rappaport, and S. Yoshida, "Propagation Measurements and Models for Wireless Communication Channels," *IEEE Communications Magazine*, vol. 32, no. 11, pp. 56-62, November 1994.

[2] S. S. Saunders, *Antennas and Propagation for Wireless Communication Systems*. Chichester, United Kingdom: John Wiley & Sons, 1999.

[3] T. S. Rappaport, J. H. Reed, and B. D. Woerner, "Position Location using Wireless Communications on Highways of the Future", *IEEE Communications Magazine*, vol. 34, no. 10, pp. 33-41, October 1996.

[4] S. Ichitsubo *et al.*, "A Statistical Model for Microcellular Multipath Propagation Environment", in *Proc. of the 47th IEEE Vehicular Technology Conference*, Arizona, USA, May 1997, pp. 61-66.

[5] F. S. Solheim, J. Vivekanandan, R. H. Ware, and C. Rocken, "Propagation Delays induced in GPS Signals by Dry Air, Water Vapor, Hydrometeors, and Other Particulates", *Journal of Geophysical Research*, vol. 104, no. D8, pp. 9663-9670, April 1999.

[6] D .A. Imel, "Evaluation of the TOPEX Dual-Frequency Ionosphere Correction", *Journal of Geophysical Research*, vol. 99, no. C12, pp. 24985-24906, December 1994.

[7] F. J. Ferrández Pastor *et al.*, "Método para la determinación de distancias mediante técnica multifrecuencial", in *Proc. of the Conferencia Internacional de Telecomunicaciones y Electrónica (TELEC'2000)*, Santiago de Cuba, Cuba, Julio 2000.

[8] J. R. Reitz, F. J. Milord, R. W. Christy, *Fundamentos de la Teoría Electromagnética*. Mexico D.F., Mexico: Addison-Wesley Iberoamericana, 1986.

Experimental Studies of the Potentialities of Backscattering Dynamical Spectroscopy for Investigating the Characteristics of Biological Particles with Different Shape and Surface Relief

A. N. Korolevich[1,2)]

1) Departamento de Física, Escola de Ciências, Universidade do Minho, Largo do Paço, 4719 Braga, Portugal. E-mail: akaralevich@fisica.uminho.pt
2) B. I. Stepanov Institute of Physics National Academy of Sciences of Belarus, Scarina Ave., 68, 220072, Minsk, Belarus

Abstract

The attempt is made to extent the applicability of dynamic spectroscopy methods, that are commonly used to investigate media with relatively low concentrations of light scattering particles, for analyzing media with high volume content of scatters where there is established the so-called multiple scattering regime. The whole blood of a person under normal and pathological state is chosen as a model medium. The dependence of characteristics of the spectrum of the temporal fluctuations of light scattered intensity on parameters of particles (the concentration, their shape, absorption coefficient, aggregation degree) is studied. It was found that the fluctuation spectrum of multiply scattered light under high concentrations of scattering particles is mainly influenced by their optical characteristics, rather than by geometrical ones.

1. Introduction

In various fields of science and technology there arise problems associated with the determination or control of the characteristics of small particles: their sizes, shapes, degree of aggregation, concentration.

Applications of methods of the light scattering media optics for solving these problems is based on their high accuracy as well as on the fact that they are not time consuming and do not exert any action on the investigated object. Thus, these methods are most actively used to investigate the characteristics of biological objects in medicine and biophysics.

One of the most important optical methods is the method of the correlation spectroscopy [1]. In contrast to other optical methods, this method is based not on the analysis of the spatial distribution of the scattered radiation field but on the analysis of its temporal fluctuations. In other words, this method is based on the fact that the statistic characteristics of scattered radiation are related to the dynamic characteristics of particles: their sizes, shape, relief of the surface.

In modern practice the method of correlation spectroscopy is successfully used for solving various problems: determination of the diffusion coefficient, drift velocity, dynamics of muscle contractions, sizes and asphericity of particles. However, it should be noted that in all applications of this method the determination of the characteristics of scatters is possible only in the case that the distance between the particles is much greater that their sizes.

There is a sufficiently great number of media with a high concentration of particles. Because of this, the necessity arose for extending the method of correlation spectroscopy to determine the

characteristics of scatters at high concentrations. The advantages of the correlation spectroscopy method make it possible to determine the characteristics of particles without the dilution of the medium, i.e., in their natural state. For a number of media, such as biological, this is the matter of principle.

For the model medium we took the whole blood, i.e., the undiluted blood. First, this is the most important biological medium. Second, its all characteristics are clearly understood. Third, the shape of the main blood elements, erythrocites, can be relatively easily changed.

2. Experimental Results

Since erythrocytes are in the aggregate state in the whole blood, the influence of aggregation on the experimentally measured spectrum of temporal fluctuations of scattered radiation $S(\omega)$ can be investigated.

The diameter of the healthy erythrocyte in the natural condition is 7-8mkm, that of the spheroidal one (i.e. its shape was changed from the disc-like to spherical) was 10-20 mkm. The use of special methods was made it possible to change the erythrocyte shape without affecting its volume. The sphericity coefficient is 3-4, the erythrocyte concentration in 1 mm^3 – 5 10^{-6}, and the relative volume concentration is 46%.

Thus, using one and the same object, we managed to investigate the potentialities of the method of correlation spectroscopy for determining various characteristics of scattering particles: size, shape, surface microrelief, of aggregation degree.

And it should be noted that this has been done in the conditions of "nontraditional " use of the method of correlation spectroscopy, at multiple scattering of light.

We investigated the influence of the change in the eruthrocyte characteristics on the spectrum line width of intensity fluctuations of multiple scattered radiation $\Delta\omega$.

The scattered radiation spectrum was measured according to the scheme of self-pulsings [1]. The laser radiation wavelength is 0.63 mkm. Intensity fluctuations of the speckle-pattern were recorded in the direction of 170 degree from the direction of laser radiation incidence. The spectrum width $\Delta\omega$ was analyzed by a spectrum analyzer.

In the Table 1 the results of the measurements of the spectrum width $\Delta\omega$ depending on the shape of the erythrocytes in the human blood are given.

Table 1 The spectrum width $\Delta\omega$ for different shapes of particles

shape	discs	discs with relief	spheroids	spheres
$\Delta\omega$, Hz	323 ±23	429 ±30	375 ±26	273 ±19

Since the particle size remained constant, the change in the spectrum width is due to the change in the shape of the particle.

This, solving the inverse problem, we can determine the shape of scattering particles at multiple scattering.

It is evident that the change in the erythrocyte shape leads to a change in the width of the recorded spectrum $S(\omega)$. Thus, it was shown, that, as in the case of small concentrations, the correlation spectroscopy methods could be used for determining the form of scatters. And in this case the method is sensitive not only to the change in the shape of particles, but to the relief of their surface as well.

Theoretical and experimental investigations of the concentration dependence of the coefficient of diffusion D show that in the region of relatively small concentrations (C < 10%) marked changes are observed for spherical particles and relatively small changes for disk-shaped particles. It was

shown that value of D spheroidal erythrocytes is greater than for disk-shaped ones with the same volume (Fig. 1).

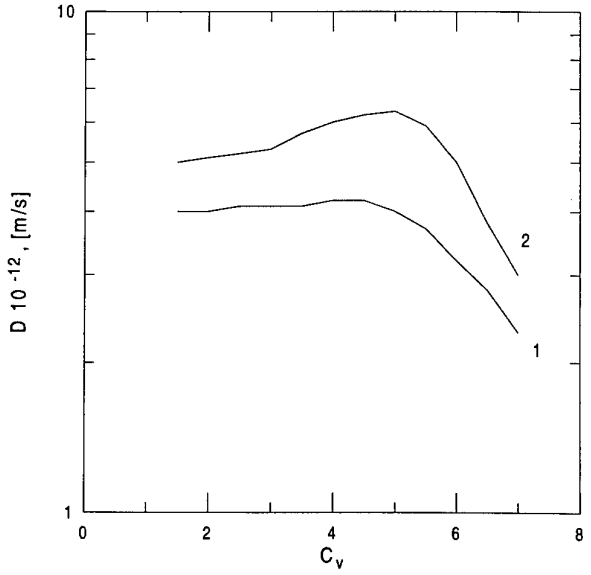

Fig. 1 Dependence of the diffusion coefficient D of disk-shaped (curve 1) and spherical particles (curve 2) on the volume concentration C_v at a constant volume. The dashed lines denote the theoretical calculation for a diluted medium.

Analogous measurements of $\Delta\omega$ have been made for erythrocytes at large concentrations. The results are diametrically opposite. The spectrum width for disc-shaped erythrocytes is smaller than for spheroidal ones. The explanation of this result is given below where the influence of optical characteristics of particles on the fluctuation spectrum of radiation scattered by them is investigated.

The result of the investigation of the influence of the optical characteristics of scattering particles (absorption and scattering coefficients) on temporal fluctuations of scattered radiation $S(\omega)$ was unexpected. It was found that in the region of high concentrations of weakly absorbing biological particles, the function $S(\omega)$ is dependent not only on their geometrical characteristics, but on the optical ones as well.

It is seen from the table (Table 2) that if the value of ε/κ is great (absorption coefficient is small).

Table 2 Dependence of the halfwidth of the scattered radiation spectrum on the form of scattering particles at different values of ε / k.

Shape of particle	$\Delta\omega$, Hz	ε / k
Spheres	429	870
Disk with relief	716	870
Disk	665	2330
Disk	377	28

The broadening of the spectrum for nonspherical particles is observed. If the absorption of the disperse phase is significant, on additional broadening of the spectrum for nonspherical particles is not observed as compared with spherical particles.

Thus, this offers possibilities of investigating not only the dynamics, but also the optical parameters of biological particles.

In this connection the question arises about the possible influence of the close packed media effects on the characteristics of scattered radiation. To solve, this problem, theoretical and experimental

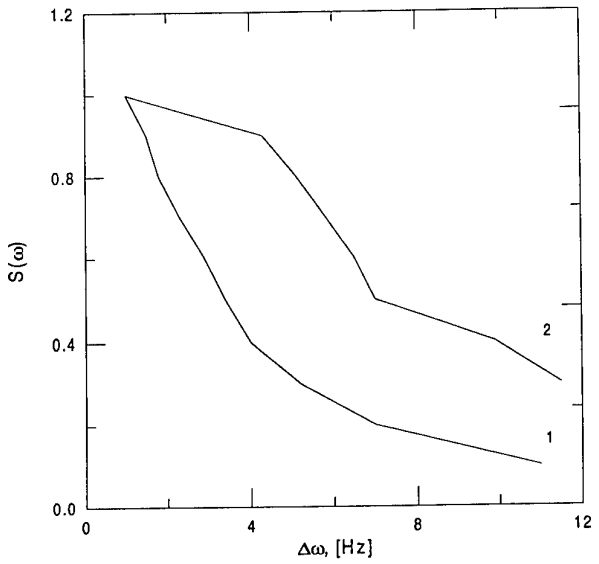

Fig.2. Spectra of fluctuations of the intensity $S(\omega)$ of the radiation scattered by the blood samples with a great (curve 1) and small (curve 2) degree of aggregation.

investigations of the influence of the volume concentrations of disk-shaped and spheroidal particles on the coefficient of the diffuse reflection R were performed at the wavelength $\lambda = 0.63\mu m$. It was found that this value practically does not depend on the volume concentration of particles for optically thick layers (semi - infinite media).

The possibility of the application of the correlation spectroscopy method to the estimation of the degree of aggregation of particles was investigated for two cases: weak aggregation - the sizes of the aggregates were < 50μm and strong aggregation - sizes of the aggregates were < 300μm. The width of the measured spectrum $S(\omega)$ in this case was two times less, than in the case of weak aggregation [2] (Fig. 2).

Thus, the possibility of the application of the correlation spectroscopy method to the investigation not only of sizes, shape, surface of particles and the degree of aggregation, but also their optical characteristics was demonstrated.

References

[1] *Photon Correlation and Light Beating Spectroscopy*, H. Z. Cummins (Ed.). Moscow: Mir, p. 583, 1978.

[2] A. N. Korolevich and N. P. Prigun, "Estimation of the possibility of using dynamical spectroscopy to analyze biological scattering media," *Journal of Applied Spectroscopy*, vol. 64, pp. 101-107, 1997.

Second Harmonic Light Scattering by the Edge Dislocation in Magnetic Crystal

I. L. Lyubchanskii, N. N. Dadoenkova, and M. I. Lyubchanskii

Donetsk Physical and Technical Institute
The National Academy of Sciences of Ukraine,
72, Luxemburg Str., 83114, Donetsk, Ukraine
Fax: + 380 – 622 – 557 462; email: igorl@kinetic.ac.donetsk.ua

Abstract

Optical second harmonic light scattering, or hyper-Rayleigh light scattering which is characterized by the electromagnetic radiation at the double frequency of an incident light in magnetic crystal with the single straight edge dislocation have been phenomenologically investigated by adopting a nonlinear photoelastic and a nonlinear magneto-optic interactions. The polarization dependencies of the light scattered at the double frequency of an incident light for the different scattering geometries are analyzed.

1. Introduction

The methods of nonlinear magneto-optics are well developed for investigating the domains in the magnetic films [1,2]. It is well known that real crystals and films contain the structural defects, for example, the dislocations [3]. The dislocations are the sources of the long-range strain field in a crystal, or in a film [3]. This strain changes the optical properties of a crystal via photoelastic interaction [3]. In magnetic films and crystals it is the magnetoelastic (ME) interaction plays very important role [4]. For example, in a magnetic crystal with a dislocation the ME interaction leads to the formation the specific kind of domain sructure, so called dislocation domains [5]. These dislocation domains are characterized by a special distribution of magnetization around a dislocation core [5].

In this communication we consider the nonlinear elastic light scattering, or hyper-Rayleigh light scattering (HRLS) by single edge dislocation in magnetic crystal. Similar to second harmonic generation (SHG), the HRLS is characterized by the electromagnertic radiation scattered at the double frequency of incident light. The nature of the HRLS phenomenon is very close to the origin of the SHG, because both these three-photon effects are described by the quadratic nonlinear polarization. However, the radiation, corresponding to the HRLS, propagates in an arbitrary direction (non-specular scattering), while for the SHG is necessary to satisfy the phase-matching conditions[6], or specular reflection (in the case of a surfaces, or thin non-transparent films).

2. Magnetization in Crystal with Dislocation

Let us consider a cubic crystal magnetized along the Y axis without an inversion center (the point symmetry $\bar{4}3m - T_d$) with the edge dislocation oriented along the Z axis with Burgers vector $\mathbf{b} = (b, 0, 0)$. In the crystallographic coordinate basis XYZ, the dislocation strain is characterized by the following non-zero components of the strain tensor $u_{ik}(\mathbf{r})$[3]:

$$u_{xx}(\mathbf{r}) = -\frac{b}{4\pi(1-\nu)}\frac{y[x^2(3-2\nu)+y^2(1-2\nu)]}{(x^2+y^2)^2}, \quad (1)$$

$$u_{yy}(\mathbf{r}) = \frac{b}{4\pi(1-\nu)}\frac{y[x^2(1+2\nu)+y^2(1-2\nu)]}{(x^2+y^2)^2}, \quad (2)$$

$$u_{xy}(\mathbf{r}) = \frac{b}{4\pi(1-\nu)}\frac{x(x^2-y^2)}{(x^2+y^2)^2}, \quad (3)$$

where ν is the Poisson's coefficient.

As mentioned above, due the ME interaction magnetization vector $\mathbf{M_0}$ changes orientation in XY plane and additional components of magnetization can be presented in the following form [5]:

$$m_x(\mathbf{r}) = \frac{bM_0}{4\pi}y[\frac{2\gamma+\pi(1-2\nu)}{2(1-\nu)}+\beta]\ln\sqrt{\frac{\alpha}{(x^2+y^2)^2}}, \quad (4)$$

$$m_y(\mathbf{r}) = \frac{bM_0(1-2\nu)x}{2\pi(1-\nu)(x^2+y^2)^2}, \quad (5)$$

where α and $\beta$are the constants of nonuniform exchange interaction and uniaxial magnetic anisotropy, respectively, and γ is the constant of ME interaction.

3. Second Harmonic Light Scattering

The second-order nonlinear optical polarization $\mathbf{P}^{NL(2)}(2\omega)$ at the double frequency of the incident light in the dipole approximation can be written in the well known form [6]:

$$P_i^{NL}(2\omega) = \chi_{ijk}^{(2)}(-2\omega:\omega,\omega)E_j(\omega)E_k(\omega), \quad (6)$$

where $\chi_{ijk}^{(2)}$ is the second-order nonlinear optical suceptibility (NOS) tensor and $\mathbf{E}(\omega)$ is the electric field of the incident light at the frequency ω. Within the phenomenological approach an influence of strain and magnetization on the second-order nonlinear polarization can be described by the nonlinear photoelastic and nonlinear magneto-optic tensors.

$$\chi_{ijk}^{(2)} = \chi_{ijk}^{(2,0)} + p_{ijklm}u_{lm} + if_{ijkl}m_l \quad (7)$$

where $\chi_{ijk}^{(2,0)}$ is the second-order NOS tensor of unstrained crystal in paramagnetic phase, p_{ijklm} is the nonlinear photoelastic tensor, and f_{ijkl} [1] is the linear on magnetization nonlinear magneto-optic tensor.

Let us determine the polarization of light scattered at the second harmonic frequency. Within the slowly varing amplitude approximation the wave equation for the second harmonic electric field can be written as [6]

$$2ik_{2\omega,l}\nabla_l E_i(2\omega,\mathbf{q}) = -\frac{\omega^2}{c^2}\chi_{ijk}^{(2)}(\mathbf{r})E_j(\omega)E_k(\omega)exp(i\mathbf{q}\cdot\mathbf{r}), \quad (8)$$

where $\mathbf{q} = 2\mathbf{k}_\omega - \mathbf{k}_{2\omega}$ is the scattering wave vector while $\mathbf{k}_\omega$ and $\mathbf{k}_{2\omega}$ are the wave vectors of the fundamental and second harmonic light, respectively. Using the infinite plane wave approximation, we obtain from Eq. (21)

$$E_l(2\omega,\mathbf{q}) = \frac{A}{V}\int_V \chi_{ijk}^{(2)}(\mathbf{r})E_j(\omega)E_k(\omega)exp(i\mathbf{q}\cdot\mathbf{r})d\mathbf{r}, \quad (9)$$

where

$$A = -\frac{i\omega}{cn_{2\omega}}.$$

The integral in Eq. (22) is taken over the interaction volume V, and $n_{2\omega}$ is the refractive index of the crystal at the second harmonic frequency.

Substituting the non-zero components of the nonlinear phootoelastic and nonlinear magneto-optic tensors for the point symmetry group $43m$ [7] and the dislocation stran tensor determined by Eqs. (18)-(20) into Eq. (22), we obtain the values of the electric fields at the second harmonic frequency for the s- and p-polarized incident light as follows:

i) $s(\omega) \rightarrow s(2\omega)$

$$E_s(2\omega, \mathbf{q}) = A[p_{yyyxy}u_{xy}(\mathbf{q}) + if_{yyyx}m_x(\mathbf{q})]E_s^2(\omega), \tag{10}$$

ii) $p(\omega) \rightarrow s(2\omega)$

$$\begin{aligned} E_s(2\omega, \mathbf{q}) &= A\{[p_{yxxxy}E_x^2(\omega) + p_{yzzxy}E_z^2(\omega)]u_{xy}(\mathbf{q}) \\ &\quad +i[f_{yxxx}E_x^2(\omega) + f_{yzzx}E_z^2(\omega)]m_x(\mathbf{q})\}, \end{aligned} \tag{11}$$

iii) $s(\omega) \rightarrow p(2\omega)$

$$E_x(2\omega, \mathbf{q}) = Aif_{yyyy}m_y(\mathbf{q})E_s^2(\omega) \tag{12}$$

$$E_z(2\omega, \mathbf{q}) = A[\chi_{zyy}^{(2,0)}f(\mathbf{q}) + p_{zyyxx}u_{xx}(\mathbf{q}) + p_{zyyyy}u_{yy}(\mathbf{q})]E_s^2(\omega). \tag{13}$$

iv) $p(\omega) \rightarrow p(2\omega)$

$$\begin{aligned} E_x(2\omega, \mathbf{q}) &= A\{[(\chi_{xxz}^{(2,0)} + \chi_{xzx}^{(2,0)})f(\mathbf{q}) + (p_{xxzxx} + p_{xzxxx})u_{xx}(\mathbf{q}) \\ &\quad +(p_{xxzyy} + p_{xzxyy})u_{yy}(\mathbf{q})]E_x(\omega)E_z(\omega) \\ &\quad +i[f_{xxxy}E_x^2(\omega) + f_{xzzy}E_z^2(\omega)]m_y(\mathbf{q})\} \end{aligned} \tag{14}$$

$$\begin{aligned} E_z(2\omega, \mathbf{q}) &= A\{[\chi_{zxx}^{(2,0)}f(\mathbf{q}) + p_{zxxxx}u_{xx}(\mathbf{q}) + p_{zxxyy}u_{yy}(\mathbf{q})]E_x^2(\omega) \\ &\quad +[\chi_{zzz}^{(2,0)}f(\mathbf{q}) + p_{zzzxx}u_{xx}(\mathbf{q}) + p_{zzzyy}u_{yy}(\mathbf{q})]E_z^2(\omega) \\ &\quad +if_{zxzy}m_y(\mathbf{q})E_x(\omega)E_z(\omega)\} \end{aligned} \tag{15}$$

The Fourier transform of the dislocation strain tensor components $u_{lm}(\mathbf{q})$, magnetization vector $\mathbf{m}(\mathbf{q})$ and factor $f(\mathbf{q})$ are determined as follows:

$$u_{lm}(\mathbf{q}) = \frac{1}{V}\int_V u_{lm}(\mathbf{r})exp(i\mathbf{q}\cdot\mathbf{r})d\mathbf{r}, \tag{16}$$

$$\mathbf{m}(\mathbf{q}) = \frac{1}{V}\int_V \mathbf{m}(\mathbf{r})exp(i\mathbf{q}\cdot\mathbf{r})d\mathbf{r}, \tag{17}$$

$$f(\mathbf{q}) = \frac{1}{V}\int_V exp(i\mathbf{q}\cdot\mathbf{r})d\mathbf{r} = 2\frac{J_1(q_\perp R)}{q_\perp R}sinc(\frac{q_z h}{2}), \tag{18}$$

where $J_1(x)$ is the first-order Bessel function, R is the diameter of the laser spot, $q_\perp$ is the in-plane component of the scattering wave vector $\mathbf{q}$, $sinc(x) = sin(x)/x$, and h is the thickness of the crystal.

As follows from Eqs. (10)-(12), the $s-$polarized component of second harmonic radiation depends on $x-$component of magnetization which is induced by ME interction for both $s(\omega) \rightarrow s(2\omega)$ and $p(\omega) \rightarrow s(2\omega)$scattering geometries. For the p-polarized second harmonic radiation, from Eqs.(13) - (15) we obtaine that only y-component of the magnetization vector contributes to the effect for both $s(\omega) \rightarrow p(2\omega)$ and $p(\omega) \rightarrow p(2\omega)$scattering geometries.

4. Conclusions

In conculsion, we shown that magnetization-induced nonlinear light scattering is sensitive to a change of orientation of magnetization in crystal. Particularly, in magnetic crystal with dislocation ME interaction leads to the change in magnetization orientation. It is possible to observe this new magnetization component via polarization analysis of reflected light at the second harmonic frequency. As mentioned above, s-polarized second harmonic radiation depends on the $x-$component of magnetization as well as p-polarized second harmonic radiation depends on the $y-$component of magnetization. This dependence can be observe via measurements of magnetic anisotropy of second harmonic sygnal whichis determined as folows

$$A_{2\omega}(\mathbf{M}) = \frac{I_{2\omega}(\mathbf{M}) - I_{2\omega}(-\mathbf{M})}{I_{2\omega}(\mathbf{M}) + I_{2\omega}(-\mathbf{M})}. \tag{19}$$

References

[1] A. V. Petukhov, I. L. Lyubchanskii, and Th. Rasing, "Theory of nonlinear magneto-optical imaging of magnetic domains and domain walls," *Phys. Rev. B*, vol. 56, no. 5, pp. 2680-2687, August 1997.

[2] V. Kirilyuk, A. Kirilyuk, and Th. Rasing, "A combined nonlinear and linear magneto-optical microscopy," *Appl. Phys. Lett.*, vol. 70, no. 17, pp. 2306-2308, November 1997.

[3] J. P. Hirth and J. Lothe, *Theory of Dislocations*. New York: McGraw-Hill, Inc., 1968.

[4] E. du Tremolet de Lacheisserie, *Magnetostriction* . Boca Raton: CRC Press, 1993.

[5] V. V. Gann and A. I. Zhukov, "Dislocation domains", *Sov. Phys. Solid State*, vol. 21, no. 7, pp. 1145-1149, July 1982.

[6] Y. R. Shen, *The Principles of Nonlinear Optics*. New York: Wiley, 1984.

[7] S. V. Popov, Yu. P. Svirko, and N. I. Zheludev, *Susceptibility Tensors for Non-Linear Optics*. Bristol: IOP Publishing, 1995.

Tensor Polarizabilities of Magnetoelectric Particles on the Base of Strip-Line-Coupled Magnetostatic Wave Resonators

S. V. Zagriadski

Radiophysics Department, St. Petersburg State Technical University
Polytekhnicheskaya 29, St. Petersburg, 195251, Russia
Fax: (7-812) 247-20-88, E-mail: zagr@radio.stu.neva.ru

Abstract

An electrodynamic description of bianisotropic particles on the base of strip-line-coupled magnetostatic wave (MSW) resonators is developed and analytical closed-form expressions for their tensor polarizabilities are obtained for an arbitrary direction of a magnetizing field and an arbitrary resonator shape. Numerical calculations are performed for a normally magnetized thin-ferrite-film disk resonator with a metal strip on its surface.

1. Introduction

Recently proposed composite non-reciprocal bianisotropic materials [1] represent ensembles of magnetized thin-ferrite-film magnetostatic wave resonators with surface metallization. Induced electric and magnetic dipole moments $\mathbf{p}_e$ and $\mathbf{p}_m$ of such artificial particles are related to the external electric and magnetic fields as

$$\mathbf{p}_e = \ddot{\alpha}_{ee}\mathbf{E} + \ddot{\alpha}_{em}\mathbf{H}\ , \quad \mathbf{p}_m = \ddot{\alpha}_{me}\mathbf{E} + \ddot{\alpha}_{mm}\mathbf{H}\ , \tag{1}$$

where $\ddot{\alpha}_{ee}$, $\ddot{\alpha}_{em}$, $\ddot{\alpha}_{me}$ and $\ddot{\alpha}_{mm}$ are corresponding tensor polarizabilities. Although a nature and qualitative physical picture of magnetoelectric coupling in these elements is quite obvious and an experimental evidence of the effect has been obtained [2], the electrodynamic description of the particles and quantitative evaluation of magnetoelectric coupling till the present time has not been performed. In this paper we consider a thin-ferrite-film resonator with a linear metal strip of the width b on its surface, as shown in the Fig.1 for a disk resonator magnetized by the field H_0 in an arbitrary direction η. Dimensions of the resonator are much less than a wavelength in the surrounding media with the permittivity ε, so electric and magnetic fields in (1) can be assumed uniform and quasi-static. Magnetization of oscillation modes $\mathbf{m}_q$ for the type q and corresponding eigenfrequencies ω_q are supposed to be known, as well the ferromagnetic resonance linewidths ΔH_q. The approach is based on the earlier obtained solutions of self-consistent electrodynamic problems of the excitation of one-port [3] and two-port [4] MSW resonators. In this formulation, in particular, dipole moments of a particle, induced by an external magnetic field are found through a resonator high-frequency magnetization, which is determined taking into account the "back" influence of the current in the strip on this magnetization. Neglecting of this interaction results in the non-accurate determination of the polarizabilities $\ddot{\alpha}_{em}$,$\ddot{\alpha}_{mm}$ and their resonant frequency. Presented electrodynamic description of magnetoelectric particles enables to obtain constitutive relations for composite media in a closed form.

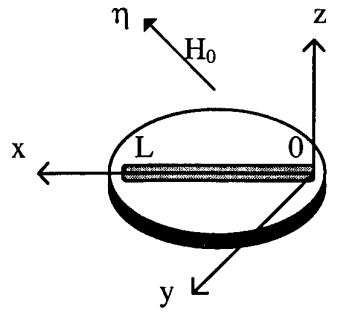

Fig. 1

2. Self-Consistent Electrodynamic Problem for $\tilde{\alpha}_{em}$ and $\tilde{\alpha}_{mm}$ Determination

Tensor polarizabilities $\tilde{\alpha}_{em}$ and $\tilde{\alpha}_{mm}$ are calculated in the assumption that $\mathbf{E} = 0$ in (1). Magnetization induced by a given magnetic field $\mathbf{H}$ is found as an expansion into the series of eigenmodes

$$\mathbf{M} = \sum_{q} c_q \mathbf{m}_q , \quad c_q = \varphi_q \int_V (\mathbf{H}+\mathbf{h}_\mu)\cdot \mathbf{m}_q^* dV \quad , \tag{2}$$

where $\varphi_q = -\dfrac{b_q}{\omega^2 - \omega_q^2 - i\omega_q^2 Q_q^{-1}}$, $b_q = \dfrac{i(\omega+\omega_q)\omega_M}{\Phi_q}$, $\Phi_q = \int_V [\mathbf{m}_q \times \mathbf{m}_q^*]_\eta \, dV$,

$Q_q = \dfrac{H_0}{2\Delta H_q}$, $\omega_M = \gamma\mu_0 M_0$, γ is the gyromagnetic ratio, μ_0 is the permeability of free space, M_0 is the saturation magnetization, and V is the resonator volume. The "back" influence of a strip current on the magnetization is taken into account by including the magnetic field $\mathbf{h}_\mu$ in (2), which can be found as a field of a transmission line excited by an equivalent given magnetic current $i\omega\mathbf{M}$

$$\mathbf{h}_\mu = c_\mu(x)\mathbf{H}_\mu^r + c_{-\mu}(x)\mathbf{H}_{-\mu}^r , \tag{3}$$

with

$$c_\mu(x) = -\frac{i\omega\omega_0}{N_\mu^r}\int_0^x dx \int_S (\mathbf{M}\cdot\mathbf{H}_{-\mu}^r)dS, \quad c_{-\mu}(x) = -\frac{i\omega\omega_0}{N_\mu^r}\int_x^L dx \int_S (\mathbf{M}\cdot\mathbf{H}_{-\mu}^r)dS$$

where $\mathbf{H}_\mu^r = \mathbf{H}_\mu + \Gamma_2\mathbf{H}_{-\mu}$, $\mathbf{H}_{-\mu}^r = \mathbf{H}_{-\mu} + \Gamma_1\mathbf{H}_\mu$, $N_\mu^r = (1-\Gamma_1\Gamma_2)N_\mu$,

$\mathbf{H}_{\pm\mu} = \mathbf{H}_{\pm\mu 0}(y,z)exp(\mp i\beta x)$ is the magnetic field of a dominant wave in a strip-line (in the absence of ferrite) with the propagation constant β, N_μ is a normalization coefficient [4], Γ_1 and Γ_2 are the reflection coefficients for a strip current at $x = 0$ and $x = L$ ($\Gamma_1 = -1$ and $\Gamma_2 = -exp(-2i\beta L)$ for our case of an open transmission line), and S is the cross section of the line. The system of integral equations (2), (3), formulating a self-consistent electrodynamic problem, has the following solution for amplitudes of electromagnetic waves in the transmission line

$$c_\mu(x) = \left[\left(e^{i\beta x}-1\right) - \Gamma_1\left(e^{-i\beta x}-1\right)\right]c_{\mu 0} , \quad c_{-\mu}(x) = \left[\left(e^{-i\beta x}-e^{-i\beta L}\right) - \Gamma_1\left(e^{i\beta x}-e^{i\beta L}\right)\right]c_{\mu 0}, \tag{4}$$

where $c_{\mu 0} = -\dfrac{i\omega\mu_0}{N_\mu}\left[i\beta(1-\Gamma_1\Gamma_2) + 2s\dfrac{i\omega\mu_0}{N_\mu}\varphi_q\left|I_{\mu q}\right|^2\right]^{-1} I_{\mu q}^*\varphi_q\int_V (\mathbf{H}\cdot\mathbf{m}_q^*)dV$, $I_{\mu q} = \int_S (\mathbf{H}_{\mu 0}\cdot\mathbf{m}_q^*)dS$

and parameter s, depending on the line length, is given in [4] ($s \approx 2i\beta L^2$ for a special case $\beta L \ll 1$). Substituting (4) in (3) and using Ampere's law (an integration extends over an arbitrary contour C in the cross section yz which includes the strip)

$$\oint_C \mathbf{h}_\mu d\,\mathbf{l} = J(x),$$

one can find an induced electric dipole moment and using (2) - a magnetic dipole moment

$$\mathbf{p}_e = \frac{1}{i\omega}\mathbf{e}_x\int_0^L J(x)dx, \quad \mathbf{p}_m = \sum_q c_q \int_V \mathbf{m}_q dV . \tag{5}$$

Polarizabilities can be written in a tensor form

$$\ddot{\alpha}_{em} = A \cdot \begin{bmatrix} m_{qx}^* & m_{qy}^* & m_{qz}^* \\ 0 & 0 & 0 \\ 0 & 0 & 0 \end{bmatrix}, \quad \ddot{\alpha}_{mm} = B \cdot \begin{bmatrix} m_{qx}m_{qx}^* & m_{qx}m_{qy}^* & m_{qx}m_{qz}^* \\ m_{yx}m_{qx}^* & m_{qy}m_{qy}^* & m_{qy}m_{qz}^* \\ m_{qz}m_{qx}^* & m_{qz}m_{qy}^* & m_{qz}m_{qz}^* \end{bmatrix}, \tag{6}$$

where for the case $\beta L << 1$ coefficients A and B are the following

$$A = \frac{i}{6}\frac{\mu_0}{\sqrt{2WN_\mu}}\varphi_q I_{\mu q}^* V \beta^2 L^3 \left(-\beta + L\frac{\omega\mu_0}{N_\mu}\varphi_q \left| I_{\mu q} \right|^2 \right)^{-1}, \tag{7}$$

$$B = \varphi_q V^2 + \varphi_q^2 V^2 \left| I_{\mu q} \right|^2 \frac{\omega\mu_0\beta^3 L^4}{3N_\mu} \left[i\beta(1-\Gamma_1\Gamma_2) + 2s\varphi_q \left| I_{\mu q} \right|^2 \frac{i\omega\mu_0}{N_\mu} \right]^{-1}, \tag{8}$$

and W is a characteristic impedance of a transmission line, which can be calculated as [5]

$$W = \frac{120}{\sqrt{\varepsilon}}\left(ln\frac{2{,}2L}{b} - 1 \right). \tag{9}$$

For a normally magnetized ferrite disk and a fundamental uniform mode of magnetization (when its components can be assumed to be $m_{qx} = 1$, $m_{qy} = -i$, $m_{qz} = 0$) calculated polarizability coefficients A (7) are shown in the Fig.2. Note that in this case an internal biasing magnetic field is uniform. The diameter of the resonator is taken equal to the length of a strip and the particle is characterized by the following set of parameters: L = 0.5mm, b = 20μm, $4\pi M_0$ = 1750 Oe, H_0 = 5320 Oe, $2\Delta H_0$ = 0.5 Oe, ε=10.

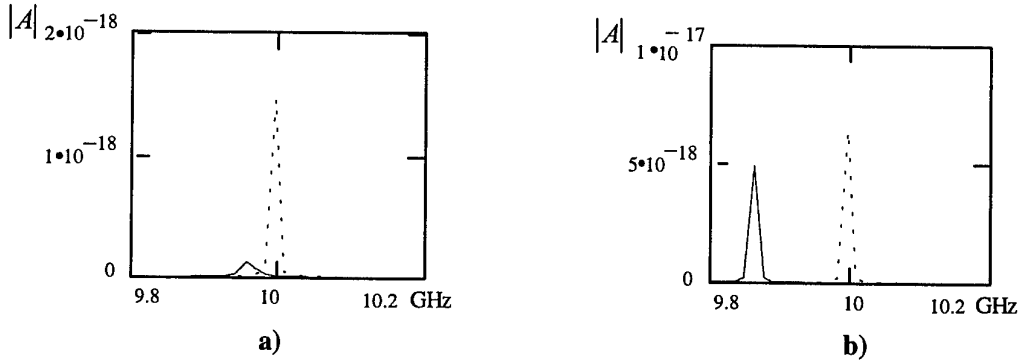

Fig. 2 Polarizability coefficient $|A|$ (ferrite film thickness: a) 10 μm, b) 50 μm). Solid curve: Self-consistent solution; Dotted: "Back" coupling neglected.

3. Calculation of Tensor Polarizabilities $\ddot{\alpha}_{ee}$ and $\ddot{\alpha}_{me}$

Tensor polarizabilities $\ddot{\alpha}_{ee}$ and $\ddot{\alpha}_{me}$ are calculated in the assumption that **H** = 0 in (1). A current distribution along a narrow strip in an external longitudinal electric field **E** is known from the antenna theory [5]

$$J(x) = J(L/2)f(x), \tag{10}$$

where $J(L/2) = \frac{2iE}{\beta W cos(\beta L/2)}\left(1 - cos\frac{\beta L}{2}\right)$, $f(x) = \frac{cos\beta(x - L/2) - cos(\beta L/2)}{1 - cos(\beta L/2)}$. Induced electric dipole moment $\mathbf{p}_e$ is obtained by integrating the current $J(x)$ according (5). A magnetic dipole moment

$\mathbf{p}_m$ of the ferrite resonator is excited by the current (10) and can be calculated using (5) with the amplitude coefficients c_q being obtained from (2) for $\mathbf{H} = 0$. It can be easily seen that the magnetic field of the transmission line is related to the current as

$$\mathbf{h}_\mu = \frac{J(x)}{J_c}\mathbf{H}_{\mu 0}, \tag{11}$$

where $J_c = \oint_C \mathbf{H}_{\mu 0} d\,\mathbf{l}$ (for this value the following relationship is valid $J_c = \sqrt{N_\mu / (2W)}$).

Performing calculations we come to the following polarizabilities for the case $\beta L \ll 1$

$$\ddot{\alpha}_{ee} = C \cdot \begin{bmatrix} 1 & 0 & 0 \\ 0 & 0 & 0 \\ 0 & 0 & 0 \end{bmatrix}, \quad \ddot{\alpha}_{me} = D \cdot \begin{bmatrix} m_{qx} & 0 & 0 \\ m_{qy} & 0 & 0 \\ m_{qz} & 0 & 0 \end{bmatrix}, \tag{12}$$

where $C = \frac{1}{6}\frac{\beta L^3}{\omega W}$, $D = \frac{i\beta L^3}{6W}\frac{\varphi_q I_{\mu q} V}{J_c}$.

4. Conclusion

Derived explicit expressions for polarizabilities show that all non-zero tensor elements, except $\ddot{\alpha}_{ee}$, have resonant character with resonance frequencies close, but not equal, to the MSW resonator eigenfrequencies. Elements of tensors of magnetoelectric coupling $\ddot{\alpha}_{em}$, $\ddot{\alpha}_{me}$ are proportional to the saturation magnetization M_0 of ferrite and to the third power of the strip length L^3 and increase with the growth of the resonator quality factor Q. For low magnetic losses these tensors are related as $\ddot{a}_{em} \approx \mu_0 \ddot{a}_{me}^{T*}$. Elements of the tensor $\ddot{\alpha}_{mm}$ are proportional to the resonator volume V. The tensor $\ddot{\alpha}_{ee}$ has no frequency dependence and is proportional to the third power of the strip length L^3. In the case when a ferrite resonator has a non-elliptic form (e.g., a straight-edge MSW resonator with a film of a rectangular form), calculations of polarizabilities must be carried out taking into account the influence of nonuniformity of the internal biasing magnetic field [6].

References

[1] E. O. Kamenetskii, "On the technology of making chiral and bianisotropic waveguides for microwave propagation", *Microwave and optical technology letters*, Vol. 11, No. 2, pp. 103-107, 1996.

[2] E. O. Kamenetskii, I. Awai, and A. K. Saha, "Experimental evidence for magnetoelectric coupling in a ferromagnetic resonator with surface metallization", *Microwave and optical technology letters*, Vol. 24, No. 1, pp. 56-60, 2000.

[3] S. V. Zagriadski, "Design theory for magnetostatic wave filters and delay lines / Theory of one port magnetostatic wave resonators", *20th European Microwave Conference Proceedings*, Vol. 2, pp. 1263-1268, 1990.

[4] S. V. Zagriadski, "Theory and applications of multiport structures using magnetostatic waves", *22nd European Microwave Conference Proceedings*, Vol. 2, pp. 1363-1368, 1992.

[5] S. A. Schelkunoff, *Advanced Antenna Theory*. New York, 1952.

[6] S. V. Bogachev and S. V. Zagriadski, "Influence of internal field nonuniformity on frequency spectrum of straight-edge forward volume magnetostatic wave resonator", *Journal of Communications Technology and Electronics*, Vol. 44, No. 7, pp. 802-806, 1999.

Hertz Potentials in Complex Medium Electromagnetics

Werner S. Weiglhofer

Department of Mathematics, University of Glasgow
University Gardens, Glasgow G12 8QW, Great Britain
Fax: + 44 - 141 - 330 4111; email: wsw@maths.gla.ac.uk

Abstract

A brief outline of the mathematical technique of scalar Hertz potentials is provided. It is shown that the technique can be successfully implemented if all four constitutive dyadics of a linear bianisotropic medium have a gyrotropic structure. A medium of that nature is a so–called Faraday chiral medium, and it may even be nonhomogeneous but of a restricted form.

1. Introduction

Approaches to solve electromagnetic field problems can be roughly divided into two categories: *direct* and *indirect*. While the former deal directly with the Maxwell equations for the electromagnetic field vectors, the latter aim to derive, and consequently solve, alternative differential equations that are fulfilled by certain functions — scalar, vector or dyadic. The field vectors themselves then follow from these functions through (relatively simple) manipulations such as differentiations and integrations.

Two of the most prominent indirect solution techniques are (i) Green function methods and (ii) potential methods. In this contribution we shall focus on potentials, and specifically on scalar Hertz potentials and their role in the solution of electromagnetic field problems in complex mediums.

Vector, scalar and Hertz potentials, in their application to (achiral) isotropic mediums, have been prominent mathematical tools since the early stages of the development of the Maxwellian formalism — a fact easily betrayed by their inclusion in the vast majority of standard textbooks on electromagnetic theory. But only in the last two decades has it been possible to extend the concept of scalar Hertz potentials into the realm of more complex mediums, which may be anisotropic, bianisotropic, nonhomogeneous, in their nature.

Here, an outline of the scalar Hertz potential method is given, necessarily short due to the limited available space. Full details including a comprehensive listing of references of the relevant research literature can be found in a recent book chapter [1].

2. Analysis

The Maxwell equations for a general, linear bianisotropic medium are[1]

$$i\omega \left[\underline{\underline{\epsilon}} \cdot \mathbf{E}(\mathbf{x}) + \underline{\underline{\xi}} \cdot \mathbf{H}(\mathbf{x}) \right] + \nabla \times \mathbf{H}(\mathbf{x}) = \mathbf{J}_e(\mathbf{x}) \,, \tag{1}$$

$$\nabla \times \mathbf{E}(\mathbf{x}) - i\omega \left[\underline{\underline{\zeta}} \cdot \mathbf{E}(\mathbf{x}) + \underline{\underline{\mu}} \cdot \mathbf{H}(\mathbf{x}) \right] = -\mathbf{J}_m(\mathbf{x}) \,. \tag{2}$$

[1]Vectors are in bold face whereas dyadics are in normal face and underlined twice. Contraction of indices is symbolized by a dot and $\mathbf{ab}$ is a dyadic product; the unit dyadic is $\underline{\underline{I}}$.

$\mathbf{E}(\mathbf{x})$ and $\mathbf{H}(\mathbf{x})$ are the electric and magnetic field vectors, whereas $\mathbf{J}_e(\mathbf{x})$ and $\mathbf{J}_m(\mathbf{x})$ are the prescribed electric and magnetic current densities (a time–dependence of $\exp(-i\omega t)$ is implicit). At this stage no restrictions are imposed on the specific form of the four constitutive dyadics in (1), (2).

To develop a field representation in terms of scalar Hertz potentials, a partial scalarization of the differential equations (1), (2), is carried out with respect to an arbitrarily chosen direction specified by a unit vector $\mathbf{c}$ — once again, full mathematical details can be found in [1]. The decompositions

$$\mathbf{E} = \mathbf{E}_t + E_c\,\mathbf{c}\,, \qquad \mathbf{H} = \mathbf{H}_t + H_c\,\mathbf{c}\,, \tag{3}$$

are introduced, whereby $\mathbf{E}_t \cdot \mathbf{c} = 0$ and $\mathbf{H}_t \cdot \mathbf{c} = 0$; $\mathbf{E}_t$ and $\mathbf{H}_t$ being called the *transverse*, E_c and H_c the *longitudinal* components of the field vectors. Similarly, for the electric and magnetic current density:

$$\mathbf{J}_e = \mathbf{J}_{et} + J_{ec}\,\mathbf{c}\,, \qquad \mathbf{J}_m = \mathbf{J}_{mt} + J_{mc}\,\mathbf{c}\,, \tag{4}$$

and also for the derivative operations:

$$\nabla = \nabla_t + \mathbf{c}\,\frac{\partial}{\partial x_c}\,, \qquad \nabla^2 = \nabla_t^2 + \frac{\partial^2}{\partial x_c^2}\,, \tag{5}$$

wherein ∇^2 is the Laplace operator.

The $\mathbf{c}$–components of (1), (2) provide two scalar expression for the components E_c and H_c and one finds, after some algebra,

$$E_c = \mathbf{P}_{ee} \cdot \mathbf{E}_t + \mathbf{P}_{eh} \cdot \mathbf{H}_t + K_e\,, \tag{6}$$

$$H_c = \mathbf{P}_{he} \cdot \mathbf{E}_t + \mathbf{P}_{hh} \cdot \mathbf{H}_t + K_h\,, \tag{7}$$

where $\mathbf{P}_{ee}$, $\mathbf{P}_{eh}$, $\mathbf{P}_{he}$ and $\mathbf{P}_{hh}$ are 2×2 dyadic operators while K_e and K_h are source terms. Now, a system for the transverse components $\mathbf{E}_t$ and $\mathbf{H}_t$ is derived in the form

$$-\frac{\partial \mathbf{E}_t}{\partial x_c} + i\omega\,\underline{\underline{M}}_{ee} \cdot \mathbf{E}_t + i\omega\,\underline{\underline{M}}_{eh} \cdot \mathbf{H}_t = \mathbf{q}_{te}\,, \tag{8}$$

$$-\frac{\partial \mathbf{H}_t}{\partial x_c} + i\omega\,\underline{\underline{M}}_{he} \cdot \mathbf{E}_t + i\omega\,\underline{\underline{M}}_{hh} \cdot \mathbf{H}_t = \mathbf{q}_{th}\,. \tag{9}$$

where $\underline{\underline{M}}_{ee}$, $\underline{\underline{M}}_{eh}$, $\underline{\underline{M}}_{he}$ and $\underline{\underline{M}}_{hh}$ are 2×2 dyadic differential operators of second order and $\mathbf{q}_{te}$ and $\mathbf{q}_{th}$ are 2–vector source terms.

The crucial step is now the introduction of scalar potentials through

$$\mathbf{E}_t = \nabla_t \Phi + \nabla_t \times \Theta\,\mathbf{c}\,, \tag{10}$$

$$\mathbf{H}_t = \nabla_t \Pi + \nabla_t \times \Psi\,\mathbf{c}\,. \tag{11}$$

Straightforward manipulation of (6), (7), then leads to formulas for the longitudinal components E_c and H_c, in symbolic form:

$$E_c = E_c\,(\Phi\,, \Theta\,, \Pi\,, \Psi\,; J_{ec}\,, J_{mc})\,, \tag{12}$$

$$H_c = H_c\,(\Phi\,, \Theta\,, \Pi\,, \Psi\,; J_{ec}\,, J_{mc})\,. \tag{13}$$

The expressions (10)–(13) constitute a representation of all field components in terms of the four scalar functions Φ, Θ, Π and Ψ; substitution into the available differential equations produces a system of four differential equations for the four scalar potentials. At that stage no direct gain has been achieved as one has simply exchanged solving a system of partial differential equations of second order for $\mathbf{E}_t$ and $\mathbf{H}_t$ with solving a corresponding system for the four scalar potentials.

The question is therefore: can two of the four scalar potentials be eliminated in a simple manner so that the field vectors $\mathbf{E}$ and $\mathbf{H}$ can be represented *in full* by two scalar Hertz potentials plus, perhaps, some auxiliary functions that are required to deal with specific source terms?

The answer to that question is that such an elimination is not possible for the general, linear bianisotropic medium characterized by $\underline{\underline{\epsilon}}$, $\underline{\underline{\xi}}$, $\underline{\underline{\zeta}}$ and $\underline{\underline{\mu}}$. Conditions on the structure of these constitutive dyadics must be imposed and the desired reduction is possible only if the constitutive dyadics are of the form

$$\begin{aligned} \underline{\underline{\sigma}} &= \sigma_t \underline{\underline{I}} + (\sigma_c - \sigma_t)\, \mathbf{c}\,\mathbf{c} - i\sigma_g\, \mathbf{c} \times \underline{\underline{I}} \\ &= \begin{pmatrix} \sigma_t & i\sigma_g & 0 \\ -i\sigma_g & \sigma_t & 0 \\ 0 & 0 & \sigma_c \end{pmatrix}, \qquad \underline{\underline{\sigma}} = \underline{\underline{\epsilon}}, \underline{\underline{\xi}}, \underline{\underline{\zeta}}, \underline{\underline{\mu}}. \end{aligned} \tag{14}$$

All four constitutive dyadics are of gyrotropic form, and a medium of that nature is called a Faraday chiral medium [2]. In the dyadics (14), σ_t and σ_c characterize the uniaxiality of the medium whereas σ_g is responsible for the gyrotropic or gyrotropic–like nature. The scalar Hertz potential formalism for homogeneous Faraday chiral mediums has been outlined in detail elsewhere [2]. The field representation, for all the types of mediums for which the scalar Hertz potential technique is then applicable, can symbolically be given by

$$\mathbf{E} = \mathbf{E}\,(\Theta\,, \Psi\,; J_{ec}\,, u_e\,, v_e\,, J_{mc}\,, u_m\,, v_m)\,, \tag{15}$$

$$\mathbf{H} = \mathbf{H}\,(\Theta\,, \Psi\,; J_{ec}\,, u_e\,, v_e\,, J_{mc}\,, u_m\,, v_m)\,, \tag{16}$$

because usually the two potentials that get eliminated are Φ and Π.

Typically, the two functions Θ and Ψ — the scalar Hertz potentials — fulfil a system of differential equations of the structure

$$L_1\Theta + L_2\Psi = s_1\,, \tag{17}$$

$$L_3\Theta + L_4\Psi = s_2\,, \tag{18}$$

where the exact form of the second order partial differential operators L_1, L_2, L_3 and L_4 depends on the specific type of bianisotropic medium being analysed; s_1 and s_2 are source terms. In general, thus, Θ and Ψ are coupled but decoupling occurs if the medium becomes sufficiently simple (as happens, for example, for a uniaxial dielectric medium [3]).

Finally, what is the significance of the functions u_e, u_m, v_e and v_m that have entered the field representation (15), (16)? These are *auxiliary* functions defined by

$$\mathbf{J}_{et} = \nabla_t\, u_e + \nabla_t \times v_e\, \mathbf{c}\,, \tag{19}$$

$$\mathbf{J}_{mt} = \nabla_t\, u_m + \nabla_t \times v_m\, \mathbf{c}\,. \tag{20}$$

Consequently, the four auxiliary functions are calculated from the differential equations

$$\nabla_t^2 u_p = \nabla_t \bullet \mathbf{J}_{pt}\,, \quad \nabla_t^2 v_p = \nabla_t \bullet (\mathbf{c} \times \mathbf{J}_{pt})\,, \quad p = e, m\,, \tag{21}$$

and it is immediately clear from these expressions that they have nothing to do with the medium as such but are simply generated by the mathematical formalism to accommodate transverse current densities.

3. Discussion

The brief outline of the scalar Hertz potential technique is concluded here with a number of observations; see [1] for more detailed discussions of the individual points.

- Not mentioned previously is the possible generalization to nonhomogeneous mediums, where the nonhomogeneity is of a restricted kind. Namely, all constitutive parameters can depend on $x_c(= \mathbf{x} \cdot \mathbf{c})$, the coordinate parallel to the distinguished axis $\mathbf{c}$. Thus, the most general type of medium that is amenable to the scalar Hertz potential technique is characterized by constitutive dyadics of the form

$$\underline{\underline{\epsilon}}(x_c) = \epsilon_t(x_c)\,\underline{\underline{I}} + \Big[\epsilon_c(x_c) - \epsilon_t(x_c)\Big]\mathbf{c}\,\mathbf{c} - i\epsilon_g(x_c)\,\mathbf{c} \times \underline{\underline{I}}, \tag{22}$$

$$\underline{\underline{\xi}}(x_c) = \xi_t(x_c)\,\underline{\underline{I}} + \Big[\xi_c(x_c) - \xi_t(x_c)\Big]\mathbf{c}\,\mathbf{c} - i\xi_g(x_c)\,\mathbf{c} \times \underline{\underline{I}}, \tag{23}$$

$$\underline{\underline{\zeta}}(x_c) = \zeta_t(x_c)\,\underline{\underline{I}} + \Big[\zeta_c(x_c) - \zeta_t(x_c)\Big]\mathbf{c}\,\mathbf{c} - i\zeta_g(x_c)\,\mathbf{c} \times \underline{\underline{I}}, \tag{24}$$

$$\underline{\underline{\mu}}(x_c) = \mu_t(x_c)\,\underline{\underline{I}} + \Big[\mu_c(x_c) - \mu_t(x_c)\Big]\mathbf{c}\,\mathbf{c} - i\mu_g(x_c)\,\mathbf{c} \times \underline{\underline{I}}. \tag{25}$$

  All constitutive dyadics have a gyrotropic structure and are spatially nonhomogeneous through the dependence on x_c and are thus nonhomogeneous Faraday chiral mediums [2].

- The auxiliary functions u_e, u_m, v_e and v_m are determined by (19)–(21); it is noted that

$$\mathbf{J}_{et} = \mathbf{0} \quad \Longrightarrow \quad u_e = 0\,,\ v_e = 0\,, \tag{26}$$

$$\mathbf{J}_{mt} = \mathbf{0} \quad \Longrightarrow \quad u_m = 0\,,\ v_m = 0\,. \tag{27}$$

  Consequently, they can be completely omitted from the mathematical formalism if the medium is free of sources, i.e., $\mathbf{J}_e = \mathbf{0}$, $\mathbf{J}_m = \mathbf{0}$, or if the current densities are purely longitudinal, i.e., $\mathbf{J}_e = J_{ec}\mathbf{c}$, $\mathbf{J}_m = J_{mc}\mathbf{c}$.

- With the fundamental system of differential equations (that for the scalar Hertz potentials) that needs to be solved being a scalar problem, Green functions that may be introduced subsequently can be of the simpler scalar rather than much more complicated dyadic nature.

- The introduction of the scalar Hertz potentials is not a unique process. New scalar Hertz potentials $\Theta^{new}(\mathbf{x})$ and $\Psi^{new}(\mathbf{x})$ may be defined via

$$\Theta^{new}(\mathbf{x}) = \gamma_1\,\Theta(\mathbf{x}) + \gamma_2\,\Psi(\mathbf{x})\,, \qquad \Psi^{new}(\mathbf{x}) = \gamma_3\,\Theta(\mathbf{x}) + \gamma_4\,\Psi(\mathbf{x})\,, \tag{28}$$

  where γ_n, $n = 1, 2, 3, 4$, are arbitrary complex constants (provided $\gamma_1\gamma_4 \neq \gamma_2\gamma_3$).

In conclusion, the scalar Hertz potential technique provides a very successful mathematical method to deal with electromagnetic field problems in complex mediums.

Acknowledgement
The author is the holder of a *RSE/SOEID Research Support Fellowship* of the *Royal Society of Edinburgh* for the year 2000.

References

[1] W.S. Weiglhofer, "Scalar Hertz potentials for linear bianisotropic mediums," in O.N. Singh and A. Lakhtakia (eds.), *Electromagnetic Fields in Unconventional Structures and Materials*. New York: Wiley, 2000, 1–37.

[2] W.S. Weiglhofer and S.O. Hansen, "Faraday chiral media revisited–I: Fields and sources," *IEEE Trans Antennas Propagat* **47**, 807–814, 1999.

[3] W.S. Weiglhofer, "Scalar Hertz potentials for nonhomogeneous, uniaxial dielectric–magnetic mediums," *Department of Mathematics, University of Glasgow*, preprint 2000/08, March 2000.

Anisotropy of Electrical Properties of Mono-Layers of Spherical Particles Located on Substrate

L.G. Grechko [1], V.V. Gozhenko [1], V.N. Malnev [2], and K.W. Whites [3]

[1] Institute of Surface Chemistry National Academy of Sciences of Ukraine
Prospekt Nauki 31, 03022 Kyiv, Ukraine
email: user@surfchem.freenet.kiev.ua

[2] Taras Shevchenko Kyiv National University
Prospect Glushkov 6, 03142 Kyiv, Ukraine
email: vmal@phys.univ.kiev.ua

[3] Department of Electrical Engineering, University of Kentucky
453 Anderson Hall, Lexington, KY 40506-0046, USA
Fax: +1 - 859 - 257 - 3092; email: whites@engr.uky.edu

Abstract

In this paper, we study the effects of a semi-infinite matrix disperse system on the external electromagnetic radiation in the electrostatic approximation. With the help of our previous technique, we obtain general expressions for the multipole expansion coefficients of the electric potential for a sphere accounting for the interaction between ambient particles and the substrate. The polarizability tensor and resonant frequencies of a single sphere show anisotropy due to the influence of a substrate.

1. Introduction

Interest in matrix disperse systems (MDS) is stimulated, first of all, by the possibility of manufacturing materials with predicted optical properties. At the same time, the properties of MDS may strongly differ from those of the materials used for the formation of MDS [1]. In the theoretical studies, MDS are usually considered as infinite systems.

In this work, we take into consideration the effects of an MDS interface. Namely, the MDS is considered as a half space of dielectric matrix with a plane interface separating it from another half space of homogeneous dielectric. The matrix is filled with spherical inclusions of different diameters that are randomly located. The results [2] obtained for the system of spheres on a dielectric substrate can be obtained from our model as a particular case. Basically, this work is a generalization of [3,4].

2. Theory

We consider the semi-infinite MDS consisting of dielectric spheres with different diameters embedded in a homogeneous dielectric (ambient) as shown in Fig. 1. The remainder of the half space is filled with another homogeneous dielectric (substrate). The system is placed in the electric field proportional to $e^{i\omega t}$. Let $\varepsilon_a(\omega), \varepsilon_s(\omega)$ and $\varepsilon_i(\omega)$ be the dielectric functions of the ambient, substrate and the i^{th} sphere, respectively, and R_i be the radius of the i^{th} sphere.

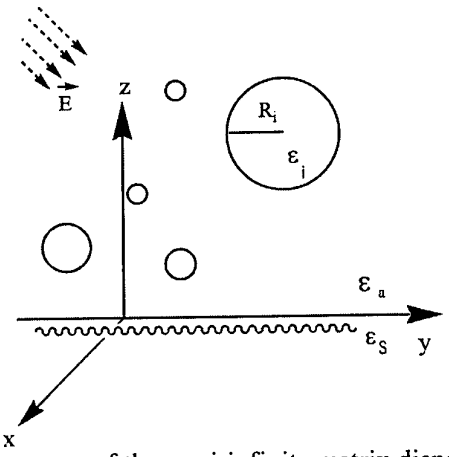

Figure 1 Geometry of the semi-infinite matrix disperse system.

Let the wavelength of the external electromagnetic field be much larger than radii of the spheres and the distances between them. In other words, we use the electrostatic approximation. In such a case, the potential of the electric field is a result of the interaction of the external field with the MDS and the substrate and satisfies the Laplace equation

$$\Delta\psi(\vec{r}) = 0 \tag{1}$$

in regions: I - inside MDS (outside of the spheres), II - inside the spheres, III - inside the substrate. We seek a solution of (1) in the following form:

$$\psi^{I} = \psi^{I}_{ext} + \sum_{i}\psi^{I}_{i-th\ spere} + \psi^{I}_{substrate} = -\vec{E}_o\vec{r} + \sum_{ilm} A_{lmi}F_{lmi}(\vec{\rho}_i) + \sum_{ilm} A'_{lmi}F_{lmi}(\vec{\rho}'_i) \tag{2}$$

$$\psi^{II}_i = \sum_{lm} B_{lm}G_{lm}(\vec{\rho}_i)\,; \tag{3}$$

$$\psi^{IIII} = \psi^{III}_{ext} + \sum_{ilm} C_{lmi}G_{lmi}(\vec{\rho}'_i)\,; \tag{4}$$

$$\begin{aligned}\psi^{I}_{ext} &= -\vec{E}_0\vec{r} = -(E_{ox}x + E_{oy}y + E_{oz}z)\\ \psi^{III}_{ext} &= -\vec{E}'_0\vec{r} = -(aE_{ox}x + bE_{oy}y + cE_{oz}z)\end{aligned} \tag{5}$$

where $F_{lm}(\vec{r}) \equiv r^{-l-1}Y_{lm}(\vec{r})$; $G_{lm}(\vec{r}) \equiv r^{l}Y_{lm}(\vec{r})$; $\vec{\rho}_i \equiv \vec{r} - \vec{r}_i$; $\vec{\rho}'_i \equiv \vec{r} - \vec{r}'_i$; $\vec{r}_i$ is a radius-vector of the center of the i^{th} sphere ; $\vec{r}'_i$ is a radius-vector of the image of the center of the i^{th} sphere.

The coefficients $A_{lmi}, A'_{lmi}, B_{lmi}, C_{lmi}, a, b, c$ are obtained after applying the boundary conditions for the continuity of the potential and its normal derivative on the limiting surfaces of regions I-II and I-III. This leads to the expressions

$$a = \frac{\varepsilon_a}{\varepsilon_s};\ b = c = 1,$$

$$A'_{lmi} = (-1)^{l+m}A_{lmi}\frac{\varepsilon_a - \varepsilon_s}{\varepsilon_a + \varepsilon_s};\ B_{lmi} = f(A_{lmi});\ C_{lmi} = A_{lmi}\frac{2\varepsilon_a}{\varepsilon_a + \varepsilon_s}, \tag{6}$$

and to the equation defining A_{lmi}

$$\sum_{\substack{il_2m_2\\ l_2\neq 0}}\left\{\delta^{l_2m_2i}_{l_1m_1j} + K^{l_2m_2i}_{l_1m_1j}\right\}A_{l_2m_2i} = V_{l_1m_1j}\,, \tag{7}$$

where

$$K^{l_2m_2i}_{l_1m_1j} \equiv \alpha_{l_1j}H^{l_2m_2}_{l_1m_1}\left\{F'_{LM}(\vec{r}_i - \vec{r}_j) + (-1)^{l_2+m_2}\frac{\varepsilon_a - \varepsilon_s}{\varepsilon_a + \varepsilon_s}F_{LM}(\vec{r}'_i - \vec{r}_j)\right\}, \tag{8a}$$

$$\alpha_{l_1 j} \equiv \frac{l_1(\varepsilon_j - \varepsilon_a)}{l_1\varepsilon_j + (l_1+1)\varepsilon_a} R_j^{2l_1+1}; \tag{8b}$$

$$H_{l_1 m_1}^{l_2 m_2} \equiv (-1)^{l_2+m_1}\left[4\pi \frac{2l_2+1}{(2l_1+1)(2L+1)} \cdot \frac{(L+M)!(L-M)!}{(2l_1+1)!(2l_1-1)!(2l_2+1)!(2l_2-1)!}\right]^{\frac{1}{2}}, \tag{8c}$$

$$L \equiv l_1 + l_2;\ \ M \equiv m_2 - m_1;\ F'_{lm}(\vec{r}_i - \vec{r}_j) \equiv \begin{cases} F_{lm}(\vec{r}_i - \vec{r}_j),\ i \neq j \\ 0,\ i = j \end{cases}, \tag{8d}$$

$$V_{l_1 m_1 j} \equiv E_0 \alpha_{l_1 j}\sqrt{\frac{2\pi}{3}}\left\{\sqrt{2}\cos\theta_0 \delta_{l_1 m_1}^{10} + \sin\theta_0 e^{i\varphi_0}\delta_{l_1 m_1}^{1-1} - \sin\theta_0 e^{-i\varphi_0}\delta_{l_1 m_1}^{11}\right\}, \tag{8e}$$

$$\vec{E}_0 = (E_{0x}, E_{0y}, E_{0z}) = E_0(\sin\theta_0\cos\varphi_0, \sin\theta_0\sin\varphi_0, \cos\theta_0). \tag{8d}$$

The explicit form of the function f in (6) is not needed for further consideration.

Equation (7) can be written in the matrix form $\hat{M}\hat{A} = \hat{V}$ or $\hat{A} = \hat{M}^{-1}\hat{V}$, that allows us to interpret

$$\hat{M}^{-1} = \left[\hat{1} + \hat{N}\right]^{-1} \tag{9}$$

as the multipole polarizability matrix of the MDS spheres.

2.1 A single sphere on the substrate; The resonant frequencies.

For the single sphere on the substrate, we can obtain the polarizability tensor in the dipole-dipole approximation using (9) and taking into account (6)

$$\hat{\alpha} = \frac{4}{3}\pi R^3 \varepsilon_a(\varepsilon - \varepsilon_a)\begin{pmatrix} \alpha_{II} & 0 & 0 \\ 0 & \alpha_{II} & 0 \\ 0 & 0 & \alpha_{\perp} \end{pmatrix}, \tag{10}$$

where $\alpha_i = \left[\varepsilon_a + L_i(\varepsilon - \varepsilon_a)\right]^{-1};\ (i = II, \perp);\ \ L_i = \frac{1}{3}\left(1 + l_i \frac{\varepsilon_a - \varepsilon_s}{\varepsilon_a + \varepsilon_s}\right);\ l_i = \eta_i x^{-3};$

$$\eta_i = \begin{cases} \eta_{II} = 1/8 \\ \eta_{\perp} = 1/4 \end{cases}; \tag{11}$$

$x = R/a$ is the dimensionless radius of the sphere (a is a typical scale of length).

Let us consider the case of Lorentz's dielectric functions and $\varepsilon_a = 1$ (vacuum):

$$\varepsilon(\omega) = 1 + \frac{\omega_p^2}{\omega_0^2 - \omega^2 - i\gamma\omega}\ \ ;\ \ \varepsilon_s(\omega) = 1 + \frac{\omega_{ps}^2}{\omega_{0s}^2 - \omega^2 - i\gamma_s\omega}. \tag{12}$$

The resonant frequency is obtained by using the condition $\alpha_i(\omega_{res}) = \infty$. In our case it reduces to the following algebraic equation with respect to the frequency

$$\omega^4 + a_3\omega^3 + a_2\omega^2 + a_1\omega + a_0 = 0, \tag{13}$$

where

$$a_3 = i(\gamma + \gamma_s)$$

$$a_2 = -\left(\omega_0^2 + \omega_{0s}^2 + \frac{1}{3}\omega_p^2 + \frac{1}{2}\omega_{ps}^2 + \gamma\gamma_s\right)$$

$$a_1 = -i\left(\gamma_s\omega_0^2 + \gamma\omega_{0s}^2 + \frac{1}{3}\gamma_s\omega_p^2 + \frac{1}{2}\gamma\omega_{ps}^2\right)$$

$$a_0 = \omega_0^2\omega_{0s}^2 + \frac{1}{3}\omega_{0s}^2\omega_p^2 + \frac{1}{2}\omega_0^2\omega_{ps}^2 + \frac{1}{6}(1-l_i)\omega_p^2\omega_{ps}^2$$

A solution to (13) neglecting damping $(\gamma = \gamma_s = 0)$ is

$$\left(\omega_{1,2}^i\right)^2 = \frac{\omega_p^2}{2}\left\{y_1 + y_2 \pm \sqrt{\left(y_1 - y_2\right)^2 + l_i y_3}\right\} \tag{14}$$

where $y_1 = \frac{1}{3} + \left(\frac{\omega_0}{\omega_p}\right)^2$; $y_2 = \left(\frac{\omega_{0s}}{\omega_p}\right)^2 + \frac{1}{2}\left(\frac{\omega_{ps}}{\omega_p}\right)^2$; $y_3 = \frac{2}{3}\left(\frac{\omega_{ps}}{\omega_p}\right)^2$.

Particularly, for a metallic sphere on the dielectric substrate from (14), using the inequality $\omega_{ps}/\omega_p << 1$, we obtain the following approximate expressions

$$\begin{cases} (\omega_{res}^{(1)})^2 = \omega_p^2/3 + l_i/6\,\omega_{ps}^2 \\ (\omega_{res}^{(2)})^2 = \omega_{0s}^2 + 1/2\,\omega_{ps}^2 - l_i/6\,\omega_{ps}^2 \end{cases} \tag{15}$$

for the two resonant frequencies.

3. Conclusion

We obtained the general expression for the resonant frequency of the model system, which is a dielectric sphere in vacuum on a dielectric substrate. The latter results in splitting and shifting of the resonant frequency depending on a direction of the external field according to (15). This allows one to suggest that mono-layers of small particles on a substrate possess anisotropic electrodynamical properties.

Acknowledgement

The authors acknowledge financial support from the National Science Foundation through the Faculty Early Career Development (CAREER) Award ECS-9624486 and an Eastern Europe Program Supplement.

References

[1] C. F. Bohren and P. R. Huffman, *Absorption and Scattering of Light by Small Particles*. New York: John Wiley & Sons, 1983.

[2] M. T. Haarmans, "The polarizability and the optical properties of lattices and random distributions of small metal spheres on a substrate," *Thin Solid Films*, vol. 224, pp. 117-131, 1993.

[3] L. G. Grechko, A. Ya Blank, V. V. Motrich, A. O. Pinchuk, and L. V. Garanina, "Dielectric function of matrix disperse systems with metallic inclusions: account of multipole interaction between inclusions," *Radio Physics and Radio Astronomy*, vol. 2, pp.19-27, 1997.

[4] L. G. Grechko, V. N. Pustovit, and K. W. Whites, "Dielectric function of aggregates of small metallic particles embedded in host insulating matrix," *Appl. Phys. Lett.*, vol. 76, no. 14, pp. 1854-1856, 2000.

Magnetostimulated Anisotropy of Conductivity and Corbino-Like Current in Composite Conductors

V.R.Sobol[1], O. N. Mazurenko[1], and M. Zoli[2]

[1] National Academy of Sciences, Institute of Solid State and Semiconductor Physics
Brovka Street 17, 220072 Minsk, Belarus
Fax: + 375-172-840888; email: sobol@ifttp.bas-net.by

[2] Istituto Nazionale Fisica della Materia,
Dipartimento di Matematica e Fisica, Universita di Camerino
Via Madonna delle Carceri, 62032 Camerino, Italy
Fax: + 39-0737-632525; email: zoli@mail.publigraphic.it

Abstract

The problem of steady field distribution in double-strip conductor having the electric contact in interface is studied. The interface is orthogonal to magnetic field. The peculiarity is that components are hyrotropic due to an action of magnetic field. Some new approaches for this problem are discussed. The analysis is based on the phenomenological macroscopic equations for steady field including the hypothesis of existence of transverse current in every strip. The expression for effective resistivity is obtained as an intermediate case between two limit geometries of the single conductor on the one hand and disk conductor on the other hand.

1. Introduction

Pure aluminum is a popular material for stabilizing of large current superconductors on the reason that aluminum shows lower resistivity and lower magnetoresistance than copper. The combination of low resistive aluminum and mechanically strong and heat conductive copper may improve the recovery currents and total functioning of superconductor. However the enhancement of magnetoresistance due to Hall currents take place because the polarity of the Hall effect in aluminum is opposite to that in copper. Here the problem of resistivity enhancement in double strip composite conductor consisted of components having opposite polarities of Hall coefficients is discussed [1, 2]. Composite components have the electric contact in the interface being orthogonal to an external magnetic field. The own magnetic field is neglected.

2. Approach

Some new approaches for this problem are developed. That is the hypothesis of an existence of transverse current similar to Corbino current in disk shaped samples is applied for this problem [3]. For the simplicity of analysis the model type of conductor is used as a conductor consisted of components having similar type of conductivity and resistivity tensor including the fact that one of component is usual aluminum conductor with hole type of conductivity (Al^+) but another component is a hypothetical quasi-aluminum conductor having electron type of conductivity (Al^-). As a result the

conductivity and resistivity tensors of these components are the same in modulo excluding of diagonal linear on magnetic field components being opposite in sign.

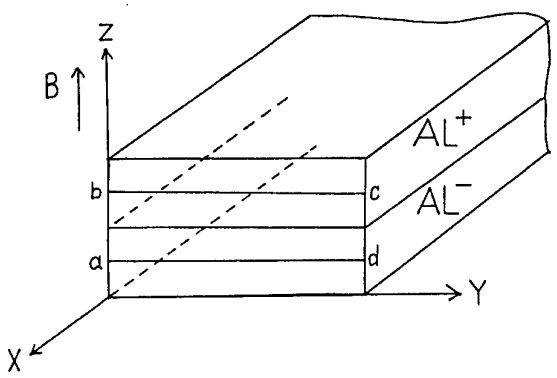

Fig. 1 Composite double strip conductor and its arrangement in an external magnetic field.

Double strip composite conductor model is displayed in Fig. 1. The conductor is uniform along transport X-direction and a primary electric field is applied along this direction. The magnetic field is oriented along Z-axis. The strips of conductor have the same dimensions. In steady state the equations that govern the transport process and transverse Hall mechanism generation are

$$\nabla \times E = 0; \quad j = \sigma E; \quad E = \rho j \tag{1}$$

Here E is electric field vector, j is current density vector, σ is conductivity tensor being equal to the reciprocal of resistivity tensor ρ. In this task

$$\rho = \begin{pmatrix} \rho_{xx} & \rho_{xy} & \rho_{xz} \\ \rho_{yx} & \rho_{yy} & \rho_{yz} \\ \rho_{zx} & \rho_{zy} & \rho_{zz} \end{pmatrix}; \quad \rho(\mathrm{Al}^+) = \rho^+; \quad \rho(\mathrm{Al}^-) = \rho^-; \tag{2}$$

$$\rho^+_{yx} = -\rho^+_{xy} = RB; \quad \rho^-_{yx} = -\rho^-_{xy} = -RB$$

All other components of ρ^+ and ρ^- are the same order of resistivity in zero magnetic field. The basic suggestion is that primary transport electric field component E_x is uniform through the double strip conductor. The total problem of this approach is to define the effective resistivity of composite conductor ρ_{ef} being the coefficient of proportionality between electric field E_x and averaged transport current density through strips $<j_x>$.

$$\rho_{eff} = \frac{E_x}{< j_x >} \tag{3}$$

3. Calculation and Results

On the base of tensor relations between current density and electric field components it is clear that the conditions for an existence of transverse current of Hall nature take place. Really the electric Hall field due to gyrotropy of one component is shorten by conducting medium of another component. Respectively the electric Hall field of another component is shorten by the conducting medium of the first component. So for the any closed counter in the plane ZX (for instance abcd, Fig.1) the

summarizing of Hall electromotive forces takes place and as a result the circular current along this counter exists. The circular current is similar to Corbino current along closed circular counter but the difference is that the current under discussion is generated in the counter being parallel to magnetic field but Corbino current is generated in the counter being orthogonal to magnetic field. Of course the transverse current is zero if the components of double strip conductor are the same in conductivity or under conditions of magnetic field absence. Using an integral form of equation for electric field circulation along closed counter of double strip conductor it is possible to get the expression for the magnetostimulated current. As a result the transverse component of this current is

$$j_y = -\frac{\rho_{yx}}{\rho_{yy} + \rho_{zy}\dfrac{z}{b}} j_x \tag{4}$$

Here b is a width of strips, z is any coordinate defining the distance from interface. In this expression the mechanism of involvement of carriers along z-direction under an action of external magnetic field is neglected because the level of a of current generation along z-direction is very small in comparison with the scope of transverse and transport current. Actually the Hall components of resistivity tensor in strong magnetic field are much higher of all other components and such an approximation is rather valid. Following equation (4) the values of current j_y and transport current j_x are the functions of geometric parameters b and z. When the ratio z/b is large the transverse current is small and for the counter having small ratio z/b the transverse current has definite non-small magnitude. For comparison Corbino current for aluminum conductor under neglecting of involvement of charge along z-direction is equal

$$j_y = -\frac{\rho_{yx}}{\rho_{yy}} j_x \tag{5}$$

This equation takes place for the thin disk samples placed in coaxial magnetic field which acts on radial carrier movements between current contacts on inner and outer diameters of disk. Taking into account tensor relations between electric field and current density vector the connection for transport current density j_x distribution with an electric field component along transport direction E_x can be obtained

$$j_x = \frac{1}{\rho_{xx}} \frac{1}{1 + \dfrac{\sigma_{xy}\rho_{yx}\dfrac{b}{z}}{\sigma_{yy}\left(\rho_{yy}\dfrac{b}{z} + \rho_{zy}\right)}} E_x \tag{6}$$

Applying the procedure of averaging of transport current through the thickness of strip the final expression for the effective resistivity is the next

$$\rho_{eff} = \frac{\rho_{xx}}{1 - \left(\dfrac{RB}{\rho_{xx}}\right)^2 \dfrac{b}{t} \ln\left\{\left[1 + \left(\dfrac{\rho_{xx}}{RB}\right)^2\right]^{-1} \dfrac{t}{b} + 1\right\}} \tag{7}$$

Here the diagonal component of resistivity tensor ρ_{xx} may be not only constant as in former suggestions but this component is allowed to have more complicated behavior close to real that of polycrystalline aluminum when not very strong linear dependence on magnetic field takes place.

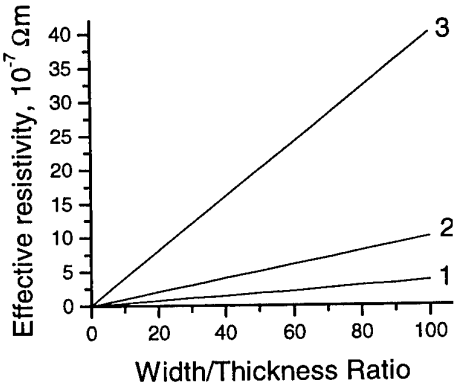

Fig. 2 Effective resistance as a function of ratio b/t at different B, T: 3(1); 5(2); 10(3); $\rho_{xx} = 5 \cdot 10^{-11} \Omega \cdot m$

In accordance with the Eq.(7) the effective resistivity is a function of ratio b/t where t is the thickness of strips. So for one limit case when $b/t \rightarrow 0$ the effective resistivity of composite conductor is equal to diagonal component of resistivity tensor ρ_{xx}. Physically it means that the main part of current flows far from the conductor interface so in accordance with the principle of the minimum of entropy generation the systems trends to such a state that ensures the minimal resistance at definite level of current flowing through cross section. The transport current density j_x and transverse current density j_y are zero near interface of conductor. Other limit case when $b/t \rightarrow \infty$ means that the thickness of every strip is so small in comparison with width that the process of shortening of transverse electric Hall field of every component with each other is a single process that can ensure the potentiality of steady electric field. As a result the transverse Hall current is generated and the path of carriers along transport direction is occupated with transverse drift so that on the unit length on path along transport direction the charge carrier has time to drift in transverse direction and the transverse path is of ρ_{yx}/ρ_{xx} higher than the path in transport direction. As a result the collisions of charge carriers with crystal structure imperfections generate a respective resistivity being higher of that mentioned above. For this second limit case the effective resistivity trends to the resistivity of Corbino that. Essentially at more realistic conditions of t/b ratio magnitude some interval case of resistivity have to take place (Fig.2).

4. Conclusion

The accepted expression for effective resistivity is rather idealized one as it operates with model composite conductor. However the approaches developed for this task here seems to be rather reliable as these allow to construct a real physical picture under the presence of opposite types of magnetostimulated gyrotropy in composite conductor consisted of double strips. The father steps in the study of this problem should be done in the direction of understanding the averaging procedure along transverse direction, the analysis of non-symmetric task on geometry and on conductive properties of components. The last thesis is adequate to the situation of real double-strip composite conductor consisted of aluminum and copper components.

References

[1] H. Kaneko and N. Yanagi, *Cryogenics,* Vol. 32, p. 1114, 1992.
[2] M. P. Krefta, O. R. Christianson, and J. H. Parker, Jr, *Cryogenics,* Vol. 36, p. 291, 1996.
[3] V. R. Sobol, O. N. Mazurenko, and A. A. Drozd, *Adv. Cryog. Eng.*, Vol. 42, p. 1063, 1996.

Spatial Inversion of Gyrotropy Parameter in Conductivity Tensor and Charge Transport Peculiarities

V.R.Sobol[1], O. N. Mazurenko[1], and M. Zoli[2]

[1] National Academy of Sciences, Institute of Solid State and Semiconductor Physics
Brovka Street 17, 220072 Minsk, Belarus
Fax: + 375-172-840888; email: sobol@ifttp.bas-net.by

[2] Istituto Nazionale Fisica della Materia,
Dipartimento di Matematica e Fisica, Universita di Camerino
Via Madonna delle Carceri, 62032 Camerino, Italy
Fax: + 39-0737-632525; email: zoli@mail.publigraphic.it

Abstract

Charge transfer is discussed for the case when gyrotropy parameter (Hall coefficient) varies along transport x-direction and inverses its sign. This situation takes place in contacts of the serially joined materials having electron and hole types of conductivity. Spatial inhomogeneity of conductivity and inversion of Hall coefficient sign are analyzed in terms of electric potential and current density distribution. It is shown that under inhomogeneous magnetic field the steady current skinning takes place in plate sample.

1. Introduction

Metal heterocontact between the conductors having electron and hole types of conductivity (for example contact similar to conjunction of Al and Cu plate sample) is an example of bianisotropic medium especially under the action of an external magnetic field. Bianisotropy is a result of opposite signs of Hall coefficients in Al and Cu. As a result such a contact has a transformation of conducting properties from the electron type to the hole that along transport direction and may be represented as an inhomogeneous medium having gradient type of conductivity. The inhomogeneity is not determined with only the electron structure via contact. The magnetic field itself is a reason of magnetostimulated inhomogeneity of conductivity and respective the potential picture rearrangement. As a result the current density redistribution through cross section of sample takes place [1, 2]. So the excessive resistance connected with current line redistribution is a result of conductivity inhomogeneity stimulated with magnetic field and heterogeneous electron conducting properties in such a conjunction. In this paper the double type of electric conductivity inhomogeneity stimulated by bianysotropy and by magnetic field is investigated. In other words the processes taking place in metal heterocontacts placed in inhomogeneous magnetic field are modeled and analysed.

2. Experimental and Theoretical Approach

The procedure of modeling of magnetic field inhomogeneity is based on the method of curving of current lines so that the normal local component of magnetic field has a variation along the transport

direction in accordance with definite law. For simplicity the heterocontact under the investigation have been chosen as a symmetric one consisted of materials not Al-Cu but Al^+-Al^- type. Here Al^+ is an usual widely used aluminum of hole type of conductivity and Al^- is an farfetched electron analogue of Al^+ which has an electron type of conductivity in magnetic field. That is Al^- has an electron type of conductivity so that its Hall coefficient R is equal $-|R|$ instead of R for usual aluminum. So Al^+ and Al^- type components used in experimental modeling process have the same electric resistivity tensors excluding the sign of Hall coefficient. Both components are realized on the base of usual aluminum.

3. Results and Analysis

In experiment two types of magnetic field inhomogeneity in bianisotropy contact medium are modeled. The first type of magnetic field structure is represented in Fig. 1-a) and the second type of magnetic field spatial structure is represented in Fig. 1-b).

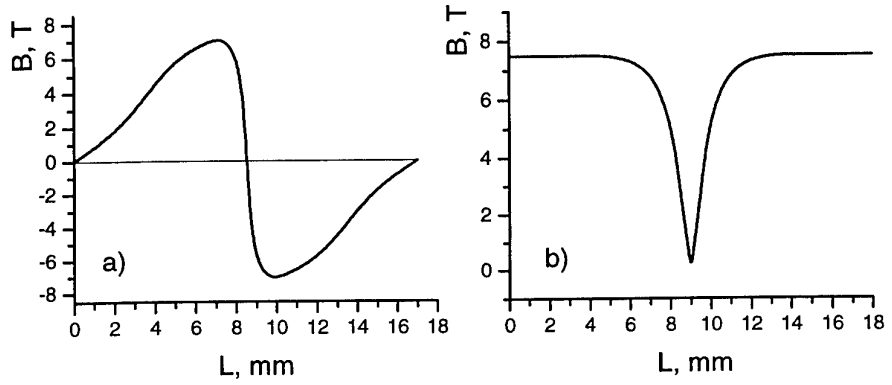

Fig. 1 The topology of magnetic field: a) The inversion type of inhomogeneity; b) The symmetric type of inhomogeneity.

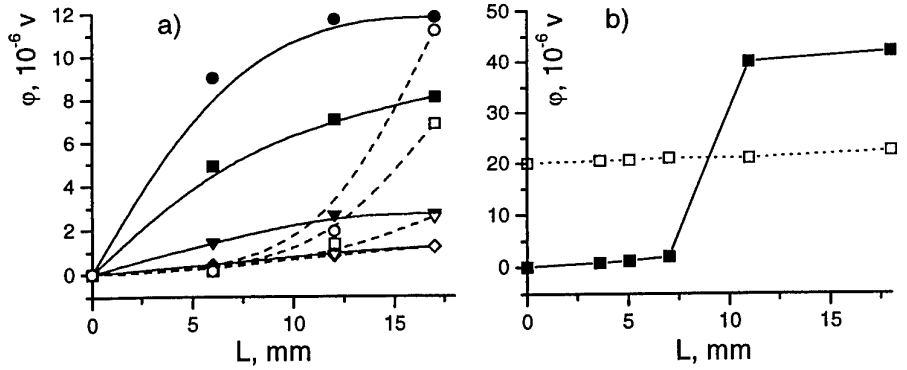

Fig. 2 The potential picture along sample length on opposite sides (solid and dashed lines) in inhomogeneous magnetic field: a) Field topology Fig. 1-a) where the maximal field B, T: 0.14 (diamonds), 1.4 (triangles), 4.3 (squares), 7.1 (circles); b) Field topology Fig. 1-b) where the maximal field is 7.5 T.

Here the potential distribution has been measured on opposite sides of sample in accordance with scheme of potential probes arrangement. Electric field potential picture is represented in Fig. 2 where the potential distribution on opposite Hall sides is shown along sample length L in contact region and close to it. It is interesting that for inversion type of inhomogeneity of magnetic field the potential picture is symmetric respectively zero field point. The strong and weak spatial dependence of potential on L takes place. For symmetric type of magnetic field inhomogeneity the potential dependence on opposite sides is different on behavior. One side has abrupt jump of potential in contact region but another side shows very weak dependence on coordinate along transport direction including the contact region. To analyze this behavior the discontinuity conditions for current density have been used to write the equation for electric potential φ. Taking into account that the thickness of samples directed along the magnetic field is rather small in comparison with other dimensions the approximation had been used that the current flow picture does not influence on potential distribution along z-direction. The carrier motion along magnetic field is neglected and the electric potential is not a function of z-coordinate. So for the two-dimensional geometry the potential equation is

$$\left(\frac{1}{\beta^2}+\frac{\alpha}{\beta}\right)_x'\varphi_x'+\left(\frac{1}{\beta^2}+\frac{\alpha}{\beta}\right)\varphi_{xx}''-\frac{\beta'}{\beta^2}\varphi_y'+\left(\frac{1}{\beta^2}+\frac{\alpha}{\beta}\right)\varphi_{yy}''=0 \qquad (1)$$

Here φ'_x , φ''_x , $(\ldots)'_x$ and so on are the derivatives of respective order, $\beta' = \partial\beta/\partial x$; $\beta = \omega\tau$, ω is Larmor frequency, τ is a relaxation time. The next type of electric conductivity tensor is used

$$\sigma=\sigma_0\begin{pmatrix}\frac{\alpha}{\beta}+\frac{1}{\beta^2} & \frac{1}{\beta} & \frac{1}{\beta}\\ -\frac{1}{\beta} & \frac{\alpha}{\beta}+\frac{1}{\beta^2} & \frac{\alpha}{\beta}+\frac{1}{\beta}\\ -\frac{1}{\beta} & \frac{\alpha}{\beta}-\frac{1}{\beta} & 1\end{pmatrix} \qquad (2)$$

Here σ_0 is the conductivity in zero magnetic field. The component $\sigma_{xx} = 1/\beta^2 + \alpha/\beta$ has such view after taking into account of the existence of a layer of open electron orbits. The term responsible for this layer is α/β which must be accepted in modulo. Following such a presentation the magnetoresistance of aluminum $\rho_{xx}=1/\sigma_0(1+\alpha\beta)$ that is has not very strong slope in linear dependence on magnetic field because the parameter α/β describing the quantity of open electron trajectory is rather small. Respectively the magnetoresistance ρ_{xx} for copper may be represented as the same expression where the linear Kapitza law takes place because the same parameter describing the width of open electron trajectories is closed to unit. The separation of variables allows to get the total decision of equation for some particular cases:

$$\varphi=C_1\left(\int\frac{\beta^2}{1+\alpha\beta}dx\right)\exp\left(\beta'\frac{1}{1+\alpha\beta}y\right)+C_2 \qquad (3)$$

Here this expression is valid when $\beta'/(1+\alpha\beta)$ = const. So for the limit case $\alpha\to 0$ one can obtain the potential distribution in approximation of free electron gas and at nonzero α the potential picture for aluminum and copper separately and for the contact of these materials can be obtained. Following Eq.(3) the potential dependence on sides of sample placed in inhomogeneous magnetic field has strong (at $y = b$, where b is the sample width) and weak (at $y = 0$) dependence on coordinate along transport direction. The direction of magnetic field gradient plays very important role in the potential distribution on the reason that magnetic gradient participates in the governing of transport process via strong exponential dependence on transverse y-coordinate. The transverse dependence of potential on

y-coordinate is much higher of that along transport x-coordinate. Here under inhomogeneity the correspondence between transport electric field and Hall field is similar to homogeneous situation. So for particular case of aluminum type conductor having very small width of elongated trajectories the potential picture and respective current density distribution along transport direction are:

$$\varphi = C_1 \int \beta^2 dx \exp(\beta' y) + C_2 ; \quad j_x = C\beta' \exp(\beta' y); \quad \beta' = const \tag{4}$$

Following this expression the potential dependence on coordinate in transverse magnetic field is rather complicated than that belonging to the homogeneous magnetic field actions which is $\varphi = C(x+\beta y)$. Respectively the steady current skinning takes place. Namely near one of side the current density is large and near opposite side the current density is small. Magnetic field gradient inversion transforms the potential picture and the current skinning center to opposite side. This type of dependence takes place in Fig.2a where the effective inversion of magnetic field gradient sign occurs near zero point because the conductivity is opposite on Hall effect. For Fig.2b the dependence of φ is governed with the effective magnetic field gradient which has the same sign via total sample. The opposite type of conductivity near zero point transforms the effective magnetic actions and the abrupt increase of potential corresponds to an action of exponent in Eq.(4) whereas the weak potential growth on opposite side is a result of decrease of exponential include. As to copper type conductor in heterocontact (experimental results we have no yet), the analysis of Eq.(3) allows to conclude that the potential picture redistribution due to double inhomogeneity also can be estimated. So for copper type conductor the width of layer of open trajectories is to be taken into account and the expressions for the potential dependence is:

$$\varphi = C_1 \int \frac{\beta}{\alpha} dx \exp\left(\frac{\beta'}{\alpha\beta} y\right) + C_2 ; \quad \frac{\beta'}{\alpha\beta} = const \tag{5}$$

The analysis shows that for copper type conductor the potential redistribution due to inhomogeneity is not so high as in aluminum type conductor. The reason of this is the large number of elongated orbits on isoenergetic surface. The carriers of these orbits are not so free to drift in gradient magnetic field and as a result more complicated movement of carriers leads to more weak degree of electric potential and current skinning.

4. Conclusion

The method of modeling of magnetic field inhomogeneity via curving of current lines allowed to create a physical picture of current flow through the aluminum based heterocontact. Aluminum based heterocontact consists of pure aluminum sample have been bent in such manner that an effective magnetic field action is equal to the presence of two heterocomponents having opposite Hall coefficient. Double type of inhomogeneity due to heteroconductivity in magnetic field and due to magnetic field action itself generates current density redistribution via contact region. This redistribution depends strongly on the topology of magnetic field and the excessive heat generation due to current skinning can be taken into account on the base of data have been analyzed here.

References

[1] Yu. A. Dreizin and A. M. Dykhne, *Zh. Eksp. Teor. Fiz.*, Vol. 63, p. 242, 1972 [*Sov. Phys. JETP*, Vol. 36, p. 127, 1972.

[2] V. R. Sobol, O. N. Mazurenko, and A. A. Drozd, *Fiz .Nizk. Temp.*, Vol. 25, p. 1211, 1999 [*Low Temp. Phys.*, Vol. 25, p. 907, 1999].

Research of Optical Activity and Circular Dichroism in Some Uniaxial Crystals in Directions Different from an Optical Axis

A.F. Konstantinova[1], Z.B. Perekalina[1], K.A. Kaldybaev[2], and V.P. Orekhova[1]

[1] Institute of Crystallography, Russian Academy of Sciences
117333 Moscow, Leninsky pr.59, Russia
Fax: +007-095-135 1011: email: afkonst@usa.net
[2] Issyk-Kul University, Karakol, Kirgysja

Abstract

The research of optical activity in some uniaxial crystals was done based on the spectropolarimeter method. The measurements were conducted on the plates cut perpendicularly to and parallel to axis in visible spectrum range. Dispersion of all components of gyration pseudotensor for a number of uniaxial crystals was determined for the first time from these measurements. The absorption spectra and circular dichroism of crystals of gallogermanate $Sr_3Ga_2Ge_4O_{14}$, undoped and doped by chromium were investigated.

1. Introduction

The special place among optical properties of crystals occupies a phenomenon of optical activity, or gyrotropy [1,2]. Two circular polarized waves propagate in absorptive isotropic media and in anisotropic crystals in the direction of optical axis. That results in rotation of the plane of polarization and circular dichroism. In directions different from optical axis two elliptically polarized waves propagate. In that case it is possible to talk about elliptical birefringence and elliptical dichroism. The optical activity is described by a gyration pseudotensor of the second rank. (a prefix pseudo we will omit). By measuring rotation of the plane of polarization it is possible to determine only one component. Other components can be determined if measurements are conducted on plates cut in directions different from optical axis. That is not a simple problem, because it is necessary to determine small components of a gyration tensor on a background of rather large birefringence. Therefore to the present time very few crystals are known, for which all components of a gyration tensor are determined even though these values are relevant characteristic of crystals.

The purpose of the present article is the research of an optical activity and also determination of components of a gyration tensor in some uniaxial crystals of a different symmetry class in directions different from direction from optical axis.

2. Theoretical Relations

All values describing optical properties of crystals are complex in absorptive gyrotropic crystals:

$$N_{1,2} = n_{1,2} + i\kappa_{1,2},\ G = G' + iG'',\ k = k' + ik'', \qquad (1)$$

where N_1, N_2- complex refractive indices, n_1 n_2 - refractive indices, κ_1 , κ_2 - absorption coefficients, G - scalar parameter gyration, which is determined by components of a gyration tensor and depends on a symmetry of crystal and propagation direction of light in crystal, ellipticity of eigen waves

propagating in crystal (b/a = tgγ) and angle of non-orthogonality (β) are determined from relation [2,3]:

$$\sin 2\gamma = 2k'/(1+ k'^2 + k''^2),\ tg2\beta = 2\,k''/(1 - k'^2 - k''^2). \quad (2)$$

In transparent crystals ellipticity of eigen waves is equal k = k'.

In uniaxial crystals in direction parallel to optical axis eigen waves are circular polarized and we have

$$k' = \pm 1,\ k'' = 0,\ G = g'_{33} + ig''_{33}. \quad (3)$$

Component of gyration tensor g'_{33} is calculated from measurement of an angle ρ of rotation of polarization plane on a spectropolarimeter: $g'_{33} = \rho\lambda n_0/\pi$. Component g''_{33} is calculated from a relation $g''_{33} = \Delta\varepsilon\ \lambda n_0/4\pi c$, where, $\Delta\varepsilon = \Delta D/d$, ΔD is optical density recorded on dichrograph, *c* is concentration of dope, d is thickness of investigated plate, λ is wavelength of incident light.

In directions perpendicular to direction of optical axis in uniaxial crystals $G = g'_{11} + ig''_{11}$, the values k' and k' are small and they are equal [3]:

$$k' = [g'_{11}\delta n_l + g''_{11}\delta\kappa_l]/[2\ n_0(\delta n_l^2 + \delta\kappa_l^2)], \quad (4a)$$

$$k'' = [g''_{11}\delta n_l - g'_{11}G'\delta\kappa_l]/[2\ n_0(\delta n_l^2 + \delta\kappa_l^2)], \quad (4b)$$

where $\delta n_l = (n_2 - n_1)$ is linear birefringence, $\delta\kappa_l = (\kappa_2 - \kappa_1)$ is linear dichroism, $\delta n_c = g'_{11}/n_0$ is a circular birefringence, $\delta\kappa_c = g''_{11}/n_0$ is a circular dichroism, n_0 is an average value of refractive indexes.

In directions, different from optical axis we can obtain the most informative expressions for the azimuth χ of passed light in cases, when the incident wave with azimuth α is linearly polarized in direction parallel to (∥) ($\alpha = 0^\circ$) or perpendicular to (⊥) ($\alpha = 90^\circ$) principal plane (that is plane, in which optical axis and normal to the surface are located). Unlike inactive crystal in these cases the light propagated through a plate is not linear but elliptically polarized with azimuth χ. When k' and k" are small we have for azimuth of transmitted light $\chi_{\parallel,\perp}$:

$$tg2\chi_{\parallel,\perp} = -2\,[e^{\pm\delta}\,k'\sin\Delta \pm k''(1 + e^{\pm\delta}\cos\Delta)], \quad (5)$$

where $\Delta = 2\pi d\ \delta n_l/\lambda$, $\delta = 2\pi d\ \delta\kappa_l/\lambda$.

The values of $tg2\chi_\perp \neq tg2\chi_\parallel$ for different a wavelength of an incident light and they oscillate, since the periodic functions sinΔ and cosΔ change. It is possible to measure the azimuth of transmitted light $\chi_{\parallel,\perp}$ on a spectropolarimeter for different wavelengths of an incident light. Thus it is necessary to know values of a birefringence and dichroism, which one can be calculate from the same experiment. In most cases k'> k", then it is possible to consider that

$$tg2\chi_{\parallel,\perp} = -2\,e^{\pm\delta}\,k'\sin\Delta. \quad (6)$$

In transparent crystals the value δ = 0. Then expression (5) becomes simpler. In these cases envelope of a curve of oscillating functions $\chi_\parallel = \chi_\perp$ and we can determine the value k' and accordingly to calculate component $g'_{11} = 2k'\ n_0\ \delta n_l$.

3. Determination of Components of Gyration Tensor in Uniaxial Crystals

We conduct the research of an optical activity of the following crystals: undoped and Cr-doped $Sr_3Ga_2Ge_4O_{14}$ and also KH_2PO_4 (KDP), $NH_4H_2PO_4$ (ADP), K_2S2O_6, $SrS_2O_6\cdot 4H_2O$.

The crystals $Sr_3Ga_2Ge_4O_{14}$, $K_2S_2O_6$, $SrS_2O_6\cdot 4H_2O$ and $Sr_3Ga_2Ge_4O_{14}$ have symmetry classes 32, 3 and 6 accordingly. Crystals of these classes of symmetry can rotate plane of polarization. The

investigated plates were cut parallel to and perpendicular to the c-axis of crystals with dimensions 10x10 mm^2 with thickness varying from 0.5 to 1.5 mm.

We conduct measurements of relations $\chi_{\parallel,\perp}(\lambda)$ for all investigated plates on spectropolarimeter [4] using method, described in [3]. The dependence of azimuth $\chi_{\parallel,\perp}$ for crystal $Sr_3Ga_2Ge_4O_{14}$:Cr is shown on Fig. 1. According to relation (6), enveloped curve of oscillations is determined by $e^{\pm\delta}k'$. After determination of dispersion of an ellipticity of eigen waves k' and value δ it is possible to calculate dispersion of components of a gyration tensor g'_{11}. In order to calculate the value g'_{11} except for measured values k' it is necessary to know values of birefringence, average refractive indices and value δ. Values g'_{33} and g'_{11} for crystal $Sr_3Ga_2Ge_4O_{14}$ are shown in Fig.2.

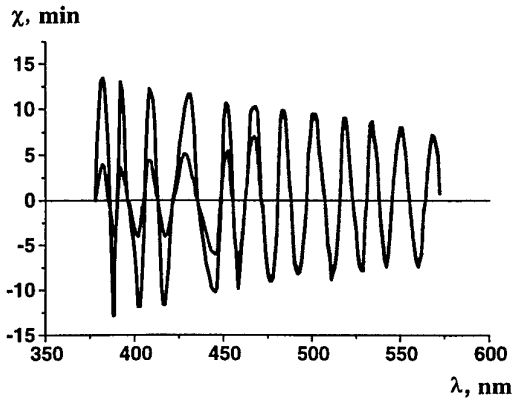

Fig. 1 Dependence of azimuth of transmitted light χ from wavelength λ for a plate cut from a crystal $Sr_3Ga_2Ge_4O_{14}$: Cr^{3+}parallel to optical axis for two polarization of incident light (d = 0.96 mm)

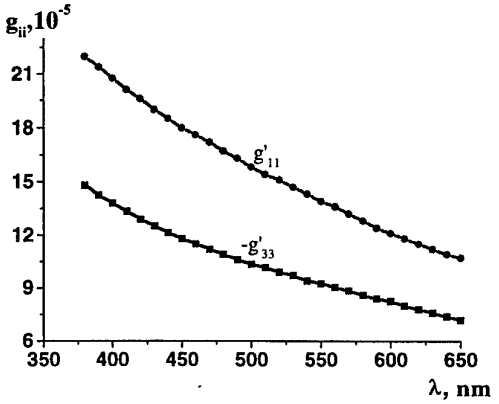

Fig. 2 A dispersion of components of gyration pseudotensor g'_{11} and g'_{33} for crystal $Sr_3Ga_2Ge_4O_{14}$: Cr^{3+}

Absorption spectra for crystals $Sr_3Ga_2Ge_4O_{14}$:Cr were measured in the range 250 - 800 nm. In absorption spectra of these crystals three bands connected with ions Cr^{3+} in octahedral coordination are found. The circular dichroism (CD) spectra were studied in the range 250 - 800 nm on dichrograph, constructed and made in Institute of Crystallography of RAS [5]. In order to calculate components of g''_{33} correctly, it is necessary to take into account concentration *c* of doped Cr. Since value *c* is not determined precisely, we present only dependence $\Delta\varepsilon$ of crystal $Sr_3Ga_2Ge_4O_{14}$:Cr on Fig. 3. It is found that CD is present in all three broad absorption bands of spectra and in the narrow R-line (~ 700nm) of Cr^{3+} ions. In spectra of circular dichroism of doped crystals the bands of absorptions connected with ions Cr^{3+} were also found. Besides that in spectra of circular dichroism the additional bands are observed. These bands are not associated with ions Cr^{3+}. In spectra circular dichroism of undoped crystals the same bands CD were also found (curve 2). Probably all bands observed in the spectra of circular dichroism of undoped crystals can be attributed to defects generated during crystal growth.

Crystals KDP, ADP and K_2S2O_6, $SrS_2O_6 \cdot 4H_2O$ were transparent in visible range of spectra. The crystals KDP and ADP belong to a symmetry class $\bar{4}2m$ and do not have optical activity in the direction optical axis of a crystal. However, in crystals of given symmetry class the gyrotropy can appear in directions different from optical axis. In order to determine the components of gyration tensor the plates were cut in crystallographic directions X and Y.

Dependences of azimuth $\chi_{\parallel,\perp}$ were obtained for these crystals. Now we have $\chi_{\parallel} = \chi_{\perp}$. From these dependences we calculated dispersion of components g'_{11}, which is shown in Fig. 4. Research was done for KDP crystals and ADP crystals on plates X and Y - cut of identical thickness. IN this case

azimuths χ (λ) have opposite phases. Therefore $g'_{11} = - g'_{22}$. This is how it should be in crystals of this symmetry class. The value of component of gyration tensor g'_{11} for KDP crystal is larger than in ADP crystal.

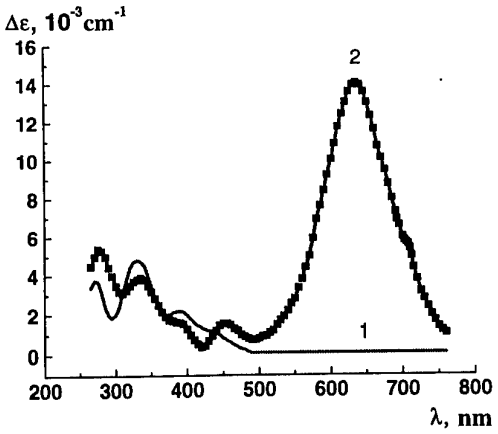

Fig. 3 Circular dichroism spectra of undoped crystal $Sr_3Ga_2Ge_4O_{14}$: (curve 1) and Cr-doped crystal $Sr_3Ga_2Ge_4O_{14}$ (curve 2)

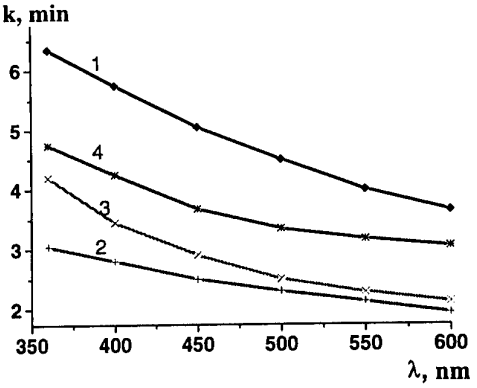

Fig. 4 A dispersion of components of gyration pseudotensor g'_{11} for crystals: 1-KH_2PO_4 (KDP), 2-$NH_4H_2PO_4$ (ADP) 3 - K_2S2O_6, 4 - $SrS_2O_6 \cdot 4H_2O$

The component g'_{11} for KDP crystal was determined in [6] for two wavelengths $\lambda = 462$ nm and 506 nm. The values g'_{11}, obtained in this article is larger than these obtained by us. At the same time in more recent article of the same authors [7] values of g'_{11} are much less than values obtained by them in [6] and values obtained by us.

Dispersion of gyration tensor components g_{11} is obtained for crystals $Sr_3Ga_2Ge_4O_{14}$, KDP, ADP, $K_2S_2O_6$, SrS_2O_6 $4H_2O$ for the first time.

The absorption spectra and circular dichroism of gallogermanate crystals $Sr_3Ga_2Ge_4O_{14}$, undoped and Cr-doped are investigated.

References

[1] T. M. Lowry, *Optical Rotatory Power*. London: Longmans, Green and Co., p. 483, 1935.

[2] F. I. Fedorov, *The Theory of Gyrotropy*. Minsk: Science and Engineering, p. 457, 1976 (in Russian).

[3] A. F. Konstantinova, B. N. Grechushnikov, D. V. Bokut', and E. G. Valjashko, *Optical Properties of Crystals*. Minsk: Science and Engineering, p. 302, 1995 (in Russian).

[4] Z. B. Perekalina, G. D. Shnyrev, A. B. Mirensky, *et al.*, *Crystallography*, Vol. 10, p. 270, 1965.

[5] Z. B. Perekalina, U. I. Vologin, I. A. Kudryashov, and K. A. Kaldybaev, *Zh. Priclad. Spectr.*, Vol. 43, p. 328, 1985.

[6] J. Kobayashi, T. Takahashi, and T. Hosokawa, *J. Appl. Phys.*, Vol. 49, p. 809, 1978.

[7] M. Takada, N. Hosogaya, Someya, and J. Kobayashi, *Ferroelectrics*, Vol. 96, p. 295, 1989.

Optical Dichroism of Homeotropically Oriented Films of Comb-shaped Liquid Crystal Polymer

D. F. Kiselev, T. M. Glushkova, S. A. Ivanov, M. M. Firsova, and A. P. Shtyrkova

Department of Physics, Lomonosov Moscow State University,
Vorob'evy Hills, Moscow, 119899, Russia.
Fax: (095) 939-14-89: E-mail kiselevdf@mail.ru

Abstract

In this work the polarization absorption spectrum of homeotropically oriented comb-shaped liquid crystal polymer (LCP) film interposed in the electrooptical cell was investigated. The optical parameters of electrodes and polymer were estimated from the observed absorption spectra of the cell with and without polymer film using the method of interferometric extrema envelopes. This method enabled us to re-establish the true polarization absorption spectrum of the polymer. For this purpose the refractive index dispersion data of the substrates and the polymer obtained by independent investigations were used. From the dichroic ratio for the absorption band at $\lambda = 405$ nm the order parameter S was estimated taking into account the effects of local fields.

1. Introduction

Recently the oriented liquid crystal (LC) and liquid crystal polymer (LCP) films have occupied an important position in modern technologies and have been widely used as a material of integral optic elements, in optical recording and optical information systems including the polarization holography also [1–5].

The important characteristic of the oriented films is the orientation degree of the anisotropic molecules in LC films or mesogenic groups in LCP films. One of the methods of orientation degree estimation is the measurements of light absorption anisotropy (optical dichroism) of the polymer itself or dye absorption bands. The method is widely used for the films with planar orientation when the crystal optical axis is situated in the film's plane [6,7,8]. For such film orientation the dichroic ratio is easily obtained as the absorption coefficients ratio for the light polarization parallel and perpendicular to the crystal optical axis. However the producing of sufficiently large homogenous LCP films with planar orientation is connected with essential technical difficulties. Therefore for LCP films the homeotropical orientation is used when the crystal optical axis is directed perpendicular to the film plane. In this case for dichroic ratio estimation it is necessary to use the oblique polarized light incidence for the absorption coefficient measurements in the samples under study. To obtain the homeotropical orientation of the LCP sample the latter is placed in the electrooptical cell. The electrooptical cell is a multilayer system (sandwich) consisting of two substrates with thin electroconducting semiconductor films (electrodes) between which a thin layer of the polymer investigated is placed. When the oblique beam incidence is used the observed polarization absorption spectra are depending on Fresnel reflection losses at all layer boundaries of the cell and besides that on the absorption of these layers. The problem is reduced to LCP absorption coefficient estimation from the experimentally observed transmission spectra for the cell with and without the polymer film investigated using the light beam with different polarization.

2. The Theory of Method

Let us consider the case of isotropic absorbing film (electrode) placed between two isotropic transparent infinite dielectric layers (air – glass). If the refractive indices of dielectric, the complex refractive index of the electrode film and its thickness are known, the energetic transmission T and reflection R coefficients may be calculated from the expression, formulated in [9] both for the case of TE wave (s - polarization) and TM wave (p – polarization). In our case the thickness of the dielectrics is finite and the cell as a whole is a symmetrical system – air (1) – substrate (3) – electrode (2) – air (4) - electrode (2) – substrate (3) – air (1). In this case the transmission I_0 of the cell without polymer may be expressed by the following formula [10].

$$I_o = J_0^2 = (T_{34}T_{31})^2 / (1 - R_{34}R_{31})^2 , \qquad (1)$$

where the transmission T_{31} and reflection R_{31} are calculated for the infinite layers [9] and T_{34} and R_{34} are the Fresnel energetic transmission and reflection coefficients on the boundary of the substrate material (glass (3) – air (4)). As the calculations show the denominator in formula (1) differs from the unity by $\approx$ 1% and therefore later on we shall neglect this difference. Also we shall assume the absorption in the electrode to be sufficiently small to neglect the k^2 quantity compared with k in the expression of electrode complex refractive index $n_2^* = n_2(1-ik)$. In this case the quantity J_0 may be transformed to the following form:

$$J_0 = (64a^2b^2c^2exp(-\gamma_2)/[(a+c)^2(b+c)^2exp(\gamma_2)+(a-c)^2(b-c)^2exp(-\gamma_2)+2(a^2-c^2)(c^2-b^2)cos\varphi](a+b)^2 \qquad (2)$$

where $a = cos\, i_0$ (i_0 – external angle of light incidence on the cell); $b_\perp^2 = n_3^2 - sin\, i_0$; $b_{||} = b_\perp / n_3^2$ (n_3 is the refractive index of substrate material (glass)); $c_\perp^2 = n_2^2 - sin\, i_0$; $c_{||} = c_\perp / n_2^2$ ($\perp$ is s - polarization and $||$ is p – polarization). The absorption in the electrode is defined by the expression $\gamma_2 = \varphi n_2^2 / c_\perp^2$, where $\varphi = 4\pi h c_\perp / \lambda$ (h is the electrode thickness, λ - light wavelength). So for any angle i_0 (if the parameters of substrate n_3, electrode n_2 and γ_2 and its thickness h are known) we can calculate the relative intensity of the polarized light transmitted though the cell. However the inverse problem solution – that is the estimation of the optical characteristics of substrate and electrode from the experimentally obtained transmission spectrum – is related to certain difficulties. In general case for the absorbing substrate and absorbing electrode this problem has not any analytical solution. For the approximate solution the most known method is the spectrophotometrical one of interferometric extrema envelops, which for the first time was suggested for transmission spectra by Valeev [11] and elaborated by Rakov [10]. The reflection spectra was worked out in detail by Filippov [12,13].

The point of the method consists in employing the interferometric extrema envelops for obtaining the wavelengths and light intensity for the maxima J_+ and minima J_- of the experimental quasi-periodic spectrum. The extremum arises at the condition (see (2)) $cos\, \varphi = (-1)^m$ (m – being an integer). In this case the expression (2) may be essentially simplified. Multiplying the numerator and the denominator by $exp(-\gamma_2)$ and extracting the square root we see that the denominator is a product of two perfect squares. Further introducing the denomination

$$A' = (I_+(a+b))^{0,25} / 8ab \qquad (3a)$$

$$A'' = (I_-(a+b))^{0,25} / 8ab \qquad (3b)$$

$$F = (a+b)+(A'-A'')/2A'A'', \qquad (3c)$$

we obtain:

$$c = 0,5(F) + (0,25F^2 - ab)^{0,5} \qquad (4a)$$

$$exp(\gamma_2) = [c - A'(a-c)(c-b)] / A'(a+c)(c+b), \quad (4b)$$

where the values c and $exp(\gamma_2)$ are defined only for the extrema wavelengths. The thickness of the electrodes h may be calculated from the condition $4h = m_i\lambda_i / c_i$. To obtain the values $c(\lambda)$ and $\gamma_2(\lambda)$ for all wavelengths it is possible to use the dispersion dependence model of Chandrasekhar-Drude:

$$n_2^2 - 1 = A\lambda^2 / (\lambda^2 - \lambda_0^2) \quad (5a)$$

$$n_2^2 k = \lambda c\gamma_2 / 4\pi h = B\lambda^3 / (\lambda^2 - \lambda_0^2)^2. \quad (5b)$$

Having the values of h and $n_2^2 k$ for the extrema, A,B, and λ_0 parameters may be obtained and functions $c(\lambda)$ and $\gamma_2(\lambda)$ accordingly.

Let us consider the second part of the problem – that is the absorption indicatrix components estimation for the LCP investigated. For this purpose we shall transform the expression (2) for the case of the cell filled with LCP

$$J_{LCP}=[64adb^2c^2exp(-\gamma_2)exp(-\gamma_{LCP})^{0,5}] / [exp(\gamma_2)(d+c)^2(b+c)^2+exp(-\gamma_2)(d-c)^2(b-c)^2 +$$

$$+2(d^2-c^2)(c^2-b^2)cos\varphi](a+b)^2 \quad (6)$$

where the d parameter was obtained from the independent measurement N_o, N_e [14,15]. This parameter is characterizing LCP as an uniaxial crystal and its value depends on incident light polarization [9,16]: $d_\perp = (N_o^2 - sin^2 i_0)^{0,5}$ (for s – polarization) and $d_{||} = (n_e^2 - sin^2 i_0)^{0,5} / n_e^2$ (for p – polarization), where N_o, N_e are the principle refractive indices of LCP, and

$$n_e^2 = N_o^2 + [(N_e^2 - N_o^2)sin^2 i_o] / N_e^2. \quad (7)$$

Dividing the equation (6) on (2) we solve the resulting equation relatively γ_2 for both types of incident light polarization. Further, using the relation $\gamma_{LCP} = \alpha_{LCP}h_{LCP}$ we obtain the values $\alpha_\perp^{angl}$ and $\alpha_{||}^{angl}$. Extracting the imaginary part from the Fresnel equation [9,16] for the uniaxial absorbing crystals we obtain absorption ellipsoid principal values $\alpha_\perp^0$ and $\alpha_{||}^0$. The ratio of absorption indicatrix principal values (for maximum of absorption band) $N = \alpha_{||}^0 / \alpha_\perp^0$ is termed the dichroic ratio.

3. Experimental Results and Discussion

The object of investigation in our work was the acryl copolymer containing easily oriented in the external electric field cyanbiphenil mesogenic groups. The structural formula and some optical properties of this LCP are presented in [14,15].

After the statistical processing of the quasi-periodical transmission spectra of the empty cell recorded for TE and TM waves at $i_0 = 0$ and $i_0=45^0$ the following electrode parameters were evaluated by the above mentioned technique:

A = 1,79±0,01; B = 0,0008±0,0005; λ_o = 0,219±0,003 μm and h = 0,45 μm.. From the transmission spectra of the cell with the polymer, using the data of the refractive index dispersion obtained in [14,15], the true polymer absorption spectra $\alpha_{||}^0(\lambda)$ and $\alpha_\perp^0(\lambda)$ were re–established. The both spectra have shown a pronounced maximum in the vicinity of λ≈0,405 nm. For this maximum the dichroic ratio N = 2,67 was obtained. As it is known [6,7,8] the orientational order parameter S is related to the effective dichroic ratio value N^* by the following expression $S = (N^* - 1) / (N^*+2)$. The dichroic effective value differs from the true one by the correction factor g, define by the local field model chosen [17]. For the simplest Vuks-Chandrasekhar-Madhusudana model [6] $g = N_e/N_o$. In this case $N^*=gN$ = 3,32 and hence S = 0,44. This value of parameter S essentially differs from the value S obtained by us formerly [15] for the same polymer from the refractometrical data. This unexpected

result has motivated us to reconsider the method of refractive index temperature dependence approximation used in [15]. These new researches carried out have led to the new value of $S = 0{,}42$ [18] which is satisfactory coinciding with the value obtained from the dichroic ratio in the present investigation.

Acknowledgment

The authors are thankful to V. P. Shibaev and S. G. Kostromin for placing in their disposal the polymer investigated and to E. Svetlischeva for assistance in the experimental process.

References

[1] V. P. Shibaev and S. V. Belyaev, *Vysokomolek. Soed. A,* vol. 32, no. 12. p. 266, 1990.
[2] *Polymer as Electrooptical and Photooptical Active Media,* V. P. Shibaev (Ed.). Berlin: Springer-Verlag, p. 37, 1996.
[3] *Side Chain Liquid Crystalline Polymers,* C. B. McArdle (Ed.). New York, 1989.
[4] V. P. Shibaev, S. G. Kostromin, and S. A. Ivanov, *Vysokomolek. Soed. A*, vol. 39, no. 1, p. 43,1997.
[5] V. P. Shibaev, I. P. Yakovlev, S. G. Kostromin, *et al.,Visokomolek. Soed A.*, vol. 32, no. 7. p. 1552, 1990.
[6] L. M. Blinov, *Electro- and Magneto-optics of Liquid Crystals (in Russian).* "Nauka", 1978.
[7] L. M. Blinov, V. A. Kisel, V. G. Rumyantsev, and V. V. Titov, *Journal de Physique,* Coll.-C1, vol. 36, p. C1-69, 1975.
[8] L. V. Blinov, V. A. Kisel, V. G. Rumyantsev, and V. V. Titiv, *Crystallografia,* vol. 20, no. 6, p. 1242, 1975.
[9] M. Born and E.Wolf, *Principles of Optics.* Oxford, 1964.
[10] A. V. Rakov, *Spectrophotometry of Semiconductor Thin-Film Structures*" (in Russian). Sov, Radio, 1975.
[11] A. S. Valeev, *Optika i Spektroskopia*, vol. 15, no. 4, 1963; vol. 18, no. 5, p. 498, 1965.
[12] V. V. Filippov, *Optica i Spertroskopya,* vol. 78, no. 5, p. 798, 1995.
[13] V. V. Filippov and V. P. Kutavichus, *Proceedings SPIE, "Polarimetry and Ellipsometry",* vol. 3094, p. 349, 1996.
[14] T. M. Glushkova, S. A. Ivanov, D. F. Kiselev, *et al,. Vestnik Mosk. Universiteta,* Ser. 3, Fisika, Astronomiya, vol. 36, no. 3, p. 33, 1995.
[15] A. P. Shtyrkova, T. M. Glushkova, S. A. Ivanov, *et al., Proc. of Bianisotropics' 97,* W. S Weiglhofer (Ed.), Glasgow, p. 289, 1997.
[16] A. F. Konstantinova, B. N. Grechushnikov, B. V. Bokut', and E. G. Valyashko. *Optical Properties of Crystal* (in Russian). Minsk, 1995.
[17] E. M. Aver'yanov and M. A. Osipov, *Uspekhi Fiz. Nauk,* vol. 160, no. 5. p. 89, 1990.
[18] T. M. Glushkova, S. A. Ivanov, D. F. Kiselev, *et al., Vestnik Mosk. Universitet,*. Ser. 3, Fisika, Astronomiya, vol. 41, no. 3, p. 24, 2000.

Effective Constitutive Tensors of Bianisotropic Multilayered Mediums

A. N. Borzdov

Department of Theoretical Physics, Belarusian State University
Fr. Skaryny avenue 4, 220050 Minsk, Belarus
Fax: + 375 - 172 - 06 60 01; E-mail: alexbor@phys.bsu.unibel.by

Abstract

Operator formalism is employed for introduction of effective constitutive tensors of bianisotropic multilayered periodic strucures in a wide wave band. It is based on the approximate calculation of the characteristic matrix of the unit cell of the system with the help of Campbell–Hausdorff series [1]. In this paper we show that effective constitutive tensors can be correctly introdused for a greate variety of mediums.

1. Introduction

One of the most fruitful approaches in the theory of propagation of waves in multilayered media is the operator formalism based on the use of intrinsic representation of vectors and operators (see [2], [3], for example). It enables one to find compact coordinate–free formulae for very complex systems and to avoid the cumbersome calculations required by usual components techniques and caused mainly by the necessity of adopting a different coordinate system for each different layer.

In this paper we use this formalism to find the effective constitutive tensors of the medium formed by a periodic set of plane bianisotropic layers with different thicknesses l_n ($n = 1, 2, \ldots N$, where N is the number of the layers which constitute the unit cell).

In what follows we assume the constitutive relations

$$\mathbf{D}_n = \varepsilon_n \mathbf{E}_n + \alpha_n \mathbf{H}_n, \ \mathbf{B}_n = \beta_n \mathbf{E}_n + \mu_n \mathbf{H}_n, \tag{1}$$

for layer's materials, where ε_n, μ_n and α_n, β_n are the dielectric permittivity, the magnetic permeability tensors and the pseudotensors of gyrotropy, respectively. These equations can be also written in matrix form, as

$$\begin{pmatrix} \mathbf{D}_n \\ \mathbf{B}_n \end{pmatrix} = \mathcal{R}_n \begin{pmatrix} \mathbf{E}_n \\ \mathbf{H}_n \end{pmatrix}, \ \mathcal{R}_n = \begin{pmatrix} \varepsilon_n & \alpha_n \\ \beta_n & \mu_n \end{pmatrix}. \tag{2}$$

If ε_n, μ_n, α_n, β_n ($n = 1, 2, \ldots N$) are complex nonsymmetric tensors, then equations (1) or (2) describe an absorbing anisotropic and gyrotropic medium, subject to the influence of external electric and magnetic fields and elastic deformations.

The main purpose of this paper is to introduce the medium's effective material tensors, feasible for the use in the wide wave band.

2. Effective Constitutive Tensors in Wide Wave Band

To treat this problem we use here an approach to introduce the effective material parameters, proposed in [4]. It is based on the approximate calculation of the characteristic matrix P of the unit cell of the system with the help of Campbell–Hausdorff series [1].

The characteristic matrix $P = \exp(ik_0 lM)$ of a layer with thickness l relates the six-vectors $(\mathbf{E}, \mathbf{H})^T$ at the layer boundaries ($k_0 = \omega/c$). The matrix M can be written in the form [5]

$$M = \mathcal{T}_q Q_\times (\mathcal{R} - \mathcal{B}_\times) \mathcal{T}_q, \tag{3}$$

$$Q_\times = \begin{pmatrix} \mathbf{0} & -\mathbf{q}^\times \\ \mathbf{q}^\times & \mathbf{0} \end{pmatrix}, \ \mathcal{B}_\times = \begin{pmatrix} \mathbf{0} & -\mathbf{b}^\times \\ \mathbf{b}^\times & \mathbf{0} \end{pmatrix}, \tag{4}$$

$$\mathcal{T}_q = \mathcal{E} - \mathcal{N}_q, \ \mathcal{E} = \begin{pmatrix} 1 & 0 \\ 0 & 1 \end{pmatrix}, \ \mathcal{N}_q = \mathcal{R}_q^{-1} Q (\mathcal{R} - \mathcal{B}_\times), \ Q = \begin{pmatrix} \mathbf{q}\otimes\mathbf{q} & \mathbf{0} \\ \mathbf{0} & \mathbf{q}\otimes\mathbf{q} \end{pmatrix}, \tag{5}$$

where operator $\mathcal{R}_q^{-1}$ is the inverse to the operator

$$\mathcal{R}_q = \begin{pmatrix} \varepsilon_q \mathbf{1} & \alpha_q \mathbf{1} \\ \beta_q \mathbf{1} & \mu_q \mathbf{1} \end{pmatrix}, \tag{6}$$

$$\varepsilon_q = \mathbf{q}\varepsilon\mathbf{q}, \mu_q = \mathbf{q}\mu\mathbf{q}, \alpha_q = \mathbf{q}\alpha\mathbf{q}, \beta_q = \mathbf{q}\beta\mathbf{q},$$

$\mathbf{q}^\times$ is the antisymmetric dyadic dual to the unit normal of the boundaries $\mathbf{q}$, $\mathbf{b}$ is the tangential component of refraction vector $\mathbf{m}$ [2],[3], $\mathbf{q}\otimes\mathbf{q}$ is the dyad and $\mathbf{1}$ is the unit dyadic.

In the case of a medium formed by two alternate layers with different thicknesses l_n and different sets of tensor constants $\varepsilon_n, \mu_n, \alpha_n, \beta_n$ $(n = 1, 2)$, the characteristic matrix of the unit cell has the form

$$P = \exp(ik_0 LM) = \exp(ik_0 l_2 M_2) \exp(ik_0 l_1 M_1), \tag{7}$$

where $L = l_1 + l_2$ is the system period and M is some matrix. This matrix can be expressed in terms of the layers parameters with the help of Campbell–Hausdorff series as follows

$$M = \begin{pmatrix} A & B \\ C & D \end{pmatrix} = f_1 M_1 + f_2 M_2 + i f_1 \frac{\pi l_2}{\lambda} [M_2, M_1] - \cdots \tag{8}$$

where $f_n = l_n/L$ is the relative thickness of the n-th layer, $\sum_{n=1}^{N} f_n = 1$, $[M_2, M_1] = M_2 M_1 - M_1 M_2$. If $\pi l_n/\lambda \ll 1$, then the series (8) quickly converges and one can drop the remainder of it after the k–th term. Here for the sake of simplicity we have limited our consideration by three terms of series. The first and the second terms correspond to the long wavelength limit.

The tensor parameters A, B, C, D can be directly used for the analysis of the wave propagation in the considered system, for example for finding the reflection and transmission tensors [3].

For the sake of simplicity we assume $\mathbf{q}$ to be the left and the right eigenvector of each of the tensors $\varepsilon_n, \mu_n, \alpha_n, \beta_n$ $(\varepsilon_n \mathbf{q} = \mathbf{q}\varepsilon_n \equiv \varepsilon_{nq}\mathbf{q}, \cdots)$. Besides, we shall use in (7)–(8) the matrices M_I, M_{1I}, M_{2I}, describing the transformation of the tangential components of the field vectors, instead of M, M_1, M_2, describing the transformation of the full six-vectors. In the majority of applications this would be ample. Under above–mentioned conditions:

$$M_{nI} = Q_\times \left[\mathcal{R}_n - \frac{1}{\delta_n} \mathcal{R}_{nq}^T \begin{pmatrix} \mathbf{a}\otimes\mathbf{a} & \mathbf{0} \\ \mathbf{0} & \mathbf{a}\otimes\mathbf{a} \end{pmatrix} \right] \mathcal{T}, \tag{9}$$

$$\mathcal{T} = \begin{pmatrix} I & 0 \\ 0 & I \end{pmatrix}, \; I = \mathbf{1} - \mathbf{q} \otimes \mathbf{q}, \tag{10}$$

where $\mathcal{R}_{nq}^T$ is the transposed operator, $\mathbf{a} = \mathbf{b}\mathbf{q}^\times$,

$$[M_{2I}, M_{1I}] = Q_\times \left[\mathcal{R}_{21} - \Delta(\mathbf{a})\right] \mathcal{T}, \tag{11}$$

$$\mathcal{R}_{21} = \mathcal{R}_2 Q_\times \mathcal{R}_1 - \mathcal{R}_1 Q_\times \mathcal{R}_2, \tag{12}$$

$$\Delta(\mathbf{a}) = \Delta_L \begin{pmatrix} \mathbf{a}\otimes\mathbf{a} & \mathbf{0} \\ \mathbf{0} & \mathbf{a}\otimes\mathbf{a} \end{pmatrix} + \begin{pmatrix} \mathbf{a}\otimes\mathbf{a} & \mathbf{0} \\ \mathbf{0} & \mathbf{a}\otimes\mathbf{a} \end{pmatrix} \Delta_R, \tag{13}$$

where

$$\Delta_L = \left[\mathcal{R}_{2I} Q_\times \frac{\mathcal{R}_{1q}^T}{\delta_1} - \mathcal{R}_{1I} Q_\times \frac{\mathcal{R}_{2q}^T}{\delta_2}\right], \; \Delta_R = \left[\frac{\mathcal{R}_{2q}^T}{\delta_2} Q_\times \mathcal{R}_{1I} - \frac{\mathcal{R}_{1q}^T}{\delta_1} Q_\times \mathcal{R}_{2I}\right], \tag{14}$$

and $\mathcal{R}_{nI} = \mathcal{T}\mathcal{R}_n\mathcal{T}, n = 1, 2$.

For the correct introduction of permittivity, permeability and gyrotropy tensors of the medium equivalent in the considered approximation to the system at hand, the matrix M_I is bound to depend on the effective tensors, angle and plane of incidence in the same way as in the homogeneous medium. From (8)–(13) it follows that these conditions are met if $\Delta(\mathbf{a}) = 0$. In this case we can find the effective material tensors in the same way as in [6]

$$\mathcal{R} = \begin{pmatrix} \varepsilon & \alpha \\ \beta & \mu \end{pmatrix} = \mathcal{T}\left(f_1\mathcal{R}_1 + f_2\mathcal{R}_2 + if_1\frac{\pi l_2}{\lambda}\mathcal{R}_{21}\right)\mathcal{T} + \mathcal{R}_q Q, \tag{15}$$

with

$$\mathcal{R}_q = \left(f_1\mathcal{R}_{1q}^{-1} + f_2\mathcal{R}_{2q}^{-1}\right)^{-1}. \tag{16}$$

For example, $\Delta(\mathbf{a}) = 0$ if $\Delta_L = \Delta_R = 0$. That takes place provided [6]

$$\mathcal{R}_{2I}\mathcal{R}_{2q} = \mathcal{R}_{1I}\mathcal{R}_{1q}, \; \mathcal{R}_{2q}\mathcal{R}_{2I} = \mathcal{R}_{1q}\mathcal{R}_{1I}, \tag{17}$$

Note, that both relations (17) are equivalent if $\alpha_i = \beta_i = 0$. Even so it is rigid enough requirement, signifying that tensors ε_{1I} and ε_{2I}, μ_{1I} and μ_{2I} bound to have the same eigenvectors.

Of course, above mentioned conditions need not be met exactly having regard to approximate nature of method. We can find valuations $\|\Delta_L\|$ and $\|\mathcal{R}_{21}\|$ instead. It should be more than sufficient if $\|\Delta_L\|, \|\Delta_R\|$ far less than $\|\mathcal{R}_{21}\|$. In what follows we shall use Euclidean valuation

$$\|X\| = \left[(XX^\dagger)_t\right]^{\frac{1}{2}}, \tag{18}$$

where $X^\dagger$ is Hermitian transposed tensor and $(XX^\dagger)_t$ is a trace of tensor $XX^\dagger$.

By way of example let us consider nongyrotropic, nonmagnetic layers with real symmetric tensors ε_i. In this instance

$$\|\Delta_L\|^2 = \left(\frac{\varepsilon_{2+}}{\varepsilon_{1q}} - \frac{\varepsilon_{1+}}{\varepsilon_{2q}}\right)^2 + \left(\frac{\varepsilon_{2-}}{\varepsilon_{1q}} - \frac{\varepsilon_{1-}}{\varepsilon_{2q}}\right)^2 + 2\sin\phi^2 \left(\frac{\varepsilon_{1+}}{\varepsilon_{1q}} - \frac{\varepsilon_{1-}}{\varepsilon_{1q}}\right)\left(\frac{\varepsilon_{2+}}{\varepsilon_{2q}} - \frac{\varepsilon_{2-}}{\varepsilon_{2q}}\right), \tag{19}$$

$$\|\mathcal{R}_{21}\|^2 = 2\left[(\varepsilon_{2+} - \varepsilon_{1+})^2 + (\varepsilon_{2-} - \varepsilon_{1-})^2 + 2\sin\phi^2 (\varepsilon_{1+} - \varepsilon_{1-})(\varepsilon_{2+} - \varepsilon_{2-})\right], \tag{20}$$

where ϕ is the angle between the preferred axes of crystals, $\varepsilon_{i+}, \varepsilon_{i-} (i = 1, 2)$ are the eigenvalues of tensors $\varepsilon_{iI} = I\varepsilon_i I$. Formulae for magnetic crystals are similarly to (19),(20). Since usually

$\|\alpha_i\|, \|\beta_i\| \ll \|\varepsilon_i\|, \|\mu_i\|$, corresponding formulas are valid also for analysis of the gyrotropic layers.

Inasmuch $\mathbf{a}^2 \sim \varepsilon_{iq}$, from (19), (20), (13) it follows that for identical layers ($\varepsilon_{1+} = \varepsilon_{2+}, \varepsilon_{1-} = \varepsilon_{2-}$) values $\|\Delta(\mathbf{a})\|$ and $\|\mathcal{R}_{21}\|$ are approximately equal. Situation changes in the case of different parameters of the layers. In this case it is possible to choose parameters of the crystals providing the fulfillment of condition

$$\|\Delta(\mathbf{a})\| \ll \|\mathcal{R}_{21}\|. \tag{21}$$

Relation (21) can be provided much easier for structures comprising more then three layers in the unit cell. Then

$$\begin{aligned} M &= f_1 M_1 + f_2 M_2 + f_3 M_3 + \\ &\frac{i\pi}{\lambda}\{f_3 l_2 [M_3, M_2] + f_3 l_1 [M_3, M_1] + f_1 l_2 [M_2, M_1]\} + \ldots, \end{aligned} \tag{22}$$

and instead of $\|\Delta(\mathbf{a})\|$, $\|\mathcal{R}_{21}\|$ (12)–(14) we shall have more complicated but more versatile expressions, which can be changed by varying thicknesses of the layers. It should be noted that sometimes the "wide wave band approximation" reduces to the long wavelength approximation. In particular, if $\mathcal{R}_1 = \mathcal{R}_3$, $l_1 = l_2 = l_3$, then $[M_3, M_1] = 0$, $[M_3, M_2] = -[M_2, M_1]$ and structure do not possess properties of form gyrotropy [6].

Formulas (15), (9)-(12) are valid for arbitrary material parameters of the layers for a small enough angles of incidence and, of course, in the case of normal incidence ($\mathbf{a} = \mathbf{0}$).

3. Conclusion

It is shown that effective constitutive tensors, not depending on the angle and plane of incidence (true constitutive tensors), can be introduced in the wide wave band for the great variety of anisotropic periodic mediums. Formulas, which enable one to determine whether it is possible to introduce true constitutive tensors for the structure at hand or not, are obtained. In the frame of considered approximation it is hardly probable to introduce correctly constitutive tensors for an arbitrary parameters of the layers. From the other hand, at normal incidence there are no limitations on the parameters of the layers and obtained effective tensors may be very useful for synthesis of new materials.

References

[1] J. P. Serre, *Lie Algebras Lie Groups*. New York–Amsterdam: Benjamin, 1965.

[2] F. I. Fedorov, *Theory of Gyrotropy*. Minsk: Nauka i Tekhnika, 1976.

[3] L. M. Barkovskii, G . N. Borzdov and A. V . Lavrinenko, "Fresnel's reflection and transmission operators for stratified gyroanisotropic media", *J. Phys. A: Math.Gen.*, vol. 20, pp. 1095–1106, 1987.

[4] A. N. Borzdov, "Effective properties of plane stratified bianisotropic systems," in *Proc. Bianisotropics'97*, University of Glasgow, Great Britain, June 1997, pp. 145–148.

[5] G. N. Borzdov, "Evolution operators of electromagnetic waves in crystals," *Sov. Phys. Cryst.*, vol. 35, no. 3, pp. 535–551, May–June 1990.

[6] A. N. Borzdov, "Operator formalism in the theory of effective parameters of plane stratified bianisotropic structures," *Electromagnetics*, vol. 19, no. 6, pp. 501–512, November–December 1999.

Effective Properties of Multilayered Bianisotropic Systems

A. N. Borzdov

Department of Theoretical Physics, Belarusian State University
Fr. Skaryny avenue 4, 220050 Minsk, Belarus
Fax: + 375 – 172 – 06 60 01; E-mail: alexbor@phys.bsu.unibel.by

Abstract

A method of introduction of the effective material tensors of bianisotropic multilayered periodic structures based on the approximate calculation of the characteristic matrix of the unit cell of the system with the help of Campbell–Hausdorff series [1] is developed. Obtained effective tensors are valid for the use in a wide wave band. This paper is primarily concerned with a comparison of the accuracy of different approximations, namely, a long wavelength approximation and approximations, using three and five terms of Campbell-Hausdorff series.

1. Introduction

Attention now frequently focuses on the study of the effective properties of plane stratified periodic media. In doing so most often a long wavelength approximation is used. For example, in [2] the coordinate-free formulae for the effective tensors of permittivity ϵ, permeability μ and pseudotensors of gyrotropy α, β of the plane stratified periodic bianisotropic systems of the most general type were obtained. But it is well known [3], [4] that some systems composed from nongyrotropic layers can possess gyrotropic properties due to their specific structure (i.e. possess form gyrotropy). Phenomena of this kind can't be explained in the framework of a long wavelength approximation. To treat such problems it is necessary to extend the wave band, in which the effective tensors can be used. One way of doing this is to employ an approach [5], based on the approximate calculation of the characteristic matrix of the unit cell with the help of Campbell-Hausdorff series. Recently it was shown that by using this approach the effects of form gyrotropy (bianisotropy) can be really explained in terms of the theory of effective parameters (see [6], for example). In [6], [7] our consideration was limited by the three terms of this series.

Here we obtain more accurate formulas using the forth and fifth terms of Campbell-Hausdorff series.

We consider systems formed by a periodic set of plane bianisotropic layers with different thicknesses l_n ($n = 1, 2, \ldots N$, where N is the number of the layers forming the unit cell). The layers are characterized by the constitutive relations

$$\mathbf{D}_n = \varepsilon_n \mathbf{E}_n + \alpha_n \mathbf{H}_n, \ \mathbf{B}_n = \beta_n \mathbf{E}_n + \mu_n \mathbf{H}_n, \tag{1}$$

where ε_n, μ_n and α_n, β_n are the dielectric permittivity, the magnetic permeability tensors and the pseudotensors of gyrotropy, respectively.

2. Effective Material Tensor Parameters

The characteristic matrix $P = \exp(ik_0 l M)$ of a layer with thickness l relates the six-vectors $(\mathbf{E}, \mathbf{H})^T$ at the layer boundaries ($k_0 = \omega/c$). M is some matrix depending on the parame-

ters of the layers, angle and plane of incidence. Matrix M is given in an explicit form in [7]. Henceforward we shall follow notation used in [7].

Let us consider the system formed by two alternate layers with different thicknesses l_n and different sets of tensor constants $\varepsilon_n, \mu_n, \alpha_n, \beta_n$ $(n = 1, 2)$. In this instance the characteristic matrix of the unit cell has the form

$$P = \exp(ik_0 LM) = \exp(ik_0 l_2 M_2) \exp(ik_0 l_1 M_1), \tag{2}$$

where $L = l_1 + l_2$ is the system period and M is the matrix to be found. This matrix can be expressed in terms of the layers parameters with the help of Campbell–Hausdorff series as follows

$$M = f_1 M_1 + f_2 M_2 + if_1 \frac{\pi l_2}{\lambda} [M_2, M_1] - \frac{\pi^2 l_1 l_2}{3\lambda^2} \{f_1 [[M_2, M_1], M_1] + f_2 [[M_1, M_2], M_2]\} + \cdots \tag{3}$$

where $[M_2, M_1] = M_2 M_1 - M_1 M_2$. If $\pi l_n / \lambda \ll 1$, then the series (3) quickly converges and one can drop the remainder of it after the k–th term. The first and the second terms correspond to the long wavelength limit. The possibilities of introduction of the effective constitutive tensors having regard the third term are discussed in [7]. In what follows we shall break the series after the fifth term.

In perfect analogy with [7] we shall use in (2)–(3) the matrices M_I, M_{1I}, M_{2I}, describing the transformation of the tangential components of the field vectors, instead of M, M_1, M_2, and we assume $\mathbf{q}$ to be the left and the right eigenvector of each of the tensors $\varepsilon_n, \mu_n, \alpha_n, \beta_n$ $(\varepsilon_n \mathbf{q} = \mathbf{q}\varepsilon_n \equiv \varepsilon_{nq}\mathbf{q}, \cdots)$.

To compare the accuracy of different approximations, namely, long wavelength approximation and approximations, using three and five terms of Campbell-Hausdorff series, let us consider the most simple case of normal incidence onto the nongyrotropic nonabsorbing layers of the same thickness $l_1 = l_2 = l$. As this takes place (3) reduces to

$$M_I = \frac{1}{2}(M_{1I} + M_{2I}) + i\frac{\pi l}{2\lambda} \{[M_{2I}, M_{1I}] + i\frac{\pi l}{3\lambda} [[M_{2I}, M_{1I}], M_{1I} - M_{2I}]\} + \cdots \tag{4}$$

Generally speaking, Campbell-Hausdorff series

$$Z = X + Y + \frac{1}{2}[X, Y] + \frac{1}{12}[X, [X, Y]] + \frac{1}{12}[Y, [Y, X]] + \cdots \tag{5}$$

converges provided $\|X\| < \frac{ln2}{2}, \|Y\| < \frac{ln2}{2}$, where $\|X\| = \left[trace\left(XX^{\dagger}\right)\right]^{\frac{1}{2}}$ is Euclidean valuation of X. In our case series converges if

$$\frac{\pi max(l_1, l_2)}{\lambda} \leq \frac{ln2}{4\ max(\|M_{1I}\|, \|M_{2I}\|)} \tag{6}$$

For example, in the case of nonmagnetic crystals with $\|\varepsilon_I\| \sim 4.5$ (eigenvalues of $\varepsilon_I \sim 3.0$) $\frac{\pi l}{\lambda} \leq 0.039$.

After simple calculation we find the effective material tensors of the system at hand

$$\alpha_I = \beta_I^{\dagger} = i\frac{\pi l}{2\lambda} R_\alpha,\ R_\alpha = (\varepsilon_{1I}\mathbf{q}^{\times}\Delta\mu_I - \Delta\varepsilon_I \mathbf{q}^{\times}\mu_{1I}), \tag{7}$$

$$\varepsilon_I = \frac{1}{2}(\varepsilon_{1I} + \varepsilon_{2I}) + \varepsilon',\ \mu_I = \frac{1}{2}(\mu_{1I} + \mu_{2I}) + \mu', \tag{8}$$

$$\varepsilon' = i\frac{\pi l}{2\lambda}\left(i\frac{\pi l}{3\lambda}\right) R'_\varepsilon,\ R'_\varepsilon = -R_\alpha \mathbf{q}^{\times}\Delta\varepsilon_I - \Delta\varepsilon_I \mathbf{q}^{\times} R_\beta, \tag{9}$$

$$\mu' = i\frac{\pi l}{2\lambda}\left(i\frac{\pi l}{3\lambda}\right) R'_{\mu},\ R'_{\mu} = R_{\beta}\mathbf{q}^{\times}\Delta\mu_I + \Delta\mu_I\mathbf{q}^{\times}R_{\alpha}, \tag{10}$$

where $\Delta\varepsilon_I = \varepsilon_{2I} - \varepsilon_{1I}$, $\Delta\mu_I = \mu_{2I} - \mu_{1I}$.

It is worth noting that third term of Campbell–Hausdorff series give rise to the effective "tensors of gyrotropy" α_I, β_I while forth and fifth terms contribute only in the effective permittivity and permeability tensors (terms ε', μ' in (8)).

¿From (7),(9), (10) it follows that

$$\|R_{\alpha}\| \leq 2\left(\|\varepsilon_{1I}\|\ \|\Delta\mu_I\| + \|\Delta\varepsilon_I\|\ \|\mu_{1I}\|\right), \tag{11}$$

$$\|R_{\beta}\| \leq 2\left(\|\varepsilon_{1I}\|\ \|\Delta\mu_I\| + \|\Delta\varepsilon_I\|\ \|\mu_{1I}\|\right), \tag{12}$$

$$\|R'_{\varepsilon}\| \leq 2\ \|\Delta\varepsilon_I\|\left(\|R_{\alpha}\| + \|R_{\beta}\|\right), \tag{13}$$

$$\|R'_{\mu}\| \leq 2\ \|\Delta\mu_I\|\left(\|R_{\alpha}\| + \|R_{\beta}\|\right). \tag{14}$$

¿From above estimations and formulae (7)-(10) it is clear that in the convergence range the contribution of the forth and fifth terms of Campbell–Hausdorff series in effective tensors is far less than the contribution of third term, and usually may be thought of as negligibly small if compared with the contribution of the first and second terms. But if in the long wavelength approximation the system under hand has transversely isotropic permittivity and permeability tensors, then contribution of the forth and fifth terms can be noticeable. The latter case is of great concern in investigation of form bianisotropy (gyrotropy), because the manifestations of gyrotropy are often suppressed due to the permeability(permittivity) being tensors, especially in the optical wave region [9].

3. Conclusion

In this paper we discussed primarily the comparative contribution of different terms of Campbell–Hausdorff series in the effective tensors of "permittivity, permeability" and "gyrotropy", analyzing the simple case of normal incidence onto the system of nongyrotropic layers. Obtained estimations holds true for gyrotropic layers too, at least for the short enough wavelengths. At normal incidence generalization of formulae (7)–(10) to the case of bianisotropic layers is not a particular problem.

Of course, derived effective tensors are not true constitutive tensors because generally they are valid only in the immediate vicinity of normal incidence. It is possible to introduce true constitutive tensors (i.e. not depending on the angle and plane of incidence) even having regard to five terms in Campbell–Hausdorff series, but only for some systems with the specific relation between the layers parameters. Therefore, proposed method is more convenient for analysis of the effective properties of systems at normal incidence, when there is no restrictions on the parameters of the layers. Extensive computations made with the use of exact and approximate formulas are in good accordance.

References

[1] J. P. Serre, *Lie Algebras Lie Groups.* New York–Amsterdam: Benjamin, 1965.

[2] A. N. Borzdov, "Effective material parameters of plane stratified bianisotropic superlattices," in *Advances in Complex Electromagnetic Materials*, NATO ASI Series, 3. vol. 28. Dordrecht: Kluwer Academic Publishers, 1997, pp. 145–154.

[3] H. J. Gerritsen, R. T. Yamaguchi, "A microwave analog of optical rotation in cholesteric liquid crystals," *Am. J. Phys.*, vol. 39, pp. 920–923, August 1971.

[4] V. V. Varadan, A. Lakhtakia and V .K . Varadan, "Reflection and transmission characteristics of a structurally chiral slab: Intrinsic anisotropy and form chirality," *Optik*, vol. 80, no. 1, pp. 27–32, January 1988.

[5] A. N. Borzdov, "Effective properties of plane stratified bianisotropic systems," in *Proc. Bianisotropics'97*, University of Glasgow, Great Britain, June 1997, pp. 145–148.

[6] A. N. Borzdov, "Operator formalism in the theory of effective parameters of plane stratified bianisotropic structures," *Electromagnetics*, vol. 19, no. 6, pp. 501–512, November–December 1999.

[7] A. N. Borzdov, "Effective Constitutive Tensors Of Bianisotropic Multilayered Mediums," in *Proc. Bianisotropics'2000*, Technical University of Lisbon, Portugal, 2000.

[8] L. M. Barkovskii, G . N. Borzdov and A. V . Lavrinenko, "Fresnel's reflection and transmission operators for stratified gyroanisotropic media", *J. Phys. A: Math.Gen.*, vol. 20, pp. 1095–1106, 1987.

[9] F. I. Fedorov, *Theory of Gyrotropy*. Minsk: Nauka i Tekhnika, 1976.

Resonant Effective Properties of Plane Stratified Structures

O. V. Ivanov

Department of Quantum Electronics and Optoelectronics, Physical Faculty,
Ulyanovsk State University, L. Tolstoy str. 42, 432700 Ulyanovsk, Russia
Fax: +7-8422-412-340; e-mail: oliv@sv.uven.ru

Abstract

Effective properties of plain stratified bianisotropic structures are found on the basis of 4x4 matrix method without restriction on the ratio of the period of structure and the wavelength of incident radiation. The effective permittivity, magnetic permeability and magnetoelectric dyadics are obtained for isotropic two-layer and anisotropic helicoidal structures in resonant case.

1. Introduction

The problem of effective properties of stratified media is known in optics for a long time [1]. The effective properties of an inhomogeneous plane stratified structure are defined as the properties of a certain homogeneous layer which cannot be distinguished from the investigated inhomogeneous structure by optical means. As a rule, periodic structures with large number of periods are considered in long wave approximation, i.e. in the case when the length of electromagnetic wave is much greater than the period of the structure. Such structures exhibit anisotropic, chiral and, generally, bianisotropic properties [1-3].

In case when the wavelength of light is approximately equal to the period of structure, the resonant interaction of light with the structure is observed. This problem is solved by various methods, for example, by the method of coupling waves or Bloch functions formalism [4]. The method of effective properties was not earlier used in this case, being limited in application by media with short period.

The purpose of the present work is to find the effective properties of periodic bianisotropic structures having the period approximately equal to the wavelength of propagating light, and also non-periodic structures made of a few layers. For solution of the given problem we apply a modification of the Berreman 4x4 matrix method.

2. Method of 4x4 Matrices; Matrix of Material Properties

Consider a medium consisting of bianisotropic layers parallel to XY plane. A plane electromagnetic monochromatic wave propagates in the medium. Its wave vector $\mathbf{k}$ is parallel to XZ plane. Maxwell equation can be transformed to the following 4x4 differential matrix equation:

$$\frac{d\mathbf{g}}{dz} = -ik_0 G\left(\hat{\varepsilon}, \hat{\mu}, \hat{\alpha}, \hat{\beta}\right)\mathbf{g}, . \tag{1}$$

where k_0 is the wave number in vacuum; the four dyadics of permittivity $\hat{\varepsilon}$, permeability $\hat{\mu}$ and magnetoelectric $\hat{\alpha}$, $\hat{\beta}$ describe the relations between electric and magnetic fields; a four-component vector $\mathbf{g} = \left(E_x, -E_y, H_x, H_z\right)$ is composed of tangential components of the fields. Here the 4x4 matrix of material properties (MMP) G is determined by local properties of the medium and the incidence angle. It is constructed on the basis of the four constitutive dyadics and allows in general way taking into account bianisotropic properties of the medium. MMP consists of the sum of three matrices which are proportional to zero, first and second degrees of the tangential component of the wave vector k_x:

$$\mathbf{G} = \mathbf{G}_0 + \frac{k_x}{k_0}\mathbf{G}_1 + \frac{k_x^2}{k_0^2}\mathbf{G}_2 . \tag{2}$$

For a homogeneous medium MMP does not depend on z, and the solution of the matrix equation (1) in this case is a superposition of eigen waves:

$$\mathbf{g} = \sum c_j \mathbf{q}_j \exp\left(-ik_{zj} z\right), \quad j = 1,..,4 \tag{3}$$

where c_j is the amplitudes of the waves corresponding to the eigen vectors $\mathbf{q}_j$ of matrix $\mathbf{G}$. The eigen numbers of this matrix $n_{zj} = k_{zj}/k_0$ are the solutions of the dispersion equation $\det(\mathbf{G} - n_z\mathbf{I})$, where $\mathbf{I}$ is the unit matrix. As follows from (3), there are four eigen waves with various polarizations determined by the fourth order equation with respect to n_{zj}.

If the structure contains several homogeneous layers, the investigation of propagation of electromagnetic waves turns into the solution of a boundary problem. The continuity conditions for tangential electrical and magnetic field components must be satisfied on the boundaries of adjoining layers, that is identical to the continuity of the four-component vector $\mathbf{g}$. Let a wave described by vector $\mathbf{g}(z_m)$ is incident on m-th layer. The vector $\mathbf{g}(z_{m+1})$ of the wave transmitted through the layer is determined by the matrix relation:

$$\mathbf{g}(z_{m+1}) = \mathbf{S}^{(m)}\mathbf{g}(z_m), \tag{4}$$

where the transformation matrix for m-th layer of thickness Δz_m has the form:

$$\mathbf{S}^{(m)} = \exp[-ik_0\mathbf{G}(z_m)\Delta z_m]. \tag{5}$$

Here the exponential function is applied to a 4x4matrix. It is known from the theory of matrices that for arbitrary matrix $\mathbf{A}$ and function f the following relation is satisfied:

$$f(\mathbf{Q}\mathbf{A}\tilde{\mathbf{Q}}) = \mathbf{Q}f(\mathbf{A})\tilde{\mathbf{Q}}, \tag{6}$$

where $\tilde{\mathbf{Q}}$ is the matrix inverse for $\mathbf{Q}$. Let's take $\mathbf{Q}$ as a matrix which are formed by columns of eigen vectors of $\mathbf{G}$: $\mathbf{Q}_{jk} = (\mathbf{q}_k)_j$. Then the lines of $\tilde{\mathbf{Q}}$ are the vectors $\tilde{\mathbf{q}}_j$ complimentary to $\mathbf{q}_k$ ($\tilde{\mathbf{q}}_j, \mathbf{q}_k = \delta_{jk}$). We substitute MMP in (5) as: $\mathbf{G} = \mathbf{Q}\tilde{\mathbf{Q}}\mathbf{G}\mathbf{Q}\tilde{\mathbf{Q}}$. Taking into account that $\tilde{\mathbf{q}}_j\mathbf{G}\,\mathbf{q}_k = \tilde{\mathbf{q}}_j n_{zk}\mathbf{q}_k$ the transformation matrix of m-th layer can by presented as:

$$S_{ij}^{(m)} = \sum_{k,l} Q_{ik}^{(m)}\delta_{kl}\exp(-ik_0 n_{zl}^{(m)}\Delta z_m)\tilde{Q}_{lj}^{(m)}. \tag{7}$$

For a system consisting of $p-1$ layers (a wave is incident from medium $n=0$, passes p boundaries and propagates to the medium $m=p$) the resulting transformation matrix is the product of transformation matrices of separate layers:

$$\mathbf{S} = \mathbf{S}^{(p)}\mathbf{S}^{(p-1)}\mathbf{L}\mathbf{S}^{(1)} \tag{8}$$

For inhomogeneous medium MMP is a continuous function of z, and the resulting transformation matrix can be found as the product of transformation matrices of indefinitesimal layers, into which the medium is divided. When the thickness of these layers tends to zero we obtain the transformation matrix as a multiplicative integral:

$$\mathbf{S} = \lim_{\Delta z \to 0}\prod_j e^{-ik_0\mathbf{G}(z_j)\Delta z} = \int e^{-ik_0\mathbf{G}(z)dz}, \tag{9}$$

where multiplicative integral is designated as:

$$\int \mathbf{A}(z)^{dz} = \lim_{\Delta z \to 0}\prod_j [\mathbf{I} + \mathbf{A}(z)\Delta z] = \lim_{\Delta z \to 0}\prod_j \mathbf{A}(z_j)^{\Delta z}.$$

The same result can be obtained by separating the variables and integrating the basic equation (1).

3. Effective Matrix of Material Properties

Arbitrary stratified bianisotropic structure accordingly to (8) can be described by a transformation matrix S, which contains the complete information on all optical characteristics of the structure as whole. This allows replacing such structure by a certain homogeneous layer with effective properties so that the transformation matrix does not changes. Thus, in order to find the effective properties of the structure it is necessary at first to find the transformation matrix from the properties of the inhomogeneous structure, then to solve the inverse problem and find effective MMP assuming the structure to be a homogeneous layer. From MMP it is possible to obtain permittivity, permeability and magnetoelectric dyadics.

Equating the transmission matrices of a homogeneous layer (5) and an inhomogeneous structure with arbitrary function $G(z)$ (9) and taking the logarithm we obtain the effective MMP:

$$G_{eff} = \frac{i}{k_0 L} \ln\left[\int_0^L e^{-ik_0 \mathbf{G}(z)dz}\right], \tag{10}$$

where L is the whole thickness of the structure. The obtained expression is exact. It allows calculating effective properties of structures both with large number of layers and few layers, for example, two or three-layer structures. For periodic medium it is enough to take integral over the period of the structure.

It is known that the logarithmic function is multivalued, in particular, for scalars it is determined up to $2\pi i m$, where m is an integer number. The multyvaluedness of logarithmic function is the result of the periodicity of exponential function. For a matrix of dimension sxs there exist s independent integer numbers m_1, K, m_s, varying which it is possible to obtain new matrices so that the exponential function upon these matrices is a constant:

$$\mathbf{A}' = \mathbf{A} + 2\pi i \mathbf{Q}\mathbf{M}\tilde{\mathbf{Q}}, \quad \mathbf{M} = \begin{pmatrix} m_1 & 0 & 0 \\ 0 & \mathbf{O} & 0 \\ 0 & 0 & m_s \end{pmatrix} \tag{11}$$

where the matrix $\mathbf{Q}$ is made of the columns of eigen vectors of the matrix $\mathbf{A}$. Thus, the logarithm of a matrix is a set of counted number of matrices. Ambiguity of determination of MMP follows from this fact. Determination of MMP is ambiguous not only when we find effective MMP for inhomogeneous structure but also for usual homogeneous medium. Really, let we transform $\mathbf{G} \to \mathbf{G}'$ so that $\exp(-ik_0\mathbf{G}) = \exp(-ik_0\mathbf{G}')$. Then the matrix $\mathbf{S}$ (5) and, therefore, and reflection and transmission coefficients will not change. Hence, the determination of constitutive dyadics of medium is ambiguous at fixed optical characteristics.

The effective MMP for an inhomogeneous medium is a complex function of k_x, and, generally, it cannot be presented in the form of (2) when $\mathbf{G}_i$ is independent on k_x. Therefore the effective dyadics $\hat{\varepsilon}$, $\hat{\mu}$, $\hat{\alpha}$ and $\hat{\beta}$ at any splitting of G into three summands depend on k_x and on the direction of wave propagation. Hence, such medium exhibit spatial dispersion.

4. Examples of Stratified Structures

Consider two most typical examples demonstrating application of the general approach of calculation of effective properties of layered bianisotropic media.

4.1 Two-layer structure

We consider a structure which consists of two dielectric layers with permittivities $\varepsilon_{1,2} = \varepsilon \pm \Delta\varepsilon/2$ ($\Delta\varepsilon = \varepsilon$) and thickness $d_{1,2}$. Non-zero components of the effective dyadics of such structure can be written as:

$$\varepsilon_{xx,yy}=\varepsilon\left[\Delta l+\left(\gamma^{(p,s)}/2\right)\sin 2l_1\right]\left(\frac{i}{\nu^{(p,s)}}+\frac{1}{\pi}\right),\quad \mu_{yy,xx}=\left[\Delta l-\left(\gamma^{(p,s)}/2\right)\sin 2l_1\right]\left(\frac{i}{\nu^{(p,s)}}+\frac{1}{\pi}\right),$$
$$\varepsilon_{zz}=\varepsilon,\quad \mu_{zz}=1,\quad \alpha_{xy,yx}=-\beta_{yx,xy}=-i\sigma\gamma^{(p,s)}\sqrt{\varepsilon}\sin^2 l_1\left(\frac{i}{\nu^{(p,s)}}+\frac{1}{\pi}\right). \tag{12}$$

where

$$\nu^{(r)}=\sqrt{\left(\gamma^{(r)}\sin l_1\right)^2-\Delta l^2}\ ,\ \gamma^{(p,s)}=\frac{\Delta\varepsilon}{2\varepsilon}\left(\frac{k_x^2}{\varepsilon k_0^2-k_x^2}\mathrm{ml}\right),\ \Delta l=\pi-l_1-l_2\ ,\ l_i=k_0\sigma_i d_i\sqrt{\varepsilon_i}\ ,\ \sigma_i^2=1-\frac{k_x^2}{\varepsilon_i k_0^2}\ .$$

The propagation constants of p and s polarized waves in such medium $k_z^{(p,s)}=\pm\sigma\sqrt{\varepsilon}\left(1-i\nu^{(p,s)}/\pi\right)k_0$ describe attenuating waves. The positive direction wave propagating in such medium attenuates and transfers its energy to the negative direction wave, i.e. Bragg reflection of light from periodic structure takes place. The penetration depth of the wave in the structure is determined by the parameter ν and equals $\pi/\left(2\sigma\nu^{(p,s)}k_0\sqrt{\varepsilon}\right)$. The effective medium exhibits the property of strong spatial dispersion, since constitutive dyadics are functions of k_x, i.e. functions of the wave vector. This is consisted with the fact that the contribution of spatial dispersion is essential when the relation between the period of structure and the wavelength is close to unit.

4.2 Helicoidal structure

A Helicoidal structure represents a twisted medium in which there is a rotation of anisotropy axes around Z axis at displacement along its direction. The effective properties of such medium correspond to a chiral medium with

$$\alpha_{xx}=\alpha_{yy}=-\beta_{xx}=-\beta_{yy}:\ i\lambda/L_0\ , \tag{13}$$

where L is the period of the structure; λ is the wavelength of the incident radiation.

5. Conclusion

On the basis of 4x4 matrix method the exact equation for effective MMP of arbitrary bianisotropic structure is obtained without restriction on the relation between the wavelength and the thicknesses of the layers constituting the structure.

The effective constitutive dyadics for a two-layer isotropic dielectric structure are found in the resonant case. It is shown that the effective magnetoelectric dyadics contain off-diagonal components which were absent for the isotropic layers of the structure. At this conditions the permittivity and permeability become complex quantities, that results in strong Bragg reflection of a wave from such structure. The effective constitutive dyadics for helicoidal medium are found. It is shown that such medium is chiral.

MMP and constitutive dyadics of any medium are determined ambiguously. The transformation for MMP which completely conserves the optical characteristic of the layered structure is found.

References

[1] S. M. Rytov, "Electromagnetic properties of thin-layer media", *J.Exp.Theor.Phys.* vol. 29, no. 11, pp. 605-608, 1955.

[2] P. S. Rees and A. Lakhtakia, "A periodic chiral arrangement of thin identical bianisotropic sheets: effective properties", *Optik*, vol. 86, no. 2, pp. 47-50, 1990.

[3] A. N. Borzdov, *Proc. Bianisotropics'98*, 3-6 June, 1998, Braunschweig, pp. 269-272; *Proc. Bianisotropics'97*, 5-7 June, 1997, Glasgow, pp. 145-148.

[4] O. V. Ivanov and D. I. Sementsov, "Magneto-optical interaction of light with a periodic bi-gyrotropic structure," *Pure Appl.Opt.*, vol.6, pp. 455-464, 1997.

Magnetization and Giant Magnetoresistance of the System of Interacting Fine Particles

C. Xu[1], Z. Y. Li[2,1] and I. E. Dikshtein[3]

[1] Department of Physics, Suzhou University, Suzhou, 215006, China

[2] CCAST(World Laboratory), P.O.Box 8730, Beijing 100080, China

[3] Institute of Radioengineering and Electronics, Russian Academy of Sciences, 103907 Moscow, Russian Federation
Fax: +7-095-2038414; email: diksh@mail.cplire.ru

Abstract

The magnetization and giant magnetoresistance (GMR) of nanosized magnetic particles embedded in a nonmagnetic metallic matrix are numerically investigated. By considering the classical dipolar interactions, we apply a Monte-Carlo simulation technique to calculate M vs H, GMR vs H, and GMR vs (M/M_s) with M, the average magnetization along the normal to the layer, M_s, the saturated magnetization, and H, the applied magnetic field. It is shown that the interfacial spin-dependent scattering of conductance electrons is dominant in GMR effect and the distance between the neighboring particles is an important parameter to obtain the GMR effect, while the size distribution only modify the shape of the curve of GMR versus H.

1. Introduction

The discovery of the giant magnetoresistance (GMR) effect in inhomogeneous alloys of magnetic and nonmagnetic metals [1] has attracted a great deal of attention to these materials. They consist of nanosized particles or clusters (e.g., Co, Fe, Ni) embedded in a nonmagnetic metallic matrix (typically Cu, Ag). The magnetic transport properties of granular metals are concerned with the size and spatial distributions of the fine particles or clusters and the interaction between the particles. Previous works studied the dependence of GMR on the size distributions [2] and successfully explained some experimental results. The interactions between particles can have a dipolar, Ruderman–Kittel–Kasuya–Yosida (RKKY), or a superexchange character, depending on the magnetic properties of the matrix. Altbir *et al.* [3] found that the classical dipolar interactions are dominant in Co-Cu systems.

2. Theory

In the present work we study the magnetization and GMR effect of the assembly of single–domain spherical ferromagnetic particles, Each particle is a saturated single domain and its magnetic moment $\vec{\mu}_i$, and the direction of its uniaxial anisotropy axis is random in space. The particles are placed in a square array consisting of 12×12 cells. The diameter of the particle i is d_i and the distance between two neighboring particles is r_0. After considering the classical dipolar interaction and crystalline anisotropy energy, the total energy of the system for a given configuration $\{\vec{\mu}_i\}$ of the magnetic moments is

$$E(\mu_i) = \sum_{i=1}^{N}[\sum_{j>i} E_{ij} + K_u V_i \sin^2 \alpha_i - \vec{\mu}_i \cdot \vec{H}], \quad (1)$$

with E_{ij}, the energy of the dipolar interaction, K_u, the effective anisotropy constant, V_i, the volume of a particle i, and α_i, the angle between the direction of the crystalline axis and $\vec{\mu}_i$. For a given temperature, the reduced magnetization $< m >$ can be calculated by averaging $m = M/M_s = |\sum_i \vec{\mu}_i|/(N\mu)$ over cluster configurations after thermal equilibrium has been reached. The crucial factor for GMR in granular system is the average value $< \cos\theta_{ij} >$, where θ_{ij} is the relative angle between the magnetic moments in sites i and j [4]. It implies that the magnetic transport properties are primarily caused by the spin–dependent scattering process of conductance electrons between magnetic particles. Namely, the spin-dependent scattering at interfaces between the magnetic particles gives rise to the GMR to a greater extent than the scattering within the magnetic particles would do [5]. In the case that the distance between the neighboring particles does not far exceed the electronic mean free path λ [6], the variation in resistivity of a granular system with the degree of field-induced magnetic order may be simply pictured as $\rho = \rho_0 - k < \cos\theta_{ij}^{(\lambda)} >$, where ρ_0 and k are constants. Assuming that there are no correlations between the magnetic moments of particles, the magnetoresistance $\Delta\rho/\rho$ can be written as $\Delta\rho/\rho = -(k/\rho_0) < \cos\theta_{ij}^{(\lambda)} >^2 = -(k/\rho_0)m^2$. Such a quadratic dependence of $\Delta\rho/\rho$ on m is actually found by some experiments [1]. However, other experiments [2] showed that $\Delta\rho/\rho$ does not vary quadratically with m because of the size distribution of magnetic particles and interaction between them.

For the system involving coupling between magnetic particles, the assumption, that the average value $< \cos\theta_{ij}^{(\lambda)} >_0$ for $H = 0$ is not vanished, gives

$$\Delta\rho/\rho = (< \cos\theta_{ij}^{(\lambda)} >_0 - < \cos\theta_{ij}^{(\lambda)} >)(Q - < \cos\theta_{ij}^{(\lambda)} >_0), \quad (2)$$

where $Q = \rho_0/k$ is the field–independent constant.

The thermal averages of the system above are obtained using the standard MC procedure and the Metropolis algorithm [7]. The system is assumed to have reached thermal equilibrium after 10^4 Monte-Carlo steps per spin. Then, we are able to get the thermal averages as an arithmetic average over the accepted configurations (500 accepted configurations for ensemble averages), and to calculate the $< m >$ and GMR. Data for our MC simulation is generated and calculated as follows. Each particle is assigned a random crystalline anisotropy ($K_u = 4.0 \times 10^6 \mathrm{erg/cm^3}$) and a random direction of magnetic moment at initial state. These particles are placed in the magnetic field $\vec{H}$ applied along the normal to the array. The distance r_0 between the particles was taken as 6.0 nm (except for the up triangles in Fig. 1) which is comparable in magnitude with λ [6]. Single–domain ferromagnetic particles exhibit the phenomenon of superparamagnetism and the blocking temperature $T_b^{(0)}$ for $H = 0$ of a particle of diameter d=4 nm is equal to 38 K [8]. So we choose T=40 K close to $T_b^{(0)}$.

3. Results

First, for simplicity, we choose the same diameter d_i(=3 nm) of all the magnetic particles, which is the typical average size of particles for granular materials [6]. In Fig. 1 we plot the graph of magnetization M/M_0 vs H. Four different sets of data are shown that correspond to a system of particles with random anisotropy only (squares; $r_0 = 6$ nm), a moderate dipolar system with random anisotropy (circles; $r_0 = 6$ nm), a system with moderate dipolar interaction only (triangles down; $K_u = 0$, $r_0 = 6$ nm), and a strong dipolar system with random anisotropy (triangles up; $r_0 = 3$ nm). We notice that M exhibits the different field dependence, depending on the interplay of the single–particle anisotropy and the dipolar interaction effects. *E.g.*, for a

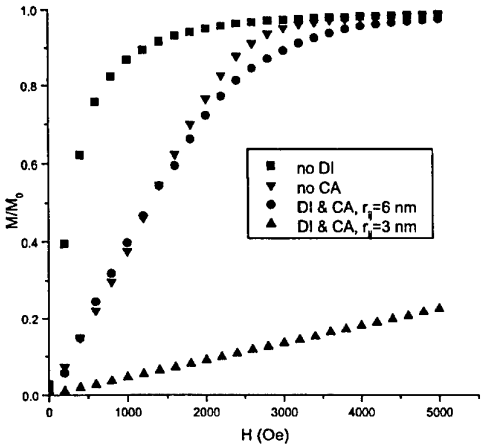

Fig.1. The dependence of M/M_s on H for T=40 K. The symbles are obtained when we do not consider the dipolar interaction(DI) (squares), or do not include the crystalline anisotropy (CA) (down triangles). The circles and up triangles are obtained by considering both the DI and CA when the r_i equals 6nm and 3nm respectively.

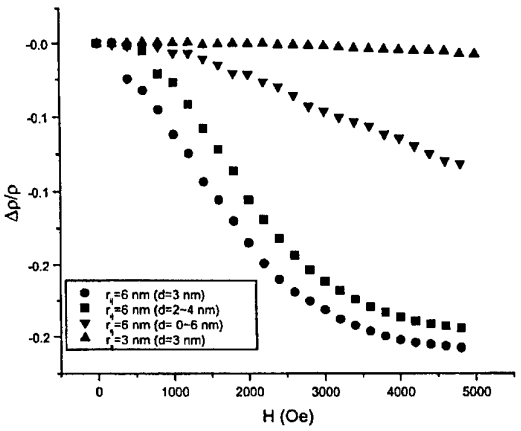

Fig.2. The dependenc of GMR on H for T=40 K. The symbles are obtained when r_i=6nm, d=3nm (circles), d=2~4nm(squares), d=0~6nm(down triangles), and r_i=3nm, d=3nm (up triangles).

system with random anisotropy only the magnetization reversal of the assembly of particles is well described by both a coherent rotation of $\vec{\mu}_i$ from the easy axes to the direction of $\vec{H}$ and by a thermally activated process over the anisotropy barrier.

A pure dipolar system ($K_u = 0$) For $H = 0$ possesses the interaction–induced anisotropy. Out–of–plane orientation $\vec{M}$ has a large energy due to the demagnetization effect. Therefore in–plane configuration of $\vec{\mu}_i$ is realized. For the free boundary conditions accepted here the ground state is antifferromagnetic due to the demagnetization effect of the lateral boundaries. This effect is not so strong compared with the demagnetization effect of the surface. Once again, if a field is applied to the array the magnetic moments $\vec{\mu}_i$ rotate coherent to the direction of $\vec{H}$.

If both the dipolar interaction and the random uniaxial anisotropy of particles are involved it is more difficult for $\vec{M}$ to reach saturation since these effects impede the collinear ordering of $\vec{\mu}_i$ and reduce the magnetization of the system. The anisotropy induced by dipolar interactions is very sensitive to the spatial arrangement of the particles (average distance between the particles and their size) and it is enhanced with decreasing r_0. Therefore in a strong dipolar system (triangles up; $r_0 = 3$ nm) the $\vec{M}$ is harder to be saturated in comparison with a moderate dipolar system (circles; $r_0 = 6$ nm).

In Fig. 2 we plot the field dependence of $\Delta\rho/\rho$ for T=40 K. All curves are calculated in terms of Eq. (2) with Q=5.2 after considering both the effects of anisotropy and interactions when the system reaches the equilibrium state. To investigate the influence of the distance r_0 and the particle–size distribution on the GMR four different sets of data are shown that correspond to particles of fixed diameter with strong (up triangles; d_i=3 nm, r_0=3 nm) and weak (circles; d_i=3 nm, r_0=6 nm) dipolar interactions, a narrow particle–size distribution from 2 to 4 nm (squares; $\bar{d}$=3 nm, r_0=6 nm), and a wide particle–size distribution from 0 to 6 nm (down triangles; $\bar{d}$=3 nm, r_0=6 nm) with $\bar{d}$ is the average particle size. From Fig. 2 it follows that the GMR effect depends crucially on the particle density. If the dipolar interaction are strong (d_i=3 nm, r_0=3 nm) all the particles are coupled to each other, and the negative GMR disappears. For a narrow particle–size distribution from 2 to 4 nm (squares) the field dependence of $\Delta\rho/\rho$ is closed to that for the system of particles with fixed diameter and a weak dipolar interection (circles). In this case the blocking temperature of the maximum particle $T_b \approx$38 K, and all the particles are superparamagnetic. This result was observed in [5]. For a wide particle–size distribution from 0 to 6 nm, certain of large particles are blocked at 40 K in the region of strong magnetic fields,

whereas the rest small particles are still in the superparamagnetic state. Then the modulus of $|\Delta\rho|/\rho$ is substantially reduced relative to the case of a narrow particle–size distribution. This effect was observed and explained in [2] for the systems with a wide particle–size distribution. So we believe that the size distribution strongly affects the shape of the curves of GMR vs H.

In order to investigate in more detail the role of a particle–size distribution in GMR effects, we show in Fig. 3 the dependence of $\Delta\rho/\rho$ vs M/M_s for a narrow (hollow squares) and wide (up triangles) particle–size distributions. From Fig. 3 it follows that for a narrow particle-size distribution from 2 to 4 nm, the behavior of GMR vs (M/M_s) is close to the parabolic line, whereas for a wide particle–size distribution from 0 to 6 nm, it is deviated essentially from the parabolic law. It indicates that the wide distribution of magnetic particles may explain the noncompliance with the parabolic law for the GMR as a function of the $\vec{M}$ [2].

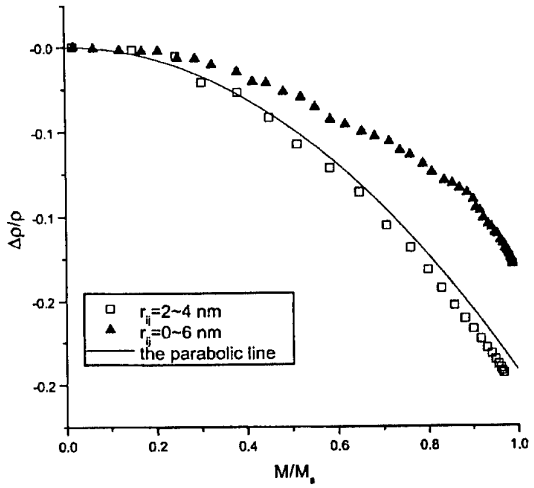

Fig.3. The dependence of GMR on M/M_s for T=40 K. The hollow squares and up triangles are obtained by varing of r_{ij} from 2 to 4 nm and 0 to 6 nm respectively. The solid line is the parabolic line.

4. Conclusion

In conclusion, we have presented the results for the field dependence of M and GMR of a granular magnetic film. We demonstrate that the magnetic properties of the system depends essentially on the particle–size distribution and the average distance between the magnetic particles. To discuss experimental data the state of single–domain magnetic particles is usually assumed to be blocked or collective at low temperatures and to be superparamagnetic at high temperatures. Within our MC approach, there is no need for making *a priori* assumptions about the particle state. However, it is likely that the high density regime favours the collective state, and the low density, wide particle–size distribution and strong magnetic field regime favours the blocked state. The collective behaviour at high particle density reveals itself in the disappearance of the negative GMR effect. A manifestation of the blocked state effects is a substantial decrease in $|\Delta\rho|/\rho$ for the low density and wide particle–size distribution in the region of strong magnetic field.

Acknowledgement

This work was supported, in part, by the National Natural Science Foundation of China under grant 19774042 and the Russian Foundation for the Basic Research (grant 99-02-39009).

References

[1] J.Q. Xiao, J.S. Jiang, and C.L. Chien, Phys. Rev. Lett. vol. 68, no. 25, pp. 3749-3752, June 1992.
[2] B.J. Hickey *et al.*, Phys. Rev. B vol. 51, no. 1, pp. 667-669, January 1995.
[3] D. Altbir *et al.*, Phys. Rev. B vol. 54, no. 10, pp. R6823-R6826, Sept. 1996.
[4] C.L. Chien, J.Q. Xian, and J.S. Jiang, J. Appl. Phys. vol. 73, no. 10, pp. 5309-5314, May 1993.
[5] P. Allia *et al.*, Phys. Rev. B vol. 52, no. 21, pp. 15398-15411, December 1995.
[6] S. Zhang, Appl. Phys. Lett. vol. 61, no. 15, pp. 1855-1857, October 1992.
[7] M.B. Stearns and Y. Cheng, J. Appl. Phys. vol. 75, no. 10, pp. 6894-6899, May 1994.
[8] K. Binder and D.W. Heermann, *Monte Carlo Simulation in Statistical Physics* (Springer Verlag, Berlin, 1992).

Analytical Models of Systems with Photoinduced Spiral Spatial Microstructure: Interaction with Polarized Optical Radiation

O. D. Asenchik and E. G. Starodubtsev

Gomel State Technical University
October av. 48, 246746 Gomel, Belarus
Fax: + 375 - 232 - 479165; email: starodub@ggtu.belpak.gomel.by

Abstract

Optical model of a photochromic medium with spiral spatial microstructure of centres distribution, which is formed at the record in photoactive materials of polarization state and intensity of two interfering light beams, is developed. The expressions for dielectric permittivity tensor are derived and the corresponding boundary problem for the photochromic layer is investigated. Some possibilities of bistability and multistability regimes for such layers are considered.

1. Creation of Systems with Photoinduced Spiral Spatial Microstructure

Important examples of media with spiral spatial microstructure are cholesteric liquid crystals (CLC). On the other hand, there is a possibility of creating spiral symmetric structures by the optical method: at interference of opposing coherent beams in layers from photochemically active materials. Such materials are polymeric solid solutions of photochromic dyes (indigoide colours, anthracenes, spiropirans, etc.) in polymeric glass (polymethyl methacrylate, polystyrene, etc.) [1,2]. Under polarized optical excitation owing to various photophysical and photochemical processes (saturation of metastable states, photoisomeric change, photoreduction, and others), in these materials dichroism and (or) birefringence is photoinduced. Thus, systems with optically controllable character of the anisotropy arise. The change of the polarized radiation characteristics allows gaining materials with given properties of optical anisotropy, which are not masked by the natural anisotropy (as a rule, initially the samples are isotropic). In this connection, it is interesting to use CLC optics methods and results for the investigation of optical properties of the photochromic layers.

The aims of the paper are: 1) development of optical model of a medium with spiral spatial microstructure of photochromic centres distribution, which is formed at the record in the material of polarization state and intensity of two interfering coherent light beams; 2) investigation of linear and nonlinear interaction of polarized optical radiation with layers from such materials.

Let us accept the following kinetic scheme describing dynamics of photophysical and photochemical processes in a plane-parallel photochromic layer: 1) excitation of molecules of photosensitive component D with rate $R(\Omega_d)$ due to absorption of photons; 2) the later conversion of the molecules D to a photoproduct DP (at monochromatic excitation $R=\sigma_D(\Omega_d)I$, where $\sigma_D(\Omega_d)$ is the interaction cross-section on the excitation frequency of the dipole oscillator with orientation Ω_d, I is photons flux density). Solving kinetic equations describing such scheme and making the corresponding averaging on the ensemble, one can derive dependencies of concentrations $[D](t,\Omega_d),[DP](t,\Omega_d)$ on time and orientation. Function of distribution $f(\Omega_d)$ of non-rotating photochromic centres on orientations Ω_d of the transitions dipole moments can be written in the form

$$f(\Omega_d)=[D](t,\Omega_d)/[D](0,\Omega_d)=f(\sigma_D(\Omega_d)It). \qquad (1)$$

According to quantum mechanics representations: $I\sigma_D(\Omega) \sim \sigma_D |\mathbf{E}\cdot\mathbf{d}|^2$, where $\mathbf{E}$ is the strength of the recording electric field in the medium, $\mathbf{d}$ is unit vector of the transition dipole moment of the photochromic center (in the spherical coordinate system $\mathbf{d} = (\sin\vartheta\cos\varphi, \sin\vartheta\cos\varphi, \cos\theta)$).

Let us make the consideration in frames of the following assumptions: 1) optical density of photochromic layer on the record frequency is small, that corresponds to the optically thin layer; 2) absorption of photon by the photoactive center occurs due to dipole-dipole transition between the main and electronically excited states; 3) initial photochromic layer is homogeneous and optically isotropic, with scalar permittivity ε_0.

The recording field in the medium is $\mathbf{E} = \mathbf{E}_+ + \mathbf{E}_-$, where vectors $\mathbf{E}_+$ and $\mathbf{E}_-$ characterize plane elliptically polarized waves with wave vectors $\mathbf{k}_+ = k(-\sin\alpha, 0, \cos\alpha)$ и $\mathbf{k}_- = k(-\sin\alpha, 0, -\cos\alpha)$ (axis Z of the square coordinate system is perpendicular to the layer boundaries), and

$$\mathbf{E}_+ = -E_0(\cos\alpha, -ib, \sin\alpha)\exp(-i\mathbf{k}_+\cdot\mathbf{r}), \quad \mathbf{E}_- = -rE_0(\cos\alpha, ib, -\sin\alpha)\exp(-i\mathbf{k}_-\cdot\mathbf{r}). \tag{2}$$

In Eq. (2) α is the angle of waves incident on the layer, $E_0=E(1+b^2)^{-1/2}$, b is the ellipticity parameter ($b = 0$ at linear and $b = \pm 1$ at circular polarizations); E is amplitude of wave $\mathbf{E}_+$; r is the relation of amplitudes of waves $\mathbf{E}_-$ and $\mathbf{E}_+$.

2. Optical Properties of the Structure: Boundary Problem

Permittivity tensor of the considered system can be written in the form ($i, j = 1,2,3$)

$$\varepsilon_{ij} = \varepsilon_0 + \frac{\Delta\varepsilon}{4\pi}\int_0^{4\pi} d_i d_j f(\Omega_d)\, d\Omega_d = \varepsilon_0 + \frac{\Delta\varepsilon}{4\pi}\sum_{m=1}^{\infty}\int_0^{4\pi} d_i d_j a_m(H)\left(\sigma_D(\Omega_d)/\sigma_D\right)^m d\Omega_d, \tag{3}$$

where function $f(\Omega_d)$ in Eq. (1) has been expanded in the Taylor series about factor $\sigma_D(\Omega_d)\phi It$ with coefficients $a_m = f^{(m)}(0)H^m/m!$ which do not depend on angle Ω_d, $H = \sigma_D I\phi t$ is the exposure and $\Delta\varepsilon$ is depth of permittivity modulation; ϕ is quantum yield of conversion.

The general form of the expression determining dependence of quantity $\sigma_D(\Omega_d)/\sigma_D$ on the angles of the spherical coordinate system is relatively awkward

$$\begin{aligned}
\sigma_D(\Omega_d)/\sigma_D = {} & \cos^2 K\left((1-r)^2\cos^2\vartheta\sin^2\alpha + (1-r^2)\cos\vartheta\sin\vartheta\cos\varphi\sin 2\alpha\right) + \\
& + \sin^2\vartheta\left((1+r)^2\cos^2\alpha\cos^2\varphi + b^2(1-r)^2\sin^2\varphi\right) + \\
& + \sin^2 K\left((1+r)^2\cos^2\vartheta\sin^2\alpha + (1-r^2)\cos\vartheta\sin\vartheta\cos\varphi\sin 2\alpha\right) + \\
& + \sin^2\vartheta\left((1-r)^2\cos^2\alpha\cos^2\varphi + b^2(1+r)^2\sin^2\varphi\right) + 2br\cos\alpha\sin 2K\sin^2\vartheta\sin 2\phi,
\end{aligned} \tag{4}$$

where $K = kz\cos\alpha$. So let us consider important particular cases when Eq. (4) is significantly simplified. At linear on exposure H expansion of function $f(\Omega_d)$ substitution of Eq. (4) to Eq. (3) gives

$$\begin{aligned}
& \varepsilon_{11} = \varepsilon_0 + (\Delta\varepsilon/15)\left[(1+r^2)(2+b^2+\cos 2\alpha) + 2r\cos(2K)(1-b^2+2\cos 2\alpha)\right]a_1, \\
& \varepsilon_{12} = \varepsilon_{21} = \varepsilon_0 + (4\Delta\varepsilon/15)(br\sin(2K)\cos\alpha)a_1, \quad \varepsilon_{13} = \varepsilon_{31} = \varepsilon_0 - (\Delta\varepsilon/15)((r^2-1)\sin(2\alpha))a_1, \\
& \varepsilon_{22} = \varepsilon_0 + (\Delta\varepsilon/15)\left[(1+r^2)(1+3b^2) + 2r\cos(2K)(\cos(2\alpha) - 3b^2)\right]a_1, \\
& \varepsilon_{33} = \varepsilon_0 + (\Delta\varepsilon/15)\left[(1+r^2)(2+b^2-\cos(2\alpha)) - 2r\cos(2K)(1+b^2-2\cos(2\alpha))\right]a_1, \\
& \varepsilon_{23} = \varepsilon_{32} = 0.
\end{aligned} \tag{5}$$

In case of arbitrary parameters describing the recording waves, tensor ε form depends on the photoreaction type and transformation extent. Even in simple model situations the derived expressions are very awkward. Moreover, analysis of Eq. (5) leads to some general conclusions: 1) $\varepsilon_{23}=\varepsilon_{32}=0$; 2) $\varepsilon_{13}=\varepsilon_{31}\neq 0$ if $r\neq 0$, and quantities ε_{13} и ε_{31} do not depend on z; 3) at $\alpha\neq 0$ there is a harmonic dependence $\varepsilon_{33}(z)$, which can be absent at the relations between parameters r, b, α: $b=\sqrt{2\cos(2\alpha)-1}$ or $r=0$.

In another particular case of $\alpha=0$, $b=1$, $r=1$ (opposing propagation of the circularly polarized waves with the equal amplitudes) we have from Eq. (4): $\sigma_D(\Omega_d)/\sigma_D=\left(\cos(K+\varphi)\sin(\vartheta)\right)^2$. Substitution of Eq. (4) in Eq. (3) gives ($(2/15)\Delta\varepsilon(H)\to\Delta\varepsilon$ at $H\to\infty$)

$$\varepsilon=\begin{pmatrix}\varepsilon_0+(2-\cos(2kz))\Delta\varepsilon(H) & \Delta\varepsilon(H)\sin(2kz) & 0\\ \Delta\varepsilon(H)\sin(2kz) & \varepsilon_0+(2+\cos(2kz))\Delta\varepsilon(H) & 0\\ 0 & 0 & \varepsilon_0\end{pmatrix}. \qquad (6)$$

Due to specific dependence of relation $\sigma_D(\Omega_d)/\sigma_D$ on angles ϑ and φ the form of the permittivity tensor in Eq. (6) does not depend on particular mechanism of the photoreaction which leads to the record of the electromagnetic field state and extent of photochemical transformations in the medium.

The form of Eq. (6) corresponds exactly to the permittivity tensor of uniaxial CLC with the spiral step $H=1/(2k)$ [3]. This analogy allows to use the known analytical expressions for the proper waves and solutions of the boundary problems for CLC [3] at analysis of optical properties of the exposed photochromic layers. In particular, one can show that the circularly polarized proper waves in the layer experience a selective diffractional reflection. In general case, it is represented to be possible investigation of the polarized waves transmission and reflection in a wide frequency range (and not only near the Bragg frequency, as at the traditional approach to investigations of polarization holograms [4]), and with account of the multiple reflections on the layer boundaries.

The calculated at using results [3] dependencies of the transmissivity of the circularly polarized light incident on the layer with thicknesses $50\lambda_0$ (1), $100\lambda_0$ (2), $430\lambda_0$ (3), and $730\lambda_0$ (4) on wavelength λ are shown in Fig. 1 (λ_0=0.44μm). The parameters values $\varepsilon_0=3$, $\Delta\varepsilon=0.01$, b=1 are taken, indexes of refraction beyond the layer are equal to 1. It is seen from Fig. 1, that with increasing the layer thickness and at small tunes from λ_0 the system is similar to the Fabry-Perot interferometer, despite of small Fresnel's reflectivities on the layer boundaries. Mutual influence of the multibeam interference and diffraction on the periodic structure cause such behaviour of the system.

Obviously, the permittivity tensor characterizing the structure, has the form similar to Eq. (6) not only in the case of parallel propagation of the recording beams ($\alpha=0$). For example, as it follows from Eq. (5), at $b^2=2\cos 2\alpha-1$ and $r=1$ this tensor has the form as in Eq. (6) with the structure period $H=1/(2k\cos\alpha)$. That allows to control the structure period at a choice of the record geometry.

The nonlinear properties of the Fabry-Perot interferometers were studied enough explicitly. One of the most interesting features of such systems is bistable and multistable responses at high incident intensities. In connection with the marked similarity of the explored system to the Fabry-Perot interferometer, it is interesting to investigate opportunities of occurrence of multistable regimes in our system. Taking into account, that the photochromic layer with spiral spatial microstructure has specific polarization properties, the analysis of the mentioned problem can have a practical interest.

Let under incident of the probe radiation on the layer of material characterized by the tensor Eq. (6) the averaged permittivity ε varies on quantity $\Delta\varepsilon_{nl}=\varepsilon_2 P$, where P is intensity, and parameter ε_2 is determined by the concrete mechanism of a nonlinearity. Figure 2 illustrates the graphical solution of the transcendental equation determining transmittance of the layer $T(\varepsilon)$:

$$T(\varepsilon)=(\varepsilon-\varepsilon_0)/(\varepsilon_2 P). \qquad (7)$$

The wavelength of the radiation differed from quantity λ_0, determining the spiral microstructure period, on quantity $\lambda_0\delta/3$, where $\delta = 4\Delta\varepsilon/(15\varepsilon_0 + 8\Delta\varepsilon)$ (see Fig. 1). From Fig. 2 it is seen, that at various intensities (straight lines 1, 2, 3, 4 correspond to increasing intensity) of incident radiation, Eq.(9) has a various number of the solutions. That corresponds to the multistable response of the system in the range of intensities relevant to curves 1-3 (Fig. 2). Taking $\varepsilon_2 = 10^{-3} cm^2/kW$ (typical value for the thermal nonlinearity [5]), from Fig. 2 one can estimate the minimal intensity for observation of the bistability and multistability effects in the considered layers: $P = 5kW/cm^2$.

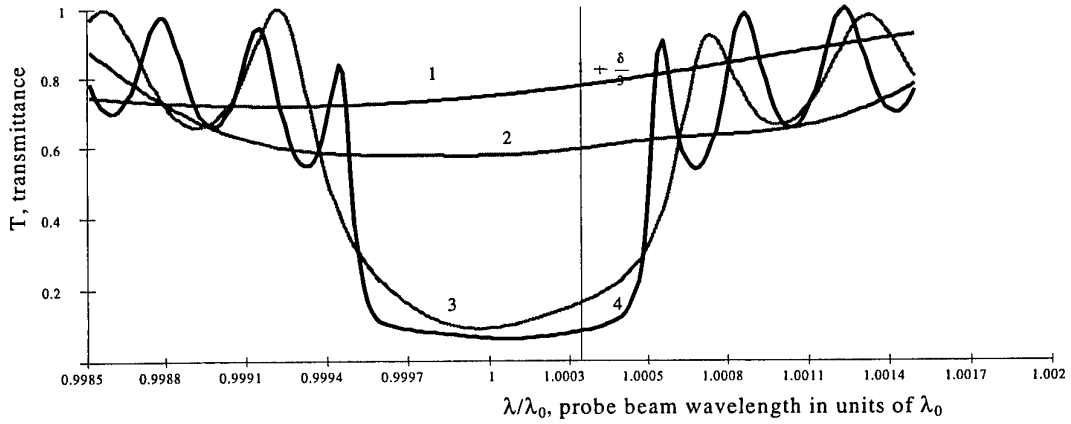

Fig. 1

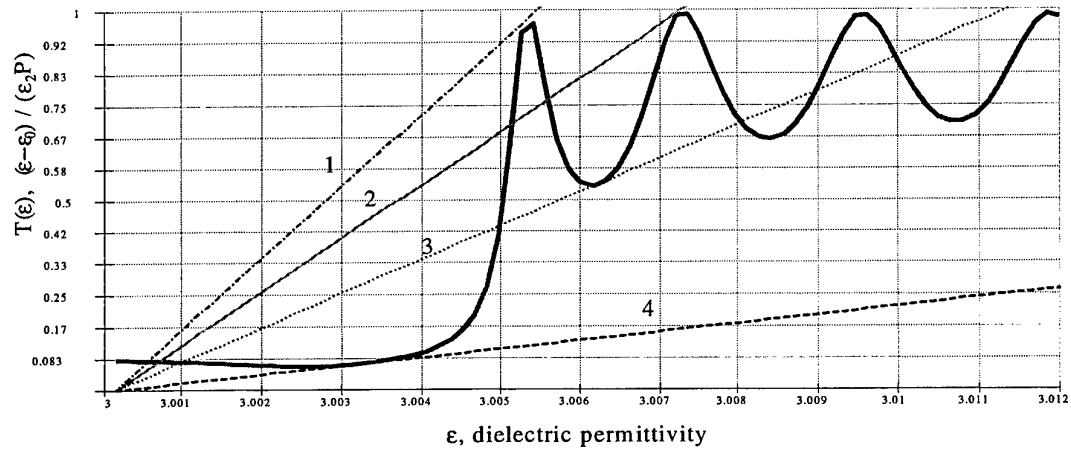

Fig. 2 $\varepsilon_0 = 3$; $\Delta\varepsilon$=0.01; $b = 1$; $\Delta\varepsilon_{nl}$=0.0053 (1), 0.0071 (2), 0.0112 (3), 0.045 (4)

References

[1] J. Gillet, *Photophysics and Photochemistry of Polymers*. Moscow: Mir, 1988.

[2] R. A. Lessard, R. Changkakoti, D. Roberg, and G. Manivannan, "Photopolymers in optical computing: materials and devices," *SPIE Proc.*, vol. 1806, pp. 2-13, 1992.

[3] V. A. Belyakov, *Diffraction Optics of Periodic Media with Complex Structure*. Moscow: Nauka, 1988.

[4] Sh. D. Kakichashvili, *Polarization Holography*. Leningrad: Nauka, 1989.

[5] H. Gibbs, *Optical Bistability*. Moscow: Mir, 1988.

Session 4

Session 4

Wednesday - September 27, 2000

16:30 - 17:40

Bianisotropic Media I

A Pedigree of Bianisotropic Media

F. Olyslager[1] and I.V. Lindell[2]

[1] Department of Information Technology, Ghent University
Sint-Pietersnieuwstraat 41, B-9000 Ghent, Belgium

[2] Electromagnetics Laboratory, Helsinki University of Technology
PO Box 3000, FIN-02015 HUT, Espoo, Finland

Abstract

During the past years we have intensively studied basic properties and field solutions in homogeneous bianisotropic media. We started from simple isotropic media to ever more general bianisotropic media. This study has led to some classification of bianisotropic media, which resembles a pedigree. The pedigree contains two branches. The first branch are so-called self-dual media, these are generalisations of the chiral medium. The second branch are factorizable media, these are generalisations of the uniaxial anisotropic media. We think to have reached some consensus with respect to the pedigree, i.e. we think to have found the most general media in each of the two branches.

1. Introduction

In this contribution we want to report on some of the findings we obtained during the past eight years. During this period we have been investigating homogeneous bianisotropic media with constitutive relations of the form

$$\mathbf{D} = \underline{\epsilon} \cdot \mathbf{E} + \underline{\xi} \cdot \mathbf{H}, \qquad \mathbf{B} = \underline{\zeta} \cdot \mathbf{E} + \underline{\mu} \cdot \mathbf{H}, \tag{1}$$

where $\underline{\epsilon}$, $\underline{\mu}$, $\underline{\zeta}$ and $\underline{\xi}$ are the medium dyadics.

We were interested in finding basic field solutions in these media. The fields for any given source can be found by integration from the fields of an elementary dipole source, i.e. from the Green dyadics. In general it is not possible to obtain the Green dyadics into closed form. Other basic solutions are plane waves. Sometimes an electromagnetic field problem can be simplified by decomposing the fields in two components. Each of these components then propagate in a "simpler" medium for which the Green dyadics are known. Another way to solve field problems is the use of duality transformations which allow us to transform field solutions in one medium to those in another medium. Our aim was to find the most general media for which decomposition of the fields was possible, for which we could find the plane wave solutions and for which the Green dyadics could be obtained in closed form. It turned out that these three problems are intimately interrelated. The common backbone behind these problems is the possibility to factorize the fourth order "Helmholtz determinant operator".

This study resulted in a hierarchical ordening – which we call a pedigree – of ever more general bianisotropic media. Basically this pedigree consists of two separate branches. In the present contribution we will first discuss some basics such as Green dyadics, factorization, plane waves, decomposition and duality. Then we will focus on the the two branches of the pedigree.

This paper gives only a small overview of the subject, a more rigorous historical overview with more references can be found in [1].

2. Green Dyadics and Factorization

The electric Green dyadic $\underline{G}_{ee}(\mathbf{r})$ is defined as the relation between the electric current density $\mathbf{J}(\mathbf{r})$ and the electric field $\mathbf{E}(\mathbf{r})$:

$$\mathbf{E}(\mathbf{r}) = -j\omega \iiint_V \underline{G}_{ee}(\mathbf{r}-\mathbf{r}') \cdot \mathbf{J}(\mathbf{r}')\mathrm{d}V'. \tag{2}$$

In a bianisotropic medium this Green dyadic satisfies the equation

$$\underline{H}_{ee}(\nabla) \cdot \underline{G}_{ee}(\mathbf{r}) = -\underline{I}\delta(\mathbf{r}), \tag{3}$$

with $\underline{H}_{ee}(\nabla)$ the vector Helmholtz operator given by [2]

$$\underline{H}_{ee}(\nabla) = -(\nabla \times \underline{I} - j\omega\underline{\xi}) \cdot \underline{\mu}^{-1} \cdot (\nabla \times \underline{I} + j\omega\underline{\zeta}) + \omega^2\underline{\epsilon}. \tag{4}$$

To solve (3) it suffices to find a scalar Green function $G(\mathbf{r})$ that is solution of

$$\det\underline{H}_{ee}(\nabla)G(\mathbf{r}) = -\delta(\mathbf{r}), \tag{5}$$

with $\det\underline{H}_{ee}(\nabla)$ the Helmholtz determinant operator. The solution of (3) then follows from

$$\underline{G}_{ee}(\mathbf{r}) = \left[\underline{H}^A_{ee}(\nabla)\right]^T G(\mathbf{r}), \tag{6}$$

with $\underline{H}^A_{ee}(\nabla)$ the adjoint operator of the vector Helmholtz operator. The Helmholtz determinant operator turns out to be a fourth order operator, which makes, in general, a closed form solution of (5) impossible. For some classes of media it is possible to factorize this operator as a product of two second order operators, i.e.

$$\det\underline{H}_{ee}(\nabla) = H_a(\nabla)H_b(\nabla). \tag{7}$$

A medium for which this is possible is called factorizable. Factorizability does not necessarily mean that we can solve (5) in closed form. However, often a closed form solution is possible or an elegant series or integral representation.

Sometimes one can factorize the second order dyadic Helmholtz operator:

$$\underline{H}_{ee}(\nabla) = \underline{H}_a(\nabla) \cdot \underline{H}_b(\nabla) \tag{8}$$

where $\underline{H}_a(\nabla)$ and $\underline{H}_b(\nabla)$ are first order dyadic operators. For these media it is possible to write $\underline{G}_{ee}$ in closed form.

3. Plane Waves

For a plane wave of the form $\mathbf{E}(\mathbf{r}) = \mathbf{E}_0 \exp(-j\mathbf{k} \cdot \mathbf{r})$ the vector $\mathbf{E}_0$ satisfies the equation

$$\underline{H}_{ee}(-j\mathbf{k}) \cdot \mathbf{E}_0 = 0. \tag{9}$$

A solution different from zero is only possible when $\mathbf{k}$ satisfies the dispersion equation

$$\det\underline{H}_{ee}(-j\mathbf{k}) = 0. \tag{10}$$

If we write $\mathbf{k}$ as $k\mathbf{u}$ with $\mathbf{u}$ a unit vector defining the phase velocity propagation direction then (10) is a fourth order polynomial equation in k and the dispersion surface will be a fourth order surface. When $\det\underline{H}_{ee}$ is factorizable the dispersion surface consists of two second order surfaces, i.e. of two quadrics. For a given value of $\mathbf{k}$ the solution of equation (9) gives the polarization of the plane waves.

4. Decomposition

With decomposition we mean that the fields can be split in two components as

$$\mathbf{E} = \mathbf{E}_a + \mathbf{E}_b, \qquad \mathbf{H} = \mathbf{H}_a + \mathbf{H}_b. \tag{11}$$

Both a and b are solution of Maxwell equations for simpler media than the original medium. These simpler media are called the equivalent media. The most well known field decomposition is the TE and TM decomposition for uniaxial anisotropic media [3] for which the equivalent media are isotropic media. This can be generalised to media where the decomposed fields satisfy the conditions

$$\mathbf{a}_1 \cdot \mathbf{E}_a + \mathbf{a}_2 \cdot \mathbf{H}_a = 0, \qquad \mathbf{b}_1 \cdot \mathbf{E}_b + \mathbf{b}_2 \cdot \mathbf{H}_b = 0, \tag{12}$$

where $\mathbf{a}_1$, $\mathbf{a}_2$, $\mathbf{b}_1$ and $\mathbf{b}_2$ are arbitrary vectors.

Another way to decompose the fields is the Bohren decomposition [4]. In this case the fields are decomposed as

$$\mathbf{E} = \mathbf{E}_+ + \mathbf{E}_-, \qquad \mathbf{H} = \mathbf{H}_+ + \mathbf{H}_-, \tag{13}$$

with

$$\mathbf{E}_\pm = Y_\pm \mathbf{H}_\pm, \tag{14}$$

with $Y_\pm$ some scalar constants. The most well known medium that allows such a decomposition is the isotropic chiral medium. Also in this case there are much more general media that allow a Bohren decomposition.

5. Duality

A duality transformation transforms original fields $\mathbf{E}$ and $\mathbf{H}$ into dual fields $\mathbf{E}_d$ and $\mathbf{H}_d$ as

$$\begin{pmatrix} \mathbf{E}_d \\ \mathbf{H}_d \end{pmatrix} = \begin{pmatrix} A & B \\ C & D \end{pmatrix} \begin{pmatrix} \mathbf{E} \\ \mathbf{H} \end{pmatrix}, \tag{15}$$

with A, B, C and D arbitrary constants. The dual fields satisfy Maxwell equations in a dual medium defined by its medium dyadics as

$$\begin{pmatrix} \underline{\epsilon}_d & \underline{\xi}_d \\ \underline{\zeta}_d & \underline{\mu}_d \end{pmatrix} = -\begin{pmatrix} A & B \\ C & D \end{pmatrix} \begin{pmatrix} 0 & 1 \\ -1 & 0 \end{pmatrix} \begin{pmatrix} \underline{\epsilon} & \underline{\xi} \\ \underline{\zeta} & \underline{\mu} \end{pmatrix} \begin{pmatrix} A & B \\ C & D \end{pmatrix}^{-1}. \tag{16}$$

Using the duality transformation it is possible to transform field solutions from the original medium to the dual medium or vice versa. For example the Green dyadics between both media are related through [5]

$$\begin{pmatrix} \underline{G}_{ee,d} & \underline{G}_{em,d} \\ \underline{G}_{me,d} & \underline{G}_{mm,d} \end{pmatrix} = \begin{pmatrix} A & B \\ C & D \end{pmatrix} \begin{pmatrix} \underline{G}_{ee} & \underline{G}_{em} \\ \underline{G}_{me} & \underline{G}_{mm} \end{pmatrix} \begin{pmatrix} 0 & 1 \\ -1 & 0 \end{pmatrix} \begin{pmatrix} A & B \\ C & D \end{pmatrix}^{-1}. \tag{17}$$

When a medium is invariant under a duality transformation we say it is a self-dual medium. Only a restricted class of bianisotropic media are self-dual.

6. The First Branch

It turns out that the class of media that are self-dual or that allow a Bohren decomposition or that allow a factorization of the vector Helmholtz operator is one and the same. These media

have been studied in [6]–[11]. The isotropic chiral medium is the simpliest representative of this class. The most general medium of this class is given by

$$\underline{\epsilon} = \epsilon\underline{\alpha}, \qquad \underline{\mu} = \mu\underline{\alpha}, \qquad \underline{\zeta} = (\chi\underline{\alpha} + j\underline{\kappa})\sqrt{\epsilon\mu}, \qquad \underline{\xi} = (\chi\underline{\alpha} - j\underline{\kappa})\sqrt{\epsilon\mu}, \tag{18}$$

with $\underline{\alpha}$ and $\underline{\kappa}$ arbitrary dyadics.

The Green dyadics for this medium can be written in closed form [11] as follows

$$\underline{G}_{ee}(\mathbf{r}) = -\frac{j\eta \exp(k\mathbf{a}_+ \cdot \mathbf{r})}{2\cos\theta}\underline{L}_+(\nabla)\left(\frac{\exp(-jkD_+)}{4\pi kD_+}\right)$$

$$-\frac{j\eta \exp(k\mathbf{a}_- \cdot \mathbf{r})}{2\cos\theta}\underline{L}_-(\nabla)\left(\frac{\exp(-jkD_-)}{4\pi kD_-}\right), \tag{19}$$

with

$$k = \omega\sqrt{\epsilon\mu}, \quad \eta = \sqrt{\frac{\mu}{\epsilon}}, \quad D_\pm = \sqrt{\det\underline{S}_\pm}\sqrt{\mathbf{r}\cdot\underline{S}_\pm^{-1}\cdot\mathbf{r}}, \quad \cos\theta = \sqrt{1-\chi^2}, \tag{20}$$

$$\underline{L}_\pm(\nabla) = \nabla\nabla \pm k(\nabla\cdot\underline{S}_\pm)\times\underline{I} + k^2\underline{S}_\pm^{-1}\det\underline{S}_\pm \tag{21}$$

and where $\underline{S}_\pm$ and $\mathbf{a}_\pm$ follow from a decomposition of $\cos\theta\underline{\alpha} \pm \underline{\kappa}$ in a symmetric and an asymmetric part of the form

$$\cos\theta\underline{\alpha} \pm \underline{\kappa} = \underline{S}_\pm + \mathbf{a}_\pm \times \underline{I}. \tag{22}$$

For more information on the media in this branch we also refer to another paper in these proceedings [12].

7. The Second Branch

The second branch is much more complicated. This branch contains the media that are decomposable. It turns out that these media are also factorizable. It took us a long while to find the medium that has all decomposable and factorisable media as special cases. This medium is described by rather complicated medium parameters [13]

$$\underline{\epsilon} = \alpha(\mathbf{z}\times\underline{I} + \mathbf{a}_1\mathbf{b}_1 + \mathbf{b}_1\mathbf{a}_1) + \eta(-\underline{B}^T + \mathbf{a}_2\mathbf{b}_1 + \mathbf{b}_2\mathbf{a}_1), \tag{23}$$

$$\underline{\xi} = \eta(\mathbf{x}\times\underline{I} + \mathbf{a}_2\mathbf{b}_2 + \mathbf{b}_2\mathbf{a}_2) + \alpha(\underline{B} + \mathbf{a}_1\mathbf{b}_2 + \mathbf{b}_1\mathbf{a}_2), \tag{24}$$

$$\underline{\zeta} = \tau(\mathbf{z}\times\underline{I} + \mathbf{a}_1\mathbf{b}_1 + \mathbf{b}_1\mathbf{a}_1) - \alpha(-\underline{B}^T + \mathbf{a}_2\mathbf{b}_1 + \mathbf{b}_2\mathbf{a}_1), \tag{25}$$

$$\underline{\mu} = -\alpha(\mathbf{x}\times\underline{I} + \mathbf{a}_2\mathbf{b}_2 + \mathbf{b}_2\mathbf{a}_2) + \tau(\underline{B} + \mathbf{a}_1\mathbf{b}_2 + \mathbf{b}_1\mathbf{a}_2), \tag{26}$$

where α, η, τ, $\mathbf{a}_1$, $\mathbf{a}_2$, $\mathbf{b}_1$, $\mathbf{b}_2$, $\mathbf{x}$, $\mathbf{z}$ and $\underline{B}$ are arbitrary scalars, vectors and dyadics. It turns out that this medium is also closed with respect to duality transformations. This means that it is not possible to generalize this medium further using a duality transformation. These observations made us conclude that (23)–(26) is the most general medium that allows decomposition and factorisation.

Special cases of the medium (23)–(26) were studied in [14]–[34]. An important special case are the anisotropic media. The most general anisotropic medium that allows factorization and decomposition is $\underline{\epsilon} = \tau\underline{\mu}^T + \mathbf{ab}$ [24], with as special case the uniaxial anisotropic medium.

Another interesting class of media are the equivalent media of the medium (23)–(26). These are of the form [13]

$$\underline{\epsilon} = -\eta\underline{B}^T + \alpha(\mathbf{z}\times\underline{I}), \qquad \underline{\mu} = \tau\underline{B} - \alpha(\mathbf{x}\times\underline{I}), \tag{27}$$

$$\underline{\xi} = \alpha\underline{B} + \eta(\mathbf{x}\times\underline{I}), \qquad \underline{\zeta} = \alpha\underline{B}^T + \tau(\mathbf{z}\times\underline{I}). \tag{28}$$

Without loss of generality we assume that $\tau\eta + \alpha^2 = 1$. The Helmholtz determinant operator for these media can be written as a square. This allows a closed form Green dyadic given by

$$\underline{G}_{ee}(\mathbf{r}) = \{\frac{\alpha}{j\omega}[(\alpha\nabla \times \underline{I} - j\omega\underline{B}) \cdot (\tau\nabla - j\omega\mathbf{x})] \times \underline{I}$$

$$-\frac{\tau}{j\omega}[(\eta\nabla + j\omega\mathbf{z})(\tau\nabla - j\omega\mathbf{x}) + \alpha^2\nabla\nabla + j\omega\alpha\nabla(\underline{B}^{T\times}\vdots\underline{I}) + \underline{I} \times (\nabla \cdot \underline{B}) - \omega^2(\underline{B}^{-1})^T \det\underline{B}]\}$$

$$\frac{e^{j\omega\mathbf{c}\cdot\underline{R}^{-1}\cdot\mathbf{r}}e^{-jkD}}{j\omega 4\pi\sqrt{\det\underline{R}}\sqrt{D}}, \tag{29}$$

with

$$\underline{R} = \frac{1}{2}(\alpha^2 + \tau\eta)(\underline{B} + \underline{B}^T), \quad \mathbf{c} = \frac{1}{2}[\eta\underline{B} \cdot \mathbf{x} + \tau\mathbf{z} \cdot \underline{B} - \alpha\mathbf{z} \times \mathbf{x} + \alpha(\det\underline{B})(\underline{B}^{-1})^{T\times}\vdots\underline{I}], \tag{30}$$

and

$$k = \omega\sqrt{\mathbf{z} \cdot \underline{B} \cdot \mathbf{x} + \det\underline{B} - \mathbf{c} \cdot \underline{R}^{-1} \cdot \mathbf{c}}, \quad D = \sqrt{\mathbf{r} \cdot \underline{R}^{-1} \cdot \mathbf{r}}, \tag{31}$$

where $\underline{A}^{\times}\vdots\underline{I}$ is shorthand for $\mathbf{u}_x \times \underline{A} \cdot \mathbf{u}_x + \mathbf{u}_y \times \underline{A} \cdot \mathbf{u}_y + \mathbf{u}_z \times \underline{A} \cdot \mathbf{u}_z$. The fact that the Helmholtz determinant operator is a square also means that the two second order dispersion surfaces coincide. Each of the equivalent media of a certain original medium have as coinciding dispersion surfaces one of the two dispersion surfaces of the original medium.

Acknowledgements

F. Olyslager is a Research Associate of the Fund for Scientific Research - Flanders (Belgium)(F.W.O.) and I.V. Lindell has the research position of Academy Professor by the Academy of Finland.

References

[1] F. Olyslager and I. V. Lindell, "Electromagnetics and exotic media – A quest to the Holy Grail," Submitted to *IEEE Antennas and Propagation Magazine*.

[2] I. V. Lindell, *Methods for Electromagnetic Field Analysis*, IEEE Press - Oxford University Press, New-York, 1995.

[3] P. C. Clemmow, "The resolution of a dipole field into transverse electric and magnetic waves," *IEE Proceedings*, Vol. 110, no. 1, pp. 107–111, 1963.

[4] G. F. Bohren, "Light scattering by an optically active sphere," *Chem. Phys. Lett.*, vol.29, no.3, pp.458-462, 1974.

[5] I. V. Lindell and L.H. Ruotanen, "Duality transformations and Green dyadics for bi-anisotropic media," *Journal of Electromagnetic Waves and Applications*, Vol. 12, no. 9, pp. 1131–1152, 1998.

[6] J. C. Monzon, "Radiation and scattering in homogeneous general biisotropic regions," *IEEE Trans. on Antennas and Propagation*, Vol. 38, no. 2, pp. 227–235, 1990.

[7] S. Bassiri, N. Engheta and C. H. Papas, "Dyadic Green's function and dipole radiation in chiral media," *Alta Frequenza*, Vol. 55, no. 2, pp. 83–88, 1986.

[8] I. V. Lindell and W. S. Weiglhofer, "Green dyadic and dipole fields for a medium with anisotropic chirality," *IEE Proceedings Part H*, Vol. 141, no. 3, pp. 211–215, 1994.

[9] I. V. Lindell and F. Olyslager, "Duality transformations, Green dyadics and plane-wave solutions for a class of bianisotropic media," *Journal of Electromagnetics Waves and Applications*, Vol. 9, no. 1/2. pp. 85–96, 1995.

[10] F. Olyslager and I. V. Lindell, "Green's Dyadics for Bi-anisotropic Media with Similar Medium Dyadics," *Microwave and Optical Technology Letters*, Vol. 17, no. 1, pp. 45–47, 1998.

[11] I. V. Lindell and F. Olyslager, "Green dyadics for self-dual bianisotropic media," *Journal of Electromagnetic Waves and Applications*, Vol. 14, pp. 153–163, 2000.

[12] I. V. Lindell and F. Olyslager, "Green dyadics for self-dual bi-anisotropic media," *Proceedings of Bianisotropics 2000*, Lisboa, Portugal, 2000.

[13] F. Olyslager and I. V. Lindell, "Field decomposition and factorization of Helmholtz determinant operator for bianisotropic media," Submitted to *IEEE Transactions on Antennas and Propagation.*
[14] F. I. Federov, Teoriya girotropii (Theory of Gyrotropy). Minsk: Nauka i tekhnika, 1976.
[15] W. S. Weiglhofer, "Dyadic Green's functions for general uniaxial media," *IEE Proc. H Microwaves, Antennas and Propagation,* Vol. 137, no. 1, pp. 5–10, 1990.
[16] I. V. Lindell, "Coordinate-independent Green Dyadic for General Symmetric Uniaxial Media," *Helsinki University of Technology, Radio Laboratory Report,* no. S61, 1974.
[17] I. V. Lindell and W.S. Weiglhofer, "Green dyadic for a uniaxial bianisotropic medium," *IEEE Trans. Antennas Propagat.*, Vol. 42, no. 7, pp. 1013–1016, 1994.
[18] W. S. Weiglhofer and I.V. Lindell, "Analytic solution for the Green's function of a nonreciprocal uniaxial bianisotropic medium," *AEÜ*, Vol. 48, no. 2, pp. 116–119, 1994.
[19] W. S. Weiglhofer, "Dyadic Green function for unbounded general uniaxial bianisotropic medium," *Int. J. Electron.*, Vol. 77, no. 7, pp. 105–115, 1994.
[20] F. Olyslager, "Time-harmonic two- and three-dimensional Green's dyadics for general uniaxial bianisotropic media," *IEEE Trans. Antennas Propagat.*, Vol. 43, no. 4, pp. 430–434, 1995.
[21] F. Olyslager, "Time-harmonic two- and three-dimensional closed form Green's dyadics for gyrotropic bianisotropic and anisotropic media," *Electromagnetics*, Vol. 17, no. 4, pp. 369–386, 1997.
[22] I. V. Lindell and F. Olyslager, "Analytic Green dyadic for a class of nonreciprocal anisotropic media," *IEEE Trans. Antennas Propagat.*, Vol. 45, no. 10, pp. 1563–1565, 1997.
[23] I. V. Lindell and F. Olyslager, "Green dyadic for a class of anisotropic media," *Helsinki Univ. Tech., Electromagnetics Lab. Rept.* 237, 1997.
[24] I. V. Lindell and F. Olyslager, "Factorization of the Helmholtz determinant operator for anisotropic media," *Archiv für Elektronik und Übertragungstechnik*, Vol. 52, no. 1, pp. 261–267, 1998.
[25] A. Kujawski and S. Przezdziecki, "Necessary condition for the splitting of electromagnetic fields into TE and TM constituents in a class of anisotropic media," *Bull. Acad. Polon. Sci., math. astr. phys.*, Vol. 21, no. 10, pp. 955–962, 1973.
[26] I. V. Lindell, "Decomposition of electromagnetic fields in bi-anisotropic media," *Journal of Electromagnetic Waves and Applications*, Vol. 11, no. 5, pp. 645–657, 1997.
[27] I. V. Lindell and F. Olyslager, "Generalized decomposition of electromagnetic fields in bi-anisotropic media," *IEEE Transactions on Antennas and Propagation*, Vol. 46, no. 10, pp. 1584–1585, Oct. 1998.
[28] I. V. Lindell, "Field decomposition in special gyrotropic media," *Microwave and Optical Technology Letters*, Vol. 12, no. 1, pp. 29–31, 1996.
[29] F. Olyslager and I. V. Lindell, "Green's dyadics for a class of bi-anisotropic media with nonsymmetric bi-anisotropic dyadics," *AEÜ*, Vol. 52, no. 1, pp. 32–36, 1998.
[30] F. Olyslager and I. V. Lindell, "Closed form Green's dyadics for a class of media with axial bi-anisotropy," *IEEE Trans. Antennas Propagat.*, Vol. 46, no. 12, pp. 1888–1890, 1998.
[31] I. V. Lindell and F. Olyslager, "Green dyadic for a class of bi-anisotropic media," *Microwave and Optical Technology Letters*, Vol. 19, no. 3, pp. 216–221, 1998.
[32] F. Olyslager and I. V. Lindell, "Green's dyadics and factorization of the Helmholtz determinant operator for a class of bi-anisotropic media," *Microwave and Optical Technology Letters*, Vol. 21, no. 4, pp. 304–309, 1999.
[33] I. V. Lindell and F. Olyslager, "Factorization of the Helmholtz determinant operator for decomposable bi-anisotropic media," *Journal of Electromagnetic Waves and Applications*, Vol. 13, pp. 431–446, 1999.
[34] F. Olyslager, I. V. Lindell and L. H. Puska, "Factorisation and Green dyadics for a new class of bi-anisotropic media using duality," Submitted to *Journal of Electromagnetic Waves and Applications*, Vol. 14, pp. 745–762, 2000.

Onsager–Casimir Principle in the Theory of Bi-Anisotropic Media

S. A. Tretyakov[1], A. H. Sihvola[1], and B. Jancewicz[2]

[1] Electromagnetics Laboratory, Helsinki University of Technology
P.O. Box 3000, FIN-02015 HUT, Finland

[2] Institute of Theoretical Physics, University of Wroclaw
pl. Maksa Borna 9, PL-50-204, Wroclaw, Poland

Abstract

In this paper we establish relation between the microscopic and macroscopic Onsager–Casimir principles. It is demonstrated that because of certain symmetries with respect to the space reversal operation, which are intrinsic to any form of the linear constitutive relations, it follows that the symmetries under time reversal expressed by the Onsager–Casimir principle are valid both on the microscopic and macroscopic levels. As one of the possible applications we show that the property of the general bi-anisotropic media to be reciprocal or non-reciprocal does not depend on the constitutive formalism.

1. Introduction

In the electromagnetic theory there is a well-established *Onsager–Casimir principle* or *the principle of the symmetry of kinetic coefficients* [1, 2, 3] which provides certain symmetry relations for microscopic polarizabilities and macroscopic constitutive parameters. The principle is based on the time-reversal symmetry properties of electromagnetic processes. In this paper we show that quite general and important conclusions can be drawn from the fact that microscopic and macroscopic electromagnetic processes possess both time-reversal symmetry (manifested in the Onsager-Casimir principle) and space-reversal symmetry. The latter is manifested by the fact that linear kinetic equations or, in electromagnetics, linear constitutive relations can connect quantities of different mathematical nature. For example, electric polarization is an even vector with respect to the space-reversal operation *(polar vector)*, but magnetic field is odd under this operation *(axial vector)*. Thus, the polarizability coefficient must possess certain mathematical properties, so that operation on an axial vector gives a polar vector. In this paper we consider the two symmetry principles dictated by the time-reversal symmetries and space-reversal symmetries together. In particular, we find that the space-inversion symmetry imposes certain restrictions on the mixing rules which connect microscopic and macroscopic parameters of electromagnetic systems. As one of the applications, we consider the Onsager–Casimir principle for the material parameters of bi-anisotropic media. Here we show that the Onsager–Casimir principle leads always to the same conclusions in all possible formal descriptions of bi-anisotropic media. In particular, if a medium is seen to be reciprocal in one set of material parameters, it is found to be reciprocal in any other set.

2. Theory

2.1 Microscopic and macroscopic Onsager–Casimir principles

On the microscopic level a small bi-anisotropic particle is described by linear relations between the induced electric $\mathbf{p}_e$ and magnetic $\mathbf{p}_m$ dipole moments and external electric $\mathbf{E}$ and magnetic $\mathbf{B}$ fields (in the frequency domain):

$$\mathsf{p} = \mathsf{A} \cdot \mathsf{e} = \begin{pmatrix} \overline{\overline{a}}_{ee} & \overline{\overline{a}}_{em} \\ \overline{\overline{a}}_{me} & \overline{\overline{a}}_{mm} \end{pmatrix} \cdot \mathsf{e}, \quad \text{where} \quad \mathsf{p} = \begin{pmatrix} \mathbf{p}_e \\ \mathbf{p}_m \end{pmatrix}, \quad \mathsf{e} = \begin{pmatrix} \mathbf{E} \\ \mathbf{H} \end{pmatrix} \tag{1}$$

(A small particle is in free space, so $\mathbf{B} = \mu_0 \mathbf{H}$). The Onsager-Casimir relations for the polarizabilities [3, Eqs. (125.14), (125.16)] read:

$$\overline{\overline{a}}_{ee}(\mathbf{H}_0) = \overline{\overline{a}}_{ee}^{T}(-\mathbf{H}_0), \qquad \overline{\overline{a}}_{mm}(\mathbf{H}_0) = \overline{\overline{a}}_{mm}^{T}(-\mathbf{H}_0), \qquad \overline{\overline{a}}_{me}(\mathbf{H}_0) = -\overline{\overline{a}}_{em}^{T}(-\mathbf{H}_0) \tag{2}$$

Here $\mathbf{H}_0$ denotes a medium parameter (or a set of several parameters) which is odd under the time reversal operation.

On the macroscopic level, we deal with the averaged quantities – *constitutive parameters* – which connect the four field quantities as in

$$\mathbf{D} = \overline{\overline{\epsilon}} \cdot \mathbf{E} + \overline{\overline{\xi}} \cdot \mathbf{H}, \qquad \mathbf{B} = \overline{\overline{\mu}} \cdot \mathbf{H} + \overline{\overline{\zeta}} \cdot \mathbf{E} \tag{3}$$

The Onsager-Casimir principle [1, 2, 3] was extended to the constitutive parameters of bi-anisotropic media in [4, 5][1]. Probably the most general proof can be based on the fluctuation-dissipation theorem [3, §124-125]. The proof is straightforward for the constitutive relations (in the frequency domain) written in the following form (for perturbations cased by small fields $\mathbf{D}$ and $\mathbf{B}$):

$$\mathsf{e} = \mathsf{F} \cdot \mathsf{d}, \qquad \text{where} \quad \mathsf{d} = \begin{pmatrix} \mathbf{D} \\ \mathbf{B} \end{pmatrix}, \qquad \mathsf{F} = \begin{pmatrix} \overline{\overline{e}} & \overline{\overline{f}} \\ \overline{\overline{g}} & \overline{\overline{h}} \end{pmatrix} \tag{4}$$

The time-derivative of the energy density is

$$\frac{dW}{dt} = \mathsf{e} \cdot \frac{d\mathsf{d}}{dt} \tag{5}$$

Thus, the same relations follow for the macroscopic parameters as well [4, 5, 8]:

$$\overline{\overline{e}}(\mathbf{H}_0) = \overline{\overline{e}}^{T}(-\mathbf{H}_0), \qquad \overline{\overline{h}}(\mathbf{H}_0) = \overline{\overline{h}}^{T}(-\mathbf{H}_0), \qquad \overline{\overline{g}}(\mathbf{H}_0) = -\overline{\overline{f}}^{T}(-\mathbf{H}_0) \tag{6}$$

For simple dielectrics described in terms of the permittivity tensor only, it is obvious that the same symmetry relation as (6) is also valid for the permittivity [9, §96], because the symmetry properties of the inverse tensor are the same as that of the original tensor.

2.2 Different formalisms

Several forms of material relations can be used to characterize bi-anisotropic media (in the frequency domain). In particular, two such forms are considered in [8]:

$$\mathbf{E} = \overline{\overline{\varepsilon}} \cdot \mathbf{D} + \overline{\overline{f}} \cdot \mathbf{B}, \qquad \mathbf{H} = \overline{\overline{g}} \cdot \mathbf{D} + \overline{\overline{h}} \cdot \mathbf{B} \tag{7}$$

[1] Probably the first formulation for bi-anisotropic media was published in [6], but an equivalent result in terms of the quantum statistics was published as early as in 1952, see Eqs. (5.3,4) in [7].

(Equations (8) in [8]) and relations (3)

$$\mathbf{D} = \overline{\overline{\epsilon}} \cdot \mathbf{E} + \overline{\overline{\xi}} \cdot \mathbf{H}, \qquad \mathbf{B} = \overline{\overline{\zeta}} \cdot \mathbf{E} + \overline{\overline{\mu}} \cdot \mathbf{H} \tag{8}$$

The Onsager–Casimir principle written in terms of the parameters in (7) reads (6). On the other hand, if relations (8) are used, which means that the macroscopic problem is such that $\mathbf{E}$ and $\mathbf{H}$ can be considered as the primary fields, the same principle gives

$$\overline{\overline{\epsilon}}(\omega, \mathbf{H}_0) = \overline{\overline{\epsilon}}^T(\omega, -\mathbf{H}_0), \qquad \overline{\overline{\mu}}(\omega, \mathbf{H}_0) = \overline{\overline{\mu}}^T(\omega, -\mathbf{H}_0), \qquad \overline{\overline{\xi}}(\omega, \mathbf{H}_0) = -\overline{\overline{\zeta}}^T(\omega, -\mathbf{H}_0) \tag{9}$$

Although the Onsager–Casimir relations look differently for different formalisms, it can be proven that one of them automatically implies the other. Indeed, let us express the material parameters from one set in terms of the other [10]. Consider, for example,

$$\begin{aligned} \overline{\overline{\epsilon}}^T(-\mathbf{H}_0) &= \left[\left(\overline{\overline{e}}(-\mathbf{H}_0) - \overline{\overline{f}}(-\mathbf{H}_0) \cdot \overline{\overline{h}}^{-1}(-\mathbf{H}_0) \cdot \overline{\overline{g}}(-\mathbf{H}_0) \right)^{-1} \right]^T \\ &= \left[\overline{\overline{e}}^T(-\mathbf{H}_0) - \overline{\overline{g}}^T(-\mathbf{H}_0) \cdot (\overline{\overline{h}}^{-1})^T(-\mathbf{H}_0) \cdot \overline{\overline{f}}^T(-\mathbf{H}_0) \right]^{-1} \end{aligned} \tag{10}$$

Using (6) we rewrite this as

$$\overline{\overline{\epsilon}}^T(-\mathbf{H}_0) = \left(\overline{\overline{e}}(\mathbf{H}_0) - \overline{\overline{f}}(\mathbf{H}_0) \cdot \overline{\overline{h}}^{-1}(-\mathbf{H}_0) \cdot \overline{\overline{g}}(\mathbf{H}_0) \right)^{-1} = \overline{\overline{\epsilon}}(\mathbf{H}_0) \tag{11}$$

Similarly, one can prove that the other relations in (6) follow from (9). From this we find that, in contrast to the main conclusion of [8], it is impossible that one of the symmetry relations is satisfied but the other one is not. The same conclusion is true for the Post relations. Effectively, this means that the notion of reciprocity or non-reciprocity always has a clear sense which is independent on the material description formalism.

2.3 Time-reversal and space-reversal symmetries

Artificial bi-anisotropic materials are designed as mixtures of many bi-anisotropic inclusions. Because the composite properties depend on that of the inclusions, we can say that the macroscopic symmetry relations (9) are "inherited" from the microscopic relations (2). Several mixture rules exist which allow to find estimates of the macroscopic parameters from the properties of inclusions. For simple mixture rules, such as the Maxwell Garnett rule, the macroscopic Onsager-Casimir principle can be proved directly from the microscopic relations, because the symmetry properties of the microscopic dyadics dictate the same properties of the macroscopic dyadics. The reason is that different coefficients in (1) and (3) are of different mathematical nature: they behave differently under mirror reflection of spatial coordinates. And this distinction must be preserved in the averaging process which leads to macroscopic constitutive relations.

3. Conclusion

On the microscopic level of consideration we have the fields $\mathbf{E}$ and $\mathbf{B}$ which act on charged particles and cause their displacements. On this level, the fundamental principles such as causality or the symmetry of kinetic coefficients (Onsager–Casimir principle) should be applied to the parameters which connect microscopic responses (such as molecular dipole moments) with the microscopic fields $\mathbf{E}$ and $\mathbf{B}$. Thus, the Fourier transform of the molecular polarizability is subject to the Kramers–Kronig relations, etc. To describe a macroscopic object we average the

fields and introduce the notions of so called induction fields **D** and **H**. Instead of the molecular polarizabilities we deal with constitutive parameters which are in a certain sense averaged values of their microscopic counterparts. Naturally, we expect that the same principles of causality and symmetry should also apply to the macroscopic parameters. If not, we would actually conclude that the way of introducing the macroscopic parameters is non-physical. From the above considerations of this paper we in fact can draw an important conclusion that all considered bi-anisotropic material relations are compatible with the Onsager–Casimir principle.

It is important for the macroscopic electromagnetics since at the macroscopic level we cannot any more distinguish between primary and induction fields as the source and reaction fields. In different situations one or the other field can be fixed by the sources and we have to treat that as the primary source field. Causality requirement leads to the conclusion that both the permittivity ϵ and its inverse ϵ^{-1} satisfy the Kramers–Kronig relations. Similarly, both these quantities are even with respect to the time reversal, according to the Onsager–Casimir principle. In the more general case we see that these principles can be universally applied to any of the sets of the bi-anisotropic parameters. If that would not be so, that would actually mean that one or more sets have no physical meaning.

Finally, we have found that the microscopic and macroscopic Onsager–Casimir principles (symmetries with respect to the time inversion) are related, since the macroscopic parameters are introduced as a result of a certain averaging procedure. In this procedure, correct mathematical relations between variables of different mathematical nature should be always maintained.

References

[1] L. Onsager, "Reciprocal relations in irreversible processes," *Phys. Rev.*, vol. 37, pp. 405-426, 1931.

[2] H. B. G. Casimir, "On Onsager's principle of microscopic reversibility," *Rev. Mod. Phys.*, vol. 17, pp. 343-350, 1945.

[3] L. D. Landau and E. M. Lifshitz, *Statistical Physics*, part 1, vol. 5 of *Course of Theoretical Physics*. Oxford: Butterworth–Heinemann, 1997, p. 366.

[4] G. T. Rado, "Reciprocity relations for susceptibilities and fields in magnetoelectric antiferromagnets," *Phys. Rev. B*, vol. 8, no. 11, pp. 5239-5242, 1973.

[5] B. V. Bokut, A. N. Serdyukov, V. V. Shepelevich, "Phenomenological theory of absorbing optically active media," *Opt. Spectrosc.*, vol. 37, no. 1, pp. 65-67(120-124), 1974.

[6] B. V. Bokut, A. N. Serdyukov, V. V. Shepelevich, "Absorption in the phenomenological theory of optical activity," *Institute of Physics, Belarussian Academy of Sciences* (Minsk, 1972, in Russian).

[7] H. B. Callen, M. L. Barasch, J. L. Jackson, "Statistical mechanics of irreversibility," *Phys. Rev.*, vol. 88, no. 6, pp. 1382-1386, 1952.

[8] E. O. Kamenetskii, "Onsager–Casimir principle and reciprocity relations for bianisotropic media," *Microw. and Optical Technol. Lett.*, vol. 19, no. 6, pp. 412-416, 1998.

[9] L. D. Landau and E. M. Lifshitz, *Electrodynamics of Continuous Media*, vol. 8 of *Course of Theoretical Physics*. 2nd edition, Oxford: Pergamon Press, 1984.

[10] I. V. Lindell, A. H. Sihvola, S. A. Tretyakov, and A. J. Viitanen: *Electromagnetic Waves in Chiral and Bi-Isotropic Media*. Boston and London: Artech House, 1994.

Green Dyadics for Self–Dual Bi–Anisotropic Media

I.V. Lindell[1] and F. Olyslager[2]

[1] Electromagnetics Laboratory
Helsinki University of Technology
PO Box 3000, FIN-02015 HUT, Espoo, Finland

[2] Department of Information Technology, University of Ghent
Sint-Pietersnieuwstraat 41, B-9000 Ghent, Belgium

Abstract

The class of self-dual linear bi-anisotropic media can be defined in three different ways. It consists of media which are invariant in a duality transformation, allow factorization of the second-order dyadic Helmholtz operator in terms of two first-order dyadic operators and allow decomposition of fields and sources in a way that is an extension of the Bohren decomposition for chiral media. It is shown that the Green dyadic can be solved in closed analytic form for any self-dual bi-anisotropic medium and its general expression is given in terms of the self-dual decomposition.

1. Introduction

The Green dyadic corresponding to the homogeneous space of a bi-anisotropic medium gives the field from an arbitrary point source in that medium and forms the basis for all computations of electromagnetic field problems. It characterizes the dependence of the electromagnetic field on the medium in question. Presently, an analytic expression of the Green dyadic is known for a very limited number of linear bi-anisotropic media. It is of interest to increase the number of media with analytic Green dyadic solutions.

The media under consideration in this study are defined by the four medium dyadics appearing in the constitutive equations

$$\begin{pmatrix} \mathbf{D} \\ \mathbf{B} \end{pmatrix} = \begin{pmatrix} \overline{\overline{\epsilon}} & \overline{\overline{\xi}} \\ \overline{\overline{\zeta}} & \overline{\overline{\mu}} \end{pmatrix} \cdot \begin{pmatrix} \mathbf{E} \\ \mathbf{H} \end{pmatrix}, \tag{1}$$

restricted by the general form

$$\begin{pmatrix} \overline{\overline{\epsilon}} & \overline{\overline{\xi}} \\ \overline{\overline{\zeta}} & \overline{\overline{\mu}} \end{pmatrix} = \begin{pmatrix} \epsilon & \sqrt{\mu\epsilon}\sin\theta \\ \sqrt{\mu\epsilon}\sin\theta & \mu \end{pmatrix} \overline{\overline{\alpha}} + \begin{pmatrix} 0 & -1 \\ 1 & 0 \end{pmatrix} j\sqrt{\mu\epsilon}\,\overline{\overline{\kappa}}_r. \tag{2}$$

Here, the dimensionless dyadics $\overline{\overline{\alpha}}$ and $\overline{\overline{\kappa}}_r$ are arbitrary. For convenience we also denote $\eta = \sqrt{\mu/\epsilon}$ and $k = \omega\sqrt{\mu\epsilon}$. The class of bi-anisotropic media (2) under consideration appears quite interesting because it can be derived in three different ways considered below.

2. Self–Dual Media

Defining the duality transformation for the electromagnetic fields as the linear mapping

$$\begin{pmatrix} \mathbf{E} \\ \mathbf{H} \end{pmatrix} \Rightarrow \begin{pmatrix} \mathbf{E}_d \\ \mathbf{H}_d \end{pmatrix} = \begin{pmatrix} A & B \\ C & D \end{pmatrix} \begin{pmatrix} \mathbf{E} \\ \mathbf{H} \end{pmatrix}, \quad AD - BC \neq 0, \tag{3}$$

for the medium dyadics it induces the transformation [1]

$$\begin{pmatrix} \overline{\overline{\epsilon}}_d \\ \overline{\overline{\xi}}_d \\ \zeta_d \\ \overline{\overline{\mu}}_d \end{pmatrix} = \frac{1}{AD-BC} \begin{pmatrix} D^2 & -CD & -CD & C^2 \\ -BD & AD & BC & -AC \\ -BD & BC & AD & -AC \\ B^2 & -AB & -AB & A^2 \end{pmatrix} \begin{pmatrix} \overline{\overline{\epsilon}} \\ \overline{\overline{\xi}} \\ \overline{\overline{\zeta}} \\ \overline{\overline{\mu}} \end{pmatrix}. \tag{4}$$

It can now be shown that (2) describes the class of media invariant in the duality transformation, by assuming first that the four medium dyadics satisfy the self-dual conditions $\overline{\overline{\epsilon}}_d = \overline{\overline{\epsilon}}$, $\overline{\overline{\xi}}_d = \overline{\overline{\xi}}$, $\overline{\overline{\zeta}}_d = \overline{\overline{\zeta}}$ and $\overline{\overline{\mu}}_d = \overline{\overline{\mu}}$ in a particular duality transformation defined by four parameters $A - D$. This leads to two independent equations

$$(A-D)\overline{\overline{\epsilon}} + C(\overline{\overline{\xi}} + \overline{\overline{\zeta}}) = 0, \qquad (D-A)\overline{\overline{\mu}} + B(\overline{\overline{\xi}} + \overline{\overline{\zeta}}) = 0 \tag{5}$$

implying that the dyadics $\overline{\overline{\epsilon}}$, $\overline{\overline{\mu}}$ and $\overline{\overline{\xi}} + \overline{\overline{\zeta}}$ must be multiples of the same dyadic, say, $\overline{\overline{\alpha}}$. There is no condition to the dyadic $\overline{\overline{\xi}} - \overline{\overline{\zeta}}$, which can be chosen independently as a multiple of another dyadic $\overline{\overline{\kappa}}_r$. Thus, the medium dyadics of a bi-anisotropic medium self dual in a specific duality transformation must be of the form (2) which is why the class is labeled as that of self-dual media.

3. Factorizable Helmholtz Operator

A second way to define the class of media (2) is by requiring that the second-order dyadic Helmholtz operator [2]

$$\overline{\overline{H}}_e(\nabla) = -(\nabla \times \overline{\overline{I}} - j\omega\overline{\overline{\xi}}) \cdot \overline{\overline{\mu}}^{-1} \cdot (\nabla \times \overline{\overline{I}} + j\omega\overline{\overline{\zeta}}) + \omega^2\overline{\overline{\epsilon}} \tag{6}$$

be factorizable in terms of two first-order dyadic operators. For two operators to be the same, they have to coincide termwise in all orders of differentiation. Let us look for a factorization of the form

$$\overline{\overline{H}}_e(\nabla) = -(\nabla \times \overline{\overline{I}} + \overline{\overline{A}}) \cdot \overline{\overline{\mu}}^{-1} \cdot (\nabla \times \overline{\overline{I}} + \overline{\overline{B}}), \tag{7}$$

because in this case the second-order terms of (6) and (7) are identically the same. By equating the first-order terms of (6) and (7) one finds the dyadics must be of the form $\overline{\overline{B}} = \alpha\overline{\overline{\mu}} + j\omega\overline{\overline{\zeta}}$, $\overline{\overline{A}} = \beta\overline{\overline{\mu}} - j\omega\overline{\overline{\xi}}$ with $\beta = -\alpha$. Equating the zeroth-order terms of (6) and (7) leads to a dyadic equation for the scalar α:

$$\alpha^2\overline{\overline{\mu}} + j\omega\alpha(\overline{\overline{\xi}} + \overline{\overline{\zeta}}) - \omega^2\overline{\overline{\epsilon}} = 0. \tag{8}$$

Now it is obvious that this has no solution unless the three dyadics $\overline{\overline{\mu}}$, $\overline{\overline{\epsilon}}$ and $\overline{\overline{\xi}} + \overline{\overline{\zeta}}$ are multiples of the same dyadic and, again, $\overline{\overline{\xi}} - \overline{\overline{\zeta}}$ can be any dyadic. Thus, we have rearrived at the class of self-dual media. Assuming medium dyadic expressions of the form (2), the solution can be written as $\alpha = \omega\sqrt{\epsilon/\mu}\, e^{-j\theta}$ and the electric Helmholtz operator dyadic has the simple factorization

$$\overline{\overline{H}}_e(\nabla) = -\overline{\overline{H}}_+(\nabla) \cdot \overline{\overline{\mu}}^{-1} \cdot \overline{\overline{H}}_-(\nabla) = -\overline{\overline{H}}_-(\nabla) \cdot \overline{\overline{\mu}}^{-1} \cdot \overline{\overline{H}}_+(\nabla), \tag{9}$$

in terms of two first-order operators defined by

$$\overline{\overline{H}}_\pm(\nabla) = \nabla \times \overline{\overline{I}} \mp k\overline{\overline{\tau}}_\pm, \qquad \overline{\overline{\tau}}_\pm = \cos\theta\, \overline{\overline{\alpha}} \pm \overline{\overline{\kappa}}_r. \tag{10}$$

4. Decomposable Fields

Finally, the same class of self-dual media can be defined by requiring that the fields be decomposable in two independent electromagnetic fields as

$$\mathbf{E}(\mathbf{r}) = \mathbf{E}_+(\mathbf{r}) + \mathbf{E}_-(\mathbf{r}), \quad \mathbf{H}(\mathbf{r}) = \mathbf{H}_+(\mathbf{r}) + \mathbf{H}_-(\mathbf{r}), \tag{11}$$

with scalar admittance relations necessary for the decomposition

$$\mathbf{H}_+(\mathbf{r}) = Y_+\mathbf{E}_+(\mathbf{r}), \quad \mathbf{H}_-(\mathbf{r}) = Y_-\mathbf{E}_-(\mathbf{r}). \tag{12}$$

Inserting $\mathbf{E}$ and $\mathbf{H}$ in terms of $\mathbf{E}_+$ and $\mathbf{E}_-$ in the Maxwell equations and requiring that there be no coupling between $\mathbf{E}_+$ and $\mathbf{E}_-$, leads to two quadratic dyadic equations for the admittances Y_+, Y_-:

$$Y_\mp^2\overline{\overline{\mu}} + Y_\mp(\overline{\overline{\xi}} + \overline{\overline{\zeta}}) + \overline{\overline{\epsilon}} = 0 \tag{13}$$

similar to (8). To be solvable, they require that the medium be of the self-dual type (2). In this notation, the admittances can be solved as $Y_\pm = \pm j/\eta_\pm$ with $\eta_\pm = \eta e^{\mp j\theta}$, and the decomposed fields become

$$\mathbf{E}_\pm = \frac{1}{2\cos\theta}(e^{\mp j\theta}\mathbf{E} \mp j\eta\mathbf{H}), \quad \mathbf{H}_\pm = \frac{1}{2\cos\theta}(e^{\pm j\theta}\mathbf{H} \pm \frac{j}{\eta}\mathbf{E}). \tag{14}$$

This approach has led us to the decomposition in bi-isotropic media alternatively labeled as the Bohren decomposition [3], self-dual decomposition or wavefield decomposition [4]. It splits the Maxwell equations in two independent sets:

$$\nabla \times \mathbf{E}_\pm = -j\omega\overline{\overline{\mu}}_\pm \cdot \mathbf{H}_\pm - \mathbf{M}_\pm, \tag{15}$$

$$\nabla \times \mathbf{H}_\pm = j\omega\overline{\overline{\epsilon}}_\pm \cdot \mathbf{E}_\pm + \mathbf{J}_\pm, \tag{16}$$

when the decomposed electric and magnetic currents are defined as

$$\mathbf{J}_\pm = \frac{1}{2\cos\theta}(e^{\pm j\theta}\mathbf{J} \mp \frac{j}{\eta}\mathbf{M}), \quad \mathbf{M}_\pm = \frac{1}{2\cos\theta}(e^{\mp j\theta}\mathbf{M} \pm j\eta\mathbf{J}), \tag{17}$$

and the equivalent permittivity and permeability dyadics as $\overline{\overline{\epsilon}}_\pm = \epsilon e^{\pm j\theta\overline{\overline{\tau}}_\pm}$, $\overline{\overline{\mu}}_\pm = \mu e^{\mp j\theta\overline{\overline{\tau}}_\pm}$, with the dyadics $\overline{\overline{\tau}}_\pm$ defined in (10). The decomposed fields and sources obey the relations,

$$\mathbf{E}_\pm = \mp j\eta_\pm\mathbf{H}_\pm, \quad \mathbf{M}_\pm = \pm j\eta_\pm\mathbf{J}_\pm. \tag{18}$$

5. Green Dyadics

The fields generated by arbitrary electric and magnetic sources in a homogeneous linear bi-anisotropic medium can be expressed as integrals of four Green dyadics $\overline{\overline{G}}_{ee}(\mathbf{r})$, $\overline{\overline{G}}_{ee}(\mathbf{r})$, $\overline{\overline{G}}_{ee}(\mathbf{r})$ and $\overline{\overline{G}}_{mm}(\mathbf{r})$ satisfying

$$\left[\begin{pmatrix} 0 & \nabla\times\overline{\overline{I}} \\ -\nabla\times\overline{\overline{I}} & 0 \end{pmatrix} - j\omega\begin{pmatrix} \overline{\overline{\epsilon}} & \overline{\overline{\xi}} \\ \overline{\overline{\zeta}} & \overline{\overline{\mu}} \end{pmatrix}\right] \cdot \begin{pmatrix} \overline{\overline{G}}_{ee}(\mathbf{r}) & \overline{\overline{G}}_{em}(\mathbf{r}) \\ \overline{\overline{G}}_{me}(\mathbf{r}) & \overline{\overline{G}}_{mm}(\mathbf{r}) \end{pmatrix} = \begin{pmatrix} \overline{\overline{I}} & 0 \\ 0 & \overline{\overline{I}} \end{pmatrix}\delta(\mathbf{r}). \tag{19}$$

For the decomposed fields in a self-dual medium we only need to consider two Green dyadics $\overline{\overline{G}}_+(\mathbf{r})$ and $\overline{\overline{G}}_-(\mathbf{r})$, which can be defined in terms of fields due to the decomposed point sources. They satisfy

$$\overline{\overline{H}}_\pm(\nabla) \cdot \overline{\overline{G}}_\pm(\mathbf{r}) = (\nabla\times\overline{\overline{I}} \mp k\overline{\overline{\tau}}_\pm) \cdot \overline{\overline{G}}_\pm(\mathbf{r}) = \mp j\eta e^{\mp j\theta\overline{\overline{I}}}\delta(\mathbf{r}). \tag{20}$$

Relations between the different Green dyadics are

$$\overline{\overline{G}}_{ee}(\mathbf{r}) = \frac{1}{2\cos\theta}\left(e^{j\theta}\overline{\overline{G}}_{+}(\mathbf{r}) + e^{-j\theta}\overline{\overline{G}}_{-}(\mathbf{r})\right), \qquad \overline{\overline{G}}_{em}(\mathbf{r}) = \frac{1}{2j\eta\cos\theta}\left(\overline{\overline{G}}_{+}(\mathbf{r}) - \overline{\overline{G}}_{-}(\mathbf{r})\right), \tag{21}$$

$$\overline{\overline{G}}_{me}(\mathbf{r}) = \frac{-1}{2j\eta}\left(e^{j\theta}\overline{\overline{G}}_{+}(\mathbf{r}) - e^{-j\theta}\overline{\overline{G}}_{-}(\mathbf{r})\right), \qquad \overline{\overline{G}}_{mm}(\mathbf{r}) = \frac{1}{2\eta^2}\left(\overline{\overline{G}}_{+}(\mathbf{r}) + \overline{\overline{G}}_{-}(\mathbf{r})\right). \tag{22}$$

To find the solutions for (20), the dyadics $\overline{\overline{\tau}}_{\pm}$ are first expressed in terms of their symmetric and antisymmetric parts as $\overline{\overline{\tau}}_{\pm} = \overline{\overline{S}}_{\pm} + \mathbf{a}_{\pm} \times \overline{\overline{I}}$. The equation (20) then becomes

$$[\overline{\overline{L}}_{\pm}(\nabla) \mp k\mathbf{a}_{\pm} \times \overline{\overline{I}}] \cdot \overline{\overline{G}}_{\pm}(\mathbf{r}) = \mp j\eta e^{\mp j\theta}\overline{\overline{I}}\delta(\mathbf{r}), \qquad \overline{\overline{L}}_{\pm}(\nabla) = \nabla \times \overline{\overline{I}} \mp k\overline{\overline{S}}_{\pm}. \tag{23}$$

The Green dyadics $\overline{\overline{G}}_{\pm}(\mathbf{r})$ can now be expressed in terms of two scalar Green functions $g_{\pm}(\mathbf{r})$ satisfying a second-order equation (for details see [6])

$$\overline{\overline{G}}_{\pm}(\mathbf{r}) = \pm j\eta e^{\mp j\theta}e^{\pm k\mathbf{a}_{\pm}\cdot\mathbf{r}}\overline{\overline{L}}_{\pm}^{(2)T}(\nabla)g_{\pm}(\mathbf{r}), \quad \det\overline{\overline{L}}_{\pm}(\nabla)g_{\pm}(\mathbf{r}) = -\delta(\mathbf{r}). \tag{24}$$

The solutions for $g_{\pm}(\mathbf{r})$ are obtained through an affine transformation [2] as

$$g_{\pm}(\mathbf{r}) = \mp\frac{e^{-jkD_{\pm}}}{4\pi kD_{\pm}}, \qquad D_{\pm}(\mathbf{r}) = \sqrt{\det\overline{\overline{S}}_{\pm}}\sqrt{\overline{\overline{S}}_{\pm}^{-1} : \mathbf{rr}}. \tag{25}$$

Thus, the two Green dyadics obey the expressions

$$\overline{\overline{G}}_{\pm}(\mathbf{r}) = -j\eta e^{\mp j\theta}e^{\pm k\mathbf{a}_{\pm}\cdot\mathbf{r}}\overline{\overline{L}}_{\pm}^{(2)T}(\nabla)\left(\frac{e^{-jkD_{\pm}}}{4\pi kD_{\pm}}\right). \tag{26}$$

Finally, the four basic Green dyadics $\overline{\overline{G}}_{ee}\cdots\overline{\overline{G}}_{mm}$ are obtained by substituting (26) in (21) – (22). For example, the expression for the electric-electric Green dyadic becomes

$$\overline{\overline{G}}_{ee}(\mathbf{r}) = -\frac{j\eta e^{k\mathbf{a}_{+}\cdot\mathbf{r}}}{2\cos\theta}\overline{\overline{L}}_{+}^{(2)T}(\nabla)\left(\frac{e^{-jkD_{+}}}{4\pi kD_{+}}\right) - \frac{j\eta e^{-k\mathbf{a}_{-}\cdot\mathbf{r}}}{2\cos\theta}\overline{\overline{L}}_{-}^{(2)T}(\nabla)\left(\frac{e^{-jkD_{-}}}{4\pi kD_{-}}\right). \tag{27}$$

As a simple check we can consider the bi-isotropic special case by choosing $\overline{\overline{\alpha}} = \overline{\overline{I}}$ and $\overline{\overline{\kappa}}_r = \kappa_r\overline{\overline{I}}$. These imply $k\overline{\overline{\tau}}_{\pm} = k\overline{\overline{S}}_{\pm} = k_{\pm}\overline{\overline{I}}$, $kD_{\pm} = k_{\pm}r$ and $k_{\pm} = k(\cos\theta \pm \kappa_r)$, whence the well-known expression for $\overline{\overline{G}}_{ee}(\mathbf{r})$, as originally presented in [5], can be obtained.

6. Conclusion

The class of self-dual bi-anisotropic medium defined by two arbitrary dyadics (2) was shown to be definable in three different basic ways. It was shown that the Green dyadic corresponding to any bi-anisotropic medium in this class can be found in explicit analytic form by applying the decomposition method.

References

[1] I. V. Lindell and L. H. Ruotanen, "Duality transformations and Green dyadics for bi-anisotropic media," *J. Electro. Waves Appl.*, vol. 12, pp. 1131-1152, 1998.

[2] I.V. Lindell, *Methods for Electromagnetic Field Analysis* (2nd ed.). Oxford: University Press, 1995.

[3] G. F. Bohren, "Light scattering by an optically active sphere," *Chem. Phys. Lett.*, vol. 29, no. 3, pp. 458-462, 1974.

[4] I. V. Lindell, A. H. Sihvola, S. A Tretyakov, and A. J. Viitanen, *Electromagnetic Waves in Chiral and Bi-Isotropic Media.* Boston: Artech House, 1994.

[5] S. Bassiri, N. Engheta, and C. H. Papas, "Dyadic Green's function and dipole radiation in chiral media," *Alta Frequenza*, vol. 55, no. 2, pp. 83-88, 1986.

[6] I. V. Lindell and F. Olyslager, "Green dyadics for self-dual bi-anisotropic media", *J. Electro. Waves Appl.*, vol. 14, pp. 143-153, 2000.

Session 5

Thursday - September 28, 2000

09:00 - 10:20

Session 5

Nanostructures and Related Topics

Filamentary, My Dear Watson!

Akhlesh Lakhtakia

CATMAS — Computational & Theoretical Materials Sciences Group
Department of Engineering Science and Mechanics, Pennsylvania State University
University Park, PA 16802–6812, USA
Tel: +1 814 863 4319; Fax: +1 814 863 7967; email: AXL4@psu.edu

Abstract

Developments that took place in the area of sculptured–thin–film technology after *Bianisotropics '98* are reviewed here. Devices addressed include: optical filters of various kinds, laser mirrors, gas–concentration sensors, optical interconnects, interlayer dielectrics, and biosensors. Pulse bleeding is related to the circular Bragg phenomenon in chiral sculptured thin films. Acoustic research is also identified.

Light from a fluorescent street lamp filtered through the soft rain, and the leaves of an ornamental maple tree on the other side of Baker Street cast muted shadows on the wall opposite the bay window in the cavernous living room of 221 B. The September night was in full glory, as Sherlock Holmes smoked a meerschaum pipe another people's princess had sent him as a token of her gratitude more than a century ago. He sat quietly, absorbed in some deep thoughts. Only the frequency with which he released smoke rings indicated his phrenetic turmoil.

* – * – *

But, what's time in our state now? Having left aside our mortal accouterments, Holmes and I still inhabit our beloved apartments in the metropolis. I continue to organize many of the cases that Conan Doyle, our literary agent in our former life, never published because they were then deemed inimical to public order. Not nowadays, however. Holmes often tells me of particularly horrid instances of murder that the modern criminal has the means and the desire to commit and does. That of a little girl in Boulder and that of a big girl in Los Angeles come to mind. Occasionally, Holmes is sufficiently intrigued to solve particularly infamous crimes, but Conan Doyle is no longer able to bring the criminals to book.

The great love of Holmes these days, however, is not crime but the science of materials. No longer able to experiment himself as he once did on the ashes of cigars of 34 different provenances and the herbs used by the Moluccans to shrink other people's heads, he spends many a night at the Imperial College library, poring over the pages of thousands of journals and other scientific and technological proceedings. He has an astonishing capacity to memorize diverse facts, and he synthesizes new constructs with uncommon fecundity. I have always felt that the gain of Victorian crime–fighters was the loss of Victorian natural philosophers. The recent discovery of materials with Möbiated bianisotropy — a truly bizarre material structure that promises a thorough rewrite of plane waves in physics textbooks — came of a suggestion Holmes had whispered in the ears of a visiting San Doggo del High physicist as he slept late one evening, in the Imperial College library, about two years ago. More often than not, he is unable to find a competent medium for his ingenious ideas; though Holmes did manage to masquerade as Daedalus for several years in the pages of *New Scientist*.

I remember clearly that in 1959 he came across a report in *Nature* by two Nottingham engineers working for a Swedish company.[1] These worthies had sought fit to outsmart nature by depositing a twisted film of fluorite on a flat glass substrate. Their method of inducing the twist was simplicity itself: just rotate the substrate while the fluorite adatoms fall obliquely on it. A stationary substrate results in columnar thin films that can act like biaxial crystals; a rotating substrate can give rise to sculptured thin films that are ever more complex.

Neither one of the Nottingham duo could have verified the true nature of their films as scanning electron microscopes had yet not made their *début*, though they did have an inkling that the microstructure was some limiting case of a Šolc filter. Holmes, who can see matters more clearly than scanning electron microscopes because he can perform wavelet transforms on his nebular personal wavefunction, returned that January dawn from the Imperial College library, declaring that he knew the microstructure.

"Filamentary, my dear Watson," he had loudly shouted for all to hear — but no person then alive did. The Nottingham paper gathered dust for many decades. Only two reports were filed over 35 years by the Baker Street Irregulars, now no longer confined to their corporeal sheaths but clad in black instead: A Scotsman living in Arizona once mentioned the paper during an antipodean seminar, and a Louisiana physicist wrote of something similar. And then in 1995, an engineer from Pencilmania and a mathematician from the nether Caledonia discussed the films in a Royal Society paper, not at all aware of the Nottingham paper. Shortly thereafter, impelled by the Pencilmaniac engineer, a Canadian undergraduate student was able to duplicate the 1959 feat and scrutinize the arrays of parallel straight curls that chiral sculptured thin films are. Two years later, the Nottingham report came to light again, and today occupies its rightful place in the scientific literature on thin films. What an amazing confirmation of Holmes' foresight!

* − * − *

Cogitating for over an hour in complete silence, Holmes said out aloud: "What do you make of the prospects of sculptured thin films, my esteemed Watson?"

Taken aback, I mumbled: "How the deuce did you know that?"

"You know my methods, Watson. Apply them. After the last gawking humans left our abode in the evening, you were nowhere to be found. Looking at your desk, I saw the letters W I L Y traced in the dust on your table, and an American envelope with a coyote stamp lying on the floor. Clearly, our transatlantic friend John had communicated with you through an infernal countryman of his who spent almost the whole day here in 221 B. I called one of my men in black, who confirmed that you had been seen crossing the Brooklyn Bridge. On your return, I detected perfume clinging to you. You must have been looking over the shoulder of a copy–editor in New York."

"Yes, but how did you know that John's missive concerned sculptured thin films?"

"Obsessed with these films you have been for some months, haven't you?"

"Yes. It does sound so simple, Holmes, when you explain it. Anyhow, there is this new book being published,[2] and I sneaked a preview of Chapter 5, just to apprise you of the latest developments."

"Pray do," quoth he, as he slowly floated up to the top of the ottoman.

I began: "Well, it seems that matters have advanced quite considerably during the past two years. You may recall, Holmes, the addresses that the Pencilmaniac engineer had delivered at *Bianisotropics'97* in Glasgow and *Bianisotropics '98* in Braunschweig. In his first address, he

[1] N.O. Young and J. Kowal, "Optically active fluorite films," *Nature* **183**, 104–105, 1959.

[2] O.N. Singh and A. Lakhtakia (eds), *Electromagnetic Fields in Unconventional Materials and Structures* (Wiley, New York, 2000).

was quite speculative about sculptured thin films. Reliable methods of producing them were still in their infancy; and the optical rotation spectrum of only one chiral sculptured thin film had been measured by then — and that too was crude and incomplete. The Pencilmaniac engineer's group took many theoretical strides following the Glaswegian meeting, which were duly reported in Germany. The theoretical basis of optical devices — such as circular polarization filters, laser mirrors, and gas–concentration sensors — was also firmed up between those two meetings.

"Several developments took place after *Bianisotropics '98*, many of which are reported in Chapter 5 of this new book. Optical interconnects as well as interlayer dielectrics are among the emerging applications of the sculptured–thin–film nanotechnology. Some acoustics research has also taken place, but it is definitely in the theoretical stage only. Most importantly, at least three types of optical devices have been made with the new serial bideposition technique in New Zealand, in collaboration with the Pencilmania group.

"The first optical device is a circular polarization filter that allows either left– or right–handed plane waves to pass through, but not both. Of course, on enquiry both Williams bragged that they have known from Wilhelm's time that such filters can work only in relatively narrow wavelength–regimes.

"The next device combines the filtering action with polarization–inversion. The circular polarization filter is capped by a columnar thin film which functions as a half–wave plate at a certain wavelength within the Bragg regime. The device thus is really the first two–section sculptured thin film ever made, and fully justifies your confidence in the concept of sculptured thin films.

"Finally, the third device is a spectral hole filter. While a chiral sculptured thin films is being deposited, the substrate rotation is temporarily stopped and then resumed after a while. This results in the production of a reflection hole that punctures the Bragg regime, when all parameters are properly chosen. The bandwidth of the hole is 11 nm, which is comparable to the 10 nm holes produced commercially by holographic techniques."

Holmes interjected: "That is a three–section sculptured thin film then, isn't it? But they have done even better with reflection holes. Instead of stopping the rotation of the substrate, they now simply give a quick orthogonal twist. They have achieved the same type of hole with a two–section sculptured thin film."

"How do you know about that?" I asked, to which Holmes replied that he had sneaked into an editorial office at a London physics department. He was also tickled pink to find that an Imperial College lecturer had joined the Pencilmania–NZ collaboration.

Holmes continued: "I can see the possibilities of highly sensitive gas–concentration sensors in those spectral holes. Did you find any evidence in the book chapter?" My reply in the negative made him pensive for a while. "Anything else in that book?" he questioned, and I mentioned that the Pencilmania group had undertaken the incorporation of further verisimilitude in their research by assuming Lorentzian dependencies for the constitutive parameters. "Good," he went on, "Hendrik will be pleased. But we must find more on what's afoot in Pencilmania."

Dawn was about to break as he uttered those words. Soon the fog would roll out of Heathrow and aeroplanes would begin landing there, bringing another clutch of Holmesians to 221 B. It was time to retire for the day, but Holmes went out to speak to one of his men in black.

* – * – *

The great merit of disembodiment is that the Baker Street Irregulars can travel quite fast. While speeds close to or more than a tenth of the speed of light are not advised, lest a blue glow be emitted, during the last few years the men in black have been able to go to almost anywhere in the world with the help of the Internet. Constantly bumping into copper atoms used to be a

hazard, but optical fibers now provide them with a smooth Alpine slide, even to Papua Niugini. Holmes and I also use the same mode of travel, incidentally.

* – * – *

As the shadows filtered in again, ushering a new twilight, Holmes began to receive reports from the Baker Street Irregulars who had combed through the editorial offices of a multitude of physics and engineering journals. That the Lorentzian route had been taken by the Pencilmaniac was confirmed not only from France but also from Germany and Italy. No less than three editorial outfits from the three countries had become the Pencilmaniacs' accomplices, so to say. Sound research had been conducted and reported.

An interesting development was the modeling of individual columns in chiral sculptured thin films as ensembles of inclusions laid out end–to–end, not unlike strings of sausages. Spectral maximums of various observable properties had been examined as functions of inclusion shape, volume fraction and orientation — for eventual use in computer–aided design.

Even more astonishingly, research had spilled over from the frequency into the time domain. After solving the Maxwell equations directly in the time domain, the spatio–temporal anatomy of the circular Bragg phenomenon exhibited by chiral sculptured thin films had been bared, much to the delight of the doctor in me. Pulse bleeding had been shown to occur in the Bragg regime under certain circumstances. Holmes rubbed his hands with glee, as he wondered about the encounter of femtosecond pulses with chiral sculptured thin films, and cautioned me to be careful: if these new materials were to be used for wavelength division multiplexing and demultiplexing, we would have to choose suitable polarizations for future Internet travel. "Better pack a few extra polarizations, Joseph, just to stand out from the hoi polloi." In some of his lighter moments, Holmes fancies himself as Sir Andrew Lloyd Webber giving stage directions!

"Watson, the Pencilmaniac engineer is moving just too fast. I fear I am unable to delve into his brain, because he never puts on the virtual reality headset I had surreptitiously suggested the head of his department to provide him with. But his thoughts cannot elude detection. Unable to remember anything for too long, he commits all his ideas to writing. Somewhere in his office, a blueprint of his plans must be hidden; and I must lay a trap for him." Holmes pronounced each word with deliberation, in his usual calm manner. Every comma and every semi–colon, not to mention full stops, were marked by pauses of the right duration. I could almost feel that gears were whirring and lights were flashing inside that powerful intellect of his. And then he went out ..... with one of his men in black.

* – * – *

Holmes did not come back in the morning, and was away the next night as well. Late in the following afternoon, as I reposed on a horsehair sofa in the attic away from the prying throngs of visitors, I became aware of a tall cylindrical object with a faint green glow making its way towards me. If I had a skin, I would have jumped out of it. Golly, whatever could that dreadful apparition be? I froze in terror, as peals of laughter rang out.

"What's up, Doc?" a guttural *patois* issued from that object. But Holmes couldn't fool me. He is certainly a master of mimicry, but long association with him helped me see right through him.

"What are you disguised as?"

"What else? A Pencil, of course."

"Aha! A pencil for the Pencilmaniac!!"

"Exactly! Let's be off to Pencilmania, where the day is just about middle–aged now. Our quarry must be working in his office, where we must corner him."

Hitching a ride on the telephone cable, we exited 221B. Milliseconds later, we swung over to a British Telecom fiber. A skip over the splicing with an MCI fiber, and we negotiated the Atlantic *via* a satellite faster than you can say 'WorldCom.'

As we were landing on the desk of the Pencilmaniac engineer through his computer, he began to raise his right hand from his lap. He opened the side–drawer. Nimble as a humming bird, Holmes slid into the pencil case lying inside the drawer. A piece of paper lay on the desk, covered with chemical symbols such as $[Ru(2,2'–bipyridine)_3]Cl_2$ and $[Ru(1,10–phenantholine)_3]Cl_2$, and with the letters A, T, C, G and U strewn all over. A firefly had been doodled in a corner, with the words *Lucifer — Son of Morning* written below in a cursive hand.

The Pencilmaniac's left hand took out a pencil and drew several parallel lines on another sheet of paper. Those lines glowed green! Holmes had been able to get inside the engineer's brain! The Pencilmaniac continued to make a schematic, occasionally labeling certain layers. I did not understand the diagram, but Holmes did.

* – * – *

An hour later, after the Pencilmaniac engineer had closed shop for the day, and his office was bathed in vivacious darkness, Holmes emerged from the pencil case. Triumphantly, he declared, "I just want to say one word to you ..... Biosensors."

Author's note: If you enjoyed the story, please write or call for the following publications:

Electromagnetic References

[1] E. Ertekin and A. Lakhtakia, "Sculptured thin film Šolc filters for optical sensing of gas concentration," *Eur. Phys. J. AP* **5**, 45–50, 1999.

[2] E. Ertekin, V. C. Venugopal, and A. Lakhtakia, "Effect of substrate and lid on the optical response of an axially excited slab of a dielectric thin–film helicoidal bianisotropic medium," *Microw. Opt. Technol. Lett.* **20**, 218–222, 1999.

[3] E. Ertekin and A. Lakhtakia, "Optical intercconects realizable with thin–film helicoidal bianisotropic mediums," *Proc. R. Soc. Lond. A*, 2000 (submitted for publication).

[4] J. B. Geddes III and A. Lakhtakia, "Reflection and transmission of optical narrow–extent pulses by axially excited chiral sculptured thin films," *Eur. Phys. J. AP*, 2000 (submitted for publication).

[5] I. Hodgkinson, Q. H. Wu, A. Lakhtakia, and R. Messier, "Linear and circular polarization filters using sculptured thin films," *OSA Opt. Photon. News* **10** (12), 30–31, Dec. 1999.

[6] I. Hodgkinson, Q. H. Wu, B. Knight, A. Lakhtakia, and K. Robbie, "Vacuum deposition of chiral sculptured thin films with high optical activity," *Appl. Opt.* **39**, 642–649, 2000.

[7] I. J. Hodgkinson, Q. H. Wu, A. Lakhtakia, and M.W. McCall, "Spectral–hole filter fabricated using sculptured thin–film technology," *Opt. Commun.* **177**, 79–84, 2000.

[8] I. J. Hodgkinson, A. Lakhtakia, and Q. H. Wu, "Experimental realization of sculptured–thin–film polarization–discriminatory light–handedness inverters," *Opt. Eng.* **39**, 2000 (at press).

[9] I. J. Hodgkinson, Q. H. Wu, K. E. Thorn, A. Lakhtakia, and M. W. McCall, "Spacerless circular–polarization spectral–hole filters using chiral sculptured thin films: theory and experiment," *Opt. Commun.*, 2000 (submitted for publication).

[10] A. Lakhtakia, "On determining gas concentrations using thin–film helicoidal bianisotropic medium bilayers," *Sens. Actuat. B: Chem.* **52**, 243–250, 1998.

[11] A. Lakhtakia, "Anomalous axial propagation in a gyrotropic, locally uniaxial, dielectric, helicoidally nonhomogeneous medium," *Arch. Elektron. Übertrag.* **53**, 45–48, 1999.

[12] A. Lakhtakia, "Energy flows in axially excited, locally biaxial, dielectric, helicoidal bianisotropic media (HBMs)," *Opt. Commun.* **161**, 275–286, 1999.

[13] A. Lakhtakia, "Capacitance of a slab of a dielectric thin–film helicoidal bianisotropic medium," *Microw. Opt. Technol. Lett.* **21**, 286–288, 1999.

[14] A. Lakhtakia, "On the quasistatic approximation for helicoidal bianisotropic mediums," *Electromagnetics* **19**, 513–525, 1999.

[15] A. Lakhtakia, "Towards sculptured thin films (STFs) as optical interconnects," *Optik* **110**, 289–293, 1999.
[16] A. Lakhtakia, "Bragg–regime absorption in axially excited slabs of dielectric thin–film helicoidal bianisotropic media," *Microw. Opt. Technol. Lett.* **22**, 243–247, 1999.
[17] A. Lakhtakia, "Spectral signatures of axially excited slabs of dielectric thin–film helicoidal bianisotropic mediums," *Eur. Phys. J. AP* **8**, 129–137, 1999.
[18] A. Lakhtakia, "Dielectric sculptured thin films for polarization–discriminatory handedness–inversion of circularly polarized light," *Opt. Eng.* **38**, 1596–1602, 1999.
[19] A. Lakhtakia, "On percolation and circular Bragg phenomenon in metallic, helicoidally periodic, sculptured thin films," *Microw. Opt. Technol. Lett.* **24**, 239–244, 2000.
[20] A. Lakhtakia and I. J. Hodgkinson, "Spectral response of dielectric thin–film helicoidal bianisotropic medium bilayer," *Opt. Commun.* **167**, 191–202, 1999.
[21] A. Lakhtakia and M. McCall, "Sculptured thin films as ultranarrow–bandpass circular–polarization filters," *Opt. Commun.* **168**, 457–465, 1999.
[22] A. Lakhtakia and V. C. Venugopal, "On Bragg reflection by helicoidal bianisotropic mediums," *Arch. Elektron. Übertrag.* **53**, 287–290, 1999.
[23] A. Lakhtakia, V. C. Venugopal, and M. W. McCall, "Spectral holes in Bragg reflection from chiral sculptured thin films: circular polarization filters," *Opt. Commun.* **177**, 57–68, 2000.
[24] A. Lakhtakia and W. S. Weiglhofer, "Significance of cross–sectional morphology for Motohiro–Taga interfaces," *Optik* **110**, 33–36, 1999.
[25] A. Lakhtakia and W. S. Weiglhofer, "A comparative study of planewave propagation in helicoidal bianisotropic mediums and isotropic chiral mediums," *J. Opt. A: Pure Appl. Opt.* **2**, 107–111, 2000.
[26] M. W. McCall and A. Lakhtakia, "Polarization–dependent narrowband spectral filtering by chiral sculptured thin films," *J. Mod. Opt.* **47**, 743–755, 2000.
[27] M. W. McCall and A. Lakhtakia, "Development and assessment of coupled wave theory of axial propagation in thin–film helicoidal bianisotropic media. Part 1: reflectances and transmittances," *J. Mod. Opt.* **47**, 973–991, 2000.
[28] M. W. McCall and A. Lakhtakia, "Development and assessment of coupled wave theory of axial propagation in thin–film helicoidal bianisotropic media. Part 2: dichroisms, ellipticity transformation and optical rotation," *J. Mod. Opt.* **47**, 2000 (at press).
[29] R. Messier and A. Lakhtakia, "Sculptured thin films–II. Experiments and applications," *Mater. Res. Innovat.* **2**, 217–222, 1999.
[30] J. A. Sherwin and A. Lakhtakia, "Nominal model for structure–property relations of chiral dielectric sculptured thin films," *Math. Comput. Model.*, 2000 (at press).
[31] V. C. Venugopal and A. Lakhtakia, "Electromagnetic plane–wave response characteristics of non–axially excited slabs of dielectric thin–film helicoidal bianisotropic mediums," *Proc. R. Soc. Lond. A* **456**, 125–161, 2000.
[32] V. C. Venugopal and A. Lakhtakia, "On absorption by non–axially excited slabs of dielectric thin–film helicoidal bianisotropic mediums," *Eur. Phys. J. AP* **10**, 173–184, 2000.
[33] V. C. Venugopal, A. Lakhtakia, R. Messier, and J.–P. Kucera, "Low–permittivity materials using sculptured thin film technology," *J. Vac. Sci. Technol. B* **18**, 32–36, 2000.
[34] V. C. Venugopal and A. Lakhtakia, "Sculptured thin films: Conception, optical properties, and applications," In: O.N. Singh and A. Lakhtakia (eds), *Electromagnetic Fields in Unconventional Materials and Structures* (Wiley, New York, 2000), pp. 151–216.
[35] Q. H. Wu, I. J. Hodgkinson, and A. Lakhtakia, "Circular polarization filters made of chiral sculptured thin films: experimental and simulation results," *Opt. Eng.* **39**, 2000 (at press).

Acoustic References

[1] A. Lakhtakia, "Shear axial modes in a PCTSCM. Part V: transmission spectral holes," *Sens. Actuat. A: Phys.* **80**, 216–223, 2000.
[2] A. Lakhtakia, "Shear axial modes in a PCTSCM. Part VI: simpler transmission spectral holes," *Sens. Actuat. A: Phys.*, 2000 (at press).
[3] A. Lakhtakia, "Axial loading of a chiral sculptured thin film," *Model. Simulat. Mater. Sci. Eng.*, 2000 (at press).
[4] A. Lakhtakia and M. W. Meredith, "Shear axial modes in a PCTSCM. Part IV: bandstop and notch filters," *Sens. Actuat. A: Phys.* **73**, 193–200, 1999.
[5] A. Lakhtakia and J. A. Sherwin, "Displacement in a continuously twisted structurally chiral medium (CTSCM) due to axial loading," *J. Acoust. Soc. Am.* **107**, 3549–3551, 2000.

Effective Boundary Conditions in Electrodynamics of Nanostructures

G. Ya. Slepyan, S. A. Maksimenko

[1] Institute for Nuclear Problems, Belarus State University
Bobruiskaya str. 11, Minsk, 220050, Belarus
Fax: +375-17-226-5124 email: maksim@inp.minsk.by

Abstract

The effective boundary condition method is extended to nano-scale mesoscopic systems. The EBCs appear as a result of the 2D-homogenezation procedure and have the form of two-side anisotropic impedance boundary conditions stated on the structure's surface. The surface impedance tensor has been evaluated for a set of typical nanostructures. It has been shown that, unlike to macroscopic electrodynamics, the surface impedance tensor exhibits sharp oscillations at frequencies of optical transitions. The EBC method supplemented with well-developed mathematical techniques of classical electrodynamics creates unified basis for solution of boundary-value problems in electrodynamics of nanostructures. A generalization of the EBC method to the quantum electrodynamics is also presented,

1. Introduction

Rapid progress in the synthesis of a variety of different kinds of spatially confined nanostructures with fascinating electronic and optical properties irreducible to properties of bulk media symbolizes a fundamental breakthrough in solid state physics. The key peculiarities of such structures are related to spatial confinement of the charge carrier motion and their nanoscale spatial inhomogeneity. Since the inhomogeneity scale is much less than the optical wavelength, in many cases it turns out to be possible under analysis to reduce the dimensionality of structure (low–dimensional structure). In this contribution we present a method of evaluation of the electromagnetic response of low–dimensional nanostructures formed by thin layers with intrinsic 2D periodicity with characteristic period much less than the optical wavelength, e.g., carbon nanotubes (CNs) [1], planar arrays of quantum dot (QDs) [2].

This method, conventionally referred to as the effective boundary condition (EBC) method, has been originally developed for microwaves and antenna theory [3]–[5], and has found a wide application in these fields, e. g., for the design of semi–transparent grid screens and helical sheaths in traveling wave tubes[1]. In essence, the EBC method is modification of the effective medium theory as applied to 2D–confined structures. The basic idea of the EBC method is that a smooth homogeneous surface is considered instead a periodic structure, and appropriate EBCs for the electromagnetic field are stated for this surface. These conditions are chosen in such a way that the spatial structures of the electromagnetic field due to an effective current induced on the homogeneous surface, and the electromagnetic field of the real current in the lattice turn out to be identical some distance away from the surface. The lattice parameters are included in coefficients of the EBCs. The applicability of the EBCs is restricted by the requirement that the lattice period be small compared with the free–space wavelength. The effectiveness of the

[1]Similar approaches have been developed in acoustics, hydrodynamics, elasticity theory.

EBC method is determined by a possibility its extension to more complicated situations. Such an extension is only possible when the parameters involved in the EBCs do not depend on the spatial structure of the irradiating field, or, in another words, the EBCs must be *local*, i.e., they must couple field components and their spatial derivatives at a given point of space. In the simplest case, the EBCs have the form of two–side impedance boundary conditions on the surface S:

$$[\mathbf{n}\,[\mathbf{n}, \mathbf{H}^{\mathrm{I}} - \mathbf{H}^{\mathrm{II}}]] = -\frac{4\pi\widehat{\boldsymbol{\sigma}}}{c}[\mathbf{n}, \mathbf{E}]\,, \tag{1}$$

$$[\mathbf{n}, \mathbf{E}^{\mathrm{I}} - \mathbf{E}^{\mathrm{II}}] = 0 \tag{2}$$

where c is the speed of light. The unit vector $\mathbf{n}$ is normal to the surface S and is directed from region I to region II. The effective conductivity tensor $\widehat{\boldsymbol{\sigma}}$ contains information about geometrical configuration and constitutive parameters of the lattice. EBCs in the form given by Eqs. (1)–(2) are obtained neglecting (i) polarization of the structure in the $\mathbf{n}$ direction, and (ii) contribution of spatial dispersion into conductivity.

2. Formulation of the EBCs for Planar Nanostructures

In order to derive the EBCs, a kernel problem must be solved in each particular case. For example, this problem is formulated for grid screens as the problem of plane wave scattering by the infinite plane screen [4]. Below we consider the kernel problems for two particular cases of low–dimensional nanostructures.

A) Carbon nanotubes.
As applied to CNs, the kernel problem is to derive the EBCs for an isolated infinitely long regular CN with an arbitrary index (m, n), i. e., to derive the EBCs for a cylindrical surface of the radius R with R as the CN radius. Neglecting indirect interband transitions in the π–electrons' motion, the conductivity tensor of the CN is given by [6]

$$\widehat{\boldsymbol{\sigma}} = \begin{pmatrix} 0 & 0 \\ 0 & \sigma_{zz} \end{pmatrix}, \tag{3}$$

where σ_{zz} is the axial conductivity of CN; this quantity appears in coupling of the microscopic properties of the CN and its macroscopic electromagnetic response. The treatment of the axial dynamical conductivity of an isolated CN has been given in Refs. [7], [8]. Both semi–classical and quantum–mechanical analyses of the conductivity have been presented in the above references. In some cases, the role of spatial dispersion for CNs turns out to be essential. In that cases, Eq. (2) keeps validity while Eq. (1) is transformed to

$$\widehat{\boldsymbol{\Lambda}}[\mathbf{n}\,[\mathbf{n}, \mathbf{H}^{\mathrm{I}} - \mathbf{H}^{\mathrm{II}}]] = -\frac{4\pi\widehat{\boldsymbol{\sigma}}}{c}[\mathbf{n}, \mathbf{E}]\,, \tag{4}$$

where

$$\widehat{\boldsymbol{\Lambda}} = \begin{pmatrix} 1 & 0 \\ 0 & 1 + \dfrac{\tilde{l}_0}{k^2(1 + i\nu/\omega)^2}\dfrac{\partial^2}{\partial z^2} \end{pmatrix}, \tag{5}$$

$\tilde{l}_0$ is the spatial dispersion parameter and ν is the relaxation frequency. In a general case, the quantities σ_{zz} and $\tilde{l}_0$ are evaluated using the quantum–mechanical transport theory. Though the CN surface possesses a periodic crystalline structure, Eqs. (4)-(5) incorporate only constant coefficients (i.e., σ_{zz} and $\tilde{l}_0$), and are devoid of any periodic functions. This is because the

technique of deriving the EBCs is equivalent to the averaging of microscopic fields over an infinitesimally small volume.

The conductivity was assumed to be quasi–one–dimensional while $\sigma_{z\phi}$, $\sigma_{\phi z}$ and $\sigma_{\phi\phi}$ were ignored in the derivation of the EBCs. As a consequence, we obtained conditions (2), (4) and (5) for the electromagnetic field across the CN surface. The polar conductivity $\sigma_{\phi\phi}$ is due to indirect interband transitions neglected in our model and will surely modify the stated EBCs. The role of $\sigma_{z\phi}$ and $\sigma_{\phi z}$ is expected to be important, for example, in chiral CNs in relation to the effect of natural optical activity exhibited by such CNs.

B) 2D–lattice of QDs.

In QDs, apart from the charge carrier confinement [2], there exist a class of electrodynamic effects related to light diffraction by QDs and QD ensembles, which strongly influence the electromagnetic response properties of such systems [9] –[11]. Here we consider 2D arrays of QDs to establish correlation between properties of such systems and homogeneous 2D structures like quantum wells. The key problem here is the diffraction by infinite planar quadratic lattice constituted by identical QDs imbedded in a host medium. The host medium is assumed to be dispersionless and transparent. Conventional phenomenological model of the dispersion and the gain of a single QD is as follows: $\varepsilon(\omega) = \varepsilon_h + g_0/(\omega - \omega_0 + i/\tau)$. Here ε_h is the host medium permittivity while the quantity g_0 is the phenomenological parameter proportional to the oscillator strength of the transition; $g_0 > 0$ in an inverted medium.

Let the normal $\mathbf{n}$ be directed along the z-axis and let the incident planewave be polarized along the x-axis. Further we restrict ourselves to the dipole approximation of the diffraction theory. In that case, the scattering field from an isolated QD can be expressed in terms of Hertz potentials by

$$\mathbf{E} = \sum_{l,m=-\infty}^{\infty} \left(\nabla\nabla\cdot + k_1^2\right) \mathbf{\Pi}^e_{lm}\,, \tag{6}$$

$$\mathbf{H} = -ik\varepsilon_h \sum_{l,m=-\infty}^{\infty} \nabla \times \mathbf{\Pi}^e_{lm}\,, \tag{7}$$

where

$$\mathbf{\Pi}^e_{lm} = \mathbf{e}_x \alpha_{xx} \mathcal{E}_x(0) \exp\{ik_1\rho_{lm}\}/\rho_{lm}\,, \tag{8}$$

$k_1 = k\sqrt{\varepsilon_h}$, $\rho_{lm} = [(ld-x)^2 + (md-y)^2 + z^2]^{1/2}$, α_{xx} is the QD polarizability tensor component, d is the lattice period, and $\mathcal{E}_x(0)$ is the electric field inside QD. This field is related to the mean field in the layer, $E_x(0)$, by $E_x(0) = (1 + \delta_1\alpha_{xx}/d^2)\mathcal{E}_x(0)$, where δ_1 is the lattice parameter:

$$\delta_1 = \int_{-d/2}^{d/2}\int_{-d/2}^{d/2} \frac{2x^2 - y^2}{(x^2+y^2)^{5/2}}\,dxdy \approx -\frac{8}{\sqrt{2}d}\,. \tag{9}$$

After some manipulations with Eqs. (6), (7) (see, e.g., [12]), in the limit $z \to \pm 0$ we come to Eqs. (1), (2) with the x0y plane as the S surface and

$$\hat{\sigma} = i\frac{4\pi\omega\varepsilon_h}{cd^2}\hat{\alpha}\left(\hat{\mathbf{I}} + \frac{\delta_1}{d^2}\hat{\alpha}\right)^{-1}. \tag{10}$$

Here $\hat{\mathbf{I}}$ is the unit tensor. Second term in the brackets is due to the depolarization related to the difference between mean and acting fields.

It should be noted that the assumption (i) which neglect polarization of the structure in the $\mathbf{n}$ direction, holds true only for QDs with planar configuration in x0y plane, e. g., discs, islands,

flattened pyramids, etc. For QDs with comparable extensions in all directions, the derivation of EBCs presented above should be generalized. Derivation method remains the same: scattered fields are described by Eqs. (6), (7), but Hertz potentials are given by

$$\Pi^e_{lm} = [\mathbf{e}_x \alpha_{xx} \mathcal{E}_x(0) + \mathbf{e}_z \alpha_{zz} \mathcal{E}_z(0)] \exp\{ik_1 \rho_{lm}\}/\rho_{lm}\,, \tag{11}$$

where α_{zz} stands for the QD polarizability in the z direction. Contribution of the transverse polarizability qualitatively modifies the EBCs: tangential components of the electric field exhibit discontinuity at the S surface.

In that case, relation between z–components of internal field of QD and mean field is given by $E^{\mathrm{I}}_z(0) + E^{\mathrm{II}}_z(0) = 2(1 + \alpha_{zz}\delta_2/d^2)\mathcal{E}(0)$, where

$$\delta_1 = \lim_{z\to 0} \int\limits_{-d/2}^{d/2} \int\limits_{-d/2}^{d/2} \frac{2z^2 - x^2 - y^2}{(x^2+y^2+z^2)^{5/2}}\, dxdy \approx \frac{2\pi\sqrt{\pi}}{d}\,. \tag{12}$$

Then, carrying out with Eqs. (6), (7) the manipulations analogous to the described above, we come to the generalized EBCs as follows:

$$[\mathbf{n}\,[\mathbf{n}, \mathbf{H}^{\mathrm{I}} - \mathbf{H}^{\mathrm{II}}]] = -\tfrac{2\pi\widehat{\sigma}}{c}[\mathbf{n}, \mathbf{E}^{\mathrm{I}} + \mathbf{E}^{\mathrm{II}}]\,, \tag{13}$$

$$[\mathbf{n}, \mathbf{E}^{\mathrm{I}} - \mathbf{E}^{\mathrm{II}}] = -\xi[\mathbf{n}, \nabla(\mathbf{n}, \mathbf{E}^{\mathrm{I}} + \mathbf{E}^{\mathrm{II}})] \tag{14}$$

with the conductivity tensor $\widehat{\sigma}$ defined by Eq. (10) and $\xi = 2\pi\alpha_{zz}/(d^2 + \delta_2\alpha_{zz})$.

The above equations constitute the complete system of EBCs for electromagnetic field in low-dimensional nanostructures. They have been obtained in the ordinary way, by the averaging of a microscopic field over a physically infinitesimal volume. The technique of macroscopic averaging is similar to one of introducing constitutive parameters for bulk media, but differing in that the averaging occurs in boundary conditions, but not in field equations. Correspondingly, the averaging was carried out over the 2–D surface (cylindrical for CNs or plane for QD sheets) but not over the 3–D spatial element. Thus, in electrodynamics of low-dimensional structures the EBCs play the same role as constitutive relations in electrodynamics of balk media.

3. EBCs in Quantum Electrodynamics of Nanostructures

As different from macroscopic microwave lattices, in nanostructures effects become valid related to quantum nature of the electromagnetic radiation (spontaneous irradiation, Kazimir forces, electromagnetic fluctuations, etc.). Obviously, quantum electrodynamics (QED) should be applied for description of such effects. In Ref. [13] a procedure of the electromagnetic field quantization in inhomogeneous Kramers–Kronig bulk dielectrics. In the framework of this approach, the electric field operator is introduced by

$$\hat{\mathbf{E}}(\mathbf{r}) = \int\limits_0^\infty d\omega\, \underline{\hat{\mathbf{E}}}(\mathbf{r}, \omega) + H.c. \tag{15}$$

Analogous expression can be written for the magnetic field. The Maxwell equations with a source term corresponding to the dissipation–assisted quantum noise have been formulated in Ref. [13] for the operators $\underline{\hat{\mathbf{E}}}(\mathbf{r}, \omega)$, $\underline{\hat{\mathbf{H}}}(\mathbf{r}, \omega)$. Physically observable quantities are found by averaging of corresponding field operators. The above mentioned source term provides necessary commutative relations for these operators. Our analysis has shown that the basic ideas presented in Ref. [13] in combination with the EBC method can be extended to the case of spatially inhomogeneous low–dimensional structures. For simplicity we neglect both the medium polarization in

the z–direction and the spatial dispersion. The conductivity tensor is assumed to be given in its eigenbasis. In such a case, the field operators $\hat{\underline{\mathbf{E}}}(\mathbf{r},\omega)$, $\hat{\underline{\mathbf{H}}}(\mathbf{r},\omega)$ satisfy to the vacuum Maxwell equations and the EBCs as follows

$$[\mathbf{n}\,[\mathbf{n},\hat{\underline{\mathbf{H}}}^{\mathrm{I}}-\hat{\underline{\mathbf{H}}}^{\mathrm{II}}]]=-\frac{4\pi\hat{\sigma}}{c}[\mathbf{n},\hat{\underline{\mathbf{E}}}]-\frac{4\pi}{c}\hat{\underline{\mathbf{J}}}_N\,, \tag{16}$$

$$[\mathbf{n},\hat{\underline{\mathbf{E}}}^{\mathrm{I}}-\hat{\underline{\mathbf{E}}}^{\mathrm{II}}]=0 \tag{17}$$

where $\hat{\underline{\mathbf{J}}}_N$ is the operator of the surface noise current density which can be presented by

$$\hat{\underline{J}}_{Ni}(\mathbf{R},\omega)=\sqrt{\frac{\hbar\omega}{\pi}\Re\{\hat{\sigma}_{ii}\}}\left[\Theta(\Re\{\hat{\sigma}_{ii}\})\hat{f}_i(\mathbf{R},\omega)+\Theta(-\Re\{\hat{\sigma}_{ii}\})\hat{f}_i^{+}(\mathbf{R},\omega)\right]\,,\quad i=1,2\,. \tag{18}$$

Here $\mathbf{R}\in S$ and $\Theta(\cdot)$ stands for the unit step function; $\hat{f}_i(\mathbf{R},\omega)$ and $\hat{f}_i^{+}(\mathbf{R},\omega)$ are the annihilation and creation operators, respectively, of the 2D bosonic field. This field satisfies to the Heisenberg equations of motions and is analogous to the 3D bosonic field described in Ref. [13]. It can easily be found that the second term in brackets in right–hand part of Eq. (18) disappears for thermodynamically equilibrium systems.

The key feature of QED EBCs (16)–(17) which distinguishes them from the classical EBCs (1)–(2) is the presence of the surface noise current $\hat{\underline{\mathbf{J}}}_N$. This current makes it possible to satisfy the commutation relations for the field operators. Corresponding proofs will be given separately elsewhere. The fundamental difference between quantum electromagnetic field and the classical one is the presence in the quantum field of zero–point vacuum oscillations. Similar to classical electromagnetic field, zero–point vacuum oscillations will diffract by spatial inhomogeneities (nanostructure). The diffraction distorts the spatial structure of zero–point oscillations as compared with the virtual photons in vacuum. This diffraction process is described by the EBC operators (16)–(17).

4. Utilization of EBCs

Potentiality of utilization of the EBCs method under consideration of particular electrodynamical problems is provided by applying the solution of the kernel problem to a variety of much more complicated situations: curved and/or bounded screens, screens placed in the vicinity of dielectric or metallic surfaces, *etc.* For example, EBCs (4)–(5) has been derived for an isolated infinitely long CN. Nevertheless, our formalism can be utilized for consideration of diffraction problems in different types of nanotubes, *viz.*, CNs of finite length (first results in this field have been presented in Ref. [14]), bent and corrugated CNs, CNs with junctions, multi-shell CNs with hexagonal cross-section, CN–based composites, etc. The derived effective boundary conditions can also serve as the basis for description of interaction of CNs with beams of electrons and other charged particles. The investigation of guided surface wave propagation in single– and multi–shell CNs carried out in [7], [8] exemplifies the application of the formalism developed, and it is of significance in its own right too. Such waves can be excited by directing laser or electron beams along a CN axis. These surface waves are characterized by strong retardation and, consequently, have large field gradients in the transverse plane. As the result, such surface waves must manifest a strong pondermotive effect.

As applied to 2D lattices of QDs, the EBC method allows us to analyze electromagnetic response of such layers (or multilayer structures) placed in microcavity: this is of importance for the design of QD–based semiconductor lasers [2]. EBCs given by Eqs. (13), (14) state mathematical equivalence of 2D periodical layer of QDs and an isolated quantum well. It should be stressed that the mechanisms of transport processes and oscillator strengths in each case

are essentially different. Nevertheless, the equivalence makes it possible to extend to QD–based planar structures the well-developed mathematical formalism of investigation of quantum wells. In particular, starting conditions for QD–based lasers can be evaluated by analogy with solution of the corresponding problem for the quantum well [15].

It should be emphasized that the extension of the EBC method to deformed or complicated structures is only possible when the modification of geometrical parameters of the structure does not change the electron transport properties in it; otherwise, modification of EBC is required. For example, too close location of two planar layers with QDs will change the energy spectrum because of overlapping of exciton wave functions, tunneling, etc. Analogously, too strong bend of CN will distort quasi–free motion of π–electrons in it and, consequently, may change the conductivity character. Thus, justification of applicability of EBCs must be given in each particular case.

Acknowledgement
The research is partially supported through INTAS under project 96-0467 and the NATO Science for Peace Program under project SfP-972614.

References

[1] M. S. Dresselhaus, G. Dresselhaus, and P. C. Eklund, *Science of Fullerenes and Carbon Nanotubes.* New York: Academic Press, 1996.
[2] D. Bimberg, M. Grundmann, N. N. Ledentsov, *Quantum Dot Heterostructures.* Chichester: John Wiley & Sons, 1999.
[3] L. A. Weinstein, *The Theory of Diffraction and the Factorization Method.* New York: Golem, 1969.
[4] D. J. Hoppe and Y. Rahmat-Samii, *Impedance Boundary Conditions in Electromagnetics.* Washington: Taylor & Francis, 1995.
[5] A. S. Ilyinsky, G. Ya. Slepyan and A. Ya. Slepyan, *Propagation, Scattering and Dissipation of Electromagnetic Waves.* London: Peter Peregrinus, 1993.
[6] G. Ya. Slepyan *et al.*, "Electronic and electromagnetic properties of nanotubes," *Phys. Rev. B*, vol. 57, no 16, pp. 9485–9497, April 1998.
[7] G. Ya. Slepyan *et al.*, "Electrodynamics of carbon nanotubes: Dynamic conductivity, impedance boundary conditions and surface wave propagation," *Phys. Rev. B*, vol. 60, no 24, pp. 17136–17149, December 1999.
[8] S. A. Maksimenko and G. Ya. Slepyan, "Electrodynamic properties of carbon nanotubes", in *Electromagnetic Fields in Unconventional Structures and Materials*, Ed. by: O.N. Singh and A.Lakhtakia, New York: John Wiley & Sons, 2000 (to be published).
[9] G. Ya. Slepyan *et al.*, "Polarization splitting of the gain band in quantum wire and quantum dot arrays," *Phys. Rev. B*, vol 59, no 19, pp. 1275-1278, May 1999.
[10] S. A. Maksimenko *et al.*, "Electromagnetic response of 3D arrays of quantum dots," *J. Electronic Materials*, vol. 29, no 5, pp.494-503, May 2000.
[11] S. A. Maksimenko *et al.*, "Light confinement in a quantum dot," *Semiconductor Sci. and Techn.*, vol. 15, no. 6, pp. 491–496, 2000.
[12] N.A. Khiznjak, *Integral Equations of Macroscopic Electrodynamics.* Kiev: Naukova Dumka, 1986 (in Russian).
[13] S. Scheel, L. Knöll, and D.-G. Welsch, "QED commutation relations for inhomogeneous Kramers–Kronig dielectrics," *Phys. Rev. A*, vol. 58, no. 1, pp. 700–706, July 1998.
[14] N. A. Krapivin *et al.*, "Electromagnetic wave scattering by the edge of a carbon nanotube," in *Proc. Bianisotropics'00*, Lisbon, Portugal, September 2000, pp.
[15] J. Pansarini *et al.*, "Exciton–light coupling in single and coupled semiconductor microcavities: Polariton dispersion and polarization splitting," *Phys. Rev. B*, vol. 59, no. 7, pp. 5082–5089, February 1999.

Space–Guides: Efficient Thin–Film Optical Interconnects

E. Ertekin and A. Lakhtakia

CATMAS — Computational and Theoretical Materials Sciences Group
Department of Engineering Science and Mechanics
Pennsylvania State University, University Park, PA 16802–6812, USA
Fax: +1 814 863 7967; email: AXL4@psu.edu

Abstract

Waveguiding in a thin–film helicoidal bianistropic medium (TFHBM) layer is investigated. A dielectric TFHBM layer bounded by isotropic dielectric half–spaces is shown to support guided wave propagation with guide wavenumbers dependent on the direction of signal propagation, thus signalling potential use as a space–guide. The modal fields and power transmission distributions associated with the guided modes in the proposed TFHBM interconnects are detailed.

1. Introduction

Implementation of optoelectronic devices requires the development of optical interconnects which, in addition to providing effective signal transmission, must be simple to fabricate on integrated circuitry. In this paper, we present a theoretical study which indicates that dielectric thin–film helicoidal bianisotropic mediums (TFHBMs) are very suitable for realizing optical interconnects. In fact, the adoption of dielectric TFHBM interconnects may result in efficient use of semiconductor real–estate in electronic chips.

2. Theory in Brief

Suppose a linear, dielectric TFHBM layer completely fills the region $|z| \leq D/2$, while the halfspaces $z \leq -D/2$ and $z \geq D/2$ are filled by an isotropic dielectric medium whose relative permittivity scalar at angular frequency ω is denoted by $\epsilon_r(\omega)$. The constitutive relation $\mathbf{D}(\mathbf{r},\omega) = \epsilon_0 \underline{\underline{\epsilon}}(z,\omega) \cdot \mathbf{E}(\mathbf{r},\omega)$ of the TFHBM layer contains the relative permittivity dyadic

$$\underline{\underline{\epsilon}}(z,\omega) = \underline{\underline{S}}_z(z - \tfrac{D}{2}) \cdot \underline{\underline{S}}_y(\chi) \cdot \underline{\underline{\epsilon}}^{\circ}_{ref}(\omega) \cdot \underline{\underline{S}}^T_y(\chi) \cdot \underline{\underline{S}}^T_z(z - \tfrac{D}{2}) \,. \tag{1}$$

Here, the *reference* relative permittivity dyadic

$$\underline{\underline{\epsilon}}^{\circ}_{ref}(\omega) = \epsilon_a(\omega)\mathbf{u}_z\mathbf{u}_z + \epsilon_b(\omega)\mathbf{u}_x\mathbf{u}_x + \epsilon_c(\omega)\mathbf{u}_y\mathbf{u}_y \,, \tag{2}$$

where $\mathbf{u}_{x,y,z}$ are the cartesian unit vectors and $\epsilon_{a,b,c}(\omega)$ are frequency–dependent scalars. The rotational non–homogeneity (along the z axis) of a structurally right–handed TFHBM is expressed by the dyadic

$$\underline{\underline{S}}_z(z) = (\mathbf{u}_x\mathbf{u}_x + \mathbf{u}_y\mathbf{u}_y)\cos\left(\frac{\pi z}{\Omega}\right) + (\mathbf{u}_y\mathbf{u}_x - \mathbf{u}_x\mathbf{u}_y)\sin\left(\frac{\pi z}{\Omega}\right) + \mathbf{u}_z\mathbf{u}_z \tag{3}$$

with 2Ω as the structural period. The so–called angle of rise χ appears in the tilt dyadic

$$\underline{\underline{S}}_y(\chi) = (\mathbf{u}_x\mathbf{u}_x + \mathbf{u}_z\mathbf{u}_z)\cos\chi + (\mathbf{u}_z\mathbf{u}_x - \mathbf{u}_x\mathbf{u}_z)\sin\chi + \mathbf{u}_y\mathbf{u}_y\,; \tag{4}$$

typically $\chi \geq 20^\circ$ for the sculptured thin films. Guided wave propagation is ensured if $\epsilon_r < \min\{\epsilon_a, \epsilon_b, \epsilon_c\}$, with both mediums assumed non–dissipative at the frequency of interest.

Knowing the constitutive relations of the chosen TFHBM layer, we can determine the guide wavenumbers which enable guided wave propagation. A specific guided wave mode can be delineated with the following equations:

$$\left.\begin{array}{rcl} \mathbf{E}(\mathbf{r}) &=& \exp\left[i\kappa\left(x\cos\psi + y\sin\psi\right)\right]\ \mathbf{e}(z,\kappa,\psi) \\ \mathbf{H}(\mathbf{r}) &=& \exp\left[i\kappa\left(x\cos\psi + y\sin\psi\right)\right]\ \mathbf{h}(z,\kappa,\psi) \end{array}\right\}, \quad -\infty \leq z \leq \infty\,. \tag{5}$$

Here, the angle ψ denotes the propagation direction $\mathbf{u}_\ell = \mathbf{u}_x\cos\psi + \mathbf{u}_y\sin\psi$, while κ is the modal guide wavenumber whose values have to be determined.

The leakage fields accompanying a guided wave mode are represented by

$$\left.\begin{array}{rcl} \mathbf{E}(\mathbf{r}) &=& (b_s\mathbf{s} + b_p\mathbf{p}_-)\exp\left[i\mathbf{k}_-\cdot(\mathbf{r} + \frac{D}{2}\mathbf{u}_z)\right] \\ \mathbf{H}(\mathbf{r}) &=& \frac{1}{\eta}(b_s\mathbf{p}_- - b_p\mathbf{s})\exp\left[i\mathbf{k}_-\cdot(\mathbf{r} + \frac{D}{2}\mathbf{u}_z)\right] \end{array}\right\}, \quad z \leq -\frac{D}{2} \tag{6}$$

in the lower halfspace, and

$$\left.\begin{array}{rcl} \mathbf{E}(\mathbf{r}) &=& (c_s\mathbf{s} + c_p\mathbf{p}_+)\exp\left[i\mathbf{k}_+\cdot(\mathbf{r} - \frac{D}{2}\mathbf{u}_z)\right] \\ \mathbf{H}(\mathbf{r}) &=& \frac{1}{\eta}(c_s\mathbf{p}_+ - c_p\mathbf{s})\exp\left[i\mathbf{k}_+\cdot(\mathbf{r} - \frac{D}{2}\mathbf{u}_z)\right] \end{array}\right\}, \quad z \geq \frac{D}{2}\,, \tag{7}$$

in the upper halfspace, with b_s, b_p, c_s, and c_p as the amplitudes of the perpendicular– and the parallel–polarized components. The various vectors introduced in (6) and (7) are given by

$$\mathbf{s} = \mathbf{u}_z \times \mathbf{u}_\ell\,,\ \mathbf{p}_\pm = \mp\left[1 - (\kappa/k)^2\right]^{1/2}\mathbf{u}_\ell + (\kappa/k)\mathbf{u}_z\,,\ \mathbf{k}_\pm = \kappa\mathbf{u}_\ell \pm \left(k^2 - \kappa^2\right)^{1/2}\mathbf{u}_z\,, \tag{8}$$

where $k = k_0\sqrt{\epsilon_r}$, $\eta = \eta_0/\sqrt{\epsilon_r}$, $k_0 = \omega\sqrt{\epsilon_0\mu_0} = 2\pi/\lambda_0$ is the free–space wavenumber, λ_0 is the free–space wavelength, and $\eta_0 = \sqrt{\mu_0/\epsilon_0}$ is the intrinsic impedance of free space. Guided wave propagation is possible only if $\kappa > k$; otherwise, energy launched into the TFHBM layer must leak into the two halfspaces.

On substituting the constitutive relations and the field expressions above into the time–harmonic Maxwell curl equations $\nabla \times \mathbf{E}(\mathbf{r}) = i\omega\mathbf{B}(\mathbf{r})$ and $\nabla \times \mathbf{H}(\mathbf{r}) = -i\omega\epsilon_0\,\underline{\underline{\epsilon}}(z,\omega)\cdot\mathbf{E}(\mathbf{r})$, a 4×4 matrix ordinary differential equation emerges for the TFHBM layer. Its solution requires the prescription of boundary values through (6) and (7). Our interest lies in determining pairs of (κ, ψ) such that not all of the coefficients b_s, b_p, c_s and c_p are null–valued; thereby the dispersion equation is obtained. For guided wave propagation, values of κ denoted by κ_ψ^r, $(r = 1, 2, 3,...)$, that satisfy the dispersion equation have to be numerically determined, the roots being indexed by the integer r in descending order of their magnitudes.

3. Guide Wavenumbers

We implemented the foregoing procedure using the C programming language and the IMSL C numerical library subroutines for complex linear algebra. The wavelength λ_0 was fixed at 600 nm for all calculations. We tested our computer program for the case of an isotropic, homogeneous, dielectric slab waveguide. Analytical solutions to the dispersion equation of this simple waveguide are well–documented – see, *e.g.*, [1]. Setting $\epsilon_r = 1$, we simulated homogeneity and isotropy by choosing $\epsilon_a = \epsilon_b = \epsilon_c$ and taking the limit $1/\Omega \to 0$. The roots κ^r that we

obtained corresponded exactly with the analytical results. Furthermore, the calculated mode shapes and power transmission characteristics of the waveguide also matched the expected power transmission and mode shape plots.

Now let us proceed to the proposed TFHBM interconnect. Most calculations were made with $\{\epsilon_a = 3.8, \epsilon_b = 4.6, \epsilon_c = 3.0\}$, in accordance with data from [2]. In general, the guide wavenumbers show a strong dependence on the propagation direction (see [3,4] for more details). This is illustrated in Figure 1, where the guide wavenumbers are indicated for various ψ for a specific TFHBM interconnect. Thus, the proposed TFHBM interconnect functions as *a space-guide through which signals can be simultaneously transported in different directions with different phase velocities*. This feature emerges from the anisotropic and non-homogeneous nature of TFHBMs, and may be exploited for efficient use of semiconductor real-estate in optoelectronic circuitry.

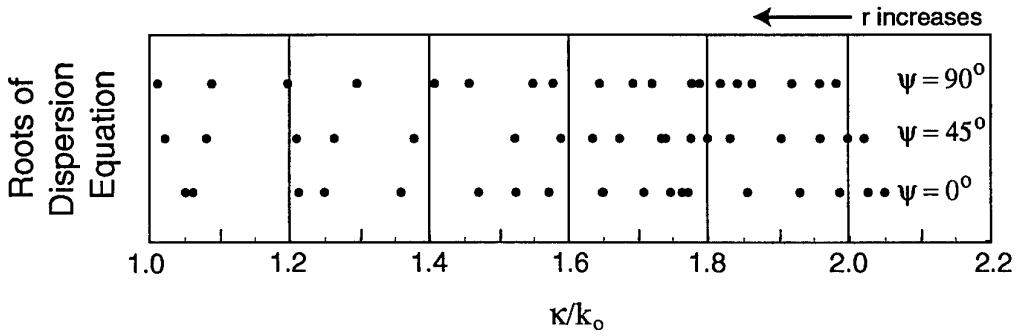

Figure 1: Roots of dispersion equation for directions of propagation denoted by the angle ψ; $\lambda_0 = 600$ nm, $\epsilon_a = 3.0$, $\epsilon_b = 4.6$, $\epsilon_c = 3.8$, $\chi = 30°$, $\Omega = 200$ nm, $D = 8\ \Omega = 1600$ nm.

Independently of all parameters, the guide wavenumbers κ_ψ^r for propagation directions $\mathbf{u}_\ell$ and $-\mathbf{u}_\ell$ are the same. When the TFHBM layer consists of an integral number of periods (*i.e.*, the ratio D/Ω is an even integer), the additional relation $\kappa_\psi^r = \kappa_{\pi-\psi}^r$ holds. This arises because all three principal axes of $\underline{\underline{\epsilon}}(z,\omega)$ rotate through an integral number of turns between the planes $z = -D/2$ and $z = D/2$, thereby imposing a symmetry constraint.

The variability of κ_ψ^r with ψ is most pronounced around the lower values of κ_ψ^r (where solutions of the dispersion equation are more widely spaced). Additionally, the directional-dependence of κ_ψ^r persists for smaller values of D/Ω, including $D/\Omega << 1$. Parenthetically, we also studied the directional-dependence of the guide wavenumbers for a locally uniaxial TFHBM layer with $\{\epsilon_a = \epsilon_c = 3.8, \epsilon_b = 4.6\}$; The guide wavenumbers κ_ψ^r still exhibit a dependence on ψ, but the dependence is weaker than for the biaxial case illustrated in Figure 1.

The number density of guided wave modes is less when D is small. The mode number density appears to be predominantly determined by the overall thickness D, and is largely unaffected by the half-period Ω. Thus, the availability of guided wave modes can be tailored by properly choosing the layer thickness D.

In TFHBM interconnects, κ_ψ^r has an upper bound which varies with ψ. For instance, $\kappa_\psi^r < 2.049\ k_0$ for $\psi = 0°$, whereas $\kappa_\psi^r < 1.981\ k_0$ for $\psi = 90°$, in Figure 1. The upper bound decreases monotonically as ψ increases from 0° to 90°. The upper bound on κ_ψ^r varies with χ, ψ, D, and Ω for given ϵ_a, ϵ_b, and ϵ_c.

4. Space–Guide Modes

The modal fields and power transmission associated with the guided wave modes were also studied. The time–averaged power flow in the propagation direction is given by $P_\ell(z) = \frac{1}{2}\mathbf{u}_\ell \cdot \mathrm{Re}\,[\mathbf{e}(z,\kappa,\psi) \times \mathbf{h}^*(z,\kappa,\psi)]$, where the asterisk denotes the complex conjugate. Detailed numerical study of the modal fields and power distributions revealed that each mode of propagation inside a TFHBM interconnect can be classified into one of two groups: *hybrid electric* (HE) and *hybrid magnetic* (HM). The modes are *hybrid*, because electric and magnetic field components are present in all directions, along the axial ($\mathbf{u}_z$) direction, as well as in the longitudinal and perpendicular directions in the xy plane. This is unlike the modes in an isotropic, dielectric, planar interconnect, wherein the modes are either transverse electric (TE) or transverse magnetic (TM). Another distinction between the HE and HM modes in the TFHBM interconnect and TE and TM modes in the isotropic interconnect is that there appears to be no apparent ordering to the occurence of the HE and HM modes, while the TE and TM modes alternate with $r = 1, 2, 3, \ldots$.

For both the HE and the HM modes, the power transmission distributions $P_\ell(z)$ are quite similar to those of the TE and the TM modes, respectively. In fact, for propagation in any direction, it is possible to order the guided modes HE_n and HM_n, $(n = 1, 2, 3, \ldots)$, based upon the similarity of $P_\ell(z)$, respectively, to $P_\ell(z)$ for TE_n and TM_n modes. $P_\ell(z)$ for a given mode (HE_n or HM_n) does not vary much with respect to ψ in the space–guide. Regarding modal field plots, however, there are distinct differences between the HE and the HM modes.

The variation of $e_\perp = \mathbf{e} \cdot \mathbf{u}_\ell$ with respect to z for the HE_n mode is similar in all directions; and, in general, the $e_\perp$ vs. z curves for all HE_n modes resemble those for a TE_n mode in an isotropic interconnect. Thus, all HE_n modes propagating in any direction $\mathbf{u}_\ell$ in a space–guide have similar modal characteristics. However, the $h_\perp$ vs. z plots for the HM_n modes do not display these characteristics. Not only are the $h_\perp$ vs. z plots for an HM_n mode different from that of the TM_n mode, but also the $h_\perp$ vs. z plots are distinctly dissimilar for the various propagation directions. Thus, the dielectric anisotropy and non–homogeneity of the space–guide impart more significant directional dependence to the mode shapes of the HM modes and less to the HE modes.

Clearly, the HE_n mode launched in one direction will not interfere with the HE_n mode launched in some other direction; and the same holds true for any HM_n mode, at least for small values of n. Indeed, several HE and HM modes of low order can be launched in different directions, while taking care that their guide wavenumbers are all different. The space–guide concept is thus well–founded. Obviously, however, hardware requirements will put a limit on the number of channels a TFHBM space–guide can realistically support in actual circuitry.

Acknowledgement
E. Ertekin acknowledges a Graduate Fellowship from the US National Science Foundation.

References

[1] M. S. Sodha and A. K. Ghatak, *Inhomogeneous Optical Waveguides.* New York, NY, USA: Plenum Press, 1977.

[2] I. J. Hodgkinson and Q. H. Wu, *Birefringent Thin Films and Polarizing Elements.* Singapore: World Scientific, 1997.

[3] E. Ertekin and A. Lakhtakia, submitted for publication in *Proc. R. Soc. Lond. A.*

[4] E. Ertekin, *Space–Guides: Efficient Optical Interconnects Made from a Thin–Film Helicoidal Bianisotropic Medium*, M.S. Dissertation. Department of Engineering Science and Mechanics, The Pennsylvania State University (August 2000).

Session 6

Thursday - September 28, 2000

10:40 - 12:40

Session 6

Bianisotropic Media II

Ubi Materia, Ibi Geometria

Ari Sihvola

Electromagnetics Laboratory, Helsinki University of Technology
P.O. Box 3000, FIN–02015 HUT, Finland
Fax: + 358–9–451 2267; email: ari.sihvola@hut.fi

Abstract

This invited presentation discusses the connection between geometry and matter. The theme of the paper, ubi materia, ibi geometria, is illuminated from the point of view of history of post-Renaissance science and also in terms of modern bi-anisotropic electromagnetics research. The citation is pinpointed in Johannes Kepler's philosophical texts, and an attempt is made to understand its meaning. The validity of 'ubi materia, ibi geometria' for the electromagnetic bi-anisotropics research is reconfirmed and a modified interpretation is proposed for it.

1. Preliminaries

Johannes Kepler declared 'Ubi materia, ibi geometria'. It is not difficult to imagine that a modern researcher in the field of chiral and bi-anisotropic electromagnetics concurs with this statement; 'where there is matter, there is geometry'. Matter and geometry, Nature and mathematics are intimately connected.

Ubi materia, ibi geometria. Citations to this formula appears often in scientific literature, sometimes with a reference to Kepler, sometimes just as it reads.[1] But it is difficult to find an exact citation from where and in what context in Kepler's writings this statement can be found. It seems to be well hidden; the only[2] place I have seen it is in the small tractate [6] *De fundamentis astrologiae certioribus*, shown with the surrounding text in Figure 1.[3] Where there is matter, there is geometry.

The observation of the connectedness of nature and mathematics was essential with the scientific revolution in the 16th and 17th centuries. In today's world where apparently nothing else than change is permanent, knowledge is said to be short-lived, and postmodernism is claimed to have replaced modernity.[4] But is it really so? Is Millennium the opening to a New Age? I would hesitate to agree. It is one of the aims of the present paper to defend Kepler's ethos which pronounces the reality of geometry in matter. If we are now going towards a new age, it should and could rather be a Renaissance of modernity.

[1] *Ubi materia, ibi geometria* can be found as a motto for chapters in mathematics books (for example, [1]), in general studies of the birth of new physics and astronomy, and as contribution to obscure rhetoric in speculative quantum physics texts. In fact, not only mathematicians and physicists use this slogan. It can be found in other environments, like of course philosophy and history, but also surveying [2], linguistics [3], and even jurisprudence [4]. A search in the world-wide-web with the string <ubi materia, ibi geometria> returns several virtual sites in rather unexpected places, most of them confusing. In the hunt for the origins of the title of the present paper, more interesting hints can be found using the digitally stored scholarly journal archive JSTOR [5].

[2] With this I do not imply that Kepler may not have written it also elsewhere in his great books (e.g., *Mysterium Cosmographicum, Astronomia Nova, Harmonices Mundi*).

[3] See footnote 12 on page 400 of [7].

[4] Physicists at large, of course, tend to have another opinion; see, for example, the delightful [8].

2. Matter and Geometry: Kepler's Platonism

Johannes Kepler (1571–1630) is rightfully seen as a central figure in the birth of the new physics. It is often said that the Copernican revolution[5] marks the end of Medieval times, and there indeed, Kepler's contribution was very essential in giving support to heliocentric cosmology and replacing the Aristotelian concepts in mechanics by new ones. For Kepler and Galileo, not to mention Newton, mathematics had to be included in the correct description of natural phenomena.

But in the case of Kepler the importance of mathematics was not only in arithmetic. Surely he was able to calculate tolerable approximations for the positions of planets. However, Kepler was in the sense Platonist that he believed in the rigorous and perfect structure of the universe. His celestial world had—at least in his early writings—a geometrically exact, nearly Pythagorean form, "his God [was] a geometer, and not an aritmetician" [7, p. 139]. This view is reflected in his models for the sizes of the planetary spheres that had harmonic ratios.[6] Kepler made ample use of various polyhedric volumes and it can be seen in the illustrations of his books, cf., e.g. Figure 2. The young Kepler was advised by Tycho Brahe to abandon his aprioristic speculations for more fruitful observational work. The incompatibility between the two approaches, the empiristic Tychonian on one hand, and geometrically ideal on the other, caused probably certain tension for Kepler during his later studies.

> ***Primam contrarietatem Aristoteles in metaphysicis recipit illam, quae est inter idem et aliud: volens supra geometriam altius et generalius philosophari. Mihi alteritas in creatis nulla aliunde esse videtur, quam ex materia aut occasione materiae, aut ubi materia, ibi geometria. Itaque quam Aristoteles dixit primam contrarietatem sine medio inter idem et aliud, eam ego in geometricis, philosophice consideratis, invenio esse primam quidem contrarietatem, sed cum medio, sic quidem, ut quod Aristoteli fuit aliud, unus terminus, eum nos plus et minus, duos terminos dirimamus.***

Figure 1: Part of Johannes Kepler's Thesis **xx** from *De fundamentis astrologiae certioribus*; (Opera Omnia, Vol. 1, p. 423). What is Kepler's intention in the second sentence?

Aside from astronomical and astrological theories, also in his Earth-bound studies Kepler was seeking causes for the form of matter. There he can be seen to follow more faithfully the metaphysics of Aristoteles.[7] For example, in his study of the snowflake (*Strena seu de Nive sexangula* ([10]),[8] Kepler searches the reason and cause for the sixfold symmetry, obvious in snow crystals (see, for example, Figure 3). His conclusion is that the cause for of the six-sided shape of a snowflake is a formative faculty already present in water in the liquid state and in vapour.

---

[5]The term 'revolution' may have overtones that pertain to certain schools of the philosophy of science; by this choice of words I am not attaching myself to any of these, nor criticising them. The reader fluent in Finnish finds the discussion in [9] enlightening in respect how literally the metaphor of revolution can be taken in connection of Copernicanism.

[6]Kepler saw that there had to be six planets (Mercury, Venus, Earth, Mars, Jupiter, Saturn) because only then the five regular polyhedra can be circumscribed between their spheres. In the earlier Ptolemaic system, there was place for seven planets (Moon, Mercury, Venus, Sun, Mars, Jupiter, Saturn); hence the Copernican system has to be valid (*Mysterium Cosmographicum*). (One might, however, with justification doubt that the system presented by Copernicus in his book *De Revolutionibus Orbium Coelestium* was simpler or aesthetically more pleasing than the theory in Ptolemy's *Almagest*.)

[7]According to the classical Aristotelian analysis, there are four causes for entities (things): material, formal, efficient, and final.

[8]See also [11, 12].

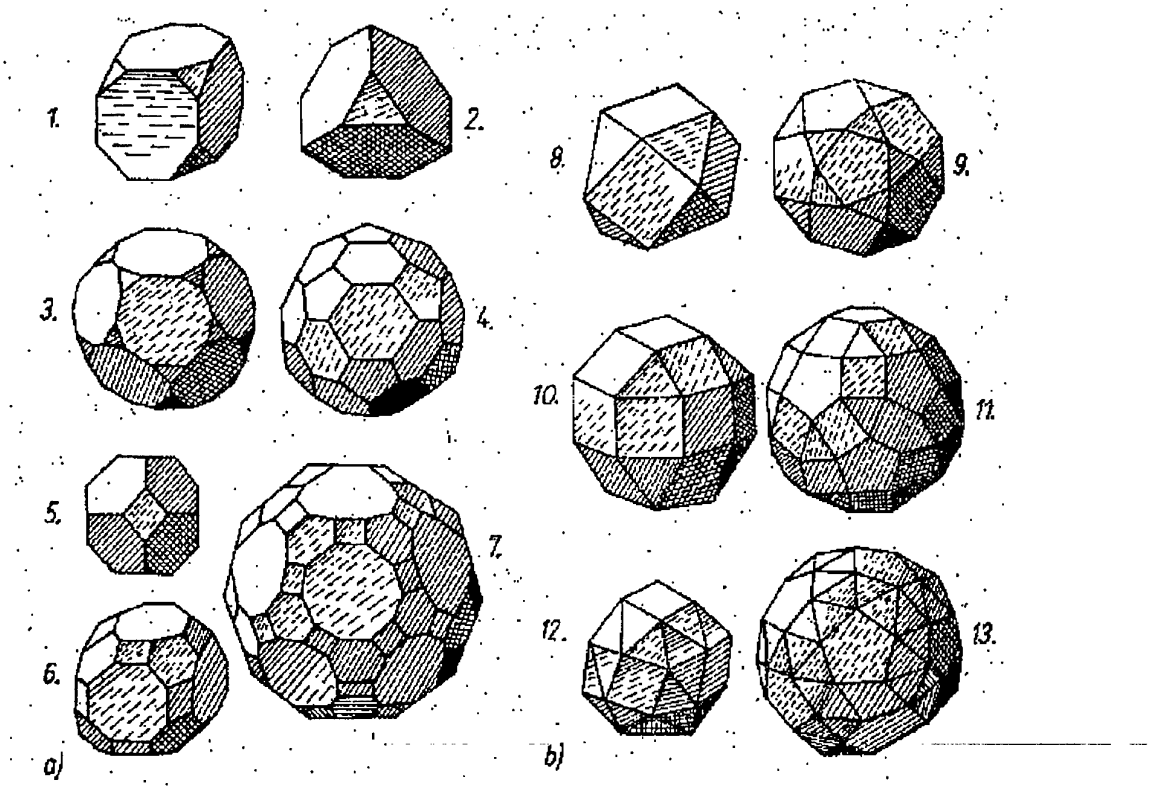

Figure 2: Archimedean polyhedra, used by Kepler in *Harmonice Mundi.*

What, then, did Kepler mean by his *Ubi materia, ibi geometria*? The citation, Figure 1 — *Mihi alteritas in creatis nulla aliunde esse videtur, quam ex materia aut occasione materiae, aut ubi materia, ibi geometria* — is not perfectly apparent. Somehow Kepler is saying that matter, and its emergence (*occasione*) is the cause of a certain property in created objects: *alteritas.* 'Alteritas' might be 'variety' or 'otherness', and this is an essential concept which in some sense in Kepler's mind gets connected with geometry, as the conclusion of the sentence ('in other words, where there is matter, there is geometry') shows. One reasonable interpretation might be just to guess that Kepler emphasises his idealistic belief in perfect shapes immanent within all matter.[9] It is probably not too bold to presume that Kepler would have loved today's solid-state physics classes, and would have much preferred them over semiconductor engineering textbooks where impurities and defects ruin the clean symmetries in solid matter.

3. Geometry and Matter: Bi-Anisotropics in the 21th Century

Ubi materia, ibi geometria. These words can a materials scientist safely speak out in the *Bianisotropics 2000* meeting in Lisbon. To calculate the effective dielectric and magnetic medium parameters of simple or complex materials, knowledge about their geometrical structure has to be made use of. The macroscopic properties of solid materials are connected to their microscopic crystallography. Kepler's maxim has even been reworded more strongly in the form of Neumann's principle: No asymmetry may be exhibited by any property of the crystal which is not possessed by the crystal itself [15]. In other words, the special characteristics of the geometrical constellation of solid matter "shine through" in the properties of its measurable properties.

[9] I welcome competing interpretations!

Pierre Curie has expressed the principle in the form 'C'est la dissymétrie, qui creé le phénomène' (It is asymmetry which creates the phenomenon).

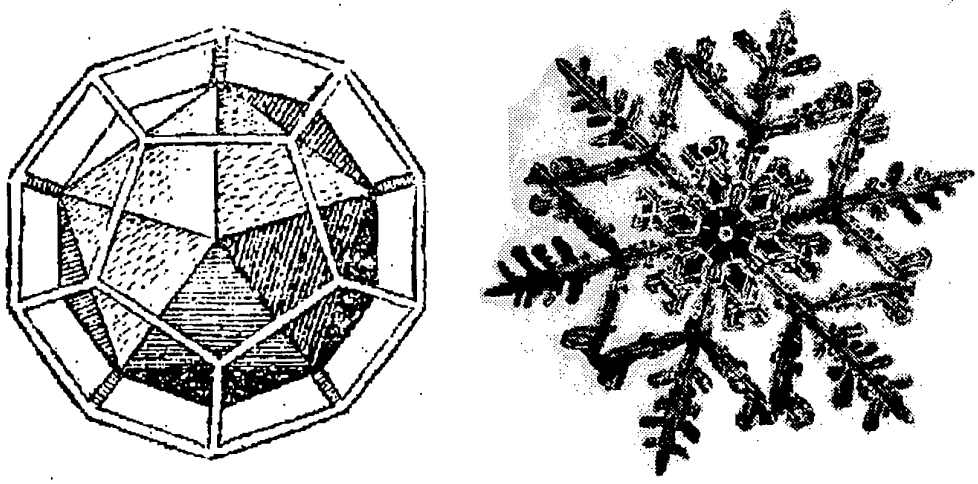

Figure 3: The togetherness of matter and geometry was obvious for Kepler also in his studies of snow [10]. On the left, one of his favourites, icosahedron in Platonic dodecahedron. To the right side, one of Wilson A. Bentley's snowflake photographs. (Spending decades during the early last century, W.A. Bentley of Jericho, Vermont (New England), patiently and skillfully took thousands of photographic images of snow crystals. These can be admired in the Dover edition [13] of his book and nowadays also on a CD-rom [14].) Note the sixfold symmetry in the snowflake.

Indeed, where a physicist or an electrical engineer needs to find out *ab initio* the effective properties of matter, the presence or absence of symmetry, that is geometry, has to be dealt with. But could Kepler's watchword be approached from another direction? What about understanding it in a way such that the role of geometry is stressed more; so that geometry begets matter? In such a reading of the principle, we in some sense surpass the Neumann–Curie interpretation. The properties of matter are determined by its geometrical description; this is then true but trivial: what is essential is that these properties can be very varied and unexpected. Why? We only need to think about engineering applications such as chirality, photonic band gap structures, or liquid crystals.

More technical support to such an interpretation for the interplay between geometry and matter is provided by the basic material relations of bi-anisotropic electromagnetics:

$$\mathbf{D} = \epsilon \bullet \mathbf{E} + \xi \bullet \mathbf{H} \tag{1}$$

$$\mathbf{B} = \zeta \bullet \mathbf{E} + \mu \bullet \mathbf{H} \tag{2}$$

The field vectors are denoted here by $\mathbf{E}$ (electric) and $\mathbf{H}$ (magnetic), and the responses in this representation are the flux densities $\mathbf{D}$ (electric) and $\mathbf{B}$ (magnetic). The relations between these vectors are given by the material parameters, permittivity ϵ, permeability μ, and the two magnetoelectric cross terms ξ and ζ.[10] The geometry of matter determines the character of the

[10]I am not discussing here the question which one of the magnetic fields ($\mathbf{H}$ or $\mathbf{B}$) is primary and should appear on the right-hand side of the constitutive relations (to read a sharp-worded argument against the above use, look [16]). Also, I am well aware of the fact that one has to be careful with the order of the magnitude and balance of electric and magnetic polarisation terms on the right-hand side of these relations (see, for example, [17]). In terms of the focus of the paper, these points are not crucial; also, the form of the relations (1)–(2) is familiar and much-used in Bianisotropics meetings [18].

quantities ϵ, μ, ξ, and ζ, and the nature of the product marked by $\bullet$ in (1)–(2). For the simplest isotropic case, the product is a plain multiplication by a scalar. The other extreme is that all four medium "parameters" are full dyadics (alternatively, tensors of second rank) and then the number of degrees of freedom in the bi-anisotropic description of such matter is $4 \times 9 = 36$.[11]

If the medium is anisotropic, its material dyadics, for example the permittivity $\overline{\overline{\epsilon}}$, have a structure which reflects faithfully the internal geometry of the matter, according to the Neumann principle. But how do the magnetoelectric effects arise? Obviously through geometry.

Chirality is one reciprocal type of these magnetoelectric effects. Chirality can be said to be present in materials that have a handed microstructure. If the medium is predominantly right- or left-handed, macroscopic effects of chirality can be observed. One observable optical or electromagnetic effect of chiral media is their ability to rotate the polarisation plane of the incident wave, and on the level of dipole moments in the medium the effect is electrically caused magnetic polarisation density and vice versa. But these effects take place because of the left–right symmetry is broken.[12]

Another affirmation for the strong interpretation of the Kepler principle is artificial magnetism. 'Natural' magnetism is present in certain materials, like iron, and in electromagnetics applications this property is taken into account by the $B - H$ relation. The origin of the magnetic properties is not important. It is not easy to talk about the geometrical cause of magnetic permeability in quantum mechanics. But because macroscopic electric loops act as magnetic moments, it is possible to synthetise a medium with magnetic permeability. Also in modelling of chiral, bi-anisotropic, and other complex materials, the observation of the appearance of magnetic properties for materials with non-magnetic constituents has been emphasised [21, 22, 23]. If interested in "artificial" magnetism in natural media, see [24] for the diamagnetic effect of wet snow due to the funicularly circling water phase in the ice matrix.

Finally, it is perhaps proper to remind of one important electromagnetics application that hinges on the geometry–matter interaction. This is the field with many names: photonic band gaps, electromagnetic or photonic superlattices, photonic crystals, periodic quasicrystal structures, etc. [25]. There, the geometry of the structure is built in such a way that from the electromagnetic point of view the medium looks transparent or opaque depending on the wavelength, thus giving access to a whole new range of material properties. With such prospects in sight, it is not overoptimistic to foresee a revival for Kepler's credo. *Ubi materia, ibi geometria.*

Acknowledgements
I acknowledge with pleasure Docent Reijo Pitkäranta's help with Latin texts. Mr. Sami Ilvonen kindly processed and edited some of the electronic illustrations. Discussions with Professor Roger Raab about crystallography some years ago have been very helpful. Officers in both the Electrical Engineering Department Library and the Main Library in the Helsinki University of Technology assisted me very much in locating old and rare texts.

References

[1] J. J. Koenderink, *Solid shape.* Cambridge (Mass): MIT Press, 1990.
[2] Integrated sensor orientation. Theory, algorithms and systems. *ISPRS–IAG–FIG–IUSM Workshop*, (International Society for Photogrammetry and Remote Sensing, and the International Association for Geodecy), Barcelona, September 4–8, 1995.
[3] K. Buehler, *Sprachtheorie*, Stuttgart, 1965.
In, `http://www.uni-essen.de/sesam/geschichte/theorie/buehler_zeichen.html`.

[11] This number is outrageously high. Brave attempts to control its freedom have found their way into the electromagnetics literature [19].

[12] In the subatomic level, physicists use the term 'parity' in connection of chirality. In the weak interaction process, parity is broken [20].

[4] H. Kaminsky, Review of "Community in historical perspective: A translation of selections from 'Das Deutsche Genossenschaftsrecht' (The German law of fellowship)," *Speculum*, vol. 67, no. 2, pp. 498-499, April 1992.
[5] `http://www.jstor.org`
[6] J. Kepler: *De fundamentis astrologiae certioribus.* In, Joannis Kepleri astronomi Opera Omnia, Vol. I. Editit Christian Frisch. Frankofurti a.M.–Erlangae, Heyder & Zimmer 1858–1871. (Johannes Kepler, Gesammelte Werke, München (C.H. Beck), Edited by Kepler-Komission der Bayerischen Akademie der Wissenschaften, Band 4: Kleinere Schriften 1602–1611; Dioptrice. Hrsg. von Max Caspar und Franz Hammer, 1941)
[7] A. Koyré, *The astronomical revolution.* Paris: Hermann, 1973.
[8] A. Sokal and J. Bricmont, *Fashionable nonsense: postmodern intellectuals' abuse of science.* New York: Picador, 1998.
[9] R. Lehti, *Tanssi Auringon ympäri.* Oulu: Pohjoinen, 1989.
[10] J. Kepler, *Strena seu de Nive sexangula*, (1611). *Vom sechseckigen Schnee*, (translated and commented by Dorothea Goetz), Leipzig: Akademische Verlagsgesellschaft Geest & Portig K.-G., 1987.
[11] R. Lehti, *Lumihiutaleet ja maailmankuvat.* Helsinki: URSA, 1998.
[12] R. Palter, "Kepler's conversation with Galileo's Sidereal Messenger; the Six-cornered Snowflake," *Renaissance Quarterly*, vol. 21, no. 3, pp. 344-349, Autumn 1968.
[13] W. A. Bentley and W. J. Humpreys, *Snow Crystals.* New York: Dover, 1962.
[14] Wilson "Snowflake" Bentley Digital Archives. The man & his images, CD-rom, Vol. 1, Photo-Graphics Multimedia production, Jericho, Vermont, USA, 1999.
[15] R. R. Birss, *Symmetry and magnetism.* Amsterdam: North Holland, 1966.
[16] R. P. Feynman, R. B. Leighton, and M. Sands, *The Feynman lectures on physics.* Vol. II, Chapter 36-2. Reading (Mass.): Addison–Wesley, 1964.
[17] R. E. Raab and J. H. Cloete, "An eigenvalue theory of circular birefringence and dichroism in a non-magnetic medium," *Journal of Electromagnetic Waves and Applications*, vol. 8, no. 8, pp. 1073-1089, 1994.
[18] W. S. Weiglhofer, "Bianisotropy and *Bianisotropics'97* – A Perspective," Proceedings of *Bianisotropics'97*, Glasgow, Great Britain, 5–7 June 1997, pp. 23-26.
[19] W. S. Weiglhofer and A. Lakhtakia, "Thirty-five is enough: A new constraint for linear, bianisotropic media," *Radio Science Bulletin*, no. 273, p. 4, 1995.
[20] T. D. Lee and C. N. Yang, "Question of parity conservation in weak interactions," *Physical Review*, vol. 104, no. 1, pp. 254-258, 1956.
[21] A. Lakhtakia, V. K. Varadan, and V. V. Varadan, "On the Maxwell-Garnett model of chiral composites," *Journal of Materials Research*, vol. 8, pp. 917-922, 1993.
[22] I. V. Lindell, A. H. Sihvola, S. A. Tretyakov, and A. J. Viitanen, *Electromagnetic waves in chiral and bi-isotropic media.* Boston: Artech House, 1994.
[23] J. B. Pendry, "Photonic band gaps and magnetism," In, CD-rom Proceedings of *AP2000*, Millennium Conference on Antennas and Propagation, Davos, Switzerland, 9–14 April 2000.
[24] C. Mätzler, "Eddy currents in heterogeneous mixtures," *Journal of Electromagnetic Waves and Applications*, vol. 2, no. 5/6, pp. 473-479, 1988.
[25] J. D. Joannopoulos, R. D. Meade, and J. N. Winn, *Photonic crystals. Molding the flow of light.* Princeton University Pres, 1995.

Nonreciprocity and Spatial Dispersion in Bianisotropic Media

E. O. Kamenetskii

Department of Electrical Engineering – Physical Electronics,
Faculty of Engineering, Tel-Aviv University, Tel-Aviv 69978, Israel
Fax: 972-3-6423508; e-mail: kmntsk@eng.tau.ac.il

Abstract

Definition of the notion of reaction in bianisotropic media is not so trivial. In this paper, we consider some important aspects of the physical admissibility to use the notion of the reaction as a "physical observable" in bianisotropic media. The questions also arise: For what kinds of the known bianisotropic media the reciprocity theorem is physically applicable? Based on what kind of the bianisotropic media, nonreciprocal microwave devices can be realized? We will show that a novel class of microwave bianisotropic materials - magnetostatically controlled bianisotropic materials (the MCBMs) - are "physically justified" materials. The Onsager-Casimir principle and the notion of reciprocity are applicable in this case. New nonreciprocal microwave devices based on the MCBMs can be realized.

1. Introduction

There are many attempts to generalize the reciprocity theorem for bianisotropic media. Gyrotropic (gyromagnetic or gyroelectric) media with non-symmetrical constitutive tensors caused by an applied dc magnetic field have been called "nonreciprocal" media because the usual reciprocity theorem [1] does not apply to them. Rumsey has introduced a quantity called the "reaction" and interpreted it as a "physical observable" [2]. This made it possible to obtain a modified reciprocity theorem based on the property of gyrotropic media that non-symmetrical constitutive tensors of permittivity or permeability are transposed by reversing the dc magnetic field [3]. Physically, the applicability of the reciprocity theorem for gyrotropic media is based on the time-reversal invariance which is described by the Onsager principle [4,5]. With formal introduction of the notion of reaction for bianisotropic media, one can formulate reciprocity conditions for medium parameters [6]. One can also extend the procedure used for a gyrotropic medium and consider the complementary [7], or the Lorentz-adjoint [8] bianisotropic medium which satisfies the reciprocity theorem. It was shown [8] that for the monochromatic electromagnetic field in the lossless bianisotropic medium, the time-reversed constitutive matrix may correspond to the Lorentz-adjoint constitutive matrix.

The questions, however, arise: Whether the time-reversal operations used for bianisotropic media are physically admissible? For what kinds of the known bianisotropic media the reciprocity theorem is physically applicable? One cannot *a priori* characterize bianisotropic media as reciprocal or non-reciprocal materials until a convincing analysis will show that microscopic properties "permit" time-reversal operations.

Recently, we have conceptualized a novel class of microwave bianisotropic materials based on a composition of ferrite magnetostatic wave (MSW) resonators with special-form surface metalizations - the magnetostatically controlled bianisotropic materials (MCBMs) [9]. The proposed MCBMs becomes not hypothetical materials after recent experimental results have verified the

fact that ferrite magnetostatic-wave resonators with special-form surface metalizations exhibit properties of bianisotropic particles [10,11]. A very important aspect arises from the fundamental point of view. The MCBMs are *local temporally dispersive bianisotropic media* in comparison with helix or Ω-particle composites characterized as media with *nonlocal* properties [12,13].

2. Reciprocity Theorem for Bianisoropic Media

Reciprocity theorem shows that nonreciprocal bianisotropic media with constitutive parameters altered by reversing the dc magnetic field $\vec{H}_0$ are described as

$$\begin{aligned} \overleftrightarrow{\epsilon}\,(\omega,\vec{H}_0) &= \overleftrightarrow{\epsilon}^{T}\,(\omega,-\vec{H}_0),\ \overleftrightarrow{\mu}\,(\omega,\vec{H}_0)=\overleftrightarrow{\mu}^{T}\,(\omega,-\vec{H}_0), \\ \overleftrightarrow{\xi}\,(\omega,\vec{H}_0) &= -\overleftrightarrow{\zeta}^{T}\,(\omega,-\vec{H}_0),\ \overleftrightarrow{\zeta}\,(\omega,\vec{H}_0)=-\overleftrightarrow{\xi}^{T}\,(\omega,-\vec{H}_0), \end{aligned} \tag{1}$$

The microscopic aspects of relations (1) will be discussed in section 4.

Reciprocity theorem is an example of quadratic relations in electrodynamics of bianisotropic media. Energy relations are another important example of quadratic relations. It is clear that these two forms of quadratic relations should not be considered independently. In particular, the correct definition of the reaction in bianisotropic media should be made, taking into account the energy balance equation. The energy relations for bianisotropic media were carefully analyzed in [14] and also discussed in [13]. One can see that energetic relations for bianisotropic media cannot be considered just as an extension of the similar relations for anisotropic media. In bianisotropic media, variation of the energy should be realized due to both types of sources, both types of currents - the electric and magnetic currents.

3. Network Reciprocity

Let us consider now some general properties of waveguide junctions containing bianisotropic samples. It is not so difficult to show that for two sets of the fields due to sources a and b we can write

$$\begin{aligned} &\int_S \left(\vec{H}_a\times\vec{E}_b-\vec{H}_b\times\vec{E}_a\right)\cdot\vec{n}\,dS - i\omega\int_{V'}\Big[\vec{E}_b\cdot\left(\overleftrightarrow{\epsilon}\cdot\vec{E}_a\right)-\vec{E}_a\cdot\left(\overleftrightarrow{\epsilon}\cdot\vec{E}_b\right)+ \\ &+\ \vec{H}_a\cdot\left(\overleftrightarrow{\mu}\cdot\vec{H}_b\right)-\vec{H}_b\cdot\left(\overleftrightarrow{\mu}\cdot\vec{H}_a\right)+\vec{E}_b\cdot\left(\overleftrightarrow{\xi}\cdot\vec{H}_a\right)+\vec{H}_a\cdot\left(\overleftrightarrow{\zeta}\cdot\vec{E}_b\right)- \\ &-\ \vec{E}_a\cdot\left(\overleftrightarrow{\xi}\cdot\vec{H}_b\right)-\vec{H}_b\cdot\left(\overleftrightarrow{\zeta}\cdot\vec{E}_a\right)\Big]\,dV=\sum_{p=1}^{N}\int_{S_p}\left(\vec{H}_a^{(p)}\times\vec{E}_b^{(p)}-\vec{H}_b^{(p)}\times\vec{E}_a^{(p)}\right)\cdot\vec{n}^{(p)}\,ds= \\ &=\ i\omega\int_{V'}\Big[2\vec{E}_b\cdot\left(\overleftrightarrow{\epsilon}_{as}\cdot\vec{E}_a\right)-2\vec{H}_b\cdot\left(\overleftrightarrow{\mu}_{as}\cdot\vec{H}_a\right)+\vec{E}_b\cdot\left(\overleftrightarrow{A}\cdot\vec{H}_a\right)-\vec{E}_a\cdot\left(\overleftrightarrow{A}\cdot\vec{H}_b\right)\Big]\,dV\equiv K \end{aligned} \tag{2}$$

where S is a surface that restricts the volume V, $\vec{n}$ is the unit vector along the external normal to the surface S, V' is a part of a volume V filled by the bianisotropic medium. We chose volume V as the volume restricted by a joint of several waveguides and cross sections of these waveguides and supposed that sources are placed beyond the volume V. We also took into account that a surface integral over metallic walls is equal to zero.

In Expr. (2) p is a number of a port, S_p and $\vec{n}^{(p)}$ are, respectively, a cross-section of port p and the unit normal vector to this cross-section, $\overleftrightarrow{\epsilon}_{as}$ and $\overleftrightarrow{\mu}_{as}$ are antisymmetric parts of tensors $\overleftrightarrow{\epsilon}$ and $\overleftrightarrow{\mu}$, respectively, and $\overleftrightarrow{A}\equiv\overleftrightarrow{\xi}+\overleftrightarrow{\zeta}^{T}$. Besides a trivial case of $\overleftrightarrow{\epsilon}_{as}=\overleftrightarrow{\mu}_{as}=\overleftrightarrow{A}=0$, the quantity

K may become equal to zero for some particular cases of the field structure and the geometry of a problem when $\overleftrightarrow{\epsilon}_{as} \neq 0, \overleftrightarrow{\mu}_{as} \neq 0$ and $\overleftrightarrow{A} \neq 0$. We suppose that, in a general case, $K \neq 0$ for $\overleftrightarrow{\epsilon}_{as} \neq 0, \overleftrightarrow{\mu}_{as} \neq 0$, and $\overleftrightarrow{A} \neq 0$.

Let all ports, besides ports p and q, be short-circuited. In this case, the left-hand side of (2) may be rewritten in terms of normalized voltages applied to ports p and q and in terms of admittance matrix [Y] [15]. As a result, we have for (2):

$$\left(V_a^{(p)} V_b^{(q)} - V_b^{(p)} V_a^{(q)}\right) \left(Y_{pq} - Y_{qp}\right) = K \tag{3}$$

Normalized voltages $V_a^{(p)}, V_b^{(q)}, V_b^{(p)}$ and $V_a^{(q)}$ are arbitrary. Therefore, the nonreciprocal difference for parameters of the admittance matrix, $Y_{pq} - Y_{qp}$, is defined by integral K.

Taking into account correlation between the admittance matrix [Y] and scattering matrix [S] [15], one can rewrite (3) as follows:

$$Q\left(S_{pq} - S_{qp}\right) = K \ , \tag{4}$$

where term Q is a coefficient determined by amplitudes of the fields. Since coefficient Q is arbitrary, nonreciprocal difference for parameters of the scattering matrix, $S_{pq} - S_{qp}$, is defined by integral K.

Now the main question arises: When devices with integral $K \neq 0$ can be really characterized as nonreciprocal devices? Let us suppose that we have an Y-circulator constructed as a three-port waveguide junction with enclosed a sample of a bianisotropic material. When in (4) $K \neq 0$, one can realize a matched nonreciprocal three-port junction [15,16]. In a case of ferrite devices, we have an example of the magnetic group of symmetry of a system: "a waveguide junction + dc magnetic field" [17]. One of the main principle of the known nonreciprocal devices [3] sounds as: simultaneous exchange of ports and dc magnetic field direction does not alter the transmission properties. This principle follows from relation (4) if K alters its sign with alteration of dc magnetic field direction. The sign of K, in turn, will be changed when tensors, $\overleftrightarrow{\epsilon}_{as}, \overleftrightarrow{\mu}_{as}$ and $\overleftrightarrow{A}$ change their signs for opposite dc magnetic field direction. It is evident that we satisfy these conditions when relations (1) take place. Is one able to realize an Y-circulation without satisfaction to the principle of nonreciprocal devices mentioned above? When an answer to this question is positive, one will have *enantiomorphic devices*: left- or right-handed Y-circulators. The MCBMs give an example of nonreciprocal bianisotropic materials that allow to realize devices which satisfy the principle of nonreciprocal devices mentioned above. In comparison with the known gyrotropic media where the effect of nonreciprocity is due to the time-reversal invariance of microscopic equations of motion in ferrites or plasmas, in the MCBMs we have the effect of *nonreciprocal magnetoelectric coupling* between electric and magnetic dipoles in every bianisotropic particle. This, our standpoints, is based on consideration of microscopic properties of the MCBM-particles [13,18].

4. Discussion and Conclusion

To ensure "physicality", we have to rely on the generalized principle of kinetic coefficient symmetry for bianisotropic media - the Onsager-Casimir principle. It was shown in [13,18] that, in a general case, reciprocity relations (1) may not correspond to dynamical constitutive symmetry obtained from Onsager-Casimir principle. The answer to the question: Whether the *microscopic properties* of a bianisotropic medium "permit" the time-reversal operations, should be found from an analysis of the symmetry of the dynamical processes in the MCBM-particles under the time-reverse operations. *Nonsymmetry of the constitutive matrix is a measure of nonreciprocity in the MCBMs.* In accordance with (4), we can characterize a measure of nonreciprocity for

a bianisotropic medium by the matrix parameter $\overleftrightarrow{A}=\overleftrightarrow{\xi}+\overleftrightarrow{\xi}^{T}$. Our analysis of the network reciprocity shows that the MCBM-devices should satisfy one of the main principle of the known nonreciprocal devices: simultaneous exchange of ports and dc magnetic field direction does not alter the transmission properties.

Can chiroferrites (chiroplasmas) be considered as nonreciprocal bianisotropic materials? Really, in this case, one has a composite medium based on the gyrotropic host material. Constitutive parameters of such media should be dependent on the external dc magnetic field. But, the question is still open: How can one consider the time-reversal operation in media with a lack of symmetry (chiral inclusions)? Any physical justifications based on dynamical constitutive symmetry (the Onsager-Casimir principle) are not applicable in this case.

References

[1] L. A. Vainstein, *Electromagnetic Waves*. Radio i Svays: Moscow, 1988 (in Russian).

[2] V. H. Rumsey, "Reaction concept in electromagnetic theory", *Phys. Rev.*, Vol. 94, pp. 1483-1491 (1954), Errata, Vol. 95, p. 1705 (1954).

[3] R. F. Harrington and A. T. Villeneuve, "Reciprocity relationships for gyrotropic media", *IRE Trans. Microw. Theory Tech.*, Vol. MTT-6, pp. 308-310 (1958).

[4] L. D. Landau and E. M. Lifshitz, *Electrodynamics of Continuous Media*, 2nd ed., Pergamon Press, Oxford, 1984.

[5] P. R. McIsaak, "A general reciprocity theorem", *IEEE Trans. Microw. Theory Tech.*, Vol MTT-27, pp. 340-342 (1979).

[6] J. A. Kong, *Theory of Electromagnetic Waves*. Wiley, New York, 1975.

[7] C. M. Krowne, "Electromagnetic theorems for complex anisotropic media", *IEEE Trans. Antennas Propag.*, Vol. AP-32, pp. 1224-1230 (1984).

[8] C. Altman and K. Suchy, *Reciprocity, Spatial Mapping and Time Reversal in Electromagnetics*, Kluwer Acad. Publisher, Dordrecht, 1991.

[9] E. O. Kamenetskii, "On the technology of making chiral and bianisotropic waveguides for microwave propagation", *Microw. Opt. Technol. Lett.*, Vol. 11, No. 2, pp. 103-107 (1996).

[10] E. O. Kamenetskii, I. Awai, and A. K. Saha, "Bianisotropic particles based on magnetostatic resonators: A way to realize microwave bianisotropic materials and devices", in *Proceedings of the 29th European Microwave Conference*, Munich, Germany, Vol. 1, pp. 40-43 (1999).

[11] E. O. Kamenetskii, I. Awai, and A. K. Saha, "Experimental evidence for magnetoelectric coupling in a ferromagnetic resonator with a surface metalization", *Microw. Opt. Technol. Lett.*, Vol. 24, No. 1, pp. 56-60 (2000).

[12] E. O. Kamenetskii, "Theory of bianisotropic crystal lattices", *Phys. Rev. E*, Vol. 57, pp. 3563-3573 (1998).

[13] E. O.Kamenetskii, "Quasistatic principles in the macroscopic electrodynamics of bianisotropic media", *Phys. Rev. E.*, Vol. 58, pp. 7965-7973 (1998).

[14] E. O . Kamenetskii, "Energy balance equation for electromagnetic waves in bianisotropic media", *Phys. Rev. E*, Vol. 54, pp. 4359-4367 (19o.6, pp. 412-416 (1996).

[15] J. L. Altman, *Microwave Circuits*, Van Nostrand, Princeton, 1964.

[16] A. Gurevich and G. Melkov, *Magnetic Oscillations and Waves*, CRC Press, New York, 1996.

[17] V. A. Dmitriev, "Generators of magnetic groups of symmetry and commutation relations", *IEEE Trans. Microw. Theory Techniq.*, Vol. 43, pp. 2668-2675 (1995).

[18] E. O. Kamenetskii, "Onsager-Casimir principle and reciprocity relations for bianisotropic media", *Microw. Opt. Technol. Lett.*, Vol. 19, No.6, pp. 412-416 (1998).

Electromagnetic Waves in Chiral Media with Compensated Anisotropy

I. V. Semchenko[1], S. A. Khakhomov[1], S. A. Tretyakov[2], and A. H. Sihvola[2]

[1] Department of General Physics, Gomel State University
Sovyetskaya Str. 104, 246019, Gomel, Belarus
Fax: + 375-232-576557; E-mail: khakh@gsu.unibel.by

[2] Electromagnetics Laboratory, Helsinki University of Technology
P.O. 3000, FIN-02015 HUT, Espoo, Finland
Fax: +358-9-451-2267; E-mails: sergei.tretyakov@hut.fi; ari.sihvola@hut.fi

Abstract

We consider and compare three different cases of anisotropy compensation in chiral media. The first case concerns natural crystals or nonmagnetic superlattices, the second case is the class of stratified-periodic structures, which are homogeneous media in the long-wave approximation and have simultaneously dielectric and magnetic properties. The third possible case can be realized as inhomogeneous structures with spiral anisotropy of dielectric and magnetic properties.

1. Natural Crystals and Nonmagnetic Superlattices

Effect of compensation of dielectric anisotropy of natural gyrotropic crystals $AgGaS_2$ (silver gallium sulphide) and $CdGa_2S_4$ (cadmium gallium sulphide) was observed for the first time by M.V. Hobden in 1967 and 1968 [1, 2]. For these crystals the dispersion curves of the main values of the uniaxial tensor of permittivity $\varepsilon_1(\omega)$ and $\varepsilon_2(\omega)$ cross each other at a certain frequency. For the light of this frequency crystal becomes isotropic and its chiral properties are not masked by linear birefringence. The crystal $AgGaS_2$ (class $\overline{4}2m$) is optically isotropic at the wavelength $\lambda_0 = 4970$ Ångström, the rotatory power is equal to 522 degrees/mm [1]. The crystal $CdGa_2S_4$ of class $\overline{4}$ has the isotropic point at the wavelength $\lambda_0 = 4872$ Ångström. This crystal shows the rotatory power of 17.3 degrees/mm and 11.6 degrees/mm for different directions of light propagation [2].

Effect of compensation of dielectric anisotropy is possible also in nonmagnetic stratified-periodic media (superlattices), where the "isotropic point" can be shifted under the action of external magnetic fields or under elastic deformation of crystal.

Media with new optical properties can be created by combination of crystals possessing necessary features. Modern technology allows to manufacture multilayered periodic systems (superlattices) with a period from 10 to 1000 Ångström [3]. Electromagnetic properties of superlattices are easily modelled in the long wavelength approximation, which is valid if the wavelength of electromagnetic or ultrasonic waves propagating in the lattice is large compared to the period of the structure. In this case it is possible to consider a superlattice as a uniform medium characterised by a set of effective parameters. Thereby, properties of superlattices can combine useful properties of their constituents, that is, crystals, from which these lattices are formed. The important property of superlattices is the difference between their crystallographic symmetry and the symmetry of crystals used as layers. For example, if layers are isotropic,

superlattice as a whole is a uniaxial crystal [4, 5]. Due to such changing of symmetry, interesting effects are possible in superlattices, for instance, acousto-optical interactions [6, 7]. In the last years effective elastic moduli of superlattices with arbitrary crystallographic symmetry of the layers [3, 8], as well as elastooptical [3, 4], piezo-electric [9, 10], electro-optical [11] and nonlinear optical [12, 13] coefficients were theoretically estimated.

Alongside with dielectric, elastic, elasto-optic, piezo-electric and nonlinear properties of superlattices [3]–[13] also their chiral properties arise interest. In particular, it is possible to create superlattices which are dielectrically isotropic for the light at a certain frequency [14, 15].

The electromagnetic properties of chiral superlattices can be described by the constitutive relations [16, 17]

$$\mathbf{D} = \epsilon_0 \overline{\overline{\varepsilon}}^{\text{eff}} \cdot \mathbf{E} - j\sqrt{\epsilon_0 \mu_0}\, \overline{\overline{\kappa}}^{\text{eff}} \cdot \mathbf{H}, \quad \mathbf{B} = \mu_0 \overline{\overline{\mu}}^{\text{eff}} \cdot \mathbf{H} + j\sqrt{\epsilon_0 \mu_0} \left(\overline{\overline{\kappa}}^{\text{eff}}\right)^T \cdot \mathbf{E} \tag{1}$$

with effective tensors of permittivity $\overline{\overline{\varepsilon}}^{\text{eff}}$, chirality $\overline{\overline{\kappa}}^{\text{eff}}$, and permeability $\overline{\overline{\mu}}^{\text{eff}}$. Here the values with index "eff" correspond to the effective medium, and the primed and nonprimed values correspond to the two layers which form the superlattice. The effect of compensation of dielectric anisotropy is possible in nonmagnetic superlattices ($\overline{\overline{\mu}} = \overline{\overline{\mu}}' = \overline{\overline{\mu}}^{\text{eff}} = 1$) formed by two crystals with uniaxial symmetry, whose optical axes are orthogonal to the boundaries of the layers. The condition of isotropy of the effective permittivity of a multilayered periodic structure has the following form:

$$\varepsilon'_{11} + x\left(\varepsilon_{11} - \varepsilon'_{11}\right) = \frac{\varepsilon'_{33}\varepsilon_{33}}{\varepsilon_{33} + x\left(\varepsilon'_{33} - \varepsilon_{33}\right)} \tag{2}$$

The axis number 3 is orthogonal to the boundaries of the layers. The period of the structure $\mathcal{D}$ is connected with the thicknesses of the layers by the relation $\mathcal{D} = d + d'$. The notations for the relative thickness of each layer have been introduced: $x = d/\mathcal{D}$, $1 - x = d'/\mathcal{D}$.

As the graphical method shows, equation (2) has a real root on the interval $0 < x < 1$, if the first layer is a positive crystal, but the second one is a negative crystal. This means that relation $\operatorname{sgn}\left(\varepsilon_{11} - \varepsilon_{33}\right) = -\operatorname{sgn}\left(\varepsilon'_{11} - \varepsilon'_{33}\right)$ holds. In this case mutual compensation of the anisotropy of the permittivity of layers takes place, and the properties of the superlattice with respect to the light of corresponding frequency are described by an effective scalar parameter of permittivity and by the effective tensor of chirality.

2. Superlattices with Dielectric and Magnetic Properties

Effect of mutual compensation of dielectric and magnetic anisotropy in nongyrotropic media was predicted by F.I. Fedorov [16]. This effect becomes possible in the medium if the tensors of its permittivity and permeability are proportional to each other at a certain frequency of light. This condition can be reached in periodic stratified structures, whose effective parameters combine dielectric and magnetic properties of the layers. In the long-wave approximation propagation of light in such media can be described by effective tensors of permittivity and permeability.

We have averaged the vectors of electromagnetic field in the volume of the crystal in accordance with the methods developed in paper [3], which allows to determine the effective parameters, characterising the optical properties of the chiral superlattice [14, 15]:

$$\frac{1}{\varepsilon_{33}}, \quad \frac{\varepsilon_{i3}}{\varepsilon_{33}}, \quad \varepsilon_{ik} - \frac{\varepsilon_{i3}\varepsilon_{k3}}{\varepsilon_{33}}, \quad \frac{1}{\mu_{33}}, \quad \frac{\mu_{i3}}{\mu_{33}}, \quad \mu_{ik} - \frac{\mu_{i3}\mu_{k3}}{\mu_{33}} \tag{3}$$

$$\frac{\kappa_{33}}{\varepsilon_{33}\mu_{33}}, \quad \frac{1}{\varepsilon_{33}}\left(\kappa_{3m} - \kappa_{33}\frac{\mu_{m3}}{\mu_{33}}\right), \quad \frac{1}{\mu_{33}}\left(\kappa_{m3} - \kappa_{33}\frac{\varepsilon_{m3}}{\varepsilon_{33}}\right) \tag{4}$$

$$\kappa_{mn} - \frac{\varepsilon_{m3}}{\varepsilon_{33}}\kappa_{3n} - \left(\kappa_{m3} - \kappa_{33}\frac{\varepsilon_{m3}}{\varepsilon_{33}}\right)\frac{\mu_{n3}}{\mu_{33}} \tag{5}$$

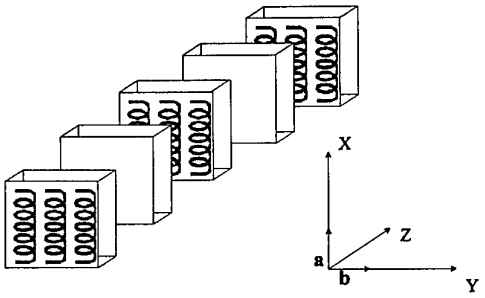

Figure 1: Geometry of the problem. The axes of the spirals are oriented along the x axis. The incident wave propagates along the z axis.

We have to substitute all these values in the generic relation

$$A^{\text{eff}} = xA + (1-x)\,A' \tag{6}$$

where indices i, k, m, n take values 1 and 2. By means of expressions (3) and relation (6) it is possible to determine the components of the effective tensor of permittivity and permeability, and by means of (4), (5), and (6) we can find the components of the effective tensor of chirality for a superlattice with arbitrary crystallographic symmetry of layers. Let us consider the case when a superlattice is formed by uniaxial crystals with the optical axes oriented perpendicularly to the boundaries of layers, i.e. along the z-axis (unit vector $\mathbf{z}_0$). The z-components are marked by index 3. The tensors of the permittivity and permeability of the first layer can be written as

$$\overline{\overline{\varepsilon}} = \varepsilon_{11}\,\overline{\overline{I}} + (\varepsilon_{33} - \varepsilon_{11})\,\mathbf{z}_0\mathbf{z}_0, \quad \overline{\overline{\mu}} = \mu_{11}\,\overline{\overline{I}} + (\mu_{33} - \mu_{11})\,\mathbf{z}_0\mathbf{z}_0 \tag{7}$$

where $\varepsilon_{11} = \varepsilon_{22}$, $\mu_{11} = \mu_{22}$. Tensors $\overline{\overline{\varepsilon}}'$ and $\overline{\overline{\mu}}'$ of the second layer have a similar type. In this case, as follows from relations (3) and (6), the superlattice is also a uniaxial crystal with the effective tensors of permittivity and permeability

$$\overline{\overline{\varepsilon}}^{\text{eff}} = \varepsilon_{11}^{\text{eff}}\,\overline{\overline{I}} + \left(\varepsilon_{33}^{\text{eff}} - \varepsilon_{11}^{\text{eff}}\right)\mathbf{z}_0\mathbf{z}_0, \quad \overline{\overline{\mu}}^{\text{eff}} = \mu_{11}^{\text{eff}}\,\overline{\overline{I}} + \left(\mu_{33}^{\text{eff}} - \mu_{11}^{\text{eff}}\right)\mathbf{z}_0\mathbf{z}_0 \tag{8}$$

where $\varepsilon_{11}^{\text{eff}} = \varepsilon_{22}^{\text{eff}}$, $\mu_{11}^{\text{eff}} = \mu_{22}^{\text{eff}}$. Mutual compensation of dielectric and magnetic anisotropies in the superlattice takes place at the condition

$$\frac{\varepsilon_{11}^{\text{eff}}}{\mu_{11}^{\text{eff}}} = \frac{\varepsilon_{33}^{\text{eff}}}{\mu_{33}^{\text{eff}}} \tag{9}$$

By means of relations (3) and (6), condition (9) can be presented in the following form:

$$\frac{x\varepsilon_{11} + (1-x)\,\varepsilon'_{11}}{x\mu_{11} + (1-x)\,\mu'_{11}} = \frac{\varepsilon_{33}\varepsilon'_{33}\left[x\mu'_{33} + (1-x)\,\mu_{33}\right]}{\mu_{33}\mu'_{33}\left[x\varepsilon'_{33} + (1-x)\,\varepsilon_{33}\right]} \tag{10}$$

Let us introduce notations for the mean values of the permittivity and permeability:

$$<\varepsilon> = \frac{1}{2}\,(\varepsilon_{11} + \varepsilon_{33}), \quad <\mu> = \frac{1}{2}\,(\mu_{11} + \mu_{33}) \tag{11}$$

and notations for the anisotropy of tensors $\overline{\overline{\varepsilon}}$ and $\overline{\overline{\mu}}$:

$$\Delta\varepsilon = \frac{1}{2}\,(\varepsilon_{11} - \varepsilon_{33}), \quad \Delta\mu = \frac{1}{2}\,(\mu_{11} - \mu_{33}) \tag{12}$$

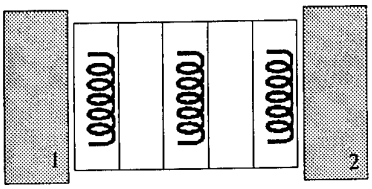

Figure 2: The scheme of the device. 1 is a polarizer, 2 is an analyzer.

Similar notations are used also for the primed and effective values. It is easy to prove (graphically) that equation (10) has a real root x on interval $0 < x < 1$, if the following conditions hold simultaneously:

$$\frac{\Delta\varepsilon'}{<\varepsilon'>} < \frac{\Delta\mu'}{<\mu'>}, \qquad \frac{\Delta\varepsilon}{<\varepsilon>} > \frac{\Delta\mu}{<\mu>} \tag{13}$$

Inequalities (13) mean that for the first layer the relative anisotropy of the permittivity exceeds the relative anisotropy of the permeability. For the other layer the inverse relation is true and the anisotropy of magnetic properties dominates. For instance, this case is possible if the first layer is a nonmagnetic crystal with parameters $\varepsilon_{11} > \varepsilon_{33}$, $\mu_{11} = \mu_{33} = 1$. At the same time the second layer is a crystal possessing only magnetic anisotropy: $\mu'_{11} > \mu'_{33}$, $\varepsilon'_{11} = \varepsilon'_{33} = 1$.

Using condition (9) in the first-order approximation on parameters $\Delta\varepsilon$ and $\Delta\mu$, we find the following relation:

$$\frac{\Delta\varepsilon^{\text{eff}}}{<\varepsilon^{\text{eff}}>} = \frac{\Delta\mu^{\text{eff}}}{<\mu^{\text{eff}}>} \tag{14}$$

This formula means that the anisotropy of dielectric properties compensates the anisotropy of magnetic properties. Because of the frequency dispersion of the parameters of the crystals the considered effect of mutual compensation of dielectric and magnetic anisotropies can exist for a certain light frequency only. Thus, superlattices with the specified properties can be used in devices with frequency-selective transmission of light.

Anisotropic chiral media with pronounced magnetic properties can be realized as a periodic superlattice (period $\mathcal{D}$) in which every period consists of two layers (see Figure 1). One layer is an array of parallel spirals, and this layer exhibits only anisotropic dielectric and chiral properties (manufacture of such media is described in [18]). The other layer has anisotropic magnetic properties (it can be a weakly magnetized ferrite such that off-diagonal components of the permeability dyadic are small, but diagonal components are electrically controlled, and losses can be neglected). The scheme of the device is presented in Figure 2 [19] for the case when optical axes of each layer and of superlattices as a whole are oriented parallelly to the boundaries of layers. Also in this case the effect of compensation of dielectric anisotropy is possible which is similar to the case considered above when the optical axes were oriented perpendicularly to the boundaries of layers.

Similar selective effects take place also in isotropic chiral slabs, since chirality parameter is frequency dependent. We see that due to anisotropy of permittivity and permeability, selectivity can be improved. Indeed, at the point of anisotropy compensation, difference between wavenumbers of two eigenmodes has a minimum. When the balance (14) is not fulfilled (due to changed frequency), this difference increases sharply. The thickness of the sample is chosen as

$$L = \frac{\pi}{2\theta} \tag{15}$$

where $\theta = k_0\kappa_{11}/2$ is the specific rotation of the polarization plane. The angle between the planes of the polarizer and analyser is $\pi/2$. On Figure 3 we demonstrate a typical dependence of the rotation angle on the effective permittivity. For the chosen parameter values the compensation

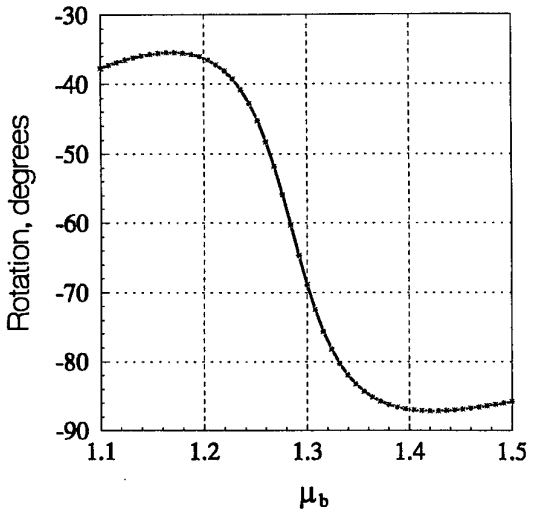

Figure 3: The rotation of the polarization ellipsis of the reflected wave as a function of $\mu_b = \mu_{22}^{\text{eff}}$. The incident wave polarization is perpendicular to the direction of the helix axes (along vector **b**), $\epsilon_{22}^{\text{eff}} = 3.9$, $\epsilon_{11}^{\text{eff}} = 3$, $\kappa_{11}^{\text{eff}} = 0.45$, $\mu_{11}^{\text{eff}} = 1$, $\omega/(2\pi) = 14$ GHz.

point (14) corresponds to $\mu_{22}^{\text{eff}} = 1.3$. We observe that close to this point the rotational power is indeed very sensitive to the material parameter values. This supports our expectation that the use of magnetically anisotropic structures can give a possibility to improve frequency selectivity of microwave and optical filters.

3. Spirally Inhomogeneous Media

Mutual compensation of dielectric and magnetic anisotropy is possible also in spirally inhomogeneous media. In the first case, investigated by Hobden, compensation of anisotropy leads to disappearance of linear birefringence of light. Now, in media with a spiral structure, disappearance of diffraction of waves becomes possible at the condition $\frac{\varepsilon_{11}}{\mu_{11}} = \frac{\varepsilon_{22}}{\mu_{22}}$ or $\frac{\Delta\varepsilon}{<\varepsilon>} = -\frac{\Delta\mu}{<\mu>}$ [20, 21]. In all three cases the properties of eigenwaves of media are considerably changed near the "isotropic point", which can be used for the design of devices for transformation of polarization of electromagnetic waves.

Acknowledgement

Sergei Khakhomov thankfully acknowledges support from the Byelorussian Fund for Basic Researhes in form of a young scientist grant (grant number F99M-055).

References

[1] M. V. Hobden, "Optical activity in a non-enantiomorphous crystal silver gallium sulphide," *Nature,* vol. 216, no. 18, p. 678, 1967.

[2] M. V. Hobden, "Optical activity in a non-enantiomorphous crystal cadmium gallium sulphide," *Nature,* vol. 220, no. 23, p. 88, 1968.

[3] B. Djafari Rouhani and J. Sapriel, "Effective dielectric and photoelastic tensors of superlattices in the long-wavelength regime," *Phys. Rev. B,* vol. 34, no. 10, pp. 7114-7117, 1986.

[4] S. M. Rytov, "Electromagnetic properties of thin-layered medium," *Zhurnal Eksp. i Teor. Fiz.,* vol. 29, no. 5, pp. 605-616, 1955.

[5] S. M. Rytov, "Acoustic properties of thin-layered medium," *Akust. Zhurn.*, vol. 2, no. 1, pp. 71-83, 1956.
[6] A. V. Vakulenko and L. A. Chernozatonskii, "Acoustooptic properties of superlattices in the long wavelength approximation," *Fiz. Tverdogo Tela,* vol. 30, no. 6, pp. 1641-1645, 1988.
[7] J. He and J. Sapriel, "Resonant acousto-optical interaction in superlattices," *Appl.Phys.Lett.*, vol. 55, no. 22, pp. 2292-2294, 1989.
[8] M. Grimsditch and F. Nizzoli, "Effective elastic constants of superlattices of any symmetry," *Phys. Rev. B.*, vol. 33, no. 8, pp. 5891-5892, 1986.
[9] E. Akcakaya and G. W. Farnel, "Effective elastic and piezo-electric constants of superlattices," *J. Appl. Phys.*, vol. 64, no. 9, pp. 4469-4473, 1988.
[10] E. M. Kikkarin and D. V. Petrov, "Effective elastic, piezoelectric and dielectric constants of superlattices," *Kristallografiya,* vol. 34, no. 5, pp. 1072-1075, 1989.
[11] A. V. Vakulenko and L. A. Chernozatonskii, "Effective electrooptic constants of dielectric superlattices," *Fiz. Tverdogo Tela,* vol. 32, no. 11, pp. 3439-3441, 1990.
[12] S. Dutta Gupta, "Validity of the long-wavelength approximation applied to a superlattice on a nonlinear substrate," *J. Opt. Soc. Amer. B.*, vol. 6, no. 8, pp. 1607-1610, 1989.
[13] W. Chen and D. L. Mills, "Optical response on nonlinear multilayer structures: Bilayers and superlattices," *Phys. Rev. B.*, vol. 36, no. 12, pp. 6269-6278, 1987.
[14] I. V. Semchenko, "Gyrotropic properties of superlattices in the long wavelength approximation," *Kristallografiya,* vol. 35, no. 5, pp. 1047-1050, 1990.
[15] V. E. Gaishun, I. V. Semchenko, and A. N. Serdyukov, "Gyrotropic properties of superlattices with magnetic structure in the wavelength approximation," *Kristallografia,* vol. 38, no. 1, pp. 24–27, 1993.
[16] F. I. Fedorov, *Theory of gyrotropy.* Minsk: Nauka i Tekhnika, 1976 (in Russian).
[17] I. V. Lindell, A. H. Sihvola, S. A. Tretyakov, and A. J. Viitanen, *Electromagnetic waves in chiral and bi-isotropic media.* Boston and London: Artech House, 1994.
[18] S. A. Kuehl, S. S. Grove, E. Kuehl, M. Bingle, and J. H. Cloete, "Manufacture of microwave chiral materials and their electromagnetic properties," in *Advances in Complex Electromagnetic Materials* (Kluwer Academic Publishers, NATO ASI Series 3,) vol. 28, pp. 317-332, 1997.
[19] I. V. Semchenko, S. A. Khakhomov, S. A. Tretyakov, and A. H. Sihvola, "Electromagnetic waves in artificial biaxial chiral structures with dielectric and magnetic properties," Helsinki University of Technology, Electromagnetics Laboratory, Report 313, October 1999.
[20] V. A. Kienya and I. V. Semchenko, "Transmission of light through crystals with spiral anisotropic permittivity and permeability," *Kristallografiya,* vol. 37, no. 4, pp. 837-844, 1992.
[21] V. N. Kapshay, V. A. Kienya, and I. V. Semchenko, "Propagation of light in the media with spiral permittivity and permeability," *Kristallografiya,* vol. 36, no. 4, pp. 822-827, 1991.

On the Constitutive Tensors for Bianisotropic Media

V. Dmitriev

University Federal of Para, PO Box 8619
AGÊNCIA UFPA, CEP 66075-900
Belem-PA, Brazil
Tel/Fax: (91) 211-16-34, E-mail: victor@ufpa.br

Abstract

We consider one of the key problems of bianisotropic materials for electromagnetic applications-constitutive relations. The discussion will be restricted to macroscopic level of the tensor description. We will discuss the constitutive tensors under the following assumptions: the media under consideration are linear, homogeneous and in general lossy, possessing space and time dispersion and in general anisotropic. Description in terms of complex field variables and complex parameters of the constitutive tensors allows one to take into account noninstantaneous and nonlocal interaction between electromagnetic fields and matter. In the case of homogeneous media (long-wave approximation), macroscopic properties of the media are described by tensors which are not changed from point to point. This allows one to exclude from consideration translational symmetry and to characterize the properties of the media (and consequently the properties of the electromagnetic field) by tensors in an arbitrary space point. But the point symmetry of the medium in such a description is preserved. Material descriptors are tensor quantities of known symmetry but of unknown numerical values. The symmetry structure of them is frequency and model-independent. The numerical values can be calculated by some physical theories or by experimentation. We will use phenomenological approach based on the first physical principles: Onsager's relations and space-time symmetry.

1. Introduction

The functional dependence **D=D(E,B)**, **H=H(E,B)** in the constitutive relations may be involved and in general contains integral-differential operators. Our discussion will be restricted to macroscopic level of the tensor description. We will consider the constitutive tensors under the following assumptions: the media under consideration are linear, homogeneous and in general lossy. Description in terms of complex field variables and complex parameters of the tensors allows one to take into account non-instantaneous and nonlocal interaction between electromagnetic fields and matter. In the case of homogeneous media (long-wave approximation), macroscopic properties of the media are described by the tensors which are not changed from point to point. This allows one to exclude translational symmetry from consideration and to characterize the properties of the media (and consequently the properties of the electromagnetic field) by the tensors in an arbitrary space point. But the point symmetry of the medium in such a formulation is preserved. Therefore, material descriptors are tensors of known symmetry but of unknown numerical values. The symmetry structure of them is frequency and model-independent. The numerical values can be calculated by some physical theories or by experimentation.

The following discussion will be based on the Tables of the second-rank constitutive tensors for bianisotropic media presented in [1,2]. These tensors have been calculated using the first physical principles: Onsager's relations and space-time symmetry (the point magnetic groups). Notice that by

virtue of the duality between the antisymmetric tensors of the third rank (polar or axial) and of the tensors of the second rank (axial or polar, respectively), we can use these Tables in the case of the media described by antisymmetric tensors of the third rank as well.

We will consider the following phenomenological form of the constitutive relations in the frequency domain:

$$\mathbf{D}=[\varepsilon]\mathbf{E}+[\alpha]\mathbf{B} \tag{1}$$

$$\mathbf{H}=[\beta]\mathbf{E}+[\mu]^{-1}\mathbf{B} \tag{2}$$

where the 3x3 tensors $[\alpha]$ and $[\beta]$ describe the cross-coupling between the electric and magnetic fields. We will call $[\alpha]$ and $[\beta]$ as crosscoupling tensors preserving the term "magnetoelectric tensor" to a special case of the magnetoelectric effect. Notice that the magnetoelectric tensors are a particular case of those published in [1,2]. The magnetoelectric tensors can be obtained using the Tables of [1,2] with an additional constraint $[\alpha]=-[\beta]^t$ where the superscript ^{t} means transposition.

The counterparts of (1) and (2) in the time-domain can be obtained by Fourier superposition. The relations (1), (2) describe a broad class of media with spatial and frequency dispersion.

2. Equivalence of Different Forms of the Constititutive Relations

Different forms of the constitutive relations can be met in literature [3]. We will use the **DH(EB)** presentation (1) and (2) where the fields **D** and **H** are written as linear functions of the fields **E** and **B**. Another form of the relations is the presentation **DB(EH)**:

$$\mathbf{D}=[\varepsilon]\mathbf{E}+[\xi]\mathbf{H} \tag{3}$$

$$\mathbf{B}=[\mu]\mathbf{E}+[\zeta]\mathbf{H} \tag{4}$$

It is not difficult to express the tensors of (1) and (2) in terms of (3) and (4) and vice versa. Moreover, from general properties of the tensors we know that any relation between the tensors expressed as a sum or a product of them, is invariant with respect to the group of the permissible coordinate transformations [4]. It means that if the tensors of the **DB(EH)**-system (3), (4) have been calculated by symmetry principles, the corresponding tensors of the system **DH(EB)** will have the same structure. Therefore the tensor for example, $[\alpha]$ of (1) expressed in terms of the tensors of (3) and (4) will have the same structure as the corresponding tensor $[\xi]$, the tensor $[\beta]$ will have the structure of the tensor $[\zeta]$, etc. Thus the tensor structure obtained by symmetry principles is invariant with respect to the presentations **DB(EH)** or **DH(EB)**. The same is valid for the presentation **EH(DB)**. Therefore, we can use the Tables of [1,2] for all these repersentations.

3. Decomposition of the Constitutive Tensors

Some of the medium properties can be deduced from the tensor decomposition. We can decompose a tensor into a sum of its symmetric and antisymmetric parts, then the symmetric part can be decompose into a sum of a spherical (scalar) one and a deviator, etc. The antisymmetric part of the tensor $[\mu]$ for example may describe an axial vector (dc magnetic field), the deviator of the tensor $[\varepsilon]$ may present the quadrupole electrical moment, etc. Thus we can evaluate the multipole contributions in the constitutive tensors and obtain additional information about the medium. One simple example of the tensor decomposition will be given in Section V.

4. Post's Constraint

During the last decade, we witnessed a strong controversy about interpretation and validity of the Post's constraint [5]. In terms of the tensors $[\alpha]$ and $[\beta]$ of (1) and (2), the Post's condition [6] can be written as follows:

$$\text{Trace } [\alpha] = \text{Trace } [\beta] \tag{5}$$

In order to discuss this constraint, we apply first to a well-recognized condition of reciprocity [3] for the crosscoupling tensors $[\alpha]$ and $[\beta]$:

$$[\alpha]=[\beta]^t \tag{6}$$

The tensors $[\alpha]$ and $[\beta]$ may always be decomposed into a sum of reciprocal and nonreciprocal parts as follows [7]:

$$[\alpha]= [\alpha]_r + [\alpha]_{nr} = ([\alpha] + [\beta]^t)/2 + ([\alpha] - [\beta]^t)/2 \tag{7}$$

$$[\beta]= [\beta]_r + [\beta]_{nr} = ([\beta] + [\alpha]^t)/2 + ([\beta] - [\alpha]^t)/2 \tag{8}$$

where the subscript $_r$ denotes reciprocal part and the subscript $_{nr}$ stands for nonreciprocal part of the tensor. Comparing (7) and (8) we see that the reciprocal parts of the crosscoupling tensors are coupled by the relation

$$[\alpha]_r = [\beta]^t_r \tag{9}$$

However for the nonreciprocal parts, we obtain another relation:

$$[\alpha]_{nr} = - [\beta]^t_{nr} \tag{10}$$

Analogous expressions obtained by quantum-mechanical calculations in the electric quadrupole-magnetic dipole approximation [8, p. 168,169, eqs. 58, 59] coincide structurally (in the sense of symmetry) with (9) and (10). Notice, that each of the magnetoelectric tensors $[\alpha]$ and $[\beta]$ may contain: 1) only reciprocal part, 2) only nonreciprocal part, 3) both reciprocal and nonreciprocal ones.

Now let us analyse the relations (9) and (10). First of all, there is no restriction on dispersion properties of $[\alpha]$ and $[\beta]$ in these identities. The relations (9) and (10) follow trivially from the condition of reciprocity (6) which is in its turn a consequence of time-reversal symmetry of the medium. Secondly, we did not make any restrictions on the losses in the medium, i.e. it may be lossy or lossless. Thirdly, we did not use in these relations any space rotation-reflection symmetry.

Taking into account that the diagonal elements of the tensors $[\beta]_r$ and $[\beta]_{nr}$ in the right-hand sides of (9) and (10) after transposition of the matrices remain in their positions, we obtain

$$(\alpha_{ii})_r = (\beta_{ii})_r \tag{11}$$

$$(\alpha_{ii})_{nr} = - (\beta_{ii})_{nr} \tag{12}$$

where the subscript i=1, 2, 3. The relation (11) means that the diagonal elements of the reciprocal parts of the tensors $[\alpha]$ and $[\beta]$, namely $(\alpha_{ii})_r$ and $(\beta_{ii})_r$ are equal in pairs. Analogously, the diagonal elements of the nonreciprocal parts of $[\alpha]$ and $[\beta]$ in (12), *i. e.*, $(\alpha_{ii})_{nr}$ and $(\beta_{ii})_{nr}$ are equal in pairs with opposite signs.

If the diagonal elements of two matrices are equal in pairs, the traces of these matrices (i.e. the sums of their diagonal elements) must be equal as well. Therefore from (11) and (12), it follows immediately

$$\text{Trace } [\alpha]_r = \text{Trace } [\beta]_r \tag{13}$$

$$\text{Trace } [\alpha]_{nr} = -\text{Trace } [\beta]_{nr} \tag{14}$$

Comparing (13) and (14) with (5) we see that the Post's constrant is fulfilled for reciprocal parts of $[\alpha]$ and $[\beta]$. But for nonreciprocal parts, this constraint is valid if only we extract from the tensors $[\alpha]_{nr}$ and $[\beta]_{nr}$ their spherical (isotropic or scalar) parts. It means that the tensors $[\alpha]_{nr}$ and $[\beta]_{nr}$ must be traceless, i.e.

$$\text{Trace } [\alpha]_{nr} = \text{Trace } [\beta]_{nr} = 0 \tag{15}$$

It corresponds to the obvious fact that the isotropic media cannot be nonreciprocal.

From the above discussion we see that the Post's constraint is a simple consequence of the more strong relations (9) and (10) between the elements of the tensors $[\alpha]$ and $[\beta]$.

5. Examples of the Constitutive Tensors for Some Artificial Media

5.1 Omegaferrites

Recently, a new artificial material which is a combination of a ferrite and chiral particles has been proposed [9]. This material has been called chiroferrite. Earliear, media based on omega-particles embedded in a dielectric host material have been suggested in [10]. Here, we will discuss a new medium with omega elements in the form of a hat embedded periodically or randomly in a magnetized ferrite. The axes of the elements are oriented along the z-axis. One of such elements is shown in Fig. 1.

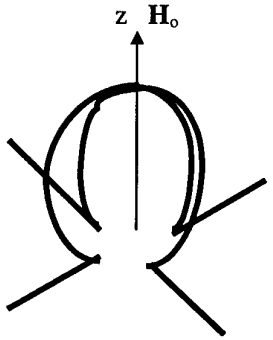

Fig. 1 Omega-element in the form of a hat

Let us first define the magnetic group of symmetry of the omegaferrite medium. The omega element has one four-fold axis of symmetry coinciding with the z-axis. This element possesses also the four plane of symmetry passing through the z-axis. If the omega elements are arranged in a three-dimensional square array with the axes of the elements along the z-axis, the resultant symmetry of the nonmagnetic medium will be $C_{\infty v}$ (in Shoenflies notations), because the four-fold axis is transformed in the axis of infinite order. A uniform dc magnetic field directed along the z-axis has the magnetic symmetry $C_{\infty v}(C_\infty)$. Using the Curie principle of symmetry superposition, we define the resultant symmetry of the omegaferrite medium as $C_{\infty v}(C_\infty)$. The constitutive tensors for media with such a symmetry calculated by the group-theoretical method of [1] are in Table 1.

Table 1

	[μ]	[ε]	[α]	[β]
Omegaferrite $C_{\infty v}(C_{\infty})$	$\begin{vmatrix} \mu_{11} & \mu_{12} & 0 \\ -\mu_{12} & \mu_{11} & 0 \\ 0 & 0 & \mu_{33} \end{vmatrix}$	$\begin{vmatrix} \varepsilon_{11} & \varepsilon_{12} & 0 \\ -\varepsilon_{12} & \varepsilon_{11} & 0 \\ 0 & 0 & \varepsilon_{33} \end{vmatrix}$	$\begin{vmatrix} \alpha_{11} & \alpha_{12} & 0 \\ -\alpha_{12} & \alpha_{11} & 0 \\ 0 & 0 & \alpha_{33} \end{vmatrix}$	$\begin{vmatrix} -\alpha_{11} & -\alpha_{12} & 0 \\ \alpha_{12} & -\alpha_{11} & 0 \\ 0 & 0 & -\alpha_{33} \end{vmatrix}$

Any of the tensors [α] and [β] in accord with (7) and (8) can be decomposed into reciprocal and nonreciprocal part. Consider for example the tensor [α]:

$$[\alpha]=[\alpha]_r+[\alpha]_{nr}=\begin{vmatrix} 0 & \alpha_{12} & 0 \\ -\alpha_{12} & 0 & 0 \\ 0 & 0 & 0 \end{vmatrix}+\begin{vmatrix} \alpha_{11} & 0 & 0 \\ 0 & \alpha_{11} & 0 \\ 0 & 0 & \alpha_{33} \end{vmatrix} \tag{16}$$

This decomposition s easily obtained using the condition of reciprocity (6). Analogous decomposition is valid for the tensor [β]. Therefore the tensors [α] and [β] for omegaferrites contain both reciprocal and nonreciprocal parts. We see from (16) that the nonreciprocity of omegaferrites is defined (along with the tensors [ε] and [μ]) by diagonal elements of the tensors [α] and [β] while the nondiagonal elements of them stipulate reciprocal crosscoupling effect. Also we see from (16) and Table 1 that the reciprocal and nonreciprocal parts of the tensors [α] and [β] satisfy the conditions (9) and (10).
As the next step in the tensor decomposition, we can calculate the spherical (scalar) parts of the diagonal tensors $[\alpha]_{nr}$ and $[\beta]_{nr}$. These parts defined by

$$\pm\frac{1}{3}\begin{vmatrix} (2\alpha_{11}+\alpha_{33}) & 0 & 0 \\ 0 & (2\alpha_{11}+\alpha_{33}) & 0 \\ 0 & 0 & (2\alpha_{11}+\alpha_{33}) \end{vmatrix} \tag{17}$$

correspond to an isotropic nonreciprocal medium which is nonphysical. Therefore, they can be extracted from the tensors. As a result we obtain a relation between the elements of the crosscoupling tensors for omegaferrites:

$$\alpha_{33}=-2\alpha_{11} \tag{18}$$

This condition means that both [α] and [β] must be traceless.

5.2 Ziolkowskii's media

We will demonstrate here how to determine the structure of the constitutive tensors of the media formed by artificial Ziolkowski's moleculas [11]. These moleculas are linear electric and/or magnetic dipole antennas loaded with some combination of passive and/or active electronic elements. The electronic elements are assumed to be nonradiative and the host material is isotropic.

First, consider the moleculas which can be presented by two-ports, i.e. every molecula has only one antenna. The simplest variant is a random distribution of such moleculas in a dilectric matrix which leads to the group of the first category K. If such moleculas are oriented along a certain axis, the medium acquires the symmetry $C_{\infty v}$ of the first category in the case of the electric dipole antennas and the symmetry $D_{\infty h}(C_{\infty h})$ for the magnetic dipole antennas.

The moleculas can have two antennas and therefore can be considered as four-ports. Several variants of the antenna-type combinations with different orientations and the corresponding symmetry groups are presented in Fig. 2. The single arrow in Fig.2 denotes the electric dipole antenna and the double arrow stands for the magnetic dipole antenna. Notice that if the host material is anisotropic

and/or magnetic, the resultant symmetry group can be defined by Curie's principle of symmetry superposition. The constitutive tensors for all the symmetries in Fig.2 are written in [1].

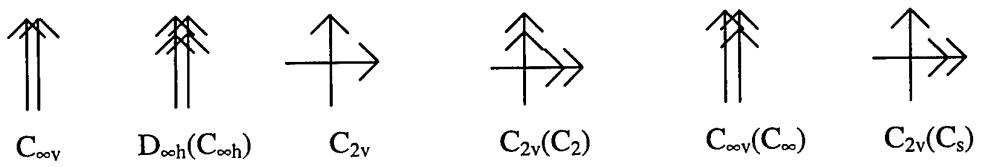

Fig. 2

6. Conclusions

The symmetry analysis presented here is essentially model-independent. Using some electromagnetic models, we can perhaps simplify the structure of the constitutive tensors. But in any case, the structure of them calculated by making use of physical models cannot be more complex that those obtained by symmetry methods.

References

[1] V. Dmitriev, "Tables of the second rank constitutive tensors for linear homogeneous media described by the point magnetic groups of symmetry," *Progress in Electromagnetic Research*, PIERS, vol. 28, 2000, pp.47-99.

[2] V. Dmitriev, "Some general electromagnetic properties of linear homogeneous bianisotropic media following from space and time-reversal symmetry of the second-rank and antisymmetric third-rank constitutive tensors", *The Eur. Phys. J.*, Appl. Phys., to be published.

[3] J. A. Kong, *Electromagnetic Wave Theory*. EMW Publishing, Cambridge, Massachusetts, USA, 1998.

[4] G. A. Korn and T.M. Korn, *Mathematical Handbook for Scientists and Engineers*. McGraw-Hill Book Company, New York, 1968, Ch.16.

[5] W. S. Weiglhofer and A. Lakhtakia, "The Post Constraint Revised", *Archiv fuer Ubertragungstechnik*, vol. 52, pp. 276-278, 1998.

[6] E. J. Post, *Formal Structure of Electromagnetics*. North-Holland, Amsterdam, 1962.

[7] A. H. Sihvola and I. V. Lindell, "Material Effects in Bi-anisotropic Electromagnetics," *IEICE Trans. on Electronics*, vol. E78-C, pp. 1383-1390, 1995.

[8] R. E. Raab and E. B. Graham, "Universal constitutive relations for optical effects in transmission and reflection in magnetic crystals," *Ferroelectrics*, vol. 204, pp. 157-171, 1997.

[9] W. S. Weiglhofer, A. Lakhtakia, and B. Michel, "On the constitutive parameters of a chiroferrite composite medium", *Microw. and Opt. Tech. Lett.*, vol. 5, N18, pp. 342-345, 1998.

[10] S. A. Tretyakov and A. A. Sochava, "Proposed composite material for nonreflecting shields and antenna radoms," *Electron. Lett.*, vol. 29, No. 12, pp. 1048-1049, 1993.

[11] R. W. Ziolkowski, "The design of Maxwellian absorbers for numerical boundary conditions and for practical applications using engineered artificial materials," *IEEE Trans.* Antennas Propagat., vol. AP-45, pp. 656-671, N4, 1997.

Magneto-Electric Jones Birefringence: A Bianisotropic Effect

T. Roth [1,2] and G. L. J. A. Rikken[1]

[1] Grenoble High Magnetic Field Laboratory, Max-Planck-Institut/CNRS
BP 166, F-38042 Grenoble Cedex 9, France
Fax: + 33 476 855610; email: roth@polycnrs-gre.fr

[2] Technische Universität Darmstadt, Germany

Abstract

In 1948, R. C. Jones showed that uniaxial media can in general show four different fundamental optical phenomena, each of which appears in refraction and absorption. Three of them are well-known: isotropic refraction and absorption, linear birefringence and dichroism, circular birefringence and dichroism. The fourth effect has remained unobserved so far. It represents an additional linear birefringence (and dichroism) with its fast and slow axes tilted by 45 degrees with respect to the axes of the standard linear birefringence. Jones birefringence should occur in several uniaxial crystal classes, and isotropic media subjected to external parallel magnetic and electric fields perpendicular to the direction of the light; $\Delta n_J = n_{+45^\circ} - n_{-45^\circ} = k_J \lambda \vec{E} \cdot \vec{B}$. We report the first experimental observation of the magneto-electric Jones birefringence, induced in liquids.

1. Introduction

Many linear optical effects in homogeneous uniaxial media are known, either intrinsic ones due to the symmetry properties of the medium, or effects induced by external influences like magnetic field, electric field, pressure etc. Jones developed a matrix formalism to classify these effects [1]. By a completeness argument, he deduced the existence of a fundamentally new effect in addition to the three known effects cited above. This fourth effect, appearing in refraction and absorption, is called Jones birefringence and Jones dichroism. Jones showed that this new effect can only exist in uniaxial media and that it represents an additional linear birefringence (with its corresponding dichroism), the optical axes of which bisect the optical axes of the standard linear birefringence. Later theoretical work on the basis of symmetry arguments [2] [3] and of generalized polarizability tensor calculations [2] showed that the Jones birefringence occurs intrinsically in many uniaxial crystal classes and can be induced in all media by simultaneously applying parallel magnetic and electric fields perpendicular to the direction of light propagation. This magneto-electric Jones birefringence Δn_J is predicted to be [2] [3]:

$$\Delta n_J \equiv n_{+45^\circ} - n_{-45^\circ} = k_J \lambda \, \vec{E} \cdot \vec{B} \tag{1}$$

where λ is the wavelength, $\vec{E}$ and $\vec{B}$ the external applied electric and magnetic fields. As the external fields can be modulated, the experimental search for the induced Jones birefringence allows high sensitivity (phase sensitive detection) and good discrimination against other effects, in particular the standard linear birefringence $\Delta n = n_{\|} - n_{\perp}$ that always accompanies the Jones birefringence. In liquids and gases subjected to electric and magnetic fields, this standard birefringence is present in the form of the Cotton-Mouton effect ($\Delta n \propto B^2$) and the Kerr effect ($\Delta n \propto E^2$). These birefringences will in general be much stronger.

2. Theory

In the following modification of a much more complete treatment of Graham *et al.* [2] [6] we will show that Jones birefringence is a bianisotropic effect. In the expressions for $\vec{D}$ and $\vec{H}$ we retain the dominant terms of the light-matter interaction:

$$D_\alpha = \epsilon_0 E_\alpha + \alpha_{\alpha\beta} E_\beta + G_{\alpha\beta} B_\beta \qquad H_\alpha = \mu_0^{-1} B_\alpha - \chi_{\alpha\beta} B_\beta - \mathcal{G}_{\alpha\beta} E_\beta \tag{2}$$

In a liquid subjected to parallel electric and magnetic fields along the x-axis, E_{ext}, B_{ext}, the tensors become field distorted, for example: $G_{\alpha\beta}(E_{ext}, B_{ext}) = G_{\alpha\beta} + \frac{\partial G_{\alpha\beta}}{\partial B_{ext}} B_{ext} + \frac{\partial G_{\alpha\beta}}{\partial E_{ext}} E_{ext} + \cdots$. The multipole polarization densities are statistical averages over the molecular orientations in the external fields. We consider only polar diamagnetic molecules and only averages proportional to $E_{ext} \cdot B_{ext}$ [2]. The dominant polar contribution is given by:

$$\langle G_{\alpha\beta}(E_{ext}, B_{ext}) \rangle = -\frac{E_{ext} B_{ext}}{kT} \langle \mu_x \frac{\partial G_{\alpha\beta}}{\partial B_{ext}} \rangle \tag{3}$$

Analogous for $\langle \mathcal{G}_{\alpha\beta} \rangle$, but $\langle \epsilon_0 \delta_{\alpha\beta} + \alpha_{\alpha\beta} \rangle = \epsilon_0 \delta_{\alpha\beta}$ and $\langle \mu_0^{-1} \delta_{\alpha\beta} + \chi_{\alpha\beta} \rangle = \mu_0^{-1} \delta_{\alpha\beta}$. We rewrite:

$$D_\alpha = \epsilon_0 \delta_{\alpha\beta} E_\beta + \frac{N E_{ext} B_{ext}}{kT} \langle \mu_x \frac{\partial G_{\alpha\beta}}{\partial B_{ext}} \rangle B_\beta \qquad H_\alpha = \mu_0^{-1} \delta_{\alpha\beta} B_\beta - \frac{N E_{ext} B_{ext}}{kT} \langle \mu_x \frac{\partial \mathcal{G}_{\alpha\beta}}{\partial B_{ext}} \rangle E_\beta \tag{4}$$

We assume plane wave eigenmodes $E_\alpha = E_{o\alpha} e^{-i\omega(t - \frac{n}{c} z)}$ and use the Maxwell equations $E_\alpha = \frac{n}{c} \epsilon_{\alpha z \beta} B_\beta$ and $D_\alpha = -\frac{n}{c} \epsilon_{\alpha z \beta} H_\beta$. This leads, with $\frac{\partial \mathcal{G}_{\alpha\beta}}{\partial B_{ext}} = \frac{\partial G_{\beta\alpha}}{\partial B_{ext}}$ [2], to the wave equation:

$$\begin{pmatrix} n^2 & -\frac{n}{c\epsilon_o} \frac{N E_{ext} B_{ext}}{kT} \langle \mu_x (\frac{\partial G_{yy}}{\partial B_{ext}} - \frac{\partial G_{xx}}{\partial B_{ext}}) \rangle \\ -\frac{n}{c\epsilon_o} \frac{N E_{ext} B_{ext}}{kT} \langle \mu_x (\frac{\partial G_{yy}}{\partial B_{ext}} - \frac{\partial G_{xx}}{\partial B_{ext}}) \rangle & n^2 \end{pmatrix} \begin{pmatrix} E_{o_x} \\ E_{o_y} \end{pmatrix} = \begin{pmatrix} E_{o_x} \\ E_{o_y} \end{pmatrix} \tag{5}$$

The eigenvectors are linearly polarized light at $\pm 45°$ with $\Delta n_J = \frac{1}{c\epsilon_o} \frac{N E_{ext} B_{ext}}{kT} \langle \mu_x (\frac{\partial G_{yy}}{\partial B_{ext}} - \frac{\partial G_{xx}}{\partial B_{ext}}) \rangle$.

3. Experiment

The experimental setup is shown in figure 1. It is a modification of a setup to measure magnetic linear birefringence, the Cotton-Mouton effect [4]. It consists of a HeNe-laser ^{L}, polarizer ^{P}, photoelastic modulator ^{PEM}, Pockels' cell ^{PC}, Fresnel rhomb ^{FR}, sample cell ^{S}, analyzer ^{A} and photodiode ^{PD}. Phase-sensitive feedback loop drives the Pockels' cell to compensate the sample birefringence. Sample lengths varied from 5 to 25 mm. Applied are a static magnetic field $\vec{B}$ and a low frequency alternating electric field $\vec{E} \cdot \cos \Omega t$. A phase sensitive detection of the resulting birefringence at the electric field frequency Ω ($\approx 60 s^{-1}$) is performed. The angle ϕ of the polarization of the light incident on the sample with respect to the magnetic field can be chosen with the Fresnel rhomb. The angle θ between $\vec{B}$ and $\vec{E}$ can be chosen by rotating the electrode assembly. By a proper choice of ϕ and θ and the external fields, the setup can measure electric linear (Kerr), magnetic linear (Cotton-Mouton) and magneto-electric Jones birefringence. The resolution is $\Delta n_J \approx 2 \cdot 10^{-12}$ with applied fields of 17 T and 2,5 $\cdot 10^5 \frac{\mathrm{V}}{\mathrm{m}}$ and a pathlength of 25 mm.

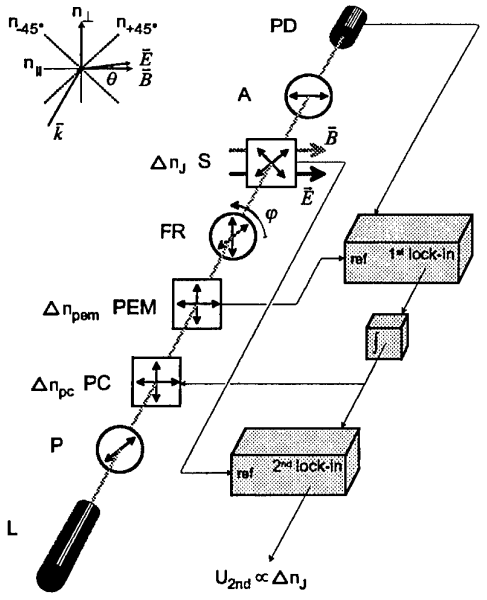

Figure 1: Experimental setup

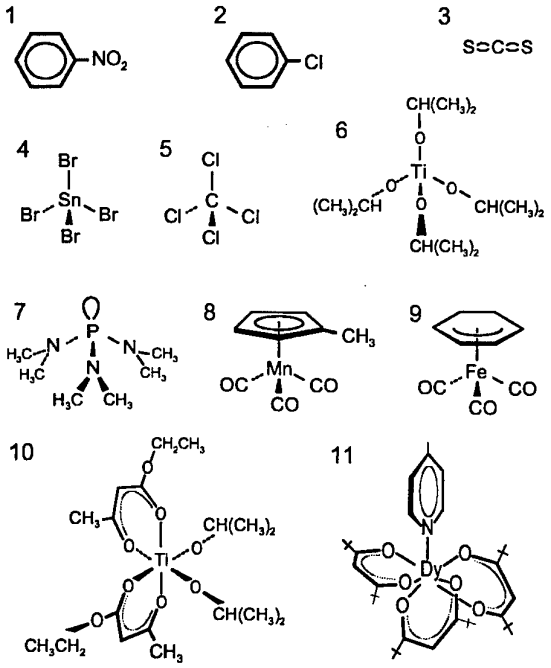

Figure 2: Investigated molecules

The samples were pure molecular liquids or concentrated molecular solutions and non-absorbing at the laser wavelength of 632 nm. They were selected based on the presence of low-lying, high oscillator strength optical transitions and the possibility to have high concentrations. Dipolar **1,2**, quadrupolar **3**, tetrahedral **4-9** and octahedral **10,11** molecules (the symmetries being only approximate) have been examined, see figure 2. Only **8**, **9** and **10** showed a significant Jones birefringence. Typical results for **8** are shown in figure 3, demonstrating explicitly the linear dependence of Δn_J on E, B and $\cos\theta$, thereby proving the existence of the Jones birefringence and confirming equation 1. The table summarizes the results for the molecules **8**, **9** and **10** (the electric field and Δn_J in the last column are rms values). It was further checked that the observed Δn_J is independent of the sample length. The temperature dependence of Δn_J for molecule **8** was measured to be $k_J(T) \propto T^{-x}, x = 0.8 \pm 0.2$. This is consistent with the alignment of a permanent molecular dipole moment by an external field, which would give $x = 1$. We suppose this moment to be the static electric dipole moment.

A further test for the validity of our experimental results consisted of measuring the magneto-electric linear birefringence of **8** and **10** in crossed magnetic and electric fields, both perpendicular to the direction of light propagation. This birefringence, which has the same optical axes as the Kerr and Cotton-Mouton effects, was predicted to have the same magnitude as the Jones birefringence [3] [5]. We found this to be indeed the case.

	μ_e [D]	μ_m [μ_B]	k_J [$\frac{1}{\mathrm{VT}}$]	$\Delta n_J^{17\mathrm{T}/1{,}9\cdot10^5\frac{\mathrm{V}}{\mathrm{m}}}$
8	≈ 4	1,7	$4{,}7 \cdot 10^{-11}$	$9{,}6 \cdot 10^{-11}$
9	≈ 4	≈ 3	$2{,}2 \cdot 10^{-11}$	$4{,}5 \cdot 10^{-11}$
10	$\neq 0$	≈ 0	$5{,}1 \cdot 10^{-12}$	$1{,}0 \cdot 10^{-11}$

We can heuristically summarize our results by noting that a relatively large Jones birefringence is observed in molecules having a low-lying strong charge transfer transition of approximately octupolar symmetry and a permanent electric dipole moment. Note that all liquids must exhibit the magneto-electric Jones birefringence, but the effect is below our detection limit for the other molecules.

Graham and Raab estimated the strength of the Jones birefringence for spherical atoms. They found the following relation between Jones, Cotton-Mouton and Kerr birefringence [2]:

$$\eta \equiv \left| \frac{\Delta n_J}{\sqrt{\Delta n_K \Delta n_{CM}}} \right| = \left| \frac{k_J}{\sqrt{k_K\, k_{CM}}} \right| = 0.016 \qquad (6)$$

The results of Ross *et al.* [3] would imply that η is of the order of α, the fine structure constant (≈ 0.0073). The values we have observed so far are $\eta = 0.0036$ for **8** and **10** and $\eta = 0.0019$ for **9** . This is within one order of magnitude of both predictions. However, values for η that are at least two orders of magnitude smaller than this were found for other molecules. The relation between η and the molecular structure is not yet understood.

Estimates of the absolute strength of Jones birefringence have been made for hydrogen atoms [5]. $k_J = 6 \cdot 10^{-17} \frac{1}{VT}$ was calculated at 1 atm. pressure, which translates to $k_J \approx 10^{-14} \frac{1}{VT}$ for the densities of our molecular liquids. Electrostatic alignment of permanent dipole moments at room temperature increases this by two orders of magnitude [2], thus $k_J \approx 10^{-12} \frac{1}{VT}$. Resonance enhancement due to the low-lying optical transitions may give another order of magnitude, leading to an estimate of $k_J \approx 10^{-11} \frac{1}{VT}$, which is in reasonable agreement with our experimental results for k_J on **8**, **9** and **10**. Empirically, this extrapolation seems only to be valid for those molecules that have optical transitions that involve truly three-dimensional motion of electrons, as is also the case for the hydrogen atom.

4. Conclusion

We have for the first time experimentally observed the Jones birefringence, induced by an electric and a magnetic field in molecular liquids. This observation provides the final validation of the Jones formalism in polarization optics. Our results confirm all qualitative predictions made for the effect. However our understanding of the relation between Jones birefringence and molecular structure is still incomplete.

Acknowledgement

We gratefully acknowledge P. Wyder, B. van Tiggelen, G. Wagnière and R. Raab for helpful discussions and C. Strohm for support. The Grenoble High Magnetic Field Laboratory is a "laboratoire conventionné aux universités UJF et INP de Grenoble".

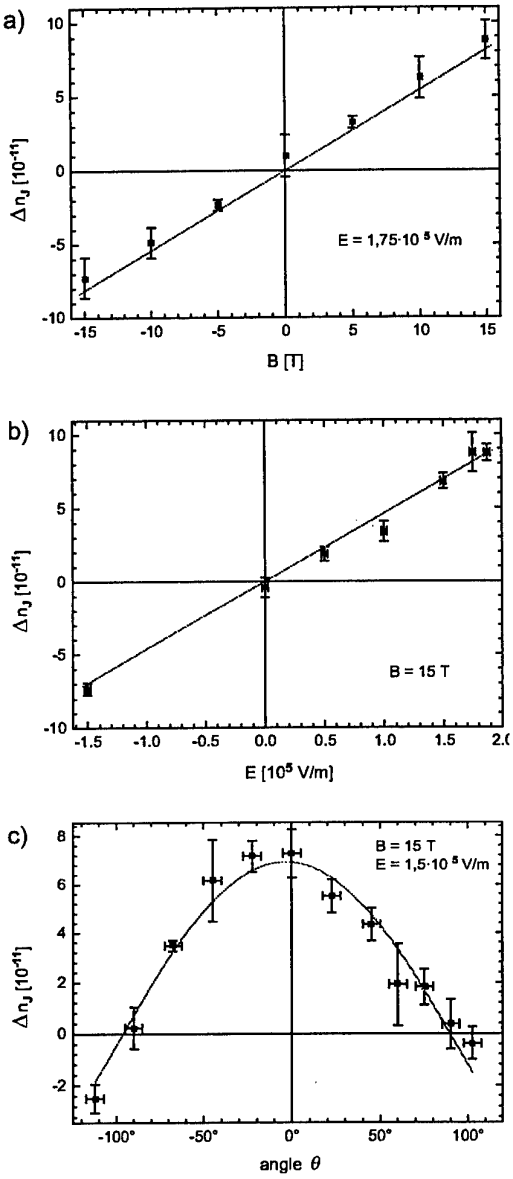

Figure 3: Characteristic dependencies

References

[1] R. C. Jones, "A new Calculus for the Treatment of Optical Systems, VII." *Journ. Opt. Soc. Am.*, vol. 38, no. 8, pp. 671-685, August 1948.

[2] E. B. Graham and R. E. Raab, "On the Jones birefringence" *Proc. R. Soc. Lond. A* vol. 390, pp. 73-90, 1983.

[3] H. J. Ross, B. S. Sherborne, and G. E. Stedman, "Selection rules for optical activity and linear birefringence bilinear in electric and magnetic fields" *Journ. Phys. B: At. Mol. Opt. Phys.*, vol. 22, pp. 459-473, 1989.

[4] G. Maret and G. Weil, "Magnetic birefringence study of the electrostatic and intrinsic persistence length of DNA" *Biopolymers*, vol. 22, pp. 2727-2744, 1983.

[5] E. B. Graham and R. E. Raab, "A molecular theory of linear birefringence induced by crossed electric and magnetic fields" *Mol. Phys.*, vol. 52, no. 5, pp. 1241-1249, 1984.

[6] C. Graham and R. E. Raab, "Eigenvector approach to the evaluation of the Jones N matrices of nonabsorbing crystalline media" *J. Opt. Soc. Am. A*, vol. 11 no. 7, pp. 2137-2144, July 1994.

Session 7

Thursday - September 28, 2000

14:00 - 15:00

Session 7

Complex Media: Random and Nonlinear

Complex Media in Complex Fields: A Statistical Approach

L. R. Arnaut

National Physical Laboratory
Queens Road, GB – Teddington TW11 0LW
Middlesex, United Kingdom
Fax: +44 - 20 - 8943 7176; e-mail: luk.arnaut@npl.co.uk

Abstract

The use of statistical techniques to characterize composite materials systems and their use in complex electromagnetic environments is discussed. Examples of the calculation of uncertainties and distribution functions of wave statistics are given.

1 Introduction

Heterogeneous media which consist of discrete inclusions of various kinds and configured in certain arrangements inside a host medium can be considered as complex electromagnetic (EM) material systems. A rigorous deterministic analytical or computational approach to their analysis is of almost forbidding complexity. Hence one usually takes recourse to simplified effective medium theories. Typically, only mean values (first-order moments) are considered, but this tends to be a significant oversimplification when correlating theoretically predicted characteristics of a composite with measured results for a realistic sample. In particular, variability between different realizations of samples proves to be a dominant factor in the uncertainty budget for the macroscopic constitutive parameters. The resulting uncertainties are furthermore important in assessing the accuracy of the measurement itself, in order to decide on the significance of certain measured effects (e.g. nonreciprocity or chirality), or on the relevant truncation point in any series expansion for their characterization in the long-wavelength regime. In crystal physics, the number of scattering centers is usually very large so as to warrant a negligible level of uncertainty. However for synthetic composites containing a relatively small number of inclusions, this is generally not the case. The uncertainty associated with sample realizations calls for new or improved methods for their characterization. Statistical characterization proves to be an especially powerful method, because the uncertainties *decrease* with increasing degree of complexity of the material system. The results find application, for example, in the characterization of adaptive material systems in active or passive mode of operation [1].

Secondly, a growing trend exists towards the use of complex EM environments as alternative measurement techniques, in order to characterize materials in their operational environment more realistically and accurately. Here, realistic excitation and illumination conditions are being generated, as opposed to the idealized case of single plane-wave illumination. The incident wave must then be considered as quasi-statistical, for the measured effect is due to an ensemble average of a multitude of different directions of incidence or polarization. The same is usually

true for the internal field inside the medium even if the externally incident wave is deterministic. One such complex EM environment simulator is the *NPL* stadium reverberation chamber, in which an ensemble of illuminations is being generated for the EMC testing of equipment or characterization of EM materials or systems [2, 3]. The most general case is of course the one of complex media subjected to complex fields.

2 Statistics of Waves and Media

2.1 Moments

In the general case of complex media subject to complex waves, both the excitation and the constitutive parameters exhibit statistical fluctuations. Sample variability can be taken into account by incorporating a continuous or discrete *realization parameter* τ. For example, in the Lorenz–Lorentz formula the number of inclusions and their dipolarizabilities α thus become random variables. At a given frequency ω:

$$\epsilon(\tau;\omega) = \epsilon_0 + \frac{N(\tau)\ \alpha(\tau;\omega)}{1 - N(\tau)\ \alpha(\tau;\omega)/(3\epsilon_0)} \tag{1}$$

The average of the macroscopic electric polarization $P_e = N\alpha/[1 - N\alpha/(3\epsilon_o)]E$ then satisfies:

$$\langle P_e \rangle = \frac{\langle N\alpha \rangle E + N\alpha\langle E\rangle + \frac{\langle N\alpha\rangle}{3\epsilon_0} P_e}{1 - \frac{N\alpha}{3\epsilon_o}} \tag{2}$$

where $\langle\cdot\rangle$ signifies ensemble averaging. Its variance then follows from $\sigma^2_{P_e} = \langle P_e^2\rangle - \langle P_e\rangle^2$, which also takes the deviation of the spatial distribution of the inclusions from a pure random distribution into account. With $\underline{D} = \epsilon_o\underline{E} + \underline{P}_e$ we can calculate σ^2_D. Its expression for general bianisotropic media has been obtained but is cumbersome. For the case of an anisotropic dielectric:

$$\begin{aligned} \sigma_D^2 &= \langle \underline{D}^\dagger \cdot \underline{D}\rangle - \langle \underline{D}^\dagger\rangle \cdot \langle \underline{D}\rangle \\ &= \left(\underline{E}^\dagger \cdot \langle \underline{\underline{\epsilon}}^\dagger\rangle \cdot \langle \underline{\underline{\epsilon}}\rangle \cdot \underline{E}\right) + \left(\langle \underline{E}^\dagger\rangle \cdot \underline{\underline{\epsilon}}^\dagger \cdot \underline{\underline{\epsilon}} \cdot \langle \underline{E}\rangle\right) + 2\left(\underline{E}^\dagger \cdot \langle \underline{\underline{\epsilon}}^\dagger\rangle \cdot \underline{\underline{\epsilon}} \cdot \langle \underline{E}\rangle\right) - \langle \underline{E}^\dagger \cdot \underline{\underline{\epsilon}}^\dagger\rangle \cdot \langle \underline{\underline{\epsilon}} \cdot \underline{E}\rangle \end{aligned} \tag{3}$$

A similar relation exist for σ^2_B. For an isotropic medium, (3) can be simplified to:

$$\sigma_D^2 = \langle D^2\rangle - \langle D\rangle^2 = \sigma_\epsilon^2 E^2 + \epsilon^2\sigma_E^2 - 2\epsilon E\langle\epsilon\rangle\langle E\rangle \tag{4}$$

where σ_ϵ represents the standard deviation resulting from differences in material processing conditions, as well as differences or uncertainties in the number, spatial distribution, size, shape, etc. of the inclusions.

2.2 Distributions

A full characterization of the wave or medium ensemble requires knowledge of all higher-order statistical moments or, equivalently, the associated probability density function (pdf). Provided the pdf of the constitutive effective medium parameters is known a priori (which is often the case owing to the central limit theorem), wave statistics such as field correlation, wave number, wave impedance, power spectral density etc. can be derived. If the medium can be considered as 'random', which presumes that the number of inclusions is sufficiently large, the ensemble permittivity and permeability exhibit an approximately Gauss normal distribution, on physical

grounds. For the random wavenumber K or random refractive index N, the resulting distribution is then obtained upon the subsequent variate transformations $x = \mu\epsilon$ and $n = \sqrt{x}$ as:

$$f_N(n) = \frac{2n}{\pi\sigma_\mu\sigma_\epsilon} K_0\left[\frac{n^2}{\sigma_\mu\sigma_\epsilon}\right] \tag{5}$$

where $K_0(\cdot)$ is the modified Bessel functions of the 2nd kind of order zero. For the wave random impedance Z, the transformations $y = \mu/\epsilon$, $z = \sqrt{y}$ yield:

$$f_Z(z) = \frac{\sqrt{z}}{\pi\left[(\sigma_\mu/\sigma_\epsilon)z^2 + (\sigma_\epsilon/\sigma_\mu)\right]} \tag{6}$$

For the mean-normalized, statistically isotropic, homogeneous and unpolarized field, whose three complex components exhibit a circular Gauss normal distribution, the real (r) and imaginary (i) parts of $\underline{D}$ and $\underline{B}$ are distributed as:

$$f_{D^{r,i}}(d^{r,i}) = (\pi\sigma_\epsilon\sigma_E)^{-1} K_0\left[\frac{d^{r,i}}{\sigma_\epsilon\sigma_E}\right] \tag{7}$$

The random power density S associated with this isotropic field satisfies, for deterministic constitutive parameters, a χ^2_{2p} pdf:

$$f_S(s) = \frac{s^{p-1}\ \exp(-s/2)}{2^p\ (p-1)!} \tag{8}$$

with $p = 1$ for a Cartesian component and $p = 3$ for the total rms power. For the field magnitude, a χ_{2p} pdf applies:

$$f_{|E_\alpha|}(|e_\alpha|) = \frac{|e_\alpha|^{2p-1}\ \exp(-|e_\alpha|^2/2)}{2^{p-1}\ (p-1)!} \tag{9}$$

Other wave statistics are obtained along similar lines, starting from basic normal random components with a Gauss normal distribution.

2.3 Spatial dispersion

Finite-size effects manifest themselves not only in the size of the material sample, but also in that of the inclusions themselves. For random fields, the effect of the latter on the effective properties can be taken into account by applying theoretical results for general local averaging [2]. The analysis then shows that finite size effects give rise to an decrease in the uncertainty of the constitutive parameters, but to an increase in the *perceived* (i.e. measured) randomness of the medium, as measured by its normalized spectral bandwidth. Typically, for sufficiently small size of the inclusions, the uncertainty will vary according the square of the characteristic length of the inclusion, or with the square of the averaging distance for the statistical field.

Acknowledgement

This work was supported by the 1997-2000 Programme of the UK National Measurement System Policy Unit.

References

[1] L. R. Arnaut, "Adaptive control and optimization of electromagnetic radiation, attenuation and scattering using self-adaptive material systems," submitted for publication.

[2] L. R. Arnaut and P. D. West, "Evaluation of the *NPL* untuned stadium reverberation chamber using mechanical and electronic stirring techniques," *NPL Report CEM 11,* Aug. 1998.

[3] L. R. Arnaut and P. D. West, "Electric field probe measurements in the *NPL* untuned stadium reverberation chamber," *NPL Report CETM 13,* Sep. 1999.

A Spectral Behavior of Fractal Aggregates in the Quasi-static Approximation

V. N. Pustovit and G. A. Niklasson

Department of Solid State Physics, University of Uppsala
The Angstrom laboratory, SE-75121 Uppsala, Sweden
Fax: +46 18 500131; email: Pustovit.Vitaly@angstrom.uu.se

Abstract

In this paper we present a method to calculate optical properties of small fractal clusters of spheres constructed in a recursive manner in the quasistatic approximation. To calculate optical properties of octahedral generator of six spheres we used the dipole-dipole approximation developed in Shalaev theory. After S iterations we received a fractal cluster of N particles with determined optical properties.

1. Introduction

Electromagnetic phenomena in random metal-insulator composites, such as rough thin films, cermets, colloidal aggregates and other, have been intensively studied for the last two decades [1]. These media typically include small nanometer – scale particles or roughness features. Often nanocomposites, within a certain interval of length-scale, are characterized by a random fractal, i.e. scale – invariant structure. Fractals look similar at different scales; in other words, a part of the object resembles the whole [2]. In this paper we study optical absorption by deterministic, recursively constructed three – dimensional fractal aggregates consisting of spherical metallic particles. Usually, it is quite difficult to calculate optical properties of fractal clusters containing a large number of particles. The most convenient way is to use the scale – invariant properties of the fractal structure. To illustrate the geometrical construction of the fractal, consider a cluster of $N = 6$ spheres as shown in Fig.1. Here we depict how the first two stages of such a construction can be built from individual spherical particles. First we calculate the optical properties of a small cluster – generator of six spheres. Further we shall use these aggregates as generators for an iterative procedure to obtain the fractal system after a number of recursive iterations. The optical parameters of these generated clusters are assigned to a new "effective particle", which instead will participate in the iteration process. Finally, after **S** iterations, we receive a fractal cluster of N particles with determined optical parameters. For generators containing six spheres we have applied a method of taking into account pair dipole-dipole interactions between particles within the cluster, developed in the works of Shalaev [3-4].

2. Polarizability of a Cluster and Recursive Approach

We assume that the fractal cluster is located in a continuous dielectric matrix with permittivity $\varepsilon_0 = 1$. We also assume that the size of generator and of the all cluster after S iterations is small compared with the wavelength of incident radiation. This fact will allow us to neglect retardation effects and describe whole system in quasi-static limit. Following the results of previous works [3-4], we can write induced dipole moments of the generator in the form:

$$d_{i,\alpha} = \alpha_0 \left(E_\alpha^{(0)} + \sum_{i \neq j} W_{ij,\alpha\beta} d_{j,\beta} \right) \tag{1}$$

$$W_{ij,\alpha\beta} = \langle i\alpha | W | j\beta \rangle = \left[\delta_{\alpha\beta} - 3 \frac{(r_{ij})_\alpha (r_{ij})_\beta}{r_{ij}^2} \right] \frac{1}{r_{ij}^3} \tag{2}$$

where $W_{ij,\alpha\beta}$ is a quasi-static interaction operator between each pair of particles; $\alpha, \beta = x, y, z$ are the coordinates of particles in three dimensional space; $r_{ij} = |r_i - r_j|$ is a distance between particles; r_i and r_j are the origins of spheres i and j, respectively.

$$\alpha_0 = Ba^3 = \frac{\varepsilon - \varepsilon_0}{\varepsilon + 2\varepsilon_0} a^3 \tag{3}$$

is the usual dipole polarizability of the spherical particle with radius a. The polarizability tensor of the i-th particle interacting with all neighboring $j \neq i$ particles can be found from Eq. (1-2) [3-4]:

$$\alpha_{i,\alpha\beta}(\omega) = \sum_{j,n} \frac{\langle i\alpha | n \rangle \langle n | j\beta \rangle}{\alpha_0^{-1}(\omega) + w_n} \tag{4}$$

where w_n and $\langle i\alpha | n \rangle \langle n | j\beta \rangle$ are eigenvalues and eigenvectors of the interaction matrix W respectively, i.e. $W|n\rangle = w_n |n\rangle$. The average polarizability of the generator is given by:

$$\alpha(\omega) = \frac{1}{3N} \sum_i Tr\left[\alpha_{\alpha\beta}^{(i)}\right] \tag{5}$$

where N is a number of particles in generator.

Consider now the octahedral cluster with $N = 6$ spheres shown in Fig. 1 with sphere radius a and distance between nearest neighbors $R = 2a\sigma$. According to the iteration scheme [5], the radius of the equivalent sphere after the first step of iteration ($S = 1$) is $a(1) = R/2 + a = a(1+\sigma)$. The same procedure can be applied, for example, to the octahedral generator with $N = 7$ spheres, where after the first iteration the equivalent radius becomes $a(1) = a\left(1+\sqrt{2}\sigma\right)$. Taking into account self-similar properties of fractal cluster, we can assume that after S iterations the radius of the single "effective sphere" in the final cluster is [6]

$$a(s) = a(1+\sigma)^s \tag{6}$$

for the $N = 6$ generator. After S steps of the iteration process for $N = 6$ generator, the recursive relation for $B^{(s)}$, which should be used for calculation of "effective sphere" polarization, has a form:

$$B^{(s)} = (1+\sigma)^{-3} \sum_n \frac{\langle i\alpha | n \rangle \langle n | j\beta \rangle}{\left(B^{(s-1)}\right)^{-1} + w_n a^3 (1+\sigma)^{3(s-1)}} \tag{7}$$

Therefore, the extinction cross-section of the fractal cluster with generator $N = 6$ after S iterations should be:

$$\sigma_e^{(s)} = 4\pi k N^s \, \mathrm{Im}\left[a^3 (1+\sigma)^{3(s-1)} \sum_n \frac{\langle i\alpha | n \rangle \langle n | j\beta \rangle}{\left(B^{(s-1)}\right)^{-1} + w_n a^3 (1+\sigma)^{3(s-1)}} \right] \tag{8}$$

where $k = 2\pi/\lambda$ and λ denotes the wavelength of incident radiation in the system.

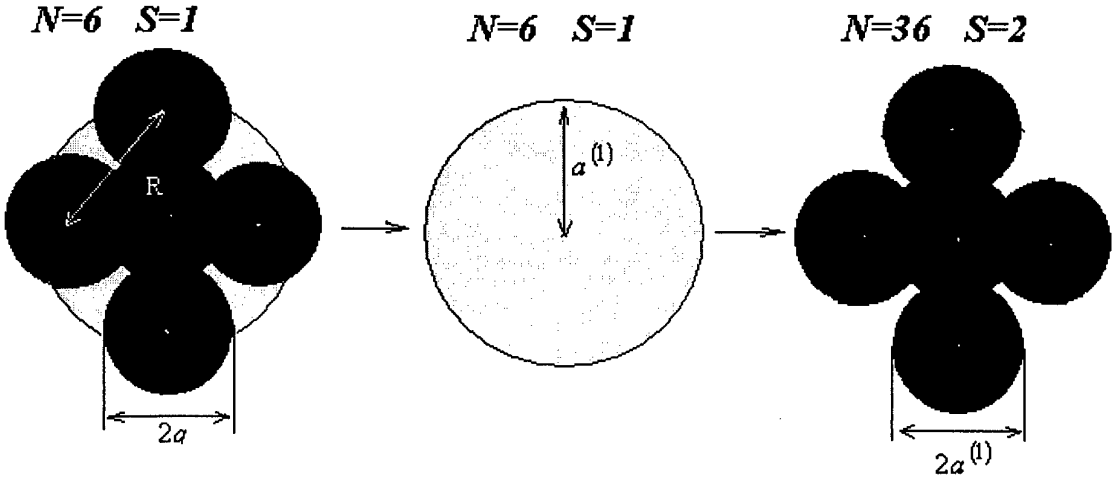

Fig. 1 .The iterative procedure of cluster construction when a cluster of spheres N=6 is replaced by a single equivalent sphere, which is used to construct a larger cluster in a self-similar manner. The fractal dimension of the resulting fractal cluster is $D = \ln(6)/\ln(1+\sigma)$

3. Results and Discussion

We have applied this theory to the deterministic fractal of metallic particles $N = 6$ depicted in Fig. 1 for the $S = 1, 2$ iteration steps. In Fig. 2 we present the results of our calculations by plotting the extinction efficiency of the fractal cluster N = 6 as a function of $\omega = \omega/\omega_p$, where ω_p is a plasma frequency of metallic particles. We have specified the properties of the particle material by the values $\omega_p = 1.37 \cdot 10^{16} s^{-1}$, $\gamma = 7.14 \cdot 10^{13} s^{-1}$. The average size of particles $a = 30\text{Å}$ and diameter $d = 61\text{Å}$, gives us the parameter $\sigma = 1.017$. We observe that the main features of the spectra are present already in the dipolar approximation of the Shalaev theory [3-4]. Our results show that the response of the system is strongly dependent on the volume fraction of particles in cluster, which decreases rapidly with arising number S of iterations. This is very interesting, because in the normal non-fractal structures the volume fraction of particles should be approximately constant with increasing number of iterations (i.e. number of particles in the cluster $N \to \infty$). In the same time the magnitude of spectra also decreases with arising number S. Indeed, the self-similar properties of fractal clusters, which save its geometrical structure, after S iterations make them more "transparent". We have also observed that, in particular, the low frequency peak shift to lower frequencies as parameter σ decreases. It should be noted that the two peaks in Fig.2. are in qualitative agreement with theoretical results obtained by application of Ausloos theory [7]. In experiments on random fractal metal aggregates, a two-peak absorption, qualitatively similar to Fig.2 has been observed [8-11]. We are not aware of any data on the behavior of these peaks as a function of aggregate size or particle separation. For linear chains, the low frequency peak shift to low frequency with increasing number of particles [12]. It would be interesting to investigate whether this is the case for anisotropic fractals also. Our method could, in principle, be used for two-scale anisotropic fractal structures. The present method has large similarities with Discrete Dipole Approximation [13] largely used by astrophysicists. This may point a way to extend the method to large particle clusters beyond the quasistatic limit.

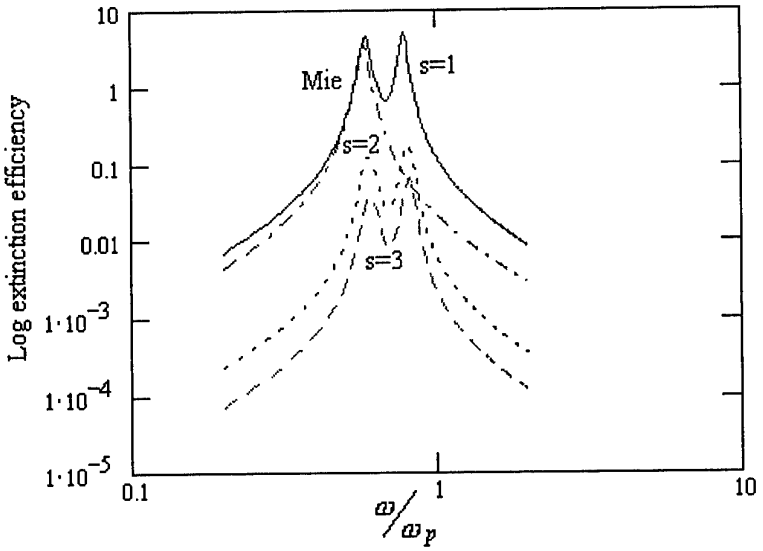

Fig.2. The logarithm of the extinction efficiency as a function of normalized frequency for the generator of 6 spheres (Fig.1.) at σ =1.017. For comparison the results at the first (s=1), second (s=2) and third (s=3) stages of iteration process are shown. The dot-dashed curve gives results of direct application of Mie theory to given cluster of 6 spheres considered as a one spherical particle.

Acknowledgement

One of the authors (V.N.Pustovit) would like to thank the WENNER-GREN foundation for the given support to his work at Uppsala University, Sweden.

References

[1] *Electron Transport and Optical Properties of Inhomogeneous Media,* J. C. Garland and D. B. Tanner (Eds.), AIP, New York, 1987; *Electron Transport and Optical Properties of Inhomogeneous Media* (ETOPIM 3), W .L. Mochan and R. G. Barrera (Eds.), North-Holland, Amsterdam, 1994; Physica A, vol. 241, no. 1-2, pp. 1-452, 1997, *Proceedings of ETOPIM 4*, A. M. Dykhne, A. N. Lagerkov, and A. K. Sarychev (Eds).

[2] B. B. Mandelbrot, *The Fractal Geometry of Nature.* Freeman, San Francisco, 1982.

[3] V. M. Shalaev, *Physics Reports*, vol. 272, no. 2-3, 1996.

[4] V. M. Shalaev, *Nonlinear Optics of Random Media.* Springer Tracts in Modern Physics, vol. 158, 1999.

[5] F. Claro and R. Fuchs, *Phys.Rev. B*, vol. 44, no. 9, pp. 4109-4116, 1991.

[6] P. M. Hui and D. Stroud, *Phys. Rev. B*, vol. 33, no. 4, pp. 2163-2169, 1985.

[7] J. M. Gerardy and M. Ausloos, *Phys.Rev. B*, vol. 25, pp. 4204-4210, 1982.

[8] D. Schonauer, M. Quinten, and U. Kreibig, *Z. Phys. D*, vol. 12, pp. 527-532, 1989.

[9] U. Kreibig, M. Quinten, and D. Schonauer, *Physica Scripta* vol. 13, pp. 84-92, 1986.

[10] J. P. Wilcoxon, J. E. Martin, and D. W. Schaefer, *Phys. Rev. A*, vol. 39, pp. 2675-2688, 1985.

[11] H. Hasegawa, N. Satoh, K. Tsujii, and K. Kimura, *Z. Phys. D*, vol. 20, pp. 325-327, 1991.

[12] M. Quinten and U. Kreibig, *Surface Science*, vol. 172, pp. 557-577, 1986.

[13] K. Lumme and J. Rahola, *Astrophys. J.*, vol. 425, pp. 653-667, 1994.

Modeling of Nonlinear Optical Activity Characteristics of Layered-Periodic Crystal Structures

E. G. Starodubtsev and O. D. Asenchik

Gomel State Technical University
October av. 48, 246746 Gomel, Belarus
Fax: + 375 - 232 - 479165; email: starodub@ggtu.belpak.gomel.by

Abstract

Analytical and numerical modeling of tensor characteristics of nonlinear optical activity for layered-periodic crystal structures (superlattices) is carried out. Calculations are executed in frames of the long wavelength approximation for electromagnetic field at neglecting of the harmonics generation and effect of the probe wave on the effective medium optical characteristics. The relations determining nonlinear optical activity, electrogyration effective tensors for the structures from bianisotropic layers are derived. The detailed analysis is made for the superlattices formed by cubic crystals of GaAs-type. Domains of parameters values at which the effective nonlinear gyrotropy characteristics exceed ones for the monocrystal components of the superlattices are ascertained.

1. General Relations

Effects of parametric crystal optics of layered-periodic structures or superlattices (SL) are intensively investigated last time. Even in frames of the long wavelength approximation for electromagnetic field (the case of short-period SL) these structures can exhibit electrooptical, gyrotropic, magnetooptical properties which are distinguished from ones for the monocrystals forming SL [1-3]. The aim of the paper is investigation of nonlinear optical activity (NLOA) and electrogyration in short-period SL. For the description of electromagnetic properties of SL with account of NLOA one can use material equations [4]

$$D_q = [\varepsilon_{qj}]E_j + i[\alpha_{qj}]H_j, \qquad B_q = \mu_{qj}H_j - i[\alpha_{jq}]E_j, \tag{1}$$

where i^2=-1, and the quantities

$$[\varepsilon_{qj}] = \varepsilon_{qj} + \chi_{qjk}E_k^0 + \theta_{qjkl}E_k^0E_l^0, \qquad [\alpha_{qj}] = \alpha_{qj} + \nu_{qjk}E_k^0 + \tau_{qjkl}E_k^0E_l^0 \tag{2}$$

are the tensors of dielectric permittivity and optical activity depending on the field of the monochromatic controlling wave $\mathbf{E}^0$, q,j,k,l=1,2,3. In Eqs. (2) tensors χ and θ describing nonlinear dielectric properties are real and symmetric relatively to any permutation of the indexes that corresponds to non-absorbing media. The forms of characterizing NLOA real pseudotensors ν and τ are determined by the crystallographic symmetry of the medium [4]. We will assume satisfying Eqs. (1) and (2) for the monocrystal layers and for the short-period SL at substitution of the corresponding

material tensors for the effective tensors. According to Eqs. (1), components of magnetic permeability tensor μ are supposed to be not depending on the controlling electric field $\mathbf{E}^0$.

The general forms of effective tensors $\varepsilon^{(e)}$, $\chi^{(e)}$, $\theta^{(e)}$ and pseudotensor $\alpha^{(e)}$ of linear optical activity were determined (see Refs. in [1,2]). Analogically to [4], let us consider NLOA in the given field approximation, at neglecting: 1) generation of harmonics in the effective medium, 2) effect of the probe wave with a low intensity on the material characteristics of SL. Moreover, the following assumptions will be used: 1) tensors ε (non-disturbed by field $\mathbf{E}^0$) and μ are diagonal, 2) $\mu >> \alpha\chi$, $\tau >> \alpha\theta$, that takes place in a wide range of parameters values [5,6].

Then the methods described in [2,3] and Eqs. (1) and (2) lead to the expressions

$$(\mu_{33}\varepsilon_{33})^{-1}v_{33j},\quad (\mu_{33}\varepsilon_{33}\varepsilon^0_{33})^{-1}v_{333},\quad \varepsilon^{-1}_{33}v_{3ij},\quad (\varepsilon_{33}\varepsilon^0_{33})^{-1}v_{3i3},\quad \mu^{-1}_{33}v_{i3j},$$
$$(\mu_{33}\varepsilon^0_{33})^{-1}v_{i33},\quad v_{ijn},\quad (\varepsilon^0_{33})^{-1}v_{ij3}, \tag{3}$$

$$(\mu_{33}\varepsilon_{33})^{-1}\tau_{33ij},\quad (\mu_{33}\varepsilon_{33}\varepsilon^0_{33})^{-1}\tau_{333i},\quad (\mu_{33}\varepsilon_{33}\varepsilon^0_{33})^{-1}\tau_{33i3},\quad (\mu_{33}\varepsilon_{33})^{-1}(\varepsilon^0_{33})^{-2}\tau_{3333},\quad \varepsilon^{-1}_{33}\tau_{3mij},$$
$$(\varepsilon_{33}\varepsilon^0_{33})^{-1}\tau_{3m3i},\quad (\varepsilon_{33}\varepsilon^0_{33})^{-1}\tau_{3mi3},\quad \varepsilon^{-1}_{33}(\varepsilon^0_{33})^{-2}\tau_{3m33},\quad \mu^{-1}_{33}\tau_{m3ij},\quad (\mu_{33}\varepsilon^0_{33})^{-1}\tau_{m33i}, \tag{4}$$
$$(\mu_{33}\varepsilon^0_{33})^{-1}\tau_{m3i3},\quad \mu^{-1}_{33}(\varepsilon^0_{33})^{-2}\tau_{m333},\quad \tau_{ijmn},\quad (\varepsilon^0_{33})^{-1}\tau_{ij3m},\quad (\varepsilon^0_{33})^{-1}\tau_{ijm3},\quad (\varepsilon^0_{33})^{-2}\tau_{ij33},$$

where i,j,m,n=1,2. Here ε and ε^0 are the permittivity tensors corresponding to the frequencies of the probe and controlling electric fields. At averaging of the form

$$A^{(e)} = xA^{(1)} + (1-x)A^{(2)}, \tag{5}$$

where $x=d^{(1)}/D$ is the relative thickness of the first layer in the SL period D, upper indexes $e,1,2$ here and below denote the quantities characterizing the effective medium, the first and the second crystal layers in the SL period, expressions (3,4) determine all the components of effective tensors $v^{(e)}$, $\tau^{(e)}$ describing NLOA. Expressions (3,4) are also true in the case of the constant controlling electric field $\mathbf{E}^0$. Then tensors $v^{(e)}$ and $\tau^{(e)}$ describe linear and quadratic electrogyration [5] in the considered media.

2. The Structures from GaAs-Type Crystals

Let us determine the form of tensor $\tau^{(e)}$ in the practically important case of SL formed by cubic crystals of class $\bar{4}3m$ (GaAs-type). According to [7,8], these crystals are characterized by the following nonzero components of tensor τ (the axes of the orthogonal coordinate system are parallel to the axes $\bar{4}$):

$$\tau_{3311}=\tau_{1122}=\tau_{2233}=-\tau_{2211}=-\tau_{3322}=-\tau_{1133}=\lambda,\quad \tau_{2323}=\tau_{3131}=\tau_{1212}=-\tau_{3232}=-\tau_{1313}=-\tau_{2121}=\lambda',$$
$$\tau_{3223}=\tau_{1331}=\tau_{2112}=-\tau_{2332}=-\tau_{3113}=-\tau_{1221}=\lambda'', \tag{6}$$

where λ, λ', λ'' are real independent parameters. From expressions (4)-(6) we have (axis Z is perpendicular to the boundaries of the layers)

$$\tau^{(e)}_{3311}=-\tau^{(e)}_{3322}=\frac{<\lambda/(\mu\varepsilon)>}{<1/\mu><1/\varepsilon>},\quad \tau^{(e)}_{3131}=-\tau^{(e)}_{3232}=\frac{<\lambda'/(\varepsilon\varepsilon^0)>}{<1/\varepsilon><1/\varepsilon^0>},\quad \tau^{(e)}_{3223}=-\tau^{(e)}_{3113}=\frac{<\lambda''/(\varepsilon\varepsilon^0)>}{<1/\varepsilon><1/\varepsilon^0>},$$

$$\tau^{(e)}_{1331} = -\tau^{(e)}_{2332} = \frac{<\lambda''/(\mu\varepsilon^0)>}{<1/\mu><1/\varepsilon^0>}, \quad \tau^{(e)}_{1212} = -\tau^{(e)}_{2121} = <\lambda'>, \quad \tau^{(e)}_{2112} = -\tau^{(e)}_{1221} = <\lambda''>, \tag{7}$$

$$\tau^{(e)}_{2323} = -\tau^{(e)}_{1313} = \frac{<\lambda'/(\mu\varepsilon^0)>}{<1/\mu><1/\varepsilon^0>}, \quad \tau^{(e)}_{1122} = -\tau^{(e)}_{2211} = <\lambda>, \quad \tau^{(e)}_{2233} = -\tau^{(e)}_{1133} = \frac{<\lambda/(\varepsilon^0)^2>}{<1/\varepsilon^0>^2}.$$

In Eqs. (7) and below the angular brackets denote averaging according to Eq. (5). It is seen from Eqs. (6) and (7) that the transition from monocrystals to SL is accompanied by increasing threefold the number of independent components of tensor τ. In this case the indexes of the nonzero components of τ do not change. According to [7,8], the general form of this tensor in Eq. (7) has no analogues among monocrystal media. That determines the main characteristic properties of exhibition of NLOA and electrogyration in the considered SL and points to wide opportunities of creating new NLOA materials on the basis of SL.

Values of some components of $\tau^{(e)}$ in Eqs. (7) can exceed the values of the analogical quantities of the monocrystals originating the SL. These components, besides ones which are equal to quantities $\pm<\lambda>$, $\pm<\lambda'>$, $\pm<\lambda''>$, can be written in the form

$$\lambda^{(e)} = \frac{<\lambda/(ab)>}{<1/a><1/b>}, \tag{8}$$

where λ and a, b are scalar parameters taking on values λ, λ', λ'' and μ, ε, ε^0 correspondingly. Then a domain of the parameters values, satisfying the condition $\lambda^{(e)}>\lambda^{(2)}>\lambda^{(1)}$, is determined by the system of inequalities

$$l<1, \quad 0<x<1, \quad \alpha>0, \quad \beta>0, \quad (1-\alpha)(1-\beta)(1-x)>1-l, \tag{9}$$

where $l=\lambda^{(1)}/\lambda^{(2)}$, $\alpha=a^{(1)}/a^{(2)}$, $\beta=b^{(1)}/b^{(2)}$.

According to system (9) an amplification of the considered induced gyrotropy properties at forming SL can take place at a small difference between the NLOA constants ($l \approx 1$) and a strong difference between the dielectric (ε, $\varepsilon^{(0)}$) and magnetic (μ) constants ($\alpha \neq 1, \beta \neq 1$) of the SL components. In particular, at nonmagnetic layers satisfying the condition $\lambda^{(e)}>\lambda^{(2)}>\lambda^{(1)}$ is not possible for all the components of tensor $\tau^{(e)}$ in Eqs. (7), besides $\tau^{(e)}_{2233} = -\tau^{(e)}_{1133}$.

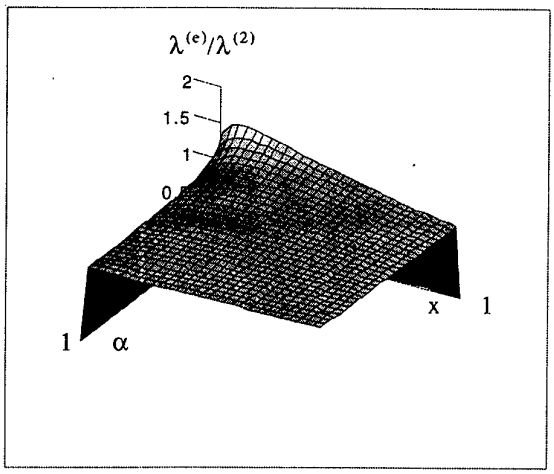

$\beta = 0.5$, $l = 0.99$
Fig. 1

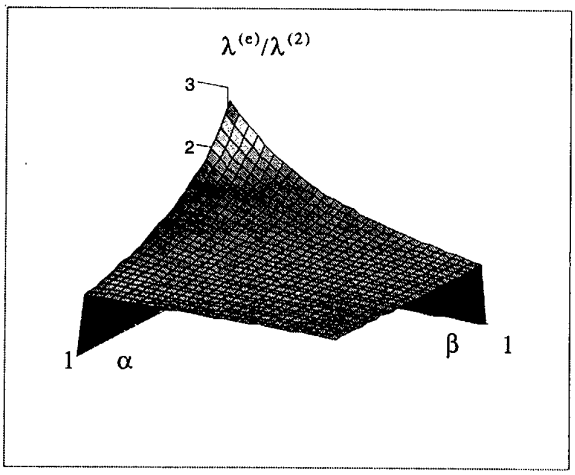

$x = 0.3$, $l = 0.99$
Fig. 2

Relations (8,9) determine also the analogical domains of parameters values for the considered SL at quadratic electrooptical and induced magnetooptical effects [2,3].

Graphs calculated on Eqs. (8) and (9) illustrate possibilities of realization of the condition $\lambda^{(e)}>\lambda^{(2)}>\lambda^{(1)}$ at various values of the parameters.

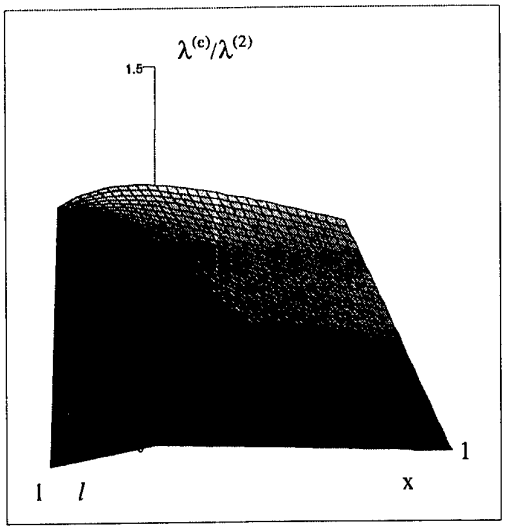

$\alpha = \beta = 0.5$

Fig. 3

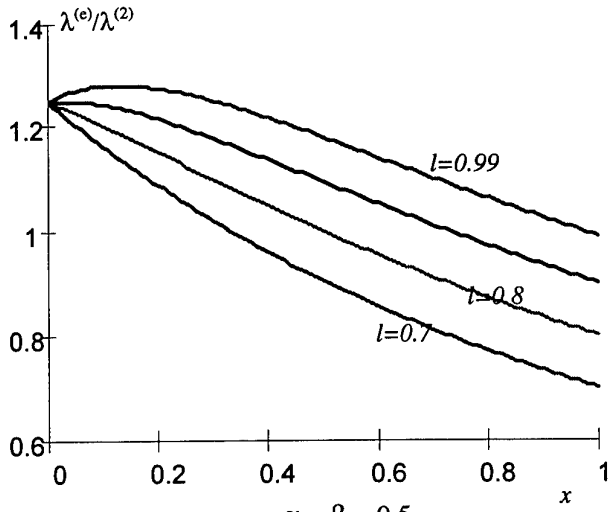

$\alpha = \beta = 0.5$

Fig. 4

References

[1] I. V. Semchenko, "Gyrotropic properties of superlattices in the long wavelength approximation", *Kristallografiya*, vol. 35, no. 5, pp. 1047-1050, 1990.

[2] E. G. Starodubtsev, I. V. Semchenko, and G. S. Mityurich, "Faraday effect and magnetogyration in superlattices in the long wavelength approximation," *NATO ASI Series, 3. High technology,* vol. 28, pp. 169-176, 1997.

[3] E. G. Starodubtsev, "Electrooptical properties of short-period superlattices," in *Proc. Bianisotropics'97*, Glasgow, Great Britain, June 1997, pp. 297-300.

[4] B. V. Bokut' and A.N. Serdyukov, "To the theory of nonlinear optical activity," *Optika i Spektroskopiya*, vol. 38, no. 2, pp. 327-331, 1975.

[5] O. G. Vlokh, *Phemomena of spatial dispersion in parametric crystal optics*, Lvov, 1984.

[6] I. R. Shen, *Principles of nonlinear optics*, Moscow: Nauka, 1989.

[7] L. M. Barkovskii and F. I. Fedorov, "Covariant form of the fourth rank tensors in crystals," *Zhurnal Prikladnoi Spektroskopii*, vol. 12, no. 4, pp. 727-734, 1970.

[8] L. M. Barkovskii, "About pseudotensors of the fourth rank in crystals," *Vestnik BGU*, series I, no. 2, pp. 42-44, 1970.

Poster Session II

Thursday - September 28, 2000

15:00 - 16:30

Poster Session II

Chiral Low Frequency Resonance on an Anisotropically Conductive Cylinder with a Thin Longitudinal Slot

P. A. Malyshkin and A. D. Shatrov

Institute of Radio Engineering and Electronics
Russian Academy of Sciences
Pl. Vvedenskogo 1, 141120 Fryazino, Moscow Region, Russia
Tel. (7-095)526 92 66; Fax (7-095) 203 84 14; E-mail palmal@mail.ru

Abstract

The problem is considered of the diffraction of a circularly polarized wave by an anisotropically conductive cylinder of small radius with a thin longitudinal slot. It is shown that, for a certain relation between the pitch angle of the helical conductive lines and the angular dimension of the slot, one can observe resonance phenomenon that manifests itself in a sharp increase in the scattering cross-section; for a right-handed helix, this resonance phenomenon occurs only when the incident wave is left circularly polarized. At the resonance frequency, the scattered field is left-circularly polarized and has a uniform directional pattern.

1. Introduction

It is known that certain cylindrical objects of small cross dimensions have resonance properties. These are, for instance, a metal cylinder with a longitudinal slot [1] and anisotropically conductive strip where the direction of conductivity makes a small angle with the edges of the strip [2]. The fields scattered by these objects are linearly polarized. In [3], a low frequency chiral resonance was observed in a hollow cylinder with the pitch angle of the helical conductive lines close to $\pi/2$. For right-handed helices, the resonance appears for right circularly polarized wave. The scattered field at the resonance is right circularly polarized and its angular directivity can be described by $\cos\varphi$.

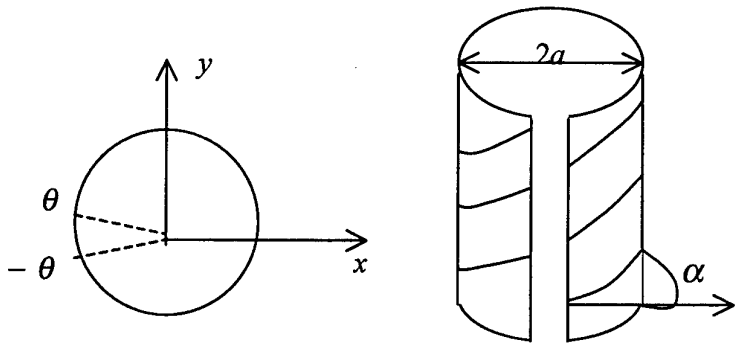

Fig. 1 Anisotropically conductive cylinder with a longitudinal slot.

2. Theory

In this work, we investigate a new electromagnetic object, which is a non-closed cylindrical surface with helical conductivity. We considered the diffraction of a circularly polarized plane wave propagating perpendicular to the z axis by the surface $r=a$, $|\varphi|<\theta$ with the following anisotropic-conductivity boundary conditions:

$$E_z^+ = E_z^-, \tag{1a}$$

$$E_\varphi^+ = E_\varphi^-, \tag{1b}$$

$$E_z \sin\alpha + E_\varphi \cos\alpha = 0, \tag{1c}$$

$$\left(H_z^+ - H_z^-\right)\sin\alpha + \left(H_\varphi^+ - H_\varphi^-\right)\cos\alpha = 0, \tag{1d}$$

where α is the pitch angle of the helix. The z-components of the incident electromagnetic field is given by the formulas

$$H_z^0 = \exp[-ikr\cos(\varphi-\varphi_0)], \tag{2a}$$

$$E_z^0 = \pm i\exp[-ikr\cos(\varphi-\varphi_0)]. \tag{2b}$$

Here and below, the upper and lower indices correspond to the right and left hand circular polarized waves.

The problem is reduced to an integral-differential equation for the surface current $f(\varphi)$, which is related to the jump in the tangential component of the magnetic field by the formulas

$$H_z^+ - H_z^- = -f(\varphi)\cos\alpha, \tag{3a}$$

$$H_\varphi^+ - H_\varphi^- = f(\varphi)\sin\alpha. \tag{3b}$$

The equation for $f(\varphi)$ is as follows:

$$\frac{d^2}{d\varphi^2}\int_{-\theta}^{\theta} A(\varphi-\varphi')f(\varphi')d\varphi' + \frac{d}{d\varphi}\int_{-\theta}^{\theta} B(\varphi-\varphi')f(\varphi')d\varphi' + \int_{-\theta}^{\theta} C(\varphi-\varphi')f(\varphi')d\varphi' = F(\varphi) \tag{4}$$

The kernels A, B, and C are determined by the Green function for open space,

$$G(r,\varphi,r',\varphi') = \frac{i}{4}H_0^{(2)}\left\{ k\left[r^2 + r'^2 - 2rr'\cos(\varphi-\varphi')\right]^{1/2} \right\}, \tag{5}$$

as follows:

$$A = \frac{\cos^2\alpha}{ka}G(a,\varphi,a,\varphi')\cos(\varphi-\varphi'), \tag{6a}$$

$$B=\frac{\cos^2\alpha}{ka}\left[G(a,\varphi,a,\varphi')+a\frac{\partial}{\partial r}G(a,\varphi,a,\varphi')\right]\sin(\varphi-\varphi'), \tag{6b}$$

$$C=ka\sin^2\alpha G(a,\varphi,a,\varphi')+ka\cos^2\alpha G(a,\varphi,a,\varphi')\cos(\varphi-\varphi'). \tag{6c}$$

The left-hand side of equation (4) is determined by the expression

$$F(\varphi)=[i\cos\alpha\cos(\varphi-\varphi_0)\mp\sin\alpha]\exp[-ika\cos(\varphi-\varphi_0)]. \tag{7}$$

The current $f(\varphi)$ obeys the conditions

$$f(\theta)=f(-\theta)=0. \tag{8}$$

For the asymptotic case

$$ka\ll 1,\ \mu=tg\alpha\ll 1,\ \pi-\theta\ll 1, \tag{9}$$

an analytical solution is derived in the following form:

$$f(\varphi)=Df_0(\varphi), \tag{10}$$

where

$$f_0(\varphi)=\ln\left[\cos\frac{\varphi}{2}+\left(\cos^2\frac{\varphi}{2}-\cos^2\frac{\theta}{2}\right)^{1/2}\right]-\ln\cos\frac{\theta}{2}, \tag{11}$$

$$D=\frac{2ka(ka\mp 2\mu)}{1+(ka)^2\left\{2-i\frac{\pi}{2}\left[(ka)^2+4\mu^2\right]\right\}\ln\cos\frac{\theta}{2}}. \tag{12}$$

3. Scattering Cross-Section

The total scattering cross-section σ calculated from the current (10) is determined by the formula

$$k\sigma=\frac{\pi^2}{8}(ka)^2\left[(ka)^2+4\mu^2\right]|D|^2\ln^2\cos\frac{\theta}{2}. \tag{13}$$

As it follows from (12), just as in the case of the problem for a metal cylinder with a longitudinal slot, the resonant frequency is determined by the formula

$$ka=\left|2\ln\cos\frac{\theta}{2}\right|^{-1/2}. \tag{14}$$

Note that, at the frequency

$$ka=2\mu, \tag{15}$$

a right circularly polarized wave does not interact with the cylinder. Therefore, a cylinder with the geometrical parameters μ and θ related by the formula

$$\mu^2 = 1 \Big/ 8 \left| \ln \cos \frac{\theta}{2} \right| \tag{16}$$

exhibits ideal chiral properties at the resonant frequency (14). It does not interact with a right circularly polarized wave and strongly scatters a left circularly polarized wave. Figure 2 shows the scattering cross-sections versus frequency for the left and right circularly polarized waves for $\theta = 175^\circ$ and $\alpha = 12^\circ$.

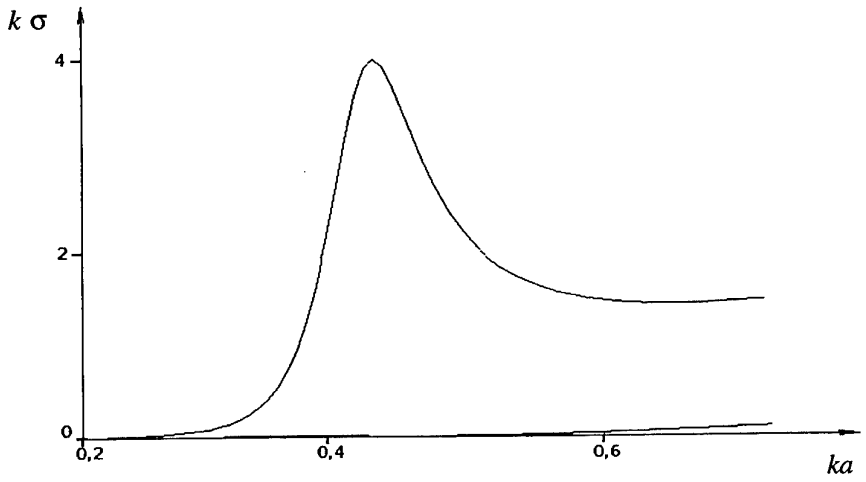

Fig. 2 Scattering cross-sections for left (resonance curve) and right circularly polarized waves for $\theta = 175^\circ$, $\alpha = 12^\circ$.

Thus, an anisotropically conductive cylinder with a longitudinal slot manifests strong polarization selectivity with respect to left and right circularly polarized waves. This fact makes it possible to use such cylinders for the design of artificial chiral media and structures [4].

Acknowledgement

This work was supported by the Russian Foundation for Basic Research, project no. 98-02-16197.

References

[1] A. I. Nosich and V. P. Shestopalov, "An electromagnetic analogue of the Helmholtz resonator," *Dokl. Akad. Nauk SSSR*, vol. 234, no. 1, pp. 53–56, 1977.

[2] P. A. Malyshkin and A. D. Shatrov, "Resonance scattering of electromagnetic waves by a Narrow anisotropically conductive strip," *Radiotekh. Elektron.*, vol. 44, no. 7, pp. 800–805, 1999.

[3] A. N. Sivov, A. D. Chuprin, and A. D. Shatrov, "Low-frequency resonance in a hollow circular cylinder with perfect conductivity along helical lines," *Radiotekh. Elektron.*, vol. 39, no. 10, pp. 1534–1538, 1994.

[4] B. Z. Katsenelenbaum, E. N. Korshunova, A. N. Sivov, and A. D. Shatrov, "Chiral electromagnetic objects," *Usp. Fiz. Nauk*, vol. 167, no. 11, pp. 1201–1212, 1997.

Scattering and Absorption Problems Solution upon the 3-D Chiral and Biisotropic Objects

F. G. Bogdanov, D. D. Karkashadze, and R. S. Zaridze

Tbilisi State University
3 Chavchavadze Ave, 380028 Tbilisi, Georgia
Tel.: +995 32 290821, fax: +995 32 290845, e-mail: rzaridze@resonan.ge

Abstract

An efficient solution to the 3-D scattering and absorption problems of chirality and biisotropy is developed using various types of expansion functions. The necessary conditions to obtain the most optimal solution are outlined. The program complex to compute and visualize scattering, absorption, polarization, energetic, and directive properties of biisotropic and chiral objects is described and applied to solve some applied scattering and antenna problems.

1. Introduction

The problems of microwave behavior of the objects of complicated shape and complex material filling, such as chiral and biisotropic, are to be important both from theoretical and applied viewpoints [1-6]. In this regard, much effort has been devoted in last few years to develop and justify new techniques and codes to solve 2D and 3D problems on chirality and biisotropy. However, most of the results declared for the time being, is restricted to the geometry of objects, the range of material parameters, the type of primary excitation and the accuracy attained and thus no longer satisfy the present-day practical needs.

In this contribution, based on the Method of Auxiliary Sources (MAS) [4-6], an efficient solution to the 3-D scattering and absorption problems of chirality and biisotropy is developed using various types of expansion functions. Farther, the necessary conditions to obtain the most optimal solution are outlined. The program complex to compute and visualize scattering, absorption, polarization, energetic, and directive properties of biisotropic and chiral objects is described. Application of the created computer code to solve the practical problems of interest is illustrated.

2. Brief Description of the Method

The problem discussed here is to find the electromagnetic response of an arbitrary homogeneous biisotropic (including, chiral) object to be excited from outside or within by the given field of primary electromagnetic sources. From the mathematical point of view, this problem can be obviously reduced to solving wave equations

$$\hat{\Im}^{e,i}\,\breve{U}(\vec{r})=0 \tag{1}$$

for unknown potential function of scattered field $\breve{U}(\vec{r})$, with providing the radiation conditions at infinity and satisfying the following boundary conditions on the surface S enclosing the object

$$W\left\{\breve{U}(\vec{r})+\breve{U}_0(\vec{r})\right\}_{r=r^s}=0,\ M(\vec{r}^{\,s})\in S \tag{2}$$

Hereinafter, superscripts e and i concern to the exterior and interior domains, respectively, $\breve{U}_0(\vec{r})$ is a given function of incident field, and W is an operator of boundary conditions ensuring the fields conjugation on the boundary surface S.

Various techniques to solve the boundary problem (1)-(2) differ actually by the method to construct the solution to the equation (1) and to determine the unknown coefficients arising from satisfying the boundary conditions (2). The MAS, in contrast to most other methods, constructs the solutions to (1)

as non-orthogonal expansions in terms of fundamental solutions of (1) with singularities out of the described domain [6]

$$\breve{\vec{U}}(\vec{r}) = \sum_{n=1}^{N^{i,e}} a_n^{i,e} \breve{\Psi}_n(\vec{r}, \vec{r}_n^{\,i,e}), \quad \vec{r} \in D^{i,e} \tag{3}$$

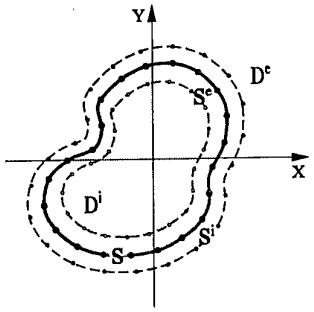

Fig. 1

The sets of points $\{\vec{r}_n^{\,i,e}\}_{n=1}^{N^{i,e}}$ to be distributed at the auxiliary surfaces $S^{i,e}$ (Fig. 1) can be interpreted as the centers of auxiliary sources associated with fundamental solutions $\breve{U}_n(\vec{r}, \vec{r}_n^{\,i,e})$. The amplitudes $a_n^{i,e}$ of these sources should be determined from the boundary conditions (2) by any numerical procedure, in particular, by the collocation method.

3. Application to the Problems of Chirality and Biisotropy

Application of the described scheme to the problems of chirality and biisotropy is of the simplest one if using constitutive relations in Post notations

$$\vec{D} = \varepsilon\vec{E} + i\alpha\vec{B}, \quad \vec{H} = i\beta\vec{E} + \mu^{-1}\vec{B}, \tag{4}$$

where ε and μ are the medium permittivity and permeability, respectively, $\alpha = \xi - i\psi$ and $\beta = \xi + i\psi$ are magnetoelectric admittances, ξ is chirality admittance and ψ is nonreciprocity susceptance.

To determine now fundamental solutions of wave equation (1) for constitutive relations (4), it is necessary first choose the type of the potential function $\breve{U}$. As such a function, any function can be employed which identically define the vectors of electromagnetic field, e.g., electric and magnetic vector potentials $\vec{A}^{e,m}$, Debye scalar potentials ${}^{e,m}\Pi$, Hertz vectors $\vec{Z}^{e,m}$, spinor dyad of Hertz potential $\bar{\bar{Z}}$, spinor dyad of electromagnetic field $\bar{\bar{F}}$ or any field vector $\{\vec{E}, \vec{H}, \vec{D}, \vec{B}\}$. It is convenient, however, to choose such a potential function, which leads to the simpler form of wave operator $\hat{\Im}$ and the relations to the field vectors.

Thus, when choosing $\vec{E}$ or $\vec{H}$ as potential function $\breve{U}$, wave operator $\hat{\Im}$ is of the form

$$\hat{\Im} = (\vec{\nabla}^2 + k^2)\bar{\bar{I}} + \omega\mu(\alpha + \beta)\vec{\nabla}\times\bar{\bar{I}}, \qquad k = \omega\sqrt{\varepsilon\mu}, \tag{5}$$

and fundamental solutions of wave equation (1) are found to be as follows

$$\breve{\Psi}(\vec{r}, \vec{r}') = \left[\hat{\gamma}^r G^r(|\vec{r} - \vec{r}'|) - \hat{\gamma}^\ell \vec{G}^\ell(|\vec{r} - \vec{r}'|)\right]\Re\vec{\tau}(\mathrm{r}'), \tag{6}$$

where $\hat{\gamma}^{r,l} = \vec{\nabla}\times\bar{\bar{I}} \pm k_{r,l}^{-1}\vec{\nabla}\vec{\nabla} \pm k_{r,l}\bar{\bar{I}}$ are vector differential operators for right-hand (r) and left-hand (ℓ) wavefields, $\Re = -\frac{1}{\omega\mu}\frac{\eta_c^\ell\eta_c^r}{\eta_c^\ell + \eta_c^r}$ is normalized coefficient, $\bar{\bar{I}}$ is a unit matrix,

$$G^{r,\ell} = \frac{1}{4\pi|\vec{r} - \vec{r}'|} e^{ik_{r,\ell}|\vec{r} - \vec{r}'|} \tag{7}$$

are scalar Green's functions for outgoing waves with wavenumbers

$$k_{r,\ell} = k\{[1 + \eta^2(\alpha + \beta)^2/4]^{1/2} \pm \eta(\alpha + \beta)/2\}, \quad \eta = \sqrt{\mu/\varepsilon}, \tag{8}$$

and wave impedances

$$\eta_c^{r,\ell} = \eta/\{1 + \eta^2(\alpha + \beta)^2/4]^{1/2} \pm \eta(\alpha - \beta)/2\}, \tag{9}$$

$\vec{\tau}(\vec{r}')$ is a unit vector tangential to the auxiliary surface at the point $\mathrm{M}'(\vec{r}')$.

If introducing as potential function the spinor dyad of electromagnetic field $\breve{U} \equiv \bar{\bar{F}}$, wave operator $\hat{\Im}$ is of the form

$$\hat{\Im} = \vec{\nabla} \times \bar{\bar{I}} - \bar{k}\,\bar{\bar{I}} \tag{10}$$

and the fundamental solutions of (1) are obtained to be as follows

$$\bar{\bar{\Psi}}(\vec{r} - \vec{r}') = \hat{\bar{\gamma}}\,\bar{G}(\vec{r} - \vec{r}')\Re\bar{\bar{\tau}} \tag{11}$$

where $\bar{k} = \begin{pmatrix} k_r & 0 \\ 0 & -k_\ell \end{pmatrix}$, $\hat{\bar{\gamma}} = \begin{pmatrix} \hat{\gamma}^r & 0 \\ 0 & -\hat{\gamma}^\ell \end{pmatrix}$ and $\bar{G} = \begin{pmatrix} G^r & 0 \\ 0 & G^\ell \end{pmatrix}$ are the matrices of wave-numbers, vector differential operators and Green's functions for right- and left-hand wavefields, respectively. The field vectors $\vec{E}$ and $\vec{H}$ can be found over the potential function via relations

$$\vec{E} = \bar{\chi}\,\bar{\bar{\mathrm{F}}},\ \vec{H} = \bar{\zeta}\,\bar{\bar{\mathrm{F}}}, \tag{12}$$

with rows of parameters

$$\bar{\chi} = (i\eta_c^r\ , -i\eta_c^\ell),\ \ \bar{\zeta} = (1,1) \tag{13}$$

The knowledge of fundamental solutions of wave equation (1) for biisotropic (including, chiral) medium formally completes the construction of solution (3) to the stated boundary problem (1)-(2).

4. Numerical Results

To numerically calculate electromagnetic characteristics of chiral or biisotropic objects by the present method, it is necessary to determine the coefficients $a_n^{i,e}$ of expansions (3) from the boundary conditions (2). To provide the quick convergence and minimal discrepancy of the solution to be sought, the proper choice of the auxiliary parameters, such as the shape and dimensions of auxiliary surface, distribution of the points on the boundary and auxiliary surfaces, *etc.*, is required. It is especially important to properly account for the character and situation of the singularities of continuously extended scattered field across the boundary of the domain to be described.

All the aspects above have been considered to produce the program complex for calculating and visualizing scattering, absorption, polarization, energetic, and directive characteristics of 3-D chiral and biisotropic objects. In the code performed, both isolated and integrated auxiliary sources have been utilized to obtain the optimized and effective solutions. We illustrate here some possibilities of the created code to calculate and visualize radiation, propagation and scattering problems of interest.

Fig. 2 and 3 compare the radiation processes produced by a linear current source placed in a back focus of biisotropic ellipsoid of revolution along (Fig. 2) and perpendicular (Fig. 3) to the axis of revolution. The geometry of ellipsoid is determined by its semi-axises: $a = 0.5$, $b = 0.4$, and medium parameters are: $\varepsilon_r = 2.00006$, $\mu_r = 2.02502$, $\alpha\eta_0 = 0.1885 + i0.754$, $\beta\eta_0 = 0.1885 - i0.754$ ($\eta_0 = 120\pi$). We are interested in distribution of energy density of right-hand (*a*) and left-hand (*b*) wavefields outside the ellipsoid for wavenumber $k = 32$. The parameters of biisotropic medium are chosen so, that mainly left-hand polarization is focused along the axis of ellipsoid. The comparison of Fig. 2 and 3 also shows, that the transverse current source manifests more focusing properties.

Fig. 4 shows the 3-D radiation pattern of ellipsoid of revolution of Fig. 2 and 3 with longitudinal (*a*) and transverse (*b*) excitation. From comparison of Fig. 4-a) and 4-b), it is obvious, that transverse current excitation leads to better directive pattern with weaker lobes. It is also clear, that this pattern is not omnidirectional, and thus one of polarization (left-hand) is dominant. Fig. 5 calculated for situation of Fig. 4-a), but with $k = 400$, shows the increase of directivity and decrease of radiation lobes with growing wavenumber (frequency).

It should be noted, that Fig. 2-5 have been calculated with rather high accuracy (about 0.5%) and only thus allow studying in detail electromagnetic properties of scattering biisotropic objects. Thus, the proper use of the method described allows one to obtain numerical results with predesigned accuracy and to study the practical problems of interest.

References

[1] A. Lakhtakia, *Beltrami Fields in Chiral Media*. World Sci. Publ. Co., pp. 1-536, 1994.

[2] I. V. Lindell, A. H. Sihvola, S. A. Tretyakov, and A. J. Viitanen, *Electromagnetic Waves in Chiral and Bi-Isotropic Media*. Artech House: Boston, London , pp. 1-332, 1994.

[3] J. C. Monzon, "Scattering by a biisotropic body," *IEEE Trans. Antennas Prop.* 43, Vol. 11, pp. 1273, 1995.

[4] F. G. Bogdanov and D. D. Karkashadze, "Conventional method of auxiliary sources in the problems of electromagnetic scattering by the bodies of complex materials," *Electromagnetic and Light Scattering - Theory and Applications*, Bremen, Germany , pp. 133-140, 1998.

[5] F. G. Bogdanov, D. D. Karkashadze., and R. S. Zaridze, "Propagation and scattering by biisotropic objects of complicated shape," in *Proc. Bianisotropics'98,* 7th International Conf. on Complex Media, Braunschweig, Germany, pp. 133-136, 1998.

[6] F. G. Bogdanov, D. D. Karkashadze, and R. S. Zaridze, "The method of auxiliary sources in electromagnetic scattering problems," in *Generalized Multipole Techniques for Electromagnetic and Light Scattering*, Th. Wriedt (Ed.). Elsevier Science B.V., pp. 143-172, 1999.

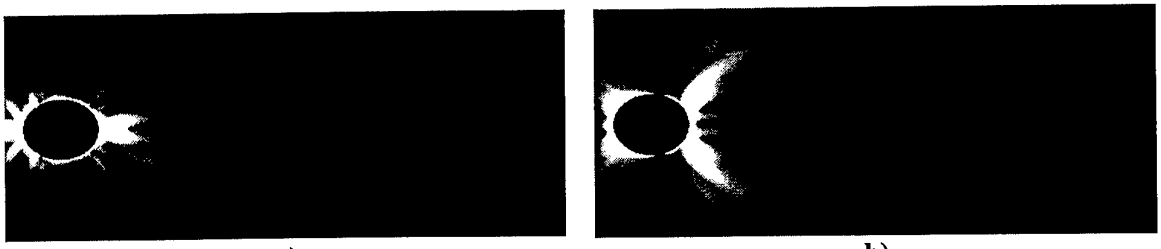

a) b)

Fig. 2

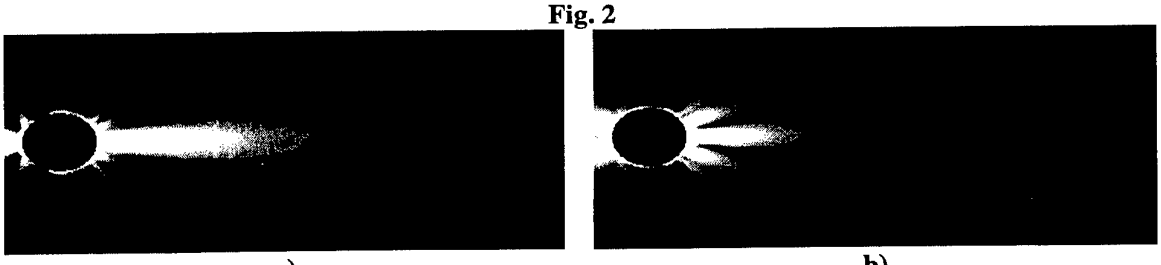

a) b)

Fig. 3

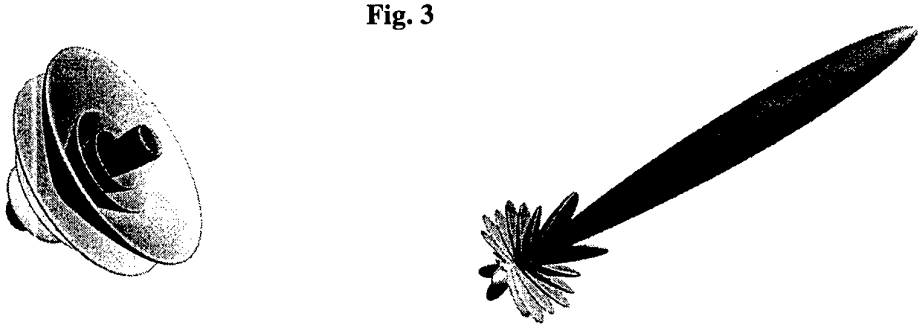

a) b)

Fig. 4

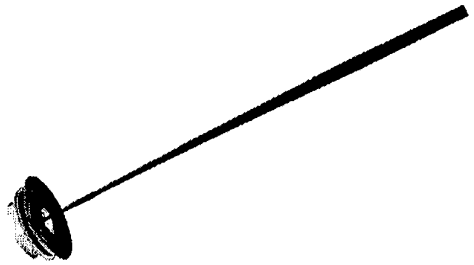

Fig. 5

Numerical Homogenization Studies of Biaxial Bianisotropic Composite Materials

T. G. Mackay and W. S. Weiglhofer

Department of Mathematics, University of Glasgow
University Gardens, Glasgow G12 8QW, Great Britain
Fax: + 44–141–330 4111; email: tm@maths.gla.ac.uk

Abstract

We explore the conceptualization of biaxial composite mediums through the process of homogenization. Biaxiality is found to arise when the component mediums undergoing homogenization present two non–collinear distinguished axes. Two possible sources of directionality in the component mediums are considered: (a) topological and (b) electromagnetic. Examples of these are investigated by considering the homogenization of particulate components with (a) non–spherical topologies and isotropic electromagnetic properties and (b) uniaxial electromagnetic properties and spherical topologies.

1. Introduction

In the context of electromagnetic material properties, the concept of *homogenization* is both scientifically and technologically important. Composite mediums with complex properties may be conceptualized through homogenizing relatively simple constituent mediums. Biaxial symmetry in such homogenized composite mediums (HCMs) is our primary concern here. We build upon the foundation laid by earlier studies of non–dissipative dielectric [1] and dissipative dielectric–magnetic [2] biaxial HCMs (wherein further background details may be found) and generalize to the bianisotropic case. By considering only component mediums of the simplest forms, we demonstrate that an elaborate HCM form can arise; and through illustrative parametric studies, we delineate symmetries in the HCM structure.

2. Preliminaries

We consider HCMs derived from only two (distinct) component mediums, each being envisioned in particulate form; we refer to them as the *host* medium and *inclusion* medium. Of the many formalisms which have been developed in order to estimate the electromagnetic constitutive properties of HCMs, here we adopt the Bruggeman formalism [3, 4, 5]. The HCMs emerging from the numerical calculations may be characterized by the bianisotropic constitutive relations[1]

$$\mathbf{D}(\mathbf{x}) = \epsilon_0 \underline{\underline{\epsilon}}_{HCM} \cdot \mathbf{E}(\mathbf{x}) + \sqrt{\epsilon_0 \mu_0}\, \underline{\underline{\xi}}_{HCM} \cdot \mathbf{H}(\mathbf{x}), \tag{1}$$

$$\mathbf{B}(\mathbf{x}) = \sqrt{\epsilon_0 \mu_0}\, \underline{\underline{\zeta}}_{HCM} \cdot \mathbf{E}(\mathbf{x}) + \mu_0 \underline{\underline{\mu}}_{HCM} \cdot \mathbf{H}(\mathbf{x}). \tag{2}$$

[1]Vector quantities are in boldface while dyadics are double underlined. The unit dyadic is denoted by $\underline{\underline{I}}$ and $(\mathbf{u}_x, \mathbf{u}_y, \mathbf{u}_z)$ is the triad of cartesian unit vectors. The permittivity and permeability of free space are denoted by ϵ_0 and μ_0, respectively.

The HCM constitutive dyadics have a biaxial form which we represent as [1, 2, 6]

$$\underline{\underline{\tau}}_{HCM} = a_\tau^r \underline{\underline{I}} + b_\tau^r(\mathbf{u}_{m\tau}^r \mathbf{u}_{n\tau}^r + \mathbf{u}_{n\tau}^r \mathbf{u}_{m\tau}^r) + i\left[a_\tau^i \underline{\underline{I}} + b_\tau^i(\mathbf{u}_{m\tau}^i \mathbf{u}_{n\tau}^i + \mathbf{u}_{n\tau}^i \mathbf{u}_{m\tau}^i)\right], \quad (\tau = \epsilon, \xi, \zeta, \mu), \tag{3}$$

where $a_\tau^{r,i}$ and $b_\tau^{r,i}$ are real–valued scalars and we describe the real–valued unit vectors in terms of spherical polar coordinates as

$$\mathbf{u}_{\kappa\tau}^\chi = \sin\theta_{\kappa\tau}^\chi \cos\phi_{\kappa\tau}^\chi \, \mathbf{u}_x + \sin\theta_{\kappa\tau}^\chi \sin\phi_{\kappa\tau}^\chi \, \mathbf{u}_y + \cos\theta_{\kappa\tau}^\chi \, \mathbf{u}_z, \quad (\chi = r, i; \;\; \kappa = m, n; \;\; \tau = \epsilon, \xi, \zeta, \mu). \tag{4}$$

With one exception, we consider here only constituent mediums with distinguished axes lying in the xy plane. Consequently, our calculations reveal that the HCM unit vector pairs $\mathbf{u}_{mc}^\chi$ and $\mathbf{u}_{nc}^\chi$ always lie in planes perpendicular to the xy plane with the xy plane bisecting the angle between $\mathbf{u}_{mc}^\chi$ and $\mathbf{u}_{nc}^\chi$. The following identities therefore hold

$$\theta_{m\tau}^\chi = \pi - \theta_{n\tau}^\chi = \theta_\tau^\chi, \qquad \phi_{m\tau}^\chi = \phi_{n\tau}^\chi = \phi_\tau^\chi, \qquad (\chi = r, i; \;\; \tau = \epsilon, \xi, \zeta, \mu). \tag{5}$$

The one exception occurs when we consider ellipsoidal inclusions of varying eccentricity; in this case one distinguished axis can lie along the z axis and we shall treat this as a special case in Section 3.1. Furthermore, since all component mediums we consider are reciprocal, results for the magnetoelectric dyadic $\underline{\underline{\zeta}}_{HCM}$ need not be explicitly presented as we find $\underline{\underline{\xi}}_{HCM} = -\underline{\underline{\zeta}}_{HCM}$.

All graphs are presented with reference to the key given in Table 1. A volumetric proportion of inclusion medium to host medium of 0.3 is taken for all calculations.

3. Numerical Homogenization Calculations

3.1 Dielectric case

We homogenize a host medium of permittivity $\underline{\underline{\epsilon}}^{host} = 1.2\,\underline{\underline{I}}$ and spherical topology with an inclusion medium of permittivity $\underline{\underline{\epsilon}}^{inc} = (3 + 3i)\,\underline{\underline{I}}$ and ellipsoidal geometry characterized by the shape dyadic $\underline{\underline{U}}^{inc} = \mathrm{diag}(2, 1, \gamma)$. For this particular example (and no others) the identities (5) do not hold; instead we take $\theta_{m\epsilon}^{r,i} = \theta_\epsilon^{r,i}$ and $\phi_{m\epsilon}^{r,i} = \phi_\epsilon^{r,i}$ and plot these angles as a function of γ in Figure 1. At points where the inclusion shape becomes spheroidal, the unit vectors $\mathbf{u}_{m\epsilon,n\epsilon}^{r,i}$ all lie on a common axis and the HCM becomes uniaxial. For all values of γ we find that $\underline{\underline{\epsilon}}_{HCM}$ is diagonal and hence the HCM belongs to the biaxial orthorhombic class [7]. This reflects the fact that in this case biaxiality arises from a geometrical structure based on three mutually perpendicular principal axes, namely those of the inclusion ellipsoid.

3.2 Dielectric–magnetic case

Here we consider constituents in which the distinguished axes have an electromagnetic, rather than topological, origin. We homogenize a host medium with constitutive dyadics $\underline{\underline{\epsilon}}^{host} = \underline{\underline{\mu}}^{host} = \mathrm{diag}(3, 1, 1)$ and an inclusion medium specified by $\underline{\underline{\epsilon}}^{inc} = (1 + i)\,\underline{\underline{A}}$ and $\underline{\underline{\mu}}^{inc} = (2 + i)\,\underline{\underline{A}}$ where

$$\underline{\underline{A}} = \begin{bmatrix} 3\cos^2\lambda + \sin^2\lambda & 2\sin\lambda\cos\lambda & 0 \\ 2\sin\lambda\cos\lambda & 3\sin^2\lambda + \cos^2\lambda & 0 \\ 0 & 0 & 1 \end{bmatrix}, \tag{6}$$

and both host and inclusion mediums have a spherical topology. Plotted in Figures 2 and 3 as functions of λ are, respectively, the defining angles for the unit vector pairs $\mathbf{u}_{m\epsilon,n\epsilon,m\mu,n\mu}^{r,i}$ and the

corresponding permittivity ($a_\epsilon^{r,i}$ and $b_\epsilon^{r,i}$) and permeability scalars ($a_\mu^{r,i}$ and $b_\mu^{r,i}$) . A uniaxial dielectric–magnetic HCM results when the distinguished axes of the constituent mediums are aligned. With the exception of the special cases $\lambda = 0$, $\pi/2$ and π, all eight angles $\theta_{\epsilon,\mu}^{r,i}$ and $\phi_{\epsilon,\mu}^{r,i}$ and all eight scalars $a_{\epsilon,\mu}^{r,i}$ and $b_{\epsilon,\mu}^{r,i}$ have distinct values and the biaxial HCM is of the monoclinic/triclinic type as regards both $\underline{\underline{\epsilon}}_{HCM}$ and $\underline{\underline{\mu}}_{HCM}$ [7].

We repeat the homogenizations of Figures 2 and 3 but now with a more general host medium characterized by $\underline{\underline{\epsilon}}^{host} = \underline{\underline{\mu}}^{host} = \mathrm{diag}(3+3i\delta, 1+i\delta, 1+i\delta)$ and with a fixed angle for the inclusion distinguished axis of $\lambda = 50°$. The angles $\theta_{\epsilon,\mu}^{r,i}$ are plotted against δ in Figure 4. Our findings for this example may be summarized by:

$$\mathrm{Re}\,\underline{\underline{\tau}}^{host} = p_\tau\,\mathrm{Im}\,\underline{\underline{\tau}}^{host},\ \ \mathrm{Re}\,\underline{\underline{\tau}}^{inc} = p_\tau\,\mathrm{Im}\,\underline{\underline{\tau}}^{inc} \ \Rightarrow\ \theta_\tau^r = \theta_\tau^i,\ \ \phi_\tau^r = \phi_\tau^i, \quad (\tau = \epsilon,\, \mu), \quad (7)$$

where $p_{\epsilon,\mu}$ are proportionality scalars. Thus, the biaxial HCM structure becomes orthorhombic with respect to permittivity (permeability) when ratios of real and imaginary parts of $\underline{\underline{\epsilon}}^{host}$ and $\underline{\underline{\epsilon}}^{inc}$ ($\underline{\underline{\mu}}^{host}$ and $\underline{\underline{\mu}}^{inc}$) are equal, despite the distinguished axes of the constituent mediums being non–perpendicular.

3.3 Bianisotropic case

Finally we consider the general bianisotropic case: the homogenization of an inclusion medium characterized by $\underline{\underline{\epsilon}}^{inc} = 2(1+i)\,\underline{\underline{A}}$, $\underline{\underline{\mu}}^{inc} = 1.5(1+i)\,\underline{\underline{A}}$ and $\underline{\underline{\xi}}^{inc} = -\underline{\underline{\zeta}}^{inc} = (1+i)\underline{\underline{A}}$ where $\lambda = 50°$, with a host medium described by $\underline{\underline{\epsilon}}^{host} = \underline{\underline{\mu}}^{host} = \underline{\underline{\xi}}^{host} = -\underline{\underline{\zeta}}^{host} = diag(3+3i\delta, 1+i\delta, 1+i\delta)$; and spherical topology is chosen for both component mediums. The computed biaxial bianisotropic HCM structure is of the generalized monoclinic/triclinic type with angles $\theta_{\epsilon,\xi,\mu}^{r,i}$ and $\phi_{\epsilon,\xi,\mu}^{r,i}$, and scalars $a_{\epsilon,\xi,\mu}^{r,i}$ and $b_{\epsilon,\xi,\mu}^{r,i}$, all taking distinct values, in general. The corresponding polar HCM unit vector angles are displayed as functions of δ in Figure 5 (the azimuthal angles behave similarly). At the point $\delta = 1$ we find that the HCM is orthorhombic biaxial with respect to all four constitutive dyadics and, as in Section 3.2, the orthorhombic state is not associated with perpendicularity of the distinguished axes in the component mediums.

Acknowledgement
The work of TGM is supported by the *Carnegie Trust for the Universities of Scotland*. WSW is the holder of a *RSE/SOEID Research Support Fellowship* of the *Royal Society of Edinburgh*.

References

[1] T. G. Mackay and W. S. Weiglhofer, "Homogenized biaxial materials: dielectric properties," *Department of Mathematics, University of Glasgow*, preprint 2000/06, February 2000.
[2] T. G. Mackay and W. S. Weiglhofer, "Homogenization of biaxial composite materials: dissipative anisotropic properties," *J. Opt. A.: Pure Appl. Opt.* **2**, 2000, in press.
[3] A. Lakhtakia (ed.), *Selected Papers on Linear Optical Composite Materials*. Bellingham, WA: SPIE Opt. Engg. Press, 1996.
[4] W. S. Weiglhofer, A. Lakhtakia, and B. Michel, "Maxwell Garnett and Bruggeman formalisms for a particulate composite with bianisotropic host medium," *Microwave Opt. Technol. Lett.* **15**, 263–266, 1997; erratum **22**, 221, 1999.
[5] B. Michel, A. Lakhtakia, and W. S Weiglhofer, "Homogenization of linear bianisotropic particulate composite media — Numerical studies," *Int. J. Appl. Electromag. Mech.* **9**, 167–178, 1998; erratum **10**, 537–538, 1999.
[6] W. S. Weiglhofer and A. Lakhtakia, "On electromagnetic waves in biaxial bianisotropic media," *Electromagnetics* **19**, 351–362, 1999.
[7] M. Born and E. Wolf, *Principles of Optics*. Cambridge, UK: Cambridge University Press, 1997.

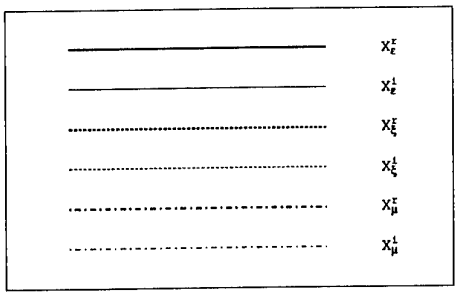

Table1: Key for Figures 1–5. $X = a, b, \theta$ or ϕ.

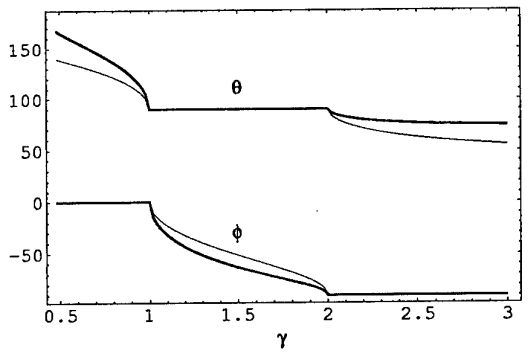

Figure 1: HCM angles $\theta_{\epsilon}^{r,i}$ and $\phi_{\epsilon}^{r,i}$ vs. inclusion ellipsoid semi–axis γ. ($X = \theta$, ϕ in Table 1).

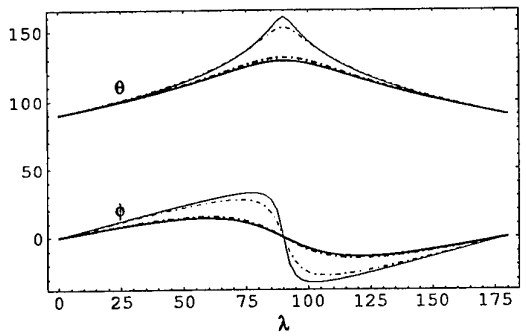

Figure 2: HCM angles $\theta_{\epsilon,\mu}^{r,i}$ and $\phi_{\epsilon,\mu}^{r,i}$ vs. inclusion distinguished axis angle λ. ($X = \theta$, ϕ in Table 1).

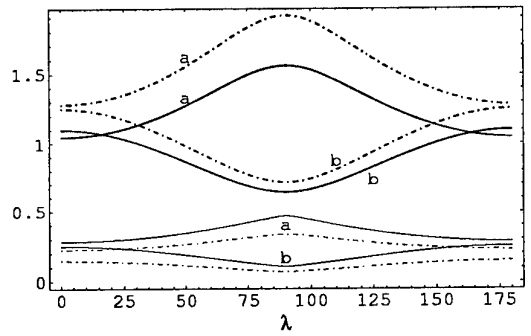

Figure 3: HCM scalars $a_{\epsilon,\mu}^{r,i}$ and $b_{\epsilon,\mu}^{r,i}$ vs. inclusion distinguished axis angle λ. ($X = a$, b in Table 1).

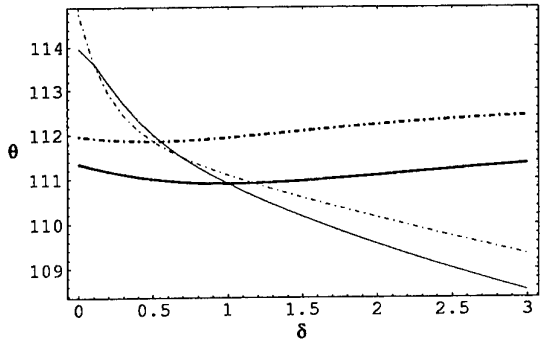

Figure 4: HCM angles $\theta_{\epsilon,\mu}^{r,i}$ vs. host medium parameter δ. ($X = \theta$ in Table 1).

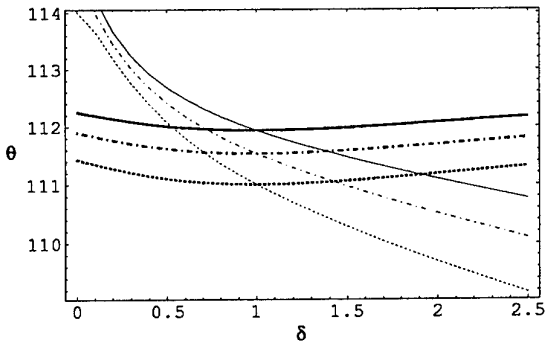

Figure 5: HCM angles $\theta_{\epsilon,\xi,\mu}^{r,i}$ vs. host medium parameter δ. ($X = \theta$ in Table 1).

Eigen Waves of Periodic Layered Structure of Complex Arrays

S. L. Prosvirnin and T. D. Vasilyeva

Institute of Radio Astronomy of National Academy of Sciences of Ukraine
Krasnoznamennaya Street 4, 61002 Kharkov, Ukraine
Fax: + 38–0572–476506; email: prosvirnin@rian.kharkov.ua

Abstract

The characteristics of eigen waves of periodical structures consist of 2-D arrays of strip particles, in particular having the shape of letters C, S and Ω are studied. Analytical and numerical results are presented. Study of eigen waves can be used for analyze property of polarization transformation by single complex array and multi-layered one.

1. Introduction

The layered periodic structure can be used as transformer of polarization of reflected and transmitted electromagnetic fields, absorber in the case a loss medium are placed between layers, and polarized and frequency selective surfaces. They has properties typical for photonic band-gap crystals. Analysis of characteristics of structure that has finite number of layers and semi infinite structure also can be carried by using the characteristics of eigen waves of infinite periodic structure [1], [2].

Let's consider an infinite layered periodic structure that is shown in the Fig. 1. Each layer represents a plane periodic on two directions array of strip particles. The particles have a complex shape, in particular, the shape of letters C, S and Ω. Mirror non-symmetric particles, such as S-shaped, are called planochiral [3]. All layers of structure are identical.

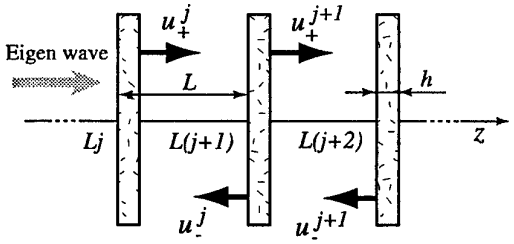

Figure 1: Infinite periodic layered structure of 2-D arrays

If the operators of reflection and transmission of a single layer are known it is easy to derive a homogeneous system of linear algebraic equations concerning vectors of amplitudes of plane waves that are propagated towards each other in every gap between layers. These form field of the eigen waves of an infinite structure. The condition of nonzero solution of a homogeneous system of equations is dispersing equation to which satisfy propagation constants of eigen waves. The distribution of electromagnetic field amplitude of an eigen wave and its polarization in gaps between layers can be derived from a solution of the system of equations.

2. Equations of Eigen Waves

For the sake of simplicity we shall confine to the most important case for applications. This case is one-wave scattering by single array on the assumption that both its periods are less than a

wavelength. Under these conditions reflection and transmission operators of a single layer can be presented by the second order square matrices. The solution of the problem of electromagnetic wave scattering by a single array of strip particles of the complex shape is known [4], [5].

Electromagnetic field of eigen wave is the field of plane waves inside layered structure that propagated along axis Oz in positive and negative directions between the boundaries of neighbor layers. The field is represented in the j gap between layers as following

$$\vec{u}^j = \vec{u}^j_+ + \vec{u}^j_-, \qquad Lj + h < z < L(j+1) \tag{1}$$

where

$$\vec{u}^j_+ = \vec{A}^j_+ e^{ik(z-Lj-h)}, \qquad \vec{u}^j_- = \vec{A}^j_- e^{-ik(z-Lj-L)},$$

L is the structure period along Oz axis, h is the thickness of layer, it is assumed field time dependence $e^{-i\omega t}$. The wave amplitudes of eigen wave between neighbor gaps are transformed in accordance with formula

$$\vec{A}^{j+1}_\pm = e^{i\beta L}\vec{A}^j_\pm \tag{2}$$

where β is propagation constant of eigen wave. Wave amplitudes in a neighbor gaps are connected by two vector equations

$$\vec{A}^{j+1}_+ = t^- e^{ik\Delta}\vec{A}^j_+ + r^+ e^{ik\Delta}\vec{A}^{j+1}_- \tag{3}$$

$$\vec{A}^j_- = r^- e^{ik\Delta}\vec{A}^j_+ + t^+ e^{ik\Delta}\vec{A}^{j+1}_- \tag{4}$$

Here $\Delta = L - h$, $r^\pm$ and $t^\pm$ are reflection and transmission operators of single layer for the cases of incident of electromagnetic wave in positive "+" and negative "-" directions of axis Oz. After take into account the Floquet condition (2) we can rewrite these equations for amplitudes plane waves that forming eigen wave of structure in the gap between layers as following

$$(I - t^- e^{ik\Delta}e^{-i\beta L})\vec{A}^j_+ - r^+ e^{ik\Delta}\vec{A}^j_- = 0 \tag{5}$$

$$r^- e^{ik\Delta}\vec{A}^j_+ - (I - t^+ e^{ik\Delta}e^{i\beta L})\vec{A}^j_- = 0 \tag{6}$$

System of equations are invariant respect to change indexes "$\pm$" by "$\mp$" and change the sign of constant of propagation β of eigen wave simultaneously. This property is consequence of the invariant of structure properties respect to choosing of direction of axis Oz.

Let us assume that layers of structure have not non-reciprocal elements and as consequence the matrix of operator reflection and transmission are symmetrical. In this case and so as we take into account only propagated partial waves the operators t^+ and t^- are equal. If the layer is symmetric regard to its average plane the matrices of operators r^+ and r^- are equal also. We shall restrict for simplicity this case only. The system of equations regard to amplitudes of eigen wave in this case is follow

$$(I - \tilde{t}e^{-i\beta L})\vec{A}^j_+ - \tilde{r}\vec{A}^j_- = 0 \tag{7}$$

$$\tilde{r}\vec{A}^j_+ - (I - \tilde{t}e^{i\beta L})\vec{A}^j_- = 0 \tag{8}$$

where $\tilde{t} = te^{ik\Delta}$, $\tilde{r} = re^{ik\Delta}$.

3. Analytical Results

If non-diagonal elements of matrices $\tilde{r}$ and $\tilde{t}$ are equal to zero there are two independent systems of equations regard to amplitudes of two line polarized along axis Ox and axis Oy eigen waves. Dispersion equations have the form

$$2\tilde{t}_{xx}\cos\beta L = 1 + \tilde{t}^2_{xx} - \tilde{r}^2_{xx} \tag{9}$$

$$2\tilde{t}_{yy}\cos\beta L = 1 + \tilde{t}_{yy}^2 - \tilde{r}_{yy}^2 \tag{10}$$

Two eigen waves have different phase velocities in general case.

Let us now suggest that elements of reflection and transmission matrices are in accord with equations

$$\tilde{r}_{xx} = \tilde{r}_{yy}, \qquad \tilde{t}_{xx} = \tilde{t}_{yy}, \qquad \tilde{r}_{xy} = \tilde{t}_{xy}$$

Dispersion equations can be wrote in the form

$$2(\tilde{t}_{xx} + \tilde{r}_{xy})\cos\beta L = 1 + \tilde{t}_{xx}^2 - \tilde{r}_{xx}^2 - 2\tilde{r}_{xy}(\tilde{r}_{xx} - \tilde{t}_{xx}) \tag{11}$$

$$2(\tilde{t}_{xx} - \tilde{r}_{xy})\cos\beta L = 1 + \tilde{t}_{xx}^2 - \tilde{r}_{xx}^2 + 2\tilde{r}_{xy}(\tilde{r}_{xx} - \tilde{t}_{xx}) \tag{12}$$

Solutions of equations 11 and 12 are accordingly β_+ and β_-

$$e^{i\beta_\pm L} = \frac{1}{2(\tilde{t}_{xx} \pm \tilde{r}_{xy})}\left[1 + \tilde{t}_{xx}^2 - \tilde{r}_{xx}^2 \pm 2\tilde{r}_{xy}(\tilde{t}_{xx} - \tilde{r}_{xx}) + \sqrt{S_\pm}\right] \tag{13}$$

where $S_\pm = 1 - 2\tilde{t}_{xx}^2 - 2\tilde{r}_{xx}^2 + \tilde{t}_{xx}^4 + \tilde{r}_{xx}^4 - 2\tilde{t}_{xx}^2\tilde{r}_{xx}^2 \mp 4\tilde{r}_{xy}(\tilde{t}_{xx} + \tilde{r}_{xx} + \tilde{r}_{xx}\tilde{t}_{xx}^2 + \tilde{t}_{xx}\tilde{r}_{xx}^2 - \tilde{t}_{xx}^3 - \tilde{r}_{xx}^3) + 4\tilde{r}_{xy}^2(\tilde{t}_{xx}^2 + \tilde{r}_{xx}^2 - 2\tilde{t}_{xx}\tilde{r}_{xx} - 1)$.

Eigen waves of structure are line polarized. Polarizations of eigen waves are mutually orthogonal. Amplitudes of field of eigen wave that correspond to solution $\beta_\pm$ of dispersion equation have values

$$A_{+x}^j = \pm A_{+y}^j = c_\pm, \quad A_{-x}^j = \pm A_{-y}^j = \frac{c_\pm}{2(\tilde{r}_{xx} \pm \tilde{r}_{xy})}\left[1 + \tilde{r}_{xx}^2 - \tilde{t}_{xx}^2 \mp 2\tilde{r}_{xy}(\tilde{t}_{xx} - \tilde{r}_{xx}) \pm \sqrt{S_\pm}\right] \tag{14}$$

Value $c_\pm$ is arbitrary constant.

4. Numerical Results

There are line polarized eigen waves only in the more complicated structures consist of arrays with C, S or Ω-shaped strip particles also. Two eigen waves are orthogonal polarized and have different phase velocities and different stop band frequencies.

Dependence of propagation constants of eigen waves in the structure of S-shaped strip particles from distance between layers is shown in Fig. 2. Directions of polarization of eigen waves don't vary when distance between arrays is varied.

One eigen wave is polarized at the angle approximately equal to 56.7 degrees regard to Ox axis. The wave has strong dependence of propagation constant from distance between arrays at resonant frequency region. There are stop band zones of this wave. The width of zone is increased with increasing reflection of single array. If frequency lower than resonant frequency a phase velocity of this wave is more than light velocity and it is smaller than light velocity in opposite case.

Other eigen wave marked by sign $\perp$ in Fig. 2 is polarized at the angle approximately equal to -33.3 degrees in regard to Ox axis. This wave has propagation constant the same as one in free space.

Similar characteristics have eigen waves of C-shaped and Ω-shaped layered structures. Both eigen waves of these structures can have stop band frequency zones.

5. Conclusion

If sizes of array cell are little than wave length in free space only two eigen waves can propagate in periodic structures of complex arrays of plane particles having any shape. The eigen waves have linearly polarized mutually orthogonal fields.

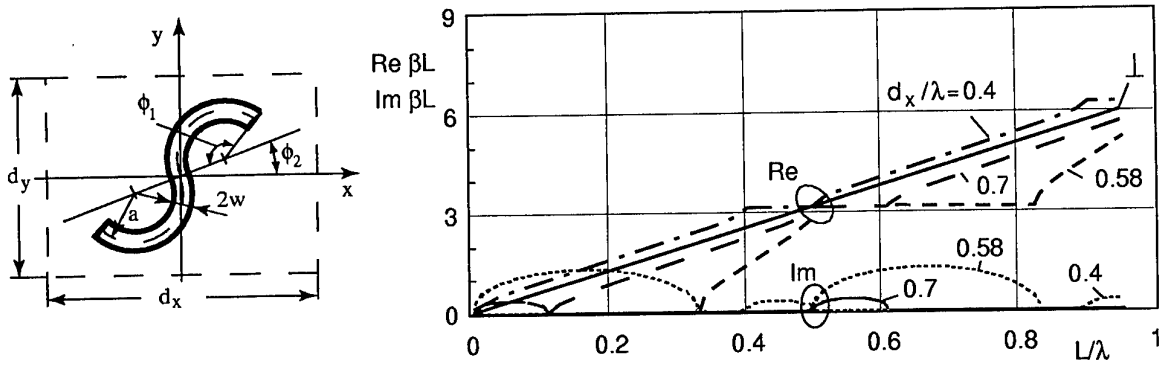

Figure 2: Propagation constant β versus distance between layers: array without substrate $h = 0$, $d_x = d_y = 10$ mm, $a = 3$ mm, $\phi_1 = \pi/2$, $\phi_2 = 0$, $w = 0.05$ mm, $d_x/\lambda_0 \approx 0.58$ is resonant value.

The field of the one eigen wave in the plano-chiral structure of S-shaped strips is polarized linearly along an average direct line that is similar to the segment of the straight line in a symbol \$. The field of another eigen wave is polarized orthogonal to this direction. The polarization of eigen waves don't vary if a distance between layers is varied. The stop band zones is extended at increasing of the single array reflection. The phase velocity of eigen wave can be both more or less than the light velocity depending on the frequency that is lower or higher than the resonance frequency of a strip element of array.

Transformation of polarization doesn't occur at reflection and transmission of normal incident plane wave from single array or multi-layer array if incident wave has line polarization coincident with polarization of eigen wave of infinite structure.

Array of any plane particles has property to transform polarization of normal incident wave the same as an array of cross-shaped plane particles oriented along directions of polarizations of eigen waves on condition that reflection and transmission coefficients of both arrays are equal in selected frequency.

References

[1] L. N. Litvinenko and S. L. Prosvirnin, "Analyzis of electromagnetic wave reflection by multi-layer periodic structures," in *Proc. of III-th Intern. Seminar/Workshop on Direct and Inverse Problems of Electromagnetic and Acoustic Wave Theory "DIPED-98"*, Tbilisi, Georgia, November 1998, pp. 28–30.

[2] D. Litvinenko, L. Litvinenko, S. Prosvirnin, and I. Reznik, "Wave diffraction by semi-infinite system of partially transmitted layers," in *Proc. of VI-th Intern. Conf. on Mathematical Methods in Electromagnetic Theory "MMET'96"*, Lviv, Ukraine, September 1996, pp. 96–99.

[3] L. R. Arnaut, "Chirality in multi-dimensional space with application to electromagnetic characterisation of multi-dimensional chiral and semi-chiral media," *J. Electromagnetic Waves and Applications*, vol. 11, pp. 1459–1482, 1997.

[4] T. D. Vasilyeva and S. L. Prosvirnin, "Electromagnetic wave diffraction by the plane array of chiral strip elements of complex shape," *Physics of wave processes and radio systems*, vol. 1, no. 4, pp. 5-9, 1998 (in Russian).

[5] S. L. Prosvirnin, "Analysis of electromagnetic wave scattering by plane periodical array of chiral strip elements," in *Proc. of 7-th Intern. Conf. on Complex Media "Bianisotropics-98"*, Braunschweig, Germany, June 1998, pp. 185–188.

Magnetic Eigenmodes in QD-Based Resonant Active Composites

S. A. Maksimenko[1], G. Ya. Slepyan[1], N. N. Ledentsov[2,3], V. P. Kalosha[1], A. Hoffmann[3], and D. Bimberg[3]

[1] Institute for Nuclear Problems, Belarus State University
Bobruiskaya str. 11, Minsk, 220050, Belarus
Fax: +375-17-226-5124 email: maksim@inp.minsk.by

[2] A.F.Ioffe Physical-Technical Institute
Politekhnicheskaya 26, 194021 St.Peterburg, Russia

[3] Institut fur Festkorperphysik, Technische Universitat Berlin
Hardenbergstr. 36, D-10623 Berlin, Germany

Abstract

The phenomenon of light confinement in an isolated quantum dot, provided by the resonant nature of exciton in QD and diffraction of electromagnetic waves at the dot boundary, is discussed. It has been shown that at a certain condition the quantum dot behaves as a microcavity those eigenmodes manifest themselves as additional, geometrical, resonances in the quantum dot electromagnetic response. The effect of induced magnetization of quantum dot is predicted and illustrated by the example of magnetic resonances in spherical quantum dots.

1. Introduction

A fundamental breakthrough in semiconductor device physics is connected with the recent progress in the synthesis of sheets of nano-scale 3D confined narrow-gap insertions in a host semiconductor, quantum dots (QDs). In particular, it was predicted that lasers based on QDs will show radically changed characteristics as compared to conventional quantum well lasers [1, 2]. The large body of recent results on physical properties of QDs and their utilization for the QD laser design has been accumulated in a monograph [3].

The key peculiarity of QDs emerges from the 3D confinement of the charge carriers determined by QD size and shape. However, there exists a class of effects governed by the QD size and shape, which have not received much attention so far. These effects are related to resonant nature of the exciton which provides a dramatic resonant discontinuity of the dielectric function at the QD boundary and, consequently, gives rise inhomogeneity of the electromagnetic field both inside and outside QD. By analogy with charge carrier confinement, redistribution of the electromagnetic field energy between the QD interior and exterior under effect of the QD boundary can be referred to as *light confinement*. Owing to this effect, diffraction of light by QDs are expected to contribute significantly to the electromagnetic response properties of QDs. In many cases the role of diffraction can be properly accounted for the formation in QD of depolarization electromagnetic field, e.g., in dipole approximation of the diffraction theory.

To our knowledge, some physical consequences of the light confinement in an individual QD first time were considered by Schmitt-Rink *et al.* [4]. Manifestation of this phenomenon

in relation to the scanning near-field optical microscopy was discussed by Martin *et al.* [5] for geometrically complex mesoscopic systems and by Hanewinkel *et al.* [6] for QDs. An asymmetry of optical absorption and gain spectra in single QD because of depolarization field has been mentioned in Ref. [6]. Recently it has been predicted and experimentally verified that the light confinement in QD arrays constituted by anisotropically shaped QDs manifests itself as polarization splitting of the gain band [7] and, in more general case, as the fine structure of this band [8]. A concept of active composite has been introduced by Ref. [7]. A set of new effects related to the light confinement in QDs is analyzed in Ref. [9]. One of them, excitation of geometrical resonances in QD arrays, we consider here in more detail.

2. Electromagnetic Response of a Single QD

Conventional phenomenological model of the gain in a QD is based on semi-classical theory of two-level systems which gives the well-known Lorentzian polarizability of QD: $\alpha(\omega) = (g_0/\varepsilon_h)[\omega - \omega_0 + i/\tau]^{-1}$, and $\varepsilon(\omega) = \varepsilon_h[1 + \alpha(\omega)]$. Here ω_0 is the exciton resonant frequency and τ is the exciton dephasing time in QD, ε_h is the frequency–independent complex–valued permittivity of the host medium. The phenomenological parameter g_0 is proportional to the oscillator strength of the transition. Such a primitive model does not take into account effect of depolarization field which makes the polarizability tensorial for anisotropically shaped QDs and shifts exciton resonance [7], [8] (for spherical QDs $\omega_N = \omega_0 - g_0/3\varepsilon_h$). The depolarization field approximation is applicable when the condition $\kappa(\omega) = kR\sqrt{\varepsilon(\omega)} \ll 1$ holds true. Beyond the scope of this condition, when the wavelength inside QD becomes comparable with its linear extension, the role of diffraction by QD is irreducible to the effect of depolarization. Below we discuss this effect restricting ourselves to the spherical QD for simplicity.

Let an isolated spherical QD of the radius R be exposed to external electromagnetic field. The problem of wave diffraction by a sphere has been exactly solved in the early of century by using the variable separation in the spherical basis. In view of the condition $kR\sqrt{\varepsilon_h} \ll 1$, which is valid for any realistic QDs, this solution is essentially simplified [10] and presents the field outside the sphere by:

$$\left\{ \begin{array}{c} \mathbf{E} \\ \mathbf{H} \end{array} \right\} = \left(\nabla\nabla\cdot + \varepsilon_h k^2\right) \left\{ \begin{array}{c} \mathbf{\Pi}^e \\ \mathbf{\Pi}^m \end{array} \right\} + ik\nabla \times \left\{ \begin{array}{c} \mathbf{\Pi}^m \\ -\sqrt{\varepsilon_h}\mathbf{\Pi}^e \end{array} \right\}, \tag{1}$$

where Hertz potentials are given by:

$$\left\{ \begin{array}{c} \mathbf{\Pi}^e \\ \mathbf{\Pi}^m \end{array} \right\} = \frac{R^3}{3r} \left\{ \begin{array}{c} \alpha^e \mathbf{E}_0 \\ \alpha^m \mathbf{H}_0 \end{array} \right\} \exp(ik\sqrt{\varepsilon_h} r)\,. \tag{2}$$

and the electric and magnetic polarizabilities of the sphere, $\alpha^{e,m}(\omega)$, are as follows:

$$\alpha^e(\omega) = 3\frac{\varepsilon(\omega)F(\kappa) - \varepsilon_h}{[\varepsilon(\omega)F(\kappa) + 2\varepsilon_h](1 - ikR\sqrt{\varepsilon_h}) + i(kR\varepsilon_h)^2 F(\kappa)}\,, \tag{3}$$

$$\alpha^m(\omega) = 3\frac{F(\kappa) - 1}{[F(\kappa) + 2](1 - ikR) + i(kR)^2 F(\kappa)}\,. \tag{4}$$

The function

$$F(\kappa) = 2\frac{\sin\kappa - \kappa\cos\kappa}{(\kappa^2 - 1)\sin\kappa + \kappa\cos\kappa} \tag{5}$$

is responsible for the diffraction effect.

It can easily be found that the depolarization field approximation comes into play in the limit $F(\kappa) \to 1$. At $|\kappa| > 1$ the wavelength inside the QD becomes comparable with its linear

extension, and, as follows from Eqs. (3)–(5), scattered wave field is generated by irradiation of both electric and magnetic dipoles indicating thus induced magnetism of QDs. Physical mechanism of magnetization of dielectrics with linear extension compared with the internal wavelength is related to the excitation of internal TE_{1q1} cavity modes ($q = \pm 1, \pm 2, \ldots$ are the polar indices of the modes) in scattering object, which thus behaves itself as a microcavity. Such modes give rise to a curl electric current in its turn inducing nonzero magnetic moment of the object [11]. The given effect is known in macroscopic electrodynamics; it is observed in macroscopic dielectric composite materials [12]. A peculiarity of the magnetism in QDs is its pronounced resonant nature. The eigenmodes indicated are called geometrical resonances. The term "geometrical" [10] is related to that the resonances occur exceptionally owing to a certain geometrical configuration of the QD.

The resonant conditions for electric and magnetic geometrical resonances are completely determined by the properties of the function $F(\kappa)$. This function demonstrates a set of resonances in the vicinity of the exciton frequency, whereas $F(\kappa) \to 1$ at $|\omega - \omega_0| \to \infty$ reducing the problem to that considered in Refs. [7], [8]. Thus, the geometrical resonances can manifest themselves in the vicinity of the exciton frequency ω_0 and certainly disappear far away this frequency region. However, concerning electrical geometrical resonances we have to conclude that they are not of interest because they can not be excited separately from the main exciton resonance ω_N. This is because both types of electric resonances are excited by electric component of the external field. Since the intensity of electrical geometrical resonance is a small portion of the main resonance intensity, its contribution results in small-amplitude beatings on the main line slope. Thus, higher electrical eigenmodes practically do not influence the main (depolarization) resonance. Unlike to electric resonances, magnetic ones are excited by magnetic component of the external field; in such situation placement of a QD in a microcavity in an antinode of magnetic field creates a possibility to make the effect evident without excitation of the main resonance.

Note also that the magnetic resonance exhibits much longer radiative lifetime as compared to the main resonance [9]. Furthermore, this lifetime is extremely longer than the intrinsic dephasing time, which therefore is crucial for possibility to observe the magnetic resonance.

3. Magnetization of QD Arrays

Occurrence of the magnetic geometrical resonance in isolated QDs must lead to magnetization of a QD array in the vicinity of the exciton frequency, essentially shifted to the blue with respect to the main resonance observable in experiments. Electromagnetic properties of composites are usually modeled in the framework of the effective–medium approach using the well–known Mossotti–Clausius formalism [12]. A homogeneous medium with effective constitutive parameters — such as conductivity, susceptibility and permittivity — is said to replace the composite. Following to conventional procedure, we present the homogenization of a QD–based composite with induced magnetic polarizabilities of inclusions.

General expression for the effective permiability tensor of a dilute composite medium comprising a regular ensemble of identical, electrically small magnetic inclusions dispersed in a host dielectric material is as follows:

$$\widehat{\mu}_{eff}(\omega) = \widehat{\mathbf{I}} + 4\pi f_V \widehat{\alpha}^m(\omega) \left[\widehat{\mathbf{I}} + f_V \widehat{\delta}\, \widehat{\alpha}^m(\omega)\right]^{-1}, \tag{6}$$

where $\widehat{\delta}$ is the lattice tensor completely determined by geometry of the array, $\widehat{\alpha}^m$ is the magnetic polarizability tensor of a single inclusion (for spherical QDs this tensor reduces to scalar quantity α^m (4)), f_V is the volume fraction of inclusions. The notation $\widehat{\delta}\widehat{\alpha}^m$ stands for the inner tensor product. Rigorous derivation of this expression based on the integral equations of macroscopic electrodynamics has been presented by Khiznjak [10]. An estimate of the array permeability can

be obtained from equation (6). Using realistic parameters, one can find $\mu - 1 \sim 0.05 - 0.1$. This is available for observation. For more correct estimate, effects of inhomogeneous broadening has to be involved in the analysis. Thus, we can conclude that the electromagnetic wave diffraction by QDs may result in manifestation by QD arrays of magnetic properties although both QD and surrounding materials are dielectric.

4. Conclusion

In this paper occurrence of magnetic geometrical resonances caused by the excitation of eigenmodes in QDs, which thus behave themselves as microcavities, is predicted. Having much smaller intensity as compared to the main exciton peak, these resonances can be evident owing to their shifts with respect to the main exciton peak and can be excited by placing of QD in a microcavity in the magnetic field antinode, where the main peak is suppressed. Measurement of the frequency shift between main exciton and magnetic resonances can be used for direct determination of the oscillator strength in QDs. In our paper we restricted ourselves to the spherical model of QD. Different QD configurations like disks or pyramids can be investigated using direct computation on the basis of the well-developed method of classical electrodynamics [13].

Acknowledgement
The research is partially supported through INTAS under project 96-0467 and the NATO Science for Peace Program under project SfP-972614.

References

[1] Y. Arakawa and H. Sakaki, "Multidimensional quantum–well laser and temperature dependence of its threshold current," *Appl. Phys. Lett.*, vol. 40, no. 11, pp. 939–941, June 1982.

[2] M. Asada, Y. Miyamoto, and Y. Suematsu, "Gain and threshold of three dimensional quantum box laser," *IEEE J. Quant. Electr.*, vol. 22, no. 9, pp. 1915–1921, September 1986.

[3] D. Bimberg, M. Grundmann, and N. N. Ledentsov, *Quantum Dot Heterostructures.* Chichester: John Wiley & Sons, 1999.

[4] S. Schmitt-Rink, D. A. B. Miller, and D. S. Chemla, "Theory of the linear and nonlinear optical properties of semiconductor microcrystallites," *Phys. Rev. B*, vol. 35, no. 15, pp. 8113–8125, May 1987.

[5] O. J. F. Martin, C. Girard and A. Dereux, "Generalized field propogator for electromagnetic scattering and light confinement," *Phys. Rev. Lett.*, vol.74, no. 4, pp. 526-529, January 1995.

[6] B. Hanewinkel *et al.*, Optical near–field response of semiconductor quantum dots," *Phys. Rev. B*, vol. 55, no. 20, 13715–13725, May 1997.

[7] G. Ya. Slepyan *et al.*, "Polarization splitting of the gain band in quantum wire and quantum dot arrays," *Phys. Rev. B*, vol 59, no 19, pp. 1275-1278, May 1999.

[8] S. A. Maksimenko *et al.*, "Electromagnetic response of 3D arrays of quantum dots," *J. Electronic Materials*, vol. 29, no 5, pp.494-503, May 2000.

[9] S. A. Maksimenko *et al.*, "Light confinement in a quantum dot," *Semiconductor Sci. and Techn.*, vol. 15, no. 6, pp. 491–496, 2000.

[10] N.A. Khiznjak, *Integral Equations Of Macroscopic Electrodynamics.* Kiev: Naukova Dumka, 1986 (in Russian).

[11] L. D. Landau and E. M. Lifshitz, *Electrodynamics Of Continuous Media.* Oxford: Pergamon Press, 1960.

[12] A. Lakhtakia (Ed.), *Selected Papers on Linear Optical Composite Materials.* Bellingham: SPIE Optical Engineering Press, 1996.

[13] A. S. Ilyinsky, G. Ya. Slepyan, and A. Ya. Slepyan, *Propagation, Scattering And Dissipation Of Electromagnetic Waves.* London: Peter Peregrinus, 1993.

Nonlinear Properties of Carbon Nanotubes in a Strong Electric Field

A. S. Maksimenko and G. Ya. Slepyan

Institute for Nuclear Problems, Belarus State University,
Bobruiskaya str. 11, Minsk, 220050, Belarus
Fax: + 375–17–226 5124; email: antonmx@inp.minsk.by

Abstract

A theoretical model and computations of the I-V characteristics of both doped and undoped long carbon nanotubes in a strong axial dc-fields at room temperatures have been presented. Negative differential conductivity has been predicted. It has been shown that $|dI/dV|$ for metal carbon nanotubes in the region of the negative differential conductivity significantly exceeds corresponding values for semiconducting ones. The predicted effect makes possible the design of wave-generating nanotube-based diods for submillimeter and infrared ranges.

1. Introduction

Since the discovery by Iijima of carbon nanotubes (CNs), a great deal of interest has been focused on these quasi-one-dimensional monomolecular structures because of their unique physical properties (mechanical, electrical, optical, etc.) and the rapid experimental progress in the controlled preparation. Processes of electron transport in strong external fields when nonlinear effects are constitutive are of a great interest for potential applications in nanoelectronics and for experimental diagnostic of CN themselves.

The current-voltage (I-V) characteristics for tunnelling electrons in individual single-wall CNs at law temperatures were measured in Refs.[1, 2]. At such temperatures $k_BT \ll \mathcal{E}_c, \Delta\mathcal{E}$ and conduction occurs through well separated discrete electron states; here k_B is the Boltzmann constant, T is the temperature, $\mathcal{E}_c$ is charging energy, $\Delta\mathcal{E} = \pi\hbar v_F/L$ is the energy level spacing with v_F as the Fermi speed and L as the CN length. At the above condition the current is produced by the electrons tunneling through CN in the presence of the Coulomb blockade induced by the long-ranged (unscreened) Coulomb interaction.

Current instability in CNs is of great interest. The instability appears due to the negative differential conductivity (NDC) in I-V curves of CNs. Nonlinear coherent transport through doped nanotube junctions was considered in Ref.[3]. It was also shown the possibility of NDC for tunelling electrons. In Ref.[4] a theoretical phenomenological analysis of the I-V characteristics of undoped CNs at room temperatures, when $k_BT > \mathcal{E}_c, \Delta\mathcal{E}$. The current was produced by free charge carriers (quasiparticles) which are π-electrons moving in the field of the crystalline lattice. The nonlinearity of the I-V characteristic appears due to the nonlinear properties of the quasiparticle gas . The *negative differential conductivity* region with $dI/dV < 0$ in CNs aws predicted in a certain range of the field strength.

2. Theory

This report extends Ref.[4] for the case of doped CNs. Let us consider an doped single-wall zigzag CN (m,0) exposed to a homogeneous axial dc-field E_z, $E_z = V/L$, where V is the voltage

between the CN ends. We shall apply the semi-classical approximation considering the motion of π-electrons as a classical motion of free quasi-particles with dispersion law extracted from the quantum theory in the tight-binding approximation [5].

The motion of quasi-particles in an external axial electric dc-field is described by the Boltzmann kinetic equation

$$eE_z\frac{\partial f(\mathbf{p})}{\partial p_z} = -\frac{1}{\tau}[f(\mathbf{p}) - F(\mathbf{p})], \tag{1}$$

where e is the electron charge, $F(\mathbf{p})$ is the equilibrium Fermi distribution function and τ is the relaxation time. The relaxation term of the equation (1) describes the electron-phonon scattering [6, 7], electron-electron collisions etc.

Utilizing the method originally developed in the theory of quantum semiconductor superlattices [8] we can construct an exact solution of kinetic equation (1) without assuming the electric field to be weak. First, note that the distribution function $f(\mathbf{p})$ is periodic in p_z with period $2\pi/a$, $a = 3b/2\hbar$, $b = 1,42$Å. Then, taking into account the transverse quantization, the distribution function can be presented by:

$$f(\mathbf{p}) = \Delta p_\phi \sum_{s=1}^{m} \delta(p_\phi - s\Delta p_\phi) \sum_{r\neq 0} f_{rs} e^{iarp_z}, \tag{2}$$

where f_{rs} are coefficients to be found, $\delta(x)$ is the Dirac delta-function, $\Delta p_\phi = \pi\sqrt{3}/am$. The equilibrium distribution function $F(\mathbf{p})$ can be expanded in the analogous series with the coefficients as follows

$$F_{rs} = \frac{a}{4\pi}\int_0^{2\pi/a}\left[\frac{e^{-iarp_z}}{1+\exp\{(\mathcal{E}_s(p_z)-\mu)/k_BT\}} - \frac{e^{-iarp_z}}{1+\exp\{(-\mathcal{E}_s(p_z)-\mu)/k_BT\}}\right]dp_z. \tag{3}$$

In this equation first term descirebes the contribution of conduction band and the second one of valence band. Here μ is a chemical potential of CN. It describes doping (μ=0 for undoped CNs [4]). μ can be varied within wide range of values. Accordingly to [3] $\mu \sim 0.3$ eV for dopping by Au substrate, -0.5 eV $< \mu <$ 0.5 eV for doping by typical alcali and halogen atoms. For the KC_8 doped CNs $\mu \sim 2.0$ eV [9]. Substitution of both expansions into Eq. (1) gives $f_{rs} = F_{rs}/(1 + i\tau r\Omega)$, where $\Omega = aeE_z$ is the Stark frequency.

The surface current density is defined by

$$j_z(E_z) = -\frac{8e\gamma_0}{\sqrt{3}\hbar bm}\sum_{r=1}^{\infty}\frac{r^2\Omega\tau}{1+(r\Omega\tau)^2}\sum_{s=1}^{m}F_{rs}\mathcal{E}_{rs}. \tag{4}$$

Here $\gamma_0 \sim 3.0$eV is the overlapping integral. This equation states the basis for the evaluation of I-V characteristics. As it has been stated above, the quasi-particles motion is described classically. Thus, both interband transitions and quantum-mechanical corrections to the intraband motion are left out of account in this model. This imposes the limitation on the external electric field strength: $|E_z| < \gamma_0/2eR$.

The Coulomb electron-electron interaction has been also left out of account in our approach. The role of this mechanism as applied to CNs was considered in a number of papers, see [10] for example. It has been established that the short-range electron-electron interaction, typical for CN arrays ('ropes'), have only a weak effects at high temperatures.

3. Numerical Results

The I-V characteristics obtained via numerical calculation of Eq.(4) are presented in Fig.1 and Fig. 2 for metal ($m = 3q$, q is an integer) and Fig. 3 and Fig. 4 for semiconducting ($m \neq 3q$) zigzag CNs.

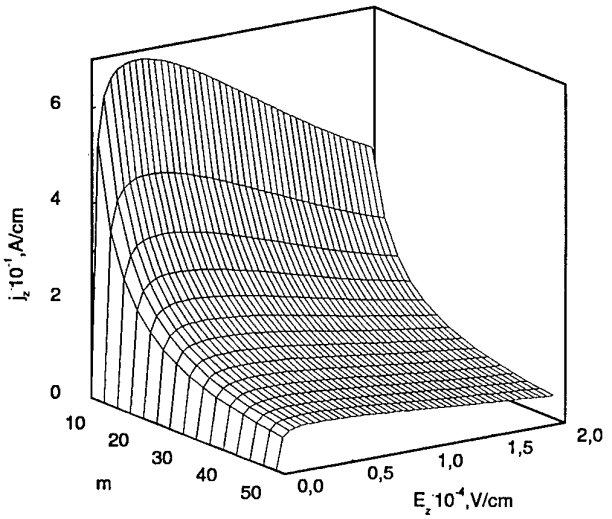

Fig. 1 Undoped metall zigzag CNs.
T=287,5°K, τ=3*10^{-12}.

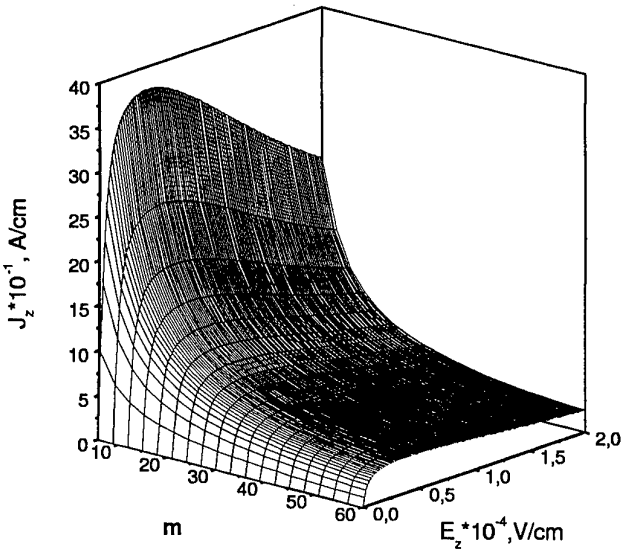

Fig. 2 Doped zigzag CNs with m=3q (q is an integer).
μ=0.2 eV, T=287,5°K, τ=3*10^{-12}.

The figures show the linear dependence of j_z on E_z at weak strengths of the external field both for doped and undoped CNs; it corresponds to the region of ohmic conductivity. As E_z increases, the value $\partial j_z/\partial E_z$ growth smaller and at $E_z = E_z^{(max)}$ the current density reaches the maximum value j_z^{max}. Further increase of E_z results in the decrease of j_z. Thus, predicted in [4] the region with the negative differential conductivity ($\partial j_z/\partial E_z < 0$), in the I-V characteristics of undoped CNs can be also observed in the case of doped CNs.

Fig.1 and Fig. 3 demonstrate that $E_z^{(max)}$ depends on neither number m nor the conductivity type (metal or semiconductor), whereas, j_z^{max} shows the different dependencies on m for undoped metal and semiconducting CNs. For metal CNs, j_z^{max} decreases with m while it increases for semiconducting ones. As $m \to \infty$, j_z^{max} for metal and semiconducting CNs tends to the same limit from opposite sides. Generally, at large m, the I-V characteristics of different CNs are coming close and in the limit case $m \to \infty$ they reduce to I-V characteristic of the plane graphite monolayer. It should be noted that the metal CNs exhibit much lager NDC as compared to semiconducting ones. Fig. 2 shows that the doping of metal CNs makes J_z^{max} some times larger. Doping of semiconducting CNs with small m does not lead to noticeable changes but as m increses, current through doped doped semiconducting CNs increases and values of current density become one order with ones for conducting undoped CNs (Fig. 4).

4. Conclusion

In Summary, we have predicted the NDC effect in both doped and undoped CNs, which is expected to be observable in sufficiently long CNs at room temperatures. I-V curves are expected to be effectevely controlled due to doping.

Acknowledgement
The research is partially supported through INTAS under project 97-2018 and BMBF under project WEI-001-98.

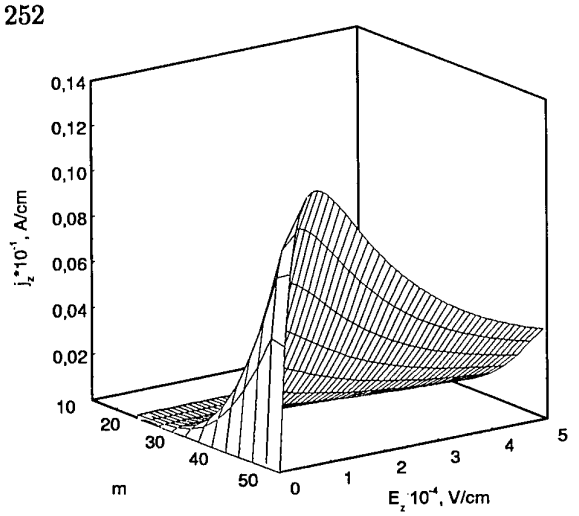

Fig. 3. Undopped semiconducting zigzag CNs. T=287,5°K, $\tau=3*10^{-12}$.

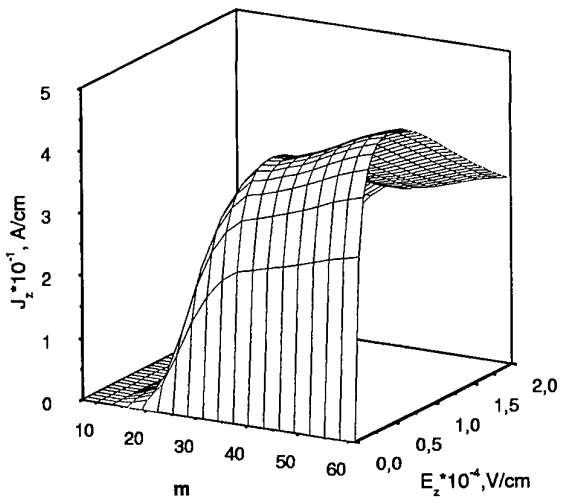

Fig. 4. Doped zigzag CNs with m=3q+1 (q is an integer). μ=0.2 eV, T=287,5°K, $\tau=3*10^{-12}$.

References

[1] S. J. Tans *et. al.*, "Individual single-wall carbon nanotubes as quantum wires," *Nature*, London, vol. 386, pp. 474-480, 1997.

[2] A. Bezryadin *et. al.*, "Multiprobe transport experiments on individual single-wall carbon nanotubes," *Phys. Rev. Lett.*, vol. 80, pp. 4036-4039, May 1998.

[3] A. A. Farajian, K. Estarjani, and Y. Kawazoe, "Nonlinear coherent transport through doped nanotube junctions," *Phys. Rev. Lett.*, vol. 82, pp. 5084-5087, June 1999.

[4] A. S. Maksimenko and G. Ya. Slepyan, "Negative differential conductivity in carbon nanotubes," *Phys. Rev. Lett.*, vol. 84, pp. 362-365, January 2000.

[5] M. F. Lin and K. W.-K. Shung, "Magnetization of graphene tubules," *Phys. Rev. B*, vol. 52, pp. 8423-8438, September 1995.

[6] R. A. Jishi, M. S. Dresselhaus, and G. Dresselhaus, "Electron-phonon coupling and electrical conductivity of fulerene nanotubes," *Phys. Rev. B*, vol. 48, pp. 11385-11389, October 1993.

[7] C. L. Kane and E. J. Mele, "Size, shape, and low energy electronic structure of carbon nanotubes," *Phys. Rev. Lett.*, vol. 78, pp. 1932-1935, March 1997.

[8] F. G. Bass and A.A. Bulgakov, *Kinetic and Electrodynamic Phenomena in Classical and Quantum Semiconductor Superlattices*. New York: Nova, 1997.

[9] Y.-K. Kwon, S. Saito and D. Tomaneck, "Effect of intertube coupling on the electronic structure of carbon nanotube ropes," *Phys. Rev. B*, vol. 58, pp. R13314-R13317, November 1998.

[10] Yu. A. Krotov, D.-H. Lee, and S. G. Louie, "Low energy properties of (n,n) carbon nanotubes," *Phys. Rev. Lett.*, vol. 78, pp. 4245-4248, June 1997.

Electromagnetic Wave Scattering by the Edge of a Carbon Nanotube

N. A. Krapivin[1], G. Ya. Slepyan[1], S. A. Maksimenko[1],
A. Lakhtakia[2], and O. M. Yevtushenko[3]

[1] Institute for Nuclear Problems, Belarus State University
Bobruiskaya str. 11, Minsk, 220050, Belarus
Fax: +375 17 226 5124; email: maksim@inp.minsk.by

[2] CATMAS, Department of Engineering Science and Mechanics
Pennsylvania State University, University Park, PA 16802–6812, USA

[3] Institute for Radiophysics and Electronics, Nat. Ac. Sci. of Ukraine
Ak. Proskura str. 12, Kharkov, 310085, Ukraine

Abstract

Scattering of a time–harmonic electromagnetic field by the edge of a semi–infinite, single–wall, zigzag carbon nanotube (CN) is considered. The Wiener–Hopf technique is applied to determine the exact solution of the problem, and the scattering pattern is numerically calculated in the vicinity of the main plasmon resonance frequency.

1. Introduction

Since the discovery by Iijima of quasi–one–dimensional cylindrical crystalline structures of carbon atoms, generally referred to as carbon nanotubes (CNs), many unique physical properties of theirs have been predicted theoretically and detected experimentally [1]. In particular, with reference to their optical properties, thin films comprising aligned CNs have been described theoretically as composite mediums [3, 4].

A composite medium consists of a homogeneous host medium with periodically or randomly dispersed inclusions. The inclusions must be electrically small for *local* homogenization to be possible, for which purpose each inclusion is represented by a polarizability tensor [5]. Furthermore, macroscopic samples of a composite medium are supposed to contain a huge number of inclusions, so that the composite medium can be replaced by an effectively homogeneous medium.

The polarizability tensor of a single CN in isolation has been treated approximately by several researchers. For instance, the 3–D polarizability tensor of a *zigzag* CN was calculated by Ma & Yang [6] when its length L and cross–sectional radius R are small compared to the free–space wavelength $\lambda = 2\pi/k$ (i.e., $kL \ll 1$ and $kR \ll 1$). The 2–D polarizability tensor (per unit length) of infinitely long CNs has also been treated [3, 4, 7]. However, in the optical frequency range, the typical geometric parameters of actual CNs satisfy the following conditions:

$$kR \ll 1, \quad L \gg R, \quad kL \sim 1. \tag{1}$$

Such conditions are characteristic of wire antennas at microwave frequencies [8]. A wire antenna cannot be characterized by a polarizability tensor, because the contribution of the

high–order multipoles to the scattered field is strong due to the last condition in Eqs. (1). Scattering by a long wire is much too complicated to be expressed *via* a dipole, and arrays of many long wires can not therefore be homogenized in the same way as arrays of electrically small inclusions can be [5]. The essential quantity required is the scattering matrix (or its equivalent) of a single wire [9]. From this quantity, the scattering pattern of a wire array can be calculated [10]. Analogously, the key problem for the optical response of CN arrays in the optical regime defined by Eqs. (1) is the calculation of the scattering pattern of an isolated CN of finite length. Of course, care must be exercised because CNs can not be necessarily assumed as perfect conductors — unlike wire antennas.

The effective boundary conditions for a CN are non–trivial [11]. Accordingly, the responses of CNs are different from those of wire antennas. For example, strongly attenuated surface polaritons [11] and plasmons [2] appear in CNs, instead of the weakly attenuated waves of longitudinal current in wire antennas. Yet the universality of macroscopic electrodynamics means that certain common effects are possible. In particular, we expect resonance effects, which can arise as a result of the interactions between the edges of a CN.

This paper addresses the electromagnetic scattering properties of CNs. We use the Wiener–Hopf technique [12] and the effective impedance boundary conditions [11] for a semi–infinite, single–shell, zigzag CN. The scattering amplitude of a finite–length CN can be expressed in terms of the scattering response of a semi–infinite CN, using the edge–wave method.

2. Theoretical Framework

Consider a CN aligned parallel to the z axis of a circular cylindrical coordinate system (r, ϕ, z) whose origin is located at the center of the circular cross–section of the CN. The edge of the CN can be either closed or open. If closed, the edge is almost hemispherical. However, the oxidation of CNs makes the open–edge configuration more probable — which is fortuitous, as that configuration is the more suitable of the two for theoretical analysis. But the scattered field is almost independent of the edge configuration if the first of Eqs. (1) holds true, in direct analogy with hollow and dense wire antennas [12]. Hence, we restrict ourselves to the open–edge configuration.

Let the incident field be E–polarized, with harmonic time–dependence of $e^{-i\omega t}$, and propagating at an angle θ_0 with respect to the z axis. This field is represented by the Hertz potential $\psi^{(i)}$. The total potential $\psi_\Sigma = \psi^{(i)} + \psi^{(s)}$, where $\psi^{(s)}$ corresponds to the scattered field as per

$$\mathbf{E}^{(s)} = -\frac{1}{ik}\frac{\partial^2\psi^{(s)}}{\partial z \partial r}\mathbf{u}_r + \frac{1}{ikr}\frac{\partial^2\psi^{(s)}}{\partial z \partial \phi}\mathbf{u}_\phi - \frac{1}{ik}\left(\frac{\partial^2\psi^{(s)}}{\partial z^2} + k^2\psi^{(s)}\right)\mathbf{u}_z\,, \tag{2}$$

$$\mathbf{H}^{(s)} = \frac{1}{r}\frac{\partial\psi^{(s)}}{\partial\phi}\mathbf{u}_r - \frac{\partial\psi^{(s)}}{\partial r}\mathbf{u}_\phi\,. \tag{3}$$

The boundary conditions satisfied are as follows (in Gaussian units) [11]:

$$\left.\begin{aligned} \left(1 + \tfrac{\tilde{l}_0}{k^2}\tfrac{\partial^2}{\partial z^2}\right)\left(\left.\frac{\partial\psi^{(s)}}{\partial r}\right|_{r=R+0} - \left.\frac{\partial\psi^{(s)}}{\partial r}\right|_{r=R-0}\right) &= \tfrac{4\pi\tilde{\sigma}_{zz}}{i\omega}\left(\frac{\partial^2\psi^{(s)}}{\partial z^2} + k^2\psi^{(s)}\right) + \Phi(\phi, z)\,, \\ & \qquad 0 < z < \infty\,, \\ \left.\frac{\partial\psi^{(s)}}{\partial r}\right|_{r=R-0} = \left.\frac{\partial\psi^{(s)}}{\partial r}\right|_{r=R+0}\,, \qquad \psi^{(s)}|_{r=R+0} &= \psi^{(s)}|_{r=R-0}\,, \qquad -\infty < z < \infty \end{aligned}\right\}, \tag{4}$$

Here, $\Phi(\phi, z) = \frac{4\pi}{c}k\tilde{\sigma}_{zz}\psi^{(i)}(R, \phi, z)\sin^2\theta_0$ emerges from the incident field; c is the speed of light in vacuum; the parameter $\tilde{l}_0$ takes spatial dispersion into account [11]; and $\tilde{\sigma}_{zz}$ is the axial

conductivity of an isolated CN. Both $\tilde{\sigma}_{zz}$ and $\tilde{l}_0$ have been calculated *via* quantum transport theory [11]. The boundary conditions (4) have to be complemented by radiation conditions as well as by edge conditions [12].

The boundary value problem may be solved with the Wiener–Hopf technique, with the Jones method employed to derive Wiener–Hopf functional equation:

$$\mathcal{J}_+(\alpha)G(\alpha) = \Psi_-(\alpha) - \frac{\breve{\Phi}(\phi,\alpha)}{\xi\gamma^2}. \tag{5}$$

Here, $\breve{\Phi}(\phi,\alpha)$ is the spatial 1–D Fourier transform of $\Phi(\phi,z)$ with α as the (complex–valued) spatial frequency corresponding to z; $K_l(\cdot)$ and $I_l(\cdot)$ are modified Bessel functions of order $l \geq 0$; $G(\alpha) = K_l(\gamma R)I_l(\gamma R)R$ $-\Gamma\xi^{-1}\gamma^{-2}$, $\xi = -4i\pi\tilde{\sigma}_{zz}/\omega$, $\Gamma = 1 - \tilde{l}_0\alpha^2k^{-2}$ and $\gamma = \sqrt{\alpha^2 - k^2}$; while $\mathcal{J}_+(\alpha)$ and $\Psi_-(\alpha)$ are two unknown functions to be determined as per the Wiener–Hopf technique. In order to solve Eq. (5) analytically, one has to apply the usual factorization and decomposition procedures, and the exact analytical expression for the scattered Hertz potential is then obtained by the inverse spatial Fourier transform.

In the far zone, application of the saddle point method leads to

$$H_\phi^{(s)},\ E_\theta^{(s)} \sim F_l(\theta,\theta_0)\,\frac{e^{ik\sqrt{r^2+z^2}}}{k\sqrt{r^2+z^2}}, \tag{6}$$

where $\theta = \pi - \tan^{-1}(r/z)$ and

$$F_l(\theta,\theta_0) = \frac{H_l^{(1)}(kR\sin\theta_0)}{G_+(k\cos\theta_0)(1+\cos\theta_0)} \times \frac{\cos(\theta/2)}{\sin(\theta/2)} \times \frac{J_l(kR\sin\theta)e^{-i\pi/4}}{(\cos\theta+\cos\theta_0)\ G_-(k\cos\theta)}; \tag{7}$$

$H_l^{(1)}(\cdot)$ is the cylindrical Hankel function and $J_l(\cdot)$ the cylindrical Bessel function of order l; while $G(\alpha) = G_+(\alpha)G_-(\alpha)$. The function $F_l(\theta,\theta_0)$ is the *scattering pattern* of the edge. The full scattering pattern of a CN includes additional components accounting for surface polaritons.

3. Numerical Results and Discussion

We calculated the far–zone scattered power density $P(\theta) \sim |F_0(\theta,\theta_0)|^2$, with $l = 0$ sufficing for most realistic incident fields. Following Ref. [11], we set the inverse relaxation time $\nu = 0.33 \times 10^{12}$ s^{-1}, which is in good agreement with the recent measurements of dynamic room–temperature conductivity of mats of single–wall CNs [13].

Let us examine $P(\theta)$ in the vicinity of $\beta = 1$, where $\beta = \hbar\omega/2\gamma_0 = 1$, $\hbar$ is the Planck constant, and γ_0 is the so–called overlap integral [11]. This case is of special interest since it corresponds to the main plasmon condition [2] for all types of CNs. All other resonant lines are interpreted as its satellites. Sample plots of $P(\theta)$ calculated in the regime $0 < \theta < \pi - \theta_0$ are presented in Figure 1. Let us point out here that the saddle point method is inapplicable in the vicinity of $\theta = \pi - \theta_0$.

It is clear from Figure 1 that a relatively weak deviation from the exact resonance condition $\beta = 1$ leads to a significant decrease in the scattered field intensity; and we deduce thereby that scattering by a semi–infinite CN is essentially due to plasmon propagation. We also infer from Figure 1 that *forward scattering* is stronger by 2 to 3 orders in magnitude than *backscattering*. This effect persists for all types of CNs in a wide frequency range.

To conclude, we have investigated the scattering of a time–harmonic electromagnetic field by a semi–infinite, single–shell, zigzag CN. We have found an exact analytical solution in the framework of the Wiener–Hopf technique. The solution found will serve as the basis of the theory of light scattering by single CNs and CN–based composites.

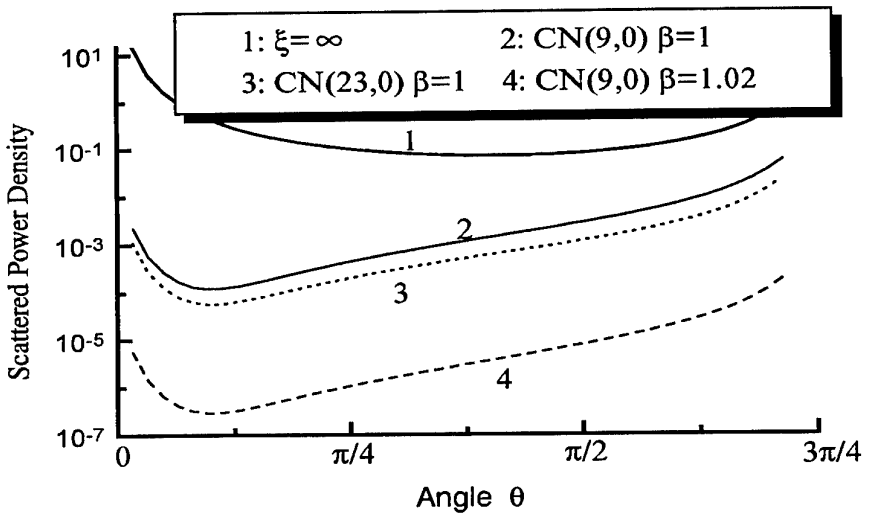

Figure 1: Sample plots of the scattered power density $P(\theta)$ for semi–infinite, single–shell, zizgag CNs (m, $n = 0$), when $\theta_0 = \pi/4$. For comparison, the results for $\xi = \infty$ (i.e., perfect conduction) are also shown.

References

[1] M. S. Dresselhaus, G. Dresselhaus, and P. C. Eklund, *Science of Fullerenes and Carbon Nanotubes*. Academic Press: New York, 1996.

[2] M. F. Lin and K. W.–K. Shung, "Magnetoconductance of carbon nanotubes," *Phys. Rev. B*, vol. 51, pp. 7592–7597, 1995.

[3] A. Lakhtakia, G. Ya. Slepyan, S. A. Maksimenko, A. V. Gusakov, and O. M. Yevtushenko, "Effective medium theory of the microwave and the infrared properties of composites with carbon nanotubes inclusions," *Carbon*, vol. 36, pp. 1833–1839, 1998.

[4] S. Tasaki, K. Maekawa, and T. Yamabe, "π–band contribution to the optical properties of carbon nanotubes: Effect of chirality," *Phys. Rev. B*, vol. 57, pp. 9301–9318, 1998.

[5] A. Lakhtakia (Ed.), *Selected Papers on Linear Optical Composite Materials*. SPIE: Bellingham, WA, USA, 1996.

[6] J. Ma and R.–k. Yang, "Electronic and optical properties of finite zigzag carbon nanotubes with and without Coulomb interaction," *Phys. Rev. B*, vol. 57, pp. 9343–9348, 1998.

[7] L. X. Benedict, S. G. Louie, and M. L. Cohen, "Static polarizabilities of single-wall carbon nanotubes," *Phys. Rev. B*, vol. 52, pp. 8541–8549, 1995.

[8] E. Hallén, "Theoretical investigations into the transmitting and receiving qualities of antennae," *Nova Acta Reg. Soc. Scient. Upsaliensis*, vol. 11, pp. 1–44, 1938.

[9] P. Newton, *Theory of Waves and Particles Scattering*. World: Moscow, 1969 (in Russian).

[10] R. C. McPhedran, L. C. Botten, A. A. Asatryan, N. A. Nicorovici, P. A. Robinson, and C. M. de Sterke, "Calculation of electromagnetic properties of regular and random arrays of metallic and dielectric cylinders," *Phys. Rev. E*, vol. 60, pp. 7614–7617, 1999.

[11] G. Ya. Slepyan, S. A. Maksimenko, A. Lakhtakia, O. Yevtushenko, and A. V. Gusakov, "Electrodynamics of carbon nanotubes: Dynamic conductivity, impedance boundary conditions, and surface wave propagation," *Phys. Rev. B*, vol. 60, pp. 17136–17149, 1999.

[12] L. A. Weinstein, *The Theory of Diffraction and the Factorization Method*. Golem: New York, 1969).

[13] O. Hilt, H. B. Brom, and M. Ahlskog, "Localized and delocalized charge transport in single-wall carbon-nanotube mats," *Phys. Rev. B*, vol. 61, pp. R5129–R5132, 2000.

On Mode Spectrum Degenerations, Quasi-Degenerations and Mode Polarization Transformations in Optical Chiral Waveguides

S.V. Demidov[1], K.V. Kushnarev[1], and V.V. Shevchenko[2]

[1] Radiophysics Department, Russian People Friendship University, Mikluho-Maklay str. 6, Moscow, 117198, Russia.

[2] Institute of Radioengineering and Electronics, Mokhovaya str. 11, Moscow, 103907, Russia.
E-mail: sto@mail.cplire.ru

Abstract

It is known [1-3], that mode spectrum degenerations take place for modes in chiral optical waveguides. Dispersion characteristics (curves) cross one another in the degeneration points, where propagation constants of two modes have the same values on some frequency. However, the more accurate analysis shows, that degeneration points are not exact but approximate only. In reality they are quasi-degeneration points. The dispersion curves do not cross one another, they close up near quasi-degeneration points. In this place, circular polarization of the modes converts: the right-handed polarization changes into left handed and on the contrary.

1. Theory

This paper deals with polarization transformations of modes in isotropic and anisotropic planar chiral optical waveguides and optical fibers. The general theory of spectral degenerations and quasi-degenerations and mode transformations is given in [4].

Let's have the dispersion equation for even modes in a symmetrical chiral planar waveguide [2,3]

$$(b - C_+ \tan C_+V)(b - C_- \tan C_-V) - \Delta^2 C_+ C_- t \tan C_+V \tan C_-V = 0, \tag{1}$$

where

$$b = \left(\frac{\gamma - kn_o}{kn_o\Delta} \right)^{\frac{1}{2}}, \tag{2a}$$

$$V = kn_g R(2\Delta)^{\frac{1}{2}}, \tag{2b}$$

$$k = \frac{\omega}{c}, \tag{2c}$$

$$\Delta = \frac{n_g - n_o}{n_g} << 1, \tag{2d}$$

$$C_{\pm} = \left(1 \mp 2\kappa V - b^2\right)^{\frac{1}{2}}, \quad \kappa = \frac{\rho}{2R\left(2\Delta^3\right)^{\frac{1}{2}}}, \tag{2e}$$

γ is a propagational constant, ω is a circular frequency, c is a velocity of light; n_g and n_o are refraction coefficients of the inside and outside media, ρ is a chirality, R is a half-thickness of the guiding layer. In [3] we used approximation $\Delta \approx 0$, and the dispersion curves were solutions of equations

$$b - C_+ \tan C_+ V = 0, \tag{3a}$$

$$b - C_- \tan C_- V = 0. \tag{3b}$$

For the solution $b = b_q$, $V = V_q$, where b_q and V_q satisfy both equations (3) simultaneously, we had a degeneration point. Now the dispersion equation (1) can be presented approximately near this point as

$$\left[\left(b - b_q\right)A_+ - \left(V - V_q\right)B_+\right]\left[\left(b - b_q\right)A_- - \left(V - V_q\right)B_-\right] - \Delta^2 b_q^2 C_{q+}^2 C_{q-}^2 = 0 \tag{4}$$

where

$$\begin{aligned} A_{\pm} &= \left(1 \mp 2\kappa\ V_q\right)\left(1 + b_q V_q\right), \\ B_{\pm} &= \left(1 \mp 2\kappa V_q\right)\left(C_{q\pm}^2 \mp \kappa V_q\right) \mp \kappa b_q, \\ C_{q\pm} &= \left(1 \mp 2\kappa V_q - b_q^2\right)^{\frac{1}{2}}. \end{aligned} \tag{5}$$

Due to (4) that point b_q, V_q is quasi-degeneration point [4].

$$\kappa = 0.1, \Delta = 0.01$$

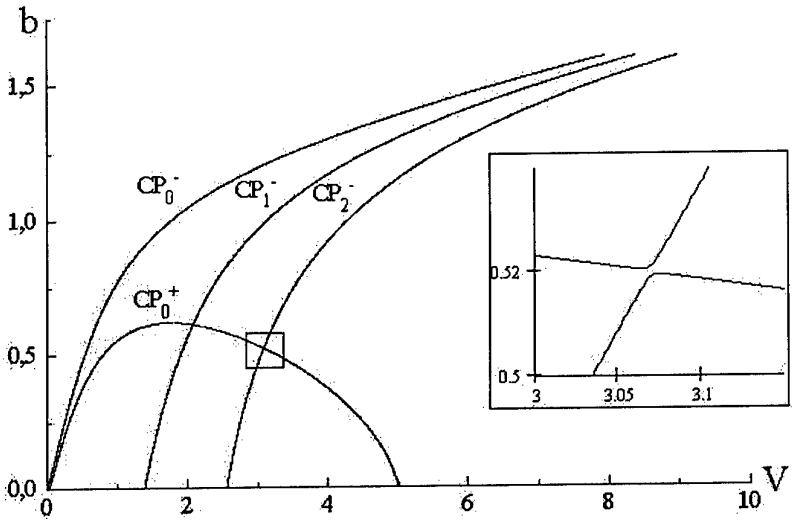

Fig. 1

It is possible to reconstruct the fine structure of dispersion curves that defines them near the points of quasi-degeneration from those results.

2. Discussion

It is interesting to consider the polarization evolution of both modes related to these curves. According to Fig. 1 while frequency increases and mode curves are passing the quasi-degeneration point of b_q, V_q the mode CP_0^+ with right-handed polarization converts into CP_2^- with left handed polarization. And how can a circular polarized mode change the direction of field rotation? It seems at first sight that it is necessary for this kind of transformation that the speed of rotation has to slow down to zero and only after this the polarization handiness changes. But this process is impossible. The frequency of rotation of a field vector and wave length of a circular polarized mode cannot change essentially on a respectively small frequency interval near the quasidegeneration point. That is why only the following process of polarization conversion can take place. Both polarizations are approximately circular they are slightly elliptical. The ellipticity grows while the dispersion curve approaches the quasi-degeneration point. In the nearest area the polarization appears to be linear and parallel to the boundary for the upper curve with a smaller phase velocity and perpendicular for the lower curve with greater phase velocity. Having passed those area the polarization becomes elliptical but with an opposite direction of field vector rotation and then approximately circular again. This takes place for optical chiral waveguides with a little difference of refraction coefficients of a guiding and external media.

Although all mentioned above dealt with even modes of a planar chiral waveguide the same relates to odd modes. But the dispersion curves' intersection points for even and odd modes are strictly degenerational because the dispersion equations for even and odd modes are exactly independent.

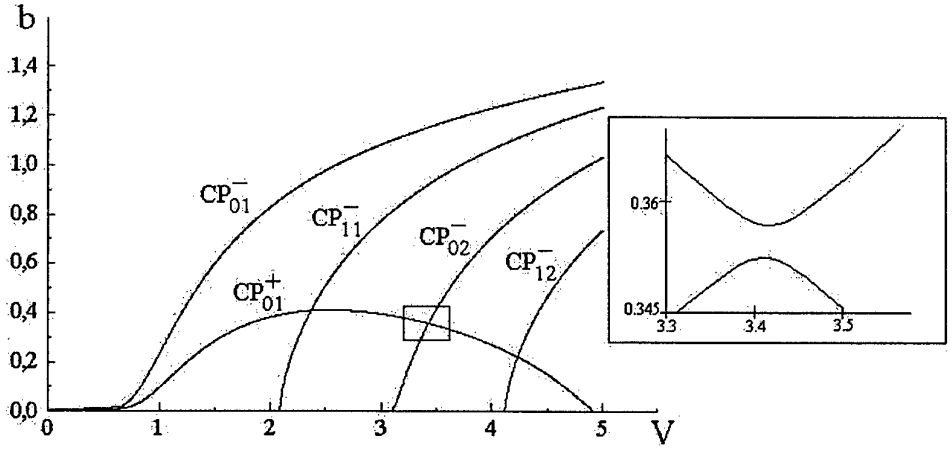

Fig. 2

We have the similar results for modes in chiral optical fiber with the same angular variations of fields (Fig. 2),

$$\kappa = 0.1, \Delta = 0.01$$

and for modes in anisotropic planar chiral waveguide (Fig. 3), where modes always have elliptical polarization [5]. In Fig. 3 $\sigma = e/4\Delta$, $\varepsilon_x = \varepsilon_g(1+e)$, $\varepsilon_y = \varepsilon_z = \varepsilon_g = n_g^2$, where x, y are transverse and z is longitudinal coordinates, x is parallel to the boundaries of the waveguide and in (2)

$$C_{\pm} = \left[1 + \sigma \mp \left(\kappa^2 V^2 + \sigma^2\right)^{\frac{1}{2}} - b^2\right]^{\frac{1}{2}}, \quad \kappa = \frac{\rho_x + \rho_y}{4R\left(2\Delta^3\right)^{\frac{1}{2}}}. \tag{6}$$

$$\kappa = 0.1, \sigma = 0.5, \Delta = 0.01$$

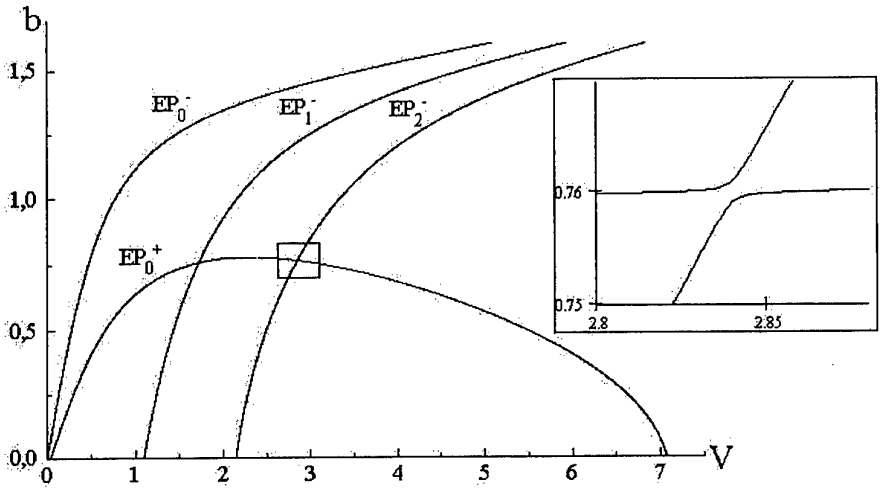

Fig. 3

References

[1] I. V. Lindell, A. H. Sihvola, S. A. Tretyakov, and A. J. Viitanen, *Electromagnetic Waves in Chiral and Bi-isotropic Media.* Boston-London: Artech House, 1994.

[2] S. V. Demidov, K. V. Kushnarev, and V. V. Shevchenko, "On mode dispersion properties of chiral optical planar waveguides", *Journal of Radioelectronics*, No. 4, 1999, http://jre.cplire.ru/jre/apr99/1/text.html.

[3] S. V. Demidov, K. V. Kushnarev, and V. V. Shevchenko, "Dispersion properties of the modes of chiral planar optical waveguides", *J. of Communications Technology and Electronics*, vol. 44, No. 7, pp. 827-832, 1999.

[4] V. V. Shevchenko, "On spectral degenerations, quasi-degenerations and wave transformations in dielectric waveguides and lightguides", *J. of Communications Technology and Electronics*, vol. 45, 2000 (in press).

[5] V. V. Shevchenko, "Waves in chiral-anisotropic medium", *J. of Communications Technology and Electronics*, vol. 44, No. 11, pp. 1198-1201, 1999.

A Uniaxial Chiral Slab Backed by Soft and Hard Surfaces Used as a Polarization Transformer

G. Öğücü and S. Uçkun

Electrical and Electronics Engineering Department, University of Gaziantep, Gaziantep, 27310, Turkey. email: savas@gantep.edu.tr

Abstract

Plane wave reflection from soft and hard surfaces coated by chiral material has recently been analyzed for normal incidence. In this study, the plane wave reflection from a uniaxial chiral slab backed by soft and hard surfaces is formulated for normal incidence and the polarization properties of the reflected field are investigated.

1. Introduction

The chiral medium is a subclass of bianisotropic media. A special type of bianisotropic chiral media is the axially chiral uniaxial medium. A uniaxial bianisotropic chiral slab can be realized by doping miniature chiral objects (such as wire spirals) into an anisotropic host medium as explained in [1]-[2]. The orientation of the chiral objects must be parallel to a unique preferred direction.

Soft and hard surface (SHS) boundaries are well known from acoustics. They have been also defined for dually polarized electromagnetic waves. Kildal [3] explained the concept of SHS in detail by considering different geometries. A common characteristic of both soft and hard surfaces is that they do not create cross polarization by geometrical optics reflection. For example, a right circularly polarized wave for a hard conducting surface is still right cicularly polarized after reflection and for a smooth conducting surface it is left circularly polarized.

In a previous paper [4], an isotropic chiral slab backed by SHS and its application to polarization transformer have been analyzed. In this study, a plane wave reflected from an infinite uniaxial chiral slab of thickness d, sandwiched between air and SHS, with axis parallel to the interfaces is considered. This characteristic of SHS and easy construction of the uniaxial chiral slab might make the study of this problem worthwhile.

2. Fields at the Interface and Reflection Dyadic

It is known that in the uniaxial chiral medium, the electromagnetic fields satisfy the constitutive relations

$$\mathbf{D} = \overline{\overline{\varepsilon}} \cdot \mathbf{E} - j\sqrt{\mu_o \varepsilon_o}\,\overline{\overline{\kappa}} \cdot \mathbf{H} \tag{1.a}$$

$$\mathbf{B} = \overline{\overline{\mu}} \cdot \mathbf{H} + j\sqrt{\mu_o \varepsilon_o}\,\overline{\overline{\kappa}} \cdot \mathbf{E} \tag{1.b}$$

with the medium parameter dyadics

$$\overline{\overline{\varepsilon}} = \varepsilon_u \hat{\mathbf{u}}\hat{\mathbf{u}} + \varepsilon_t (\hat{\mathbf{v}}\hat{\mathbf{v}} + \hat{\mathbf{z}}\hat{\mathbf{z}}) \tag{2.a}$$

$$\overline{\overline{\mu}} = \mu_u \hat{\mathbf{u}}\hat{\mathbf{u}} + \mu_t (\hat{\mathbf{v}}\hat{\mathbf{v}} + \hat{\mathbf{z}}\hat{\mathbf{z}}) \tag{2.b}$$

$$\overline{\overline{\kappa}} = \kappa \hat{\mathbf{u}}\hat{\mathbf{u}}\,. \tag{2.c}$$

where κ is the chirality parameter and the nonreciprocity parameter χ of [5] is assumed zero. In Eq. (2), u and v are the transverse axes to z-axis with $\hat{\mathbf{u}} = \hat{\mathbf{z}} \times \hat{\mathbf{v}}$. They are chosen such that they are the natural coordinates from the geometrical optics point of view. Moreover, the direction of corrugation on SHS is along v-axis.

To find the reflection coefficient of the plane wave for normal incidence, consider a uniaxial slab which is confined between two infinitely extended planes at $z=-d$ and $z=0$, as shown in Figure 1. The plane wave solutions of the Maxwell's equations for the chiral medium are [2]

$$\mathbf{E}_{\pm}(\mathbf{r}) = E_{\pm} e^{-jk_{\pm}z} \tag{3.a}$$

$$\mathbf{H}_{\pm}(\mathbf{r}) = \frac{k_{\pm}}{k_t \eta_t} \hat{\mathbf{z}} \times \mathbf{E}_{\pm}(\mathbf{r}) \tag{3.b}$$

where + and – indicate the right-hand and left-hand polarization, respectively. In Eq. (3), the corresponding propagation factors are given by

$$k_{\pm} = k_t \sqrt{A_{\pm}} \tag{4.a}$$

where

$$k_t = \omega\sqrt{\mu_t \varepsilon_t}\ ,\ \eta_t = \sqrt{\mu_t/\varepsilon_t}\ ,\ A_{\pm} = \frac{1}{2}\left(\frac{\mu_u}{\mu_t} + \frac{\varepsilon_u}{\varepsilon_t}\right) \pm \sqrt{\frac{1}{4}\left(\frac{\mu_u}{\mu_t} - \frac{\varepsilon_u}{\varepsilon_t}\right)^2 + \frac{\kappa^2 \mu_o \varepsilon_o}{\mu_t \varepsilon_t}} \tag{4.b}$$

After writing the fields inside the uniaxial chiral slab and using boundary conditions at z=-d and z = 0 the following equation can be obtained:

$$\mathbf{E}^r = \overline{\overline{\mathbf{R}}} \cdot \mathbf{E}^i \tag{5}$$

where

$$\overline{\overline{\mathbf{R}}} = \begin{bmatrix} R_{uu} & R_{uv} \\ R_{vu} & R_{vv} \end{bmatrix} = e^{j2k_o d} \begin{bmatrix} \dfrac{U-X}{Y+X} & \dfrac{Z}{Y+X} \\ \dfrac{T}{Y+X} & \dfrac{S-X}{Y+X} \end{bmatrix}. \tag{6}$$

In Eq. (6)

$$S = -AD(k_+ + k_-)^2 + j\frac{k_t \eta_t}{\eta_o}(A+D)(k_+ + k_-)\sin(k_+ + k_-)d + \frac{k_t^2 \eta_t^2}{\eta_o^2}\sin^2(k_+ + k_-)d \tag{7.a}$$

$$T = j2(k_- B - k_+ C)\frac{k_t \eta_t}{\eta_o}\sin(k_+ + k_-)d \tag{7.b}$$

$$U = -AD(k_+ + k_-)^2 - j\frac{k_t \eta_t}{\eta_o}(A+D)(k_+ + k_-)\sin(k_+ + k_-)d + \frac{k_t^2 \eta_t^2}{\eta_o^2}\sin^2(k_+ + k_-)d \tag{7.c}$$

$$X = (B^2 + C^2)k_+ k_- - BC(k_+^2 + k_-^2) \tag{7.d}$$

$$Y = AD(k_+ + k_-)^2 + j\frac{k_t \eta_t}{\eta_o}(A-D)(k_+ + k_-)\sin(k_+ + k_-)d + \frac{k_t^2 \eta_t^2}{\eta_o^2}\sin^2(k_+ + k_-)d \tag{7.e}$$

$$Z = j2(k_+ B - k_- C)\frac{k_t \eta_t}{\eta_o}\sin(k_+ + k_-)d \tag{7.f}$$

where

$$A = \sin k_+ d \sin k_- d\ ,\ B = \sin k_+ d \cos k_- d \tag{8a}$$

$$C = \cos k_+ d \sin k_- d\ ,\ D = \cos k_+ d \cos k_- d \tag{8b}$$

For the isotropic achiral slab, $k_+ = k_- = k_t = k$, and therefore $Z = T = X = 0$ which contributes to the vanishing of the crosspolarized reflection coefficients. The copolarized reflection coefficients are

$$R_{uu} = e^{j2k_o d}\frac{\left(\dfrac{\eta_t^2}{\eta_o^2} - 1\right)\sin 2kd - j2\dfrac{\eta_t}{\eta_o}}{\left(\dfrac{\eta_t^2}{\eta_o^2} + 1\right)\sin 2kd - j\dfrac{\eta_t}{\eta_o}2\cos 2kd} \quad \text{and} \quad R_{vv} = e^{j2k_o d}\frac{\left(\dfrac{\eta_t^2}{\eta_o^2} - 1\right)\sin 2kd + j2\dfrac{\eta_t}{\eta_o}}{\left(\dfrac{\eta_t^2}{\eta_o^2} + 1\right)\sin 2kd - j\dfrac{\eta_t}{\eta_o}2\cos 2kd} \tag{9}$$

Thus, the incident field does not change polarization after it is reflected, but the phases of the field components are shifted as expected.

For the uniaxial chiral slab there is not always such simple expressions. If we consider a special case for the uniaxial chiral slab with $(k_+ + k_-)d = \pi$ and $(k_+ - k_-)d = \pi/2$, then $R_{uv} = R_{vu} = 0$ and

$$R_{uu} = R_{vv} = -e^{j2k_o d}\frac{2k_+k_- + (k_+ + k_-)^2}{2k_+k_- - (k_+ + k_-)^2} \tag{10}$$

Hence, in this case, as for the isotropic achiral slab, linearly polarized wave is reflected as linearly polarized wave.

3. Polarization Transformer

Let us study the possibility of defining the uniaxial medium backed by SHS as polarization transformer, by appropriate choice of the medium parameter values and thickness of the slab. Assume that the incident field linearly polarized along $\hat{\mathbf{u}}$, reflects right-hand circularly polarized, and that polarized along $\hat{\mathbf{v}}$, reflects left-hand circularly polarized. Then $\overline{\overline{\mathbf{R}}} \cdot \hat{\mathbf{u}}$ will be parallel to $-\hat{\mathbf{u}} + j\hat{\mathbf{v}}$ and $\overline{\overline{\mathbf{R}}} \cdot \hat{\mathbf{v}}$ will be parallel to $-\hat{\mathbf{u}} - j\hat{\mathbf{v}}$. These lead to

$$\mathrm{Re}\left\{-\frac{U-X}{Y+X}\right\} = \mathrm{Re}\left\{\frac{T}{j(Y+X)}\right\}, \text{ and } \mathrm{Re}\left\{\frac{Z}{Y+X}\right\} = \mathrm{Re}\left\{-\frac{S-X}{j(Y+X)}\right\} \tag{11.a}$$

$$\mathrm{Im}\left\{-\frac{U-X}{Y+X}\right\} = \mathrm{Im}\left\{\frac{T}{j(Y+X)}\right\} = 0, \text{ and } \mathrm{Im}\left\{\frac{Z}{Y+X}\right\} = \mathrm{Im}\left\{-\frac{S-X}{j(Y+X)}\right\} = 0 \tag{11.b}$$

to be more explicit these equations give

$$\cos(k_+ + k_-)d = 0 \quad \text{and} \quad \sin(k_+ - k_-)d = \pm\left(\frac{\frac{2k_+k_-}{k_t\eta_t/\eta_o} - 2\frac{k_t\eta_t}{\eta_o} + k_+ - k_-}{k_+ + k_-}\right) \tag{12}$$

With the conditions in Eq. (12), the reflection dyadic will be

$$\overline{\overline{\mathbf{R}}} = e^{j2k_o d}\left(\frac{1}{\sqrt{2}}(-\hat{\mathbf{u}} + j\hat{\mathbf{v}})\hat{\mathbf{u}} + \frac{1}{\sqrt{2}}j(-\hat{\mathbf{u}} - j\hat{\mathbf{v}})\hat{\mathbf{v}}\right)R_0 \tag{13}$$

where

$$R_0 = \frac{\sqrt{2}\left((k_+k_-)^2 - \left(k_t\eta_t/\eta_o\right)^4\right)}{(k_+k_-)^2 + 4(k_+k_-)\left(k_t\eta_t/\eta_o\right)^2 + \left(k_t\eta_t/\eta_o\right)^4} \tag{14}$$

As can be deduced from Eq. (13), the incident polarization $\hat{\mathbf{u}}$ gives rise to right-hand circularly polarized, and $\hat{\mathbf{v}}$ to left-hand circularly polarized reflected field.

The ratio $\dfrac{k_+k_-}{(k_t\eta_t/\eta_o)^2}$ in Eq.(12) is not arbitrary. We can impose some conditions on it. From the expression in Eq. (12)

$$-1 \le \frac{\frac{2k_+k_-}{k_t\eta_t/\eta_o} - 2\frac{k_t\eta_t}{\eta_o} + k_+ - k_-}{k_+ + k_-} \le 1 \tag{15}$$

and hence

$$\left(\frac{\sqrt{5}-1}{2}\right)\leq\frac{k_+k_-}{\left(k_t\eta_t/\eta_o\right)^2}\leq\left(\frac{\sqrt{5}+5}{2}\right) \tag{16}$$

The graph of the reflection coefficient, $|R_0|$, as a function of Ratio = $\frac{k_+k_-}{(k_t\eta_t/\eta_o)^2}$ is shown in Figure 2. When the Ratio is one, $|R_0|$ vanishes and hence there is no reflection at this point. With the condition in Eq. (16), a highly efficient polarization transformer cannot be achieved by using a uniaxial chiral slab.

4. Conclusion

In this study, the normal incidence of the electromagnetic waves to lossless uniaxial chiral slab backed by SHS is analyzed. The reflection dyadic is derived. It is shown that the slab can be used as polarization transformer if the suitable medium parameters and slab thickness are chosen.

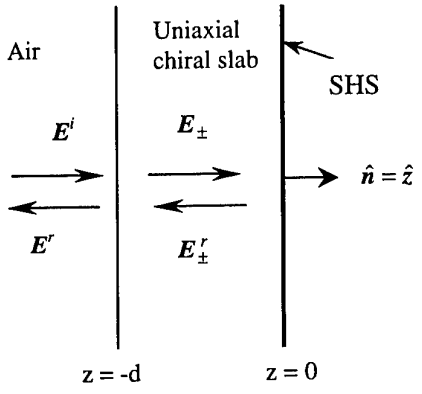

Fig. 1 Geometry of the problem.

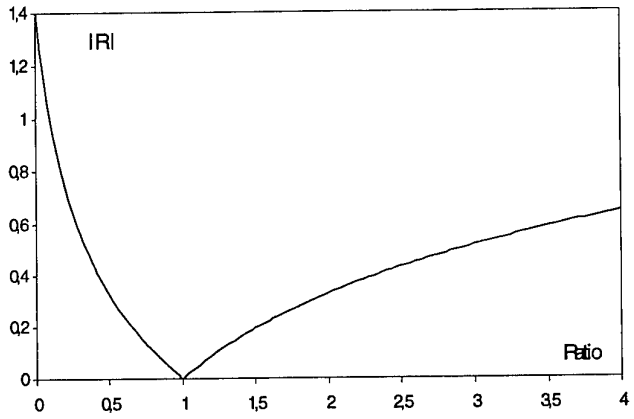

Fig. 2 The reflection coefficient R as a function of the Ratio = $\frac{k_+k_-}{(k_t\eta_t/\eta_o)^2}$.

References

[1] A. J. Viitanen and I. V. Lindell, "Uniaxial chiral quarter-wave polarisation transformer," *Electron. Lett.*, Vol. 29, pp. 1074-1075, June 1993.

[2] I. V. Lindell and A. H. Sihvola, "Plane-wave reflection from uniaxial chiral interface and its application to polarization transformation," *IEEE Trans. Antennas Propagat.*, Vol. 43, pp. 1397-1404,.Dec. 1995.

[3] P.-S. Kildal, "Artificially soft and hard surfaces in electromagnetics," *IEEE Antennas Propagat.*, vol. 38, no. 10, pp. 1537-1544, Oct. 1990.

[4] A. J. Viitanen and P. P. Puska, "Plane wave reflection from a chiral slab backed by soft and hard surfaces with application to polarisation transformers," *IEE Proc.-Microw. Antennas Propagat.*, Vol. 145, no. 4, pp. 299-302, Aug. 1998.

[5] A. J. Viitanen, "Reflected and transmitted fields of uniaxial bianisotropic slab," *Proc. URSI 1995*, Int. Symp. EM Theory, pp. 649-651, 1995.

Anisotropic Electromagnetic Properties of RF Sputtered Ni–Al_2O_3 Composite Thin Films

T. S. Sathiaraj[1] and B. Michel[2]

[1] Department of Physics, University of Botswana,
Private Bag 0022, Gaborone, Botswana
e-mail: sathiara@mopipi.ub.bw, Fax: 267-585097

[2] Scientific Consulting,
Kirchenstraße 13, D–90537 Feucht–Moosbach, Germany
e–mail: BEST.michel@t–online.de

Abstract

Experimental data of the permittivity of RF sputtered Ni-Al_2O_3 thin films were studied in the wavelength region from 300 to 2500 nanometers [1]. The data were analyzed in the framework of the Bergman-Milton theory and it was shown that they lie inside the Hashin-Shtrikman bounds, but outside the Bergman-Milton bounds. The latter indicates a strong electromagnetic anisotropy of the composite thin film. For a more detailed theoretical study, we performed calculations using the Maxwell Garnett, Bruggeman and Incremental Maxwell Garnett homogenization formalisms for uniaxial dielectric composites [2–4]. A comparison between the calculated and measured permittivities was made on the basis of a least-square fit. In this paper, we interpret the results and suggest models for the microstructures of the Ni-Al_2O_3 thin films.

1. Introduction

The dielectric properties of composite thin films made of a mixture of two particulate materials are of great practical interest with potential applications in many disciplines of science and technology. Composite thin films can be fabricated by a variety of vacuum techniques. In order to obtain the desired optical properties, the film microstructure has to be optimized in terms of concentration, size and shape of the inclusions. If the nonhomogeneities of the composite thin film are electrically small, homogenization theory can be used to obtain estimates of its effective permittivity, provided the permittivities of the component materials and some details about its microstructure are known ("direct problem"). Conversely, if the effective permittivity of the composite thin film has been determined experimentally, homogenization formalisms can be applied for microstructural characterization ("inverse problem").

The Bergman-Milton theory [5, 6] provides rigorous bounds for the effective permittivity in the complex plane [7] and therefore is an important tool for a preliminary analysis of experimental data [8]. Homogenization formalisms, such as the Maxwell Garnett and Bruggeman formula and their extensions, can be used for more detailed studies.

Due to the axial symmetry of the thin film geometry, we expect its effective permittivitiy dyadic $\underline{\underline{\epsilon}}^{\text{eff}}$ to be uniaxial

$$\underline{\underline{\epsilon}}^{\text{eff}} = \epsilon_0 \left[\epsilon_u^{\text{eff}} \underline{u}\,\underline{u} + \left(\underline{\underline{I}} - \underline{u}\,\underline{u} \right) \epsilon_t^{\text{eff}} \right], \tag{1}$$

with the free-space permittivity ϵ_0, the unit dyadic $\underline{\underline{I}}$, and the unit vector $\underline{u}$ perpendicular to the surface of the thin film; ϵ_u^{eff} and ϵ_t^{eff} are the axial and transverse components of the relative

effective permittivity dyadic, respectively. The electromagnetic anisotropy of the film may be caused by an anisotropic growth of the film on the substrate, by the non-spherical shape of the particulates the film is made of, and by an anisotropic spatial arrangement of these particulates. Homogenization formalisms that are able to take the anisotropy into account have become available only recently; see [9] for a review. The main intention of this paper is to interpret measured permittivities obtained for Ni-Al_2O_3 composite thin films in the framework of these formalisms.

2. Theory

The Al_2O_3 host material of the thin film is taken to be uniaxial dielectric with a permittivity dyadic $\underline{\underline{\epsilon}}^a$ of the form

$$\underline{\underline{\epsilon}}^a = \epsilon_0 \epsilon^a \left[\gamma \underline{u}\underline{u} + \left(\underline{\underline{I}} - \underline{u}\underline{u} \right) \right], \tag{2}$$

where the parameter γ specifies the degree of anisotropy. The permittivity dyadic $\underline{\underline{\epsilon}}^b$ of the inclusions (Ni particulates in our case) is isotropic:

$$\underline{\underline{\epsilon}}^b = \epsilon_0 \epsilon^b \underline{\underline{I}}. \tag{3}$$

For the reasons discussed before, the effective permittivity dyadic $\underline{\underline{\epsilon}}^{\text{eff}}$ of the composite thin film is assumed to be uniaxial, having the form specified in (1).

Let us first assume that the host material is isotropic ($\gamma = 1$ in equation (2)). The Bergman-Milton theory is then applicable. Accordingly, the scalar relative permittivities ϵ_t^{eff} and ϵ_u^{eff} must lie inside a region of the complex permittivity plane which is bounded by the so-called Hashin-Shtrikman (HS) bounds. Failure of measured permittivities to fulfill this constraint indicates serious inconsistencies of the data. If the microstructure of the composite medium is isotropic, the effective permittivity will be isotropic too ($\epsilon_u^{\text{eff}} = \epsilon_t^{\text{eff}}$). The value of the effective permittivity can then be further restricted by the so-called Bergman-Milton (BM) bounds. If the measured effective permittivities lie outside the BM bounds, the thin film must be anisotropic.

Homogenization formalisms can be used to get a more detailed description of the experimental data. For dilute composites in which one component exists as inclusions embedded in the other one, the Maxwell Garnett (MG) formalism is expected to produce good results. For non-dilute, mutually isolated inclusions, the Incremental Maxwell Garnett (IMG) formalism (or, alternatively, the Differential Maxwell Garnett formalism) is an appropriate choice [4], whereas for composites with percolated inclusions the Bruggeman (Br) formalism is recommendable. In these homogenization formalisms, anisotropy can be implemented in two ways: by using uniaxial permittivity dyadics for the component materials ($\gamma \neq 0$ in eq. (2)), and by assigning the host and inclusion particulates a spheroidal effective shape with a certain aspect ratio $a : b$, the latter quantitiy being > 1 for prolate and < 1 for oblate spheroids (and 1 for spheres). The effective shape is a parametrization of both shape *and* relative spatial arrangment of the particulates.

3. Experiment

The Ni-Al_2O_3 composite films were deposited in a planar magnetron assisted RF sputtering system. The fill factor f of Ni was found to be 0.21, 0.42 and 0.61 in the examples studied here. Detailed reports on the experimental set-up and characterization techniques have been given elsewhere [10]. The optical constants n and k of the composite films in the wavelength range from 300 to 2500 nm were calculated from the measured near-normal incidence reflectance (R), transmittance (T) and thickness (t) values as described elsewhere [1]. Because of the near-normal incidence technique used, the electromagnetic field is approximately parallel to the surface of the film; therefore only the transverse component of the relative permittivity ϵ_t^{eff} can be deduced from this experiment. The relation between n, k, and ϵ_t^{eff} is $\epsilon_t^{\text{eff}} = (n + ik)^2$.

4. Results and Discussion

For all fill factors and wavelengths, the measured permittivities were compared with the HS and BM bounds. All experimental data lie within the HS bounds, but outside the BM bounds. The latter provides evidence that the composite is anisotropic. Typical results for various fill factors f are shown in Figure 1, where we used the optical constants for Ni and Al_2O_3 at wavelength $\lambda = 500$ nm. Assuming isotropy (γ=1, a:b=1), we computed the MG, Br, IMG estimates, which turned out to lie far off the experimental results (Figure 1). Allowing for an oblate spheroidal effective shape of the particulates ($a : b < 1$), the agreement between theory and experiment is greatly improved. This is also shown in Figure 1 in the case of the IMG estimate.

A further comparison between the calculated and measured permittivites of the thin film was made on the basis of a least-square fit, minimizing the quantity

$$\chi^2 = \sum_i \left| \epsilon_t^{\text{eff}}(\lambda_i) - \epsilon_t^{exp}(\lambda_i) \right|^2, \tag{4}$$

where the sum extends over all measured wavelengths λ_i, ϵ_t^{exp} is the measured and ϵ_t^{eff} the computed value of the transverse component of the permittitivity. Assuming that the Al_2O_3 host material is anisotropic ($\gamma \neq 0$ in equation (2)) does not lead to a significant improvement of the fit between experiment and calculations. The effective shape of the particulates, however, significantly influences the quality of the fit.

For $f = 0.21$ and $f = 0.42$ the IMG formalism performs best while for $f = 0.61$ the Br formalism leads to the smallest χ^2-values (Figure 2). The best fit is obtained, when the *effective* shape of the particulates is oblate spheroidal with aspect ratios in the range from 0.1 to 0.6, depending on the fill factor. This strong dependence on the fill factor cannot be explained by assuming a non-spherical shape of the particulates itself. Rather it must be due to their anisotropic arrangement in the film. A possible interpretation of these findings is that the Ni inclusions form planar structures parallel to the surface of the thin film. For larger fill factors ($f = 0.62$) percolation sets in and therefore the Br estimate is in better agreement with experiment.

References

[1] T. S. Sathiaraj and R. Thangaraj, "The experimental and calculated optical properties of Ni–Al_2O_3 coatings using effective medium theories", *J. Phys. D*, 30, p. 769, 1997.

[2] A. Lakhtakia, B. Michel, and W. S. Weiglhofer, "The role of anisotropy in the Maxwell Garnett and Bruggeman formalisms for uniaxial particulate composite media," *J. Phys. D*, 30, pp. 230–240, 1997.

[3] B. Michel, A. Lakhtakia, W. S. Weiglhofer, and T. G. Mackay, "Incremental and differential Maxwell Garnett formalisms for bianisotropic composites," *Comp. Sci. Technol.*, 2000, at press.

[4] B. Michel, A. Lakhtakia, W. S. Weiglhofer, and T. G. Mackay, "The incremental and differential Maxwell Garnett formalisms for bianisotropic composites," in *Proc. Bianisotropics 2000*, A. M. Barbosa and A. L. Topa (Eds.), Lisbon, Portugal, pp. 27–30, 2000.

[5] D. J. Bergman, "The dielectric constant of a composite material — a problem in classical physics", *Phys. Rept.*, 43, pp. 377–407, 1978.

[6] G. W. Milton, "Bounds on the complex permittivity of a two–component composite material", *J. Appl. Phys.*, 52, pp. 5286–5293, 1981.

[7] B. Michel, http://www.unternehmen.com/Bernhard-Michel/ejava.html (Online program for the calculation of the HS and BM bounds).

[8] G. A. Niklasson and C. G. Granqvist, "Optical properties and solar selectivity of coevaporated Co-Al_2O_3 composite films", *Journal Appl. Phys.*, 55, pp. 3382–3410, 1984.

[9] B. Michel, "Recent developments in the homogenization of linear bianisotropic composite materials," in O. N. Singh and A. Lakhtakia (Eds.), *Electromagnetic Fields in Unconventional Materials and Structures*. Wiley: New York, 2000, pp. 39–82.

[10] T. S. Sathiaraj, R. T Thangaraj , H. Al Sharbaty, and O. P. Agnihotri, " Optical properties of selectively absorbing R.F. sputtered Ni–Al_2O_3 composite films", *Thin Solid Films*, 195, 33,1991.

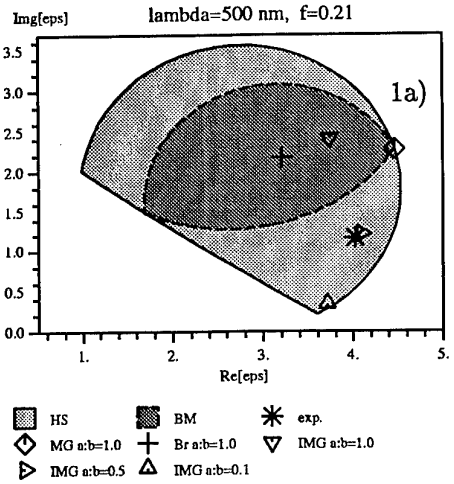

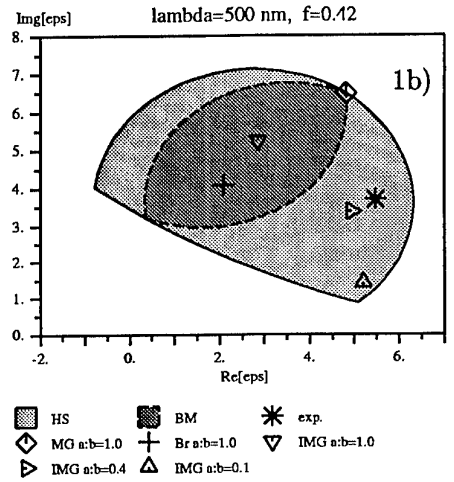

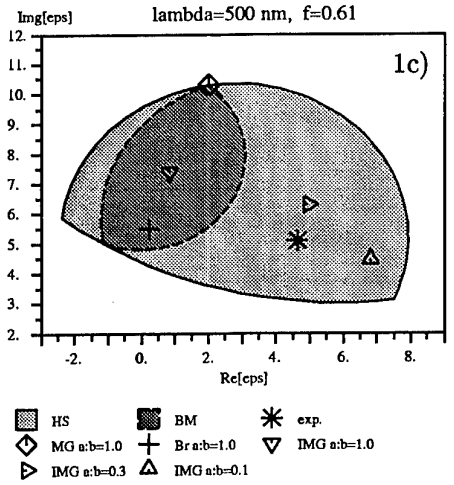

Figure 1: Comparison of experimental data (exp.), HS and BM bounds, and various homogenization estimates calculated for different aspect ratios $a : b$.
a) $f = 0.21$, b)$f = 0.42$, c) $f = 0.61$.

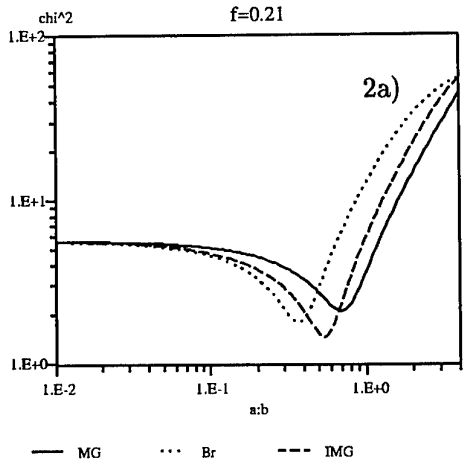

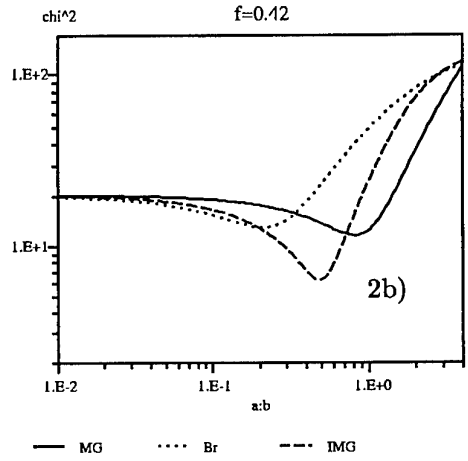

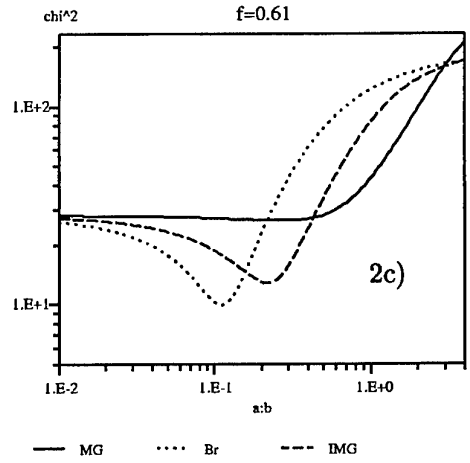

Figure 2: χ^2 as function of the aspect ratio $a : b$ for the MG, Br, and IMG homogenization formalisms.
a) $f = 0.21$, b)$f = 0.42$, c) $f = 0.61$.

Diffraction by a Conducting Half-Plane in a Chiroplasma

D. A. Marakassov[1] and V. V. Fisanov[2]

[1] Department of Radiophysics, Tomsk State University
Lenin Avenue 36, 634050 Tomsk, Russia;
Electromagnetics Laboratory, Helsinki University of Technology
P.O. Box 3000, FIN-02015 HUT, Finland

[2] Siberian Physical and Technical Institute, Tomsk State University
Revolution Square 1, 634050 Tomsk, Russia
Fax: + 7-3822-233-034; email: kanc@spti.tsu.ru

Abstract

The scattering of a plane eigenwave normally incident on a half-plane placed in a chiroplasma whose distinguished axis is parallel to the edge of the screen is considered. The formulation of the problem leads to the vector functional equation which is exactly solved by the Wiener–Hopf–Hilbert method. Some distinct properties of the diffraction problem are noted.

1. Introduction

Diffraction of waves as an item of bianisotropy research in electromagnetics is in need of a unimaginative but adequate model description. As for chiral media subjected to an external magnetic field, the constitutive relations of a chiroplasma [1] are rather simple. They differ favorably from a previous ones [2] by what properly furnish the transition to an isotropic chiral medium. Therefore we use the chiroplasma model in the attempt to obtain an exact analytical solution of a half-plane canonical diffraction problem with reference to complex birefringent medium. As opposed to its nonchiral [3], nongyrotropic chiral [4] and biisotropic [5] counterparts, the problem is led to the vector Wiener–Hopf equation. The matrix factorization is fulfilled by virtue of the Wiener–Hopf–Hilbert method. Some features of the obtained exact closed-form solution are discussed then.

2. Statement of the Diffraction Problem

A perfectly conducting screen $x \geq 0$, $y = 0$ is embedded in a chiroplasma whose distinguished z-axis is parallel to the edge. The medium is described by the constitutive relations (time-harmonic factor $\exp(-i\omega t)$ is meant)

$$\begin{cases} \mathbf{D} &= \bar{\bar{\varepsilon}} \cdot \mathbf{E} + i\xi \mathbf{B} \\ \mathbf{H} &= i\xi \mathbf{E} + \mathbf{B}/\mu \,. \end{cases} \tag{1}$$

The permittivity $\bar{\bar{\varepsilon}}$ depends on the reduced frequencies Ω and R, see explicit definition in [6].

One of two plane eigenwaves with the wave numbers $\varkappa_{1,2}$ where

$$\varkappa_{1,2}^2 = \frac{k_\infty^2}{2}\left[\varepsilon_\perp + \varepsilon_z + a \pm \sqrt{(\varepsilon_\perp + \varepsilon_z - a)^2 + 4a\varepsilon_z}\right], \quad a = 4\mu\varepsilon_\infty^{-1}\xi^2, \quad k_\infty = \omega\sqrt{\varepsilon_\infty \mu} \tag{2}$$

propagates in the sagittal plane $z = 0$ and falls on the half-plane under an angle θ. In this case, the electromagnetic field may be described via the sum of two scalar functions $\varphi_j(x,y)$ $(j = 1,2)$ representing the eigen polarizations with the wave numbers according to Eq. (2). The total field must satisfy the boundary conditions on the screen, where $\hat{\mathbf{e}}_y \times \mathbf{E}^{(t)}(x,0) = 0$, and on its sequel, where $\hat{\mathbf{e}}_y \times \mathbf{E}^{(t)}$ and $\hat{\mathbf{e}}_y \times \mathbf{H}^{(t)}$ are continuous. The scattered field is subjected to the edge condition [7] and the radiation condition at infinity.

The secondary field is sought in the form of the Fourier integral

$$\varphi(x,y) = \frac{1}{2\pi} \int_{-\infty}^{\infty} \Phi(\alpha,y) e^{i\alpha x} d\alpha \tag{3}$$

where $\Phi(\alpha,y)$ yields to the equation

$$\left[\left(\frac{d^2}{dy^2} + \gamma_1^2\right)\right]\left[\left(\frac{d^2}{dy^2} + \gamma_2^2\right)\right]\Phi(\alpha,y) = 0 \tag{4}$$

with non-coincident $\gamma_j = \sqrt{\alpha^2 - \varkappa_j^2}$, $j = 1,2$. The solution of Eq. (4) is

$$\Phi(\alpha,y) = \begin{cases} A_1(\alpha)e^{-\gamma_1 y} + B_1(\alpha)e^{-\gamma_2 y}, & \text{if } y \geq 0 \\ A_2(\alpha)e^{\gamma_1 y} + B_2(\alpha)e^{\gamma_2 y}, & \text{if } y \leq 0 \end{cases} \tag{5}$$

where $A_j(\alpha)$, $B_j(\alpha)$ are amplitude functions to be found. Using Eqs. (3)–(5) we translate the boundary conditions into the spectral domain and present in the matrix form

$$\overline{\overline{\boldsymbol{Q}}}(\alpha) \cdot \boldsymbol{L}(\alpha) = \boldsymbol{E}(\alpha) + \boldsymbol{U}(\alpha) \tag{6}$$

where the two-element column-vectors $\boldsymbol{U}(\alpha)$ and $\boldsymbol{L}(\alpha)$ represent the functions of α which are regular in the regions Π_U, Π_L of the complex α-plane, respectively. The symbols Π_U (Π_L) indicate the upper (lower) half-plane of α including the common regularity strip along the $\mathrm{Re}\,\alpha$-axis. The elements of $\boldsymbol{U}(\alpha)$, $\boldsymbol{L}(\alpha)$ include the unknown amplitude functions whereas the vector $\boldsymbol{E}(\alpha)$ consists of elements relating to components of the transformed electric field of the incident plane wave $\mathbf{E}^{(i)}(x,y)$. Eq. (6) is the vector Wiener–Hopf equation with the matrix kernel $\overline{\overline{\boldsymbol{Q}}}(\alpha) \equiv (Q_{ij}(\alpha))$ where

$$Q_{11}(\alpha) = \frac{k_\infty^2\varepsilon_\perp - \varkappa_1^2}{\gamma_1} - \frac{k_\infty^2\varepsilon_\perp - \varkappa_2^2}{\gamma_2}, \quad Q_{12}(\alpha) = \frac{g\alpha}{\varepsilon\gamma_2}(\varkappa_1^2 - \varkappa_2^2)$$

$$Q_{21}(\alpha) = \frac{g}{\varepsilon}\left(\frac{1}{\gamma_2} - \frac{1}{\gamma_1}\right), \quad Q_{22}(\alpha) = \gamma_1 - \gamma_2\frac{k_\infty^2\varepsilon_\perp - \varkappa_1^2}{k_\infty^2\varepsilon_\perp - \varkappa_2^2} - \frac{g^2\alpha^2}{\varepsilon^2\gamma_2}\frac{\varkappa_1^2 - \varkappa_2^2}{k_\infty^2\varepsilon_\perp - \varkappa_2^2}.$$

3. Solution of the Functional Vector Equations

In order to perform the fundamental step in the Wiener–Hopf technique, that is to decompose the matrix $\overline{\overline{\boldsymbol{Q}}}(\alpha)$ in the form of a product $\overline{\overline{\boldsymbol{Q}}}(\alpha) = \overline{\overline{\boldsymbol{Q}}}_U(\alpha) \cdot \overline{\overline{\boldsymbol{Q}}}_L(\alpha)$ we use the Hurd idea [8] and re-formulate the homogeneous version of Eq. (6) as a vector Hilbert problem on the branch cuts $\Gamma_{1,2}$ due to the branch points $\alpha = \varkappa_{1,2}$ in Π_U. Let the "+" and "−" subscripts indicate the values of functions at the opposite sides of $\Gamma_{1,2}$. After elimination of $\boldsymbol{U}(\alpha)$, one obtains a vector Hilbert problem

$$\boldsymbol{L}_+(\alpha) = \overline{\overline{\boldsymbol{H}}}(\alpha) \cdot \boldsymbol{L}_-(\alpha), \quad \text{where } \overline{\overline{\boldsymbol{H}}}(\alpha) = \overline{\overline{\boldsymbol{Q}}}_+^{-1}(\alpha) \cdot \overline{\overline{\boldsymbol{Q}}}_-(\alpha). \tag{7}$$

The matrix $\overline{\overline{\boldsymbol{H}}}(\alpha)$ has zero trace and contains only polynomial elements. We have for the contours Γ_1 and Γ_2

$$\overline{\overline{\boldsymbol{H}}}(\alpha)_{|\Gamma_1} = -\overline{\overline{\boldsymbol{H}}}(\alpha)_{|\Gamma_2} = \frac{1}{\Delta_+}\begin{pmatrix} l & m \\ n & -l \end{pmatrix} \tag{8}$$

where

$$\begin{cases} l &= \gamma_2^2(k_\infty^2\varepsilon_\perp - \varkappa_1^2)^2 - \gamma_1^2(k_\infty^2\varepsilon_\perp - \varkappa_2^2)^2 - \frac{g^2}{\varepsilon^2}\alpha^2(\varkappa_1^2 - \varkappa_2^2)^2 \\ m &= 2\frac{g}{\varepsilon}\alpha\gamma_1^2(\varkappa_1^2 - \varkappa_2^2)(k_\infty^2\varepsilon_\perp - \varkappa_2^2) \\ n &= -2\frac{g}{\varepsilon}\alpha(\varkappa_1^2 - \varkappa_2^2)(k_\infty^2\varepsilon_\perp - \varkappa_2^2) \end{cases} \tag{9}$$

and

$$\Delta(\alpha) = \frac{g^2}{\varepsilon^2}\alpha^2(\varkappa_1^2 - \varkappa_2^2)^2 - [\gamma_1(k_\infty^2\varepsilon_\perp - \varkappa_2^2) - \gamma_2(k_\infty^2\varepsilon_\perp - \varkappa_1^2)]^2. \tag{10}$$

According to the Wiener–Hopf–Hilbert method, we introduce another unknown vector $\boldsymbol{V}(\alpha) = \overline{\overline{\boldsymbol{T}}}(\alpha)\cdot\boldsymbol{L}(\alpha)$ in order to receive a new vector Hilbert problem for $\boldsymbol{V}(\alpha)$. Due to special choice of $\overline{\overline{\boldsymbol{T}}}(\alpha)$, the latter may be separated into two uncoupled standard Hilbert problems [9], whereupon the vectors $\boldsymbol{V}(\alpha)$ and $\boldsymbol{L}(\alpha)$ are found. These vectors should be regular in the domain $\Pi_U + \Pi_L - \Gamma_1 - \Gamma_2$. Farther, one may construct two vectors $\boldsymbol{L}^{(1,2)}(\alpha) \equiv (L_i^{(1,2)}(\alpha))$ which fulfil the condition $L_1^{(1)}L_2^{(2)} - L_1^{(2)}L_2^{(1)} \neq 0$. We use them in order to form the matrix $\overline{\overline{\boldsymbol{Q}}}_L^{-1}(\alpha)$ which also should satisfy Eq. (7). The matrices $\overline{\overline{\boldsymbol{Q}}}_L(\alpha)$ and $\overline{\overline{\boldsymbol{Q}}}_U^{-1}(\alpha) = \overline{\overline{\boldsymbol{Q}}}_L(\alpha)\cdot\overline{\overline{\boldsymbol{Q}}}^{-1}(\alpha)$ have not branch points in Π_L and Π_U, respectively, but temporarily have poles there. The next step is to cancel the undesirable singularities in these matrices using a properly chosen rational matrix $\overline{\overline{\boldsymbol{F}}}(\alpha)$, namely

$$\overline{\overline{\boldsymbol{Q}}}_U^{-1}(\alpha) = \overline{\overline{\boldsymbol{F}}}(\alpha)\cdot\overline{\overline{\boldsymbol{Q}}}_U^{-1}(\alpha), \quad \overline{\overline{\boldsymbol{Q}}}_L(\alpha) = \overline{\overline{\boldsymbol{F}}}(\alpha)\cdot\overline{\overline{\boldsymbol{Q}}}_L(\alpha)\,. \tag{11}$$

To define the elements of $\overline{\overline{\boldsymbol{F}}}(\alpha)$ we have to take into account the number of roots of $\Delta(\alpha)$ located on its branch, which is given via the conditions at infinity. It turns out, that at least four constants can be chosen arbitrary. The correct definition allows to simplify essentially the further complicated calculations.

4. Completion and Analysis of the Solution

When the matrix factors $\overline{\overline{\boldsymbol{Q}}}_{U,L}(\alpha)$ are found the solution of Eq. (6) is straightforward. It is rearranged so that to receive the left- and right-hand sides which are regular in Π_U and Π_L, respectively, and define an integral function $J(\alpha)$. According to the edge condition, the asymptotic behaviour of both sides of the equation at $|\alpha| \to \infty$ permits to put $J(\alpha) = 0$. This makes it possible to find the spectral amplitudes $A_j(\alpha)$, $B_j(\alpha)$ and to complete the solution of the problem.

It turns out that the integrand of Eq. (3) is quite cumbersome. Yet the related integrals are suitable for the asymptotic evaluation of far fields by the method of steepest descent. The singularities of the integrands give rise to the distinct wave species. The pole contributions are coupled with the geometrical optics field which in the illuminated region $y \geq 0$ consists of the reflected basic mode and the concominant mode excited due to reflection coupling between

modes. An additional pole originated from the dispersion relation $\Delta(\alpha) = 0$ (see Eq. (10)) contributes a surface-wave term. The unidirectional surface wave [6] propagates along a face of the half-plane. Reversion of the external magnetic field shifts it on the other face. The saddle-point contributions are interpreted as two congruences of diffracted rays. At last, in principle, one needs to consider the branch-point contributions that lead to the such manifestation of modal coupling and total reflection as lateral waves.

5. Conclusion

A problem of plane wave diffraction by a perfectly conducting screen in a homogeneous chiroplasma is solved for the case of normal incidence on the edge which is parallel to the external magnetic field. The formulation leads to the vector Wiener–Hopf equation which is solved by the Wiener–Hopf–Hilbert method. Because of numerous wave species involved, the problem has certain versatility. An outline is conducted on the example of both propagating bulk eigenwaves of the medium. A unidirectional surface wave and lateral waves are the most notable features of the far field in the diffraction problem under consideration.

Acknowledgement
D. Marakassov thanks the Helsinki University of Technology for a study term in the year 2000 and financial support.

References

[1] N. Engheta, D. L. Jaggard, and M .W. Kowarz, "Electromagnetic waves in Faraday chiral media," *IEEE Trans. Antennas Propagat.*, vol. 40, no. 4, pp. 367–374, 1992.

[2] H. S. Eritsian, "The optics of naturally gyrotropic media in the presence of a magnetic field," *Izv. AN Armjan. SSR. Fizika*, Vol. 3, no. 3, pp. 217–219, 1968. (in Russian)

[3] E. V. Jull, "Diffraction by a conducting half-plane in an anisotropic plasma," *Canad. J. Phys*, vol. 42, no. 8, pp. 1455–1468, 1964.

[4] S. Przeździecki, "Diffraction by a half-plane in a chiral medium (normal incidence)," *Acta Physica Polonica A*, vol. 83, no. 6, pp. 739–750, 1993.

[5] S. Asghar and A. Lakhtakia, "Planewave diffraction by a perfectly conducting halfplane in a homogeneous biisotropic medium," *Int. J. of Applied Electromagnetics in Materials*, vol. 5, pp. 181–188, 1994.

[6] V. V. Fisanov and D. A. Marakasov, "Electromagnetic surface waves at a plane boundary of semi-infinite Faraday chiral media," in A. Priou *et al.* (eds.), *Advances in Complex Electromagnetic Materials*, Dordrecht: Kluwer Academic Publishers, 1997, pp. 239–248.

[7] V. V. Fisanov, "Singularity exponent of the electromagnetic field near the chiroplasma edge", in *Proc. CHIRAL'95*, State College, USA, October 1995, pp. 109–112.

[8] R. A. Hurd, "The Wiener–Hopf–Hilbert method for diffraction problems", *Canad. J. Phys.*, vol. 54, no. 7, pp. 775–780, 1976.

[9] R. A. Hurd and S. Przeździecki, "Diffraction by a half-plane perpendicular to the distinguished axis of a gyrotropic medium," *J. Math. Phys.*, vol. 17, no. 10, pp. 1838–1847, 1976.

A Hybrid FDFD-BIE Approach to Two-dimensional Scattering from an Inhomogeneous Biisotropic Cylinder

M. Norgren

Department of Electromagnetic Theory, Royal Institute of Technology
Osquldas väg 6, SE-100 44 Stockholm, Sweden
Fax + 46 8 10 83 27; e-mail: martin@tet.kth.se

Abstract

The scattering problem for an inhomogeneous two-dimensional biisotropic cylinder is solved in the frequency-domain by means of a hybrid method, in which finite difference equations in the interior region are combined with a mesh truncation in terms of a boundary integral equation. Numerical results for the bistatic echo widths are presented and compared with a reference solutions in the circular cylinder cases and it is found that the method yields more accurate results than what can be achieved with a local absorbing boundary condition.

1. Introduction

A scattering problem involving inhomogeneous media can be solved using a volume integral equation (VIE) that is discretized into a matrix equation by using the method of moments (MoM). However, a drawback with VIE is that the integral operator discretizes into a filled matrix, that becomes very large and exceedingly time consuming to invert if the geometry is several wavelengths in size. An alternative is to use a partial differential equation (PDE) method, in which the differential operator discretizes into a sparse matrix by using finite differences (FD) or by using the finite element method (FEM). However, when using FD or FEM in an open region a radiation condition must be supplemented by truncating the computational domain with an absorbing boundary condition (ABC), which can be either an approximate (local) ABC or an exact (global) ABC. One example of a local ABC is the perfectly matched layer (PML), which has been extended recently to include bianisotropic media [1]. A global ABC is usually formulated in terms of an integral operator on the boundary of the computational domain, which yields that the FD or FEM equations then must be solved in conjunction with a boundary integral equation (BIE). Examples of such combined methods, referred to as hybrid methods, are e.g. FEM-BIE [2] and FDTD-BIE [3]. In this paper, we consider a hybrid FD FrequencyDomain-BIE approach to a two-dimensional scattering problem for an inhomogeneous cylinder of a biisotropic material. Interior to the region containing the biisotropic cylinder, we use finite differences and on the boundary of the region we use a BIE, which reduces to a contour integral equation.

2. The Scattering Problem

Consider an in free space located biisotropic scatterer (see figure 1) described by the following constitutive relations in the frequency-domain:

$$\boldsymbol{D}(\boldsymbol{r}) = \varepsilon_0 \varepsilon(\boldsymbol{r})\,\boldsymbol{E}(\boldsymbol{r}) + \sqrt{\varepsilon_0\mu_0}\,\xi(\boldsymbol{r})\,\boldsymbol{H}(\boldsymbol{r}), \qquad \boldsymbol{B}(\boldsymbol{r}) = \mu_0 \mu(\boldsymbol{r})\,\boldsymbol{H}(\boldsymbol{r}) + \sqrt{\varepsilon_0\mu_0}\,\zeta(\boldsymbol{r})\,\boldsymbol{E}(\boldsymbol{r}), \quad (1)$$

where the parameters ε, μ, ξ and ζ are arbitrary functions of the position variable $\boldsymbol{r}$.

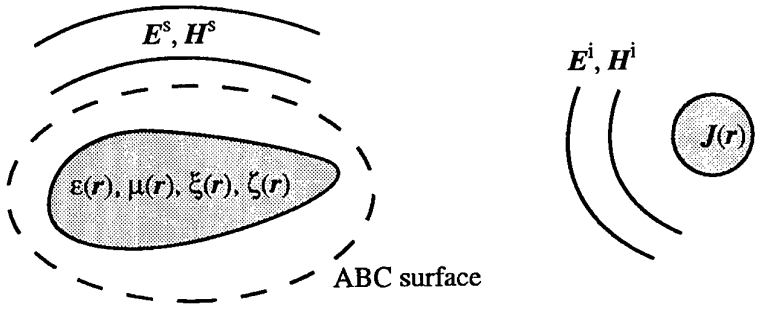

Figure 1: The scattering configuration.

The scattering problem is to determine the scattered fields $\boldsymbol{E}^{\mathrm{s}}, \boldsymbol{H}^{\mathrm{s}}$ when the scatterer is excited by known incident fields $\boldsymbol{E}^{\mathrm{i}}, \boldsymbol{H}^{\mathrm{i}}$, created by an extraneous time-harmonic ($\exp(\mathrm{j}\omega t)$) current density $\boldsymbol{J}$; see figure 1. Substituting the constitutive relations (1) into the Maxwell's equations, we eventually arrive at the following equations for the scattered fields:

$$\nabla \times \boldsymbol{E}^{\mathrm{s}} + \mathrm{j}k_0 \left(\mu\eta_0 \boldsymbol{H}^{\mathrm{s}} + \zeta \boldsymbol{E}^{\mathrm{s}}\right) = -\mathrm{j}k_0 \left(\left(\mu - 1\right)\eta_0 \boldsymbol{H}^{\mathrm{i}} + \zeta \boldsymbol{E}^{\mathrm{i}}\right), \tag{2}$$

$$\nabla \times \eta_0 \boldsymbol{H}^{\mathrm{s}} - \mathrm{j}k_0 \left(\varepsilon \boldsymbol{E}^{\mathrm{s}} + \xi\eta_0 \boldsymbol{H}^{\mathrm{s}}\right) = \mathrm{j}k_0 \left(\left(\varepsilon - 1\right)\boldsymbol{E}^{\mathrm{i}} + \xi\eta_0 \boldsymbol{H}^{\mathrm{i}}\right). \tag{3}$$

3. The FDFD Equations in the Two-dimensional Case

The 2D FDFD equations are derived in a similar way as in [4]. The region containing the scatterer is divided into square cells (see figure 2), in which the constitutive parameters are approximated as homogeneous and equal to their true values at the mid points. In the outermost layer of cells, the parameters are $\varepsilon = \mu = 1, \xi = \zeta = 0$. The FDFD approximation results in a linear system of equations for the everywhere continuous z-components of the fields [5]:

$$\mathrm{M}'_{\mathrm{EE}} \bar{E}^{\mathrm{s}}_{z,\mathrm{inside}} + \mathbf{B} \bar{E}^{\mathrm{s}}_{z,\mathrm{outside}} + \mathrm{M}_{\mathrm{EH}} \bar{H}^{\mathrm{s}}_{z,\mathrm{inside}} = \bar{J}^{\mathrm{E}}_{\mathrm{inside}}, \tag{4}$$

$$\mathrm{M}'_{\mathrm{HH}} \bar{H}^{\mathrm{s}}_{z,\mathrm{inside}} + \mathbf{B} \bar{H}^{\mathrm{s}}_{z,\mathrm{outside}} + \mathrm{M}_{\mathrm{HE}} \bar{E}^{\mathrm{s}}_{z,\mathrm{inside}} = \bar{J}^{\mathrm{H}}_{\mathrm{inside}}, \tag{5}$$

where $\bar{E}^{\mathrm{s}}_{z,\mathrm{inside}}, \bar{H}^{\mathrm{s}}_{z,\mathrm{inside}}$ are evaluated at the interior FDFD points, indicated with filled circles in figure 2, and $\bar{E}^{\mathrm{s}}_{z,\mathrm{outside}}, \bar{H}^{\mathrm{s}}_{z,\mathrm{outside}}$ are evaluated at the extruding FDFD points, indicated with blank circles in figure 2. $\mathrm{M}'_{\mathrm{EE}}, \mathrm{M}_{\mathrm{EH}}, \mathrm{M}_{\mathrm{HE}}$ and $\mathrm{M}'_{\mathrm{HH}}$ are sparsely filled square matrices, describing the FDFD operators at the interior points and the matrix $\mathbf{B}$ describes the FDFD operators on the extruding points. $\bar{J}^{\mathrm{E}}_{\mathrm{inside}}$ and $\bar{J}^{\mathrm{H}}_{\mathrm{inside}}$ are excitation vectors, obtained as linear combinations of the components of the incident fields at the interior points.

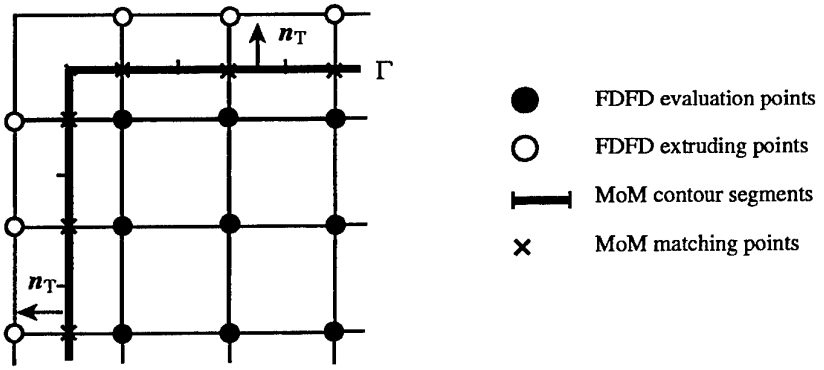

Figure 2: One corner region of the computational domain. Γ is the contour at which the global absorbing boundary condition is calculated.

4. Absorbing Boundary Condition in Terms of a BIE

With all their sources inside the contour Γ, depicted with a thick solid line in figure 2, the z-component of the scattered fields satisfy the integral equation

$$\frac{1}{2}F_z^{\mathrm{s}}(\boldsymbol{r}) + \fint_\Gamma \left[G(\boldsymbol{r},\boldsymbol{r}') \frac{\partial F_z^{\mathrm{s}}}{\partial n'}(\boldsymbol{r}') - F_z^{\mathrm{s}}(\boldsymbol{r}') \frac{\partial G}{\partial n'}(\boldsymbol{r},\boldsymbol{r}') \right] \mathrm{d}\Gamma' = 0, \quad \boldsymbol{r} \text{ on } \Gamma, \tag{6}$$

where F_z^{s} denotes E_z^{s} or H_z^{s} and $G(\boldsymbol{r},\boldsymbol{r}') = -\frac{j}{4}\mathrm{H}_0^{(2)}(k_0|\boldsymbol{r}-\boldsymbol{r}'|)$ is the 2D free space Green's function. After a simple MoM approximation using pulse functions and point-matching at the points indicated with crosses in figure 2, we obtain the following relation (the numerical ABC) between the scattered field and its normal derivative:

$$\mathbf{P}\bar{F}_z^{\mathrm{s}} = \mathbf{Q}\partial_n \bar{F}_z^{\mathrm{s}}, \tag{7}$$

where $\bar{F}_z^{\mathrm{s}}$ and $\partial_n \bar{F}_z^{\mathrm{s}}$ are vectors containing the field and its normal derivative, respectively, and where $\mathbf{P}$ and $\mathbf{Q}$ are matrices. To connect the ABC to the FDFD scheme, the elements in $\bar{F}_z^{\mathrm{s}}$ and $\partial_n \bar{F}_z^{\mathrm{s}}$ are approximated from the two nearest FDFD points on each side of Γ by linear interpolations and central differences, respectively, i.e.

$$F_z^{\mathrm{s}} \approx \frac{F_{z,\mathrm{outside}}^{\mathrm{s}} + F_{z,\mathrm{inside}}^{\mathrm{s}}}{2}, \qquad \partial_n F_z^{\mathrm{s}} \approx \frac{F_{z,\mathrm{outside}}^{\mathrm{s}} - F_{z,\mathrm{inside}}^{\mathrm{s}}}{h}, \tag{8}$$

where h (the mesh parameter) is the side-length of a cell. With (8) in (7), we obtain a matrix relation between the field values at the different side of Γ:

$$\mathbf{D}\bar{E}_{z,\mathrm{outside}}^{\mathrm{s}} = \mathbf{C}\bar{E}_{z,\mathrm{inside}}^{\mathrm{s}}, \qquad \mathbf{D}\bar{H}_{z,\mathrm{outside}}^{\mathrm{s}} = \mathbf{C}\bar{H}_{z,\mathrm{inside}}^{\mathrm{s}}, \tag{9}$$

where the square matrix $\mathbf{D}$ appears to be well-conditioned and hence invertible. Using (9) in (4) and (5), it thus follows that the fields at the interior points are obtained from the following matrix equation:

$$\begin{bmatrix} \mathbf{M}_{\mathrm{EE}} & \mathbf{M}_{\mathrm{EH}} \\ \mathbf{M}_{\mathrm{HE}} & \mathbf{M}_{\mathrm{HH}} \end{bmatrix} \cdot \begin{bmatrix} \bar{E}_{z,\mathrm{inside}}^{\mathrm{s}} \\ \bar{H}_{z,\mathrm{inside}}^{\mathrm{s}} \end{bmatrix} = \begin{bmatrix} \bar{J}_{\mathrm{inside}}^{\mathrm{E}} \\ \bar{J}_{\mathrm{inside}}^{\mathrm{H}} \end{bmatrix}, \tag{10}$$

where

$$\mathbf{M}_{\mathrm{EE}} = \mathbf{M}'_{\mathrm{EE}} + \mathbf{B}\mathbf{D}^{-1}\mathbf{C}, \qquad \mathbf{M}_{\mathrm{HH}} = \mathbf{M}'_{\mathrm{HH}} + \mathbf{B}\mathbf{D}^{-1}\mathbf{C}. \tag{11}$$

Note that since neither $\mathbf{B}$ nor $\mathbf{C}$ nor $\mathbf{D}$ depend on the properties of the scatterer, the operation $\mathbf{B}\mathbf{D}^{-1}\mathbf{C}$ in (11) has to be carried out only once. Thus, for a given mesh and frequency the ABC can be precalculated and stored for further usage when considering different properties of the scatterer, as long as the scatterer is confined within the boundary Γ.

5. Numerical Example

In this one example, consider a circular chiral cylinder with the radius $= \lambda$, where λ is the wavelength in free space. The constitutive parameters are chosen to be $\varepsilon = 2.6 - 0.2\mathrm{j}, \mu = 1.5 - 0.1\mathrm{j}, \xi = -\zeta = -\mathrm{j}\kappa = -\mathrm{j}(0.6 - 0.1\mathrm{j})$. For the computational region we consider two different mesh sizes, 41×41 FDFD points with spacing $h = 0.05\lambda$ and 81×81 FDFD points with spacing $h = 0.025\lambda$. The numerical results are compared with a reference solution obtained by means of an expansion in cylindrical eigenwaves. The cross-polarized bistatic echo width $\sigma_{\mathrm{cross}}^{\mathrm{E}} = \sigma_{\mathrm{cross}}^{\mathrm{H}}$ for waves impinging in the direction $\phi = 0$ is depicted in figure 3, with the solid lines for the reference solution, the dotted lines for $h = 0.05\lambda$ and the dashed lines for $h = 0.025\lambda$. The numerical results indicate convergence and are in good agreements with the reference solution.

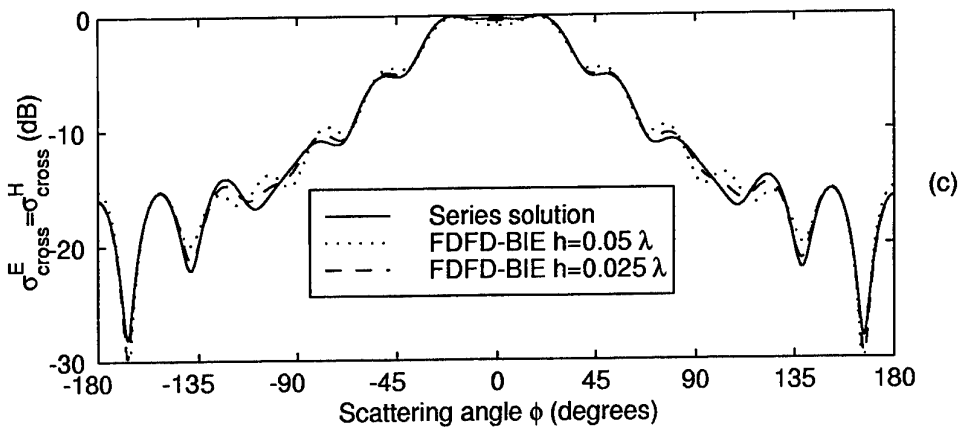

Figure 3: The cross-polarized bistatic echo width for a chiral circular cylinder with the radius $= \lambda$ and the parameters $\varepsilon = 2.6 - 0.2\mathrm{j}, \mu = 1.5 - 0.1\mathrm{j}$ and $\kappa = 0.6 - 0.1\mathrm{j}$. The cylinder is illuminated in the direction $\phi = 0°$.

6. Conclusion

The scattering problem for inhomogeneous two-dimensional biisotropic cylinders has been considered. Finite difference equations for the interior region as well as a contour integral equation realizing a global absorbing boundary condition have been derived and implemented numerically.

Computationally, the present FDFD-BIE method is much faster than a moment method using a filled matrix of the same size. Hence, the present method can be used for solving 2D scattering problems involving scatterers of intermediate sizes (i.e. a couple of wavelengths) in both directions whereas MoM under, the same computation time, only can be used for considerably smaller or thinner structures.

Since our global ABC is unlikely to generate artifacts from the boundary in the solution, the usefulness of the hybrid method as a fast solver in an optimization approach for solving the corresponding inverse problem is of interest for forthcoming research.

References

[1] M. Kuzuoglu and R. Mittra, "A systematic approach to the derivation of constitutive parameters of a perfectly matched absorber", *IEEE Microw. Guided Wave Lett.*, vol. 8, no. 9, pp. 313-315, June 1998.

[2] X.-Q. Sheng *et al.*, "On the formulation of hybrid finite-element and boundary-integral methods for 3-D scattering", *IEEE Trans. Ant. Prop.*, vol. 46, no. 3 , pp. 303-311, March 1998.

[3] H. Rogier *et al.*, "A new hybrid FDTD-BIE approach to model electromagnetic scattering problems", *IEEE Microw. Guided Wave Lett.*, vol. 8, no. 3, pp. 138-140, March 1998.

[4] W. Hong *et al.*, "Application of the measured equation of invariance to solve scattering problems involving a penetrable medium", *Radio Science*, vol. 29, no. 4, pp. 897-906, July-August 1994.

[5] M. Norgren, "A hybrid FDFD-BIE approach to two-dimensional scattering from an inhomogeneous biisotropic cylinder", Technical Report TRITA-TET 00-1, Royal Institute of Technology, SE-100 44, Stockholm.

Characterization of Rectangular Waveguide with a Pseudochiral Ω Slab

K. Dorko[1] and J. Mazur[1]

[1] Technical University of Gdańsk,
Faculty of Electronics, Telecommunication and Informatic,
(ETI) Narutowicza 11/12 str., 80-952 Gdańsk Poland,
email: jem@pg.gda.pl

Abstract

Mode matching approach is applied to a rectangular waveguide containing a pseudochiral Ω slab. From waveguide measurements carried over a few placement of the slab in the guide the constitutive parameters are extracted. The extraction is performed numerically by a algorithm minimizing the differences between theoretical and measured values of scattering parameters.

1. Introduction

The study of the pseudochiral Ω guides is important for several reasons. Electromagnetic properties introduced by Ω media can enhance the guide performance [1] or provide some added field phenomena over the guide behaviour [2],[3]. Therefore it is important to predict the effect that the Ω medium has on their propagation and scattering characteristics. This paper investigates the structure of the rectangular waveguide loaded with an Ω slab as shown in Fig. 1. We assume that the Ω slab is extended over the waveguide height and can be arbitrary placed in the guide. The excitation is chosen to be TE_{no} modes of the input rectangular waveguides so that due to the localization of the Ω particles in the slab the scattered fields can be defined only by TE_{no} waves [3]. Taking into account the above restrictions the problem is solved using the mode matching approach. It yields very reliable and accurate values for scattering parameters. The knowledge of this scattering characteristics for a few different localizations of the slab in the rectangular guide is basis for the extraction of the dispersive, complex Ω medium parameters.

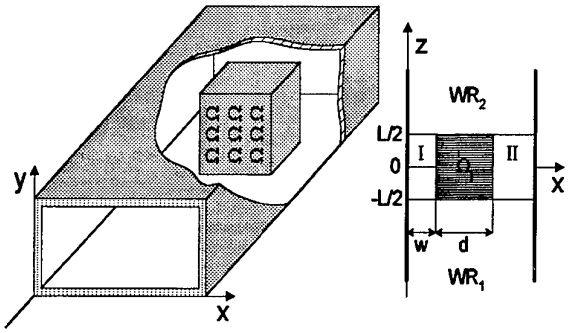

Figure 1: Rectangular waveguide with Ω slab and geometry of the investigated structure.

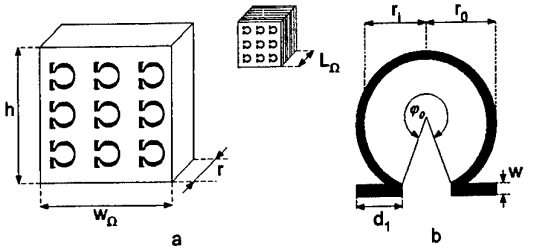

Figure 2: (a) - An Ω sample used in experiment, parameters: $w_\Omega = 10mm$, $l_\Omega = 10mm$, $h = 10.2mm$, $r = 0.2mm$; (b) - A single Ω element, parameters: $r_i = 0.915mm$, $r_o = 1.046mm$, $w = 0.131mm$, $d = 2 * d_1 = 1.6mm$, $\varphi_0 = 5.96rad$

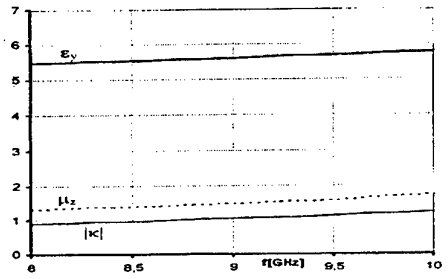

Figure 3: Material parameters computed for static capacity and inductance.

2. Specification of the Slab

Let us consider a three dimensional (3-D) slab of Ω medium as shown in Fig. 1 whose the relative electric permittivity and magnetic permeability tensors are of the diagonal form: $\bar{\bar{\varepsilon}} = \varepsilon(\vec{i}_x\vec{i}_x + \vec{i}_z\vec{i}_z) + \varepsilon_y\vec{i}_y\vec{i}_y$ and $\bar{\bar{\mu}}_c = \mu(\vec{i}_x\vec{i}_x + \vec{i}_y\vec{i}_y) + \mu_z\vec{i}_z\vec{i}_z$. For the considered pseudochiral slab the magnetoelectric coupling tensors have the following dyadic representation $\bar{\bar{\Omega}}_{yz} = \Omega\vec{i}_y\vec{i}_z$ and $\bar{\bar{\Omega}}_{zy} = \Omega\vec{i}_z\vec{i}_y$, where Ω is a coupling admitance between electric and magnetic field along y and z axis respectively. This Ω sample is composed of unilaterally metallized duroid plates ($\varepsilon = 2.2$) with chemically etched matrix of nine Ω particles as illustrated in Fig. 2a. To obtain the Ω block the plates are stuck together using the polystyren glue ($\varepsilon \sim 2.4$).

To calculate the unknown material parameters we used the static method based on the equivalent $L - C$ circuit from M. Saadoun Dr dissertation [2]. Fig. 3 shows plots of the set of material parameters as function of frequency.These values will be used in next steps of extraction as initial parameters.

3. Transfer Matrices Formulation

The problem is solved by using transfer matrix approach (TMA) presented in [3]. Here the TMA is modified to the cases where pseudochiral materials, such as Ω media, are involved. In this paper we get a following transfer matrix equation that defines the relation between the tangential fields components $\underline{F} = (H_z, E_y)^T$ at the side interfaces $x_i = a$ and $x_{i-1} = 0$.

$$\begin{bmatrix} H_z \\ E_y \end{bmatrix}_a = \underbrace{\begin{vmatrix} T_{11}^{II} & T_{12}^{II} \\ T_{21}^{II} & T_{22}^{II} \end{vmatrix}}_{T^{II}} \underbrace{\begin{vmatrix} T_{11}^{\Omega} & T_{12}^{\Omega} \\ T_{21}^{\Omega} & T_{22}^{\Omega} \end{vmatrix}}_{T^{\Omega}} \underbrace{\begin{vmatrix} T_{11}^{I} & T_{12}^{I} \\ T_{21}^{I} & T_{22}^{I} \end{vmatrix}}_{T^{I}} \begin{bmatrix} H_z \\ E_y \end{bmatrix}_0 \tag{1}$$

where: T^I and T^{II} are tangential matrices in free space sectors (I) and (II); T^Ω is a tangential matrix in Ω slab designed in [3].

4. The Scattering Matrix

The knowledge of the results obtained by TMA gives us a possibility calculation of the scattering parameters for the considered structure. The continuity of the transverse electric and magnetic fields over each aperture cross section (see Fig. 1) is expressed as follows:

$$\begin{aligned}
\sum_n (a_{1n} + b_{1n})\vec{e}_n &= \sum_n (A_n + B_n e^{-\gamma_{\Omega n} L})\vec{e}_{\Omega n} \\
\sum_n (a_{1n} - b_{1n})\vec{h}_n &= \sum_n (A_n - B_n e^{-\gamma_{\Omega n} L})\vec{h}_{\Omega n} \qquad (2) \\
\sum_n (a_{2n} + b_{2n})\vec{e}_n &= \sum_n (A_n e^{-\gamma_{\Omega n} L} + B_n)\vec{e}_{\Omega n} \\
\sum_n (-a_{2n} + b_{2n})\vec{h}_n &= \sum_n (A_n e^{-\gamma_{\Omega n} L} - B_n)\vec{h}_{\Omega n} \qquad (3)
\end{aligned}$$

where: a_{in} and b_{in}, $i = 1, 2$ are complex coefficients of the incident and reflected wave and $\vec{e}_n$, $\vec{h}_n$ are the transverse electric and magnetic field functions in $WR_{1,2}$. A_n and B_n are the forward and backward wave complex coefficients, $\gamma_{\Omega n}$ is the propagation constant and $\vec{e}_{\Omega n}$, $\vec{h}_{\Omega n}$ are the transverse field functions in the Ω_J section which can be solved by TMA described before. Equations (2) for z = -L/2 and (3) for z = L/2 are converted into a linear matrix form taking the inner products of both side of these equations with eigenfields of orthonormal set of modes in WR guides. In this approach the Ω_J fields are orthogonalized by eigenfields of WR guides. The resulting matrices, truncated to a total of N modes in each of the region, we manipulate so that the amplitudes of the fields in the Ω_J are eliminated. Finally, the solution is expressed in the scattering matrix formulation as

$$\begin{bmatrix} \underline{b}_1 \\ \underline{b}_2 \end{bmatrix} = \begin{bmatrix} \underline{\underline{S}}_{11} & \underline{\underline{S}}_{12} \\ \underline{\underline{S}}_{21} & \underline{\underline{S}}_{22} \end{bmatrix} \begin{bmatrix} \underline{a}_1 \\ \underline{a}_2 \end{bmatrix} \qquad (4)$$

If the measured and calculated scattering parameters at fixed frequency for a few positions of pseudochiral slab in the guide are known we can use optimization method to determine the parameters of the Ω medium investigated.

5. Optimization

For extraction of the Ω material parameters we use a procedure based on a modified Levenberg-Marquardt algorithm. In this case the problem is stated as follows:

$$\min_{\underline{x} \in \mathbf{R}} \frac{1}{2} \sum_{i=1}^{m} f_i(\underline{x})^2 \qquad (5)$$

where $\underline{x}$ is a search vector of the material dispersive parameters. The considered medium is characterized by three unknown complex values; permittivity $\varepsilon_y = \varepsilon_y' - j\varepsilon_y''$, permeability $\mu_z = \mu_z' - j\mu_z''$ and coupling coefficient $\kappa = \kappa' - j\kappa''$. So we get:

$$\underline{x} = [\varepsilon_y', \varepsilon_y'', \mu_z', \mu_z'', \kappa', \kappa'']^T \qquad (6)$$

Other material parameters ($\varepsilon_x = \varepsilon_z = \varepsilon$ and $\mu_x = \mu_y = \mu$) are taken from duroid parameters used in experiment. The goal of optimization procedure is minimization of (5) with

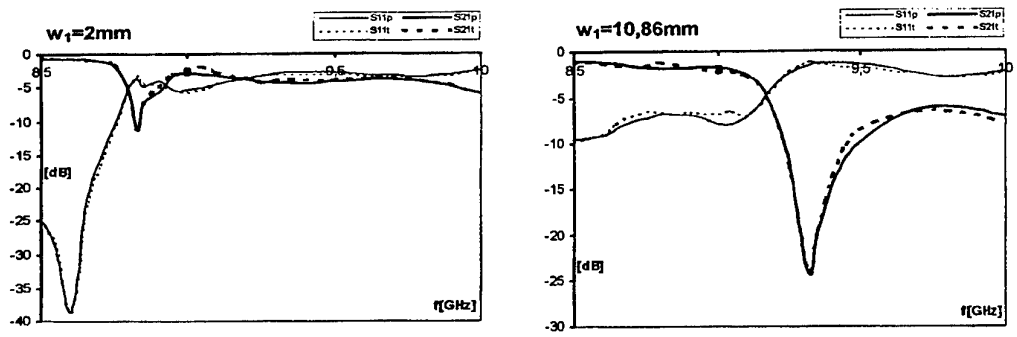

Figure 4: Comparison between optimized and measured performance of the section for a two opposite positions (w) of the Ω slab in the guide.

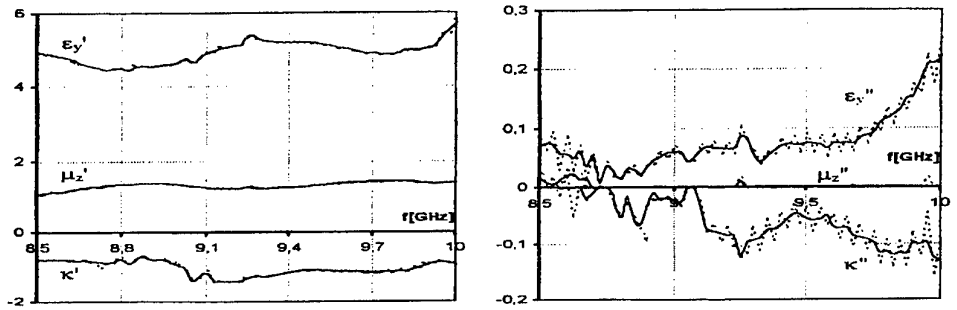

Figure 5: The final material parameters with added noise characteristics.

$f_i(\underline{x}) = |S_{p_i}| - |S_{t_i}|$ where $S_p[dB], S_t[dB]$ - are the measured and calculated scattering parameters, respectively. It is taken as a dominant mode reflection S_{11} and transmission S_{21} coefficients which are measured at fixed frequency and one position of the slab in the guide. Although six goal functions are sufficient for solution of the problem we used twenty six equations in order to correct the slab position errors. One should note from Fig. 4 that after optimization process good agreement between the theoretical and measured characteristics is obtained. In this case the extraction of the Ω material parameters is performed. These results are shown in Fig. 5 as a function of frequency.

6. Conclusion

This paper present the theoretical and measured scattering characteristics of the rectangular waveguide with slab of the Ω medium. These characterisctics are used in the Levenberg-Marquardt optimization algorithm to extract all three constitutive parameters of the Ω material.

References

[1] N. Engheta and M. M. Saadoun, "Novel pseudochiral or Ω – *medium* and its applications," *Proc. of PIERS'91*, Cambrige, MA, p. 339, July 1991.

[2] M. M. Saadoun, "The pseudochiral Ω – *medium* : Theory and potencial applications," *PhD Disertation*, University of Pennsylvania, USA, September 1992.

[3] J. Mazur and J. Michalski, "Pseudochiral omega medium in rectangular waveguides," in *Proceedings of BIANISOTROPICS'98*, 7^{th} International Conference on Complex Media, Braunschweig, Germany, pp. 155-158, 1998.

Static Image Principle for the Sphere in Bi-Isotropic Space

J. J. Hänninen[1] and I. V. Lindell

Electromagnetics Laboratory, Helsinki University of Technology
P.O. Box 3000, FIN-02015 HUT, Finland

[1] Fax: +358 9 451 2267; e-mail: jari@eml.hut.fi

Abstract

The classical inversion transformation in a sphere was originally introduced by Lord Kelvin to formulate the electrostatic image principle for the perfectly electrically conducting sphere. Here it shown that the inversion principle can be used as the basis of an extended electrostatic image principle for a perfectly magnetically conducting sphere and for a sphere with an impedance boundary condition. Any of these spheres may even reside in the most general linear isotropic medium, namely in the bi-isotropic medium, as will be shown.

1. Introduction

Inversion in a sphere (also called the Kelvin transformation) is one of the transformations that keep the Maxwell equations invariant in the static case. This conformal transformation involves one parameter—the radius a of the reference sphere. In spite of the basic limitation to statics, the inversion is applicable to time-harmonic problems, even at microwave frequencies. This requires that the region of interest be small enough in wavelengths, what is known as the quasi-static approximation. In this case the medium parameters are not the static ones but those taken at the frequency in question, in general with complex values.

The inversion method was introduced by William Thomson (later known as Lord Kelvin) in 1845 for solving static problems involving a perfectly electrically conducting (PEC) grounded sphere. The inversion method arises from the observation that one of the equi-potential surfaces (the one of zero potential) of two given point charges of different magnitude and opposite sign happens to be a sphere enclosing one of the charges, which can be seen through simple geometric reasoning. Because the sphere of zero potential can be covered by PEC material without changing the fields on either side of it, this immediately leads to an image principle for a point charge either inside or outside the PEC sphere.

In the present paper the inversion principle is first applied to the PEC sphere in an isotropic dielectric space for finding the classical Kelvin image priciple. Then, after some adjustment, it is applied to the perfectly magnetically conducting (PMC) sphere and to spherical surfaces with an impedance (mixed) boundary condition ('impedance spheres'). In these two cases the image of a point charge becomes a combination of point and line charges. The same approach is then used for an impedance sphere enclosed in bi-isotropic space. The result will include the images for the PEC and PMC spheres in bi-isotropic space and all types of spheres in isotropic space as special cases.

2. Kelvin's Inversion in Isotropic Dielectric Medium

The potential $\phi(\mathbf{r})$ from a source $\varrho(\mathbf{r})$ satisfies in homogeneous dielectric medium the Poisson equation

$$\nabla^2\phi(\mathbf{r}) = -\frac{\varrho(\mathbf{r})}{\epsilon}. \tag{1}$$

It can be shown [1, Appendix] that the same charge and potential functions also satisfy the equation

$$\nabla^2\left(\frac{a}{r}\phi(\frac{a^2}{r^2}\mathbf{r})\right) = -\frac{1}{\epsilon}\frac{a^5}{r^5}\varrho(\frac{a^2}{r^2}\mathbf{r}). \tag{2}$$

This is of the form (1) if we define the Kelvin-inverted potential and source functions as

$$\phi_{\mathrm{K}}(\mathbf{r}) = \frac{a}{r}\phi(\frac{a^2}{r^2}\mathbf{r}), \qquad \varrho_{\mathrm{K}}(\mathbf{r}) = \frac{a^5}{r^5}\varrho(\frac{a^2}{r^2}\mathbf{r}). \tag{3}$$

In the following discussion we assume the source function $\varrho(\mathbf{r})$ to be either completely outside or inside the spherical surface $r = a$.

2.1 PEC sphere

When $\mathbf{r}$ lies on the spherical surface $r = a$, we have from (3)

$$\phi_{\mathrm{K}}(\mathbf{r})|_{r=a} = \phi(\mathbf{r})|_{r=a}. \tag{4}$$

This means that the potential for the difference-charge $\varrho_{\mathrm{d}}(\mathbf{r}) = \varrho(\mathbf{r}) - \varrho_{\mathrm{K}}(\mathbf{r})$ vanishes on the sphere $r = a$:

$$\phi_{\mathrm{d}}(\mathbf{r})|_{r=a} = [\phi(\mathbf{r}) - \phi_{\mathrm{K}}(\mathbf{r})]_{r=a} = \left[\phi(\mathbf{r}) - \frac{a}{r}\phi(\frac{a^2}{r^2}\mathbf{r})\right]_{r=a} = 0. \tag{5}$$

Thus, the charge

$$\varrho_{\mathrm{PEC}}(\mathbf{r}) = -\varrho_{\mathrm{K}}(\mathbf{r}) \tag{6}$$

is the image of the charge $\varrho(\mathbf{r})$ in a grounded (zero-potential) PEC sphere $r = a$. This is the classical Kelvin image principle.

2.2 PMC sphere

The PMC boundary condition requires vanishing of the normal component of the electric field or the normal derivative of the electrostatic potential. Let us denote $\partial/\partial r$ by ∂_r for brevity. For the combined sum-charge

$$\varrho_{\mathrm{s}}(\mathbf{r}) = \varrho(\mathbf{r}) + \varrho_{\mathrm{K}}(\mathbf{r}) \tag{7}$$

the normal derivative of the corresponding potential on the sphere $r = a$ is (prime denotes the inverse radius $r' = a^2/r$)

$$\partial_r\phi_{\mathrm{s}}(\mathbf{r})|_{r=a} = \left[\partial_r\phi(\mathbf{r}) - \frac{a}{r^2}\phi(\mathbf{r}') - \frac{a^3}{r^3}\partial_{r'}\phi(\mathbf{r}')\right]_{r=r'=a} = -\phi(\mathbf{r})|_{r=a} \tag{8}$$

and, as we see, the right-hand side does not vanish in general. However, it can be canceled by adding the source $(a\partial_r)^{-1}\varrho_{\mathrm{K}}(\mathbf{r})$. For the new sum-source $\varrho_{\mathrm{s}}(\mathbf{r}) = \varrho(\mathbf{r}) + (1 + 1/(a\partial_r))\varrho_{\mathrm{K}}(\mathbf{r})$ the normal derivative of the total potential on the sphere $r = a$ vanishes and the image of the charge function $\varrho(\mathbf{r})$ in the PMC sphere is thus

$$\varrho_{\mathrm{PMC}}(\mathbf{r}) = (1 + \frac{1}{a\partial_r})\varrho_{\mathrm{K}}(\mathbf{r}), \tag{9}$$

where the operator $1/\partial_r$ must be understood as integration along the r coordinate:

$$\varrho_{\mathrm{PMC}}(\mathbf{r}) = \varrho_{\mathrm{K}}(\mathbf{r}) + \frac{1}{a}\int_a^r \varrho_{\mathrm{K}}(\mathbf{r})\, dr. \tag{10}$$

Here the integration limit is chosen so that the image does not extend to the wrong side of the sphere $r = a$.

For example, for a point charge $\varrho(\mathbf{r}) = Q\delta(\mathbf{r} - \mathbf{r}_0)$ outside the sphere we have an image source consisting of a point charge $Q_{\mathrm{K}} = Qr_{\mathrm{K}0}/a$ at the Kelvin image point $\mathbf{r}_{\mathrm{K}0} = (a^2/r_0^2)\mathbf{r}_0$ plus a line charge of density $-Q_{\mathrm{K}}/a$ on the line connecting the Kelvin point to the center of the sphere.

2.3 Impedance sphere

A sphere with general linear boundary conditions is the impedance sphere on which the (total) potential satisfies

$$(\alpha + \beta\partial_r)\phi_{\mathrm{t}}(\mathbf{r})|_{r=a} = 0. \tag{11}$$

Here α and β are parameters which may have complex values in the quasi-static approximation. Inspired by the preceding theory, and after some algebraic manipulation, we find the image of the source $\varrho(\mathbf{r})$ in the operational form

$$\varrho_{\mathrm{imp}}(\mathbf{r}) = \left[1 + \frac{\beta - 2\alpha a}{a(\alpha + \beta\partial_r)}\right]\varrho_{\mathrm{K}}(\mathbf{r}). \tag{12}$$

The PEC and PMC cases above are obtained for $\beta \to 0$ and $\alpha \to 0$, respectively. The general impedance conditions of the form considered here are encountered, for example, in the radiation condition for time-harmonic potentials in the far zone where $\alpha/\beta = j\omega\sqrt{\mu_0\epsilon_0}$.

An inverse operator expression of the form

$$\frac{1}{\alpha + \beta\partial_r} f(r) = g(r) \tag{13}$$

can be expressed as the integral

$$g(r) = \frac{1}{\beta}\int_a^r e^{\alpha(q-r)/\beta} f(q)\, dq. \tag{14}$$

Again, the integration limit is chosen so that the image does not enter the wrong side of the sphere.

3. Kelvin's Inversion in Bi–Isotropic Medium

The most general linear and isotropic medium is characterized by a four-parameter constitutive equation of the form

$$\begin{pmatrix} \mathbf{D} \\ \mathbf{B} \end{pmatrix} = \begin{pmatrix} \epsilon & \xi \\ \zeta & \mu \end{pmatrix}\begin{pmatrix} \mathbf{E} \\ \mathbf{H} \end{pmatrix}, \tag{15}$$

and the medium is called bi-isotropic. It is worth noting that because there is no coupling for static fields, the following analysis must be understood in a quasi-static sense.

The Poisson equations for the electric and magnetic scalar potential functions $\phi_{\mathrm{e}}(\mathbf{r})$, $\phi_{\mathrm{m}}(\mathbf{r})$ and the corresponding charge densities $\varrho_{\mathrm{e}}(\mathbf{r})$, $\varrho_{\mathrm{m}}(\mathbf{r})$ can be written in the matrix form

$$\nabla^2 \mathsf{f}(\mathbf{r}) = -\mathsf{M}^{-1}\mathsf{g}(\mathbf{r}), \tag{16}$$

where

$$\mathsf{f}(\mathbf{r}) = \begin{pmatrix} \phi_{\mathrm{e}}(\mathbf{r}) \\ \phi_{\mathrm{m}}(\mathbf{r}) \end{pmatrix}, \qquad \mathsf{M} = \begin{pmatrix} \epsilon & \xi \\ \zeta & \mu \end{pmatrix}, \qquad \mathsf{g}(\mathbf{r}) = \begin{pmatrix} \varrho_{\mathrm{e}}(\mathbf{r}) \\ \varrho_{\mathrm{m}}(\mathbf{r}) \end{pmatrix}. \tag{17}$$

The Kelvin-inverted quantities are now

$$\mathsf{f}_{\mathrm{K}}(\mathbf{r}) = \begin{pmatrix} \phi_{\mathrm{eK}}(\mathbf{r}) \\ \phi_{\mathrm{mK}}(\mathbf{r}) \end{pmatrix} = \frac{a}{r}\mathsf{f}(\frac{a^2}{r^2}\mathbf{r}), \qquad \mathsf{g}_{\mathrm{K}}(\mathbf{r}) = \begin{pmatrix} \varrho_{\mathrm{eK}}(\mathbf{r}) \\ \varrho_{\mathrm{mK}}(\mathbf{r}) \end{pmatrix} = \frac{a^5}{r^5}\mathsf{g}(\frac{a^2}{r^2}\mathbf{r}). \tag{18}$$

We shall study case of the impedance sphere directly, because it contains the previous PEC and PMC conditions as special cases. We combine two boundary operators in terms of two coefficients α and β as was done for the sphere in the dielectric medium, and get the generalized operator

$$\mathsf{B} = \begin{pmatrix} \alpha + \beta\epsilon\partial_r & \beta\xi\partial_r \\ \alpha\zeta\partial_r & \alpha\mu\partial_r + \beta \end{pmatrix} = \begin{pmatrix} \alpha & 0 \\ 0 & \beta \end{pmatrix} + \begin{pmatrix} \beta & 0 \\ 0 & \alpha \end{pmatrix} \mathsf{M}\partial_r. \tag{19}$$

Applying the previous line of thought we assume an image of the form

$$\mathsf{g}_{\mathrm{imp}}(\mathbf{r}) = \eta\mathsf{g}_{\mathrm{K}}(\mathbf{r}) + \mathsf{B}^{-1}\mathsf{C}\mathsf{g}_{\mathrm{K}}(\mathbf{r}). \tag{20}$$

When the boundary condition

$$\mathsf{B}\left[\mathsf{f}(\mathbf{r}) + \eta\mathsf{f}_{\mathrm{K}}(\mathbf{r})\right]_{r=a} + \mathsf{C}\mathsf{f}_{\mathrm{K}}(\mathbf{r})|_{r=a} = 0 \tag{21}$$

is expanded, η and C can be solved as

$$\eta = 1, \qquad \mathsf{C} = \begin{pmatrix} -2\alpha + \beta\epsilon/a & \beta\xi/a \\ \alpha\zeta/a & -2\beta + \alpha\mu/a \end{pmatrix} = -2\begin{pmatrix} \alpha & 0 \\ 0 & \beta \end{pmatrix} + \frac{1}{a}\begin{pmatrix} \beta & 0 \\ 0 & \alpha \end{pmatrix} \mathsf{M}. \tag{22}$$

Equation (20) is the most general image expression considered here and it gives all the other images as special cases. For example, setting $\alpha = 1$ and $\beta = 0$ leads to the PEC sphere case in a bi-isotropic medium, while setting $\xi = \zeta = 0$ leads to the impedance sphere in a dielectric and magnetic medium. The result coincides with (12) of the previous section when the difference in the definition of the parameter β is taken into account.

4. Conclusion

The inversion (Kelvin) transformation is known to produce the classical image principle for the PEC sphere even if in textbooks it is generally replaced by simpler geometric arguments allowing solving for the image of a point charge. However, the transformation is more applicable as it can produce images for the sphere with PMC and impedance boundary conditions. The latter result, given here, appears to be new. Also, as shown here, the method can be easily extended for generalizing a novel image principle to spheres in the bi-isotropic medium. Because the static approach can be used for time-harmonic problems as an approximation (quasi-static approximation), the image principle appears applicable whenever the radius of the sphere is small in terms of the wavelength.

References

[1] I. V. Lindell and J. J. Hänninen, "Static image principle for the sphere in isotropic or bi-isotropic space," *Radio Science*, vol. 35, no. 3, pp. 653–660, May–June 2000.

Modelling Photonic Bandgap Structures using FDTD

T. Uusitupa[1] and K. Kärkkäinen[2]

[1] Electromagnetics Laboratory / Helsinki University of Technology
P.O. Box 3000 FIN-02015-HUT, Finland
Fax: + 358-9-451 2267; email: tero@eml.hut.fi

[2] same address

Abstract

FDTD modelling of dielectric PBG structures is considered. In this paper PBGs are assumed to be related to layered structures which are especially used in optical waveguiding applications. Many essential features can be modelled 2-dimensionally.

1. Introduction

Photonic bandgap (PBG) material is periodically inhomogeneous material, in which electromagnetic waves having frequency in the bandgap range, can't propagate. Due to the periodical structure, PBGs are often called photonic crystals, too [1]. An example of 2-D PBG material is a uniform lattice of cylindrical air holes inside dielectric host material. In real 3-D world this might correspond to a silicon plate having cylindrical air holes. Properly manufactured PBG material can be used as a frequency selective reflective surface. Potential applications are highly efficient optical lasers and sharp bends in optical waveguides, for example. In this paper purely dielectric PBG structures are considered, even though a PBG can also be manufactured using metal rods. The chosen PBG lattice is triangular, formed by cylindrical air holes in dielectric host medium (figure 1). The main interest is in 2-D modelling of the PBG waveguides and waveguide bends.

The behaviour of EM fields in space-time in a PBG structure can be modelled using FDTD (Finite-Difference Time-Domain) which essentially means solving Maxwell's equations in discretized space and time co-ordinates [2]. FDTD has been widely used in PBG research during the last few years, see [3], [4], for example.

2. Modelling PBG Waveguides

Modelling PBG structures requires some important properties from the FDTD software used:

- model for a dielectric cylinder
- freedom to describe complicated excitation fields i.e. the time-domain behaviour and the field distribution in space.
- possibility to store "measured" fields, at certain points and time intervals, to hard disk. Stored time-dependent fields are analyzed later (F-transforms, power flow analysis etc.)

The modelling scheme in general can be considered as a "virtual measurement setup". There must be a source i.e. a field excitation, for which time and spatial dependence is properly chosen. The space-time behaviour of EM fields is governed by Maxwell's equations which are solved using FDTD. Also, there must be measurement surfaces, on which time-dependent fields are sampled

and stored to hard disk for later analysis. Figure 1 shows measurement setup involving straight PBG waveguide.

When analyzing the performance of a guiding structure, computing power flow, instead of just measuring field values, should be preferred. Just inspecting field strenght does not tell, how well the power is actually propagating. For example, with a standing or evanescent wave, field value near the output can be $\neq 0$ but power is not propagating.

Power flow is computed by spatially integrating the normal poynting vector $\mathbf{S}$. The integration is done over a surface (3-D simulation) or over a line (2-D). Using simple and fast trapezoidal rule integration leads to weighted sum of poynting vector values. For example, in 2-D, when computing power flow in $+x$-direction through measurement line $M1$ ($x = x_1$, $y \in [y_1, y_2]$, see figure 1), one uses stored fields $E_y(x_1, y, t)$ and $H_z(x_1, y, t)$. Poynting $S_x(x_1, y, t) = E_y(x_1, y, t)H_z(x_1, y, t)$ and time-dependent power flow (per-unit-length) is

$$P(t) = \int_{y_1}^{y_2} S_x(x_1, y, t)dy \approx \Delta y \left[\sum_{j=2}^{N-1} S_{x,j}(t) + \frac{1}{2}\left(S_{x,1}(t) + S_{x,N}(t)\right) \right], \quad y_2 - y_1 = (N-1)\Delta y, \quad (1)$$

where the approximation corresponds to trapezoidal rule integration, and Δy is FDTD cell-size.

By computing power flow in frequency domain, $P(f)$, one can effectively obtain, for example, power transmission $T(f) = P_2(f)/P_1(f)$ for a certain waveguide bend. This requires stored fields $E_i(r_i, t)$ and $H_i(r_i, t)$, $i = 1...M$, where M is the number of measurement planes (often $M = 2$). Performing Fourier transform from time to frequency domain one gets $E_i(r_i, f)$ and $H_i(r_i, f)$. Then for every point r_i (essential field components of E and H depend on the plane i orientation),

$$S(r_i, f) = \frac{1}{2}\Re[E(r_i, f)\ H^*(r_i, f)] \quad (2)$$

is computed. Via integration of S, one gets power flow through measurement planes, $P_i(f)$, $i = 1...M$. Power flow analysis in frequency domain is efficient, because only one simulation, using pulse-like excitation, is needed to get the transmission $T(f)$.

The absolute values are not needed for power flow at different frequencies or locations, because only the spectrum of power flow matters or $T(f) = P2(f)/P1(f)$, for example. Hence, formulas such as 1 and 2, are used without coefficients Δy and $1/2$. Such simplifications are used also with 3-D analysis. Also, the P(f)-functions are divided by the power spectrum of the input signal, to actually see the filtering effect caused by the waveguide itself.

In the formulas above it was quietly assumed that E, H and S sharing the same co-ordinate (x, y, t) are also physically at the same point in space-time, which is not exactly true due to Yee's FDTD cell [2]. Additionally to numerical dispersion error, also this may cause some error at higher frequency range.

3. Numerical Examples

The numerical examples are done in 2-D and assuming TE_z polarisation i.e. $\mathbf{H} = H(x, y, t)\mathbf{u}_z$ and $\mathbf{E} = E_x(x, y, t)\mathbf{u}_x + E_y(x, y, t)\mathbf{u}_y$.

First example is a power flow analysis of a straight PBG waveguide (linear lattice defect). Figure 2 shows a H_z-field snapshot at one time instant and figure 3 (left) $P(f)$ at one measurement plane, with waveguide width w as a varying parameter. PBG material remains same i.e. frequency bandgap is same in every case. When f belongs to bandgap, PBG works as a reflecting surface or as a boundary as far as energy flow is conserned. A mode can't propagate power in the waveguide, if $f < f_{cut-off}$. Cut-off frequency goes up as the waveguide is made narrower. This effect can be seen in figure 3. It may be practical solution to determine the channel width so that only fundamental mode propagates in the bandgap frequency region.

Second example deals with determining the wavelength $\lambda(f)$ of a propagating wave, in a straight PBG waveguide which can be approximately considered as a lossless periodic waveguide, when f is in the bandgap (small radiation loss). As in example 1, narrow-band pulse-like excitation was used, and F-transformed fields at two planes were computed. Using the field phase-difference between the planes (plane separation was a i.e. the waveguide period), wavelength $\lambda(f)$ was obtained. Figure 3 (right) shows the plot $\lambda(f)$, again w as a parameter. The results were checked at some frequencies using time-harmonic excitation.

Note that in examples 1 and 2 a PEC-boundary at $y = 0$ (figure 2) was used to exclude the antisymmetric modes. So, when f is in the bandgap and small enough, the field roughly corresponds to fundamental mode. Willing to investigate antisymmetric modes, one should use PMC-boundary.

Third example is a transmission analysis of a 60^o waveguide bend. $P(f)$ was computed at two planes. The H_z-field snapshot and transmission $T(f)$ are shown in figure 4.

Due to some unwanted reflections the field sampling time window must often be limited. This causes some decrease in accuracy in F-transformed fields, $P(f)$ and $T(f)$. Considering practical modelling and design, a complicated structure is much more easily descibed using integer-like dimensions. The results, a frequency response etc., can be easily transformed later into the frequency range of interest which corresponds to the real-world physical dimensions.

4. Conclusion

2-D modelling of PBG structures was demonstrated by way of few examples. Using pulse-like excitation and after the simulation F-transforming the fields at measurement planes, one can effectively study the features of a PBG structure. It seems that 2-D simulation is often suitable for design purposes, when dealing with layered structures where the field is mostly consentrated in one layer (PBG plate). Taking the third dimension into account often means just higher radiation loss and a bit frequency-shifted response, due to a different effective refraction index seen by the wave.

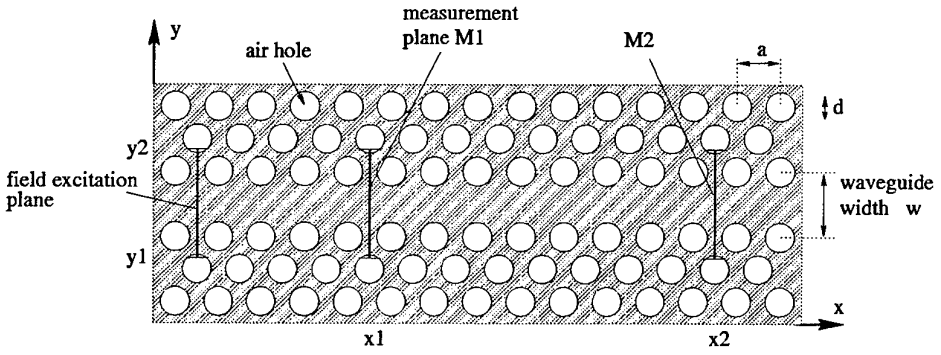

Figure 1: Triangular lattice PBG. Straight waveguide measurement setup.

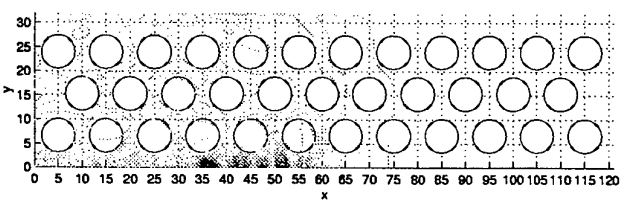

Figure 2: H_z-field snapshot. Computation domain was halved using PEC-boundary at $y = 0$. Consequently only symmetric modes can exist. The excitation field was chosen to support 1. symm. mode i.e. the fundamental mode.

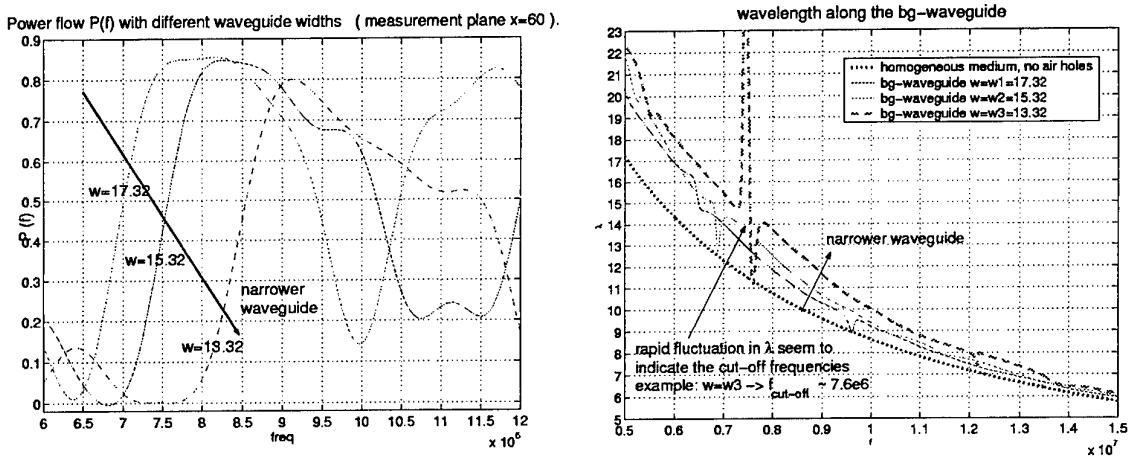

Figure 3: Left: power flow at $x = 60$. Right: wavelength in the PBG waveguide.

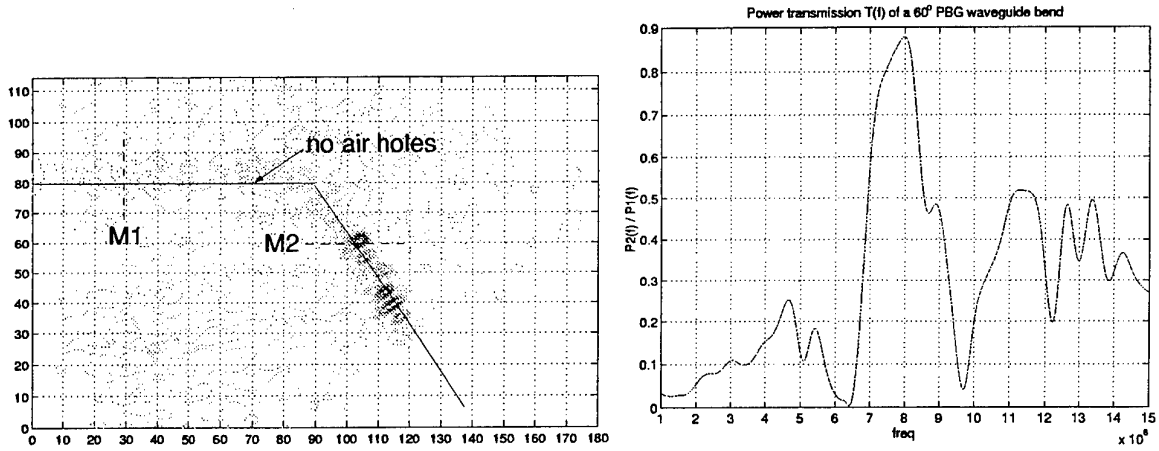

Figure 4: Left: H_z-field snapshot. Right: power transmission of a 60^o bend.

References

[1] J. D. Joannopoulos *et al.*, *Photonic Crystals, Molding the Flow of Light.* Princeton: University Press, 1995.

[2] A. Taflove, *Computational Electrodynamics, The Finite Difference Time Domain Method.* Artech House, 1995.

[3] J. G. Maloney *et al.*, "A simple description for waveguiding in photonic bandgap materials", *Microwave Opt. Technol. Lett.*, vol. 14, no. 5 , pp. 261-266, April 1997.

[4] I. El-Kady *et al.*, "Dielectric Waveguides in Two-Dimensional Photonic Bandgap Materials", *J. Lightwave Technol.*, vol. 17, no. 11, pp. 2042-2049, Nov. 1999.

Optical Fibre Embedded in a Composite Laminated with Applications to Sensing

O. Frazão[1], N. Correia[2], C. Novo[2], A. Vieira[2], A. N. Costa[2], F. M. Araújo[3,1], and A. T. Marques[2]

[1] INESC Porto – Unidade de Optoelectrónica e Sistemas Electrónicos,
Rua Campo Alegre, 687, 4169 – 007 Porto, Portugal,
Tel.: +351 226 082 601; Fax: +351 226 082 799. Email: ofrazao@goe.fc.up.pt

[2] INEGI – Instituto de Engenharia Mecânica e Gestão Industrial,
Rua do Barroco, 174, 4465-591 Leça do Balio, Portugal,
Tel.: +351 229 578 713; Fax: +351 229 537 352.

[3] Departamento de Física da Faculdade de Ciências da Universidade do Porto,
Rua Campo Alegre, 687, 4169 – 007 Porto, Portugal,
Tel.: +351 226 082 601; Fax: +351 226 082 799.

Abstract

A smart sensor was fabricated using a carbon-epoxy composite laminate in which fibre Bragg gratings were embedded. These instrumented carbon fibre laminates can be used for reinforcement and protection of concrete/metallic structures, playing an important role in monitoring repaired or reinforced constructions.

1. Introduction

Fibre Bragg grating sensors (FBG) can be very useful in applications where layered materials, such as composites, are involved, because they provide a basis for the development of smart structures. These sensors allow measurement of parameters such as load/strain, vibration, temperature and detection of cracks and delamination phenomena tests [1], which are chiefly related with the monitoring of concrete loading/failure behaviour. Based on these properties we have conducted experiments by adhesively bonding smart sensors onto polymeric concrete samples, which where then submitted to standard loading tests. The work performed was aimed at the evaluation of stiffness and detection of fissures in carbon reinforced concrete, both through experimental tests and development of analytical models. Because of the recent interest in repairing metallic/concrete structures with composite laminates, it is safe to assume that such applications will be an appealing field for FBG sensors, since these are cases where monitoring is extremely important.

2. FBG Theory

An FBG is a periodic modulation of the refractive index of the core of a single mode optical fibre, written by exposure to UV light in the region around 248nm [2]. This fabrication process is based on the photosensitive mechanism, which is observed in Ge-doped optical fibres [3]. If broadband light is travelling through an optical fibre containing such a periodic structure, its diffractive properties promote that a very narrow wavelength band is reflected back. The centre wavelength of this band can be represented by well known the Bragg condition:

$$\lambda_B = 2n_{eff}\Lambda\,, \tag{1}$$

where λ_B is the centre wavelength, n_{eff} is the effective index of the guided mode and Λ is the period of the index modulation. The FBG ressonance wavelength will vary accordingly with temperature or strain changes experienced by the fibre. For a temperature change ΔT, the corresponding wavelength shift is given by:

$$\Delta\lambda_B = \lambda_B\left(\frac{1}{\Lambda}\frac{\partial\Lambda}{\partial T}+\frac{1}{n}\frac{\partial n}{\partial T}\right)\Delta T = \lambda_B(\alpha+\xi)\Delta T\,, \tag{2}$$

where α is the fibre thermal-expansion coefficient, and ξ is the fibre thermo-optic coefficient. The wavelength shift, induced by a longitudinal strain variation $\Delta\varepsilon$ is given by,

$$\Delta\lambda_B = \lambda_B\left(\frac{1}{\Lambda}\frac{\partial\Lambda}{\partial\varepsilon}+\frac{1}{n}\frac{\partial n}{\partial\varepsilon}\right)\Delta\varepsilon = \lambda_B(1-p_e)\Delta\varepsilon\,, \tag{3}$$

where p_e is the photoelastic coefficient of the fibre. For a silica fibre, the wavelength-strain and wavelength-temperature sensitivities are ~13pm°C^{-1} and ~1.15pmμε^{-1}, for a Bragg wavelength centred at 1555nm [4].

3. Smart Sensors Plate Fabrication and Characterization

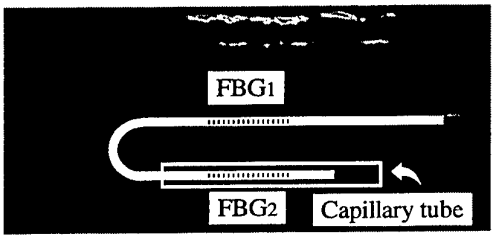

Fig. 1 Smart sensor plate with illustration of FBG sensor placement.

Two fibre Bragg gratings were embedded between layers of pre-impregnated carbon fibre/epoxy resin to produce a smart sensor plate. The laminate had three layers with dimensions of 150×70×1mm^3 and was cured inside an autoclave at 100°C during 1 hour with 0.8×10^5Pa pressure. The FBG_1 (λ_{B1}=1539nm) was used for measuring strain and temperature, while the FBG_2 (λ_{B2}=1530nm) was only sensitive to temperature. The FBG_2 sensor was properly isolated from strain inside a steel capillary tube with $\varnothing_{ext}$=0.8 mm, $\varnothing_{int}$=0.5mm and length L=40mm. The characterization of the smart sensor consisted in temperature measurements holding strain constant (ε=0) and strain measurements with constant temperature (T=20°C). Fig. 2-a) and 2-b) show the response of the two FBGs to temperature variation under constant strain and bending strain variation at constant temperature, respectively.

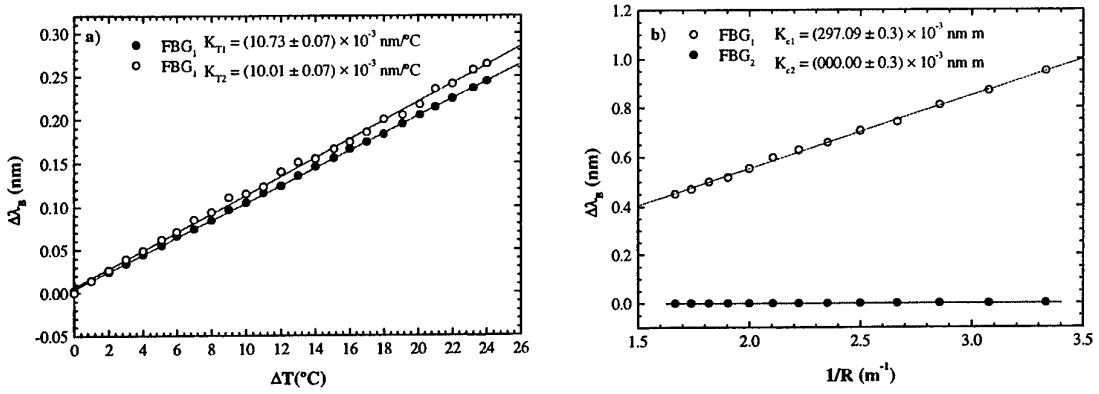

Fig. 2 Response of smart sensor plate to: **a)** Temperature; **b)** Inverse curvature radius (1/R).

As expected different sensitivities were obtained for strain, while similar ones were obtained for temperature. The small difference observed between the thermal sensitivities can be attributed mainly to the additional strain effect of the material's thermal expansion. Monitoring both Bragg grating wavelengths allow us to determine simultaneous temperature and bending strain. In fact, from data contained in Fig. 2 the following relationship can be expressed:

$$\begin{bmatrix}\Delta T\\ \Delta C\end{bmatrix}=\frac{1}{\Delta}\begin{bmatrix}K_{C2} & -K_{C1}\\ -K_{T2} & K_{T1}\end{bmatrix}\begin{bmatrix}\Delta\lambda_{B1}\\ \Delta\lambda_{B2}\end{bmatrix}=-336.3\begin{bmatrix}0.0000 & -297.09\\ -10.01 & 10.73\end{bmatrix}\begin{bmatrix}\Delta\lambda_{B1}\\ \Delta\lambda_{B2}\end{bmatrix}, \quad (4)$$

where $\Delta = K_{T1}K_{c2} - K_{c1}K_{T2}$, ΔT and ΔC are temperature and curvature variations. Based on this equation and from the experimental evaluation of $\Delta\lambda_{B1}$ and $\Delta\lambda_{B2}$ we are then able to determine both ΔT and ΔC.

4. Experimental Results

Experiments were conducted on instrumented and/or reinforced polymer concrete plates, with dimensions of 600×100×20mm^3, using a test machine INSTRON Universal (mod. 4208). All three point bending tests performed had a span length of 500mm. Fig. 3 shows two types of plates tested. In a Fig. 3-a) we can observe a CFRP (Carbon Fibre Reinforced Polymer) concrete plate. The CFRP was used to increase the tension strength and reduce the crack propagation rate of the plate, and it contained 3 FBG sensors. One was located at the centre and the others two at 150mm to each side. In Fig. 3-b) it is shown a concrete plate instrumented with the smart sensor plate described in the previous section.

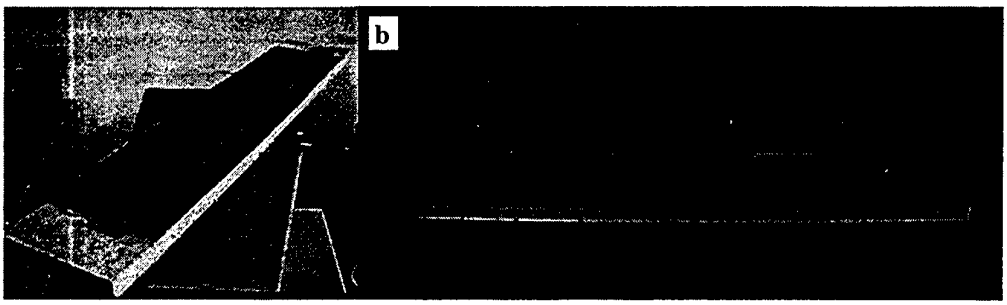

Fig. 3 **a)** CFRP reinforced concrete plate containing FBG sensors, and **b)** smart sensor plate adhesively bonded to polymer concrete plate.

The system used for monitoring the smart sensor plates is presented in Fig. 4. The system included an OSA – optical spectrum analyser (ANDO AQ 6330), an EBOS – erbium broadband optical source (PHOTONETICS), a 3 dB coupler and a computer data acquisition system.

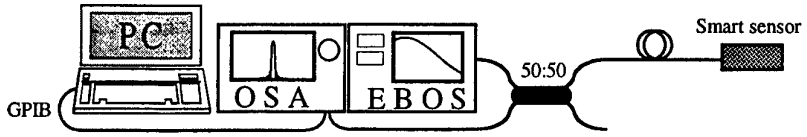

Fig. 4 Experimental set-up used for monitoring smart sensor plates.

Fig. 5-a) and 5-b) show test results of reinforced and non-reinforced polymer concrete plates (strain vs. time). The temperature evolution measured through the sensor FBG_2 during the test, in the smart sensor plate is also presented. The non-reinforced concrete plate showed no cracking before failure and presented an ultimate strain of 280με at the sensor location (see Fig. 5-a). The reinforced concrete plate, on the other hand, endured a much higher strain (about 7×) and failed in compression developing 4 compression cracks. The FBG monitoring system also allowed the detection of these

cracks as can be observed in peak (1) of Fig. 5-b) – here (2) denotes a failure of sensors 1 and 3 due rupture of the optical fibre containing FBG sensors. The crack detection is shown in detail in Fig. 6 using data extracted from the peak (1) in Fig. 5-a).

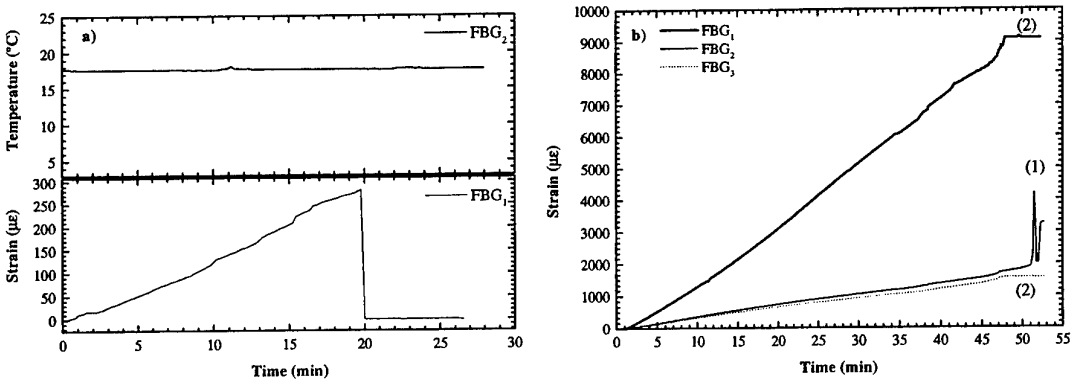

Fig. 5 Test results of the strain and temperature evolution of the: **a)** Non-reinforced concrete plate; **b)** Reinforced concrete plate containing 3 FBG sensors.

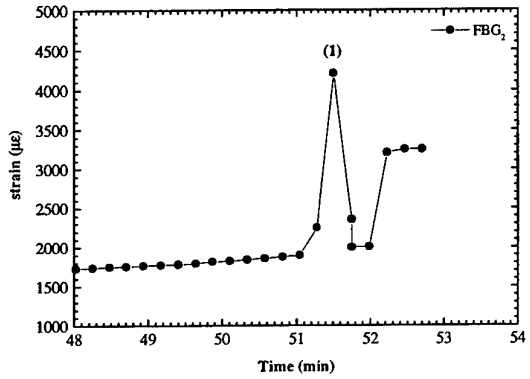

Fig. 6 Detail of crack detection and final failure extracted from peak (1) in Fig. 5-a).

5. Conclusion

FBG sensors showed the ability to detect strain and cracks in concrete plates. A 1mm thick CFRP laminate reinforcement allowed an increase of 7 times in strain and induced compressive cracking in the concrete polymer. The monitoring system failed when the optical fibres were forced to endure strain values in excess of 9000με, causing signal loss due to rupture of the optical fibres. The possibility of using fibre optic instrumented plates in rehabilitation of civil structures was demonstrated, since strain measurements and compressive cracking can be effectively detected.

References

[1] A. D. Kersey, M. A. Davis, H. J. Patrick, M. LeBlanc, K. P. Koo, C. G. Askins, M. A. Putnam, and E. J. Friebele, "Fiber grating sensors", *J. Lightwave Technol.* vol. 15, pp. 1442-1463, 1997.

[2] K. O. Hill, B. Malo, F. Bilodeau, D. C. Johnson, and J. Albert, "Bragg gratings fabricated in monomode photosensitive optical fiber by UV exposure through a phase mask", *Appl. Phys. Lett.*, Vol. 62, pp. 1035-1037, 1993.

[3] K. O. Hill, B. Malo, F. Bilodeau, and D. C. Johnson, "Photosensitivity in optical fibers", *Annu. Rev. Mater. Sci.* vol., 23, pp. 125-157, 1993.

[4] W. W. Morey, G. Meltz, and W. H. Glenn, "Fibre optic bragg grating sensors", in *Fiber Optic and Laser Sensors VII*, in Proc. SPIE 1169, Boston, USA, pp. 98-107, 1989.

Mode Transformers for Soft and Hard Surface Waveguides by using Chiral Material

A. J. Viitanen

Electromagnetics Laboratory, Department of Electrical and Communications Engineering,
Helsinki University of Technology, P.O. Box 3000, FIN-02015 HUT, Finland
Fax: + 358–9–451 2267; email: ari.viitanen@hut.fi

Abstract

The field propagation in soft and hard surface waveguide, also called balanced corrugated waveguide, filled with chiral medium is considered. The eigenfields inside the waveguide are circularly polarized and are propagating separately. For small chirality parameter values the eigenfields are slightly coupled and the polarization of the propagating field is changed. This effect causes a mode transformation between TM and TE modes.

1. Introduction

Wave propagation in cylindrical corrugated waveguide filled with chiral medium is considered. The corrugation on the surface of the waveguide is such that the boundary condition is equal to the soft and hard surface boundary [1]. These kind of waveguides are used, for example, in antenna feed horns. It is known that the eigenfields associated to the soft and hard surfaces are circularly polarized. Also the eigenwaves propagating in chiral medium are circularly polarized, denoted by + and − waves [2] - [4]. When the corrugation in a waveguide structure is in transverse direction the waveguide is called soft surface waveguide, and when the corrugation is in axial direction it is called hard surface waveguide [1]. Inside the chiral soft and hard surface waveguide there are propagating + and − waves separately. However, when the chirality parameter of the medium is very small these two eigenwaves are propagating almost with the same propagation factor which results in a change in polarization of the propagating field.

2. Theory

The electric and magnetic fields in waveguide depend on z as $e^{-j\beta z}$ where β is the propagation factor. The waveguide is filled with chiral material with the constitutive relations [4]

$$\mathbf{D} = \varepsilon\mathbf{E} - j\kappa\sqrt{\mu_o\varepsilon_o}\,\mathbf{H}, \qquad \mathbf{B} = \mu\mathbf{H} + j\kappa\sqrt{\mu_o\varepsilon_o}\,\mathbf{E}, \tag{1}$$

where ε, μ and κ are permittivity, permeability and the chirality parameter of the medium, respectively. In the waveguide structure the electric and magnetic fields are written with transverse and axial parts as

$$\mathbf{E} = \mathbf{e} + E_z\mathbf{u}_z, \qquad \mathbf{H} = \mathbf{h} + H_z\mathbf{u}_z, \tag{2}$$

which are inserted into the Maxwell equations

$$\nabla \times \mathbf{E} = -j\omega\mathbf{B}, \qquad \nabla \times \mathbf{H} = j\omega\mathbf{D}. \tag{3}$$

On the other hand, the fields in chiral medium are expressed in terms of right hand and left hand circularly polarized waves denoted by + and − waves. After eliminating the transverse

fields $\mathbf{e}$ and $\mathbf{h}$ and using the decomposition into $+$ and $-$ parts the Maxwell equations reduce to the Helmholtz equation for axial field components

$$[\nabla_t^2 + k_{c\pm}^2]E_{z\pm}(\rho,\varphi) = 0, \tag{4}$$

where $E_{z\pm} = \frac{1}{2}(E_z \mp j\eta H_z)$, $k_{c\pm} = \sqrt{k_\pm^2 - \beta^2}$ and $k_\pm = k \pm k_o\kappa$. The ∇_t operator is the transverse part of ∇. The general solutions of the Helmholtz equation in cylindrical coordinates are Bessel functions of the first kind

$$E_{z\pm}(\rho,\varphi) = A_{n\pm}J_n(k_{c\pm}\rho)e^{jn\varphi}. \tag{5}$$

The all other field components can be expressed with these two axial field components. The partial transverse fields are obtained from the axial parts as

$$\mathbf{e}_\pm = [-\frac{j\beta}{k_{c\pm}^2}\nabla_t \mp \frac{k_\pm}{k_{c\pm}^2}\mathbf{u}_z \times \nabla_t]E_{z\pm}. \tag{6}$$

The coefficients $k_{c\pm}$ and $A_{n\pm}$ are determined by the boundary and initial conditions.

The two partial transverse fields $\mathbf{e}_+$ and $\mathbf{e}_-$ are elliptically polarized of opposite handedness with respect to the direction of propagation. The total fields are obtained as a combination of transverse and axial $+$ and $-$ waves as

$$\mathbf{E} = \mathbf{e}_+ + \mathbf{e}_- + (E_{z+} + E_{z-})\mathbf{u}_z \tag{7}$$

and

$$\mathbf{H} = \frac{j}{\eta}[\mathbf{e}_+ - \mathbf{e}_- + (E_{z+} - E_{z-})\mathbf{u}_z]. \tag{8}$$

The parameters $k_{c\pm}$ are determined by the boundary condition for the soft and hard surface at $\rho = a$

$$\mathbf{u}\cdot\mathbf{E} = 0, \qquad \mathbf{u}\cdot\mathbf{H} = 0, \tag{9}$$

where $\mathbf{u} = \mathbf{u}_\varphi$ for soft surface and $\mathbf{u} = \mathbf{u}_z$ for hard surface boundary [1]. For the soft surface waveguide with index $n = 0$ and for the hard surface waveguide with all index n the boundary conditions (9) lead to the eigenvalue equation [5]

$$J_n(k_{c+}a)\,J_n(k_{c-}a) = 0. \tag{10}$$

The solution of the eigenvalue equation is

$$k_{c\pm} = \frac{p_{ns}}{a}, \tag{11}$$

where p_{ns} are the zeros of the Bessel functions. The propagation factors for $+$ and $-$ waves are now obtained

$$\beta_\pm = \sqrt{k_\pm^2 - \left(\frac{p_{ns}}{a}\right)^2}. \tag{12}$$

The value of the propagation factor is different for $+$ and $-$ waves when the waveguide is filled with chiral material. In a nonchiral case these two values reduce to $\beta = \sqrt{k^2 - (p_{ns}/a)^2}$.

3. Mode Transformation

The polarization properties of the propagating fields inside the chiral soft and hard surface waveguides are considered when the value of the chirality parameter of the medium is small. It will be shown that the small chirality value affects mainly to the polarization of the propagating field. Chiral media can be fabricated by incerting small helices into the base material and the chirality parameter is proportional to the density of chiral inclusions. High density of inclusions increases losses [6]. Now, the requered chirality parameter is small and is achieved with small density of inclusions and also the losses are small.

Denoting the wave numbers of partial waves in chiral medium as

$$k_{\pm} = k(1 \pm \kappa_r), \tag{13}$$

where $\kappa_r = \kappa\sqrt{\frac{\mu_o\varepsilon_o}{\mu\varepsilon}}$ and assuming that $|\kappa_r| \ll 1$, the propagation factors are approximated as

$$\beta_{\pm} = \sqrt{k^2(1 \pm \kappa_r)^2 - \left(\frac{p_{ns}}{a}\right)^2} \approx \beta \pm \frac{k^2}{\beta}\kappa_r. \tag{14}$$

Here, the parameters $\beta = \sqrt{k^2 - k_c^2}$ and $k_c = \frac{p_{ns}}{a}$ are the same as for a nonchiral waveguide. The axial field components reduce now to the form

$$E_{z\pm}(\rho, \varphi, z) \approx A_{n\pm} J_n(k_c\rho) e^{jn\varphi} e^{\mp j\frac{k^2}{\beta}\kappa_r z} e^{-j\beta z} \tag{15}$$

and, similarly, the transverse partial waves are approximated as

$$\mathbf{e}_{\pm}(\rho, \varphi, z) \approx [-\frac{j\beta}{k_c^2}\nabla_t \mp \frac{k}{k_c^2}\mathbf{u}_z \times \nabla_t] E_{z\pm}(\rho, \varphi, z). \tag{16}$$

The total axial field components are

$$E_z = E_{z+} + E_{z-}$$

$$= [(A_{n+} + A_{n-})\cos(\frac{k^2}{\beta}\kappa_r z) - j(A_{n+} - A_{n-})\sin(\frac{k^2}{\beta}\kappa_r z)] J_n(k_c\rho) e^{jn\varphi} e^{-j\beta z} \tag{17}$$

and

$$H_z = \frac{j}{\eta}[E_{z+} - E_{z-}]$$

$$= \frac{j}{\eta}[(A_{n+} - A_{n-})\cos(\frac{k^2}{\beta}\kappa_r z) - j(A_{n+} + A_{n-})\sin(\frac{k^2}{\beta}\kappa_r z)] J_n(k_c\rho) e^{jn\varphi} e^{-j\beta z}. \tag{18}$$

In these expressions the fields are written in terms of right hand and left hand circularly polarized components. The general field inside a waveguide can also be presented as a combination of TE and TM fields. Denoting at $z = 0$ the axial field components as

$$E_z(0) = A_{n+} + A_{n-} = E_n \tag{19}$$

and

$$H_z(0) = \frac{j}{\eta}[A_{n+} - A_{n-}] = H_n, \tag{20}$$

the axial electric field is

$$E_z(z) = [E_n \cos(\frac{k^2}{\beta}\kappa_r z) - \eta H_n \sin(\frac{k^2}{\beta}\kappa_r z)] J_n(k_c\rho) e^{jn\varphi} e^{-j\beta z} \tag{21}$$

and the axial magnetic field is

$$H_z(z) = [H_n \cos(\frac{k^2}{\beta}\kappa_r z) + \frac{E_n}{\eta}\sin(\frac{k^2}{\beta}\kappa_r z)]J_n(k_c\rho)e^{jn\varphi}e^{-j\beta z}. \quad (22)$$

The coefficients E_n and H_n are determined by the initial conditions.

The mode transformation effect is clearly seen by considering the axial field components as a function of z. If, for example, at $z = 0$ we have $H_n = 0$, there exists the axial electric field but no axial magnetic field, we have then TM_{ns} fields. At the distance

$$z = \frac{\pi\beta}{2k^2\kappa_r}, \quad (23)$$

which is denoted by $\lambda_p/4$, there exists the axial magnetic field but no axial electric field which means that we have TE_{ns} fields. So, after the distance $z = \lambda_p/4$ the original TM mode is changed to TE mode.

When the length of the chiral soft and hard surface waveguide is twice the value of (23), denoted by $\lambda_p/2$, the field configuration is at 180° phase shift of its original value. This means that the chiral soft and hard surface waveguide of length $\lambda_p/2$ works as a 180° phase shifter. In a general case, inside the soft and hard surface waveguide there can propagate a hybrid mode. With other choice of the length for the waveguide as done in the previous examples the original hybrid mode propagating inside the waveguide can be transformed to another hybrid mode.

4. Conclusion

The mode transformation effect in chiral soft and hard surface cylindrical waveguide are considered. The soft and hard surface waveguide is filled with slightly chiral material. The small chirality affects to the polarization of the propagating field. The eigenvalue equation for the chiral hard surface waveguide is evaluated. Also, the eigenvalue equation for the chiral soft surface waveguide for the spherically symmetric mode is similar as for the hard surface waveguide. It is demonstrated that with a proper length of the chiral soft and hard surface waveguide the TM mode is changed to TE mode and vice versa. Also when the length is twice of this proper length the original field pattern is suffered a 180° phase shift. This kind of mode transformers and phase shifters may be used as matching elements between different kind of waveguides or between waveguides and antennas.

References

[1] P-S. Kildal, " Artificially soft and hard surfaces in electromagnetics," *IEEE Trans. Microwave Theory Tech.*, vol. 38, no. 10, pp. 1537–1544, 1990.

[2] P. Pelet and N. Engheta, "The theory of chirowaveguides," *IEEE Trans. Antennas Propagation,* vol. 38, no. 1, pp. 90–97, January, 1990.

[3] S. F. Mahmoud, "Mode characteristics in chirowaveguides with constant impedance walls," *J. Electromag. Waves Appl.,* vol. 6, no. 5/6, pp. 625–640, 1992.

[4] I. V. Lindell, A. H. Sihvola, S. A. Tretyakov, and A. J. Viitanen, *Electromagnetic Waves in Chiral and Bi-Isotropic Media.* Norwood, NY: Artech House, 1994.

[5] A. J. Viitanen, "Chiral hard-surface waveguide mode transformer," *IEEE Trans. Microwave Theory Tech.*, vol. 48, no. 6, June 2000, to appear.

[6] F. Mariotte, S. A. Tretyakov, and B. Sauviac, "Isotropic chiral composite modeling: Comparison between analytical, numerical, and experimental results," *Microwave Opt. Technol. Lett.*, vol. 7, no. 18, pp. 861–864, 1994.

Polarisability Analysis of Layered Bi-Anisotropic Ellipsoids

J. Avelin and A. Sihvola

Electromagnetics Laboratory, Helsinki University of Technology
P.O.Box 3000, FIN-02015 HUT, Finland
Fax: + 358–9–451 2267; email: juha.avelin@hut.fi

Abstract

Using six-vector formalism, the polarisability problem of a layered bi-anisotropic ellipsoid is solved. The polarisability six-dyadic is explicitly calculated for the case of a two-component ellipsoid where the core is fully bi-anisotropic but the shell and the environment are bi-isotropic at most. It is reasonably straightforward to include more bi-isotropic layers on the ellipsoid. The limitation of the analysis is that all ellipsoidal boundaries for the composite structure have to be confocal.

1. Introduction

In this presentation we treat and analyse the calculation of the polarisability of a small scatterer. The polarisability is defined as the linear relation between the dipole moment and the uniform incident field that induces this moment. For anisotropic or non-spherical scatterers, the polarisability is generally a dyadic: $\mathbf{p} = \overline{\overline{\alpha}} \cdot \mathbf{E}$, where $\mathbf{p}$ is the dipole moment and $\mathbf{E}$ is the incident electric field. In the present paper we will concentrate on the case of bi-anisotropic scatterers in which case the polarisability is a matrix relation between the induced electric and magnetic dipole moments and the incident electric and magnetic fields. The concept of polarisability is important in the low-frequency applications [1]: the size of the scatterer has to be small in comparison of the wavelength of the operating field.

In the bi-anisotropic case we will use the six-vector formalism [2]. The electric and magnetic vector quantities are collected into a six-vector, and the relation between two six-vectors is a six-dyadic. Thus, for example, the polarisability is a six-dyadic (consisting of four ordinary three-dyadics, or 36 scalar parameters): $\mathsf{p} = \mathsf{A} \cdot \mathsf{e}$, where the field and dipole moment six-vectors are

$$\mathsf{p} = \begin{pmatrix} \mathbf{p_e} \\ \mathbf{p_m} \end{pmatrix} \quad \text{and} \quad \mathsf{e} = \begin{pmatrix} \mathbf{E} \\ \mathbf{H} \end{pmatrix} \tag{1}$$

In this presentation, the particular emphasis is on inhomogeneous scatterers; especially layered ellipsoidal scatterers. We will show how the polarisability six-matrix of a layered ellipsoidal scatterer can be calculated with the six-matrix formalism: the equations are shown for the case of core-plus-shell ellipsoid but the method works for any number of ellipsoidal layers. There is, however, one limitation: all the ellipsoidal boundaries in the structure have to be confocal. In other words, the foci of the various ellipsoids have to coincide. The results allow the layers (and the environment) to be bi-isotropic; in addition, the core of the layered ellipsoid can be arbitrarily bi-anisotropic.

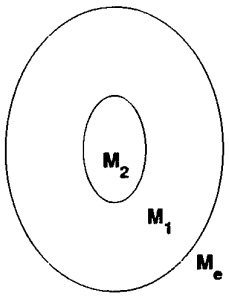

Figure 1: Layered ellipsoid with the core and shell

The results form a considerable generalisation of the previous studies where the corresponding polarisability problem for layered ellipsoidal dielectric scatterers [3] and for the two-layer chiral sphere [4] was solved.

2. Polarisability Six-Dyadic for the Core–Plus–Shell Ellipsoid

Consider the scatterer illustrated in Figure 1 where an ellipsoid is located in bi-isotropic environment. The ellipsoid consists of a bi-anisotropic core and a bi-isotropic layer (shell). It has to be remembered that the ellipsoidal boundaries have to be confocal, which roughly means that the core is less "rounded" than the whole scatterer. The material parameters in the problem are contained in the three material six-dyadics

$$\mathsf{M}_e = \begin{pmatrix} \epsilon_e \bar{\bar{I}} & \xi_e \bar{\bar{I}} \\ \zeta_e \bar{\bar{I}} & \mu_e \bar{\bar{I}} \end{pmatrix}, \qquad \mathsf{M}_1 = \begin{pmatrix} \epsilon_1 \bar{\bar{I}} & \xi_1 \bar{\bar{I}} \\ \zeta_1 \bar{\bar{I}} & \mu_1 \bar{\bar{I}} \end{pmatrix}, \qquad \mathsf{M}_2 = \begin{pmatrix} \bar{\bar{\epsilon}}_2 & \bar{\bar{\xi}}_2 \\ \bar{\bar{\zeta}}_2 & \bar{\bar{\mu}}_2 \end{pmatrix} \tag{2}$$

How to calculate the six-dyadic polarisability for this ellipsoid? Using the three-vector analysis as was done in [4] for the layered chiral sphere would lead to a large set of coupled vector equations from which the polarisability would be extremely tedious to solve. Here the six-vector analysis shows its power, because the analysis remains formally on the same level of complexity as in the three-vector case, and we can follow the steps in the layered dielectric studies.

The result is that the polarisability six-dyadic

$$\mathsf{A} = \begin{pmatrix} \bar{\bar{\alpha}}_{ee} & \bar{\bar{\alpha}}_{em} \\ \bar{\bar{\alpha}}_{me} & \bar{\bar{\alpha}}_{mm} \end{pmatrix} \tag{3}$$

of a layered bi-anisotropic ellipsoid can be expressed in a compact form:

$$\mathsf{A} = V\mathsf{M}_e \cdot \left\{ \mathsf{K} \cdot [(\mathsf{M}_1 - \mathsf{M}_e) \cdot \mathsf{L}_1 + \mathsf{M}_e] + w(\mathsf{M}_2 - \mathsf{M}_1) \cdot \mathsf{L}_1 \right\}^{-1} \cdot [\mathsf{K} \cdot (\mathsf{M}_1 - \mathsf{M}_e) + w(\mathsf{M}_2 - \mathsf{M}_1)] \tag{4}$$

with the following definitions:

$$\mathsf{K} = (\mathsf{M}_2 - \mathsf{M}_1) \cdot (\mathsf{L}_2 - w\mathsf{L}_1) \cdot \mathsf{M}_1^{-1} + \mathsf{I}$$

and the unit six-dyadic is defined obviously by

$$\mathsf{I} = \begin{pmatrix} \bar{\bar{I}} & 0 \\ 0 & \bar{\bar{I}} \end{pmatrix}$$

The depolarisation factors of the two ellipsoidal boundaries are contained in the six-dyadics

$$\mathsf{L}_1 = \begin{pmatrix} \overline{\overline{L}}_1 & 0 \\ 0 & \overline{\overline{L}}_1 \end{pmatrix} \quad \text{and} \quad \mathsf{L}_2 = \begin{pmatrix} \overline{\overline{L}}_2 & 0 \\ 0 & \overline{\overline{L}}_2 \end{pmatrix}$$

and w is fraction of the core from the total volume V of the particle.

The present analysis can be generalized to ellipsoids having more layers than the core and the shell, as in [3, 5].

3. Special Cases

3.1 Homogeneous sphere

It is important to check the result with special cases known earlierly. A trivial test could be to have a homogeneous isotropic sphere in isotropic environment, for which the scalar polarisability is

$$\alpha = 3V\epsilon_e \frac{\epsilon_i - \epsilon_e}{\epsilon_i + 2\epsilon_e} \tag{5}$$

It is quite easy to see that (4) passes this test.

3.2 Layered dielectric ellipsoid

The second special case is the layered dielectric (or magnetic) ellipsoid (see [3]): $\xi_e = \xi_1 = \zeta_e = \zeta_1 = 0$, $\overline{\overline{\xi}}_2 = \overline{\overline{\zeta}}_2 = 0$, $\overline{\overline{\epsilon}}_2 = \epsilon_2 \overline{\overline{I}}$, and $\overline{\overline{\mu}}_2 = \mu_2 \overline{\overline{I}}$. In this case the polarisability six-dyadic reduces to

$$\mathsf{A} = \begin{pmatrix} \overline{\overline{\alpha}}_{ee} & 0 \\ 0 & \overline{\overline{\alpha}}_{mm} \end{pmatrix}$$

where the electric polarisability is

$$\overline{\overline{\alpha}}_{ee} = V\epsilon_e \sum_{i=x,y,z} \frac{(\epsilon_1 - \epsilon_e)(\epsilon_1 + N_{2i}(\epsilon_2 - \epsilon_1)) + w(\epsilon_1 + N_{1i}(\epsilon_e - \epsilon_1))(\epsilon_2 - \epsilon_1)}{(\epsilon_e + N_{1i}(\epsilon_1 - \epsilon_e))(\epsilon_1 + N_{2i}(\epsilon_2 - \epsilon_1)) + wN_{1i}(1 - N_{1i})(\epsilon_1 - \epsilon_e)(\epsilon_2 - \epsilon_1)} \mathbf{u}_i \mathbf{u}_i \tag{6}$$

and the magnetic polarisability $\overline{\overline{\alpha}}_{mm}$ is, mutatis mutandis, the same as $\overline{\overline{\alpha}}_{ee}$. N_{1i} and N_{2i} are the depolarisation factors of the ellipsoids:

$$\overline{\overline{L}}_1 = N_{1x}\mathbf{u}_x\mathbf{u}_x + N_{1y}\mathbf{u}_y\mathbf{u}_y + N_{1z}\mathbf{u}_z\mathbf{u}_z \quad \text{and} \quad \overline{\overline{L}}_2 = N_{2x}\mathbf{u}_x\mathbf{u}_x + N_{2y}\mathbf{u}_y\mathbf{u}_y + N_{2z}\mathbf{u}_z\mathbf{u}_z.$$

3.3 Other special cases

Among the other possible special cases to test the result, the following ones can be considered: homogeneous chiral sphere and layered chiral sphere. The result (4) passes also these tests, but the resulting lengthy expressions are not shown here.

4. Maxwell Garnett Mixing Formula

With (4) we can build the Maxwell Garnett (Clausius–Mossotti) mixing formula for aligned layered ellipsoids:

$$\mathsf{M}_{eff} = \mathsf{M}_e + n\mathsf{M}_e \cdot \left(\mathsf{M}_e - n\mathsf{A} \cdot \mathsf{L}_1\right)^{-1} \cdot \mathsf{A} \tag{7}$$

where n is the number density of the layered ellipsoidal inclusions.

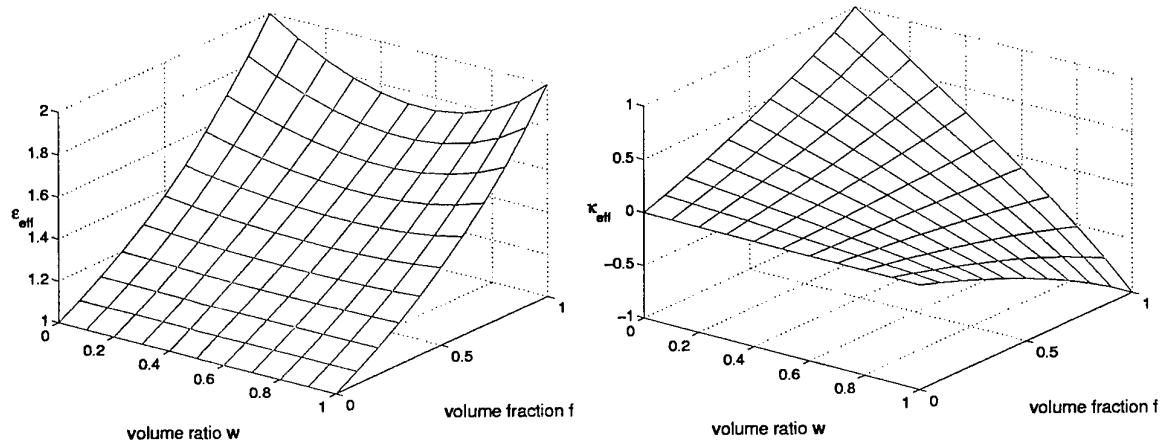

Figure 2: Effective relative permittivity (left) and chirality (right) of the mixture.

Numerical Example

Let us assume a mixture, which consists of layered chiral spheres in an isotropic background. The cores in the spheres are bi-isotropic: $\overline{\overline{\epsilon}}_2 = 2.0\epsilon_0\overline{\overline{I}}$, $\overline{\overline{\mu}}_2 = 1.5\mu_0\overline{\overline{I}}$, and $\kappa_2 = -1.0$, so that $\overline{\overline{\xi}}_2 = j\sqrt{\mu_0\epsilon_0}\overline{\overline{I}}$ and $\overline{\overline{\zeta}}_2 = -j\sqrt{\mu_0\epsilon_0}\overline{\overline{I}}$. The shells are also bi-isotropic: $\overline{\overline{\epsilon}}_1 = 2.0\epsilon_0\overline{\overline{I}}$, $\overline{\overline{\mu}}_1 = 1.5\mu_0\overline{\overline{I}}$, but $\kappa_1 = +1.0$. In other words: the materials in the layered spheres are almost the same, but the cores are right-handed and the shells are left-handed. For the background medium: $\epsilon_e = \epsilon_0$ and $\mu_e = \mu_0$.

It is a quite simple task to write a short Matlab-code and use (4) and (7), to calculate the effective material properties of the given mixture. In Figure 2 is shown the effective relative permittivity and chirality of the mixture. The volume fraction f is defined as $f = nV$, where n is the number density of the inclusions in the mixture and V is the total volume of an inclusion.

Figure 2 shows that although both components of the spheres have the same electric permittivity, the mixture permittivity ϵ_{eff} is not the same in the case $f = 1$ (no background, everything just inclusions). The strange effect on permittivity is caused by the magnetoelectric coupling.

References

[1] A. Sihvola, *Electromagnetic Mixing Formulas and Applications* (Electromagnetic Waves Series, Vol. 47, pp. 284). London: The Institution of Electrical Engineers, 1999.

[2] I. V. Lindell, A. H. Sihvola, and K. Suchy, "Six-vector formalism in electromagnetics of bi-anisotropic media," *J. Electromag. Waves Appl.*, Vol. 9, No. 7/8, pp. 887-903, 1995.

[3] A. H. Sihvola and I. V. Lindell, "Polarizability and effective permittivity of layered and continuously inhomogeneous dielectric ellipsoids," *J. Electromag. Waves Appl.*, Vol. 4, No. 1, pp. 1-26, 1990.

[4] M. E. Ermutlu and A. Sihvola, "Polarizability matrix of layered chiral sphere," in *Progress in Electromagnetics Research*, PIER 9, 1994, pp. 87–101.

[5] W. Ren, "Bi-isotropic layered mixtures," in *Progress in Electromagnetics Research*, PIER 9, 1994, pp. 103–116.

Electromagnetic Wave Propagation in Circular Waveguide Containing Chiral Rod

J. Popik and J. Mazur

Telecommunications Research Institute, Gdańsk Division
al. Gen. J.Hallera, 80–401 Gdańsk, Poland
Fax: + 48–(0)58–341 80 07; emails: jpopik@pit.gda.pl, jem@pg.gda.pl

Abstract

Here we study the scattering properties of the section of circular waveguide containing lossy isotropic chiral rod. The effects of the chirality on the polarisation state (electromagnetic field rotation and axial ratio) of fundamental mode propagate in the guide are discussed and verified experimentally.

1. Introduction

The effects of the chirality on the polarization state of the waves propagating in the circular guides filled with chiral medium have been intensively studied in the last few years [1] ÷ [6]. Such an effect allows the determination of the chiral material parameters and can be utilized in a number of novel applications. The theoretical and experimental investigation of the scattering properties of the chiral guide section allows the development of inversion method to determine the constitutive chiral material parameters [3, 4, 5]. In this paper we investigate analytically the problem of the circular waveguide containing a lossy chiral rod. The relevant research includes the complete description of the modal spectrum. Furthermore the scattering matrix of the chiral section is derived using the mode matching approach. The analysed junction consists of the chiral section and two transitions connecting this section with empty circular waveguides. In our experiments we use the chiral rod for which the constitutive parameters are closed to reported in [3]. The scattering characteristics were investigated and subsequently applied to calculate the polarisation state parameters of the fundamental waves transmitted through the chiral section. In the proof of principle experiment the performance of a chiral structure was measured and good agreement with theory was obtained.

2. Theory

The cross section of the chiral circular guide here analysed is shown in Figure 1*a*. The structure consists of the helix loaded chiral rod of length 20 mm and radius 5 mm, which is introduced into teflon sleeve entirely filling the cylindrical guide of the radius 10 mm. The chiral rods were fabricated in Sowerby Research Centre British Aerospace, England by dispersing stainless steel helices in an epoxy resin matrix. The helices have three turns of 1mm outside diameter, and a pith of 0.5 mm. The wire gauge is 0.15 mm. The rod contains 70 helices in total giving the metallic fraction of 0.6 %. In our experiments we use the values of the chiral material parameters as permeability, permittivity and chirality shown in Figure 2. It is closed to presented in [3] where they are extracted for similar chiral medium.

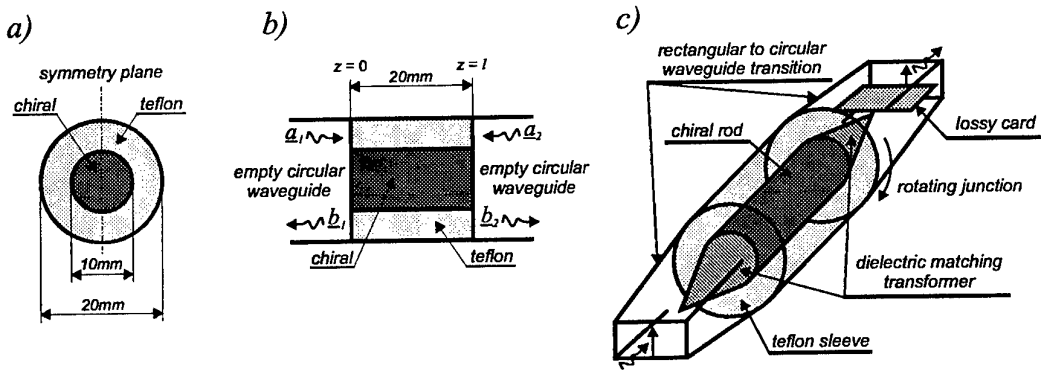

Figure 1: Cylindrical guide containing lossy chiral rod: *a)* cross–section; *b)* investigated structure; *c)* experimental setup

The transfer matrix procedure proposed in [6] for general solution of the circular waveguide containing chiroferrite rods has been applied to derive rigorous dispersion relation for the considered guide. The dispersion characteristics of the two fundamental left (LCP)and right (RCP) circularly polarised modes appearing in the guide are shown in the Figure 3. The differences observed between the modes propagation coefficients indicate that chiral material responds differentially to left and right handed circularly polarised waves. It means that the polarisation state of the wave propagated along the chiral guide is changes.

To determine the scattering matrix of a lossy chiral rod inside a circular waveguide the structure is subdivided as shown in Figure 1*b* into two transitions from the empty to the chiral

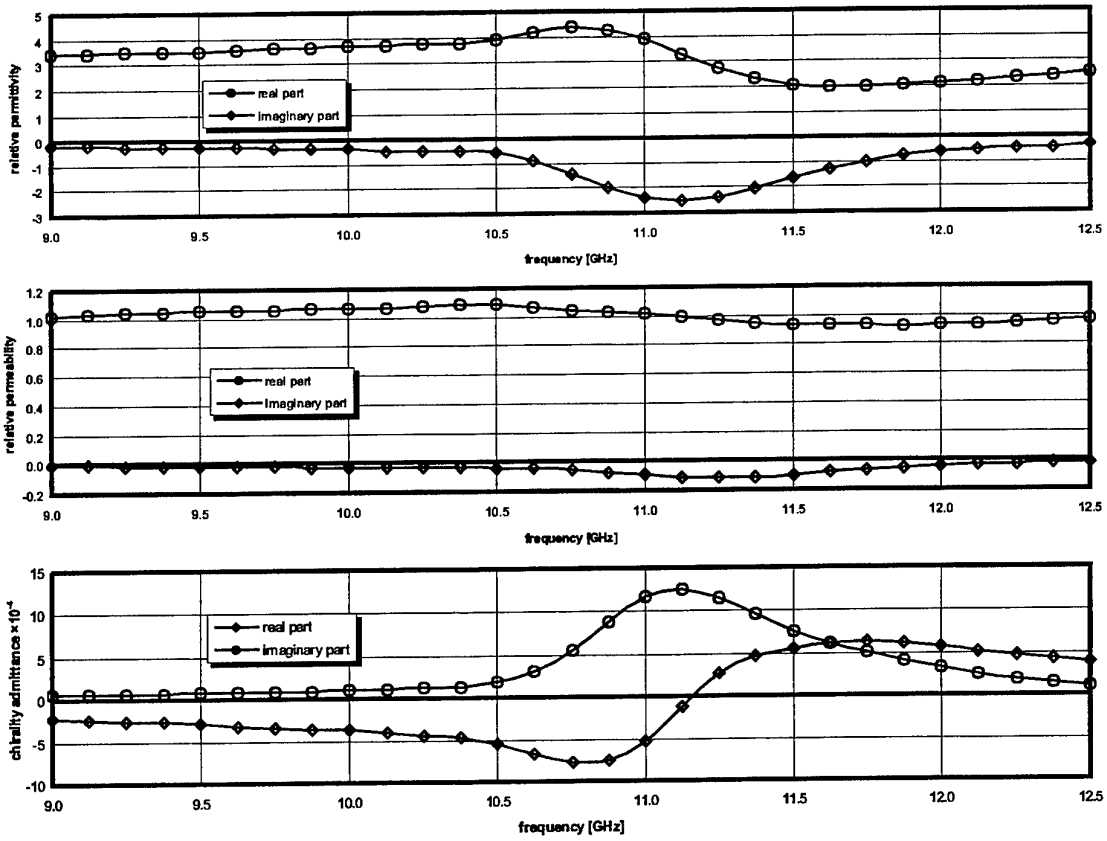

Figure 2: Constitutive parameters of the chiral material (data follows from [3])

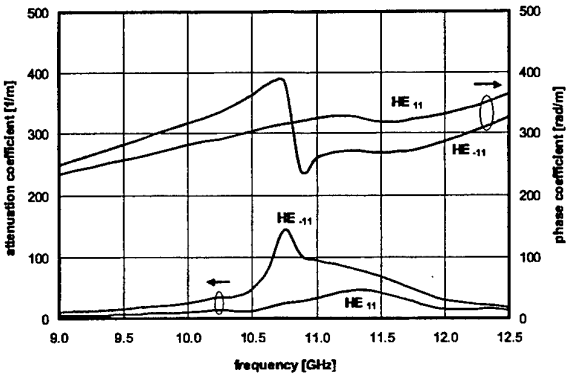

Figure 3: Dispersion characteristics of the fundamental modes in considered circular guide

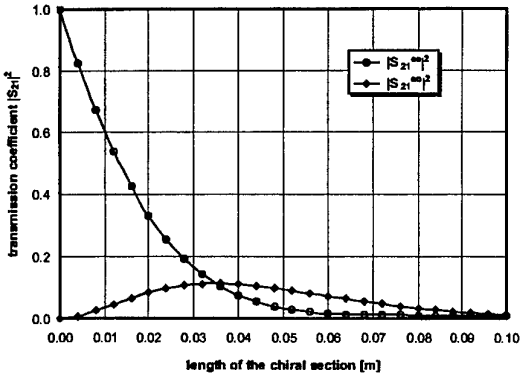

Figure 4: Transmission coefficients versus length of the chiral section

section at $z = 0$ and $z = l$ and the connecting chiral guide. In the current problem we assume that only two circularly polarised modes can propagate in the chiral section and the empty waveguides can support only two orthogonal TE_{11} modes being co–polar (even) and cross–polar (odd) with respect to the chosen symmetry plane of the guide cross–section. Imposing the boundary conditions for the tangential electric and magnetic fields at interfaces $z = 0$ and $z = l$ and orthogonalizing the fields with respect to the modes of the lossless empty waveguide, leads to the set of eight linear algebraic equations from which the scattering matrix is obtained as:

$$\begin{bmatrix} b_1^e \\ b_1^o \\ b_2^e \\ b_2^o \end{bmatrix} = \begin{bmatrix} S_{11}^{ee} & S_{11}^{oe} & S_{12}^{ee} & S_{12}^{oe} \\ S_{11}^{eo} & S_{11}^{oo} & S_{12}^{eo} & S_{12}^{oo} \\ S_{21}^{ee} & S_{21}^{oe} & S_{22}^{ee} & S_{22}^{oe} \\ S_{21}^{eo} & S_{21}^{oo} & S_{22}^{eo} & S_{22}^{oo} \end{bmatrix} \begin{bmatrix} a_1^e \\ a_1^o \\ a_2^e \\ a_2^o \end{bmatrix} \tag{1}$$

Here the superscripts and the subscripts refer to the empty waveguide co–polar (e) and cross–polar (o) modes and port respectively. One should note from Figure 4 that in dependence of the chiral section length the variation of the transmission coefficients S_{21}^{ee} and S_{21}^{eo} is observed. It means that the input of dominant co–polar TE_{11} mode at port (1) causes the output at the port (2) both fundamental co– and cross–polar modes. This coupling effect is possible because the rotation phenomenon occurs in the chiral waveguide section. Moreover the equal values of $S_{21}^{ee(oo)}$ and $S_{12}^{ee(oo)}$ indicate the reciprocal behaviour of the considered structure. The knowledge of the S_{21}^{ee} and S_{21}^{eo} elements allows to determine the polarization state parameters of the wave transmitted across the chiral section. From Stokes equations defined as [2, 7]:

$$\begin{aligned} S_0 &= S_{21}^{ee} S_{21}^{ee*} + S_{21}^{eo} S_{21}^{eo*} \;;\; S_2 = -2\,Re\left(S_{21}^{ee} S_{21}^{eo*}\right) \\ S_1 &= S_{21}^{ee} S_{21}^{ee*} - S_{21}^{eo} S_{21}^{eo*} \;;\; S_3 = 2\,Im\left(S_{21}^{ee} S_{21}^{eo*}\right) \end{aligned} \tag{2}$$

the rotation angle is:

$$\theta = \frac{1}{2} arctan\left(\frac{S_2}{S_1}\right) \tag{3}$$

and the axial ratio is written as:

$$AR = tan\left[\frac{1}{2} arcsin\left(\frac{S_3}{S_0}\right)\right] \tag{4}$$

3. Numerical and Experimental Results

Figure 1*c* shows the experimental setup used for measurement of polarization state parameters of the wave propagated along the considered chiral guide. The section of chiral circular guide is

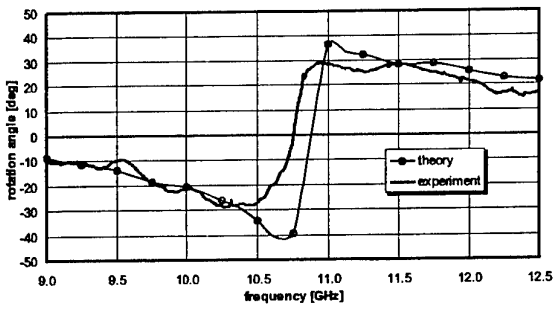

Figure 5: Characteristics of the rotation angle

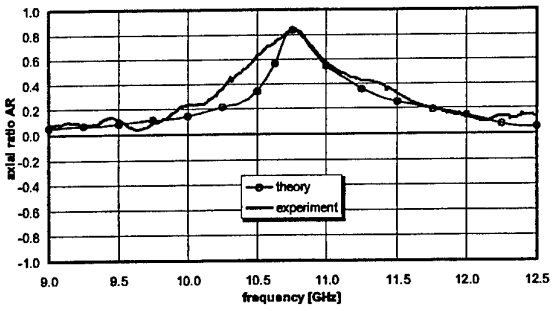

Figure 6: Characteristics of the axial ratio

placed between two circular to rectangular waveguide transitions with tapered dielectric transformers matching the chiral rod. For characterization of the polarization state parameters of the wave transmitted across the chiral sample the measurement of co– and cross–polar transmission coefficients are required. The co–polar transmission coefficient is derived when the input and output rectangular waveguides are parallel. The cross–polar coefficient is measured when output waveguide is rotated 90° relative to the input waveguide. The setup (Hewlett–Packard) was calibrated using the TRL calibration in the co–polarization configuration.

Figure 5 shows the theoretical and experimental frequency dependent characteristics of the angle of rotation for the considered chiral guide of the length 20 mm. The change of the sign of rotation angle above the resonance frequency is observed. The resonance occurs near the frequency 10.75 GHz. This frequency is in agreement to the half–wavelength resonance frequency 10.8 GHz of the current in the helix wire. As shown in Figure 6, where axial ratio characteristics are presented, near the resonance frequency the axial ratio approaches the value of 0.8. Here, the wave at the output of the chiral section is nearly circularly polarised.

4. Conclusion

The experimental results agree well with the theoretical prediction for both examined polarization state parameters. It means that the proposed solution sufficiently describes the scattering properties of the considered chiral waveguide.

References

[1] R. D.Hollinger, V. V.Varadan, and V. K.Varadan: "Eigenmodes in a Circular Waveguide Containing an Isotropic Chiral Material", *Radio Science*, vol. 26, no. 5, pp. 1335–1344, September-October 1991.

[2] R. D. Hollinger *et al.*: "Experimental Characterization of Isotropic Chiral Composites in Circular Waveguides", *Radio Science*, vol. 27, no. 2, pp. 161–168, March-April 1992.

[3] C. R. Brewitt-Taylor *et al.*: "Comparison of Theory and Measurements of the Properties of Helix-Loaded Chiral Composites", in *Proceedings of Bianisotropic '97 – Int. Conf. and Workshop Electromagnetics of Complex Media*, Glasgow, Scotland, pp. 55–58, June 1997.

[4] J. Reinert, G. Busse, and A. F. Jacob: "Waveguide Characterization of Chiral Material: Theory", *IEEE Trans. Microwave Theory Tech.*, vol. 47, no. 3, pp. 290–296, March 1999.

[5] J. Reinert, G. Busse, and A. F. Jacob: "Waveguide Characterization of Chiral Material: Experiments", *IEEE Trans. Microwave Theory Tech.*, vol. 47, no. 3, pp. 297–301, March 1999.

[6] J. Popik, J. Mazur, and S. Haq: "Characterization of Circular Waveguide Containing Chiral Rod", in *Proceedings of Microwave Conference MIKON '98*, Kraków, Poland, pp. 318–323, May 1998.

[7] S. Bassiri, C. H. Papas, and N. Engheta: "Electromagnetic Wave Propagation Through a Dielectric-Chiral Interface and Through a Chiral Slab", *J. Optical Soc. Amer.*, vol. 5, no. 9, pp. 1450–1458 September 1988.

Electromagnetic Wave Scattering by Fractal Surface

A. O. Pinchuk and V. Gozhenko

Institute of Surface Chemistry
National Academy of Science of Ukraine
Kyiv, Nauki av., 31, Ukraine, 03022
Fax: (380) 44 264 04 46, e-mail: onmf@serv.biph.kiev.ua

Abstract

We have considered some peculiarities of light reflection by several types of fractal surfaces. The two-dimensional Weierstrass function for modeling of fractal surfaces was used. The computer simulation of real rough surfaces was performed by means of this function. The electromagnetic waves scattering indicatrix was obtained for the concrete fractal surfaces based on the scalar Kirchhoff theory. The computer simulation of light reflection by fractal surfaces was performed.

1. Introduction

All the surfaces are rough in some way or another. Therefore the studying of the scattering of electromagnetic waves by rough surfaces is an important and interesting theoretical and experimental task. The investigation of the peculiarities of such scattering is an important first of all for a non-destructive control of real surfaces. Real surfaces are most adequately described by fractal functions as they are neither pure deterministic nor pure casual. Last time the fractal nature of a number of different surfaces have been experimentally determined (sea surface and sea bottom, Earth relief, cloud surfaces, thin film surfaces, deposited on the substrate, etc.).

The aim of this work was the simulation of the electromagnetic waves scattering indicatrix based on the scalar Kirchhoff theory for particular surfaces. The analogues calculations were performed by others authors [2], but our results have some distinctive features, particularly in the expression for the averaged scattering coefficient there are some additional terms which can significantly influence on the resulting scattering indicatrix at a certain geometry of the experiment.

2. Theory

We have chosen the two-dimensional Weierstrass function $z(x,y)$ for the simulation of rough surfaces

$$z(x,y)=c_w\sum_{n=0}^{N-1}\sum_{m=1}^{M}q^{(D-3)n}\sin\left\{Kq^n\left[x\cos\frac{2\pi m}{M}+y\sin\frac{2\pi m}{m}\right]+\phi_{nm}\right\}, \qquad (1)$$

were c_w is a normalizing factor; $q>1$ is the fundamental spatial frequency; K is the fundamental wavenumber of the surface; D is the fractal dimension ($2<D<3$); N,M are numbers of tones; ϕ_{nm}

is a phase term. The example of a rough surface simulated using the function (1) is shown on Fig. 1(a).

Let us consider the wave falling on the rough surface S at an angle Θ_1 and scattering at a polar angle Θ_2 and at an azimuth angle Θ_3. We will be finding the scattered field $E_s(\vec{r},t)$ based on the scalar Kirchhoff method [4]:

$$E_s(\vec{r}) = -ikrF(\Theta_1,\Theta_2\Theta_3)\frac{\exp(ikr)}{2\pi r}\int_{S_0}\exp[ik\phi(x_0,y_0)]dx_0dy_0 + E_e(\vec{r}), \tag{2}$$

where k is the wavenumber of the incident wave,

$$F(\Theta_1,\Theta_2,\Theta_3) = -\frac{R}{2C}(A^2+B^2+C^2)$$

is the angle factor, R is the reflection coefficient,

$$A = \sin\Theta_1 - \sin\Theta_2\cos\Theta_3,$$

$$B = -\sin\Theta_2\sin\Theta_3,$$

$$C = -\cos\Theta_1 - \cos\Theta_2,$$

$$\phi(x_0,y_0) = Ax_0 + By_0 + Ch(x_0,y_0)$$

is the phase function,

$$h(x_0,y_0) = z(x_0,y_0),$$

$$E_e(\vec{r}) = -\frac{R}{C}\cdot\frac{\exp(ikr)}{4\pi r}(AI_1 + BI_2)$$

is the bound term,

$$I_1 = \int_{-Y}^{Y}\left[e^{ik\phi(X,y_0)} - e^{ik\phi(-X,y_0)}\right]dy_0,$$
$$I_2 = \int_{-X}^{X}\left[e^{ik\phi(x_0,Y)} - e^{ik\phi(x_0,-Y)}\right]dx_0. \tag{3}$$

The above formalism is valid under the following conditions[4]: the incident wave is monochromatic and plane; the scattering surface is rough inside a certain square and smooth outside its; the surface dimensions are much large than the incident wavelength; all the surface points have finite gradient; the reflection coefficient is a constant across the surface area; the scattered field is observed far from the surface.

After some transformations from Eq.(2) considering Eq.(1) we obtain the expression for the average scattering coefficient

$$\langle\rho_s\rangle \equiv \frac{\langle I_s\rangle}{I_0} \tag{4}$$

where $\langle I_s \rangle = \langle \vec{E}_s \vec{E}_s^* \rangle$, $I_0 = \left(\frac{2kXY \cos\Theta_1}{\pi r} \right)^2$ is the intensity of a wave reflected from the respective smooth surface. Neglecting the terms higher than $\xi_u^2 (\xi_u \equiv kc_w Cq^{(D-3)u})$, this expression has the following approximate form

$$\langle \rho_s \rangle \approx \left[\frac{F(\Theta_1, \Theta_2, \Theta_3)}{\cos\Theta_1} \right]^2 \{ \left[1 - (k\sigma C)^2 \right] \mathrm{sinc}^2(kAX) \mathrm{sinc}^2(kBY) +$$

$$+ \frac{1}{2} c_f^2 \sum_{nm} q^{2(D-3)n} \mathrm{sinc}^2 \left[\left(kA + Kq^n \cos\frac{2\pi m}{M} \right) X \right] \mathrm{sinc}^2 \left[\left(kB + Kq^n \sin\frac{2\pi m}{M} \right) Y \right] \} +$$

$$+ \left[\frac{R}{2C\cos\Theta_1} \left(A^2 + B^2 \right) \right]^2 \mathrm{sinc}^2(kAX) \mathrm{sinc}^2(kBY), \qquad (5)$$

where, σ is the root mean square height of the surface roughness, X and Y are the dimensions reflecting area

$$c_f \equiv kc_w C = k\sigma C \left[\frac{2}{M} \cdot \frac{1 - q^{2(D-3)}}{1 - q^{2N(D-3)}} \right]^{\frac{1}{2}},$$

$$\mathrm{sinc}\, x \equiv \frac{\sin x}{x}; \quad \sum_{nm} \equiv \sum_{n=1}^{N-1} \sum_{m=0}^{M} .$$

3. Numerical results

We have calculated the averege reflected coefficient $\langle \rho_s \rangle$ as a function of Θ_2 and Θ_3 (the scattering indicatrix) based on Eq. (5). We have assumed that $R = 1$, in other words we have not considered the real dependence of the reflectance R on the wavelength λ and on the incident angle Θ_1. The example of the scattering indicatrix is shown on Fig. 1 (b).

4. Conclusion

The analysis of the obtained results leads to some inferences:

- The waves scattering is symmetrical relatively the plane of incidence;
- The most intensity of the scattered waves is observed in the specular direction;
- There are others directions, where some splashes of intensity are observed;
- The picture of the reflection complicates with increasing of the surface large scale homogeneity.

These peculiarities are due to combination of chaotic character and self-similarity of the real surface relief.

Acknowledgement

The authors have benefited from useful and stimulating discussions with Dr. L. G. Grechko.

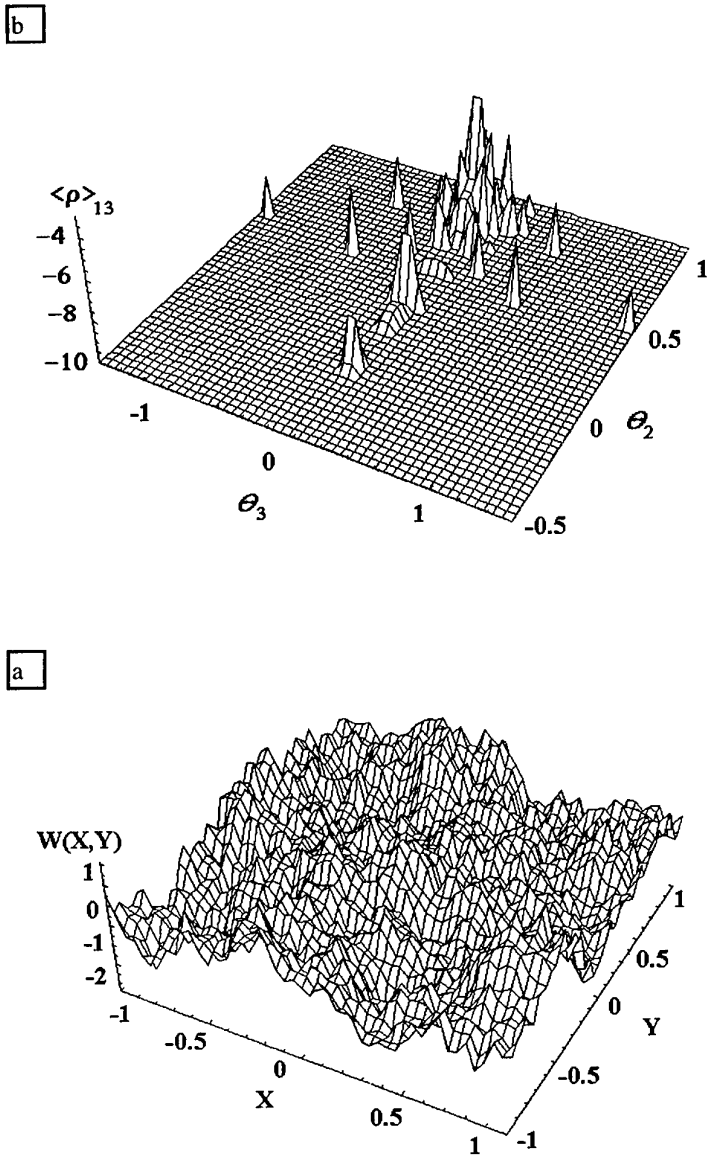

Fig. 1 **a)** The simulation of the fractal surface by means of Weierstrass function $K = 6.3$, $N = M = 5$, $D = 2.5$; **b)** The reflection coefficient $\log\langle \rho_s \rangle$ for the fractal surface with $D = 2.5$, $q = 1.8$; $N = M = 10$.

References

[1] M. V. Berry and Z. V. Lewis, *Proc. R. Soc. London A*, vol. 370, p. 459, 1980.
[2] N. Lin *et al.*, *J. Mod. Opt.*, vol. 42, No. 1, p. 225, 1995.
[3] D. L. Jaggard and Y. Kim, *J. Opt. Soc. Am. A*, vol. 4, p. 1055, 1987.
[4] J. A. Ogilvy, *Theory of Wave Scattering from Random Rough Surfaces*. New York: Adam Hilger, 1991.

Inhomogeneous Bianisotropic Materials for Antenna and Circuit Applications in Microwave and Millimetre Wave Ranges

A. Toscano, L. Vegni, and F. Bilotti

Department of Electronic Engineering, University of "Roma Tre"
Via della Vasca Navale 84, 00146 Rome, Italy
Tel. +39.06.55177003, Fax +39.06.5579078
E-mail: toscano@ieee.org, vegni@uniroma3.it, bilotti@uniroma3.it

Abstract

In this contribution we propose the use of general bianisotropic inhomogeneous materials for both radiating (i.e. microstrip antennas) and transmissive (i.e waveguides, transmission lines, filters, etc.) components in the microwave and millimetre wave frequency ranges. The analysis of such components is essentially developed via a rigorous full-wave approach in the spectral or in the spatial domain depending on the complexity of the boundary value problem to be solved and on the numerical technique to be used. For the transmissive components a fundamental mode approximate analysis is also employed in order to obtain very fast design formulas.

1. Introduction

Nowadays, materials with a continuous spatial variation of the refraction index can be easily synthesized in the optical field for graded index optical fibers and planar waveguides. Also in the solide – state applications we can control the carrier concentrations on the atomic scale, allowing, thus, the synthesis of components with an essentially continuous conductivity profile. Since in the microwave and millimetre wave frequency ranges the technological processes used in the optical and solid – state applications cannot be effective, the synthesis of such materials could be realized only by means of artificial dielectrics.

Artificial dielectrics with electromagnetic properties varying with the spatial coordinates can be synthesized via non-uniform metallic inclusions in a host material. In addition, by using, for instance, omega metallisations, we can think to introduce an anisotropic behaviour together with a magneto–electric effect. In such a way, thus, we can obtain a general inhomogeneous bianisotropic material.

The use of the inhomogeneous materials has been recently considered in some works [1-9] and, as shown, leads to some improvements both in circuit and in antennas applications. The dielectric inhomogeneity, for instance, can be used to control the filtering and matching properties of a transmission line [1-4] or the radiation properties of microstrip antennas (directivity, efficiency and bandwidth) [5-9].

The analysis of such components has been developed by means of the rigorous full-wave approach both in the spectral domain associated to the Method of Moments (MoM) and in the spatial domain associated to a variational formulation and a Finite Element Boundary Integral (FE-BI) numerical procedure. Moreover, in certain cases, especially when the propagation characteristics of a component are investigated an approximate approach based on the TEM or quasi-TEM propagation can be used together with the non-uniform transmission line theory.

The aim of this contribution is to extend the previous works [1-9] to the case of inhomogeneous bianisotropic materials leading to a closed form representation of the Green's dyads in the spectral domain and to a new variational formulation in the spatial domain.

2. Theory

The constitutive relations for an inhomogeneous bianisotropic material are:

$$\begin{cases} \mathbf{D} = \underline{\varepsilon}(\mathbf{r}) \bullet \mathbf{E} + \underline{\xi}(\mathbf{r}) \bullet \mathbf{H} \\ \mathbf{B} = \underline{\zeta}(\mathbf{r}) \bullet \mathbf{E} + \underline{\mu}(\mathbf{r}) \bullet \mathbf{H} \end{cases} \tag{1}$$

Assuming a harmonic time dependence exp[jωt] the Maxwell equations in a source free region can be written as:

$$\begin{cases} \nabla \times \mathbf{E} = -j\omega \underline{\zeta}(\mathbf{r}) \bullet \mathbf{E} - j\omega \underline{\mu}(\mathbf{r}) \bullet \mathbf{H} \\ \nabla \times \mathbf{H} = j\omega \underline{\varepsilon}(\mathbf{r}) \bullet \mathbf{E} + j\omega \underline{\xi}(\mathbf{r}) \bullet \mathbf{H} \\ \nabla \bullet \left[\underline{\varepsilon}(\mathbf{r}) \bullet \mathbf{E} + \underline{\xi}(\mathbf{r}) \bullet \mathbf{H} \right] = 0 \\ \nabla \bullet \left[\underline{\zeta}(\mathbf{r}) \bullet \mathbf{E} + \underline{\mu}(\mathbf{r}) \bullet \mathbf{H} \right] = 0 \end{cases} \tag{2}$$

Since the analysis of radiating and transmissive components is developed in different ways we will present it in two separate sub-sessions.

2.1 Radiating components

Here we consider planar integrated antennas of the kind depicted in Fig.1.

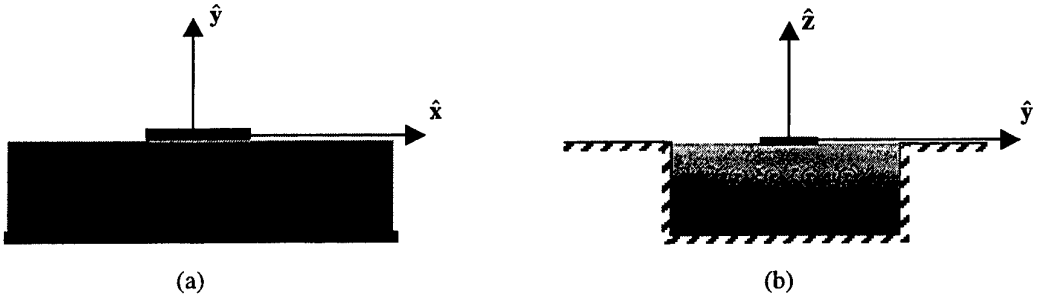

Fig. 1 Microstrip patch antenna configuration: Open planar integrated patch antenna (a); Cavity backed patch antenna (b).

The electromagnetic formulation of the antenna in Fig.1a is based on the full-wave analysis in the spectral domain and the numerical solution of the associated boundary-value problem is obtained via the method of moments (MoM). The fundamental step in this approach is the derivation of the spectral Green's dyad for the planar structure. In this case we consider the variation of the electromagnetic parameters only along the stratification direction and, starting from the curl Maxwell equations, we obtain, after a change of the reference system [6], the following relations in the spectral domain:

$$\begin{cases} \dfrac{d\mathbf{V}(y)}{dy} = \underline{C}_{VV}(y) \bullet \mathbf{V}(y) + \underline{C}_{VI}(y) \bullet \mathbf{I}(y) \\ \dfrac{d\mathbf{I}(y)}{dy} = \underline{C}_{IV}(y) \bullet \mathbf{V}(y) + \underline{C}_{II}(y) \bullet \mathbf{I}(y) \end{cases} \tag{3}$$

where $\mathbf{V} = \left[\tilde{E}_v, \tilde{E}_u\right]^T$, $\mathbf{I} = \left[\tilde{H}_u, \tilde{H}_v\right]^T$ and the elements of the matrices $\underline{C}_{VV}(y), \underline{C}_{VI}(y), \underline{C}_{IV}(y), \underline{C}_{II}(y)$ are complicate ratios involving the electromagnetic parameters. In order to decouple system (3) we impose $\underline{C}_{VV}(y) = 0$ and $\underline{C}_{II}(y) = 0$ obtaining, thus, after three derivative operations, the following fourth order decoupled differential equations:

$$\begin{cases} \dfrac{d^4\tilde{E}_v}{dy^4} + A_{v3}(y)\dfrac{d^3\tilde{E}_v}{dy^3} + A_{v2}(y)\dfrac{d^2\tilde{E}_v}{dy^2} + A_{v1}(y)\dfrac{d\tilde{E}_v}{dy} + A_{v0}(y)\tilde{E}_v = 0 \\ \dfrac{d^4\tilde{E}_u}{dy^4} + A_{u3}(y)\dfrac{d^3\tilde{E}_u}{dy^3} + A_{u2}(y)\dfrac{d^2\tilde{E}_u}{dy^2} + A_{u1}(y)\dfrac{d\tilde{E}_u}{dy} + A_{u0}(y)\tilde{E}_u = 0 \end{cases}$$

where the non constant coefficient $A_u(y)$ and $A_v(y)$ depend on the elements of the matrices $\underline{C}_{ij}(y)$. Once the solutions of such equations are found, the overall spectral electromagnetic field is also known in the grounded inhomogeneous slab and the Green's dyad can be easily determined.
The application of the MoM in order to calculate the unknown current density on the patch, is now a straightforward matter [7-8].

On the other hand the electromagnetic formulation for the antenna in Fig.1b is based on a variational approach together with the implementation of the Finite Element Boundary Integral (FE-BI) numerical method. The functional F(**E**) that has to be stationary for arbitrary variations of the **E** field is given by:

$$\begin{aligned} F(\mathbf{E}) = &< \underline{\mu}(\mathbf{r})^{a^{-1}} \bullet \left(\nabla \times \mathbf{E}^a + j\omega \underline{\xi}(\mathbf{r}) \bullet \mathbf{E}^a\right), \nabla \times \mathbf{E} + j\omega \underline{\zeta}(\mathbf{r}) \bullet \mathbf{E} > + \omega^2 < \mathbf{E}^a, \underline{\varepsilon}(\mathbf{r}) \bullet \mathbf{E} > - \\ &- < \mathbf{E}^a, j\omega \mathbf{J} > - < j\omega \mathbf{J}^a, \mathbf{E} > + 2\omega \frac{k_0}{\eta_0} \int_{S_{ap}} \left(\hat{\mathbf{n}} \times \mathbf{E}^a\right)^* \bullet \left[\int_{S_{ap}} \underline{\mathbf{G}}(\mathbf{r}, \mathbf{r}') \bullet \left[\hat{\mathbf{z}} \times \mathbf{E}(\mathbf{r}')\right] dS'\right] dS \end{aligned} \tag{3}$$

For the meaning of the apex a, of the vector **J**, of the surface S_{ap}, please, refer to [5].

After discretizing the cavity into finite elements of proper shapes (in this case bricks are used), and after expanding the electric field by using the edge-based vector basis functions as in [5] we obtain an algebraic system to be solved of the form $\underline{\mathbf{A}} \bullet \mathbf{X} = \mathbf{B}$. The solution of such a linear system returns the electromagnetic field in the cavity and on the aperture surface and, thus, the derivation of the antenna characteristics is, now, a straightforward matter.

2.2 Transmissive components

Here we consider both planar and not planar waveguides as shown in Fig.2. These waveguides have been studied by means of different approaches. When the variation of the electromagnetic parameters is only along the stratification axis striplines and microstriplines have been analyzed in the spectral domain by using the same approach previously shown simply introducing the z dependence $\exp[-jk_z z]$ in the Maxwell equations. The integral equation written on the strip can be solved again via the MoM leading to an eigenvalue algebraic system whose solution returns the propagation characteristics of the waveguides. Striplines, microstriplines and rectangular waveguides with arbitrary variations of the parameters only on the cross sections have been analyzed by means of the full-wave approach in the spatial domain together with the Method of Lines (MoL) numerical procedure [10]. Finally, when the

parameter variation is only along the power flow direction, for the striplines and microstriplines the approximation of a TEM or quasi-TEM propagation has been used and the solution has been obtained by means of the non uniform transmission line theory as in [1-4].

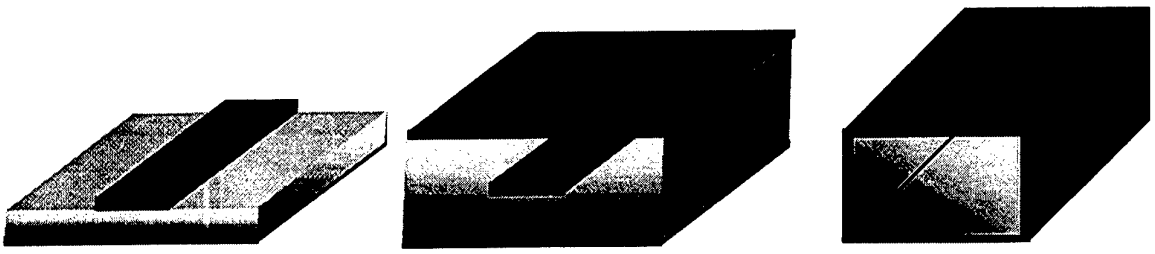

(a) (b) (c)

Fig. 2 Three different kinds of waveguides here considered: Microstripline (a); Stripline (b); Rectangular Waveguide (c).

3. Conclusion

In this contribution we have proposed the use of general bianisotropic inhomogeneous materials for both radiating and transmissive components in the microwave and millimetre wave frequency ranges. The analysis of such components has been essentially developed via a rigorous full-wave approach in the spectral or in the spatial domain together with different numerical techniques (MoM, FE-BI, MoL, etc.). Particularly, a new variational formulation for cavity backed microstrip patch antennas loaded with general inhomogeneous bianisotropic dielectrics and new analytical expressions of the spectral dyadic Green's functions for grounded slab loaded with the same materials have been derived as extensions of works previously published.

References

[1] F. Bilotti, A. Toscano, and L. Vegni, "Very fast design formulas for microwave non-homogeneous media filters," *Microwave Opt. Tech. Lett.*, pp. 218-221, Vol. 22, No. 3, Aug. 1999.

[2] L. Vegni, A. Toscano, and F. Bilotti, "Tapered stripline embedded in inhomogeneous media as microwave matching line," to appear on *IEEE Trans. Microwave Theory Tech.*

[3] F. Bilotti, L. Vegni, and A. Toscano, "A new stripline microwave high pass filter layout," *J. Electromag. Waves Applicat.*, pp. 423-439, Vol. 14, 2000.

[4] A. Toscano, L. Vegni, and F. Bilotti, "Generalized reflection coefficient for nonuniform transmission lines," *J. Electromag. Waves Applicat.*, pp. 945-959, Vol. 14, 2000.

[5] A. Toscano, L. Vegni, and F. Bilotti, "Scattering properties of antennas residing in cavities filled by inhomogeneous materials via a variational formulation," *J. Modern Opt.*, Vol. 46, No. 14, pp. 1995-2005, Nov. 1999.

[6] A. Toscano and L. Vegni, "Very general full-wave analysis of planar stratified media with inhomogeneous layers", *IEEE Trans. Antennas Propagat.*, Vol. 48, No. 4 pp. 631-632, Apr. 2000.

[7] L. Vegni, F. Bilotti, and A. Toscano, "Scattering properties of patch antennas loaded with inhomogeneous substrates via a combined spectral domain-moment method," to appear on *J. Modern Opt.*

[8] L. Vegni, F. Bilotti, and A. Toscano, "Microstrip disk antennas with inhomogeneous artificial dielectrics," *J. Electromag. Waves Applicat.*, pp. 1203-1227, Vol. 14, 2000.

[9] L. Vegni, A. Toscano, and F. Bilotti, "Mutual coupling between two circular patch antennas integrated in an inhomogeneous grounded slab," *Microwave Opt. Tech. Lett.*, pp. 294-297, Vol. 25, No. 5, Jun. 5, 2000.

[10] R. Pregla and W. Pascher, "The method of lines," in *Numerical Techniques for Microwave and Millimeter – Wave Passive Structures*, T. Itoh (Ed.). New York: Wiley, pp. 381-446, 1991.

Fabrication Effects on the Resonance Bandwidth of Chiral Materials

J. Psilopoulos, J. Reinert, and A.F. Jacob

Institut für Hochfrequenztechnik, Technische Universität Braunschweig,
Schleinitzstr. 22, 38106 Braunschweig, Germany
Tel: +49 531 391 2012, Fax: +49 531 391 2045, e-mail: j.psilopoulos@tu-bs.de

Abstract

A comparison between measured and simulated characteristics of helix loaded media reveals a good agreement for the resonance frequency but significant differences with respect to the resonance bandwidth. This phenomenon is related to the geometrical variations of the commercially available helices due to tolerances. This is confirmed by two models developed to describe these effects.

1. Introduction

A good prediction of the effective constitutive parameters of artificial chiral materials is of basic importance for the development of applications. Because of the great number of inclusions involved this is, in principle, quite a demanding task. The tools developed so far model a large quantity of helices and/or use appropriate averaging procedures [1, 2]. In these studies, however, helices of a given type are always assumed to be identical. As could be observed in various experiments this allows to predict the resonance frequency but leads to significant discrepancies between the simulated and the measured resonant bandwidth. In the following, the causes of this phenomenon will be discussed and modeled.

2. Measurements and Simulations

The chiral material used in this study consists of commercially available 5-turn metal helices embedded in PU-foam spheres. It was fabricated by means of the foam injection procedure presented in [3]. The helices have a nominal radius $r = 0.92$ mm and pitch $p = 0.37$ mm.

The three complex effective constitutive parameters ε_r, μ_r and κ (according to the Lindell-Sihvola notation [4]) were extracted using the circular waveguide setup described in [5]. With three waveguides of different diameter it was possible to cover the frequency range from 2.75 to 5.70 GHz that includes the chiral resonance at 4.2 GHz. As an example Fig. 1 displays the measured complex permittivity ε_r.

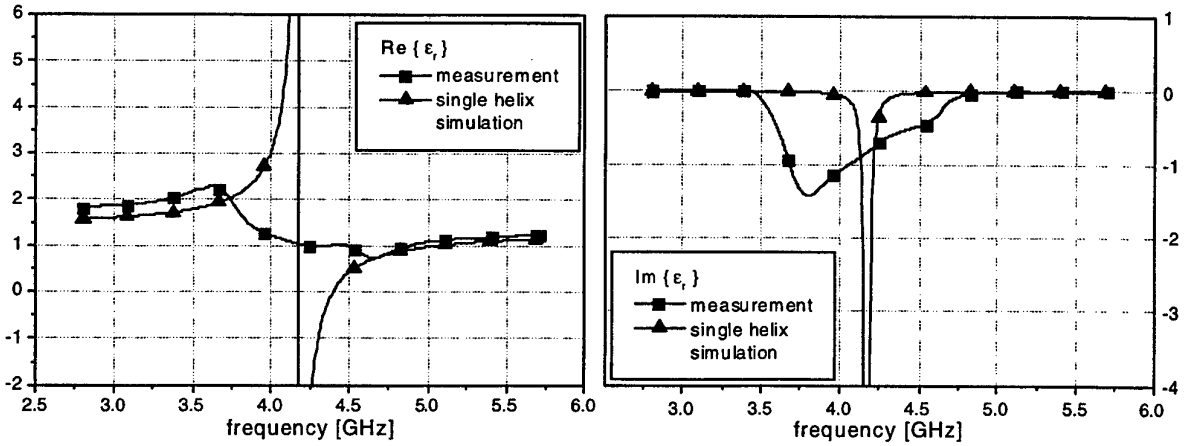

Fig. 1 Measured and simulated permittivity of the chiral material. The simulation assumes identical helices.

In addition, the average polarizabilities of a helix with nominal dimensions were calculated [2]. The constitutive parameters were computed using Maxwell-Garnett mixing rules [4]. As in the experiment the volume fraction of the chiral inclusions was set to 0.45. As can be seen from Fig. 1 predicted and measured resonance frequencies are in good agreement while the resonance width and the magnitude differ significantly.

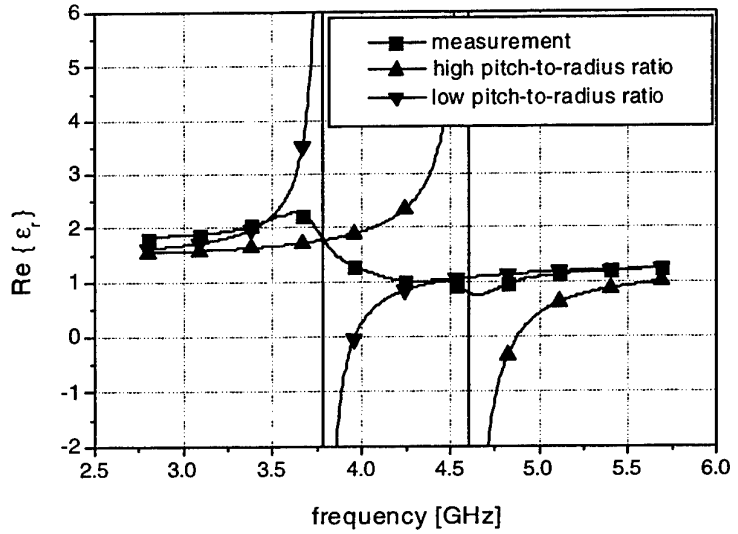

Fig. 2 Measured resonance bandwidth of a chiral material and resonance shift of a single helix due to geometrical tolerances

This phenomenon is possibly caused by the tolerances of the helix dimensions: According to the manufacturer's data sheet the tolerances of helix radius and pitch are approximately ±2.5% and ±10%, respectively. To check this assumption, the material parameters were calculated for different radius and pitch values within these limits. The computed resonance frequencies cover the measured resonance bandwidth. The highest (lowest) resonance frequency corresponds to the largest (smallest) pitch-to-radius ratio (Fig. 2).

To substantiate the above hypothesis further investigations were necessary. A direct experimental check of the material simulation would call for a medium made of identical helices. As this is not available single helices were investigated, instead. To this end individual helices were placed in both a coaxial and a circular waveguide and fixed in a Rohacell™ plug. From the measured scattering parameters S_{11} and S_{21} the quantity $\alpha=|S_{11}|^2+|S_{21}|^2$ was calculated. This is a measure of the energy dissipated in the chiral object. It provides information on the resonance frequency and the resonance bandwidth.

A single helix is only a small disturbance; therefore the measured reflection is generally small while the transmission is close to unity. Further, the scattering parameters are highly sensitive to the helix orientation. Still, the achievable measurement accuracy is satisfactory. For a further discussion, see [6]. Fig. 3 shows, as a representative example, α for a single helix. For comparison, the response obtained with a representative sample of bulk chiral material in the same waveguide is also included. For the latter the absorption bandwidth and the resonance bandwidth of the material parameters (Fig. 1) are in close agreement. The absorption bandwidth of the single helix fits the resonance bandwidth predicted for a material made of geometrically identical helices (Fig. 1). Measurements on different helices show that all resonance frequencies lie within the absorption bandwidth of the bulk material.

The above findings support the hypothesis concerning the tolerances. Still, a model is needed that allows to predict the resonance behavior of the bulk material. This is the scope of the following section which deals with the calculation of the effective constitutive parameters.

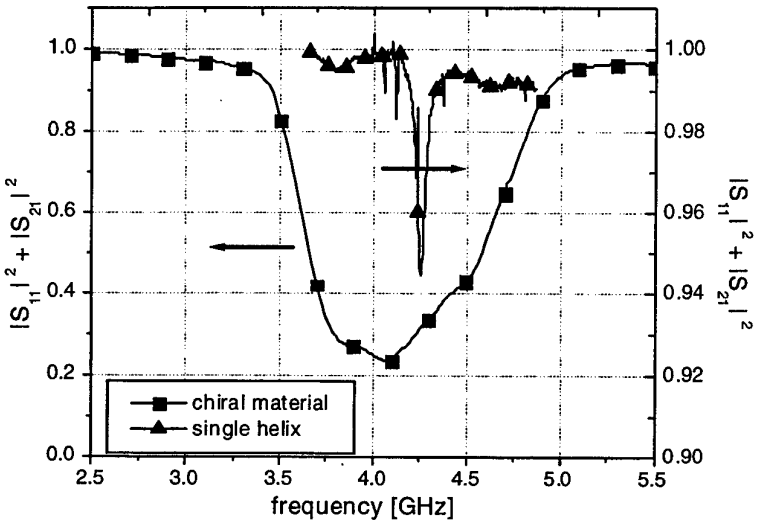

Fig. 3 Coaxial measurements: resonance bandwidth of a single helix and the chiral material

3. Modeling the Effective Chiral Material

As was shown in the previous section a chiral material is a mixture of helices with slightly differing geometry which leads to a noticeable shift of their resonance frequencies. The effective constitutive parameters follow from a superposition of the individual helix properties. Two approaches were developed to predict the material parameters. In the first one, a discrete set of helices with radius and pitch being equally distributed within the tolerance range was assumed. The average polarizabilities of each helix type were computed next. Finally, multi-phase mixing rules were applied to obtain the constitutive parameters [4]. The second method calculates the average polarizabilities for the helix of nominal dimensions, only. The results are then shifted along the frequency axis within the required resonance bandwidth. The latter can be determined either by measurements (provided the chiral material has already been realized) or by two additional calculations using the helices with smallest and largest pitch-to-radius ratio (see above). As long as the broadening of the resonance frequency is not too large both approaches yield almost identical results. Because the second method is much faster and easier to implement it was preferred in the following.

Fig. 4 shows the computed and measured permittivity of the chiral material mentioned above. The resonance frequencies were assumed to be equally distributed. It can be seen that the model predicts well the measured response. The good fit of the resonance bandwidth is of course inherent to the model. But it is interesting to note how well the model renders the dispersion characteristic of the permittivity. Also the quantitative agreement is satisfactory. This holds for all other constitutive parameters as well. Still, some differences can be observed. For instance, the peak modeled at the low frequency end is not confirmed by the measurements. It may be due to several effects. First, the assumption that the resonances are equally distributed is probably unrealistic. A Gaussian distribution together with a finer discretization is likely to give a better fit, here. Second, the electromagnetic model of the chiral inclusion is based on (the usual) simplifications. Third, the mixing formulas are only approximate. And finally, also errors of the measurement procedure have to be taken into account. Indeed, because at resonance the material is quite lossy, only thin slabs could be characterized in the waveguide setup. As, then, the number of helices was too small to yield

statistically meaningful results the material was virtually homogenized and randomized by averaging

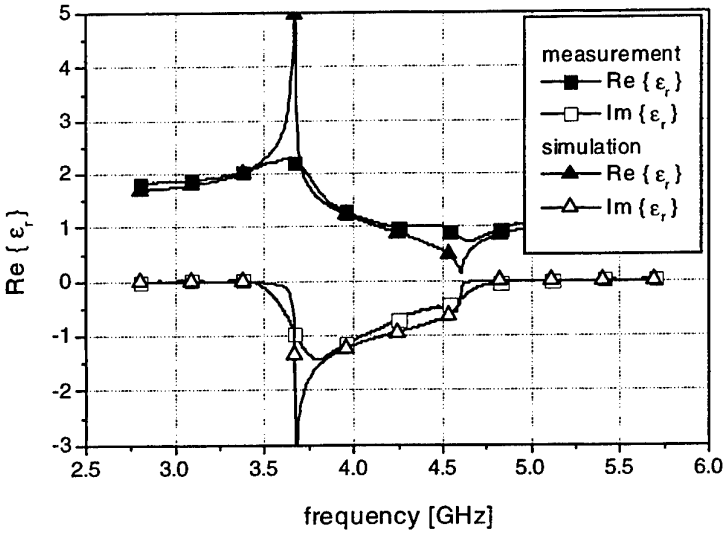

Fig. 4 Measured and simulated effective complex permittivity

the measured responses of several samples with different chiral inclusions, as was suggested in [5].

4. Conclusion

In this contribution fabrication effects on the resonance bandwidth of chiral materials were investigated. The calculated constitutive parameters of a chiral material consisting of helices with nominal pitch and radius were compared to the data extracted from circular waveguide measurements. It was observed that although the resonance frequency can be well predicted significant differences occur regarding the resonance bandwidth. It was shown that this discrepancy is related to tolerance effects of the pitch and the radius of the helices. Two models were developed that allow to accurately predict the constitutive parameters of a realistic chiral material.

References

[1] K. W. Whites, "Full-wave computation of constitutive parameters for lossless composite chiral materials", *IEEE Trans. Antennas Propagat.*, vol. 43, no. 4, pp. 376--384, 1995.

[2] J. Reinert and A. F. Jacob, "Multi-polarizability tensors of thin-wire scatterers: A direct calculation approach," submitted for publication, 2000.

[3] G. Busse, J. Reinert, M. Klemt, and A. F. Jacob, "On the chirality measurements in circular waveguides," *Advances in Complex Electromagnetic Materials* (Proceedings of the NATO Advanced Research Workshop 951552), Chiral '96, 1996.

[4] A. H. Sihvola and I. V. Lindell, "Analysis of chiral mixtures," *Journal of Electromagnetic Waves and Applications*, Vol. 6, No. 5/6, p. 553-572, 1992.

[5] G. Busse, J. Reinert, and A. F. Jacob, "Waveguide characterization of chiral material: experiments," *IEEE Trans. Microwave Theory Tech.*, vol. MTT-47, no 3, p.297-301, 1999.

[6] J. Reinert and A. F. Jacob, "Theoretical and waveguide characterization of small wire scatterers," submitted for publication, 2000.

Faraday Effect and Selective Reflection of Electromagnetic Waves in Absorbing Stratified Periodic Media

I. V. Semchenko and V. E. Kaganovich

Department of General Physics, Gomel State University
Sovyetskaya Str. 104, 246019, Gomel, Belarus
Fax: + 3-75-232-576557; email: khakh@gsu.unibel.by

Abstract

In this paper we calculate the optimum parameters of a stratified periodic structure. We obtaine the dependences of intensity, ellipticity and angle of turn of the main axis of polarization ellipse of reflected and transmitted waves on the quantity of the cells, on the frequency of the electromagnetic waves and on the magnetic field strength. We show there is the possibility of use of such structure, having selective reflection of electromagnetic waves, as the polarization converter controlled by a magnetic field.

1. Theory

One of the possibilities of creation of controlled converters of electromagnetic waves polarization is the use of stratified periodic structures, combining the properties of their components. We consider stratified periodic structure, consisting of any quantity of repeating elementary cells, placed in an external magnetic field. It is supposed, that the first layer of such cell is isotropic, and does not possess the chiral properties. The second layer is also isotropic, but adsorbing and however possesses the magnetic gyrotropy, that brings about to circular birefringence of waves inside a layer. For a gyrotropic layer of such structure the constitutive equation have the form

$$\vec{D} = \varepsilon \vec{E} + i \vec{g} \times \vec{E} \tag{1}$$

$$\vec{B} = \mu \vec{H} \tag{2}$$

where $\vec{g}$ is the vector of gyrotropy.

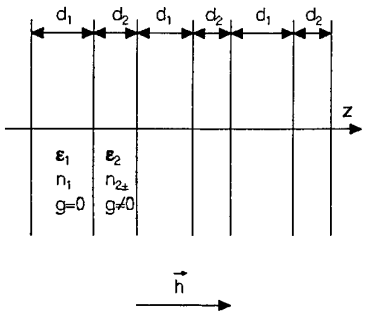

Figure 1: Schematic representation of stratified periodic medium.

For the description of absorbing gyrotropic crystals, except complex tensor of permittivity, it is necessary to introduce also complex tensor of gyrotropy. The real part of tensor of gyrotropy describes circular birefringence, and the imaginary part describes circular dichroism. Using boundary conditions for waves in each layer, we have calculated a matrix M, which connects a incident wave to transmitted and reflected waves [1]-[3]

$$M = I_{21} D_1 I_{12} D_2 \tag{3}$$

where I_{ij} is the matrix of transmission of wave through the boundary of media, D_j is the matrix of propagation of wave in medium.

If the stratified periodic structure consist of N elementary cells, we have to raise the matrix M to power N. The matrix M^{eff} for the whole stratified periodic structure can be written down as product

$$M^{eff} = I_a M^N I_b \tag{4}$$

where I_a and I_b are matrixes of transmission of electromagnetic wave through the boundaries between air and structure. Through elements of this matrix the complex coefficients of transmission and reflection of waves for all layered structure are expressed

$$T = \frac{1}{M^{eff}_{(1,1)}}, R = \frac{M^{eff}_{(2,1)}}{M^{eff}_{(1,1)}} \tag{5}$$

To obtain the maximum of reflection by each cell, the thicknesses of layers have to satisty to following relations

$$2k_1 d_1 = (2m_1 + 1)\pi, 2k_2 d_2 = (2m_2 + 1)\pi \tag{6}$$

where m_1 and m_2 are integer numbers, k_1 and k_2 are wave numbers of right- or lefthanded circularly polarized waves in the first and the second layer. Selecting the thickness of gyrotropic layer, depending on frequency of electromagnetic waves and strength of a magnetic field we can obtain the maximum reflection for one circularly polarized wave and simultaneously minimum for opposite polarization. Then at increase of number of cells of structure the intensity of one reflected circularly polarized wave monotonously increases and reaches the saturation. The value of saturation of intesity depends on a sign of imaginary part of the tensor of gyrotropy. Intensity of other circularly polarized reflected wave oscillates, periodically accepting close to the zero value. It enables to obtain the polarization of a reflected wave close to circular.

2. Numerical Calculation

One can see on fig. 3, that the maximum of ellipticity both for reflected and transmitted waves take place at calculated value of external magnetic field strength.

As is obvious on fig. 4, at the calculated value of the external magnetic field strength the intensity of reflected lefthanded wave is maximum, while the intensity of righthanded wave is close to the zero. When changing an external magnetic field or the frequency of electromagnetic waves the polarization properties change both of transmitted and of reflected waves.

3. Conclusion

As result there is the possibility of use of such structure, having selective reflection of electromagnetic waves, as the polarization converter controlled by a magnetic field.

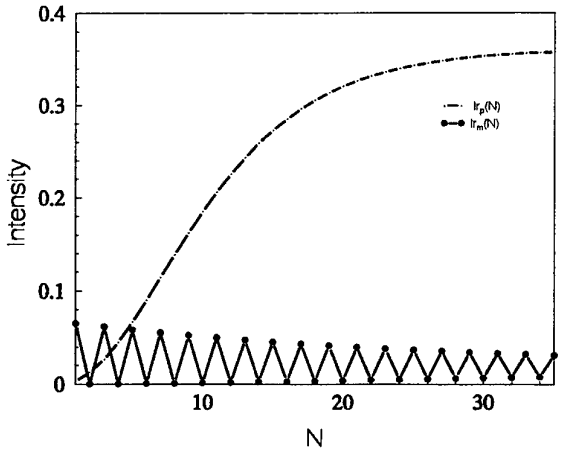

Figure 2: Dependence of normalized intensity of reflected and transmitted waves on the number of cells.

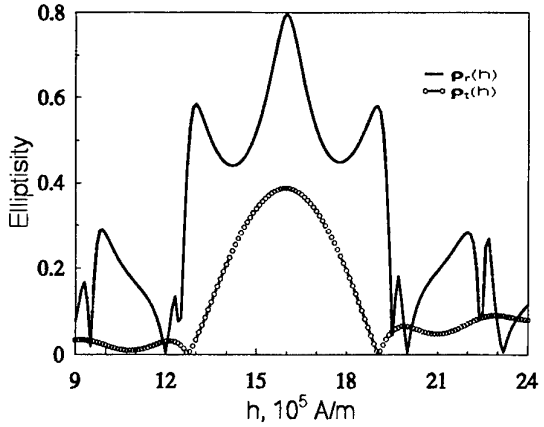

Figure 3: Dependence of ellipticity of reflected and transmitted waves on the strength of an external magnetic field.

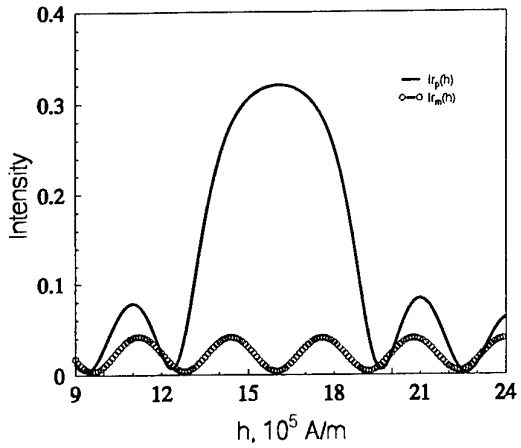

Figure 4: Dependence of intensity of reflected left- and righthanded circularly polarized waves on the strength of an external magnetic field.

References

[1] R. M. A. Azzam and N. M. Bashara, *Ellipsometry and Polarized Light.* North-Holland Publishing Company, 1977.

[2] Amnon Yariv and Pochi Yeh, *Optical Waves in Crystals.* A Wiley-Interscience Publication, John Wiley and Sons, 1984.

[3] J. Zak, E. R. Moog, C. Liu, and S. D. Bader, "Additivity of the Kerr effect in thin-film magnetic systems", *J. Magn. and Magn. Mater*, vol. 88, no. 3, pp. 261–266, May 1990.

Bandwidth Control for Photonic Bandgap Waveguides

A. Boag[1], M. Gafni[2], and B. Z. Steinberg[2]

[1] Faculty of Engineering, Department of Physical Electronics, Tel Aviv University, Tel Aviv 69978, Israel
Fax: + 972-3-6423508; E-mail: boag@eng.tau.ac.il

[2] Faculty of Engineering, Department of Interdisciplinary Studies, Tel Aviv University, Tel Aviv 69978, Israel
E-mail: steinber@eng.tau.ac.il

Abstract

A widely spaced periodic array of defects in the photonic band gap crystal is studied with the goal of designing a waveguide with a prescribed narrow bandwidth. Tunnelling of radiation between the defect sites allows wave propagation along the line of the defects. A design procedure based on the weakly coupled cavity model is proposed. The frequency shift and the band structure of the periodic defect waveguide are linked by an analytic relationship to the distance between the defect sites and therefore can be tuned by varying the latter. Sections of such waveguides can be employed as ultra narrow band filters in optical routing devices.

1. Introduction

Photonic band gap materials attracted much attention in the context of designing optical and microwave devices. Recently numerical experiments have shown that line defects in photonic crystals can be used not only to guide but also to multiplex and demultiplex optical signals [1]. Most researchers studying the wave guiding by line defects employ photonic band waveguides obtained by removal or modification of consecutive posts in the periodic structure. The strong coupling between the adjacent defects produces relatively wideband waveguides.

In this paper, we address the issue of designing photonic bandgap waveguides with a prescribed narrow bandwidth. Specifically, we concentrate on a problem of a waveguide formed by widely spaced periodic defects in the photonic band gap crystal. Tunnelling of radiation between the defect sites allows wave propagation along the line of defects. Sections of such waveguides can be employed as ultra narrow band filters in optical routing devices. Here, we propose a design procedure based on the weakly coupled cavity model. This approach resembles the tight binding perturbation theory of the solid-state physics. A single defect mode with a resonant frequency in the band gap is analyzed first. Coupling between the periodic defects causes a discrete spectral line to turn into a narrow band of guided frequencies shifted from the original frequency of a single defect. The perturbation theory facilitates an approximate calculation of both the frequency shift and the band structure of the periodic defect waveguide. Furthermore, these parameters are linked by an analytic relationship to the distance between the defect sites. Consequently, the latter distance can be directly tuned to achieve the desirable waveguide properties. The design results are verified by a comparison with numerically rigorous computations employing the current model technique [2].

2. Formulation

Consider a problem of designing a narrow band waveguide formed by widely spaced periodic defects in the photonic band gap crystal. The time harmonic electromagnetic problem in an inhomogeneous dielectric can be cast in an eigenvalue form for the magnetic field $\boldsymbol{H}$ [3]:

$$\Theta \boldsymbol{H}(\boldsymbol{r}) = \left(\frac{\omega}{c}\right)^2 \boldsymbol{H}(\boldsymbol{r}) \tag{1}$$

where ω is the frequency, c is the free space speed of light, and Θ denotes a Hermitian operator defined by

$$\Theta \boldsymbol{H} = \nabla \times \left(\frac{1}{\varepsilon(\boldsymbol{r})} \nabla \times \boldsymbol{H}\right) \tag{2}$$

In (2), $\varepsilon(\boldsymbol{r})$ denotes the relative permittivity. Alternatively, the eigen-frequencies can be expressed in the variational form:

$$\left(\frac{\omega}{c}\right)^2 = \frac{\langle \boldsymbol{H}, \Theta \boldsymbol{H} \rangle}{\langle \boldsymbol{H}, \boldsymbol{H} \rangle} \tag{3}$$

where $\langle \cdot, \cdot \rangle$ denote the inner product defined by

$$\langle \boldsymbol{F}, \boldsymbol{G} \rangle = \int \boldsymbol{F}^* \cdot \boldsymbol{G} \, d\boldsymbol{r} \tag{4}$$

The unperturbed crystal is characterized by a periodic relative permittivity $\varepsilon_{\mathrm{p}}(\boldsymbol{r})$. First, consider a single defect within the periodic structure arbitrarily centered at the origin of the coordinate system. The localized defect can be characterized by the change in the reciprocal permittivity $d(\boldsymbol{r}) = 1/\varepsilon_{\mathrm{d}}(\boldsymbol{r}) - 1/\varepsilon_{\mathrm{p}}(\boldsymbol{r})$, where $\varepsilon_{\mathrm{d}}(\boldsymbol{r})$ denotes the permittivity of the photonic crystal with a single defect. We assume that this defect allows for a localized mode $\boldsymbol{H}_o(\boldsymbol{r})$ with a frequency ω_o falling in the band gap of the unperturbed crystal. Specifically by analogy to (1),

$$\left(\Theta_{\mathrm{p}} + \Theta_o\right) \boldsymbol{H}_o(\boldsymbol{r}) = \left(\frac{\omega_o}{c}\right)^2 \boldsymbol{H}_o(\boldsymbol{r}) \tag{5}$$

Θ_p is the operator of the periodic structure and Θ_o is the defect operator. The operators Θ_p and Θ_o are defined by analogy to (2) via replacing $1/\varepsilon(\boldsymbol{r})$ by $1/\varepsilon_p(\boldsymbol{r})$ and $d(\boldsymbol{r})$, respectively.

Now, we turn to the case of a linear array of defects obtained by a periodic repetition of the defect. The reciprocal permittivity of the photonic crystal with the linear array of non-overlapping defects is given by

$$\frac{1}{\varepsilon(\boldsymbol{r})} = \frac{1}{\varepsilon_p(\boldsymbol{r})} + \sum_{n=-\infty}^{\infty} d(\boldsymbol{r} - n\boldsymbol{b}) \tag{6}$$

where the vector $\boldsymbol{b}$ is assumed to be an integral multiple of the lattice vector $\boldsymbol{a}$, $\boldsymbol{b} = \ell \boldsymbol{a}$, $\ell \in N$. The operator Θ,

$$\Theta = \Theta_p + \sum_{n=-\infty}^{\infty} \Theta_n \tag{7}$$

which comprises a superposition of Θ_p and shifted operators Θ_n defined by analogy with (2) via replacing $1/\varepsilon(\boldsymbol{r})$ by $d(\boldsymbol{r} - n\boldsymbol{b})$ for $n \in \mathbf{Z}$.

Following the strong binding perturbation theory [4] for the linear array, we seek a modal solution of the form

$$\boldsymbol{H}(\boldsymbol{r}) = \sum_{n=-\infty}^{\infty} A_n \boldsymbol{H}_n(\boldsymbol{r}) \tag{8}$$

where $\boldsymbol{H}_n(\boldsymbol{r}) = \boldsymbol{H}_o(\boldsymbol{r} - n\boldsymbol{b})$ and $\{A_n\}$ is a set of yet to be determined coefficients. Substitution of (7) and (8) in (3) yields

$$\left(\frac{\omega}{c}\right)^2 = \frac{\sum_{n=-\infty}^{\infty} \sum_{m=-\infty}^{\infty} A_n^* A_m T_{n-m}}{\sum_{n=-\infty}^{\infty} \sum_{m=-\infty}^{\infty} A_n^* A_m H_{n-m}} \tag{9}$$

where

$$H_{n-m} = \left\langle \boldsymbol{H}_n, \boldsymbol{H}_m \right\rangle \tag{10}$$

and

$$T_{n-m} = \left\langle \boldsymbol{H}_n, \Theta \boldsymbol{H}_m \right\rangle \tag{11}$$

Note that due to the periodicity of the array the integrals in (10) and (11) depend only on *n-m*. According to variational principle the frequency expressed by (9) is stationary with respect to the coefficients $\{A_n\}$. We have

$$\forall n \quad \frac{\partial \left(\frac{\omega}{c}\right)^2}{\partial A_n} = 0 \quad \Rightarrow \quad \sum_{m=-\infty}^{\infty} \left[T_{n-m} - \left(\frac{\omega}{c}\right)^2 H_{n-m} \right] A_m = 0 \tag{12}$$

Discrete shift invariant nature of (12) suggest that modal solution of the form $A_m = Ae^{jkm}$ whose use in (12) yields

$$\sum_{m=-\infty}^{\infty} \left[T_m - \left(\frac{\omega}{c}\right)^2 H_m \right] e^{jkm} = 0 \tag{13}$$

Using (5), we have

$$T_m = \left(\frac{\omega_o}{c}\right)^2 H_m + T_m' \tag{14}$$

where

$$T_m' = \int \boldsymbol{H}_m^* \cdot \sum_{\substack{n=-\infty \\ n\neq 0}}^{\infty} \Theta_n \boldsymbol{H}_o \, d\boldsymbol{r} = \sum_{\substack{n=-\infty \\ n\neq 0}}^{\infty} \left\langle \boldsymbol{H}_m, \Theta_n \boldsymbol{H}_o \right\rangle \tag{15}$$

Substituting (14) in (13) we obtain

$$\left(\frac{\omega}{c}\right)^2 - \left(\frac{\omega_o}{c}\right)^2 = \frac{\sum_{m=-\infty}^{\infty} T_m' e^{jkm}}{\sum_{m=-\infty}^{\infty} H_m e^{jkm}} \tag{16}$$

namely, an expression for the frequency shift of the linear array mode with wavenumber k/b relative to the frequency of the localized mode. For sufficiently spaced defects we can make the first order approximation by retaining only the nearest neighbor interactions. Specifically, we have $\forall m \neq 0 \quad |H_m| << |H_0|$ and $\forall |m| > 1 \quad |T_m'| << |T_0'|$. On the other hand, T_1' and T_0' can be comparable in magnitude. With this approximations and assuming $|\omega - \omega_o| << \omega_o$ we obtain

$$\omega - \omega_o = \frac{c^2}{2\omega_o H_0}\left[T_0' + 2T_1' \cos(k)\right] \tag{17}$$

The total bandwidth of the waveguide formed by the periodic array for propagating modes $0 < k < \pi$ is given by

$$\Delta\omega = \frac{2c^2}{\omega_o H_0} T_1' \tag{18}$$

Furthermore due to weak coupling and Hermitian property of Θ_1,

$$T_1' \approx 2\left\langle \boldsymbol{H}_1, \Theta_1 \boldsymbol{H}_o \right\rangle = 2\left\langle \Theta_1 \boldsymbol{H}_1, \boldsymbol{H}_o \right\rangle = 2\int (\Theta_1 \boldsymbol{H}_1)^* \boldsymbol{H}_o d\boldsymbol{r} \tag{19}$$

Once the localized modal solution is known, equations (18)-(19) allow for straightforward estimation of the waveguide bandwidth for various spacings between defects, $\boldsymbol{b} = \ell \boldsymbol{a}$. Note that in (19), $\boldsymbol{H}_1(\boldsymbol{r}) = \boldsymbol{H}_o(\boldsymbol{r} - \boldsymbol{b})$ and Θ_1 is a local operator. For sufficiently large $\boldsymbol{r}$, the localized magnetic field $\boldsymbol{H}_o(\boldsymbol{r})$ is decaying exponentially away from the origin. Thus, (19) indicates that increasing ℓ can reduce the waveguide bandwidth. The bandwidth control by varying defect spacing will be demonstrated via numerical examples.

References

[1] E. Centeno, B. Guizal, and D. Felbacq, *J. Opt. A.: Pure Appl. Opt.*, No. 1, pp. L10-L13, 1999.

[2] A. Boag, Y. Leviatan, and A. Boag, *Radio Science*, Vol. 23, pp. 612-624, 1988.

[3] J. D. Joannopoulos, R. D. Meade, and J. N. Winn, *Photonic Crystals: Molding the Flow of Light.* Princeton University Press, 1995.

[4] R. E. Peierls, *Quantum Theory of Solids*. Oxford Clarendon Press.

Radiation Control on a Step Discontinuity of a Grounded Chiral Slab

A. L. Topa, C. R. Paiva, and A. M. Barbosa

Instituto Superior Técnico, Technical University of Lisbon
Av. Rovisco Pais 1, 1049-001 Lisboa, Portugal
Fax: + 351 - 21 - 8417284; E-mail: antonio.topa@lx.it.pt

Abstract

In this paper, we analyse the radiation on a step discontinuity of a grounded chiral slab, and we show that it can be enhanced due to the effect of chirality. In addition to the surface modes, the continuous spectrum of radiation modes is also taken into account. In fact, it is the coupling between these two types of modes that is responsible for the radiation occurring on the step. We show that chirality may increase such coupling and, therefore, improve radiation. The complete spectral representation includes two subsets of continuous hybrid modes: Incident Transverse Electric (ITE) and Incident Transverse Magnetic (ITM) radiation modes. The scattering matrix of the step is determined by minimizing the boundary residual error in the sense of the least squares. The influence of chirality on the characterization of the step is demonstrated and we show that some control on the radiation pattern is achieved, mainly in the angle and width of the radiation beam.

1. Introduction

Step discontinuities play an important role in optical and millimeter wave components, as constituent blocks of several interacting structures. In dielectric planar waveguides involving chiral media, such discontinuities have been already analyzed, either isolated [1-2], or in periodic structures [3].

This paper extends the previous analysis to consider the radiation effect, and shows that the radiation of the step discontinuity can be enhanced due to the inclusion of chirality. Since the grounded chiral slab is an open structure, in addition to the surface modes, the continuous spectrum of radiation modes must be taken into account. Moreover, appreciable coupling may take place between the surface and the radiation modes of the waveguide, and so the continuous spectrum will be responsible for the radiation from the step. Chirality may affect such coupling and increase radiation from the step.

In order to calculate the radiated field, a rigorous description of the problem must be achieved, by selecting a complete spectral field representation. Two subsets of continuous hybrid modes may be considered: (i) a pair of Incident Transverse Electric (ITE) and Incident Transverse Magnetic (ITM) radiation modes; (ii) a pair of Reflected Transverse Electric (RTE) and Reflected Transverse Magnetic (RTM) radiation modes. These sets of modes were found to be mutually orthogonal and have the advantage of presenting a clear physical interpretation [4]. To apply a discrete mode matching technique, the continuous spectral amplitudes are discretized and the residual error in the boundary conditions is minimized in the sense of the least squares. Finally, the accuracy of the solution is checked by means of a power balance criterion.

The reflection and transmission coefficients of the incident fundamental surface mode, as well as the fully characterization of the radiation effect are presented. The analysis includes the influence of the chirality on the radiation control of the step. Finally, by using the saddle-point technique, the

radiation pattern is calculated. The effect of the chiral parameter on both the angle and width of the radiation beam is also considered.

2. Problem Formulation and Solution

The step discontinuity in a grounded chiral slab, shown in Fig. 1, is considered. By introducing normalized fields $\mathscr{D} = \mathbf{D}/\varepsilon_0$, $\mathscr{B} = Z_0\mathbf{B}/\mu_0$ and $\mathscr{H} = Z_0\mathbf{H}$, the constitutive relations in the chiral medium, for time-harmonic fields ($e^{j\omega t}$), may be written as [5]

$$\mathscr{D} = \varepsilon\,\mathbf{E} - j\chi\,\mathscr{H} \tag{1a}$$

$$\mathscr{B} = j\chi\,\mathbf{E} + \mu\,\mathscr{H} \tag{1b}$$

where χ is the chirality parameter, ε is the permittivity and μ is the permeability.

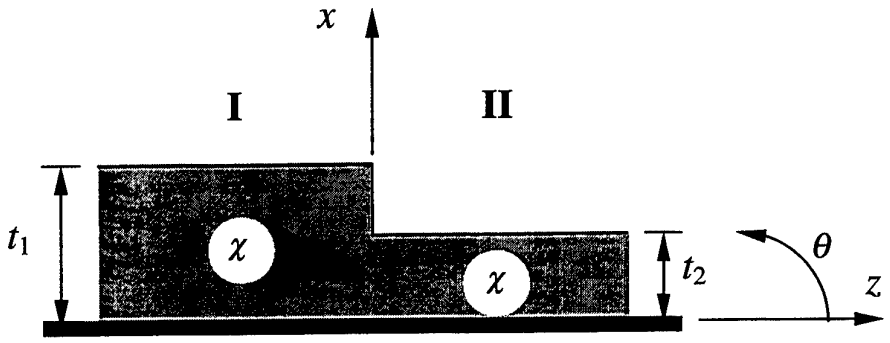

Fig. 1 Step discontinuity a grounded planar chiral slab.

According to the boundary conditions at the discontinuity plane, the transverse field components must be continuous. In this case, since all the modes are six-component hybrid modes, it is very convenient to introduce the two following transverse state vectors:

$$\phi = [E_y,\ j\mathscr{H}_y]^{\mathrm{T}} \tag{2.a}$$

$$\psi = [\mathscr{H}_x,\ -jE_x]^{\mathrm{T}}, \tag{2.b}$$

where ϕ is the transverse field supporting vector. In addition, we may introduce the boundary residual vector as

$$\varepsilon = \begin{bmatrix} \phi^I - \phi^{II} \\ \alpha\,(\psi^I - \psi^{II}) \end{bmatrix}, \tag{3}$$

where α represents a dimensionless weighting factor between the two boundary residual components. This residual can be minimized according to the least squares method. However, in order to apply this discrete mode matching technique, the spectral amplitudes of the radiation mode must be discretized

within a complete set of orthogonal basis functions. Legendre polynomials and Gauss-Laguerre functions have been used in this procedure.

The complete spectral field representation includes two types of radiation modes. In the present analysis, Incident Transverse Electric (ITE) and Incident Transverse Magnetic (ITM) radiation modes were considered [4]. The radiation pattern of the chiral step was calculated by the use of the steepest descent method.

3. Numerical Results and Discussion

For numerical simplicity we have considered monomodal slabs on each side of the step discontinuity (waveguides I and II), which means that we will only have the fundamental surface mode propagating on the structure. Fig. 2 shows the variation of the reflection and transmission coefficients Γ_0 and T_0 of the fundamental incident surface mode, as a function of the chirality parameter χ. The suddenly decrease of the value of $|T_0|$ for χ near 1.8, is due to the fact that the fundamental mode propagating in waveguide II is approaching cutoff.

The variation of the reflected and radiated power P_r and P_{rad} with chirality parameter χ, is depicted in Fig. 3. The radiated power is much higher than the reflected power, which shows that, due to the discontinuity, there is a strong coupling between the incident surface mode and the continuous spectrum of radiation modes. Moreover, one should note the monotonous increase in the value of radiated power, whenever the chirality is increased. This value may reach 80% of the total incident power, which proves that, on any circumstance, one may disregard the contribution of the radiation modes to the total fields. Only when the surface mode in waveguide II approaches cutoff, the reflected power becomes significant.

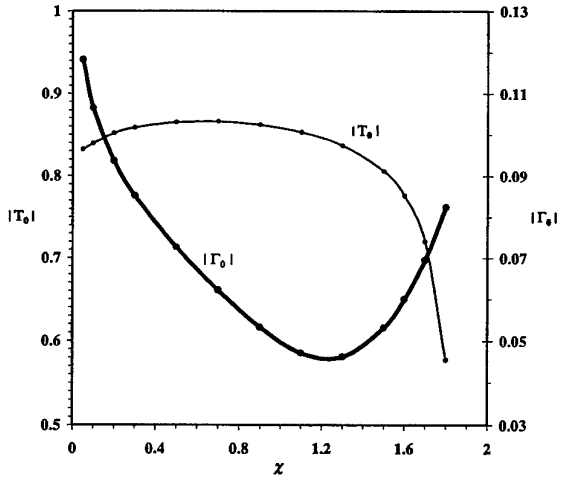

Fig. 2 Reflection and transmission coefficients for the incident surface mode as a function of the chirality parameter χ.

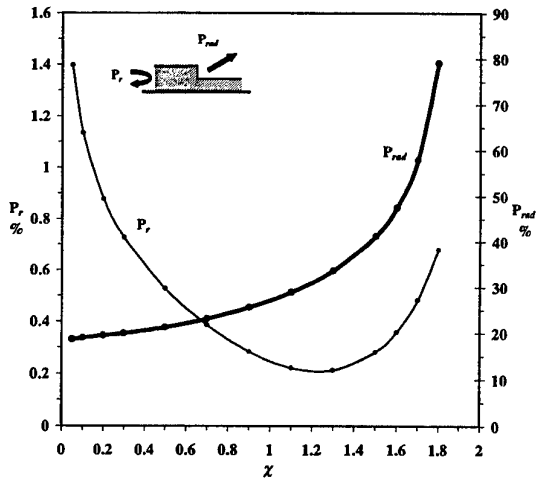

Fig. 3 Reflected and radiated power in a chiral step discontinuity as a function of the chirality parameter χ.

The forward radiation pattern of the chiral step is depicted, in Fig. 4, for different values of the chirality parameter χ. A strong increase in the radiation intensity can be clearly seen, as far as chirality is raised. Meanwhile, the beam angle observes a slightly decrease. Backward radiation pattern does not differ significantly in shape of the forward pattern, although being considerably small. Forward-backward ration is about 20 dB, which shows that, in the present case, radiation is mainly in the propagation direction.

Finally, Fig. 5 shows the variation of the beam angle θ_{max} and the 3dB beam width $\Delta\theta_{3dB}$, as a function of χ. For small values of the chirality parameter, θ_{max} and $\Delta\theta_{3dB}$ suffer a linear increase with χ. As far as the fundamental mode in waveguide II approaches cutoff, those values suddenly decay.

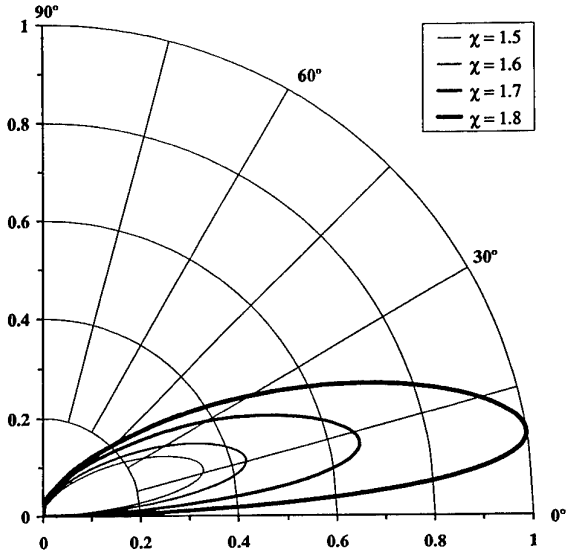

Fig. 4 Forward radiation pattern for different values of the chirality parameter χ.

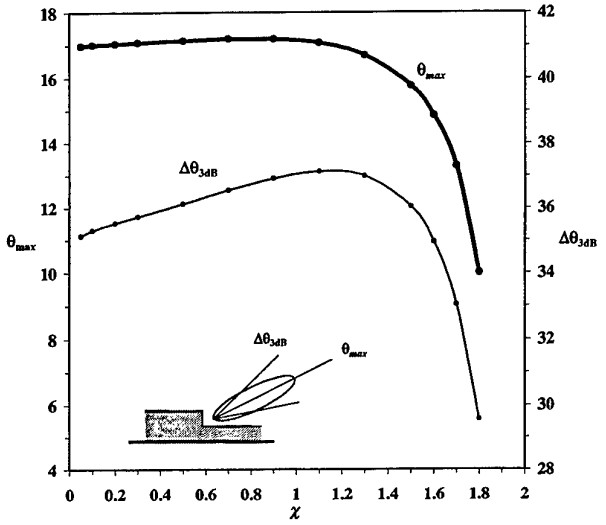

Fig. 5 Beam angle and 3 dB beam width as a function of the chirality parameter χ.

4. Conclusion

We have shown that the power radiated from a step discontinuity in a planar dielectric slab can be significantly increased with the inclusion of chirality in the dielectric substrate. On the other hand, this may cause a slightly decrease in the beam radiation angle as well as a reduction of its width. Therefore, we have proven that chirality represents an extra degree of freedom for the radiation control of a step discontinuity in a planar dielectric waveguide.

References

[1] A. L. Topa, C. R. Paiva, and A. M. Barbosa, "Rigorous analysis of a step discontinuity in a planar dielectric chiral slab," in *Proc. CHIRAL'95* - 4th International Conference on Chiral, Bi-isotropic and Bi-anisotropic Media, State College, PA, pp. 131-134, October 1995.

[2] A. L. Topa, C. R. Paiva, and A. M. Barbosa, "Step discontinuity in a planar dielectric slab," in *Proc. PIERS'96* - Progress in Electromagnetic Research Symposium, Innsbruck, Austria, p. 495, July 1996.

[3] X. Wu and D. L. Jaggard, "Discontinuities in planar chirowaveguides," *IEEE Trans. Microwave Theory Tech.*, vol. 45, pp. 641-647, May 1997.

[4] A. L. Topa, C. R. Paiva, and A. M. Barbosa, "Radiation modes of an asymmetric chiral slab waveguide: A general approach to a new canonical problem," in *Proc. PIERS' 97* - Progress in Electromagnetic Research Symposium, Kowloon, Hong Kong, p. 684, Jan. 1997.

[5] C. R. Paiva and A. M. Barbosa, "A linear-operator formalism for the analysis of inhomogeneous biisotropic planar waveguides," *IEEE Trans. Microwave Theory Tech*, vol. 40, pp- 672-678, Apr. 1993.

Polarized Spatial Soliton in a Chiral Optical Fiber

H. Torres–Silva and M. Zamorano

Departamento de Electrónica, Facultad de Ingeniería, Univesidad de Tarapacá
Casilla *6* D, Av. 18 de Septiembre 2222, Arica - Chile
email: htorres@socoroma.electa.uta.cl

Abstract

The problem of soliton propagation in nonlinearity Kerr medium with linear optical activity and cubic anisotropy is considered. It is shown that the balance between the nonlinearity and linear girotropic results in the existence of spatial polarized solitons with fixed states of polarization. The chirality effect is characterized through the Born-Fedorov formalism and the results show modifications of the attenuation and nonlinear coefficient compared with the tipical coefficients in a nonlinear Schrödinger equation for a normal fiber in a regime of 1,55 and 1,3 μm.

1. Introduction

Chirality was firstly observed as optical activity and it corresponds to the rotation of the polarization plane, in a linear isotropic material. Phenomenonlogical studies establishes that the polarization plane rotation may be predicted by Maxwell's equations adding to the polarization P an additional term proportional to $\nabla \times \vec{E}$. The Drude-Born-Fedorov equations by satisfying the edge conditions[1], allows us to characterize the nonlinear chiral media through by the equations $D = \epsilon_n \vec{E} + \epsilon\zeta \nabla \times \vec{E}$ and $B = \mu_0(\vec{H} + \zeta \nabla \times \vec{H})$, where ϵ_n is the permittivity and ζ is the chiral coefficient. The pseudo scalar ζ represent the measure of chilarity and it has length units. [2]-[3]. It should also be considered the non local character of theses equations, since the polarization P (magnetization M) depent not only of E (H) but also of the rotor of E (rotor of H). Even though from an electromagnetic point of view a homogeneous chiral material may be discrete by different specific equations [3], in this work we will use the Drude-Born-Fedorov equations in optical fiber since they are the most adequate for the applications of our interest.

2. Basic Propagation Equation

Using equations the above equations, the corresponding Maxwell's equations are

$$\nabla \times \vec{H} = \frac{\partial\left(\epsilon_n \vec{E}\right)}{\partial t} + \sigma\vec{E} + \frac{\partial}{\partial t}\epsilon\zeta\left(\nabla \times \vec{E}\right) = \frac{\epsilon_n \partial \vec{E}}{\partial t} + \sigma\vec{E} + \epsilon\zeta\nabla \times \frac{\partial \vec{E}}{\partial t} \tag{1}$$

$$\nabla \times \vec{E} = -\frac{\partial \vec{B}}{\partial t} = -\mu_0 \frac{\partial \vec{H}}{\partial t} - \mu_0\zeta \frac{\partial\left(\nabla \times \vec{H}\right)}{\partial t} \tag{2}$$

If we make the follow considerations:

- The chiral media has a Kerr type non-linearity characterized by the refraction index such that the permittivity is $\epsilon_n = \epsilon_o + \epsilon_2 \left|\vec{E}\right|^2$ [4], were ϵ_o is the lineal part and ϵ_2 is the non linear part, respectively, of ϵ_n.

- That the optical electric field E represent a located wave propagating in the direction

$$\vec{E}(\vec{r},t) = (\hat{x} + j\hat{y})\Psi(\vec{r},t)\, e^{-j(kz-\omega_0 t)} = \vec{\Psi} e^{-j(kz-\omega_0 t)} \tag{3}$$

were $\vec{\Psi}$ represents the complex envelop.

- That the condition of a slowly variant envelop conditions its may be

$$\left|\frac{\partial^2\vec{\Psi}}{\partial z^2}\right| \ll \left|j2k\frac{\partial\vec{\Psi}}{\partial z}\right|; \left|\frac{\partial\vec{\Psi}}{\partial t}\right| \ll \left|j\omega_0\vec{\Psi}\right|; \left|\frac{\partial^2\left|\vec{\Psi}\right|^2\vec{\Psi}}{\partial t^2}\right| \ll \left|j\omega_0\frac{\partial\left|\vec{\Psi}\right|^2\vec{\Psi}}{\partial t}\right| \ll \left|j\omega_0\left|\vec{\Psi}\right|^2\vec{\Psi}\right| \tag{4}$$

- That the phenomenon of dispersion is included in heuristic form through the relation $\Delta k = \frac{1}{v}\frac{\partial}{\partial t} = \frac{\partial k}{\partial\omega}\frac{\partial}{\partial t} - j\frac{1}{2}\frac{\partial^2 k}{\partial\omega_0^2}\frac{\partial^2}{\partial t^2} - j\frac{1}{6}\frac{\partial^3 k}{\partial\omega_0^3}\frac{\partial^3}{\partial t^3} = \frac{k_0}{\omega_0}\frac{\partial}{\partial t}$

we obtain the following wave equation

$$j\left(\frac{\partial\phi}{\partial z^*} + \frac{1}{v_g}\frac{\partial\phi}{\partial t}\right) + \frac{1}{2}k''\frac{\partial^2\phi}{\partial t^2} - j\frac{1}{6}k'''\frac{\partial^3\phi}{\partial t^3} + (1-\zeta k_0)\left[\frac{j\omega\alpha}{2k_0}\phi - \frac{\beta\omega_0^2}{(2k_0)^3}|\phi|^2\phi\right] + (1-\frac{\zeta k_0}{2})\zeta k_0^2\phi = 0 \tag{5}$$

where $k' = \frac{\partial k}{\partial\omega} = \frac{1}{v_g}$; $k'' = \frac{\partial^2 k}{\partial\omega^2}$; $k''' = \frac{\partial^3 k}{\partial\omega^3}$. Equation (5) describes the propagation of pulses in a chiral dispersive and nonlinear optical fiber. The analysis of each term is has follows [4]: The first term represent the evolution of pulse with distance; The second, third and fourth terms represent the dispersion of the optical fiber $k'(=1/v_g)$ and k'' correspond to the chromatic dispersion; k' indicates that the pulses moving which the group velocity, while that the dispersion of the group velocity (GVD) is represented by k'', which alters the relative phases of the frequency components of pulses producing its temporal widening. k'' is null in the region of 1.3 μm, For values of λ less than 1.3 μm, k'' is positive (normal dispersion region) and for values higher than 1.3 μm, is negative (anomalous dispersion region). k''' represent the slope of the group velocity dispersion, also denominated cubic dispersion and correspond to a higher order dispersion; important in ultra short pulses and in the second optical window where k'' is null (1.3 μm region). The cubic dispersion, besides, is important in fiber with shifted dispersion to the region of 1.5 μm. The fifth term is associated with the attenuation of the fiber (α), in this case those losses are weighed by the chirality of the fiber. $|\phi|^2\phi$ represent the nonlinear effect, and are due to the Kerr effect, which is characterized by having a refraction index depending on the intensity of the applied field. An index of this type for the case of optical fiber, means that there is a phase shift depending on the intensity and since the temporal changes of phase are also temporal changes of frequency, Its have that the Kerr type non linearity may alter and widening frequency spectrum of the pulse. This term also depends on the chirality of the fiber. The last term is highly associated to the chirality of the fiber.

3. Nonlinear Schrödinger Equation

In order to ease up the solution of the propagation equation the following changes of variables is introduced: $t' = t - \frac{z^*}{v_g}$ and $z' = z^*$, thus the original reference system will be $t = t' + \frac{z^*}{v_g}$ and $z^* = z'$ the equation (5) takes the form

$$j\frac{\partial\phi}{\partial z'} + \frac{1}{2}k''\frac{\partial^2\phi}{\partial t'^2} - j\frac{1}{6}k'''\frac{\partial^3\phi}{\partial t'^3} + j\frac{\alpha\omega_0}{2k_0}(1-\zeta k_0)\phi - \frac{\beta\omega_0^2}{(2k_0)^3}(1-\zeta k_0)|\phi|^2\phi + \zeta k_0^2(1-\frac{\zeta k_0}{2})\phi = 0 \tag{6}$$

Defining the new variables

$$q = \frac{\omega_0}{2k_0}\beta^{\frac{1}{3}}\phi, \quad \xi = \frac{\beta^{\frac{1}{3}}}{2k_0}z', \quad \tau = \sqrt{\frac{1}{2k_0k''}}\beta^{\frac{1}{6}}t', \quad \partial\tau^2 = \frac{\beta^{\frac{1}{3}}}{2k_0k''}\partial t'^2, \quad \partial\tau^3 = \frac{\beta^{\frac{1}{2}}}{(2k_0k'')^{3/2}}\partial t'^3$$

$$\gamma = \frac{\beta^{\frac{1}{6}}k'''}{6k''}\frac{1}{\sqrt{2k_0k''}}, \quad C = 1-\zeta k_0, \; \Gamma = \frac{\omega\alpha}{\beta^{1/3}}$$

and operating algebraically we get the non linear Schrödinger equation for a chiral optical fiber.

$$j\frac{\partial q}{\partial \xi} + \frac{1}{2}\frac{\partial^2 q}{\partial \tau^2} - i\gamma\frac{\partial^3 q}{\partial \tau^3} + j\Gamma Cq - C|q|^2 q + \frac{k_0}{\beta^{1/3}}\left(1-C^2\right)q = 0 \tag{7}$$

4. Analysis of Results

The equation (7) represents the basic modeling of the pulse propagations in a chiral optical fiber dispersive and nonlinear. This is applicable both in the second and third optical windows. For the numerical calculation we use $k'' = -17,4$ ps^2/km, $\gamma = 0$, $\Gamma = 0$, which correspond to the anomalous region for a fiber length equal to 2.9 km . Fig. 1 and Fig. 2 correspond to one-order soliton with input power peak $P_0 = 0,87$ W and C=0,85 and 1,15 respectively. Fig. 2 shows an increasse of the intensity when the pulse propagates. This effect appears when ζk_0 is negative so if the losses (Γ) are included the chirality factor can compensate the typical decrease of the power pulse of the normal optical fiber. Fig. 3 and Fig. 4 correspond to the second-order solitons. Here we put $P_0 = 3,49$ W, this peak power is required to sopport the second order soliton. If we compare Fig. 3 and Fig. 4 , we see that with ζk_0 positive the signal is less distorted. Finally, Figs. 5 and 6 shows the behavior of the third-order solitons, $P_0 = 7,86$ W.

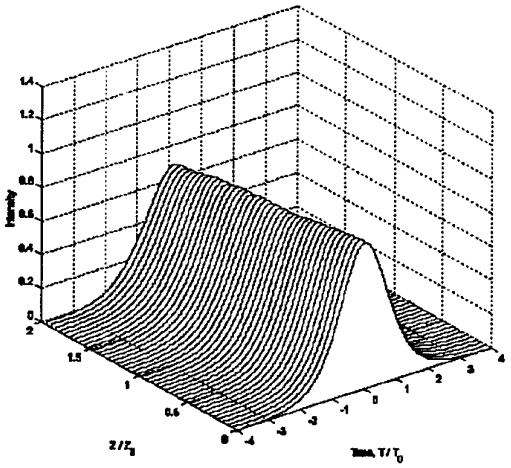

Fig. 1

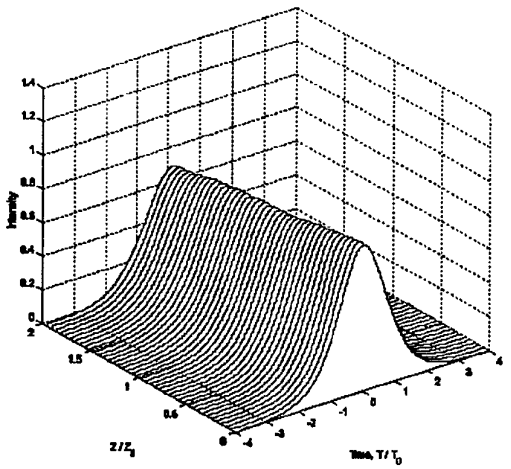

Fig. 2

5. Conclusion

In this work we have obtain the nonlinear Schrödinger equation for an optical fiber whose core is chiral dispersive and have nonlinear behavior. The effect of chirality is shown over the term associate to fiber lossy and to the nonlinear coefficient. The phenomenons that produce the dispersive effect and nonlinear in a non-chiral optical fiber (which produce the soliton propagation for example), are affected in case of using a chiral fiber, since to produce the same effect it will be necessary to operate the fiber in the normal dispersion regimen. The most important

result in our work it the possibility to use the chirality of the fiber to cancel out losses and non linearitys of the optic fiber, which would allow to modify radically their behavior as channel of communications.

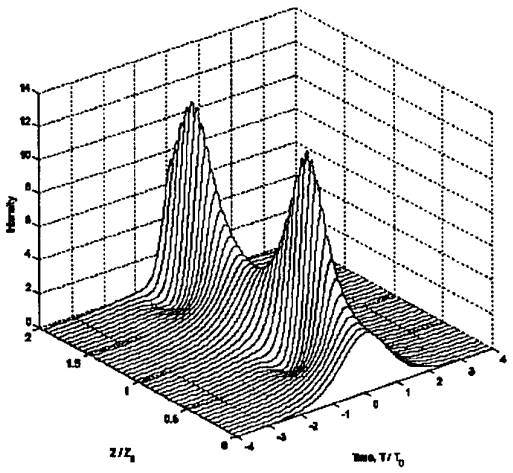

Fig. 3

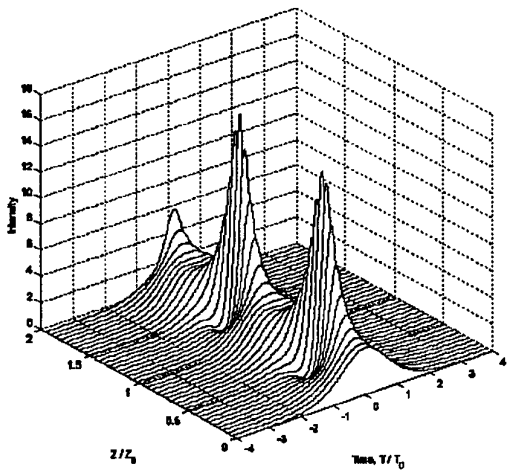

Fig. 4

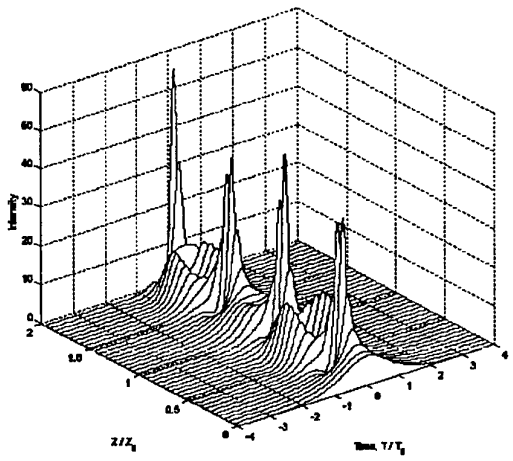

Fig. 5

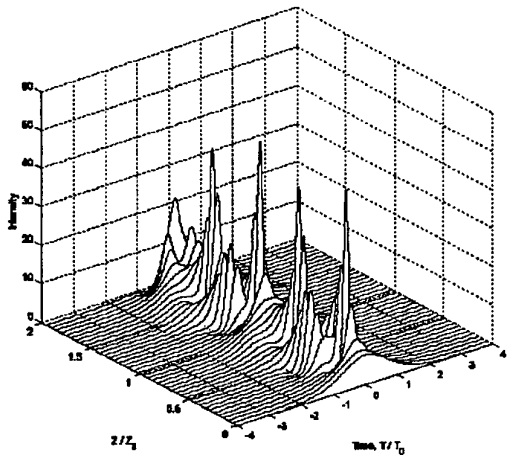

Fig. 6

Acknowledgement
This work have been financed by proyects N°8721-98, 8822-99 and 8723-99 of the Universidad de Tarapacá.

References

[1] A. Lakhtakia, V. K. Varadan, and V. V. Varadan, *Time-Harmonic Electromagnetic Fields in Chiral Media.* Lecture Notes Physics, 335, Springer-Verlag, 1985.
[2] H. Torres-Silva, P. H. Sakanaka, N. Reggiani, and C. Villarroel, "Electromagnetic properties of a chiral-plasma," *Pramana Journal of Physics*, 48, No. 1, 1997.
[3] H. Torres-Silva, "Chiro-plasma surface wave," *Advances in Complex Electromagnetic Materials.* Kruwer Academic Publishers, 38, Netherlands, 249, 1997.
[4] G. Agrawal, *Nonlinear Fiber Optics.* Academic: New York, 1995.
[5] M. Zamorano, H. Torres y C. Villarroel, "Ecuación de Schrödinger para una fibra óptica quiral," *R. Mexicana de Fisica*, 46(1),62, 2000.

Analytical and Numerical Study of Reflection of Plane Waves from Two-dimensional Bianisotropic Array Substrated by a Dielectric Shield

M. S. Kondratjev[1] , P. A. Belov[1], and C.R. Simovski[1]

[1] Physics Department, St. Petersburg Institute of Fine Mechanics and Optics,
Sablinskaya 14, 197101 St. Petersburg, Russia
Phone/fax: 7-812-3456198 ; email: kondrat@green.ifmo.ru

Abstract

This work is devoted to the problem of the electromagnetic wave reflection from regular two-dimensional infinite array of bianisotropic particles situated near the surface of a dielectric shield (a metal-backed dielectric layer). We have to study the individual particle response separately in terms of the particle polarizabilities using antenna model. Then we study the analytical model of electromagnetic interaction between particles and between particles and dielectric shield. Finally we express dipole moments of arbitrary particle via an incident plane electromagnetic wave using self-consistency model and it leads us to reflection coefficient of structure. The numerical calculations are made for the structure with omega-particles.

1. Introduction

The problem of the plane electromagnetic wave reflection from various arrays (grids) of scatterers substrated by dielectric half-space or multilayer dielectric or dielectric-metal structures has been studied in the abundant literature. These works have a common feature: the problem can be strictly solved numerically within the frame of the so-called cell formulation. This formulation is based on the periodicity of the grid and yields to the boundary integral equations (BIE) for a unit cell. However, if one deals with the grids of bianisotropic particles or particles with three-dimensional geometry this problem hardly be explicitly solved using boundary conditions for the scatterer surface together with the boundary conditions for the shield. This way is very complicated for numerical solving therefore we propose to consider particles as dipoles and to study analytically the electromagnetic interaction in the grid in the presence of shield to evaluate their dipole moments and then to evaluate reflection coefficient of structure.

2. Theory

To solve the problem consider the particles as a couple of electric p and magnetic m dipoles with four known polarizabilities, expressing **p** and **m** via local fields **E** and **H** (If the particles are small compared to the wavelength but have a complex shape their response can be described by a couple of an electric dipole and magnetic dipole):

$$\begin{cases} \mathbf{p} = \overline{\overline{a}}_{ee}\mathbf{E} + \overline{\overline{a}}_{em}\mathbf{H} \\ \mathbf{m} = \overline{\overline{a}}_{me}\mathbf{E} + \overline{\overline{a}}_{mm}\mathbf{H} \end{cases} \quad (1)$$

In the theory of the arrays in free-space, that we developed in [3,4], the local fields can be splitted in two parts: the incident wave fields $\mathbf{E}_0, \mathbf{H}_0$ and the fields $\mathbf{E}_g, \mathbf{H}_g$ produced by all other particles:

$$\begin{cases} \mathbf{E} = \mathbf{E}_0 + \mathbf{E}_g \\ \mathbf{H} = \mathbf{H}_0 + \mathbf{H}_g \end{cases} \tag{2}$$

for $\mathbf{E}_g, \mathbf{H}_g$ we obtain:

$$\begin{cases} \mathbf{E}_g = \sum\limits_{m,n=-\infty}^{+\infty} \mathbf{E}_p^{m,n} + \sum\limits_{m,n=-\infty}^{+\infty} \mathbf{E}_m^{m,n} \\ \mathbf{H}_g = \sum\limits_{m,n=-\infty}^{+\infty} \mathbf{H}_p^{m,n} + \sum\limits_{m,n=-\infty}^{+\infty} \mathbf{H}_m^{m,n} \end{cases} \tag{3}$$

there upper index is the position of particle in array (we exclude zero-particle, so $m^2 + n^2 \neq 0$), and lower index is the type of dipole produced field.

In the case of the normal incidence the dipole moments of different particles are simply equal to each other. In the case of oblique incidence we have a phase shift between fields acting on particles. It allows to express $\mathbf{E}_g, \mathbf{H}_g$ via **p**, **m:**

$$\begin{cases} \mathbf{E}_g = \overline{\overline{A}}_{ee}\mathbf{p} + \overline{\overline{A}}_{em}\mathbf{m} \\ \mathbf{H}_g = \overline{\overline{A}}_{me}\mathbf{p} + \overline{\overline{A}}_{mm}\mathbf{m} \end{cases} \tag{4}$$

there $A_{\alpha\beta}$ are double sums of fields of dipoles. And then, solving an algebraic set, to evaluate **p**, **m** through $\mathbf{E}_0, \mathbf{H}_0$:

$$\begin{cases} \mathbf{p} = \overline{\overline{F}}_{ee}\mathbf{E}_0 + \overline{\overline{F}}_{em}\mathbf{H}_0 \\ \mathbf{m} = \overline{\overline{F}}_{me}\mathbf{E}_0 + \overline{\overline{F}}_{mm}\mathbf{H}_0 \end{cases} \tag{5}$$

Then we can easily obtain reflection coefficient of structure [4]:

$$\begin{aligned} \overline{\overline{R}} &= Z_e \overline{\overline{T}}\,\overline{\overline{F}}_{ee} + Z_e \eta \overline{\overline{T}}\,\overline{\overline{F}}_{em}\,\overline{\overline{S}} + Z_{em}^{me} \overline{\overline{S}}\,\overline{\overline{F}}_{me} + Z_{em}^{me} \eta \overline{\overline{S}}\,\overline{\overline{F}}_{me}\,\overline{\overline{S}} \\ \overline{\overline{T}} &= \overline{\overline{I}} + Z_e \overline{\overline{T}}\,\overline{\overline{F}}_{ee} + Z_e \eta \overline{\overline{T}}\,\overline{\overline{F}}_{em}\,\overline{\overline{S}} - Z_{em}^{me} \overline{\overline{S}}\,\overline{\overline{F}}_{me} - Z_{em}^{me} \eta \overline{\overline{S}}\,\overline{\overline{F}}_{me}\,\overline{\overline{S}} \end{aligned} \tag{6}$$

where $Z_e, Z_m, Z_{em}^{me}, \overline{\overline{T}}, \overline{\overline{S}}$ are known constants and dyadics [4].

For the structures that we consider in present work (array substrated by dielectric shield) we apply the same procedure to solve the problem.

Split the fields **E**, **H** in (1) on three parts: the incident wave fields $\mathbf{E}_0, \mathbf{H}_0$, the fields $\mathbf{E}_g, \mathbf{H}_g$ produced by all the grid particles except the reference one and the fields $\mathbf{E}_s, \mathbf{H}_s$ produced by the shield:

$$\begin{cases} \mathbf{E} = \mathbf{E}_0 + \mathbf{E}_g + \mathbf{E}_{sh} \\ \mathbf{H} = \mathbf{H}_0 + \mathbf{H}_g + \mathbf{H}_{sh} \end{cases} \tag{2'}$$

Here $\mathbf{E}_{sh}, \mathbf{H}_{sh}$ are results of the shield polarization by the incident wave and by particles of the grid, so:

$$\begin{cases} \mathbf{E}_{sh} = \mathbf{E}_1 + \mathbf{E}_2 \\ \mathbf{H}_{sh} = \mathbf{H}_1 + \mathbf{H}_2 \end{cases} \tag{7}$$

Here the first terms are fields of the first part of the shield polarization, induced by incident wave:

$$\begin{cases} \mathbf{E}_1 = \overline{\overline{R}}_s \mathbf{E}_0 \\ \mathbf{H}_1 = \overline{\overline{R}}_s \mathbf{H}_0 \end{cases} \tag{8}$$

where R_S is the known reflection coefficient of the shield (see [2]). $\mathbf{E}_2, \mathbf{H}_2$ are fields produced by second part of the shield polarization (induced by all the particles of the grid). We can split $\mathbf{E}_2, \mathbf{H}_2$ into two parts:

$$\begin{cases} \mathbf{E}_2 = \mathbf{E}_{g'} + \mathbf{E}_s \\ \mathbf{H}_2 = \mathbf{H}_{g'} + \mathbf{H}_s \end{cases} \tag{9}$$

there $\mathbf{E}_{g'}, \mathbf{H}_{g'}$ are the fields of the shield polarization induced by all the particles of the grid except zero-particle and $\mathbf{E}_s, \mathbf{H}_s$ are the fields of the shield polarization induced by zero-particle.

Substituting (7)-(9) into (2') we obtain:

$$\begin{cases} \mathbf{E} = \mathbf{E}_0 + (\mathbf{E}_g + \mathbf{E}_{g'}) + R_s \mathbf{E}_0 + \mathbf{E}_s \\ \mathbf{H} = \mathbf{H}_0 + (\mathbf{H}_g + \mathbf{H}_{g'}) + R_s \mathbf{H}_0 + \mathbf{H}_s \end{cases} \tag{2''}$$

For $(\mathbf{E}_g + \mathbf{E}_{g'}), (\mathbf{H}_g + \mathbf{H}_{g'})$ we can write the following expression:

$$\begin{cases} \mathbf{E}_g + \mathbf{E}_{g'} = \sum\limits_{m,n=-\infty}^{+\infty} \tilde{\mathbf{E}}_p^{m,n} + \sum\limits_{m,n=-\infty}^{+\infty} \tilde{\mathbf{E}}_m^{m,n} \\ \mathbf{H}_g + \mathbf{H}_{g'} = \sum\limits_{m,n=-\infty}^{+\infty} \tilde{\mathbf{H}}_p^{m,n} + \sum\limits_{m,n=-\infty}^{+\infty} \tilde{\mathbf{H}}_m^{m,n} \end{cases} \tag{3'}$$

there $\tilde{\mathbf{E}}_{p,m}, \tilde{\mathbf{H}}_{p,m}$ are the fields of dipoles in presence of dielectric shield. Analytical expressions for $\tilde{\mathbf{E}}_{p,m}, \tilde{\mathbf{H}}_{p,m}$ we can obtain from [1]. In this work we find out the analytical expression for $\mathbf{E}_s, \mathbf{H}_s$ (so called self-action field) through **p**, **m**:

$$\mathbf{E}_s(z) = -\frac{\omega\mu_0}{4\pi k_0} e^{2ik_0 z} \left[\frac{ik_0}{2z} - \frac{1}{4z^2} - \frac{i}{8k_0 z^3} - \varepsilon\left(\frac{ik_0}{z} - \frac{1}{2z^2} \right) + \varepsilon^2 \left(\frac{ik_0(2\varepsilon+1)}{z(\varepsilon+1)} - \frac{1}{2z^2} - \frac{i}{4k_0 z^3} \right) \right] \mathbf{p}$$

So, finally substituting (2") with (3') and (9) into (1) we express induced dipole moments of the particle via incident wave (5). The wave reflected from the structure is considered as a sum of re-radiation of the electric and magnetic dipoles of the array particles and re-radiation of the shield. Though the shield is excited by all the spatial harmonics produced by the grid the shield contribution into the reflected wave is results from the wave transmitting through the grid. Therefore we obtain for the reflection coefficient:

$$R_\Omega = R + TR_S e^{2jkh} \tag{10}$$

where R and T are grid reflection and transmission coefficients, h is the grid altitude.

3. Numerical Calculations

The numerical calculation based on the formulae given above have been carried out for grid of omega-particles over metal-backed dielectric layer with following parameters (see Fig.1): grid periods a=b=15 mm, h=1..15 mm, l=1 mm, $\varepsilon = 5+2j$ (relative permittivity). Geometrical parameters of particles: R=2 mm (radius of loop), l=2 mm (length of the stem), r=0.05 mm (wire radius). The individual polarizabilities of particles calculated with use of antenna model and results [5]. On Figure 2 we present the absolute value of reflection coefficient of structure for h=1 (mark as 1), 5 (2), 10 (3) mm for frequency band f=5..15 GHz. Notice that the self-action model describe the resonance frequency shift (well-known experimental effect). Also we see that the reflectance from the shield (with weak attenuation) is reduced by the grid to 20-25% of initial value.

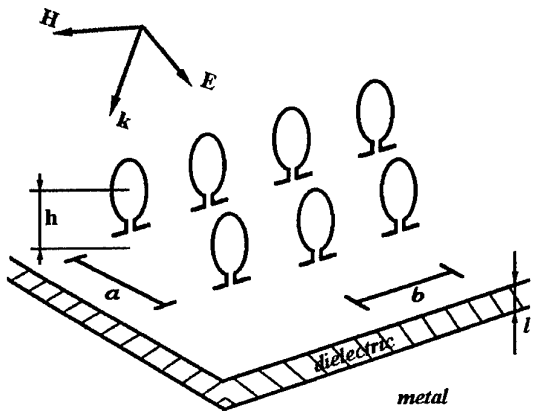

Fig. 1 Grid of omega-particles over dielectric shield.

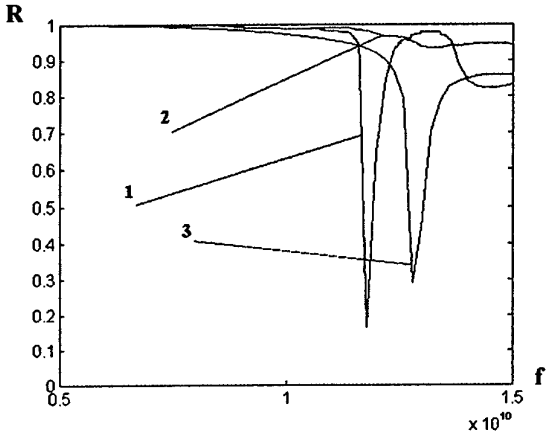

Fig. 2 Reflection coefficient depending on frequency.

4. Conclusion

We obtain analytical describing of reflection coefficients and induced dipole moment of structures consisting of regular two-dimensional infinite array of bianisotropic particles situated near the surface of a dielectric shield (a metal-backed dielectric layer). The theory taking into account electromagnetic interaction between scatterers and dielectric.

References

[1] R. W. P. King, "The electromagnetic field of a horizontal electric dipole in the presence of a three-layered region", *J. Appl. Phys.*, vol. 69, no. 12, pp. 7987-7995, 1991.

[2] C. R. Simovski, M. S. Kondratjev, and S. He, "Array of C-shaped wire elements for the reduction of reflection from a conducting plane", *Microwave and Optics Tech. Letters*, vol. 22, no. 6, 2000.

[3] C. R. Simovski, M. S. Kondratjev, P. A. Belov, and S. A. Tretyakov, "Interaction effects in two-dimensional bianisotropic arrays", *IEEE Transactions on Antennas and Propagation*, vol. 47, no. 9, pp. 1429-1439, 1999.

[4] M. S. Kondratjev, C. R. Simovski, and P. A. Belov, "Reflection and transmission of plane waves in bianisotropic planar grids", in *Proc. of SPIE 5th Symp. on Smart Structures and Materials*, San Diego, USA, pp. 669-678, 1998.

[5] S. A. Tretyakov, C. R. Simovski, F. Mariotte, and T. G. Kharina, "Scattering by a single omega-shaped conductive particle and omega composite modeling", in *Proc. of URSI Intern. Symp.*, St. Petersburg, Russia, pp. 639-635, 1995.

Session 8

Thursday - September 28, 2000

16:30 - 17:30

Complex Media II

Session 8

Interaction of Bianisotropic Particles and Energy Conservation in Regular Arrays

S. I. Maslovski[1], S. A. Tretyakov[2], and V. V. Yatsenko[1]

[1] Radiophysics Department
St. Petersburg State Technical University
Politekhnicheskaya 29, 195251 St. Petersburg, Russia
E-mail: stas@radio.stu.neva.ru

[2] Electromagnetics Laboratory, Helsinki University of Technology
P.O. Box 3000, FIN-02015 HUT, Finland
E-mail: sergei.tretyakov@hut.fi

Abstract

Interaction of bianisotropic particles in plane regular arrays is under investigation in this paper. We give a recipe on how to use the particle polarizabilities and the interaction constants obtained from approximate models so that the energy balance is satisfied and the physics of the phenomena is kept. Numerical examples are given for arrays of omega particles.

1. Introduction

To solve a diffraction problem for an array of scattering particles one should, at first, know the properties of an isolated inclusion given by its polarizability and, second, how the inclusions interact in the array. The polarizabilities as well as the interaction fields often cannot be calculated exactly. The aim of this paper is to give a method which will allow us to use the polarizabilities and the interaction coefficients obtained by approximate models so that the reflection and transmission coefficients will satisfy the energy conservation principle.

2. Energy Conservation in Bianisotropic Arrays

Consider a plane regular array of scattering particles. We will assume that the particles may be represented as combinations of electric and magnetic dipoles. Thus, every particle is characterized by its dyadic polarizability factors $\overline{\overline{\alpha}}$:

$$\begin{aligned} \mathbf{p} &= \overline{\overline{\alpha}}_{ee} \cdot \mathbf{E}_{\text{loc}} + \overline{\overline{\alpha}}_{em} \cdot \mathbf{H}_{\text{loc}} \\ \mathbf{m} &= \overline{\overline{\alpha}}_{me} \cdot \mathbf{E}_{\text{loc}} + \overline{\overline{\alpha}}_{mm} \cdot \mathbf{H}_{\text{loc}} \end{aligned} \tag{1}$$

We assume that the array is excited by a normally incident plane wave with the fields $\mathbf{E}_{\text{ext}}$ and $\mathbf{H}_{\text{ext}}$. Every particle is excited by the local fields

$$\mathbf{E}_{\text{loc}} = \mathbf{E}_{\text{ext}} + \overline{\overline{\beta}}_e \cdot \mathbf{p}, \qquad \mathbf{H}_{\text{loc}} = \mathbf{H}_{\text{ext}} + \overline{\overline{\beta}}_m \cdot \mathbf{m} \tag{2}$$

Here $\overline{\overline{\beta}}_e$ and $\overline{\overline{\beta}}_m$ are the interaction dyadics. These dyadics take into account interaction of the particles in the array. Under our assumptions the array of electric dipoles does not produce any magnetic interaction field and the array of magnetic dipoles does not produce any electric

interaction field. Due to this there are no cross terms in (2). As it was shown in our recent work [1] the interaction dyadics for the considered problem can be represented as

$$\overline{\overline{\beta}}_e = \mathrm{Re}(\overline{\overline{\beta}}_e) + j\frac{\eta\epsilon_0\mu_0\omega^3}{6\pi}\overline{\overline{I}} - j\frac{\eta\omega}{2S_0}\overline{\overline{I}}_t, \qquad \overline{\overline{\beta}}_m = \mathrm{Re}(\overline{\overline{\beta}}_m) + j\frac{\epsilon_0\mu_0\omega^3}{6\pi\eta}\overline{\overline{I}} - j\frac{\omega}{2\eta S_0}\overline{\overline{I}}_t \tag{3}$$

Here S_0 is unit cell area. As one can see, the last terms in the above relations correspond to the plane wave field contribution. We can express the local fields in terms of the induced dipole moments:

$$\begin{aligned} \mathbf{E}_{\mathrm{loc}} &= \left(\overline{\overline{\alpha}}_{ee} - \overline{\overline{\alpha}}_{em}\cdot\overline{\overline{\alpha}}_{mm}^{-1}\cdot\overline{\overline{\alpha}}_{me}\right)^{-1}\cdot\left(\mathbf{p} - \overline{\overline{\alpha}}_{em}\cdot\overline{\overline{\alpha}}_{mm}^{-1}\cdot\mathbf{m}\right) \\ \mathbf{H}_{\mathrm{loc}} &= \left(\overline{\overline{\alpha}}_{mm} - \overline{\overline{\alpha}}_{me}\cdot\overline{\overline{\alpha}}_{ee}^{-1}\cdot\overline{\overline{\alpha}}_{em}\right)^{-1}\cdot\left(\mathbf{m} - \overline{\overline{\alpha}}_{me}\cdot\overline{\overline{\alpha}}_{ee}^{-1}\cdot\mathbf{p}\right) \end{aligned} \tag{4}$$

The external fields, as follows from (2), can be written as

$$\begin{aligned} \mathbf{E}_{\mathrm{ext}} &= \left(\overline{\overline{\alpha}}_{ee} - \overline{\overline{\alpha}}_{em}\cdot\overline{\overline{\alpha}}_{mm}^{-1}\cdot\overline{\overline{\alpha}}_{me}\right)^{-1}\cdot\left(\mathbf{p} - \overline{\overline{\alpha}}_{em}\cdot\overline{\overline{\alpha}}_{mm}^{-1}\cdot\mathbf{m}\right) - \overline{\overline{\beta}}_e\cdot\mathbf{p} \\ \mathbf{H}_{\mathrm{ext}} &= \left(\overline{\overline{\alpha}}_{mm} - \overline{\overline{\alpha}}_{me}\cdot\overline{\overline{\alpha}}_{ee}^{-1}\cdot\overline{\overline{\alpha}}_{em}\right)^{-1}\cdot\left(\mathbf{m} - \overline{\overline{\alpha}}_{me}\cdot\overline{\overline{\alpha}}_{ee}^{-1}\cdot\mathbf{p}\right) - \overline{\overline{\beta}}_m\cdot\mathbf{m} \end{aligned} \tag{5}$$

The total averaged fields (plane wave fields) in the array plane read

$$\begin{aligned} \mathbf{E}_{\mathrm{tot}} &= \mathbf{E}_{\mathrm{ext}} - j\tfrac{\eta}{2}\tfrac{\omega}{S_0}\overline{\overline{I}}_t\cdot\mathbf{p} = \overline{\overline{Z}}_{ee}\cdot\mathbf{J} + \overline{\overline{Z}}_{em}\cdot\mathbf{J}_m \\ \mathbf{H}_{\mathrm{tot}} &= \mathbf{H}_{\mathrm{ext}} - j\tfrac{1}{2\eta}\tfrac{\omega}{S_0}\overline{\overline{I}}_t\cdot\mathbf{m} = \overline{\overline{Z}}_{me}\cdot\mathbf{J} + \overline{\overline{Z}}_{mm}\cdot\mathbf{J}_m \end{aligned} \tag{6}$$

Here, the currents $\mathbf{J}$ and $\mathbf{J}_m$ are not the average surface electric and magnetic currents. These vectors can be arbitrarily directed and they represent the normalized electric and magnetic dipole moments. The dyadic coefficients in (6) can be easily identified from the above formulas:

$$\overline{\overline{Z}}_{ee} = -j\frac{S_0}{\omega}\left[\left(\overline{\overline{\alpha}}_{ee} - \overline{\overline{\alpha}}_{em}\cdot\overline{\overline{\alpha}}_{mm}^{-1}\cdot\overline{\overline{\alpha}}_{me}\right)^{-1} - \overline{\overline{\beta}}_e - j\frac{\eta}{2}\frac{\omega}{S_0}\overline{\overline{I}}_t\right] \tag{7}$$

$$\overline{\overline{Z}}_{mm} = -j\frac{S_0}{\omega}\left[\left(\overline{\overline{\alpha}}_{mm} - \overline{\overline{\alpha}}_{me}\cdot\overline{\overline{\alpha}}_{ee}^{-1}\cdot\overline{\overline{\alpha}}_{em}\right)^{-1} - \overline{\overline{\beta}}_m - j\frac{1}{2\eta}\frac{\omega}{S_0}\overline{\overline{I}}_t\right] \tag{8}$$

$$\overline{\overline{Z}}_{em} = j\frac{S_0}{\omega}\left[\left(\overline{\overline{\alpha}}_{ee} - \overline{\overline{\alpha}}_{em}\cdot\overline{\overline{\alpha}}_{mm}^{-1}\cdot\overline{\overline{\alpha}}_{me}\right)^{-1}\cdot\overline{\overline{\alpha}}_{em}\cdot\overline{\overline{\alpha}}_{mm}^{-1}\right] \tag{9}$$

$$\overline{\overline{Z}}_{me} = j\frac{S_0}{\omega}\left[\left(\overline{\overline{\alpha}}_{mm} - \overline{\overline{\alpha}}_{me}\cdot\overline{\overline{\alpha}}_{ee}^{-1}\cdot\overline{\overline{\alpha}}_{em}\right)^{-1}\cdot\overline{\overline{\alpha}}_{me}\cdot\overline{\overline{\alpha}}_{ee}^{-1}\right] \tag{10}$$

Although different terms have different dimensions, we use the same notation Z for all of them. Indeed, only $\overline{\overline{Z}}_{ee}$ has the meaning of impedance.

Let us now suppose that the particles have no dissipation losses. Then, the energy conservation condition

$$\mathrm{Re}\{\mathbf{E}_{\mathrm{tot}}\cdot\mathbf{J}^* + \mathbf{J}_m\cdot\mathbf{H}_{\mathrm{tot}}^*\} = 0 \tag{11}$$

can be written in the dyadic form as

$$\begin{pmatrix}\mathbf{J}\\ \mathbf{J}_m\end{pmatrix}\cdot\begin{pmatrix}\overline{\overline{Z}}_{ee}^T + \overline{\overline{Z}}_{ee}^* & \overline{\overline{Z}}_{em}^* + \overline{\overline{Z}}_{me}^T\\ \overline{\overline{Z}}_{em}^T + \overline{\overline{Z}}_{me}^* & \overline{\overline{Z}}_{mm}^T + \overline{\overline{Z}}_{mm}^*\end{pmatrix}\cdot\begin{pmatrix}\mathbf{J}^*\\ \mathbf{J}_m^*\end{pmatrix} = 0 \tag{12}$$

Since this should be valid identically for all currents, we find that in lossless arrays

$$\overline{\overline{Z}}_{ee} + \overline{\overline{Z}}_{ee}^\dagger = 0, \qquad \overline{\overline{Z}}_{mm} + \overline{\overline{Z}}_{mm}^\dagger = 0 \tag{13}$$

$$\overline{\overline{Z}}_{em} + \overline{\overline{Z}}_{me}^{\dagger} = 0 \tag{14}$$

where † denotes the Hermite conjugate. Consider reciprocal particles. Then $\overline{\overline{Z}}_{ee}$ and $\overline{\overline{Z}}_{mm}$ are symmetric dyadics. Thus, (13) means that these dyadics are purely imaginary (and the bracketed expressions are purely real). In other words,

$$\mathrm{Im}\left\{\left(\overline{\overline{\alpha}}_{ee} - \overline{\overline{\alpha}}_{em}\cdot\overline{\overline{\alpha}}_{mm}^{-1}\cdot\overline{\overline{\alpha}}_{me}\right)^{-1}\right\} = \frac{\eta\epsilon_0\mu_0\omega^3}{6\pi}\overline{\overline{I}} \tag{15}$$

$$\mathrm{Im}\left\{\left(\overline{\overline{\alpha}}_{mm} - \overline{\overline{\alpha}}_{me}\cdot\overline{\overline{\alpha}}_{ee}^{-1}\cdot\overline{\overline{\alpha}}_{em}\right)^{-1}\right\} = \frac{\epsilon_0\mu_0\omega^3}{6\pi\eta}\overline{\overline{I}} \tag{16}$$

and similarly from (14):

$$\mathrm{Re}\left\{\left(\overline{\overline{\alpha}}_{ee} - \overline{\overline{\alpha}}_{em}\cdot\overline{\overline{\alpha}}_{mm}^{-1}\cdot\overline{\overline{\alpha}}_{me}\right)^{-1}\cdot\overline{\overline{\alpha}}_{em}\cdot\overline{\overline{\alpha}}_{mm}^{-1}\right\} = 0 \tag{17}$$

$$\mathrm{Re}\left\{\left(\overline{\overline{\alpha}}_{mm} - \overline{\overline{\alpha}}_{me}\cdot\overline{\overline{\alpha}}_{ee}^{-1}\cdot\overline{\overline{\alpha}}_{em}\right)^{-1}\cdot\overline{\overline{\alpha}}_{me}\cdot\overline{\overline{\alpha}}_{ee}^{-1}\right\} = 0 \tag{18}$$

The last two relations are equivalent since in reciprocal media $\overline{\overline{Z}}_{me} = -\overline{\overline{Z}}_{em}^{T}$. For a special case of omega particles with

$$\overline{\overline{\alpha}}_{ee} = a_{ee}^{xx}\mathbf{x}_0\mathbf{x}_0 + a_{ee}^{yy}\mathbf{y}_0\mathbf{y}_0, \quad \overline{\overline{\alpha}}_{mm} = a_{mm}\mathbf{z}_0\mathbf{z}_0, \quad \overline{\overline{\alpha}}_{me} = a_{me}\mathbf{z}_0\mathbf{y}_0, \quad \overline{\overline{\alpha}}_{em} = -a_{me}\mathbf{y}_0\mathbf{z}_0 \tag{19}$$

relations (15) and (16) give

$$\mathrm{Im}\left\{\frac{1}{a_{ee}^{xx}}\right\} = \frac{\eta\epsilon_0\mu_0\omega^3}{6\pi}, \qquad \mathrm{Im}\left\{\frac{a_{mm}}{a_{ee}^{yy}a_{mm} + a_{me}^2}\right\} = \frac{\eta\epsilon_0\mu_0\omega^3}{6\pi}$$
$$\mathrm{Im}\left\{\frac{a_{ee}^{yy}}{a_{ee}^{yy}a_{mm} + a_{me}^2}\right\} = \frac{\epsilon_0\mu_0\omega^3}{6\pi\eta} \tag{20}$$

Conditions (17) and (18) lead to the same result, which reads

$$\mathrm{Re}\left\{\frac{a_{me}}{a_{ee}^{yy}a_{mm} + a_{me}^2}\right\} = 0 \tag{21}$$

3. Reflection and Transmission Coefficients

Let us now make the final step. Our main goal is to find the reflection and transmission coefficients. It is easy to see that they can be found in terms of the introduced parameters (7)–(10). The parameters are expressed via the particle polarizabilities. In the usual practice we have the polarizabilities dyadics found from the antenna model or numerically. This gives approximate results and the values of alphas are not quite correct. We should somehow "correct" the polarizabilities to find the reflection and transmission coefficients which satisfy the energy conservation law.

From the other hand, the correction should not lead to significant difference in the array reflective properties. If we simply skip the scattering terms from the polarizabilities and the interaction dyadics, i.e. we take α_{ee} and α_{mm} as purely real, α_{em} and α_{me} as purely imaginary, and leave only plane wave contribution in the imaginary parts of betas, we easily satisfy the energy conservation conditions (15)–(18). But the frequency behaviour of the array reflection will change dramatically. It follows from (7)–(8): equating the scattering terms in the alphas to zero we change the values of dyadics $\overline{\overline{Z}}$. It suggests us to apply additional conditions to

avoid that. These conditions will keep the non-scattering terms of (7)–(8) unchanged when the scattering terms in alphas and betas are skipped. Doing so we obtain a system of equations on the new "corrected" polarizabilities $\overline{\overline{\alpha}}'_{ee}$, $\overline{\overline{\alpha}}'_{mm}$, $\overline{\overline{\alpha}}'_{em}$, and $\overline{\overline{\alpha}}'_{me}$. In more detail, the system is

$$\mathrm{Im}(\overline{\overline{\alpha}}'_{ee}) = \mathrm{Im}(\overline{\overline{\alpha}}'_{mm}) = 0, \qquad \mathrm{Re}(\overline{\overline{\alpha}}'_{em}) = 0 \tag{22}$$

and

$$\begin{aligned}
\left(\overline{\overline{\alpha}}'_{ee} - \overline{\overline{\alpha}}'_{em} \cdot \overline{\overline{\alpha}}'^{-1}_{mm} \cdot \overline{\overline{\alpha}}'_{me}\right)^{-1} &= \mathrm{Re}\left\{\left(\overline{\overline{\alpha}}_{ee} - \overline{\overline{\alpha}}_{em} \cdot \overline{\overline{\alpha}}^{-1}_{mm} \cdot \overline{\overline{\alpha}}_{me}\right)^{-1}\right\} \\
\left(\overline{\overline{\alpha}}'_{mm} - \overline{\overline{\alpha}}'_{me} \cdot \overline{\overline{\alpha}}'^{-1}_{ee} \cdot \overline{\overline{\alpha}}'_{em}\right)^{-1} &= \mathrm{Re}\left\{\left(\overline{\overline{\alpha}}_{mm} - \overline{\overline{\alpha}}_{me} \cdot \overline{\overline{\alpha}}^{-1}_{ee} \cdot \overline{\overline{\alpha}}_{em}\right)^{-1}\right\} \\
j\left(\overline{\overline{\alpha}}'_{ee} - \overline{\overline{\alpha}}'_{em} \cdot \overline{\overline{\alpha}}'^{-1}_{mm} \cdot \overline{\overline{\alpha}}'_{me}\right)^{-1} \cdot \overline{\overline{\alpha}}'_{em} \cdot \overline{\overline{\alpha}}'^{-1}_{mm} &= \\
-\mathrm{Im}\left\{\left(\overline{\overline{\alpha}}_{ee} - \overline{\overline{\alpha}}_{em} \cdot \overline{\overline{\alpha}}^{-1}_{mm} \cdot \overline{\overline{\alpha}}_{me}\right)^{-1} \cdot \overline{\overline{\alpha}}_{em} \cdot \overline{\overline{\alpha}}^{-1}_{mm}\right\}
\end{aligned} \tag{23}$$

The "corrected" polarizabilities together with the "corrected" betas (only plane wave contribution is included) will give the reflection and transmission satisfying the energy conservation law.

4. Numerical Results

We have numerically investigated the case of a double array of omega particles under the plane wave excitation. The polarizabilities were obtained from the antenna model described in [2]. The reflection coefficient values via the frequency together with the energy balance plot are given on Figure 1 and Figure 2. The solid lines correspond to the corrected alphas and betas, the dashed lines correspond to the original ones.

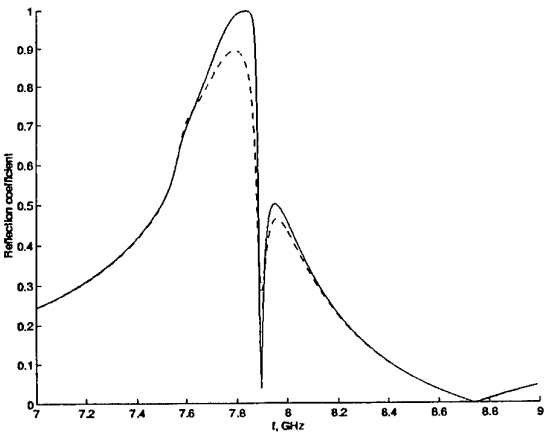

Figure 1: Reflection coefficient as function of frequency.

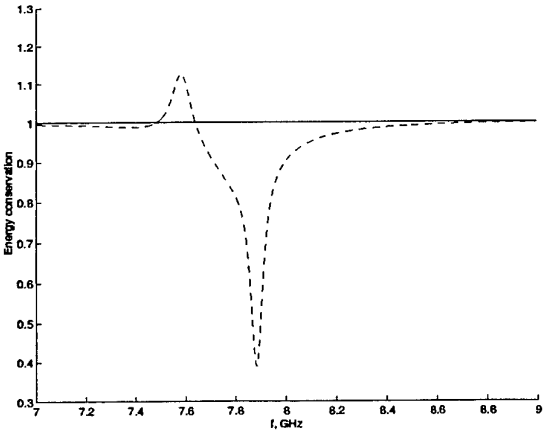

Figure 2: Energy conservation as function of frequency.

References

[1] S. A. Tretyakov, A. J. Viitanen, S. I. Maslovski, and I. E. Saarela, "Impedance boundary conditions for regular arrays of dipole scatterers," *Report 304*, Electromagnetics Laboratory, HUT, Helsinki, Finland, 1999, ISBN 951-22-4509-4.

[2] C. R. Simovski, S. A. Tretyakov, and A. A. Sochava, "Antenna model for conductive omega particles," *J. Electromagnetic Waves Applic.*, vol. 11, no. 11, pp. 1509-1530, 1997.

Effects of Anisotropy in Light Scattering by Anisotropic Layer around a Spherical Particle in Uniaxial Medium

A. D. Kiselev[1], V. Yu. Reshetnyak[2], and T. J. Sluckin[3]

[1] Department of Pure & Applied Mathematics,
Chernigov State Technological University,
Shevchenko Street 95, 14027 Chernigov, Ukraine
Fax: +380–46–22 34244; Email: kisel@elit.chernigov.ua

[2] Department of Theoretical Physics, Kiev State University,
Prospect Glushkova 6, 03680 Kiev, Ukraine

[3] Faculty of Mathematical Studies, University of Southampton,
Southampton SO17 1BJ, United Kingdom

Abstract

We have used a Mie–type theory to study the light scattering from an annular anisotropic layer around a spherical colloidal particle. We have derived an exact solution of the scattering problem in the case when the distribution of the optical axes around the particles posses some special transformation properties under rotation and, outside of the layer, the ambient medium is isotropic. We have then calculated the dependence of the the scattering cross-section on particle size, anisotropy parameter, and layer thickness for different optical axis distributions. We find that the scattering cross-section is strongly affected by the type of anisotropy. The presence of disclinations enhances scattering efficiency. We determine the region of validity of Rayleigh–Gans approximation by comparing approximate values of the scattering cross-section with the results computed from the exact solution. As an additional effect specific to anisotropic scatterer, it is found that for structures with broken central symmetry there is the phase shift proportional to the logarithm of layer thickness that enters the scattering amplitudes.

In order to study the case of anisotropic ambient medium, approximate theory has been developed. The phase shift is found to affect the scattering amplitudes even if the central symmetry is unbroken.

1. Introduction

There are a large number of physical contexts in which it is useful to understand light scattering by impurities [1]. A particular example of recent interest concerns liquid crystal devices. There are now a number of systems in which liquid crystal droplets are suspended in a polymer matrix – the so-called PDLC systems – or the inverse system, involving colloids now with a nematic liquid crystal solvent. The latter systems are commonly known as filled nematics [2, 3].

In such systems it is required to calculate the scattering of light by composite anisotropic particles embedded in an isotropic matrix. In this paper we discuss some model cases of light scattering by such particles, which may be supposed to represent local liquid crystalline director structures, using both the Mie and the Rayleigh-Gans (R-G) approaches.

The large majority of exact solutions of the single-scattering problem have been derived for isotropic scatterers [4]. However, there are a few cases for which Mie theory has been extended to the case of anisotropic scatterers[5, 6, 7, 8].

In order that the problem have an analytic solution, we find it necessary to restrict consideration to cases in which the optical axis distributions within the anisotropic layer around the core possess some special symmetry properties under rotation. The analysis is then based on a systematic expansion of the electromagnetic field over vector spherical harmonics [9, 10]. The specific form of the expansions is known as the T-matrix ansatz. This has been widely used in the related problem of light scattering by nonspherical particles [11].

In this study we investigate the dependence of light scattering from the layer on the internal structure of the optical tensor, and implicitly on the liquid crystal director texture. We also compare our exact results with those obtained by the simpler but less accurate R-G method. For brevity, in what follows we shall leave aside the details on this comparison and do not discuss extensions of the theory.

2. Scatterers

We consider scattering by a spherical particle of radius R_1 embedded in a uniform isotropic dielectric medium with dielectric constant $\epsilon_{ij} = \epsilon\delta_{ij}$ and magnetic permeability $\mu_{ij} = \mu\delta_{ij}$. The scattering particle consists of an inner isotropic core of radius R_2, surrounded by an anisotropic annular layer of thickness $d = R_1 - R_2$.

Within the inner core of the scatterer the dielectric tensor ϵ, and the magnetic permittivity μ take the values $\epsilon_{ij} = \epsilon_2\delta_{ij}$, $\mu_{ij} = \mu_2\delta_{ij}$. The dielectric tensor within the annular layer is locally uniaxial. The optical axis distribution is defined by the vector field $\hat{\mathbf{n}}$. (Hats will denote unit vectors.) Then within the annular layer $\epsilon_{ij}(\mathbf{r}) = \epsilon_1\delta_{ij} + \Delta\epsilon_1(\hat{\mathbf{n}}(\mathbf{r}) \otimes \hat{\mathbf{n}}(\mathbf{r}))_{ij}$ and $\mu_{ij} = \mu_1\delta_{ij}$. The unit vector $\hat{\mathbf{n}}$ corresponds to a liquid crystal director for material within the annular region.

We shall suppose that the director field can be written in the following form

$$\hat{\mathbf{n}} = n_r\hat{\mathbf{r}} + n_\varphi\hat{\boldsymbol{\varphi}} + n_\vartheta\hat{\boldsymbol{\vartheta}}, \tag{1}$$

where $\hat{\mathbf{r}}$ is the unit radial vector and $\hat{\boldsymbol{\varphi}}$, $\hat{\boldsymbol{\vartheta}}$ are the vectors tangential to the unit sphere. The components $n_r, n_\varphi, n_\vartheta$ are constants.

3. Generalized Mie Theory

The electromagnetic field can be expanded using the vector spherical harmonic basis, $\mathbf{Y}_{j+\delta\, jm}(\phi,\theta) \equiv \mathbf{Y}_{j+\delta\, jm}(\hat{\mathbf{r}})$ $(\delta = 0, \pm 1)$ [9] as follows:

$$\mathbf{E} = \sum_{jm}\mathbf{E}_{jm} = \sum_{jm}\left[p^{(0)}_{jm}(r)\mathbf{Y}^{(0)}_{jm}(\hat{\mathbf{r}}) + p^{(e)}_{jm}(r)\mathbf{Y}^{(e)}_{jm}(\hat{\mathbf{r}}) + p^{(m)}_{jm}(r)\mathbf{Y}^{(m)}_{jm}(\hat{\mathbf{r}})\right], \tag{2a}$$

$$\mathbf{H} = \sum_{jm}\mathbf{H}_{jm} = \sum_{jm}\left[q^{(0)}_{jm}(r)\mathbf{Y}^{(0)}_{jm}(\hat{\mathbf{r}}) + q^{(e)}_{jm}(r)\mathbf{Y}^{(e)}_{jm}(\hat{\mathbf{r}}) + q^{(m)}_{jm}(r)\mathbf{Y}^{(m)}_{jm}(\hat{\mathbf{r}})\right], \tag{2b}$$

where $\mathbf{Y}^{(m)}_{jm} = \mathbf{Y}_{jjm}$ and $\mathbf{Y}^{(e)}_{jm} = [j/(2j+1)]^{1/2}\mathbf{Y}_{j+1\,jm} + [(j+1)/(2j+1)]^{1/2}\mathbf{Y}_{j-1\,jm}$ are electrical and magnetic harmonics respectively, and $\mathbf{Y}^{(0)}_{jm} = [j/(2j+1)]^{1/2}\mathbf{Y}_{j-1\,jm} - [(j+1)/(2j+1)]^{1/2}\mathbf{Y}_{j+1\,jm}$ are longitudinal harmonics.

Outside the scatterer $p^{(\alpha)}_{jm}(r)$ and $q^{(\alpha)}_{jm}(r)$ can be expressed in terms of linear combinations of spherical Bessel functions and spherical Hankel functions. For the incident and scattered waves

in the far field region we have:

$$\mathbf{E}_{inc} = \sum_{jm} \left(\alpha_{jm}^{(inc)} j_j(\rho) \mathbf{Y}_{jm}^{(m)} + \tilde{\alpha}_{jm}^{(inc)} D j_j(\rho) \mathbf{Y}_{jm}^{(e)} \right), \tag{3}$$

$$\mathbf{E}_{sca} = \sum_{jm} \left(\beta_{jm}^{(sca)} h_j^{(1)}(\rho) \mathbf{Y}_{jm}^{(m)} + \tilde{\beta}_{jm}^{(sca)} D h_j^{(1)}(\rho) \mathbf{Y}_{jm}^{(e)} \right), \tag{4}$$

where $\rho = kr$ and $Df(x) \equiv x^{-1} \dfrac{\mathrm{d}}{\mathrm{d}x}(xf(x))$. Since the scattering problem is linear, the coefficients $\{\beta_{jm}^{(sca)}, \tilde{\beta}_{jm}^{(sca)}\}$ are linearly related to $\{\alpha_{jm}^{(inc)}, \tilde{\alpha}_{jm}^{(inc)}\}$ through the elements of the T–matrix.

In order to derive the T–matrix, we need to find the general expressions for the electromagnetic field inside the anisotropic layer and the isotropic core. The ingoing and outgoing waves then can be related by using continuity of the tangential components of the electric and magnetic fields at $r = R_2$ and $r = R_1$ as boundary conditions.

Substituting the expansions (2) into the Maxwell equations gives a system of equations for the components $p_{jm}^{(\alpha)}$ and $q_{jm}^{(\alpha)}$. For the distributions (1) we have found that the system can be reduced to a system of coupled Bessel equations for the magnetic components: $\{p_{jm}^{(m)}, q_{jm}^{(m)}\}$. For the structures $\hat{\mathbf{n}} = \hat{\boldsymbol{\vartheta}}$ and $\hat{\mathbf{n}} = \cos\gamma\,\hat{\mathbf{r}} + \sin\gamma\,\hat{\boldsymbol{\varphi}}$ solutions of this system can be obtained in the closed form. The result for transverse components is

$$p_{jm}^{(m)} = \alpha_{jm} j_j(\rho_e) + \beta_{jm} h_j^{(1)}(\rho_e), \quad q_{jm}^{(e)} = n_e/\mu_1 \, D p_{jm}^{(m)}(\rho_e), \tag{5a}$$

$$q_{jm}^{(m)} \equiv \tilde{\rho}_e^{i\delta_j} \tilde{q}_{jm}^{(m)} = \tilde{\rho}_e^{i\delta_j} \left[\tilde{\alpha}_{jm} j_{\tilde{j}}(\tilde{\rho}_e) + \tilde{\beta}_{jm} h_{\tilde{j}}^{(1)}(\tilde{\rho}_e) \right], \quad p_{jm}^{(e)} = -\mu_1/\tilde{n}_e \, \tilde{\rho}_e^{i\delta_j} \, D\tilde{q}_{jm}^{(m)}(\tilde{\rho}_e), \tag{5b}$$

$$\tilde{j}(\tilde{j}+1) = \frac{1 + u_1(1 - n_\vartheta^2)}{(1 + u_1 n_r^2)^2} j(j+1), \quad \delta_j = \tilde{u}_1 \tilde{m}_e^2 \sqrt{j(j+1)}\, n_\varphi n_r, \tag{5c}$$

$$u_1 \equiv \Delta\epsilon_1/\epsilon_1, \quad m_e^2 = \frac{1 + u_1}{1 + u_1(1 - n_\vartheta^2)}, \quad \tilde{m}_e^2 = \frac{1 + u_1(1 - n_\vartheta^2)}{1 + u_1 n_r^2}, \tag{5d}$$

where α_{jm} and β_{jm} are integration constants; $\rho_e = m_e \rho_1 = m_e k_1 r$ and $\tilde{\rho}_e = \tilde{m}_e \rho_1$. For brevity, the corresponding rather cumbersome expressions for the T–matrix have been omitted. It is seen, that anisotropy affects the analytical expressions in the following manner: (a) it renormalizes the order of corresponding Bessel functions; (b) it changes the arguments of the functions by replacing k_1 with k_e; (c) it leads to the appearance of the geometric factor $\propto \rho^{i\delta_j}$ for the tilted configuration.

4. Scattering Efficiency

In this section we discuss briefly the results concerning the scattering efficiency, Q, that is the ratio of the total scattering cross section C_{sca} and area of the composite particle, $S = \pi R_1^2$.

Dependence of the scattering efficiency Q on the dimensionless size parameter kR_2, is depicted in Figs. 1. It is assumed that refractive indexes of the surrounding medium and the isotropic core are equal, $n = n_2$. Clearly, the scattering cross section is strongly affected by the type of anisotropy characterizing by the unit vector $\hat{\mathbf{n}}$. Fig. 1 shows that the structure $\hat{\mathbf{n}} = \hat{\boldsymbol{\varphi}}$ has the largest value of Q at small kR_2, whereas the least scattering efficiency corresponds to the configuration with $\hat{\mathbf{n}} = \hat{\boldsymbol{\vartheta}}$. We found that the helical structure $\hat{\mathbf{n}} = \hat{\boldsymbol{\varphi}}$ remains the most efficient scatterer with increase in the anisotropy parameter u_1 for sufficiently small particle size. On the other hand, Fig. 1 reveals that the configuration $\hat{\mathbf{n}} = \hat{\boldsymbol{\vartheta}}$ becomes the most efficient scatterer as size of the scatterer increases.

Acknowledgement
This work is performed under INTAS grant 97–1315.

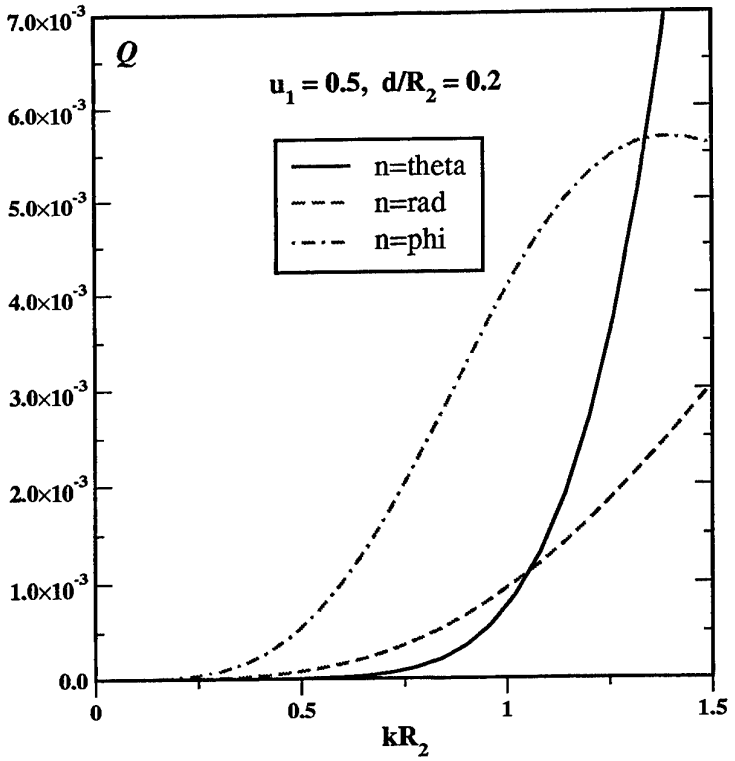

FIGURE 1: Dependence of Q on the size parameter kR_2 at $u_1 = 0.5$ and $d/R_2 = 0.2$ for different types of anisotropy. It is shown that the scattering efficiency reveals crossover behaviour in this range of size parameters.

References

[1] A. Ishimaru, *Wave Propagation and Scattering in Random Media.* London: Academic Press, 1978.

[2] M. Kreuzer and R. Eidenschink, in *Liquid Crystals in Complex Geometries*, G. P. Crawford and S. Žumer (Eds.), Chap. 15. London: Taylor & Francis, 1996.

[3] T. Bellini, N. A. Clark, V. Degiorgio, F. Mantegazza, and G. Natale, "Light scattering measurement of the nematic correlation length in a liquid crystal with quenched disorder," *Phys. Rev. E.*, vol. 57, pp. 2996-3006, 1998.

[4] C. F. Boren and D. R. Huffman, *Absorption and Scattering of Light by Small Particles.* New York: Wiley, 1983.

[5] J. Roth and M. J. Digman, "Scattering and extinction cross sections for a spherical particle coated with an oriented molecular layer," *JOSA*, vol. 63, pp. 308–311, 1973.

[6] B. Lange and S. R. Aragon, "Mie scattering from anisotropic thin spherical shells," *J. Chem. Phys.*, vol. 92, pp. 4643–4650, 1990.

[7] D. K. Hahn and S. R. Aragon, "Mie scattering from anisotropic thick spherical shells," *J. Chem. Phys.*, vol. 101, pp. 8409–8417, 1994.

[8] H. Karacali, S. M. Risseler, and K. F. Ferris, "Scattering of light from small nematic spheres with radial dielectric anisotropy," *Phys. Rev. E.*, vol. 56, pp. 4286–4293, 1997.

[9] L. C. Biedenharn and J. D. Louck, *Angular Momentum in Quantum Physics.* Massachusetts: Addison–Wesley, 1981.

[10] R. G. Newton, *Scattering Theory of Waves and Particles.* London: McGraw Hill, 1966.

[11] M. I. Mishchenko, L. D. Travis, and D. W. Mackowski, "T–matrix computations of light scattering by nonspherical particles: A review," *J. of Quant. Spectr. & Radiat. Transf.*, vol. 55, pp. 535–575, 1996.

Switching and Rectification of Phonon Polaritons of an Insulator at its Boundary with a Metal

I. E. Chupis[1] and D. A. Mamaluy[2]

[1] B. Verkin Institute for Low Temperature Physics & Engineering
47 Lenin Avenue, 61164 Kharkov, Ukraine
E-mail: Chupis@ilt.kharkov.ua

[2] E-mail: Mamaluy@ilt.kharkov.ua

Abstract

The existence of surface polaritons in an insulator at its boundary with an ideal metal or a superconductor in a constant electric or magnetic field is predicted. The modes of these surface polaritons appreciably differ in opposite directions of the field, so that a change in the direction of the field signifies "switching on" or "switching off" of surface polaritons. In the presence of a magnetic field polaritons of a given frequency propagate only in one direction with respect to the magnetic field, which is the effect of rectification. The existence of a radiant surface polariton modes is predicted.

1. Introduction

It is well known that in massive insulator at its boundary with an ideal metal, surface polaritons do not exist [1]. We have shown that surface polaritons appear in the presence of a constant electric field directed along a normal to the contact plane [2] or in a magnetic field oriented in a contact plane [3]. Surface phonon polaritons appear due to a dynamic magnetoelectric (ME) interaction [4] and their penetration depth is inversely proportional to the value of the field. The modes of these polaritons belong to IR or optical regions of the spectrum and substantially depend on the directions of the fields and the propagation of the wave.

2. The Energy of Optical Phonons

For definiteness, we assume the insulator to be uniaxial (Z is the easy axis). The energy density W of optical phonons in external electric $\vec{E}$ and magnetic $\vec{H}$ fields can be written as

$$W = \frac{C_1}{2} P_z^2 + \frac{C_2}{2}\left(P_x^2 + P_y^2\right) + \frac{\Pi^2}{2\rho} - \vec{P}\vec{E} + \frac{1}{c\rho}\vec{P}\left[\vec{\Pi}\times\vec{H}\right] \qquad (1)$$

Here $\vec{P}$ is the electric polarization, $\vec{\Pi}$ is the momentum density, $\vec{E} = \vec{E}_0 + \vec{e}$, $\vec{H} = \vec{H}_0 + \vec{h}$; $\vec{E}_0, \vec{H}_0$ are constant fields, $\vec{e}$ and $\vec{h}$ are alternating electric and magnetic fields; c is velocity of light; $\rho = m/V_0$, where m is the mass of a charge, V_0 is the elementary cell volume. Generally the electric polarization consists of ion and electron parts. In the IR region of the spectrum the contribution of ions to the

polarization is predominant, then m is the reduced mass of an ion-cation pair and $\vec{\Pi}$ is the elementary-cell moment. In the optical region of the spectrum the electron contribution to the polarization is much greater than the ionic one, then m is the electron mass and $\vec{\Pi}$ is the electron momentum. The last term in (1) corresponds to the dynamic ME energy [4]. This energy is a scalar so it is present in the energy of any crystal.

ME energy gives the contribution in an electric ($\vec{d}$) and magnetic ($\vec{b}$) inductions,

$$d_i = \varepsilon_{ik} e_k + 4\pi\chi_{ik}^{em} h_k,\ b_i = \mu_{ik} h_k + 4\pi\chi_{ik}^{em} e_k, \tag{2}$$

where ME susceptibility

$$\chi_{ik}^{em} = \frac{\partial P_i}{\partial h_k} = \left(\chi_{ki}^{me}\right)^* = \left(\frac{\partial m_k}{\partial e_i}\right)^* \tag{3}$$

3. Surface Phonon Polaritons in Electric Field

We consider a semi-infinite insulator ($z>0$) which is in contact with an ideal metal ($z<0$) in a constant electric field $\vec{E}_0$ directed along the Z axis. Polaritons propagate along the X axis. The solution of the Maxwell equations for an insulator with inductions (2) and $\mu_{ik} = \delta_{ik}$ in the absence of damping we take in the form

$$\vec{e}, \vec{h} \propto \exp\left[i(kx - \omega t) - k_0 z\right],\ k_0 \geq 0,\ z \geq 0 \tag{4}$$

where $k_0^{-1} = \delta_E$ is the depth of penetration of the field. At the boundary with an ideal metal $e_x = e_y = 0$ and without ME susceptibility surface polaritons do not exist because $d_x = 0$. In the presence of a constant electric field $\vec{E}_0$ directed along a normal to a contact plane the ME susceptibility χ_{ik}^{em} appears and takes the contribution in electric induction d_x,

$$\chi_{xy}^{em} = \frac{i\omega g P_0}{\omega^2 - \omega_0^2},\ P_0 = C_1^{-1} E_0,\ \delta_E = \frac{c\left(\omega^2 - \omega_0^2\right)}{4\pi\omega^2 g P_0}$$
$$\omega_0 = \tilde{\omega}_0 \sqrt{C_2},\ g = e/mc,\ \tilde{\omega}_0^2 = e^2/mV_0. \tag{5}$$

Surface polaritons appear with the penetration depth δ_E which is inversely proportional to the value of electric field $\vec{E}_0$. For these polaritons only components of fields e_z and h_y are not zero. In our case $b_z = h_z = 0$, therefore all the results will be also hold true when an insulator is in a contact with a superconductor. The dispersion relation has the same form as for volume polaritons in the case of absence of electric field (Fig. 1)

$$k^2 = \frac{\omega^2}{c^2}\varepsilon_{zz}(\omega),\ \varepsilon_{zz} = \frac{\Omega_e^2 - \omega^2}{\omega_e^2 - \omega^2},\ \Omega_e^2 = \omega_e^2 + 4\pi\tilde{\omega}_0^2,\ \omega_e = \tilde{\omega}_0\sqrt{C_1} \tag{6}$$

The figure 1 corresponds to electron excitations (the optical region, $g<0$, m is the electron mass). The modes of surface polaritons are different for opposite orientations of the electric field. In a field directed into the insulator, the lower branch is excited, while in a field with opposite orientation

the upper branch is excited. The situation is reversed for ionic excitations ($g<0$). Thus surface polaritons with a fixed frequency can be "switched on and off" by changing the direction of the static electric field.

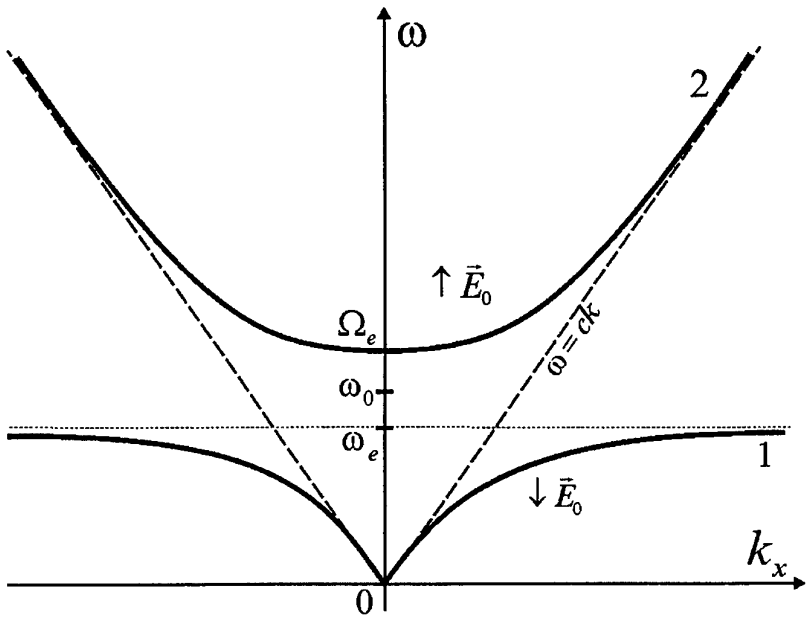

Figure 1

4. Surface Polaritons in Magnetic Field

In the presence of magnetic constant field $\vec{H}_0$, directed in the contact plane along Y axis the dynamic ME interaction induces the non-diagonal component of a dielectric tensor ε_{xz}.

$$\varepsilon_{xz} = -i\varepsilon' = -\frac{i8\pi\omega\omega_H\vec{\omega}_0^2}{\left(\omega^2-\omega_1^2\right)\left(\omega^2-\omega_2^2\right)},\ \omega_H = gH_{0y}$$
$$\omega_{1,2}^2 = \frac{1}{2}\left[\omega_0^2+\omega_e^2+2\omega_H^2 \mp \sqrt{\left(\omega_0^2-\omega_e^2\right)^2+8\omega_H^2\left(\omega_0^2+\omega_e^2\right)}\right] \quad (7)$$

The penetration depth of polaritons δ_H is inversely proportional to the value of magnetic H_{0y}. The dispersion relation and the depth of penetration are following:

$$k_x^2 = \frac{\omega^2}{c^2}\frac{\left(\omega^2-\Omega_1^2\right)\left(\omega^2-\Omega_2^2\right)}{\left(\omega^2-\omega_1^2\right)\left(\omega^2-\omega_2^2\right)},\ \delta_H = \frac{c^2k_x}{\omega^2\varepsilon'(\omega)} > 0 \quad (8)$$

where the expressions for $\Omega_{1,2}$ we obtain from (7) by the replacement ω_e on Ω_e. Surface polariton modes in magnetic field are shown in Fig. 2.

In optical region ($g<0$) for $H_{0y}>0$ the polariton modes are thick solid curves. The modes are not close to each other and the spectrum is strongly nonreciprocal: there are two modes for polaritons

running to the left and one mode for polaritons running to the right. Surface polaritons with a given frequency propagate only in one direction with respect to magnetic field. This is the effect of the rectification. The substitution of $-k_x$ for k_x in Fig. 2 corresponds to the inversion of the magnetic field $H_{0y} \to -H_{0y}$. In this case, the dashed curves are the modes of surface polaritons.

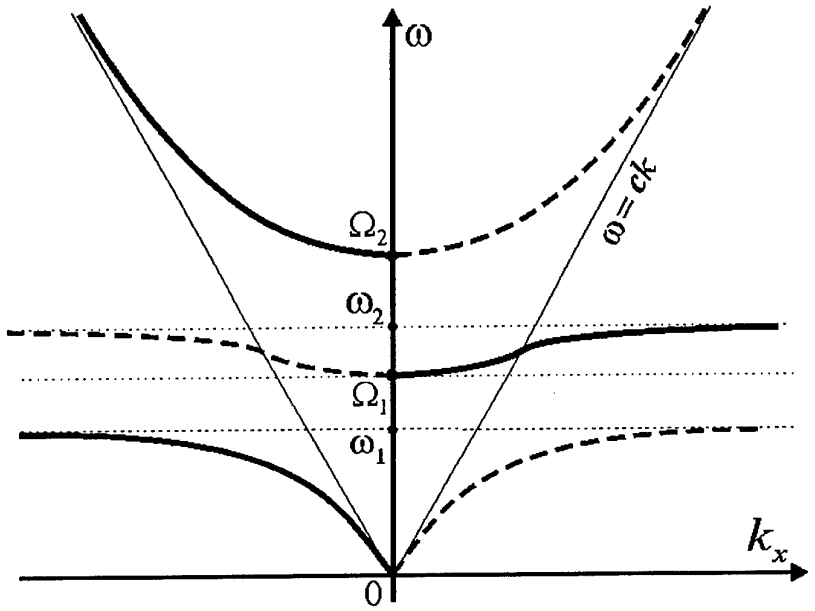

Figure 2

5. Conclusions

Thus, in the presence of a constant electric or magnetic fields the surface polaritons exist in a semi-infinite insulator, which is in contact with an ideal metal or a superconductor. The depth of penetration of polariton field into the insulator is inversely proportional to the value of the field and it is less in optical region than the one for IR region. So, in the optical region of the spectrum $\delta_H \propto c/gH_0$. If $H_0 = 10\,\mathrm{T}$, $\delta = 10^{-2}\,\mathrm{cm}$.

The frequency regions in which surface polaritons exist depend strongly on the direction of the field so a change of the sign of the field signifies the "switching off" or "switching on" of polaritons with a given frequency. In the presence of magnetic field the spectrum is a strong nonreciprocal: surface polaritons propagate only in one direction with respect to magnetic field (the effect of rectification).

The upper modes are radiant modes and may be excited by a direct interaction with electromagnetic wave.

References

[1] V. M. Agranovich and D. L. Mills (Eds.), *Surface Polaritons.* Amsterdam: North-Holland, 1982.
[2] I. E. Chupis and D. A. Mamaluy, *Pis'ma Zh. Eksp. Teor. Fiz.*, vol. 68, p. 876, 1998, [*JETP Letters*, vol. 68, p. 922, 1998].
[3] I. E. Chupis and D. A. Mamaluy, *J. Phys.: Condensed Matter*, vol. 12, p. 1413, 2000.
[4] I. E. Chupis, *Ferroelectrics*, no. 204, p. 173, 1997.

Session 9

Friday - September 29, 2000

09:00 - 10:30

Chiral Materials and Structures: Theory and Experiments

Session 9

Scattering and Absorption by Thin Metal Wires in Rectangular Waveguide – Chiral Cranks versus Non-Chiral Staples

J. H. Cloete, M. Bingle, and D. B. Davidson

Department of Electrical and Electronic Engineering, University of Stellenbosch
Stellenbosch 7600, South Africa. email: jhcloete@ing.sun.ac.za

Abstract

We investigate the physical validity of the claims about chiral microwave absorbers which have appeared in the engineering literature of the last decade. These assert that the performance of synthetic microwave absorbing materials (RAM) may be significantly enhanced by the addition of chiral inclusions, such as wire helices. We compare the performance of chiral, non-chiral and racemic absorbers by embedding unit cells—which are designed to be geometrically closely related—in an absorbing dielectric. We have found no physical mechanism to support the assertions that chirality is the key to improved microwave absorbers. Instead, in synthetic composites which employ thin metal wires in a lossy dielectric or magnetic host, it is the half-wave resonance of the inclusions—not their geometric shape—which plays the crucial role in absorption.

1. Jagadis Chunder Bose and the First Artificial Chiral Materials

Last year we became aware of the work done more than a century ago, in about 1897, on optical activity by the Indian scientist Jagadis Chunder[1] Bose [1, 2]. Until then we—like many others who have been working on artificial chiral materials during the past decade or so—mistakenly gave Lindman [3, 4] the credit for the first microwave experiments on artificial chiral materials.

Priority, however, belongs by about two decades to Bose whose remarkable experiments were conducted in the centimeter and millimeter regime [2]. A reading of his original paper leaves us in no doubt that Bose fully appreciated the role of chirality in optical activity, and that he built artificial chiral and racemic materials to simulate optical activity. A photograph of one of his jute elements is shown in [2, Figure 12].

2. Chiral Microwave Absorbers—Champions and Skeptics

Bose and Lindman, and subsequently Tinoco and Freeman [5], were interested in that most familiar of chiral phenomena—the rotation of the polarisation plane of linearly polarised waves.

Instead, much of the recent attention of microwave and antenna engineers to synthetic chiral materials was attracted by claims in refereed journals which promised microwave absorbers endowed with significantly improved properties. For example "... the possibility of designing anti-reflection coatings using chiral composites" [6]; "It is concluded that chirality can be used as a sensitive parameter to control EM wave propagation characteristics in dielectric composites" [7]; "... a novel material which reduces target RCS, through electromagnetic chirality, and makes it invisible to radar" [8]; "By incorporating electromagnetic chirality these screens offer unique

[1] Also spelled Chandra in the literature.

advantages, such as increased absorption in thin layers for a relatively wide range of frequencies, over conventional designs" [9]. A number of patents were issued in the same period.

In 1992 Bohren *et al.* challenged these claims about the efficacy of chiral absorbers [10]. After studying the effect of chirality on the reflection coefficient of a chiral slab backed by a conducting surface—the chiral Dällenbach layer—for normal incidence, they conclude that "while chiral inclusions may be advantageous, any absorber performance that can be obtained from a chiral composite may be obtained from its non-chiral counterpart." In 1994 Brewitt-Taylor independently came to a similar conclusion after an optimization study. He found "that the shape of the reflection curve is not much affected by the aspect ratio of the included helices, including the non-chiral extreme cases of a straight wire and a flat loop. Thus by this test the introduction of chirality by wire helices has not yielded any improvement" [11]. In a study, conducted between 1993 and 1997 and which used Kuehl's [12] mass production technique for helical inclusions, Cloete *et al.* find that "tiny copper helices can somewhat enhance the performance of dielectric absorbers about the frequency where the helices are one half-wave resonant, and that a racemic absorber is as effective as its purely chiral counterpart." They also find "that, unlike straight filaments (chaff), the helix makes a conveniently compact resonator." However, like Bohren *et al.* and Brewitt-Taylor they conjecture that chirality does not play an essential role in absorbers [13]. Recent network theoretical studies by Rozanov [14] and Brewitt-Taylor [15] on the fundamental limits of the bandwidth of layered absorbers are also relevant because they imply that chirality can not improve on the performance of an optimally designed dielectric-magnetic absorber.

A round table discussion, with participation from the audience, was held in June 1997 at Bianisotropics'97 in Glasgow to review whether or not chiral absorbers could yield superior performance to conventional dielectric-magnetic absorbing materials. (It is unfortunate that none of the chiral absorbing material protagonists were present[2].) The outcome of this discussion is summarized by Weiglhofer: "There seemed to be general consensus—certainly as far as technological significance is concerned—that chirality has not delivered the superior radar-absorption capabilities that some researchers had promised" [16].

We, however, did not consider the matter to be closed after this meeting. Also, to the best of our knowledge, none of the original claims in the refereed literature [6, 7, 8, 9] have been retracted. Fundamental questions remain to be answered—and consensus opinions by panels of scientists and engineers have sometimes turned out to be wrong in the past. Weiglhofer continues: "Yet, at the same time, one must recognize that the number of research groups involved in experimental research on chiral composites is comparatively small, so that many avenues that can lead to the proverbial "pot of gold at the end of the rainbow" still need to be explored" [16].

In this light—despite our negative findings and those of others—we decided in 1996 to embark on a more fundamental theoretical and experimental investigation. Our goal was to find a link—if any—between chirality and enhanced absorption.

The key phrases of Pasteur's scientific thinking are inscribed on the chapel walls of the Pasteur Institute in Paris—among them are the words *dissymétrie moléculaire* [17]. Geometry is the essence of chirality. Both Bohren *et al.* and Brewitt-Taylor had considered the geometry of the individual inclusions as a parameter. Bohren *et al.* compared an array of three-turn helices with an array of non-chiral inclusions made of three coaxial loops, presumably connected by a straight wire. Brewitt-Taylor varied the geometry of a wire parametrically from a straight wire (dipole) to a helix to a broken loop. In previous experimental work the chiral absorbers were invariably composed of randomly oriented helical resonators, which explains the emphasis on helical inclusions in the studies of Bohren *et al.* and Brewitt-Taylor.

[2]Members of the panel were *inter alia* Arne Jacob, Colin Brewitt-Taylor, Udo Unrau, Akhlesh Lakhtakia and Johannes Cloete.

3. Anisotropic Absorbers: Chiral, Racemic and Non-chiral

Instead, in search of deeper physical understanding, we decided to study periodic arrays of thin, bent wires, of resonant length, embedded in a dielectric host [18]. The resulting synthetic anisotropic media are amenable to deterministic numerical analysis, to simple physical realisation, and to microwave experiments. Most important is the clarification of the role of chirality in microwave absorbers which the new "crystalline" systems allow.

The three segment wire hook [20] was chosen as the basic element, instead of the helix, because of the simple geometrical relationship between the chiral enantiomorphs and the non-chiral structures depicted in Figure 1. Rotation of one of the outside segments in steps of $\pi/2$, in the plane normal to the central segment, transforms the non-chiral staple into a chiral crank; then a non-chiral crank; then a chiral crank of opposite hand; and back to the non-chiral staple. An obvious feature of this simple topological relationship between them is that the unwrapped length of the wire remains invariant. This turns out to be an important property because it is known that the unwrapped length of thin wires is a dominant parameter in determining their resonant scattering frequencies. As will be seen, resonance—not chirality—is the key to enhanced absorption in our systems.

Four uniaxial unit cells—one chiral, two non-chiral, and one racemic—were invented and classified according to their point group symmetry [18]. Two of them are shown in Figures 2 and 3. The unit cells were designed to fit into rectangular or square waveguide, with their optic axes parallel to the waveguide axis. This allows accurate measurement of their reflection and transmission coefficients for comparison with numerically simulated data.

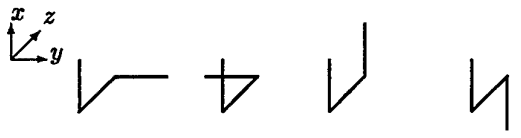

Figure 1: Basic wire structures. Two chiral cranks of opposite handedness (enantiomorphs), a non-chiral staple and a non-chiral crank.

The cells were especially studied around resonance. Because the hooks do not each occupy an electrically small volume in their resonant regime, a constitutive parameter description of the "crystals" cannot be used [21]. This does not matter, because we wished to make a direct physical study of absorption—the phenomenon of interest. This was done by using the measured or computed scattering parameters for a unit cell of the synthetic material, and the law of energy conservation, to determine the absorption spectrum. (The metal walls of the waveguide provide a well-defined and controlled environment for this approach, in contrast to a free space illumination

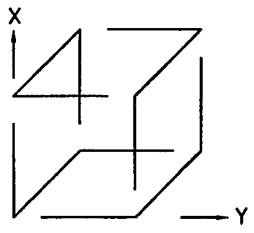

Figure 2: Chiral unit cell of point group 422 symmetry.

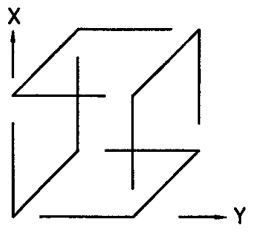

Figure 3: Non-chiral unit cell of point group 4/m symmetry.

system where out-of-beam scattering may occur.)

A finite-difference time-domain (FDTD) code was developed for the full-Maxwellian numerical analysis of thin-wire structures—with finite conductivity—embedded in an absorbing dielectric host in a rectangular or square waveguide [18]. The code was validated against physical experiments in the S-band (2–4 GHz). Figure 4 shows the results for the chiral (422 point group) unit cell of Figure 2. The measured data were obtained with an HP 8510C automatic network analyzer [18]. Agreement between the measured and simulated data for wires, made of both copper and steel, is sufficiently accurate for our purpose.

Further numerical experiments were then confidently performed in a square waveguide on the chiral, non-chiral, and racemic wire unit cells to study their absorption properties. Square waveguide was chosen so as to impose no constraints on the propagation of the cross-polarised TE_{01} mode.

4. Resonant Copper Wire Unit Cells Embedded in a Microwave Absorber

Synthetic chiral microwave absorbers usually consist of a conventional microwave absorber which contains suitable macroscopic chiral objects, such as our hooks or the more fashionable wire helix.

During the experiments to validate the FDTD code it was found that copper hooks embedded in a microwave absorber are just as effective as steel hooks[3] [18]. Therefore only the interaction between copper wire unit cells and the microwave absorbing host was studied in the square waveguide by means of the FDTD code. The microwave absorber had material parameters $\epsilon_r = 1.67$ and $\sigma = 0.04$ S/m, and an effective thickness of 18 mm. Each hook had a total length of $L = 48$ mm $= 3 \times 16$ mm ($f_0 \approx 2.4$ GHz for a deeply embedded, isolated hook), and the centre legs of the hooks were separated by 24 mm in a unit cell. The wire conductivity was 5.7×10^7 S/m.

The absorption spectra of the four uniaxial unit cells are compared in Figure 5. The microwave absorber, without any wire inclusions, absorbs on average about 25 % of the power across the band. The absorption is strikingly enhanced by the inclusion of *resonant* wire structures in the microwave absorber. This is observed whether the inclusions are chiral, non-chiral or racemic. Half-wave resonance of the wires, in the case of the chiral cell, is associated with the Cotton effect—circular dichroism—as also observed by Lindman, and Tinoco and Freeman [3, 5]. Maximum circular dichroism usually coincides with peak absorption [19], but nevertheless absorption at the Cotton frequencies of our chiral unit cell is not superior to absorption at the half-wave resonance of the non-chiral (cranks) or racemic unit cells. Evidently the unit cell of non-chiral cranks couples the incident field to the loss mechanisms of the host as effectively as the chiral and racemic unit cells.

5. Chirality is not a Geometrical Requirement for Absorption

Our experiments show that absorption by a lossy host is significantly enhanced by the inclusion of *resonant* metal-wire structures—whether the inclusions are chiral or non-chiral. Although there were differences in the enhancement of absorption by the four unit cells, the important insight is that the unit cell of non-chiral cranks couples the incident field to the loss mechanisms of the host just as effectively as does the unit cell of chiral hooks and the racemic unit cell of enantiomorphous hooks.

The essence of the claims about chiral absorbers is that the chirality of the inclusions affords an additional degree of freedom for the design of composite materials with enhanced microwave absorption. The implication is that chirality somehow provides the key to improved absorbers.

[3]There is however a marked and important difference when the hooks are embedded in a low loss host. The steel hooks, as expected, make much more efficient absorbers than the copper hooks.

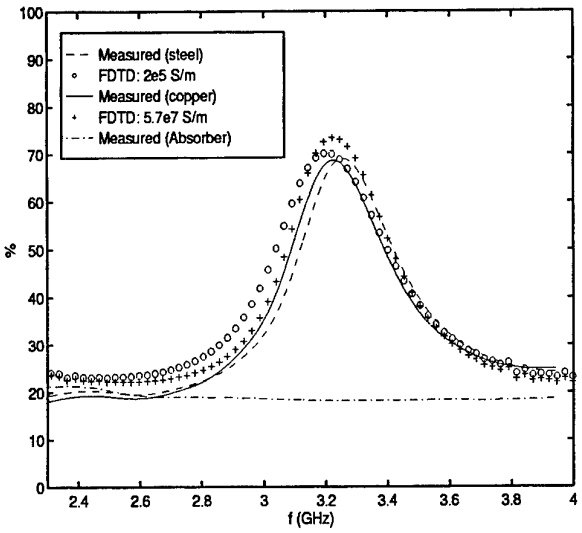

Figure 4: Point group 422 chiral unit cell in an absorber, in rectangular waveguide. Comparison of the percentage power absorbed by a copper and a steel unit cell, measured and predicted.

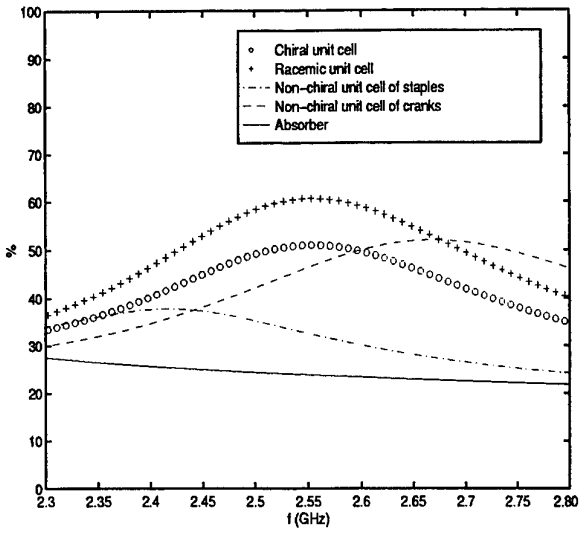

Figure 5: Theoretical absorption spectra of the four uniaxial copper wire unit cells embedded in a microwave absorber, in a square waveguide.

We have found no evidence in support of this. Although—as is well known—chirality is a geometrical requirement for optical activity, we assert that chirality is not a relevant geometrical requirement for absorption.

Instead we propose that in synthetic absorbers, which employ thin metal wires in a lossy dielectric or magnetic host, it is the half-wave resonance of the inclusions, not their shape, which plays the crucial role in absorption. The inclusion of conducting wire structures, whether chiral or not, in a microwave absorber serves only to couple the incident field to the local ohmic, dielectric and magnetic loss mechanisms of the host [13]. Unlike straight chaff-like filaments, the helix makes a conveniently compact resonator, but its chirality does not play a fundamental role in absorption. This contention is supported by the work of Brewitt-Taylor [11], which also provides evidence of enhanced absorption in the region of half-wave resonance for helices.

We recognize that our comparative study of chiral, non-chiral and racemic unit cells is thorough but not exhaustive. However, if a chiral absorber can significantly outperform an equivalent non-chiral counterpart we think that our experiments would reveal this. We are also unaware of any convincing experimental evidence from other researchers that chiral inclusions can markedly improve the performance of an *a priori* well-designed physical absorber using non-chiral conductive, dielectric and magnetic ingredients. Significantly, despite the patent applications made between September 1988 and June 1992, chiral microwave absorbers are apparently not yet available from commercial manufacturers.

Acknowledgement
The written version of this paper is an adapted version of [22]. In the oral presentation we will also draw on results which were presented in [23]. We thank Professor Afonso Barbosa for the kind invitation to present this material at Bianisotropics 2000.

References

[1] J. C. Bose, "On the rotation of plane of polarisation of electric waves by a twisted structure," *Proc. Roy. Soc.*, vol. 63, pp. 146–152, 1898.

[2] D. T. Emerson, "The work of Jagadis Chandra Bose: 100 years of millimeter-wave research," *IEEE Trans. Microwave Theory and Techniques*, vol. 45, no. 12, December 1997, pp. 2267–2273.

[3] K. F. Lindman, "Über eine durch ein isotropes System von spiralförmigen Resonatoren erzeugte Rotationspolarisation der elektromagnetischen Wellen," *Annalen der Physik*, vol. 63, no. 4, pp. 621–644, 1920.

[4] I. V. Lindell, A. H. Sihvola, and J. Kurkijärvi, "Karl F. Lindman—the last Hertzian and a harbinger of electromagnetic chirality," *The Radioscientist*, vol. 3, no. 2, pp. 38, 44–48, 52–53, June 1992.

[5] I. Tinoco, Jr. and M. P. Freeman, "The optical activity of oriented copper helices. I. Experimental," *J Physical Chemistry*, vol. 61, pp. 1196–1200, Sept. 1957.

[6] V. K. Varadan, V. V. Varadan, and A. Lakhtakia, "On the possibility of designing anti-reflection coatings using chiral composites," *J Wave-Material Interaction*, vol. 2, no. 1, pp. 71–81, 1987.

[7] T. Guire, V. V. Varadan, and V. K. Varadan, "Influence of chirality on the reflection of EM waves by planar dielectric slabs," *IEEE Trans. Electromagnetic Compatibility*, vol. 32, no. 4, pp. 300–303, 1990.

[8] D. L. Jaggard and N. Engheta, "CHIROSORB^{TM} as an invisible medium," *Electronics Letters*, vol. 25, no. 3, pp. 173–174, 1989.

[9] D. L. Jaggard, N. Engheta, and J. Liu, "Chiroshield: a Salisbury/Dallenbach shield alternative," *Electronics Letters*, vol. 26, no. 17, pp. 1332–1334, 1990. Correction: *ibid.* vol. 27, no. 6, p. 547, 1991.

[10] C. F. Bohren, R. Luebbers, H. S. Langdon, and F. P. Hunsberger, "Microwave-absorbing chiral composites: Is chirality essential or accidental?," *Applied Optics*, vol. 31, pp. 6403–6407, 20 Oct. 1992.

[11] C. R. Brewitt-Taylor, "Modeling of helix-loaded chiral radar-absorbing materials," in A. Priou (Ed.), *Progress in Electromagnetic Research, PIER 9: Bianisotropic and Bi-isotropic Media and Applications*, EMW Publishing, Cambridge, Massachusetts, USA, 1994, pp. 289–310.

[12] S. A. Kuehl, S. S. Grové, E. Kuehl, M. Bingle, and J. H. Cloete, "Manufacture of microwave chiral materials and their electromagnetic properties," in A. Priou *et al.* (Ed.), *Advances in Complex Electromagnetic Materials*, Kluwer, Dordrecht, 1996, pp. 317-332.

[13] J. H. Cloete, S. A. Kuehl, and M. Bingle, "The absorption of electromagnetic waves at microwave frequencies by synthetic chiral and racemic materials," *Int. J Applied Electromagnetics Mechanics*, vol. 9, pp. 103–114, 1998.

[14] K. N. Rozanov and S. N. Starostenko, "Ultimate thickness to bandwidth ratio of single-layer and multi-layer dielectric radar absorbers," in *Proceedings International Conference on Electromagnetics in Advanced Applications* (ICEEA99), Torino, Italy, 13–17 September 1999, pp. 167–170.

[15] C. R. Brewitt-Taylor, "Fundamental limit on the performance of radar absorbing material," in *Digest of the IEEE Antenna and Propagation Symposium*, Orlando, Florida, July 1999, pp. 1938–1941.

[16] W. S. Weiglhofer, "A report on Bianisotropics'97," *IEEE Antennas and Propagation Magazine*, vol. 39, no. 4, pp. 74–75, August 1997.

[17] J. Applequist, "Optical activity: Biot's bequest," *American Scientist*, vol. 75, pp. 59–67, Jan./Feb. 1987.

[18] M. Bingle, *The Role of Chirality in Synthetic Microwave Absorbers.* PhD thesis, Stellenbosch University, Stellenbosch, 1998.

[19] L. D. Barron, *Molecular Light Scattering and Optical Activity*, Cambridge University Press, 1982.

[20] I. P. Theron and J. H. Cloete, "The electric quadrupole contribution to the circular birefringence of nonmagnetic anisotropic chiral media: A circular waveguide experiment," *IEEE Trans. Microwave Theory and Techniques*, vol. 44, no. 8, pp. 1451–1459, 1996.

[21] R. E. Raab and J. H. Cloete, "An eigenvalue theory of circular birefringence and dichroism in a nonmagnetic chiral medium," *J Electromagnetic Waves and Applications*, vol. 8, no. 8, pp. 1073–1089, 1994.

[22] J. H. Cloete, M. Bingle, and D. B. Davidson, "The role of chirality in synthetic microwave absorbers," in *Proceedings International Conference on Electromagnetics in Advanced Applications* (ICEEA99), Torino, Italy, 13–17 September 1999, pp. 55–58.

[23] M. Bingle, D. B. Davidson, and J. H. Cloete, "FDTD simulation of scattering by conducting wires in rectangular waveguide," in *Abstracts Millenium Conference on Antennas & Propagation*, AP2000, Davos, Switzerland, 9–14 April 2000, Volume 1, p. 92. (Full paper on CD-ROM SP-444.)

Mode Spectrum of Chiral Resonators

Gerald Busse[2] and Arne F. Jacob[1]

[1] Institut für Hochfrequenztechnik, Technische Universität Braunschweig,
Postfach 3329, 38023 Braunschweig, Germany
Tel.: +49 531 391 2002, Fax: +49 531 391 2074, e-mail: a.jacob@tu-bs.de

[2] Now with: Delphi Delco Electronics Systems, TecCenter, 31162 Bad Salzdetfurth, Germany
Tel.: +49 5063 990 632, Fax: +49 5063 990 721, e-mail: Gerald.Busse@delphiauto.com

Abstract

The mode spectrum of a circular waveguide resonator filled with chiral material is calculated. For verification purposes the model is fed with chiral material parameters extracted from standard waveguide measurements. The resonance frequencies computed for different lengths of the resonator are in good agreement with those obtained from an experimental resonator setup.

1. Introduction

Cavity resonators are in general well suited for high precision material characterization. This is because their resonant frequency and quality factor depend sensitively on the electromagnetic properties of the enclosed material. To extract the constitutive parameters of chiral media from such experiments, however, is a complicated and demanding task, both experimentally and theoretically [1]. An alternative use of the resonator is therefore proposed here. Considering a completely filled cavity the material parameters cannot be extracted because the measurement does not provide enough information. The measured resonator characteristics, however, can still be used to accurately verify the material parameters obtained from other experiments. This has to be done indirectly by comparing the measured and the computed responses of the resonator. For an accurate check a field theoretical description of the resonator must be used. This model is fed with the data to be verified.

A full-wave theory of circular waveguide resonators filled with chiral material was developed in [2]. In this contribution the model is extended to cover the whole mode spectrum, in particular the modes with no length dependence. Next, the experimental setup is described and, finally, both the computed and the measured resonant frequencies are compared for different lengths of the resonator.

2. Theory

The resonator consists of a lossless circular waveguide of length l and radius a. It is short-circuited at both ends and filled with chiral material. As was explained in [2] the non-degeneracy of left and right circulating modes in circular chirowaveguides calls for a mode expansion at the short-circuited ends of the resonator. Since modes of different azimuthal order m are decoupled they can be treated separately. On a round-trip through the resonator the eigenmodes must be transmitted self-consistently at resonance. The characteristic equation can be formulated from this condition. For a given geometry of the resonator and a known material its solutions are the complex resonance frequencies $f = f' + jf''$ of modes C_{mnq}. The subscripts denote the azimuthal (m), the radial (n), and the longitudinal (q) order. Alternatively, for instance, f' may be set, l and f'' being the unknowns [2]. This approach offers numerical advantages as the number of time-consuming mode expansions at the short-circuits is reduced by about 50%. However, it only works for length-dependent modes. An in-depth discussion of the results is found in [2] for modes with $m = 1$.

For completeness and in order to fully understand experimental findings it is necessary to explore the whole mode spectrum in the considered frequency range, including, in particular, the length-independent modes. As these are purely transversal $k_z^+ = k_z^- = 0$ must be fulfilled. Here, k_z^+ and k_z^- are the (longitudinal) propagation constants of the underlying left and right circulating waveguides modes. Interestingly, only modes with no azimuthal dependence, i.e. with m=0 satisfy the above

condition. This becomes clear from a look at the dispersion characteristics of circular chirowaveguides [3]. Because of mode-splitting the conditions $k_z^+ = 0$ and $k_z^- = 0$ cannot be satisfied simultaneously, i.e. at the same frequency, except for the degenerate modes: These have no azimuthal dependence, that is $m = 0$, and are the only ones that give rise to length-independent resonator modes ($q = 0$). The characteristic equation then reads: $|k_z^+| = |k_z^-| = 0$. It is solved for the complex frequency. The unloaded quality factor is given by $Q \equiv f'/2f''$.

Fig.1 depicts as a typical numerical result the dependence between the resonator length and the real part of the resonance frequency f' for different values of the chirality parameter β (Drude-Born-Fedorov notation). The permittivity and permeability were set to $\varepsilon_r = 1\text{-}j0.001$ and $\mu_r = 1\text{-}j0.001$, respectively. The radius a is 0.025 m. The figure displays C_{11q}-modes of different longitudinal order and shows how the mode coupling at the short-circuits increases with the chirality parameter when the next higher order waveguide mode (C_{12}) becomes propagating [1]. The cutoff frequencies of the fundamental C_{11}- and the C_{12}-mode of the chirowaveguide are indicated for reference. Fig.2 shows the Q-factor of the C_{11q}-mode. It decreases with increasing chirality parameter and exhibits strong variations in the vicinity of the C_{12}-cutoff.

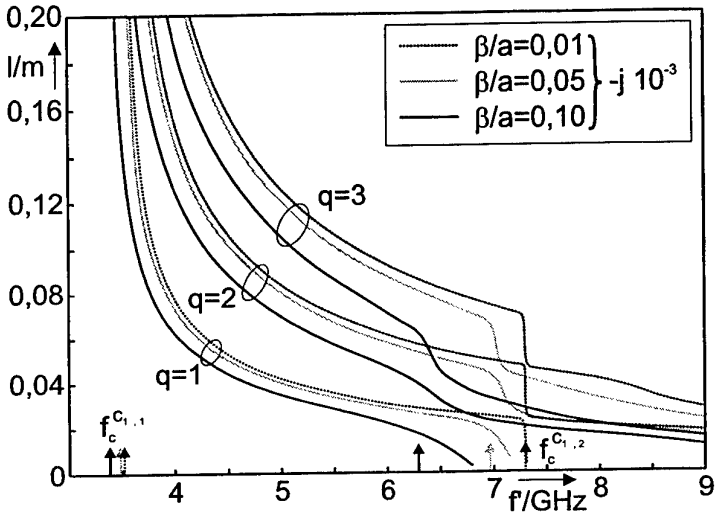

Fig. 1 Resonator length vs. frequency for different chiral parameters and longitudinal orders.

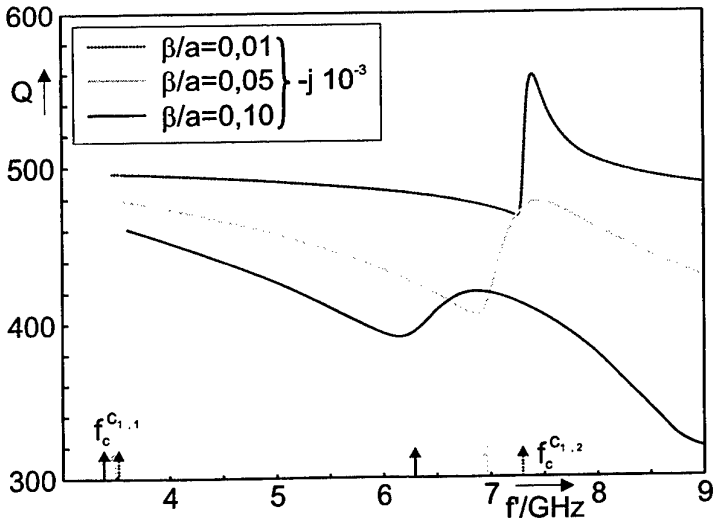

Fig. 2 Resonator quality factor Q for different values of the chirality parameter (longitudinal order $q = 2$)

3. Experimental Setup

The experimental setup is shown in Fig.3. It consists of a short-circuited piece of circular waveguide of radius $a = 0.025$ m. To allow a verification over a broad frequency range rather than at only a few discrete frequencies one of the shorts is realized as movable plunger. The length can be extended up to $l = 0.5$ m. The resonator is operated in transmission mode. To this end a microstrip antenna (22 mm long) is mounted radially on each short. This flat design allows to rotate the antennas azimuthally for optimum measurement sensitivity without damaging them or the chiral material.

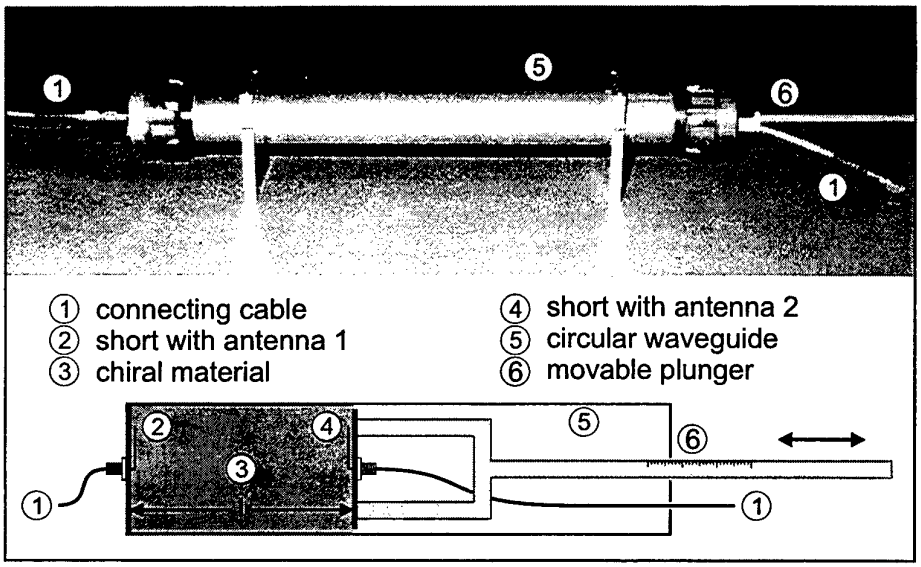

Fig. 3 Experimental setup.

4. Experimental Results

To validate the apparatus it was filled with a composite, non-chiral medium, i.e. spheres of PU-foam. The resonator was characterized with respect to its first four modes. Their resonance frequency is shown in Fig.4 versus the length of the resonator. The measured results correlate well with the values calculated on the basis of the dielectric constant ($\varepsilon_r = 1.11\text{-}j0.003$) of the foam, that was obtained from an independent precision resonator measurement. In general, only slight variations can be observed. They are randomly distributed and are due to local changes of the density. They become reproducible only for the TM_{010}-mode at very short resonator length when the disturbance caused by the antennas becomes noticeable.

Next the resonator was filled with the chiral material of [4], and the resonator characteristics were recorded versus its length. The results are marked by crosses in Fig.4. They display a noticeable uncertainty which is attributable to the inhomogeneity of the material. Still, the general behavior is qualitatively in good agreement with the theoretical results presented above. The setup was then simulated with the model sketched above. The parameters of the (same) chiral material were taken from waveguide measurements as in [4]. Six different sets of data were used. When computing the resonance frequency of the C_{010}-mode one has to take into account the dispersion of the material parameters. The results are displayed as solid lines in Fig.4. The difference of the measured and the computed resonant frequencies remains within a few percent. Because of the comparably high sensitivity of the resonator measurement, this confirms the quality of the waveguide experiments. Due to larger measurement uncertainties the agreement is less pronounced in the cases where the samples used for the waveguide measurement had small differences in length [4]. The uncertainties observed in [4] when determining ε_r and μ_r of the chiral material do not appear, here. They were related to the

measurement errors on the ratio μ_r/ε_r, a quantity that does not affect the characteristic equation of the resonator.

The results obtained for the quality factor are less satisfactory. On the one hand, the values calculated from the measured material parameters decrease in average from 120 to 25 with the wavelength. On the other hand, the measured results exhibit a rather erratic behavior. They vary between 100 and 250 and show no significant frequency dependence. This is only to some extent attributable to the uncertain assessment of losses inherent to transmission measurements as in [4]. The measured Q appears to be much more sensitive to material inhomogeneities.

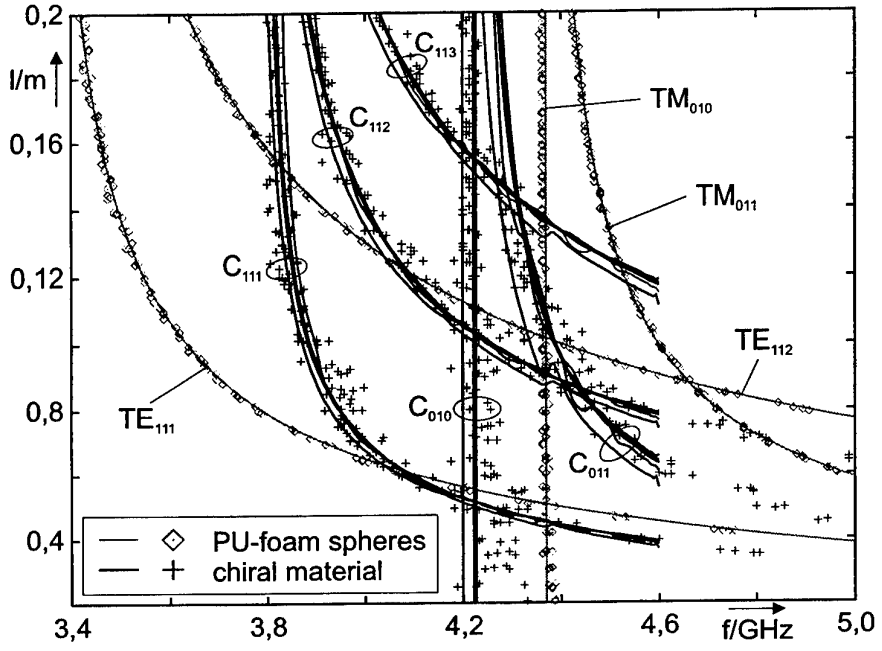

Fig. 4 Resonator length vs. measured and simulated resonance frequencies for PU-foam spheres and chiral material (modes of different order).

5. Conclusion

A resonator experiment was proposed to partially validate the constitutive parameters of a chiral material determined from waveguide measurements. To this end the resonator theory was extended to also include length-independent modes. These turn out to have no azimuthal dependence. The good correlation between the measured resonance frequencies and the ones calculated from the constitutive parameters confirms the quality of the waveguide experiments.

References

[1] S. A. Tretyakov and A. J. Viitanen, "Waveguide and resonator perturbation techniques measuring chirality and nonreciprocity parameters of biisotropic materials," *IEEE Trans. Microwave Theory Tech.*, MTT-43, no. 1, pp. 222–225, 1995.

[2] G. Busse, M. Hoffmeister, M. Kunze, and A. F. Jacob, "Properties of Chiral Filled Circular Cylindrical Resonators," *Proc. Chiral '95*, 4th Int. Conference on Chiral, Bi-isotropic and Bi-anisotropic Media, State College, PA, Oct. 1995, pp. 135–138.

[3] R. Hollinger, V. V. Varadan, and V. K Varadan: "Eigenmodes in a Circular Waveguide Containing an Isotropic Chiral Material," *Radio Science*, **26**, no. 5, pp. 1335–1344, 1991.

[4] G. Busse, J. Reinert, and A. F. Jacob, "Waveguide Characterization of Chiral Material: Experiments," *IEEE Trans. Microwave Theory and Tech.*, MTT-47, no. 3, pp. 297–301, 1999.

Fundamental Limitation on the Performance of Chiral Radar Absorbing Materials

C. R. Brewitt-Taylor

Defence Evaluation and Research Agency
St. Andrew's Road, Malvern, Worcs WR14 3PS, U.K.,
Tel: +44–1684–895091; fax: +44–1684–894185; email: crbtaylor@dera.gov.uk

Abstract

We show that a fundamental limitation exists on the integral of the dB-reflection coefficient over wavelength for a passive metal-backed absorber, whose value is determined by the low-frequency behaviour only. This limit is the same for dielectric absorbers, and for chiral and omega absorbers.

1. Introduction

Standard designs of radar absorbing material on a conducting backplane become inconveniently thick for the absorption of longer wavelength radiation. Attempts to reduce the thickness of the absorber, for example by increasing the dielectric constant of the materials, often also result in a decrease of the bandwidth of good absorption, proportional to the thickness reduction achieved (figure 1).

A possible method of overcoming this problem is the use of artificial materials. Both chiral and omega materials have been proposed to provide improved absorbers. We have previously performed broadband numerical optimisations of various composite material absorbers, including helix loaded chiral composites. As a comparison, we also performed similar optimisations using a material loaded with straight dipoles or circular loops, which give a frequency-dependent dielectric constant (and permeability, for loops), but are not chiral. These optimisations incorporated a method-of-moments analysis of the polarisabilities of a single included object, to ensure that the constitutive parameters used were physically realisable. The general validity of the modelling has been tested against measurements of the constitutive parameters of various helix-loaded composites [1].

In these optimisations it was found that for a fixed layer thickness the curve of absorption with frequency was quite similar for various aspect ratios of helix, including the degenerate cases of a straight dipole and an (almost) flat loop (see figure 2). Variations of the composite allow the shape of the absorption-frequency curve to be adjusted, but do not allow the area enclosed by the curve to be increased without limit. No great advantage was found for a chiral medium [2]. Similar computations have been performed by Wallace [3] for magnetic materials: he also raised the possibility that there is fundamental limitation arising from the Kramers-Kronig relations.

To see how such a limitation might arise, consider a single-layer absorber with frequency-dependent dielectric constant $\epsilon(f)$. An ideal frequency variation can be found by computing at each frequency what value of $\epsilon(f)$ gives zero reflection for a fixed layer thickness. The real part is roughly proportional to $1/f^2$, and the imaginary part to $1/f$. This preserves phase relationships between the front and rear of the layer and attenuation through the layer. But since any real material is causal (it cannot react to an electromagnetic pulse before the pulse arrives), the real

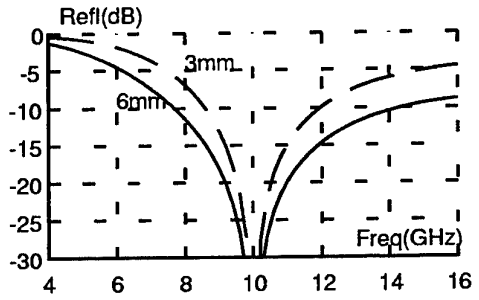

Fig. 1: Single-layer absorbers of two thicknesses

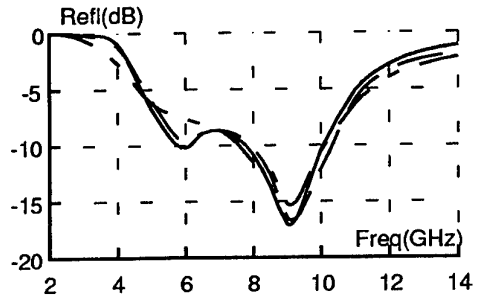

Fig. 2: Layer of two-turn helices (Full=dipole, broken=tall helix, dot-dash=flat helix)

and imaginary parts of its dielectric constant are connected by the Kramers-Kronig relations. We cannot independently specify the real and imaginary parts, as our ideal frequency variation requires, and so this variation may be unrealisable.

2. Derivation of the Limit

It has been known for a long time that a similar limitation on broadband performance exists in the design of matching circuits (e.g. [4]). We originally adapted that theory to the problem of a Salisbury screen radar absorber [5]. We construct a transmission line model of the electromagnetic problem, with a frequency-dependent shunt impedance $Z(f)$ to represent the absorbing layer, and terminated with a short circuit for the metal backplane. We also approximated the transmission line representing the spacer material by a single-stage of an LC ladder network. Using a contour integral method similar to that to be described shortly, we obtained an upper limit on the reflection coefficient of:

$$\frac{1}{f_0}\int_0^\infty |R_{dB}(f)|\,df \le \frac{320}{\ln 10}\frac{h}{\lambda_0}, \tag{1}$$

where f_0 and λ_0 are the frequency and wavelength at the centre of the absorption band, and h is the thickness of the layer. A Salisbury screen has an infinite series of absorption bands (figure 3), and the integral of the dB-reflection coefficient is clearly infinite. So this limitation cannot be rigorously true. But the approximation of using only a single step of ladder network has the effect of confining attention to the first absorption band of a Salisbury screen, and the limitation does work with this restriction. We found that in all our optimisations of dielectric and chiral materials, this limit was never violated, and integrals of up to 70% of the limit could be achieved. A scaling argument shows that if the magnetic materials were involved, the limit increases by the permeability μ.

At the PIERS-98 Conference, K. N. Rozanov published an independent paper on this topic [6]. He wrote the integral over frequency rather than wavelength. This overcomes the problem of the infinite frequency integral. Thus the method will be described here in wavelength terms.

Consider a planar absorber, with a frequency-dependent field reflection coefficient $R_f(f)$, which can also be expressed as a function of wavelength $R_\lambda(\lambda)$. We calculate the integral $\int_0^\infty \ln[1/R_\lambda(\lambda)]d\lambda$ around a contour in the complex plane, consisting of the entire real axis, closed by a large-radius semi-circle in the positive imaginary half-plane. Since $R_f(f)$ is the Fourier transform of a real and causal impulse response, it is analytic in the lower half-plane, and has the symmetry $R_f(-f^*) = R_f^*(f)$. The wavelength reflection coefficient $R_\lambda(\lambda)$ has the

same symmetry, and is analytic in the upper half-plane. Using the symmetry, the integral along the real axis is equal to $2\int_0^\infty \ln[1/|R_\lambda(\lambda)|]d\lambda$. This is proportional to the integral of the magnitude of the reflection coefficient measured in dB.

To compute the integral around the large semicircle, we expand $\ln[1/R_\lambda]$ as a power series $\sum_1^\infty A_n\lambda^{-n}$. Any positive or zero powers of λ are excluded since $|R_\lambda| \to 1$ as $f \to 0$ ($\lambda \to \infty$). The integral around the large semicircle is then $i\pi A_1$, with contributions for $n > 1$ vanishing as the radius of the semicircle tends to infinity.

We wish to use Cauchy's theorem around the contour. But singularities can arise within the contour if $R_\lambda(\lambda)$ is either zero or infinite. An infinity is excluded because the absorber is causal and passive. But the reflection coefficient can be zero, say at some wavelength λ_z. By the symmetry in the complex plane, there is another zero at $-\lambda_z^*$. These two zeros are removed by multiplying the reflection coefficient by a factor $(\lambda - \lambda_z^*)(\lambda + \lambda_z)/(\lambda - \lambda_z)(\lambda + \lambda_z^*)$ for each such zero point λ_z. This factor moves the two zeros into the lower half of the complex plane, outside the contour. The factor has unit magnitude for wavelengths along the real axis, and so does not modify the real-axis integral. It does introduce an extra term in the integral around the large semicircle. Having done this, Cauchy's theorem gives:

$$\int_0^\infty \ln[1/|R_\lambda(\lambda)|]\,d\lambda = -i\pi A_1/2 - 4\pi \sum \operatorname{Im} \lambda_z\,. \tag{2}$$

Since λ_z is in the upper half-plane, the last term is always negative. Then we have:

$$\int_0^\infty \ln[1/|R_\lambda(\lambda)|]\,d\lambda \le -i\pi A_1/2\,. \tag{3}$$

Since the left-hand side is clearly real and positive, this equation only makes sense if A_1 is positive imaginary. We have obtained an upper limit on an integral of the reflection coefficient, which depends only on the first term of its low-frequency expansion.

3. Application to Chiral Materials

The reflection coefficient at normal incidence of a single-layer absorber can be written:

$$R = \frac{iZ_1 \tan(k_1 h) - Z_0}{iZ_1 \tan(k_1 h) + Z_0}\,. \tag{4}$$

Here Z_0 is the impedance of free space, Z_1 is the impedance in the medium, and k_1 is the wavenumber in the medium. With low-frequency approximations, this becomes $R \approx -1 + 4\pi i\mu_1 h/\lambda$. This gives the value of A_1 in the expansion, and leads to the limit quoted by Rozanov:

$$\int_0^\infty \ln[1/|R_\lambda(\lambda)|]\,d\lambda \le 2\pi^2\mu_1 h\,. \tag{5}$$

He also remarks that for a narrow-band absorber the factor of $2\pi^2$ should be replaced by 16. If this is done, and the variable changed from λ to f, we recover our limitation above. In a wavelength integral, the absorption bands of a Salisbury screen have decreasing width with a finite sum (figure 3), and they account for the difference between 16 and $2\pi^2$.

The calculation can be generalised to a multi-layer absorber, using a standard recursive process of computing the upward and downward going waves in each layer, starting at the back with the zero electric field boundary condition, and applying suitable propagation factors through each layer and field continuity conditions at each interface. At each stage one makes low-frequency approximations, keeping only the first order term. The algebra is lengthy, and the result is the same as for a single layer, except that we have a sum over the layers $\sum \mu_i h_i$ instead of a single term.

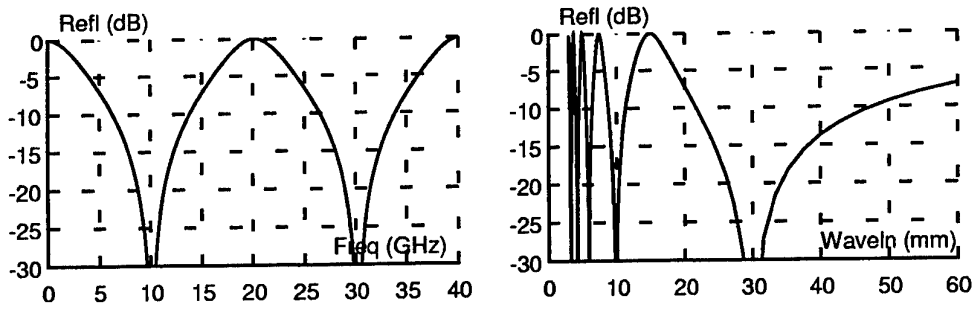

Figure 3: Reflection from single-layer absorber
((a) Function of frequency, (b) function of wavelength)

Turning to chiral materials, the details depend on the formalism used. If we use the form generally used by Lindell and Sihvola, we find that the reflection is given by equation 4, and the chirality does not appear [7]. Thus we immediately obtain the same value of A_1, and the same limit, as for a non-chiral medium. If we use the Post-Jaggard or the Lakhtakia-Varadan formalism, we find that the chirality only enters in the second order in frequency. Again, it does not affect the value of the first-order coefficient A_1, and we arrive at the same limit.

The omega medium (e.g. [8]) contains wires shaped like a Greek letter Ω, and provides a different electric-magnetic coupling than the usual chiral effect. However, taking the formulae for the reflection coefficient, and making low-frequency approximations, we find that that coupling parameter only enters in the second order in frequency. Again, it does not affect the value of the first-order coefficient A_1, and we arrive at the same limit.

4. Conclusions

We have shown that there is a fundamental limit on the broadband performance of a planar absorbing structure on a metal back, proportional to the total thickness and the permeability only. The same limit is found for chiral and omega materials as for purely dielectric materials.

References

[1] C. R. Brewitt-Taylor, P. G. Lederer, F. C. Smith, and S. Haq, "Measurement and prediction of helix-loaded chiral composites," *IEEE Trans. Antennas and Propagation*, Vol. 47, No. 4, pp. 692–700, April 1999.

[2] C. R. Brewitt-Taylor, "Modelling of helix-loaded chiral radar-absorbing layers," p. 289–310, in Priou, A. (Editor), *Bianisotropic and Bi-Isotropic Media and Applications*, PIER Book Series no. 9, 1994.

[3] J. L. Wallace, "Broadband magnetic microwave absorbers: Fundamental limitations," *IEEE Trans. Magnetics*, Vol. 29, pp. 4209–14, 1993.

[4] H. W. Bode, *Network Analysis and Feedback Amplifier Design*. Van Nostrand: NY, 1945.

[5] C. R. Brewitt-Taylor, in *Proceedings of IEEE Antennas and Propagation Symposium*, pp. 1934–1937, Orlando, USA, July 1999.

[6] K. N. Rozanov, in *PIERS 1998 Proceedings*, p. 229, Nantes, France, July 1998.

[7] S. A. Tretyakov *et al.*, "Conductor backed Tellegen slab as a twist polarizer," *Electronics Letters*, Vol. 28, 281–2, 30 Jan 1992.

[8] S. A. Tretyakov and A. A. Sochava, "Novel unixaial bianisotropic materials: reflection and transmission in planar structures," pp. 157-179, in A. Priou (editor) *Bianisotropics and Bi-Isotropic Media and Applications*, PIER Book Series No. 9, EMW Publications, Cambridge MA, 1994.

Exact and Approximate Modeling of Helices with Core

J. Reinert and A. F. Jacob

Institut für Hochfrequenztechnik, TU Braunschweig
Postfach 3329, 38023 Braunschweig, Germany
Phone: +49 531 391 2017, Fax: +49 531 391 2045, email: J.Reinert@tu-bs.de

Abstract

A model for the direct calculation of the dipole polarizability tensors of a helix with spherical core based on the exact field solution is introduced. Motivated by this model, an approximate one relying on the dipole moments of the core is developed. Results obtained with both models are compared and verified by measurements.

1. Introduction

Recently, chiral materials consisting of complex inclusions — for example perfectly electrically conducting (PEC) thin wire helices with a dielectric and/or magnetic core different from the host material — were proposed and investigated [1]. In this paper the essentially exact model of a helix with spherical core used for the calculations in [1] is outlined. Because the governing equations are lengthy and their derivation mathematically involved only the Ansatz is displayed here. It reveals a problem concerning cores with both dielectric and magnetic properties. The (approximate) solution of this problem motivates a second model relying on a dipole approximation of the core. This model is developed in the following. Note, that cartesian coordinates are used throughout the whole paper.

2. Model

Consider a helix with spherical core both centered at the coordinate origin. The current flowing on the helix wire can be calculated from a Method of Moments (MoM) solution of the scattering problem [2]. If a thin-wire Galerking MoM is employed, the (symmetric) system matrix $\underline{\underline{Z}}$ and the exciation vector $\underline{V}$ read for plane wave incidence (electric field $\underline{E}^0$)

$$\begin{aligned} Z_{mn} &= j\omega\mu \int_u \int_{u'} \underline{t}(u)(\underline{\underline{G}}^0 + \underline{\underline{G}}^s)\underline{t}'(u')B_m(u')B_n(u)\,du'\,du \\ V_n &= \int_u \underline{t}(u)(\underline{\underline{I}} + \underline{\underline{S}}(u))\underline{E}^0 \exp\{-j\underline{k}\,\underline{r}\}\,B_n(u)\,du \quad . \end{aligned} \tag{1}$$

Here, $\underline{\underline{I}}$ is the unity tensor, $\underline{\underline{G}}^0$ stands for the free space dyadic Greens function, $\underline{\underline{G}}^s$ describes the scattering correction caused by the spherical core [3], $\underline{t}$ ($\underline{t}'$) is the tangential vector on the wire in the observation (source) point, and B stands for the basis/testing functions. The term $\underline{\underline{S}}$ that describes the plane wave scattering of the spherical core can be derived from the scattering correction $\underline{\underline{G}}^s$ by plane wave normalization as described in [4, 5]; it is, in essence, identical to the Mie solution for the scattering of a plane wave by a sphere [6, 7].

The total field scattered by this helix with core can be split into four parts, each corresponding to an individual multipole series. These parts are: 1) The field scattered by the wire caused by the incident plane wave, 2) the field scattered by the core caused by the incident plane wave, 3)

the field scattered by the wire caused by the diffraction field of the core, and 4) the field scattered by the core caused by the diffraction field of the wire.

Following the procedure introduced in [8], the incident plane wave in (1) can be expanded into a Taylor series and the different terms arising can be separated into their electric and magnetic origin. This procedure gives results identical to those obtained with the method of counter-propagating waves [9], but removes the information on the direction of incidence analytically instead of using different angles of incidence to separate the polarizabilities. The Taylor series expansion produces unambiguous results if the spherical core is either purely dielectric or purely magnetic. If it possesses both properties, the tight coupling of magnetic and electric fields within the core prohibits an exact solution. One way to circumvent this problem is the following: The inclusion under investigation is intended to form the basic building block of a chiral material; thus, the inclusion itself and all of its constituents must be electrically small. Then, electric and magnetic effects are decoupled nearly entirely (static limit) and can be treated separately by applying the series expansion of the excitation vector $\underline{V}$ (see above).

This idea leads directly to a further simplification of the problem: As the core is electrically small, only the first term of the infinite series defining $\underline{\underline{G}}^s$ contributes significantly [3]. This term represents the dipole contributions to the scattered field. This means that for the description of the interaction between wire and core the latter can effectively be replaced by its electric and magnetic dipole moments in the origin. The expression for the total electric field together with the boundary condition on the PEC wire surface then reads

$$\begin{aligned} Z_{mn} &= j\omega \int_u \int_{u'} \left(\mu_0\, \underline{t}\, \underline{\underline{G}}^0\, \underline{t}' - \omega^2 \mu_0^2\, \underline{X}\, \underline{\underline{G}}^0(0,u')\, \underline{t}' - \underline{Y}\, \nabla \times \underline{\underline{G}}^0(0,u')\, \underline{t}'\right) B_m(u)\, B_n(u')\, du'\, du \\ V_n &= \int_u \left(\underline{t}\, \underline{\underline{E}}^0 \exp\{-j\underline{k}\,\underline{r}\} + \omega^2 \mu_0\, \underline{X}\, \underline{\underline{E}}^0(0) - j\omega\, \underline{Y}\, \underline{\underline{H}}^0(0)\right) B_n(u)\, du \\ \underline{X} &= \underline{t}\, \underline{\underline{G}}^0(u,0)\, \underline{\underline{\alpha}}^e \quad , \quad \underline{Y} = \underline{t}\, \nabla \times \underline{\underline{G}}^0(u,0)\, \underline{\underline{\alpha}}^m \quad , \end{aligned} \tag{2}$$

where $\underline{\underline{\alpha}}^e$ and $\underline{\underline{\alpha}}^m$ are the symmetric electric and magnetic dipole polarizability tensors of the core, respectively. To ensure reciprocity, the identities $\underline{t}(u) = \underline{t}'(u)$ and $\underline{r}(u) = \underline{r}'(u)$ must be fulfilled when considering V_n as derived in [8].

Together with the abbreviations

$$\Gamma = \sum_{m,n} B_m(u)\, Z_{mn}^{-1}\, B_n(u') \quad , \quad \langle f(u,u') \rangle = \int_u \int_{u'} f(u,u')\, du'\, du$$

the expansion of the plane wave contained in (2) now leads to the following dipole polarizabilities of the inclusion (the numbering refers to the different scattered fields discussed above):

$$\underline{\underline{\alpha}}_1^{ee} = \frac{1}{j\omega} \langle \underline{t}\, \Gamma\, \underline{t}' \rangle \, , \qquad \underline{\underline{\alpha}}_1^{em} = -\frac{\mu_0}{2} \langle \underline{t}\, \Gamma\, (\underline{r}' \times \underline{t}') \rangle$$

$$\underline{\underline{\alpha}}_1^{me} = \frac{\mu_0}{2} \langle (\underline{r} \times \underline{t})\, \Gamma\, \underline{t}' \rangle \, , \quad \underline{\underline{\alpha}}_1^{mm} = -\frac{j\omega\mu_0^2}{4} \langle (\underline{r} \times \underline{t})\, \Gamma\, (\underline{r}' \times \underline{t}') \rangle$$

$$\underline{\underline{\alpha}}_2^{ee} = \underline{\underline{\alpha}}^e \, , \quad \underline{\underline{\alpha}}_2^{mm} = \underline{\underline{\alpha}}^m$$

$$\underline{\underline{\alpha}}_3^{ee} = -j\omega\mu_0 \langle \underline{t}\, \Gamma\, \underline{X}' \rangle \, , \qquad \underline{\underline{\alpha}}_3^{em} = -\langle \underline{t}\, \Gamma\, \underline{Y}' \rangle$$

$$\underline{\underline{\alpha}}_3^{me} = \frac{\omega^2 \mu_0^2}{2} \langle (\underline{r} \times \underline{t})\, \Gamma\, \underline{X}' \rangle \, , \quad \underline{\underline{\alpha}}_3^{mm} = -\frac{j\omega\mu_0}{2} \langle (\underline{r} \times \underline{t})\, \Gamma\, \underline{Y}' \rangle$$

$$\underline{\underline{\alpha}}_4^{ee} = -j\omega\mu_0\langle \underline{X}\,\Gamma\,\underline{t}'\rangle - j\omega^3\mu_0^2\langle \underline{X}\,\Gamma\,\underline{X}'\rangle\,, \quad \underline{\underline{\alpha}}_4^{em} = -\frac{\omega^2\mu_0^2}{2}\langle \underline{X}\,\Gamma\,(\underline{r}'\times\underline{t}')\rangle - \omega^2\mu_0\langle \underline{X}\,\Gamma\,\underline{Y}'\rangle$$

$$\underline{\underline{\alpha}}_4^{me} = \langle \underline{Y}\,\Gamma\,\underline{t}'\rangle + \omega^2\mu_0\langle \underline{Y}\,\Gamma\,\underline{X}'\rangle\,, \qquad \underline{\underline{\alpha}}_4^{mm} = -\frac{j\omega\mu_0}{2}\langle \underline{Y}\,\Gamma\,(\underline{r}'\times\underline{t}')\rangle - j\omega\langle \underline{Y}\,\Gamma\,\underline{Y}'\rangle$$

Note, that

$$\underline{X} = \underline{t}\,\underline{\underline{G}}^0(u,0)\,\underline{\underline{\alpha}}^e = \underline{\underline{\alpha}}^e\,\underline{\underline{G}}^0(0,u)\,\underline{t}\,, \quad \underline{Y} = \underline{t}\,\nabla\times\underline{\underline{G}}^0(u,0)\,\underline{\underline{\alpha}}^m = \underline{\underline{\alpha}}^m\,\nabla\times\underline{\underline{G}}^0(0,u)\,\underline{t}\quad .$$

Summing up all these individual contributions, the polarizability tensors of the whole inclusion are obtained. It can be proved, that the resulting tensors represent a reciprocal inclusion, i.e. $\underline{\underline{\alpha}}^{ee} = (\underline{\underline{\alpha}}^{ee})^T$, $\underline{\underline{\alpha}}^{me} = -(\underline{\underline{\alpha}}^{em})^T$, $\underline{\underline{\alpha}}^{mm} = (\underline{\underline{\alpha}}^{mm})^T$.

3. Verification

If the core is purely magnetic or purely dielectric the approximate model can be directly compared to the exact solution. Furthermore, results derived from the system matrix $\underline{\underline{Z}}$ of eq.(1) — for example the resonance frequency of the inclusion — are exact, even for cores with both dielectric and magnetic properties. Thus, these quantities can be compared to the approximate ones obtained from eq.(2) for a partial check of the accuracy. All tests performed showed, that the results calculated from the exact and the approximate model are in very good agreement. As an example, the change in resonance frequency due to a spherical core (diameter: $2a = 3\,\mathrm{mm}$, helix dimensions: diameter 4 mm, height 4 mm, three turns) with magnetic and/or electric properties is displayed in Fig. 1. As can be seen, the errors occurring in the curves for either purely dielectric or purely magnetic cores add up for cores with both properties. As expected, the error increases with electrically larger cores. As a consequence of the neglected electric quadrupole moment this is more pronounced for dielectric cores. Although for ε_r, $\mu_r > 5$ the cores are no longer electrically small ($0.2 \le k\,a \le 0.91$), the results are in good agreement, too (maximum difference: 0.04 GHz).

Fig. 2 displays the scattering parameter S_{11} of a helix (dimensions as above) with a spherical dielectric core ($\varepsilon_r = 4.7 - j1.6$, diameter: 3 mm). It was measured using the method described in [10] and calculated using the approximate model. Apart from a small shift in the resonance frequency (see [11] for explanations) the results fit quite well, in particular if one takes into account the measurement accuracy [10].

4. Conclusion

The approximate model for helices with spherical core developed above produces meaningful results, both theoretically (reciprocity) and numerically. Although the model has its origin in the exact solution of the helix/spherical core problem, it contains no restrictions regarding the geometry of the core or the wire. The inclusion should only be electrically small so that higher order multipole moments of the core can be neglected. Thus, the model should be able to handle other than spherical cores, provided their electric and magnetic polarizability tensors are known, either analytically or from numerical calculations.

References

[1] J. Reinert and A. F. Jacob, "Chiral materials consisting of helices with core – A case study," *Proc. URSI'99*, Toronto, Canada, p. 187, 1999.

[2] R. F. Harrington, *Field Computation by Moment Methods*. IEEE Press, New York, 1993.

[3] C. T. Tai, *Dyadic Greens Functions in Electromagnetic Theory*. IEEE Press, New York, 1994.

[4] L. B. Felsen and N. Marcuwitz, *Radiation and Scattering of Waves*. IEEE Press, New York, 1994, Ch. 5.4.

[5] D. S. Jones, *The Theory of Electromagnetism*. Pergamon Press, Oxford, 1964, Ch. 8.24.

[6] G. Mie, "Beiträge zur Optik trüber Medien, speziell kolloidaler Metallösungen," *Ann. d. Physik*, Vol. 24, pp. 377–445, 1908.
[7] J. A. Stratton, *Electromagnetic Theory*. McGraw-Hill, New York, 1941.
[8] J. Reinert and A. F. Jacob, "Direct calculation of multi-polarizability tensors for thin-wire scatterers," submitted for publication, 2000.
[9] C. R. Brewit-Taylor, P. G. Lederer, F. C. Smith, and S. Haq, "Measurement and prediction of helix-loaded chiral composites," *IEEE Trans. Antennas Propagat.*, vol. 47, no. 4, pp. 692–700, 1999.
[10] J. Reinert and A. F. Jacob, "Theoretical and experimental characterization of small wire scatterers," submitted for publication, 2000.
[11] J. Psilopoulos, J. Reinert, and A. F. Jacob, "Fabrication effects on the resonance bandwidth of chiral materials," in *Proc. Bianisotropics 2000*, pp. 313-316, Lisbon, Sep. 2000.

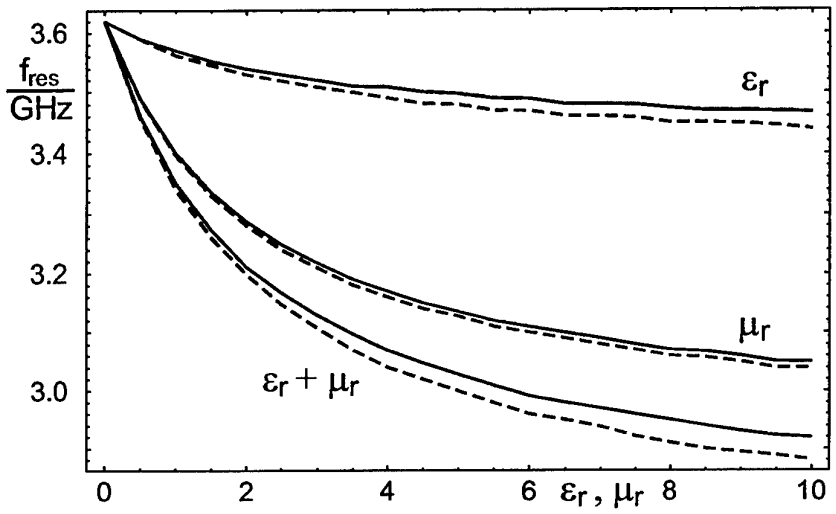

Figure 1: Change in resonance frequency due to a spherical dielectric and/or magnetic core. (——) Approximate model, (– – –) exact model.

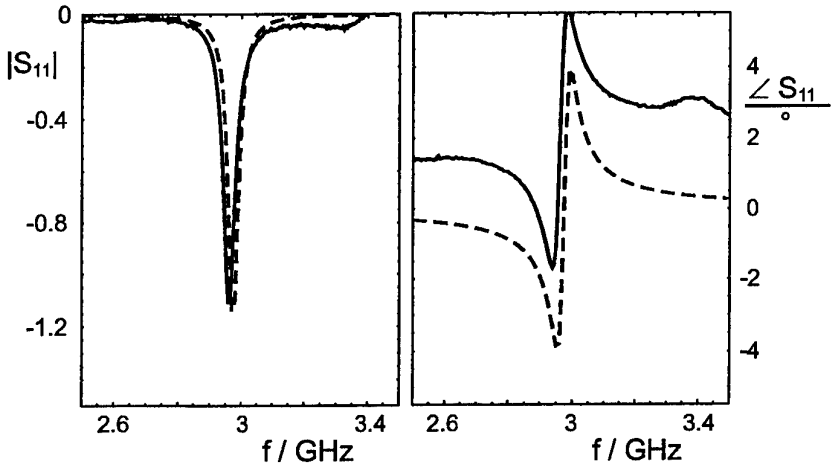

Figure 2: Scattering parameter S_{11} of a helix with dielectric core. Measured (——) and theoretical (– – –) response (approximate model).

Session 10

Friday - September 29, 2000

10:50 - 12:10

Propagation and Scattering

Reflection from a Bianisotropic Dielectric

E. B. Graham and R. E. Raab

School of Chemical and Physical Sciences, University of Natal
P/Bag X01, Scottsville, Pietermaritzburg 3209 South Africa
Fax: +27 33 260 5876; email: raab@nu.ac.za

Abstract

The well-known surface densities of bound charge $\sigma = \mathbf{P} \cdot \mathbf{n}$ and current $\mathbf{K} = \mathbf{M} \times \mathbf{n}$, which give rise to discontinuities in fields at a surface, are inconsistent in their multipole order. The electric quadrupole contribution is missing from each. A consequence of including this is the appearance of a surface density of electric dipole moment $\mathcal{P}$. Its effect on the boundary conditions is derived, and a reflection experiment on a bianisotropic crystal is proposed, which in conjunction with a transmission experiment, allows the $\mathcal{P}$ contribution to be measured.

1. Introduction

The contribution to a physical effect of electric quadrupoles induced in matter by long wavelength radiation is known to compare in magnitude with that of induced magnetic dipoles [1, 2, 3]. Consequently, there is an inconsistency in the surface densities of bound charge and current [4]

$$\sigma = \mathbf{P} \cdot \mathbf{n}, \qquad \mathbf{K} = \mathbf{M} \times \mathbf{n}, \tag{1}$$

where $\mathbf{n}$ is the outward unit normal at a macroscopic point on the surface and $\mathbf{P}$ and $\mathbf{M}$ are the electric and magnetic dipole moments per unit macroscopic volume. An electric quadrupole term should be included in $\mathbf{K}$ alongside $\mathbf{M}$, and also one in σ.

This paper derives these two contributions and then shows their effect on the boundary conditions on the fields at a vacuum-dielectric interface. In particular, the electric dipole surface density also emerges and its role is examined, as well as its contribution to a physical effect.

2. Theory of Bound Source Contributions

The retarded vector potential outside a bounded distribution of currents in vacuum is [4]

$$\mathbf{A}(\boldsymbol{\mathcal{R}}, t) = (\mu_0/4\pi) \int_v \mathbf{J}(\mathbf{r}, t - |(\boldsymbol{\mathcal{R}} - \mathbf{r}|/c)/|(\boldsymbol{\mathcal{R}} - \mathbf{r}|dv. \tag{2}$$

By expanding $\mathbf{J}$ for $\mathcal{R} \gg r$, applying the condition $\lambda \gg \mathcal{R}$ and averaging over a macroscopic volume element dV, we obtain the macroscopic vector potential due to a bounded dielectric of volume V and surface area S. To order electric quadrupole (E2)-magnetic dipole (M1) it is [5]

$$A_\alpha(\mathbf{R}, t) = (\mu_0/4\pi)\{\int_V (1/R)(\dot{P}_\alpha - \tfrac{1}{2}\nabla_\beta \dot{Q}_{\alpha\beta} + \epsilon_{\alpha\beta\gamma}\nabla_\beta M_\gamma)dV + \int_S (1/R)(\tfrac{1}{2}\dot{Q}_{\alpha\beta} - \epsilon_{\alpha\beta\gamma}M_\gamma)n_\beta da\}. \tag{3}$$

In this $\mathbf{R} = -\boldsymbol{\mathcal{R}}$ is the displacement of dV from the field point and $Q_{\alpha\beta} = \sum qr_\alpha r_\beta/dV$ is the electric quadrupole moment per unit volume. The multipole moment densities P_α, M_α, $Q_{\alpha\beta}$ are

relative to an arbitrary origin in dV at the time $t - R/c$. Similarly for the scalar potential [5]

$$\begin{aligned}\phi(\mathbf{R},t) &= 1/(4\pi\epsilon_0)\left\{\int_V (1/R)\nabla_\alpha(-P_\alpha + \tfrac{1}{2}\nabla_\beta Q_{\alpha\beta})dV\right. \\ &+ \left.\int_S [(1/R)\{(P_\alpha - \tfrac{1}{2}\nabla_\beta Q_{\alpha\beta})n_\alpha + \nabla_{||}\mathcal{P}_{||}\} + (R_\perp/R^3)\mathcal{P}_\perp]da\right\}, \qquad (4)\end{aligned}$$

where $\nabla_{||}$ denotes differentiation parallel to the surface element da and

$$\mathcal{P}_\alpha = -\tfrac{1}{2}Q_{\alpha\beta}n_\beta \qquad (5)$$

is a contribution of E2 order. From the volume integrals in (3) and (4), with their $1/R$ dependence, the bound source volume densities of current and charge are

$$J_\alpha = \dot{P}_\alpha - \tfrac{1}{2}\nabla_\beta \dot{Q}_{\alpha\beta} + \epsilon_{\alpha\beta\gamma}\nabla_\beta M_\gamma, \quad \rho = -\nabla_\alpha P_\alpha + \tfrac{1}{2}\nabla_\alpha\nabla_\beta Q_{\alpha\beta}. \qquad (6)$$

These satisfy the equation of continuity for bound sources $\nabla \cdot \mathbf{J} = -\dot{\rho}$. From the $1/R$ terms in the surface integrals in (3) and (4) the surface densities of bound current and charge are

$$K_\alpha = (\tfrac{1}{2}\dot{Q}_{\alpha\beta} - \epsilon_{\alpha\beta\gamma}M_\gamma)n_\beta, \quad \sigma = (P_\alpha - \tfrac{1}{2}\nabla_\beta Q_{\alpha\beta})n_\alpha + \nabla_{||}\mathcal{P}_{||}. \qquad (7)$$

There still remains in the surface integral in (4) the term with a $\mathbf{R}/R^3$ dependence. As this is characteristic of the potential due to an electric dipole, we interpret $\mathcal{P}$ in (4) as the surface density of electric dipole moment due to bound charge on the surface.

If the bound sources in (6) are used in the two inhomogeneous Maxwell equations

$$\nabla \cdot \mathbf{E} = (\rho_c + \rho)/\epsilon_0, \quad \nabla \times \mathbf{B} = \mu_0(\epsilon_0\dot{\mathbf{E}} + \mathbf{J}_c + \mathbf{J}), \qquad (8)$$

where ρ_c and $\mathbf{J}_c$ are the corresponding free source terms, one obtains by comparison with

$$\nabla \cdot \mathbf{D} = \rho_c, \quad \nabla \times \mathbf{H} = \dot{\mathbf{D}} + \mathbf{J}_c, \qquad (9)$$

the multipole expressions for $\mathbf{D}$ and $\mathbf{H}$ to order E2–M1

$$D_\alpha = \epsilon_0 E_\alpha + P_\alpha - \tfrac{1}{2}\nabla_\beta Q_{\alpha\beta}, \quad H_\alpha = B_\alpha/\mu_0 - M_\alpha. \qquad (10)$$

The densities P_α, M_α, $Q_{\alpha\beta}$ are induced by the wave fields and their space and time derivatives

$$E_\alpha,\ \dot{E}_\alpha,\ \nabla_\beta E_\alpha,\ \nabla_\beta \dot{E}_\alpha,\ \ldots; \quad B_\alpha,\ \dot{B}_\alpha,\ \nabla_\beta B_\alpha,\ \nabla_\beta \dot{B}_\alpha,\ \ldots. \qquad (11)$$

Then to E2–M1 order

$$P_\alpha = \alpha_{\alpha\beta}E_\beta + \omega^{-1}\alpha'_{\alpha\beta}\dot{E}_\beta + \tfrac{1}{2}a_{\alpha\beta\gamma}\nabla_\gamma E_\beta + \tfrac{1}{2}\omega^{-1}a'_{\alpha\beta\gamma}\nabla_\gamma \dot{E}_\beta + G_{\alpha\beta}B_\beta + \omega^{-1}G'_{\alpha\beta}\dot{B}_\beta, \qquad (12)$$

$$Q_{\alpha\beta} = a_{\gamma\alpha\beta}E_\gamma + \omega^{-1}a'_{\gamma\alpha\beta}\dot{E}_\beta, \qquad (13)$$

$$M_\alpha = G_{\beta\alpha}E_\beta - \omega^{-1}G'_{\beta\alpha}\dot{E}_\beta, \qquad (14)$$

where ω is the angular frequency. From their definitions $\mathbf{E}$, ∇, $\mathbf{P}$, $Q_{\alpha\beta}$ are time-even and $\mathbf{B}$, $\mathbf{M}$ time-odd. Thus $\alpha'_{\alpha\beta}$, $a'_{\alpha\beta\gamma}$, $G_{\alpha\beta}$ are time-odd and belong only to magnetic crystals. With (13)–(14) in (10), constitutive relations for $\mathbf{D}$ and $\mathbf{H}$ are obtained. However, these do not satisfy Post's covariance requirement for a plane time-harmonic wave for negligible absorption [6]

$$D_\alpha = A_{\alpha\beta}E_\beta + T_{\alpha\beta}B_\beta, \quad H_\alpha = U_{\alpha\beta}E_\beta + X_{\alpha\beta}B_\beta, \quad A_{\alpha\beta} = A^*_{\beta\alpha}, \quad X_{\alpha\beta} = X^*_{\beta\alpha}, \quad U_{\alpha\beta} = -T^*_{\beta\alpha}. \qquad (15)$$

From $\nabla \times \mathbf{E} = -\dot{\mathbf{B}}$ and with (10), (12)–(14) substituted into (9), one can show that

$$\begin{aligned} P_\alpha &= \alpha_{\alpha\beta}E_\beta + \omega^{-1}[\alpha'_{\alpha\beta}]\dot{E}_\beta + \tfrac{1}{6}\omega^{-1}[a'_{\alpha\beta\gamma} + a'_{\beta\gamma\alpha} + a'_{\gamma\alpha\beta}]\nabla_\gamma \dot{E}_\beta \\ &+ [G_{\alpha\beta} - \tfrac{1}{3}\delta_{\alpha\beta}G_{\gamma\gamma} - \tfrac{1}{6}\omega\epsilon_{\beta\gamma\delta}a'_{\gamma\delta\alpha}]B_\beta + \omega^{-1}(G'_{\alpha\beta} - \tfrac{1}{2}\omega\epsilon_{\beta\gamma\delta}a_{\gamma\delta\alpha})\dot{B}_\beta, \quad (16) \\ Q_{\alpha\beta} &= -\tfrac{1}{3}\omega^{-1}[a'_{\alpha\beta\gamma} + a'_{\beta\gamma\alpha} + a'_{\gamma\alpha\beta}]\dot{E}_\gamma = -S_{\alpha\beta\gamma}\dot{E}_\gamma, \quad (17) \\ M_\alpha &= [G_{\beta\alpha} - \tfrac{1}{3}\delta_{\alpha\beta}G_{\gamma\gamma} - \tfrac{1}{6}\omega\epsilon_{\alpha\gamma\delta}a'_{\gamma\delta\beta}]E_\beta - \omega^{-1}(G'_{\beta\alpha} - \tfrac{1}{2}\omega\epsilon_{\alpha\gamma\delta}a_{\gamma\delta\beta})\dot{E}_\beta. \quad (18) \end{aligned}$$

Terms in brackets [ ] are time-odd. From (10), (16)–(18) and with $\mathbf{E} = \mathbf{E}_0 \exp\{-i(\omega t - \mathbf{k}\cdot\mathbf{r})\}$ the covariant forms in (15) are satisfied. Then from (6) the Ampère-Maxwell equation in (8) is

$$\epsilon_{\alpha\beta\gamma}\nabla_\beta B_\gamma + i\omega\mu_0\epsilon_{\alpha\beta}E_\beta = 0 \quad (19)$$

for a dielectric, where $\epsilon_{\alpha\beta}$ is the dynamic permittivity tensor, which to order E2–M1 is

$$\begin{aligned} \epsilon_{\alpha\beta} &= \epsilon_0\delta_{\alpha\beta} + \alpha_{\alpha\beta} - i\alpha'_{\alpha\beta} + \omega^{-1}k_\gamma(A_{\alpha\beta\gamma} - iA'_{\alpha\beta\gamma}), \quad (20) \\ A_{\alpha\beta\gamma} &= -\epsilon_{\beta\gamma\delta}G_{\alpha\delta} + \epsilon_{\alpha\gamma\delta}G_{\beta\delta} + \tfrac{1}{2}\omega(a'_{\alpha\beta\gamma} + a'_{\beta\alpha\gamma}), \quad (21) \\ A'_{\alpha\beta\gamma} &= -\epsilon_{\beta\gamma\delta}G'_{\alpha\delta} + \epsilon_{\alpha\gamma\delta}G'_{\beta\delta} - \tfrac{1}{2}\omega(a_{\alpha\beta\gamma} - a_{\beta\alpha\gamma}). \quad (22) \end{aligned}$$

We now show that the surface discontinuities in (7) alter the usual Maxwell boundary conditions.

3. The Boundary Conditions

To derive these, unit step functions are used instead of the integral forms of Maxwell's equation. With the surface element in the xy plane and $+z$ axis into the medium, these functions and their derivatives are, using the Dirac δ-function and its derivative δ',

$$u(z) = \begin{cases} 1 \text{ for } z > 0 \\ 0 \text{ for } z < 0 \end{cases}, \; u(-z) = \begin{cases} 0 \text{ for } z > 0 \\ 1 \text{ for } z < 0 \end{cases}, \; \frac{\partial u(\pm z)}{\partial z} = \pm\delta(z), \; \frac{\partial^2 u(\pm z)}{\partial z^2} = \pm\delta'(z), \quad (23)$$

The total bound current and charge densities are then

$$\begin{aligned} \mathbf{J}_t(\mathbf{R}) &= u(z)\mathbf{J}_1(\mathbf{R}) + u(-z)\mathbf{J}_2(\mathbf{R}) + \delta(z)\mathbf{K}(\mathbf{r}), \quad (24) \\ \rho_t(\mathbf{R}) &= u(z)\rho_1(\mathbf{R}) + u(-z)\rho_2(\mathbf{R}) + \delta(z)\sigma(\mathbf{r}) + \delta'(z)\hat{\mathbf{z}}\cdot\boldsymbol{\mathcal{P}}(\mathbf{r}), \quad (25) \end{aligned}$$

where medium 2 is the vacuum, $\mathbf{n} = -\hat{\mathbf{z}}$, and $\mathbf{r}$ lies in the xy plane. Using (23)–(25) in $\nabla\cdot\mathbf{J} = -\dot{\rho}$ and equating the coefficients of $\delta(z)$ one obtains σ in (7) and of $\delta'(z)$ one finds

$$K_z = -\dot{\mathcal{P}}_z = \tfrac{1}{2}\dot{Q}_{zz}, \quad (26)$$

which is $\mathbf{K}$ in (7) for $\alpha = z$. Since these two results confirm (24) and (25), we similarly take

$$\begin{aligned} \mathbf{E}(\mathbf{R}) &= u(z)\mathbf{E}_1(\mathbf{R}) + u(-z)\mathbf{E}_2(\mathbf{R}) + \delta(z)\boldsymbol{\mathcal{E}}(\mathbf{r}), \quad (27) \\ \mathbf{B}(\mathbf{R}) &= u(z)\mathbf{B}_1(\mathbf{R}) + u(-z)\mathbf{B}_2(\mathbf{R}) + \delta(z)\boldsymbol{\mathcal{B}}(\mathbf{r}), \quad (28) \end{aligned}$$

where $\boldsymbol{\mathcal{E}}(\mathbf{r})$ and $\boldsymbol{\mathcal{B}}(\mathbf{r})$ are surface fields. With these in (8) one obtains the boundary conditions

$$\begin{aligned} E_{1x} - E_{2x} &= \nabla_x\mathcal{E}_z, \;\; E_{1y} - E_{2y} = \nabla_y\mathcal{E}_z, \;\; E_{1z} - E_{2z} = (\sigma - \epsilon_{1\alpha z}\nabla_{\Sigma\alpha}\mathcal{E}_z)/\epsilon_0, \quad (29) \\ B_{1x} - B_{2x} &= \mu_0(K_y + \epsilon_{1yz}\dot{\mathcal{E}}_z), \;\; (B_{1y} - B_{2y}) = -\mu_0(K_x + \epsilon_{1xz}\dot{\mathcal{E}}_z), \;\; B_{1z} = B_{2z}, \quad (30) \end{aligned}$$

$$\mathcal{E}_z = \mathcal{P}_z/\epsilon_{1zz} = -\tfrac{1}{2}Q_{zz}/\epsilon_{1zz}. \quad (31)$$

Thus to order E2–M1 the tangential components of $\mathbf{E}$ are no longer continuous across a boundary, whereas the normal component of $\mathbf{B}$ is.

4. The Role of the Surface Density of Electric Dipole Moment

As is evident from (29)–(31) the boundary conditions reduce to the Maxwell forms when $\mathcal{P}$ (or $Q_{\alpha\beta}$) is zero. In the electric dipole (E1) order $Q_{\alpha\beta} = 0$. Thus the Maxwell conditions are an approximation, applying only in the E1 order. From (5) and (17), $\mathcal{P}$ exists only for magnetic media. Also, the tensor $S_{\alpha\beta\gamma}$ in (17) may vanish for symmetry reasons, as for propagation along the main axis of antiferromagnetic Cr_2O_3, even though it possesses the time-odd tensor $a'_{\alpha\beta\gamma}$.

5. Application

The simplest magnetic crystal is an antiferromagnet (since $\alpha'_{\alpha\beta} = 0$) that is centrosymmetric (since its time-even odd-rank polar tensor $a_{\alpha\beta\gamma}$ and even-rank axial tensor $G'_{\alpha\beta}$ vanish). The only such symmetry for which an effect exists at normal incidence is $\underline{4}/\underline{m}\underline{m}\underline{m}$. Its Fresnel reflection matrix for normal incidence parallel to its C_2 axis can be shown to be [7]

$$R = \begin{bmatrix} (n_o - 1)/(n_o + 1) & r_{ps} \\ r_{sp} & -(n_e - 1)/(n_e + 1) \end{bmatrix}, \tag{32}$$

where n_o and n_e are the ordinary and extraordinary refractive indices,

$$r_{sp} = r_{ps} = \mu_0 c[Kn_e/(n_o + n_e) - S_{123}]/(n_o + 1)(n_e + 1), \quad K = 2G_{11} + \omega(a'_{123} + a'_{312}), \tag{33}$$

and S_{123} is the only component that exists of the tensor in (17) which, because of (5), is the surface electric dipole term. The components in (33) are relative to crystallographic axes. The matrix in (32) is identical in form to that of Cr_2O_3 for the same geometry. The effect in Cr_2O_3 is a rotation of the plane of linearly polarized light, which has previously been measured, yielding an experimental value of r_{sp}. Thus r_{sp} should be measurable for a $\underline{4}/\underline{m}\underline{m}\underline{m}$ crystal. A different combination of K and S_{123} enters the birefringence in transmission

$$n_+ - n_- = c\mu_0(3S_{123} - K). \tag{34}$$

From these reflection and transmission experiments a value can be obtained of S_{123} and hence of the contribution of the surface density of electric dipole moment $\mathcal{P}$ to the boundary conditions. This would provide a test of our theory.

References

[1] A. D. Buckingham and M. B. Dunn, "Optical activity of oriented molecules," *J. Chem. Soc.* A, pp. 1988–1991, 1971.

[2] I. M. B. de Figueiredo and R. E. Raab, "A molecular theory of new differential light-scattering effects in a fluid," *Proc. R. Soc. Lond.* **A375**, pp. 425–441, 1981.

[3] I. P. Theron and J. H. Cloete, "The electric quadrupole contribution to the circular birefringence of nonmagnetic anisotropic chiral media: A circular waveguide experiment," *IEEE Trans. Microwave theory and Techniques*, **44**, pp. 1451–1459, 1996.

[4] D. J. Griffiths, *Introduction to Electrodynamics.* New Jersey: Prentice Hall, 1989.

[5] E. B. Graham and R. E. Raab, "Multipole solution for the macroscopic electromagnetic boundary conditions at a vacuum-dielectric interface," *Proc. Roy. Soc. Lond.* A, **456**, pp. 1193–1215, 2000.

[6] E. J. Post, *Formal Structure of Electromagnetics.* Amsterdam: North-Holland, 1962.

[7] E. B. Graham and R. E. Raab, "The role of the macroscopic surface density of bound electric dipole moment in reflection," *Proc. R. Soc. Lond.*, submitted for publication.

Frequency Selective Structures on a Bianisotropic Slab

G. Kristensson[1], S. Poulsen[2], and M. Akerberg[1]

[1] Department of Applied Electronics, Electromagnetic Theory
Lund Institute of Technology, P.O. Box 118, SE-221 00 Lund, Sweden
Fax: +46 46-222 75 08; E-mail: gerhard@teorel.lth.se & martin@teorel.lth.se

[2] Applied Composites AB
P.O. Box 163, SE-341 23 Ljungby, Sweden
Fax: +46 372-672 01; E-mail: soren.poulsen@celsius.se

Abstract

In this paper a method for the analysis of a frequency selective surface (FSS) supported by a bianisotropic substrate is presented. The frequency selective structure is a thin metallic pattern—the actual FSS—on a plane supporting substrate. Integral representations of the fields in combination with the method of moments carried out in the spatial Fourier domain are shown to be a fruitful way of analyzing the problem with a complex substrate.

1. General Equations

The geometry of interest in this paper is depicted in Figure 1. The sources of the problem are assumed to be confined to a region located to the left of the bianisotropic slab, which extends from $z = z_1$ to $z = z_{N-1}$. The depth parameter z is defined by the normal of the interfaces as shown in the figure. The scatterer is a periodic pattern of metal—frequency selective surface (FSS)—located at $z = z_0$ on the left hand side of the slab. The space outside the slab is assumed to be homogeneous, lossless and isotropic with relative permittivity ϵ, permeability μ, and relative impedance $\eta = \sqrt{\mu/\epsilon}$.

The integral representation of the solution to the Maxwell equations in an isotropic region is used to characterize the electric field in the region outside the slab and the scatterer. The stratified geometry also suggest that an expansion of the Green's dyadic in plane vector waves is pertinent [1]. A systematic use of these two concept gives the following representations of the scattered electric field [3] ($\eta_0 = \sqrt{\mu_0/\epsilon_0}$ and $k = \sqrt{\epsilon\mu}\omega/c_0$):

$$
\boldsymbol{E}^s(\boldsymbol{r}) = \begin{cases}
-\dfrac{1}{4\pi^2}\displaystyle\iint_{-\infty}^{\infty}\left(\frac{k\eta_0\eta}{2k_z}\mathbf{P}^+(\boldsymbol{k}_t)\cdot\boldsymbol{J}(\boldsymbol{k}_t)e^{-ik_z z_0}\right)e^{i\boldsymbol{k}_t\cdot\boldsymbol{\rho}+ik_z z}\,dk_x\,dk_y \\
\qquad -\dfrac{1}{4\pi^2}\displaystyle\iint_{-\infty}^{\infty}\left(\gamma^-\cdot\mathbf{r}(\boldsymbol{k}_t)\cdot\boldsymbol{F}^+(\boldsymbol{k}_t,z_1)e^{ik_z z_1}\right)e^{i\boldsymbol{k}_t\cdot\boldsymbol{\rho}-ik_z z}\,dk_x\,dk_y, \quad z_0 < z < z_1 \\
-\dfrac{1}{4\pi^2}\displaystyle\iint_{-\infty}^{\infty}\Big(\frac{k\eta_0\eta}{2k_z}\mathbf{P}^-(\boldsymbol{k}_t)\cdot\boldsymbol{J}(\boldsymbol{k}_t)e^{ik_z z_0} \\
\qquad +\gamma^-(\boldsymbol{k}_t)\cdot\mathbf{r}(\boldsymbol{k}_t)\cdot\boldsymbol{F}^+(\boldsymbol{k}_t,z_1)e^{ik_z z_1}\Big)e^{i\boldsymbol{k}_t\cdot\boldsymbol{\rho}-ik_z z}\,dk_x\,dk_y, \quad z < z_0
\end{cases}
$$

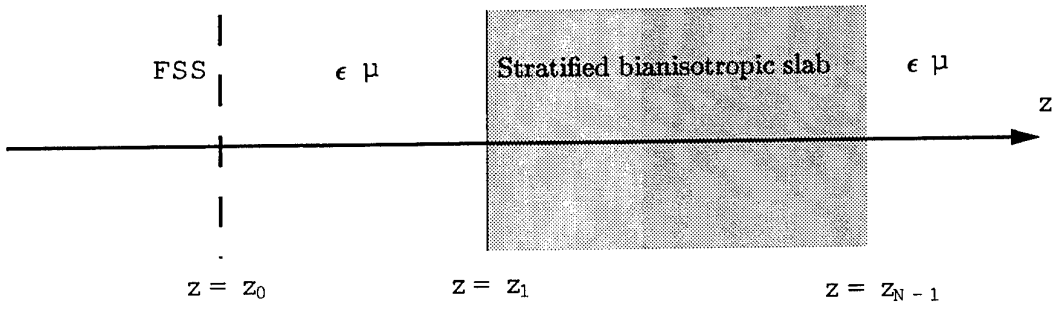

Figure 1: The geometry of the problem.

where the Fourier variable in the x-y-plane is denoted $\boldsymbol{k}_t$ and the normal (longitudinal) wave number, k_z, is defined by $k_z = \left(k^2 - k_t^2\right)^{1/2}$, $(\mathrm{Im}\, k_z \geq 0)$. $\boldsymbol{J}(\boldsymbol{k}_t)$ denotes the Fourier transformed surface currents of the plane $z = z_0$, and the projection dyadic $\mathbf{P}^{\pm}(\boldsymbol{k}_t)$ is defined by [3]

$$\mathbf{P}^{\pm}(\boldsymbol{k}_t) = \frac{k_z^2}{k^2}\hat{\boldsymbol{e}}_{\parallel}\hat{\boldsymbol{e}}_{\parallel} + \hat{\boldsymbol{e}}_{\perp}\hat{\boldsymbol{e}}_{\perp} \mp \frac{k_t k_z}{k^2}\left(\hat{\boldsymbol{z}}\hat{\boldsymbol{e}}_{\parallel} + \hat{\boldsymbol{e}}_{\parallel}\hat{\boldsymbol{z}}\right) + \frac{k_t^2}{k^2}\hat{\boldsymbol{z}}\hat{\boldsymbol{z}}$$

and the reflection dyadic $\mathbf{r}(\boldsymbol{k}_t)$ of the slab and

$$\boldsymbol{\gamma}^{\pm}(\boldsymbol{k}_t) = \pm\left(\mathbf{I}_2 \mp \frac{\boldsymbol{k}_t}{k_z}\hat{\boldsymbol{z}}\hat{\boldsymbol{e}}_{\parallel}\right)$$

where $\mathbf{I}_2$ is the identity dyadic in the x-y-plane. The two (real) unit vectors in the x-y-plane

$$\hat{\boldsymbol{e}}_{\parallel}(\boldsymbol{k}_t) = \boldsymbol{k}_t/k_t, \qquad \hat{\boldsymbol{e}}_{\perp}(\boldsymbol{k}_t) = \hat{\boldsymbol{z}} \times \hat{\boldsymbol{e}}_{\parallel}(\boldsymbol{k}_t)$$

and the split field $\boldsymbol{F}^{+}(\boldsymbol{k}_t, z)$ at the interface is [6]

$$\boldsymbol{F}^{+}(\boldsymbol{k}_t, z) = \frac{1}{2}\boldsymbol{E}_{xy}(\boldsymbol{k}_t, z) - \frac{\eta\eta_0}{2}\left(\hat{\boldsymbol{e}}_{\parallel}\hat{\boldsymbol{e}}_{\parallel}\frac{k}{k_z} + \mathit{unite}_{\perp}\hat{\boldsymbol{e}}_{\perp}\right) \cdot \hat{\boldsymbol{z}} \times \boldsymbol{H}_{xy}(\boldsymbol{k}_t, z)$$

2. Integral Equation for the Surface Current

We employ the Floquet's theorem [2] to the surface current $\boldsymbol{J}(\boldsymbol{r})$ on the FSS and the Fourier transform of this current is [5]

$$\boldsymbol{J}(\boldsymbol{k}_t) = \frac{4\pi^2}{A_E}\sum_{m,n=-\infty}^{\infty} \boldsymbol{J}_E(\boldsymbol{k}_{mn})\delta^2(\boldsymbol{k}_t - \boldsymbol{k}_{mn}), \quad \boldsymbol{k}_t \in \mathbb{R}^2$$

where A_E is the area of the unit cell (sides a and b with the angle Ω between the axis) and $\boldsymbol{k}_{mn} = \hat{\boldsymbol{x}}\alpha_m + \hat{\boldsymbol{y}}\beta_{mn}$ with

$$\alpha_m = \frac{2\pi m}{a} + k_x^i, \qquad \beta_{mn} = \frac{2\pi n}{b\sin\Omega} - \frac{2\pi m}{a}\cot\Omega + k_y^i$$

where k_x^i and k_y^i are the x- and the y-components of the wave vector of the incident field, respectively, and where $\boldsymbol{J}_E(\boldsymbol{k}_{mn})$ is the Fourier transform of $\boldsymbol{J}(\boldsymbol{r})$ over the unit cell E evaluated at $\boldsymbol{k}_{mn}$.

The boundary conditions on the FSS imply that

$$\left(\mathbf{I}_2 + \mathbf{r}(\boldsymbol{k}_{00})e^{2ik_{z00}h}\right) \cdot \boldsymbol{E}_{xy}^i(\boldsymbol{r})\big|_{z=z_0} = \sum_{m,n=-\infty}^{\infty}\left(\mathbf{I}_2 + \mathbf{r}(\boldsymbol{k}_{mn})e^{2ik_{zmn}h}\right) \cdot \boldsymbol{x}_{mn}e^{i\boldsymbol{k}_{mn}\cdot\boldsymbol{\rho}}$$

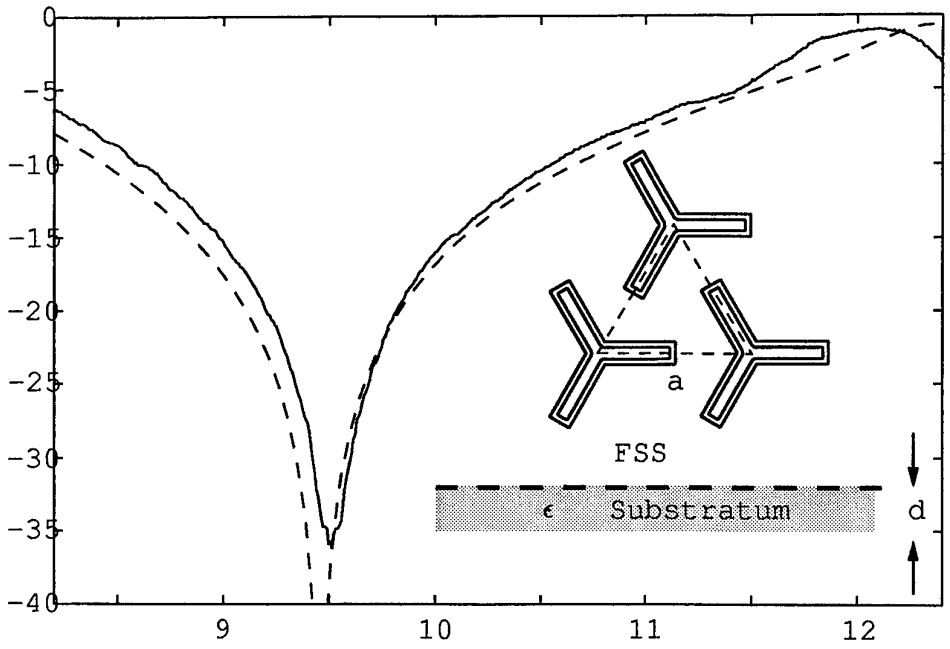

Figure 2: Power transmission (in dB scale) of the co-polarization for a hexagonal pattern of loaded tripoles on an isotropic slab as a function of frequency (GHz). The angle of incidence is $\theta = 60°$ and $\phi = 0°$, and the polarization is TE. The tripoles are 9 mm long with 3 mm long ends. The width of the metallic strips is 0.5 mm. The elements are arranged in an equilateral lattice with side 16.5 mm. The polarization of the incident field perpendicular with one of the sides in the hexagonal pattern. The thickness of the isotropic substrate is $d = 0.12$ mm and the permittivity is $\epsilon = 4.3(1 + i0.021)$. The dashed line shows the computed values and the solid line shows the measurements.

where $h = z_1 - z_0 > 0$ and where $k_{zmn} = \left(k^2 - |\boldsymbol{k}_{mn}|^2\right)^{1/2}$, $(\mathrm{Im}\, k_{zmn} \geq 0)$ and where we have introduced the vector field

$$\boldsymbol{x}_{mn} = \frac{k\eta_0\eta}{2A_E k_{zmn}} \left(\frac{k_z^2}{k^2} \hat{\boldsymbol{e}}_{||} \hat{\boldsymbol{e}}_{||} + \hat{\boldsymbol{e}}_{\perp} \hat{\boldsymbol{e}}_{\perp} \right) \cdot \boldsymbol{J}_E(\boldsymbol{k}_{mn})$$

to simplify the notation. This relation is the basic equation used for the determination of the unknown quantity $\boldsymbol{x}_{mn}$, which is solved by a method of moments technique in the spatial Fourier domain [3]. Once this quantity is determined, all other fields can be obtained.

3. Results

We illustrate the effect of an isotropic, homogeneous dielectric substrate on the transmission properties of the FSS in Figure 2. The effect of a bianisotropic substrate is illustrated in Figure 3. The constitutive relations used here are [6]

$$\boldsymbol{D} = \epsilon_0 \{ \boldsymbol{\epsilon} \cdot \boldsymbol{E} + \eta_0 \boldsymbol{\xi} \cdot \boldsymbol{H} \}, \qquad \boldsymbol{B} = \frac{1}{c_0} \{ \boldsymbol{\zeta} \cdot \boldsymbol{E} + \eta_0 \boldsymbol{\mu} \cdot \boldsymbol{H} \}$$

The material parameters of the slab is [4]

$$\boldsymbol{\epsilon} = \begin{pmatrix} 3 & 0 & 0 \\ 0 & \epsilon_{yy} & 0 \\ 0 & 0 & 3 \end{pmatrix} \quad \boldsymbol{\mu} = \begin{pmatrix} 1 & 0 & 0 \\ 0 & 1 & 0 \\ 0 & 0 & 1 \end{pmatrix} \quad \boldsymbol{\xi} = \begin{pmatrix} 0 & 0 & 0 \\ 0 & 0 & i\Omega \\ 0 & 0 & 0 \end{pmatrix} \quad \boldsymbol{\zeta} = \begin{pmatrix} 0 & 0 & 0 \\ 0 & 0 & 0 \\ 0 & -i\Omega & 0 \end{pmatrix} \qquad (1)$$

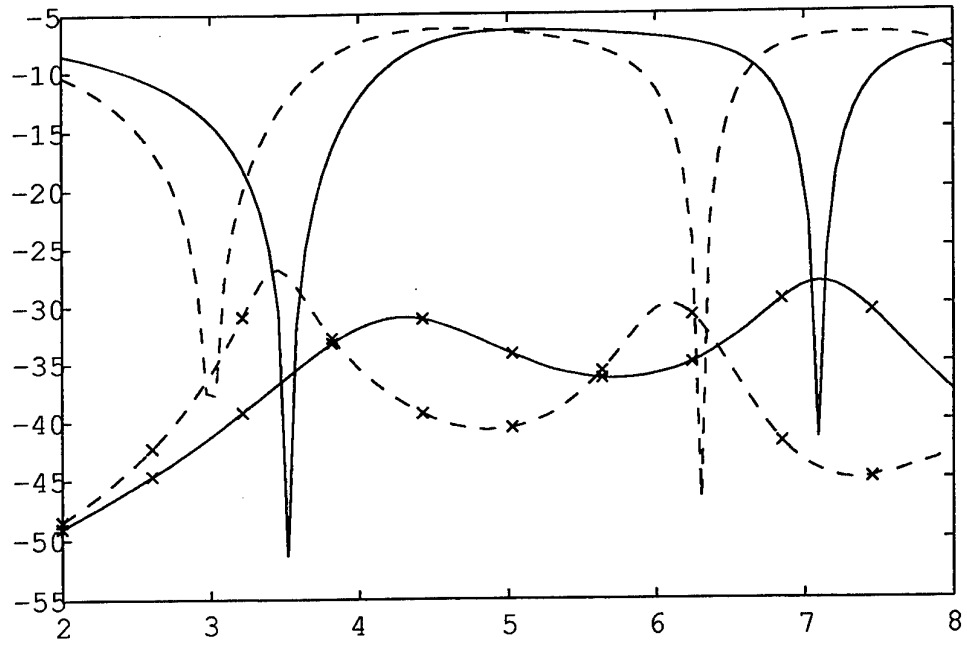

Figure 3: The same element and unit cell geometry as in Figure 2 but the substrate is bianisotropic. The material parameters is given in (1) and the thickness of the substrate is $d = 6$ mm. The curves that correspond to the co-polarization are given by lines without crosses and the cross-polarization curves are given by lines with crosses. The solid lines show the cases where $\epsilon_{yy} = 3$ and $\Omega = 0$ (*i.e.*, an isotropic substrate), and the dashed lines show the cases where $\epsilon_{yy} = 10$ and $\Omega = 0.9$. The angle of incidence is $\theta = 30°$ and $\phi = 0°$, and the polarization is TM.

References

[1] A. Boström, G. Kristensson, and S. Ström, "Transformation properties of plane, spherical and cylindrical scalar and vector wave functions," in V. V. Varadan, A. Lakhtakia, and V. K. Varadan, Editors, *Field Representations and Introduction to Scattering*, Acoustic, Electromagnetic and Elastic Wave Scattering, Chapter 4, pp. 165–210. Elsevier Science Publishers, Amsterdam, 1991.

[2] A. Ishimaru, *Electromagnetic Wave Propagation, Radiation, and Scattering.* Prentice-Hall, Inc.: Englewood Cliffs, New Jersey, 1991.

[3] G. Kristensson, M. Åkerberg, and S. Poulsen, *Scattering from a frequency selective surface supported by a bianisotropic substrate.* Technical Report LUTEDX/(TEAT-7085)/1–28/(2000): Lund Institute of Technology, Department of Applied Electronics, Electromagnetic Theory, P.O. Box 118, S-211 00 Lund, Sweden, 2000.

[4] M. Norgren and S. He. "Electromagnetic reflection and transmission for a dielectric-Ω interface and a Ω slab," *Int. J. Infrared and MM Waves*, **15**(9), 1537–1554, 1994.

[5] S. Poulsen, "Scattering from frequency selective surfaces: A continuity condition for entire domain basis functions and an improved set of basis functions for crossed dipole," *IEE Proc.-H Microwaves, Antennas and Propagation*, **146**(3), 234–240, 1999.

[6] S. Rikte, G. Kristensson, and M. Andersson, *Propagation in bianisotropic media—reflection and transmission.* Technical Report LUTEDX/(TEAT-7067)/1–31/(1998): Lund Institute of Technology, Department of Electromagnetic Theory, P.O. Box 118, S-211 00 Lund, Sweden, 1998.

Singular Guided Waves in a Chiroplasma

V. V. Fisanov[1] and D. A. Marakassov[2]

[1] Siberian Physical and Technical Institute, Tomsk State University
Revolution Square 1, 634050 Tomsk, Russia
Fax: +7–3822–233–034; email: kanc@spti.tsu.ru

[2] Department of Radiophysics, Tomsk State University
Lenin Avenue 36, 634050 Tomsk, Russia;
Electromagnetics Laboratory, Helsinki University of Technology
P.O. Box 3000, FIN-02015 HUT, Finland

Abstract

Waves with linearly distance-dependent amplitude (singular waves) directed by one and two plane boundaries in a chiroplasma are investigated for the Voigt geometrical configuration. Specially selected values of the chirality parameter give a transparent and an opaque version of the medium with twofold wave numbers for bulk eigenwaves. Dispersion relations are derived and solved with respect to electric or magnetic walls and an interface of two media.

1. Introduction

Waves with distance-dependent amplitude (so-called *singular waves*) correspond to multiple roots of the related secular equation. They are known in optics of absorbing and transparent crystals (see e.g. [1], [2]). Such a form of solution is suitable especially well for waves guided by different boundaries. In particular, singular surface polaritons and magnetoplasmons may propagate along the plane surface of an anisotropic crystal [3] and a magnetoplasma interface in the Faraday geometric configuration [4]. We consider singular guided waves in a chiroplasma in the case of the Voigt configuration, when these waves do not exist in a nonchiral magnetoplasma [5].

2. Transverse Propagating Singular Eigenwaves

A chiroplasma is the gyroelectric version of the Faraday chiral media described by the well-known constitutive relations [6]

$$\begin{cases} \mathbf{D} = \bar{\bar{\varepsilon}} \cdot \mathbf{E} + i\xi\mathbf{B} \\ \mathbf{H} = i\xi\mathbf{E} + \mathbf{B}/\mu \end{cases} \tag{1}$$

where

$$\bar{\bar{\varepsilon}} = \varepsilon_\infty \begin{pmatrix} \varepsilon & -ig & 0 \\ ig & \varepsilon & 0 \\ 0 & 0 & \varepsilon_z \end{pmatrix} \tag{2}$$

is the permittivity tensor for the biasing magnetostatic field directed along the z-axis. Its elements depend on reduced frequency parameters Ω and R as usual [7]. The time-harmonic $\exp(-i\omega t)$ dependence is meant.

We study transverse to the z-axis eigenwave propagation. In this case, one can introduce a scalar function $\varphi(x,y)$ satisfying the fourth-order wave equation

$$\left\{\Delta_\perp^2 + \left[k_\infty^2\left(\varepsilon_\perp + \varepsilon_z\right) + 4\omega^2\mu^2\xi^2\right]\Delta_\perp + k_\infty^4\varepsilon_\perp\varepsilon_z\right\}\varphi\left(x,y\right) = 0 \tag{3}$$

where $\Delta_\perp = \partial^2/\partial x^2 + \partial^2/\partial y^2$, $k_\infty = \omega\sqrt{\varepsilon_\infty\mu}$, and $\varepsilon_\perp = \varepsilon - g^2/\varepsilon$ is the Voigt permittivity. The differential operator allows to fulfil the factorisation procedure

$$\left[\left(\Delta_\perp + k_\infty^2\kappa_+^2\right)\left(\Delta_\perp + k_\infty^2\kappa_-^2\right)\right]\varphi\left(x,y\right) = 0 \tag{4}$$

where the eigenvalues

$$\kappa_\pm^2 = \frac{1}{2}\left[\varepsilon_\perp + \varepsilon_z + 4a^2 \pm \sqrt{\left(\varepsilon_\perp - \varepsilon_z + 4a^2\right)^2 + 16a^2\varepsilon_z}\right] \tag{5}$$

define two possible kinds of field polarization, $a = \xi\sqrt{\mu/\varepsilon_\infty}$ is the normalized chirality admittance. Unlike an isotropic chiral medium, the wave numbers κ_+ and κ_- can be equal here under condition that the square root in Eq. (5) is zero. This gives critical values of $a = \pm a_{1,2}$ where

$$a_{1,2} = \tfrac{1}{2}\left(\sqrt{-\varepsilon_z} \pm \sqrt{-\varepsilon_\perp}\right) \tag{6}$$

if both $\varepsilon_\perp$ and ε_z are negative. It is valid inside the frequency range

$$0 < \Omega^2 < \frac{1}{2}\left[R^2 + 2 - \sqrt{R^2\left(R^2+4\right)}\right]. \tag{7}$$

Both values of a (6) make possible to consider a chiroplasma as a nonchiral gyroelectric unirefringent medium characterized by the wave equation

$$\left[\left(\Delta_\perp + k_\infty^2\kappa^2\right)^2\right]\varphi\left(x,y\right) = 0 \tag{8}$$

with the twofold wave number $\kappa = \kappa_1 = \sqrt[4]{\varepsilon_z\,\varepsilon_\perp}$ (this is the geometric mean between the indices of the ordinary and extraordinary waves in a nonchiral magnetoplasma) or $\kappa = \kappa_2 = i\sqrt[4]{\varepsilon_z\,\varepsilon_\perp}$.

The general form of solution of Eq. (8) differs from the usual homogeneous plane-wave representation in respect of the amplitude factor which is now distance-dependent. Hereafter, we intend to concentrate on waves guided along the x-axis (it is referred to as the Voigt geometric configuration), therefore we prefer to write down the partial solution of Eq. (8) as follows:

$$\varphi\left(x,y\right) = \left(Z_1 + Z_2 y\right)\exp\left[ik_\infty\left(\alpha x + \beta y\right)\right], \qquad \alpha^2 + \beta^2 = \kappa^2 \tag{9}$$

where Z_1 and Z_2 do not depend on the coordinates. Expressions for the singular-wave components of $\mathbf{E}$ and $\mathbf{H}$ are derived from the Maxwell and Helmholtz equations in conjunction with Eq. (1).

3. Singular Surface Waves Guided by a Boundary or an Interface

Let the half-space of the medium $y > 0$ be bounded by a plane screen or an interface of infinite extent. The boundary is able to trap a singular surface wave having real α and pure imaginary β because the exponential attenuation exceeds the linear growth in the y direction.

An electric wall. The boundary condition $\mathbf{e}_y \times \mathbf{E}\left(x,0\right) = 0$ leads to the set of linear algebraic equations

$$\begin{cases} Z_2 + k_\infty\left(\frac{g}{\varepsilon}\alpha + i\beta\right)Z_1 &= 0 \\ 2i\beta Z_2 + k_\infty\left(\varepsilon_\perp - \kappa^2\right)Z_1 &= 0. \end{cases} \tag{10}$$

To find nontrivial solutions of Eq. (10) its determinant should be set equal to zero. This allows to obtain the secular equation

$$\varepsilon_\perp - \kappa^2 - 2i\beta\left(\frac{g}{\varepsilon}\alpha + i\beta\right) = 0\,. \tag{11}$$

This equation is solved exactly. A unidirectional surface wave exists only if $\varepsilon > 0$ and it propagates with the coefficient $\alpha = |\alpha|\,\mathrm{sgn}\,g$ where

$$\begin{pmatrix}|\alpha|\\ |\beta|\end{pmatrix} = \frac{1}{2}\left[\left(\sqrt{\varepsilon-\varepsilon_z}+\sqrt{\varepsilon-\varepsilon_\perp}\right)^2 - \left(\sqrt{-\varepsilon_z}\mp\sqrt{-\varepsilon_\perp}\right)^2\right]^{1/2}. \tag{12}$$

Eq. (12) is valid for the case of the transparent medium ($\kappa = \kappa_1$). Option $\kappa = \kappa_2$ (the case of the opaque medium) needs to interchange $|\alpha|$ and the decrement $|\beta|$.

It is worthwhile to compare this hybrid singular wave with the unidirectional TEM surface wave on a perfectly conducting electric screen placed in a magnetoplasma [5]. That wave has $|\alpha| = \sqrt{\varepsilon}$, its low-frequency branch exists for $\Omega < R$ where bulk waves do not propagate ($\kappa = \sqrt{\varepsilon_\perp}$ is purely imaginary).

A magnetic wall. Applying the boundary condition $\mathbf{e}_y \times \mathbf{H}(x,0) = 0$ we receive the dispersion equation

$$2\left(\sqrt{-\varepsilon_z}\pm 3\sqrt{-\varepsilon_\perp}\right)\beta^2 \mp \sqrt{-\varepsilon_\perp}\,(\varepsilon_\perp - \varepsilon_z) - 2i\frac{g}{\varepsilon}\frac{\left(\sqrt{-\varepsilon_z}\pm\sqrt{-\varepsilon_\perp}\right)^2}{\sqrt{-\varepsilon_z}\mp\sqrt{-\varepsilon_\perp}}\alpha\beta = 0 \tag{13}$$

which describes also a unidirectional singular surface wave. Here the upper sign corresponds to $\kappa = \kappa_1$ and the lower one to $\kappa = \kappa_2$. After a hyperbolic substitution, Eq. (13) is transformed to a quadratic equation. For $\kappa = \kappa_1$, the direction of propagation is defined according to $\mathrm{sgn}(g\varepsilon\alpha) = 1$, and the wave exists inside the band (7). For $\kappa = \kappa_2$, there is a gap in the dispersion diagram if R is small.

An interface of two enantiomorphous media. In order to find the dispersion relation in the case of an interface of two mirror-conjugate media

$$\left(1\pm\frac{\sqrt{\varepsilon_\perp\varepsilon_z}}{\varepsilon}\right)\left(\sqrt{-\varepsilon_z}\pm\sqrt{-\varepsilon_\perp}\right)^2\beta^2 + \frac{1}{4}(\varepsilon_\perp-\varepsilon_z)^2 - \left(4+\frac{\left(\sqrt{-\varepsilon_z}\pm\sqrt{-\varepsilon_\perp}\right)^2}{\varepsilon}\right)\beta^4 = 0 \tag{14}$$

(where the upper and lower signs correspond to the transparent and nontransparent media, respectively) one has to require continuity of tangential electric and magnetic fields at the interface $y = 0$. Singular surface wave propagates symmetrically in both directions within the band (7). In the opaque medium the pass band has the lower cut off bound if $R^2 < 4(4+3\sqrt{2})$.

4. Singular Waves of a Parallel–Plate Waveguide

Let us consider two parallel electric or magnetic walls $y = 0$ and $y = d$ bounding the waveguide region entirely filled by chiroplasma. In order to describe the singular field one needs to take a superposition of two countersolutions in the form of Eq. (9). Transcendental dispersion relations

$$4\frac{\varepsilon_\perp}{\varepsilon\left(\varepsilon_\perp-\kappa^2\right)^2}\beta^2\left(\beta^2+\varepsilon-\kappa^2\right)+1-\left[\frac{k_\infty\beta d}{\sin\left(k_\infty\beta d\right)}\right]^2 = 0 \tag{15}$$

(for electric walls) and

$$8\beta^2\frac{2\beta^2\left[\left(\varepsilon_\perp+a^2\right)^2 - a^4\frac{g^2}{\varepsilon^2}\right] - \left(\varepsilon_\perp+a^2\right)\left(\varepsilon_\perp+\kappa^2\right)\left(\varepsilon_\perp+2a^2-\kappa^2\right) + 2a^4\frac{g^2}{\varepsilon^2}\kappa^2}{\left(\varepsilon_\perp+2a^2-\kappa^2\right)^2\left(\varepsilon_\perp+\kappa^2\right)^2}$$
$$+1-\left[\frac{k_\infty\beta d}{\sin\left(k_\infty\beta d\right)}\right]^2 = 0 \tag{16}$$

(for magnetic walls) contain a common trigonometric part. Dispersion features of singular waves are quite different in the cases with $\kappa = \kappa_1$ and $\kappa = \kappa_2$. For the opaque medium, the waveguide slightly resembles the appropriate perfectly conducting screen, however an additional frequency stop-band appears for the variant with magnetic walls. The behaviour of singular guided waves in the transparent medium is more complicated because their transverse wave numbers may have real values. Under certain conditions, a singular waveguide supports one slow and a few fast waves.

5. Conclusion

The singular surface electromagnetic waves are guided by a plane boundary of a chiroplasma half-space if chirality and plasma parameters are properly matched. They form a complete set of surface polaritons jointly with the Rayleigh surface waves and generalized surface waves [7], [8] in the Voigt geometry. It is shown that a parallel-plate waveguide supports under certain conditions singular propagating modes whose characteristics drastically depend on the type of the boundary conditions.

Acknowledgement
D. Marakassov thanks the Helsinki University of Technology for a study term in the year 2000 and financial support.

References

[1] A. P. Khapaliuk, "Circular optical axes in absorbing crystals," *Kristallografiya*, vol. 7, no. 5, pp. 724–729, 1962. (in Russian)

[2] F. I. Fedorov and N. S. Petrov, "A special case of non-uniform electromagnetic waves in the transparent crystals," *Opt. Spektrosk.*, vol. 14, no. 2, pp. 256–261, 1963. (in Russian)

[3] F. N. Marchevskii, V. V. Strizhevskii, and S. V. Strizhevskii, "Singular electromagnetic waves in bounded anisotropic media," *Solid State Physics*, vol. 26, no. 5, pp. 1501–1503, 1984. (in Russian)

[4] S. T. Ivanov, N. I. Nikolaev, and R. W. Thomae, "Magnetoplasmons along the interface of gyrotropic plasma surface – longitudinal propagation," *Physica Scripta*, vol. 57, no. 6, pp. 645–651, 1998.

[5] S. R. Seshadri, "Excitation of surface waves on a perfectly conducting screen covered with anisotropic plasma," *IRE Trans. Microwave Theory and Techniques*, vol. 10, no. 6, pp. 573–578, 1962.

[6] N. Engheta, D. L. Jaggard, and M. W. Kowarz, "Electromagnetic waves in Faraday chiral media," *IEEE Trans. Antennas Propagat.*, vol. 40, no. 4, pp. 367–374, 1992.

[7] V. V. Fisanov and D. A. Marakasov, "Electromagnetic surface waves at a plane boundary of semi-infinite Faraday chiral media," in A. Priou *et al.* (eds.), *Advances in Complex Electromagnetic Materials*, Dordrecht: Kluwer Academic Publishers, 1997, pp. 239–248.

[8] V. V. Fisanov and D. A. Marakasov, "Surface waves at a plane interface of semi-infinite Faraday chiral media," in *Proc. BIANISOTROPICS'97*, Glasgow, Great Britain, June 1997, pp. 137–140.

Analysis of Reflection of Electromagnetic Waves by Multi-Layered Arrays of Complex-Shaped Elements: Application to Electronically Controllable PBG

S. L. Prosvirnin[1] and S. Zouhdi[2]

[1] Institute of Radio Astronomy of National Academy of Sciences of Ukraine
Krasnoznamennaya Street 4, 61002 Kharkov, Ukraine
Fax: + 38–0572–476506; email: prosvirnin@rian.kharkov.ua

[2] Laboratoire de Genie Electrique de Paris LGEP, Supelec
Plateau de Moulon, 91192 GIF SUR YVETTE Cedex, France
Fax: + 33–1–69 41 83 18; email: sz@ccr.jussieu.fr

Abstract

The results of the numerical analysis of reflecting and transmitting properties of multi-layered structures composed of doubly periodic arrays of metallic strips are presented in the paper. Strip elements have been selected, having a shape of letters C, S and Ω. The strips of the arrays are placed on a thin dielectric substrate. Strip elements can have bulk impedance loading, included in the break of strip. The interference of multi-layered array systems, due to multiple reflections of waves between layers, combined with the resonance properties of single layers lead the structure to acquire properties typical for photonic band gap crystals (PBG).

1. Introduction

Photonic band gap (PBG) crystals made with a few layers of periodic arrays of metal strip particles placed on thin dielectric substrate are useful for a wide range of applications in the microwave region such as novel antenna structures, frequency selective surfaces, filters with alternate frequency stop bands and pass bands. Frequent PBG structures are constructed with arrays of thin PEC disks [1] and thin metal rods [2]. A complex shape of strip particles of PBG structures gives various new resources. First of all, a complex shape particle can have a total length greater than the size of array's unit cell. This is important for making substrates of tiny microwave devices. Secondly, PBG consisting of complex shape particles can effectively transform the polarization of reflected wave in comparison with polarization of incident wave. Structures of plano-chiral elements such as strip having the shape of letter S have properties similar to true chiral structures [3]. Third of advantages of complex shaped particles is controllability of their electromagnetic properties by connecting active electronic loads such as PIN diodes to the complex particles.

The reflection properties of complex layered metal strip arrays placed in free space was studied recently [4]. Now our main goal is the study of reflection of more practical PBG layered array structures on dielectric substrates and arrays consisting of strip particles having bulk impedance loading, included in the break of strip.

2. Operators of Reflection and Transmission of Single Array Layer

Let us assume a plane electromagnetic wave incident on an plane double periodic array. The reflected and transmitted fields can be represented as superposition of partial waves of TE and TM polarizations. It is convenient to confront set of amplitudes of reflected partial waves and transmitted ones with a set of amplitudes of incident field by using operators $r_1^{\pm}$ and $t_1^{\pm}$ of reflection and transmission a single array placed on dielectric substrate. The indices plus and minus respectively are denoted the operators for the wave incident from the side of metal strip and opposite side of dielectric slab. Method of moments was used practically in the cases of wave scattering by arrays of thin narrow strips. The method of works [5], [6] was modified for simulation wave scattering by array on substrate.

3. Operators of Reflection and Transmission of a Finite Number of Arrays

A system of a finite number of arrays is shown in Fig. 1. The structure is assumed to be equidistant and to consist of identical arrays having identical orientations of the elements. Electromagnetic field in each gap between planar arrays may be represented in the form of a set of partial TE - and TM - waves propagating or exponentially decaying from one array plane to another. Amplitudes of the transverse components of the partial waves are denoted as following: q for the incident field, $r_n^+ q$ for the reflected field, $t_n^+ q$ for the transmitted field, and A, B for the fields in the gap between the next to the last array and the last array of the structure, see Fig. 1.

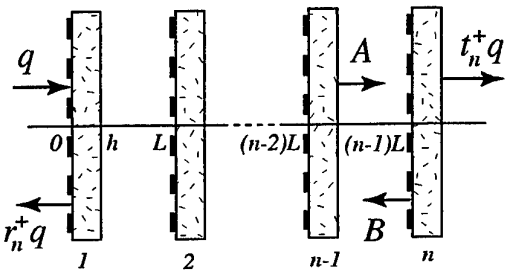

Figure 1: Layered structure

Let us assume operators $r_1^{\pm}$, $t_1^{\pm}$ for a single array to be known, as well as $r_{n-1}^{\pm}$, $t_{n-1}^{\pm}$ for the system of $(n-1)$ arrays, and show that the operators for the whole system can then be found recursively. The amplitudes of the partial waves satisfy equations

$$\begin{cases} A &= t_{n-1}^+ q + r_{n-1}^- eB \\ B &= r_1^+ eA \\ r_n^+ q &= r_{n-1}^+ q + t_{n-1}^- eB \\ t_n^+ q &= t_1^+ eA \end{cases} \tag{1}$$

where operator e is the plane-wave propagator operator from the plane of one array to the next array plane along the direction of propagation. The quite similar equations can be wrote in the case of electromagnetic wave incidence from right side of layered structure. After elimination of vectors A and B from (1) and the corresponding vectors of second set of equations one obtains recurrent expressions which allow to find operators $r_n^{\pm}$ and $t_n^{\pm}$ in the form

$$\begin{aligned} r_n^{\pm} &= r_{n-1}^{\pm} + t_{n-1}^{\mp} e r_1^{\pm} e (I - r_{n-1}^{\mp} e r_1^{\pm} e)^{-1} t_{n-1}^{\pm} \\ t_n^{\pm} &= t_1^{\pm} e (I - r_{n-1}^{\mp} e r_1^{\pm} e)^{-1} t_{n-1}^{\pm} \end{aligned} \tag{2}$$

In this way we can find any scattering characteristics of the array system, i.e. amplitudes of partial waves reflected and transmitted by the layered system using operators $r_n^{\pm}$ and $t_n^{\pm}$.

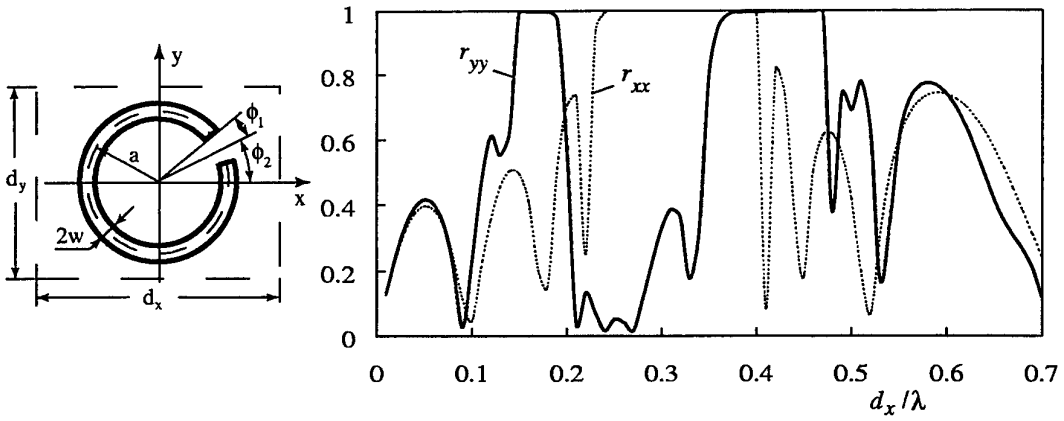

Figure 2: Absolute values of the reflection coefficients: C-shaped particles, 4 layers, $\varepsilon = 3$, $h = 0.25$ mm, $d_x = d_y = 3$ mm, $a = 1.25$ mm, $\phi_1 = 10°$, $\phi_2 = 0$, $w = 0.05$ mm, $L = 2.5$ mm

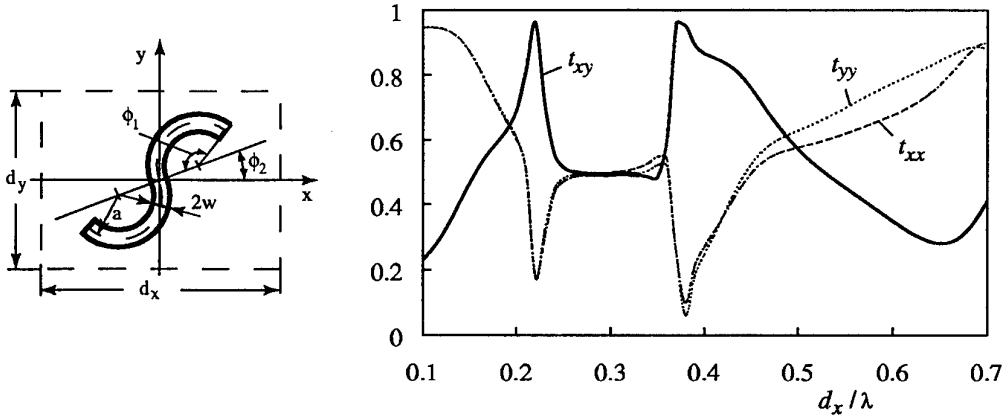

Figure 3: Absolute values of the transmission coefficients: S-shaped particles, 3 layers, $\varepsilon = 3$, $h = 0.25$ mm, $d_x = d_y = 3$ mm, $a = 1$ mm, $\phi_1 = 120°$, $\phi_2 = 0$, $w = 0.05$ mm, $L = 2.5$ mm

4. Numerical Results and Discussion

A system with two wide zones of full reflection can be made using a 4-layer structure with C-shaped particles on substrate. Its frequency characteristics are shown on Fig. 2. The first reflection zone is in the low frequency area. It is the first resonance (polarization along axis Oy) depending on the element length with the resonance between the first and the fourth layers. The second zone is the second length resonance with resonances between layers: layer 1 and layer 2 ($L_{12} \approx \lambda/2$), layer 1 and layer 3 ($L_{13} \approx \lambda$), layer 1 and layer 4 ($L_{14} \approx 3\lambda/2$), when $d_x/\lambda \approx 0.6$.

Similar behavior of frequency dependence of the reflection coefficient is observed in the case of a 4-layer structure with Ω-shaped elements.

Layered arrays of plano-chiral S-shaped particles have ability of effective transformation of polarization of incident wave near resonant frequency of strip particle. There is a wide frequency zone of equal levels of absolute values of transmission and reflection coefficients, see Fig. 3.

Frequency dependencies of reflection coefficients of layered arrays of loaded particles are shown on Fig. 4. Inductive loading leads to increase the electric length of particle. The resulting particle resonances and the resonances due to interference between layers give a complex system

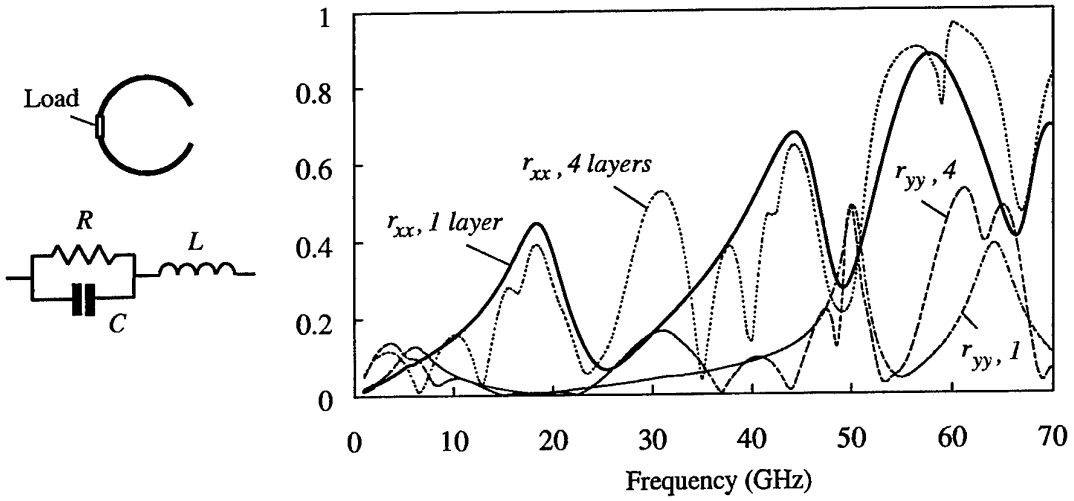

Figure 4: Absolute values of the reflection coefficients: C-shaped loaded particles, array without substrate, $d_x = d_y = 6$ mm, $a = 2.5$ mm, $\phi_1 = 10°$, $\phi_2 = 0$, $w = 0.1$ mm, $L = 5$ mm, parameters of load are $R = 0.136\ \Omega$, $L = 1.2$ pH, $C = 0$ F

of reflection and transmission zones. There is possibility to control frequency characteristics of structure by using active electronic devices as load.

4. Conclusion

Using layered structures instead of single array of complex shape particles enable to give the opportunity to have more sharp and wide band frequency zones of full reflection and polarization transformation. Controlling the frequency characteristics of layered arrays can be achieved by associating electronic loads to the array particles.

References

[1] H. F. Contopanagos, C. A. Kyriazidou, W. M. Merrill, and N. G. Alexopoulos, "Effective response functions for photonic bandgap materials," *J. Opt. Soc. Am. A*, vol. 16, no. 7, pp. 1682–1699, July 2000.

[2] J. -M. Lourtioz, A. de Lustrac, F. Gadot, S. Rowson, A. Chelnokov, T. Brillat, A. Ammouche, J. Danglot, O. Vanbesien, and D. Lippens, "Toward controllable photonic cristals for centimeter- and millimeter-wave devices," *J. Lightwave Technol.*, vol. 17, no. 11, pp. 2025–2031, November 1999.

[3] S. L. Prosvirnin, "Analysis of electromagnetic wave scattering by plane periodical array of chiral strip elements," in *Proc. of 7-th Intern. Conf. on Complex Media "Bianisotropics-98"*, Braunschweig, Germany, June 1998, pp. 185–188.

[4] S. L. Prosvirnin, S. A. Tretyakov, T. D. Vasilyeva, A. Fourrier-Lamer, and S. Zouhdi, "Analysis of reflection and transmission of electromagnetic waves in complex layered arrays," *Journal of Electromagnetic Waves and Applications*, vol. 14, pp. 805–824, 2000.

[5] T. D. Vasilyeva and S. L. Prosvirnin, "Electromagnetic wave diffraction by the plane array of chiral strip elements of complex shape," *Physics of wave processes and radio systems*, vol. 1, no. 4, pp. 5-9, 1998 (in Russian).

[6] S. Zouhdi, G. E. Couenon, and A. Fourrier-Lamer, "Scattering from a periodic array of thin planar chiral structures - calculations and measurements," *IEEE Trans. Antennas and Propagat.*, vol. 47, no. 6, pp. 1061-1065, June 1999.

Session 11

Friday - September 29, 2000

13:30 - 14:40

Unconventional Media: Wire, Turbid and Chiroferrite

An Overview of the Theory of Wire Media

C. A. Moses and N. Engheta

University of Pennsylvania
Moore School of Electrical Engineering
Philadelphia, Pennsylvania 19104, U.S.A.
Tel: +1-215-898-9777, Fax: +1-215-573-2068
E-mail: engheta@ee.upenn.edu
Web: http://www.ee.upenn.edu/~engheta/

Abstract

We present an overview of the electromagnetic theory of wire media. One can conceptually envision this class of media as composite media composed of thin wire inclusions that need not be necessarily electrically short, but can be from a fraction of a wavelength in length to multiple wavelengths in length. One can suggest several different forms and geometries for these wire inclusions; as one example of these media, we have considered the case of a medium that could be synthesized by embedding many identical, finite-length (with some arbitrary identical length), parallel, thin wire inclusions within an otherwise isotropic host medium. In this talk, we review the modeling and analysis of electromagnetic wave propagation in such media, present some results of such analysis, discuss their salient features and physical justifications, and mention some other novel inclusion geometries and shapes for wire media.

1. Introduction

The investigation of wave interaction with complex electromagnetic materials has been a subject of great interest over the past several years. Such interest has arisen from various perspectives---from mathematical, analytical, and computational techniques in treating radiation, scattering, and guidance of electromagnetic waves in complex media, to suggestions for potential applications, and to ideas for fabrication of some types of complex media, especially as connected to experimental verifications of their electromagnetic properties. Application of novel electromagnetic complex materials in future devices may provide new opportunities to solve some of the challenges in various fields such as wireless personal communication systems and mobile services.

Traditionally, analysis of the electromagnetic features of complex media has been more focused on realizations where the dispersed inclusions have been assumed to be small compared to the operating wavelength. However, can one suggest novel geometries for material inclusions such that while they would not necessarily be electrically short the entire ensemble may still be macroscopically considered as a *medium*? One possible scenario would be to imagine a class of artificial materials in which the inclusions are permitted to be electrically long in one dimension and yet still electrically small in the other two dimensions (i.e., the inclusions have small transverse cross sections that might vary along their length). Such inclusions can then all be positioned in parallel and in close proximity to each other so the entire structure may be macroscopically regarded as a *medium*. How then do we analyze and model electromagnetic wave propagation in such complex media?

2. Modeling

As an illustrative case, we consider one conceptualization of these media in which the wire inclusions are taken to be identical, but arbitrary finite-length, parallel, thin wire inclusions within an otherwise isotropic host medium. This case is an example of a larger class of complex media in which the inclusions are permitted to be electrically long in one dimension but still electrically small in the other two dimensions (e.g., the feedforward-feedbackward (FFFB) medium [1]). Furthermore, for the sake of mathematical simplicity in our analysis, we assume that these wire inclusions have been positioned on a 3-D periodic structure. However, since we want to allow the wire inclusions to have arbitrary (but identical) electrical length and at the same time we want to keep the spatial periodicities of the structure small (so an ensemble of such wires would form a macroscopic *medium*), the wire axes should be titled away from the lattice axis.

The theoretical approach we use here considers the medium as concatenation of many closely-spaced elementary planes, each of which contains a distribution of parallel identical wire inclusions located on a 2-D periodic lattice. (The types of surfaces resembling these elementary planes have been called Super-Dense dipole surfaces or Gangbuster surfaces in the context of frequency-selective surfaces (FSS) by Schneider and Munk [2], Larson and Munk [3], Kornbau [4].) The interaction of electromagnetic waves with the elementary planes is studied numerically using the standard periodic method of moments (MoM), and then, from knowledge of the wave interaction with a single elementary plane, periodic-structure theory is used to analyze wave propagation within the entire medium. Our theoretical studies have shown some interesting features connected to plane wave propagation in these media. Here we present some sample results. More results and details of our analysis of wire media are reported in [5, 6].

3. Reflection Properties of a Single Plane

Consider, as an example, an elementary plane where parallel identical wire inclusions are positioned on a 2-D periodic lattice as shown in Fig. 1. The periodicities of the square lattice structure is chosen as $D = 0.13\Lambda$ where Λ is some reference length (not the wavelength) that may be selected to scale this surface to any desired physical size. The length and radius of these identical wires are selected as $L = 0.533\Lambda$ and $a = 0.001\Lambda$, respectively. The "tilt angle" for this example is $\alpha = 14°$. The operating wavelength λ_o can be chosen from a fraction of the reference length Λ to multiples of Λ.

After going through a series of mathematical steps and MoM analyses [5, 6], one can find the reflection coefficient of this elementary plane when illuminated by an incident plane wave. In our investigation, we noticed that the variation of the reflection coefficient was greater as a function of angle of incidence in the E-plane (i.e., where the plane of incidence is parallel with the wire inclusions) than in the H-plane (where the plane of incidence is perpendicular to the wire inclusions) [5], so here, in the interest of space, we only present the results for the E-plane. More results can be found in [5].

Furthermore, we only consider TM^z waves (where the z-axis is parallel with the wire axes), because for these waves the incident electric field interacts appreciably with the thin wire inclusions. For the TE^z waves the thin wires do not interact with the incident wave since the incident electric field is perpendicular to the wires (the wire medium is effectively transparent to TE^z waves). Figure 2a shows the reflection coefficient of this elementary plane as a function of λ_o / Λ for a normally incident TM^z wave in the E-plane [5, 6]. At the smallest relative wavelength in this figure, $\lambda_o / \Lambda = 0.25$, the wires are just over two wavelengths long (i.e., $L = 2.13\lambda_o$) and at the largest relative wavelength in this figure, $\lambda_o / \Lambda = 2$, the wires are about $L = 0.27\lambda_o$.

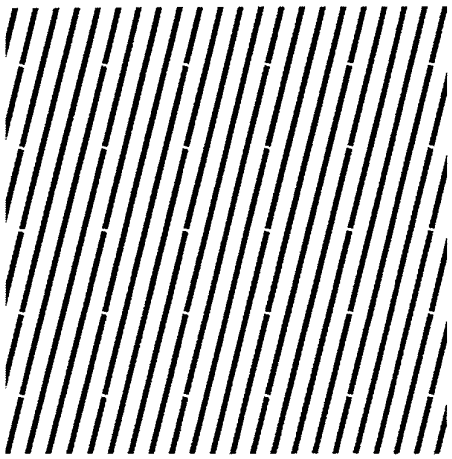

Fig. 1 An example of an elementary plane of a wire medium. The radius of these wires is taken to be very thin in our analysis. However, in this illustration, the wire radius is exaggerated five times in order to make it visible in print. See the text for the geometrical parameters for this example.

Note that grating lobes are not present for normal incidence throughout this range of relative wavelengths because the periodicities of the structure are chosen short enough to prevent this effect. Some of the interesting features of this figure, which are expected for the FSS, should be mentioned. (1) Two points on the reflection curve reach the point of complete reflection, i.e., $R=-1$. The first point occurs at $\lambda_o/\Lambda=0.83$ (which indicates that $L=0.64\lambda_o$), and the second point at $\lambda_o/\Lambda=0.34$ (i.e., $L=1.57\lambda_o$); (2) a deep null occurs near the point $\lambda_o/\Lambda=0.39$ (i.e., $L=1.37\lambda_o$), and this is between the two wavelengths for complete reflection.

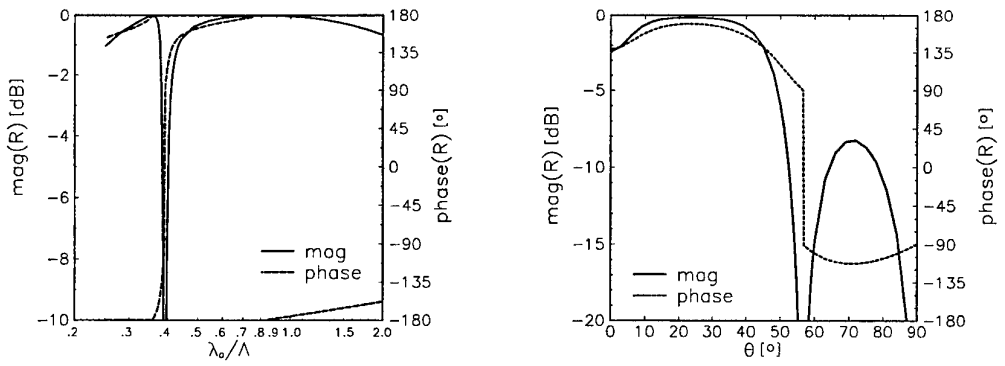

(a) **(b)**

Fig. 2 (a) Reflection coefficient of the example of single elementary plane (in Fig. 1) for a normally incident TM^z wave, as a function of relative wavelength, λ_o/Λ; (b) the E-plane specular plane wave reflection coefficient as a function of incidence angle for the same elementary plane, with the wavelength fixed at $\lambda_o=0.41\Lambda$.

This phenomenon is known in the literature as a modal interaction null [3]. Figure 2b shows the reflection coefficient as a function of incidence angle in the E-plane when the wavelength of the TM^z incident wave is kept fixed (here at $\lambda_o / \Lambda = 0.41$). As expected, the reflection coefficient is large for angles near normal incidence, and vanishes near $\theta = 57°$ and again at grazing (i.e., $\theta = 90°$).

4. Wave Propagation in a Wire Medium

To extend the above example to a medium, the elementary surface described above is used as the elementary plane of a wire medium. In our study, these planes are assumed to be separated far enough apart that the evanescent waves of neighboring planes do not significantly interact, but close enough that the period is small compared to the wavelength. Taking into account these points, the interplanar spacing for the example here is chosen to be at $D_x = \Lambda/15$ [5]. We then model the medium as a periodically loaded transmission line with the elementary planes accounted for by appropriate equivalent sheet admittances. By applying the Floquet theorem to the analysis of the periodically loaded transmission line [7], we find the propagation constant and the effective transverse impedance at the midpoint between any two adjacent elementary planes [5, 6].

To illustrate some interesting characteristics of wave propagation in this example wire medium, consider the case where a TM^z plane wave is illuminating the interface of a semi-infinite slab of this wire medium. The wire inclusions are taken to be all parallel with the z-axis. The electric field vector of the incident plane wave is in the x-z plane. (The x-axis is normal to the interface of the medium.) One of the interesting quantities to analyze is the propagation constant inside the wire medium, particularly its component normal to the interface, denoted by κ. Owing to the phase-matching requirements, the tangential components (i.e., the y and z components) of the vector wave number inside the medium are the same as those components of the incident vector wave number. Figure 3a shows the normalized x-component of wave vector inside this medium as a function of relative wavelength λ_o / Λ, for a normally incident plane wave when the interplanar spacing is taken to be $D_x = \Lambda/15$.

In addition, this figure shows the corresponding x-component of wavenumber as determined by the effective media theory [5, 6]. We see from this figure that the normalized x-component of the wave vector in this sample wire medium is purely real for $\lambda_o / \Lambda > 1.3$. In this region, the equivalent sheet reactance for each elementary plane is large and negative. As the wavelength decreases and reaches the range $0.8 < \lambda_o / \Lambda < 1.3$, the x-component of wavenumber becomes complex. In this region, the equivalent sheet reactance is small and negative, but the wave is experiencing the bandgap effect of periodic media, mainly due to the change in the equivalent sheet reactance. In such regions, there is significant coupling between the traveling wave and the backward wave and so the energy of the forward wave is mainly transferred into the backward wave.

For this reason, the effective-media approximations are not valid in these regions (as can be seen from Fig. 3a) and, as is done here, the full periodic-media approach must be utilized. As the wavelength decreases further, κ is eventually purely imaginary for $0.4 < \lambda_o / \Lambda < 0.8$. In this region, the equivalent sheet reactance becomes positive, and hence it represents inductive loading. Here, the wave evanescence is not due to the band-gap phenomena, but instead it is due to the heavy inductive loading of the medium. Both effective-media theory and periodic-structure theory are applicable for this region. As the wavelength continues to become shorter, one may speculate that this progression repeats, and also that the bandgap effects of the periodic lattice may appear. Figure 3b presents the normalized x-component of vector wavenumber inside this medium in the E-plane, as a function of angle of incidence of the TM^z plane wave when the wavelength is kept at $\lambda_o / \Lambda = 0.41$.

In this case, the interior wave in the E-plane is evanescent for the incidence angles in the E-plane between $\theta = 0^\circ$ and $\theta \square 52^\circ$. However, for the incidence angles greater than $\theta \square 52^\circ$, the wave can penetrate into the wire medium. Thus, it is evident that there is exclusion of wave propagation from certain angular regions in such a medium; essentially, wave propagation is restricted to certain "angular windows" that depend upon the chosen design parameters (e.g., number density, orientation, length, and volume fraction of inclusions).

Furthermore, these media, as expected, are frequency dependent and polarization dependent. In other words, wire media effectively behave as angle-selective, frequency-selective, and polarization-selective media. There are several other interesting features, which we obtained through our analysis of this sample, and which are mentioned in [5, 6].

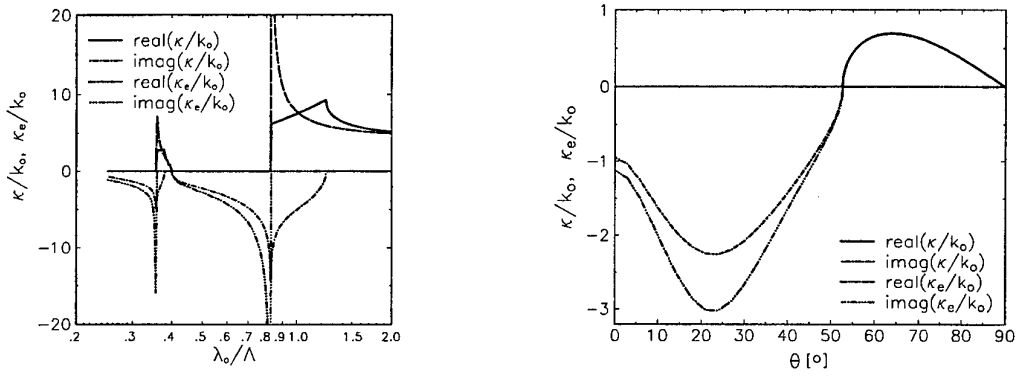

(a) (b)

Fig. 3 (a) Normalized x-component of vector wave number, κ / k_o, obtained from the periodic-structure theory and its effective-media counterpart, κ_e / k_o, inside our example of wire media, as a function of relative wavelength, λ_o / Λ for a normally incident wave. The interplanar spacing between the elementary surfaces is taken to be $D_x = \Lambda / 15$; (b) The quantities κ / k_o and κ_e / k_o in the E-plane as a function of angle of incidence of a TM^z plane wave in the E-plane, at the wavelength $\lambda_o / \Lambda = 0.41$.

5. Summary

The conceptualization of wire media presents an idea for a class of complex media in which the inclusions may, under certain constraints, be chosen to be electrically long. We have presented some of the results of our analysis for a case of wire media in which inclusions are taken to be identical, arbitrary finite-length, parallel, thin wires. It is important to note that even though there seems to be many wire inclusions on each elementary plane, the volume fraction is still very small, since the wires are taken to be very thin. For instance, for the example wire medium discussed here, the volume fraction is just less than 0.15%. Despite the small volume fraction of the metal inclusions, the resulting medium may have significantly different electromagnetic properties than the host medium.

If one were to compare two blocks of dielectric---one with wire inclusions and the other without---substantial differences in the electromagnetic properties would be noticed, even though they may have almost identical weight. Owing to the interesting features of electromagnetic wave propagation in

such media, wire media, or media similar to wire media, may find some potential applications in the design of future microwave devices and components; examples include substrates for micromachined and miniature antennas, radome for beam shaping, and waveguides for mode selection.

References

[1] C. A. Moses and N. Engheta, "An idea for electromagnetic 'feedforward-feedbackward' media," in *IEEE Transactions on Antennas and Propagation*, Vol. 47, No. 5, pp. 918-928, May 1999

[2] S. W. Schneider and B. A. Munk, "The scattering properties of "super dense" arrays of dipoles," *IEEE Transactions on Antennas and Propagation*, vol. 42, pp. 463-472, 1994.

[3] C. J. Larson and B. A. Munk, "The broad-band scattering response of periodic arrays," IEEE *Transactions on Antennas and Propagation*, vol. AP-31, pp. 261-267, 1983.

[4] T. W. Kornbau, *Analysis of Periodic Arrays of Rotated Linear Dipoles, Rotated Crossed Dipoles, and Biplanar Dipole Arrays in Dielectric*, Ph.D. dissertation, The Ohio State University, 1984.

[5] C. A. Moses, *A Theoretical Study of Electromagnetic Feedforward/Feedbackward Media and Wire Media*, Ph.D. dissertation, University of Pennsylvania, 1998.

[6] C. A. Moses and N. Engheta, "Electromagnetic wave propagation in the wire medium: A complex medium with long thin inclusions," submitted on May 1999 to *Wave Motion*, special issue on "Electrodynamics in Complex Environments."

[7] R. E. Collin, *Field Theory of Guided Waves*, IEEE Press, New York, 1991.

Resonant Response of Chiro-Ferrite Media under FMR and Chiro-FMR Conditions

G. Kraftmakher, Y. Kazantsev, and A. Kozyrkov

Institute of Radioengineering and Electronics
Russian Academy of Sciences
11, Mokhovaya str., 103907, Moscow, Russia
Fax: (095)2038414; E-mail: vsolosin@ms.ire.rssi.ru

Abstract

We present here the experimental results about some features of the microwave resonant `effects which can be excited in chiro-ferrite media under a constant magnetic field. These results are obtained from the measurement of the transmission, reflection and absorption coefficients in rectangular waveguides, using cylindrical samples of many isolated oriented multistart helices with ferrite core inside. Here we show that in the case of the FMR excitation the resonant effects are displayed as two coupled resonances (the main chiral resonance and the FMR), which interfere with each other. If the conditions of the Chiro-FMR excitation are fulfilled, the chiral resonance is controlled in a limited frequency band. For a certain value of the constant magnetic field the Chiro-FMR experiences bifurcation with large frequency separation, which can be more than one order larger than the chiral resonance width. The reflection anti-resonance and absorption decrease are observed under bifurcation. The resonant response to governing magnetic field depends essentially on the ferrite concentration.

1. Introduction

As it was shown in [1], the chiro-ferrite composite media, which combine the properties of chiral and ferrite components, are considerably more complicated than originally envisioned.
Indeed, the resonant effects are specific. Even the well-known ferromagnetic resonance (FMR), resonant interaction of the microwave magnetic field with a magnetized ferrite, is unusual because of the influence of the chiral resonance (ChR). Chiro-FMR is the resonant interaction of the magnetic moment of a chiral inclusion (induced by the microwave fields) with a magnetized ferrite. Chiro-FMR is unique as it excited only in chiro-ferrite media. In our previous works [2,3] we investigated the excitation conditions and the possibility to separately observe FMR and Chiro-FMR, using cylindrical samples with oriented multistart helical structures with ferrite core inside. Here we use similar samples. The samples (Figure 1) were made, rolling a piece of material with parallel copper (tungsten) threads to helical tube around the O-axis. Each of the threads forms the isolated helix, and one-dimensional chiral medium of many oriented multistart helices (much less than wavelength) with common O-axis is created. When we add ferrite core inside helical tube, the chiro-ferrite is formed.

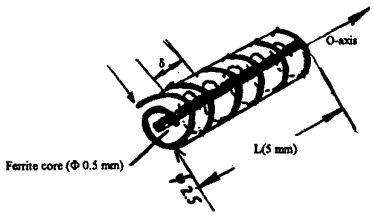

Fig. 1

2. Chiro-FMR

The Chiro-FMR features are investigated in rectangular waveguides for two cases of chiral resonance excitation. The first case is H-excitation, when the microwave magnetic field h is parallel to the O-axis, and the resonant losses are displayed as magnetic losses. The second case is E-excitation, when the microwave electric field E is parallel to the O-axis of helices, and the resonant losses are

displayed as dielectric losses. To observe the Chiro-FMR it is necessary to apply the constant magnetic field H_0 perpendicular to the O-axis

Figure 2 shows evolution of frequency dependencies of Transmission (a) and Reflection (b) with variations of the constant magnetic field in the case of H-excitation. We see that main chiral resonance moves away from the primary resonant frequency to high frequencies, and its intensity (the resonance level) decreases. Under a certain value of the constant magnetic field (H_B = 3200 Oe) the Chiro-FMR experiences bifurcation, and two identical weak resonances can be observed: previous first resonance at high frequency and a new, second resonance. The second resonance appears at low frequency about a primary resonance and moves to the primary frequency with increasing intensity, while the first resonance continues to weak and becomes invisible at all. It is observed coexistence of two resonances in a limited area of a constant magnetic field about the bifurcation field: $H_{coex} = H_B \pm$ 200 Oe. Under bifurcation we see a deep minimum of the Reflection resonance instead of traditional maximum (anti-resonance in presence of absorption).

In Figures 3 and 4, dependencies of resonance intensity (Fig. 3a), resonance frequency (Fig. 3b), and resonant absorption (Fig. 4) on the constant magnetic field H_0 are demonstrated in the form of two branches connected with both the first resonance (before bifurcation) and the second resonance (under bifurcation and after it). In Figure 3b, frequency dependence of the FMR for single ferrite core (without the chiral sample, but in Chiro-FMR geometry, $H_0 \perp$ to the core axis and $H_0 \perp$ to the h-field) is presented also. Analyzing frequency dependencies of the Chiro-FMR and the FMR (Fig. 3b), one can note the correlation between bifurcation field (H_B = 3200 Oe) and the FMR field of single ferrite at the frequency equal to the primary chiral resonance, f = 10,4 GHz at $H_0 = 0$.

3. FMR

The FMR features are investigated in the case of E-excitation, when one can observe separately the FMR under $H_0 \perp$ to the h-field ($\|$ to the O-axis). In Figure 5 we illustrate the frequency dependence of Transmission at different values of the constant magnetic field H_0. When $H_0 = 0$, only chiral resonance (ChR) is observed. Applying a constant magnetic field, the FMR is excited and moves to high frequencies. Till frequencies of the FMR and the ChR are far from each other, influence of ChR on FMR is very weak. When the FMR is near the ChR, two coupled resonances and interaction between them are observed, as Figure 6 confirms. When the FMR approaches the ChR, its intensity decreases while ChR intensifies. Next, increasing the constant magnetic field, we observe intensification of the FMR and decrease of the ChR intensity (Fig. 6a). Frequency shift of ChR caused by the FMR influence is weak, as Figure 6(b) shows.

4. Conclusion

The Chiro-FMR Features	The FMR Features
1. Controlled ChR in limited frequency band. Strong frequency shift.	1. Two resonances: main ChR and moving FMR.
2. Bifurcation effect, coexistence of two resonances. Decrease of resonant absorption.	2. Interaction between FMR and ChR near the main resonance frequency.
3. Correlation between bifurcation and FMR fields.	3. Weak frequency shift of ChR.
4. Influence of ferrite concentration on frequency band.	

Acknowledgement

The work is supported by the Russian Fund of Basic Research, Grant N 99-02-39009.

References

[1] W. S. Weiglhofer, A. Lakhtakia, and B. Michel. "On chiroplasmas and chiroferrites," *Proc. of Bi anisotropics'98*, Braunschweig, Germany, pp. 9 – 12.

[2] Y. N. Kazantsev and G. A. Kraftmakher, "Chiral medium-ferrite and electric dipole-ferrite structures: Chiral-ferromagnetic, dipole-ferromagnetic and ferromagnetic resonances," *Proc. of Chiral'95*, Pennsylvania, USA, pp. 161-170.

[3] G. A. Kraftmakher and Y. N. Kazantsev, "Experimental investigation of response of chiral media and chiral media-ferrite structures to microwave radiation and governing magnetic field," *Advances in Complex Electromagnetic Materials*, Dordrecht Kluwer Academic Publishers, 1997, pp. 341-358.

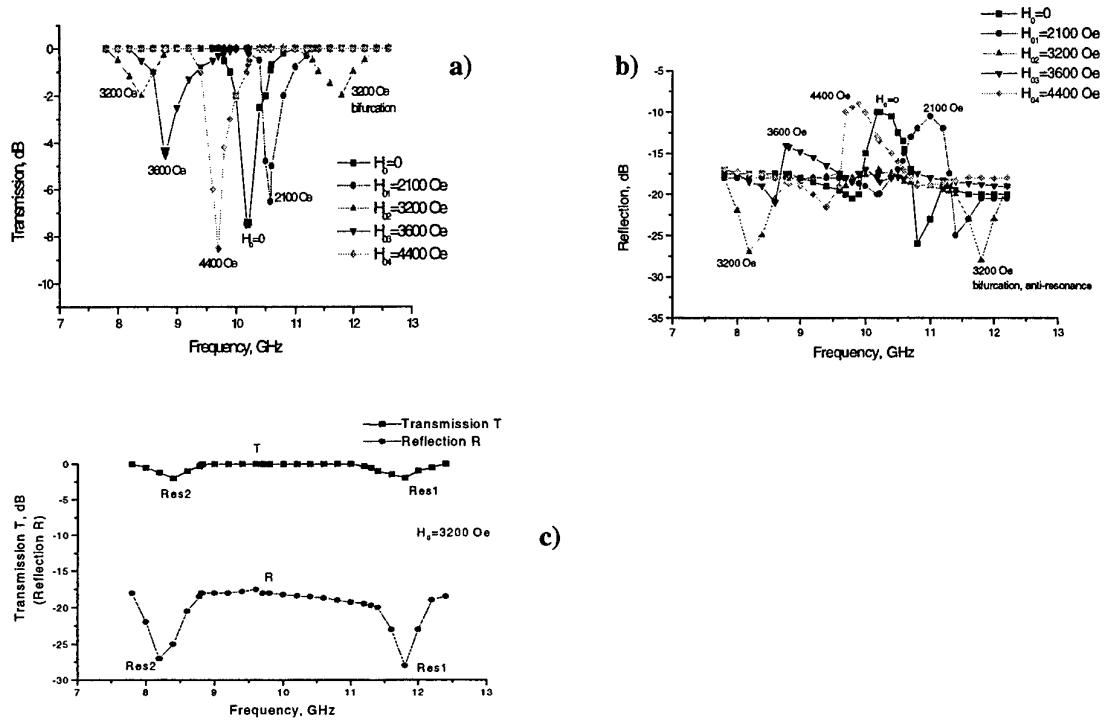

Fig. 2 Chiro-FMR - Evolution of frequency dependences with variations of the constant magnetic field H_0 (H-excitation): **(a)** Transmission; **(b)** Reflection; **(c)** Bifurcation of transmission resonance and reflection anti-resonance by $H_0 = 3200$ Oe.

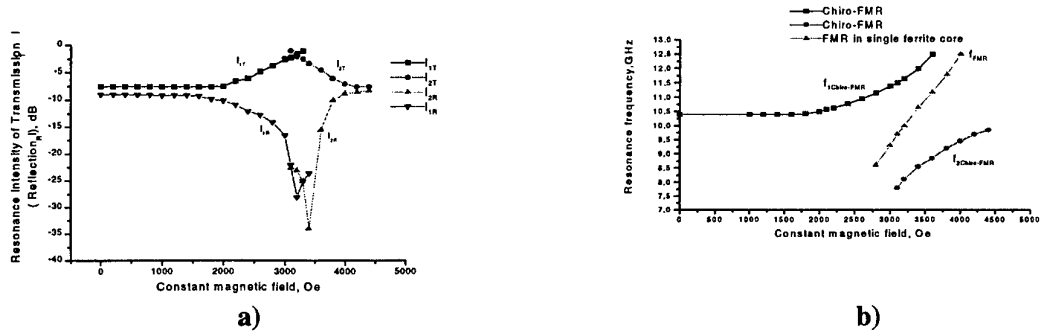

Fig. 3 Chiro-FMR: **(a)** Resonance intensity of transmission (reflection) I_T (I_R); **(b)** Resonance frequencies.

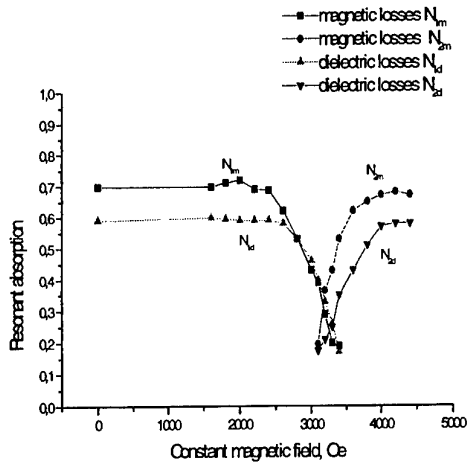

Fig. 4 Chiro-FMR: Magnetic resonant losses N_m and dielectric resonant losses N_d.

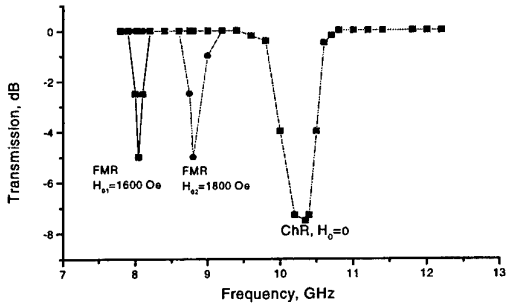

Fig. 5 Moving FMR and main chiral resonance (ChR) with variations of the constant magnetic field H_0.

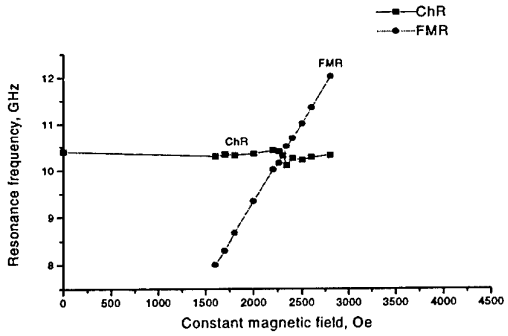

a)

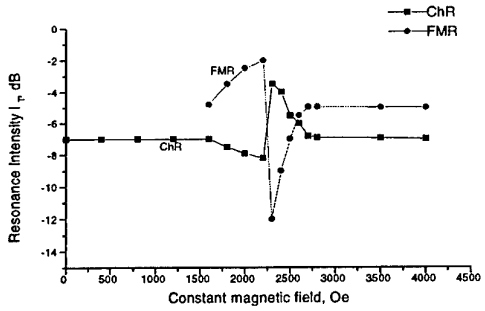

b)

Fig. 6 FMR-conditions, FMR and ChR: **(a)** Resonance intensities of transmission; **(b)** Resonance frequencies.

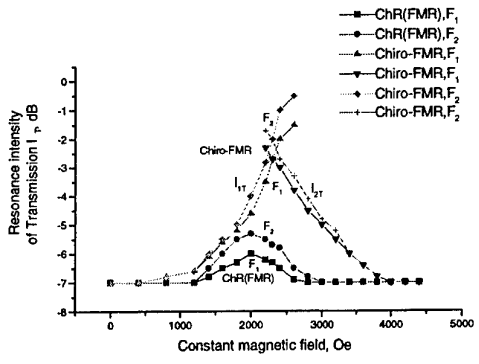

a)

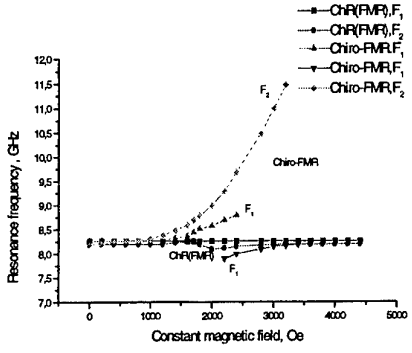

b)

Fig. 7 Influence of ferrite concentration F_1 and F_2 on ChR under FMR and Chiro-FMR: **(a)** ChR intensities of transmission under FMR and Chiro-FMR; **(b)** ChR frequencies under FMR and Chiro-FMR.

Chiroptical Spectroscopy of Turbid Media

A. A. Kokhanovsky

Institute of Physics
70 Skarina Avenue, Minsk 220072, Belarus
Fax: 375-172-840879, E-mail: alex@zege.bas-net.by

Abstract

The influence of the size of particles on the circular dichroism (CD) and optical rotatory dispersion (ORD) spectra of turbid layers with spherical globules of chiral substances is studied. Simple equations for the values of CD and ORD of dispersed slabs with optically soft large spheres are obtained and analyzed. Equations derived can be used for the solution of the inverse problem, namely for deriving intrinsic spectra of substances inside small particles from measurements of spectra for turbid layers.

1. Introduction

Circular dichroism (CD) and optical rotatory dispersion (ORD) spectra are fingerprints of molecular asymmetries of chiral substances [1,2]. They have already been studied both for homogeneous [2] and particulate [3-8] media. It was found, in particular, that both ORD and CD spectra of turbid layers with Rayleigh-Gans particles coincide with correspondent spectra of chiral molecules in solutions. This is not the case for Rayleigh particles, where a multiplier $\frac{\overline{m}^2+2}{3}$ ($\overline{m}=\frac{m_L+m_R}{2}$), $m_L=n_L+i\chi_L$ and $m_R=n_R+i\chi_R$ are the relative refractive indices for left-handed and right-handed circularly polarized beams) should be used to relate the intrinsic spectra of substances to the spectra measured for turbid layers.

One should expect even more profound distortion of spectra in the case of large ($x>>1$, $x=ka$, $k=\frac{2\pi}{\lambda}$, a is the radius of particles, λ is the wavelength of the incident wave) chiral particles. The task of this paper is to relate intrinsic CD and ORD spectra of substances inside large particles to spectra measured for dispersed layers. It is assumed that the refractive index of a host medium is close to the refractive index of particles, which is usually the case for bio-liquids. It should be pointed out that the refractive index of a surrounding medium could be always adjusted to satisfy the criteria of the optical softness: $|\overline{m}-1|<<1$.

2. Large Optically Soft Chiral Spheres

For the sake of simplicity we will consider turbid layers with spherical optically active particles. Also we combine ORD $\varphi(\lambda)$ and CD $\theta(\lambda)$ spectra in one complex function:

$$\Psi(\lambda)=\varphi(\lambda)+i\theta(\lambda). \tag{1}$$

This function can be found with the following equation in the case of turbid layers with chiral spheres [3,4]:

$$\Psi(\lambda)=\frac{2\pi N}{k^2}\int_0^\infty S(\lambda,a)f(a)da, \tag{2}$$

where N is the number concentration of particles, $f(a)$ is the particle size distribution and

$$S(\lambda,a)=\sum_{l=1}^{\infty}(2l+1)c_l. \tag{3}$$

Amplitude coefficients c_l are complex functions of the refractive index and size of particles [3,4]. These coefficients rapidly decrease at $l>M$, where $M\approx x$. Functions $S(\lambda,a)$ depend on the intrinsic ORD $\varphi_0(\lambda)$ and CD $\theta_0(\lambda)$ spectra of chiral substances bounded in small particles. Thus, Eqs. (1)-(3) can be used for the derivation of intrinsic spectra $\varphi_0(\lambda)$ and $\theta_0(\lambda)$ from measurements of the complex function $\Psi(\lambda)$, provided that the information on the particle size distribution and concentration of particles N is available.

The solution of the inverse problem is simplified for optically soft ($|\overline{m}-1|<<1$) large ($x>>1$) particles, where simple expressions for the amplitude function $S(\lambda,a)$ can be obtained. Let us show it.

It follows for the amplitude coefficients of large soft spherical particles in the framework of the van de Hulst approximation [4]:

$$c_l=\frac{1}{2}x\sin\tau\Delta m\exp(i\rho\sin\tau), \tag{4}$$

where

$$\rho=2x(\overline{m}-1),\tau=\arccos\left(\frac{l+\frac{1}{2}}{x}\right),\Delta m=m_L-m_R.$$

The value of ρ is called the phase shift. Eq. (4) allows to evaluate series (3) for the amplitude function $S(\lambda,a)$ analytically. Namely, replacing the sum in Eq. (3) by integral [4]: $\sum_{l=1}^{\infty}\to\int_0^x dl$, where $l+\frac{1}{2}=x\cos\tau$ and $dl=-x\sin\tau d\tau$, one obtains:

$$S(\lambda,a)=x^3\Delta m\int_0^1\sigma^2\exp(i\rho\sigma)d\sigma$$

or

$$S(\lambda,a)=\frac{x^3\Delta m}{3}\mathrm{H}(\rho), \tag{5}$$

where the complex function $\mathrm{H}(\rho)=\mathrm{v}(\rho)+i\mathrm{w}(\rho)$ has the following simple form:

$$\mathrm{H}(\rho)=-\frac{6i(1-e^{i\rho})}{\rho^3}+\frac{6e^{i\rho}}{\rho^2}-\frac{3ie^{i\rho}}{\rho}. \tag{6}$$

The expansion of the function $H(\rho)$ as $\rho\to 0$ for monodispersed spheres is given by:

$$H(\rho)=1-\frac{3}{10}\rho^2+\frac{1}{56}\rho^4+i\left(\frac{3}{4}\rho-\frac{1}{12}\rho^3+\frac{1}{320}\rho^5\right)+o(\rho^6). \tag{7}$$

It follows from Eqs. (2), (5):

$$\Psi(\lambda)=\overline{H}(\rho)\Psi_0(\lambda), \tag{8}$$

where

$$\overline{H}(\rho)=\frac{\int_0^\infty H(\rho)f(\rho)\rho^3 d\rho}{\int_0^\infty f(\rho)\rho^3 d\rho},$$

$$\Psi_0(\lambda)=\varphi_0(\lambda)+i\theta_0(\lambda),\ \ \varphi_0(\lambda)=\frac{\pi c\Delta n(\lambda)}{\lambda},$$

$$\theta_0(\lambda)=\frac{\pi c\Delta\chi(\lambda)}{\lambda},\ \Delta n(\lambda)=n_L-n_R,\ \Delta\chi(\lambda)=\chi_L-\chi_R$$

and c is the volumetric concentration of a chiral substance in a turbid layer.

Eq. (8) is the main result of this paper. It follows from Eq. (8) that

$$\Psi_0(\lambda)=\overline{H}^{-1}(\rho)\Psi(\lambda). \tag{9}$$

Thus, the solution of the inverse problem is greatly simplified. It follows at small values of the phase shift (see Eq.(7)): $H(\rho)\to 1$ and $\Psi(\lambda)\to\Psi_0(\lambda)$ as it should be in the framework of the Born approximation [8].

Eq. (8) can be used for studies of the dependence of spectra $\Psi(\lambda)$ on the size of chiral particles. Spectra $\Psi_0(\lambda)$ depend on the substance in question. They can be measured or found from quantum mechanical calculations.

3. Conclusion

Turbid bio-liquids and other light scattering chiral media can be characterized by their ORD and CD spectra. It was shown here how to relate ORD and CD spectra of disperse media with intrinsic spectra of particles using simple approximate equations. This could be of importance for monitoring bio-particles during their life cycles.

The case of large soft spherical particles was studied in detail. However, results can be easily generalized on the more important and practically relevant case of nonspherical particles. The diameter of a spherical particle should be changed to the maximal length of an incident beam inside of a nonspherical particle to approximately account for the effects of nonsphericity. The account for inhomogenity and internal structure of particles is also straightforward in the framework of the approximation proposed.

References

[1] L. Pasteur, Ann. Chemie Phys., vol. 28, p. 56, 1850.

[2] P. Crabbe, *Optical Rotatory Dispersion and Circular Dichroism in Organic Chemistry*. Holden-Day, San-Francisco, 1965.

[3] C. F. Bohren and D. Huffman, *Light Scattering and Absorption by Small Particles*. Wiley, New York, 1983.

[4] A. A. Kokhanovsky, *Light Scattering Media Optics: Problems and Solutions*. Wiley-Praxis, Chichester, 1999.

[5] D. W. Urry, T. A. Hinners, and L. Masotti, *Arch. Biochem. Biophys.*, no. 137, p. 214, 1970.

[6] D. J. Gordon, *Biochemistry*, no. 11, p. 413, 1972.

[7] *Selected Papers on Natural Optical Activity*, SPIE Milestone Series, v. MS15, A. Lakhtakia (Ed.). SPIE Optical Engineering Press, Bellingham, 1990.

[8] C. F. Bohren, *J. Theor. Biology*, no. 65, p. 755, 1977.

Session 12

Friday - September 29, 2000

16:00 - 17:10

Complex Media III

Bloch Wave Approach to the Optics of Crystals: The Role of Spatial Dispersion

S. Ponti, C. Oldano, and M. Becchi

Dipartimento di Fisica del Politecnico di Torino
Corso Duca degli Abruzzi 24, 10129 Torino, Italy
Fax: + 39-011-564 7399; email: ponti@polito.it

Abstract

In this work we give new results in the framework of a research on the macroscopic optical properties of crystals whose period p is shorter than the light wavelength but large on the molecular scale, so that they can be treated in the framework of a continuum theory. More precisely, we assume that the optical properties of the crystal are fully defined by a perfectly periodic function $\varepsilon(\vec{r})$, representing the local permittivity of the medium (assumption of locality). To define the effective permittivity tensor $\widetilde{\varepsilon}$ we use a method based on the analysis of the normal modes for the electromagnetic field propagating within of the periodic medium (Bloch waves).

1. Introduction

A perfect crystal is generally treated in optics as a homogeneous medium, despite the fact that in crystals the time harmonic solutions of Maxwell equations (*i.e.* the normal modes of the electromagnetic field) are Bloch waves, whereas in homogeneous media they are plane waves. We recall that a Bloch wave can be considered as a plane wave whose amplitude is a periodic function of $\vec{r}$, or equivalently as a superposition of plane waves, obtained by expanding the amplitude in a Fourier series. The dielectric tensor $\widetilde{\varepsilon}$ of the homogeneous (*macroscopic*) model for crystals is defined by considering as a starting point the Bloch wave, and neglecting the space dependence of its amplitude. This means that only the plane wave component with $\vec{q} = \vec{0}$, that defines the *macroscopic field* [1, 2, 3], is taken into account, and considered as the best 'plane wave approximation' of the actual Bloch wave. The homogeneous medium, where this plane wave can freely propagate, is the *effective macroscopic* medium. Its tensor $\widetilde{\varepsilon}$ is therefore implicitly defined by the equation

$$\vec{D}_{\vec{0}} = \widetilde{\varepsilon}\left(\epsilon_0 \vec{E}_{\vec{0}}\right), \tag{1}$$

where $\vec{D}_{\vec{0}}$, $\vec{E}_{\vec{0}}$ define the zeroth order Fourier components of the Bloch wave and ϵ_0 is the vacuum permittivity.

Here we discuss the application of the Bloch wave method to the study of a short period crystal whose optical properties are assumed as perfectly known and fully defined by a periodic tensor field $\varepsilon(\vec{r})$. This field represents a *mesoscopic model* for the actual crystal, where its molecular (*microscopic*) structure is neglected, and the assumption of *locality* is explicitly made. Despite this last assumption, the spatial dispersion plays a main role in our theory, since $\widetilde{\varepsilon}$ explicitly depends on the wave vector $\vec{k}$ of the internal plane wave, *i.e.* $\widetilde{\varepsilon} = \widetilde{\varepsilon}(\vec{k})$. The

tensor field $\varepsilon(\vec{r})$ is well known for many periodic liquid crystal (LC) phases and for artificially made structures (as for instance Reusch piles). Our problem reduces therefore to the search of equations relating $\tilde{\varepsilon}(\vec{k})$ to $\varepsilon(\vec{r})$. Fully analytic expressions for $\tilde{\varepsilon}(\vec{k})$ will be given, that allow for a quantitative analysis of the approximations required to define homogeneous models for non-homogeneous and periodic media. This is the main motivation of our research. The found equations will be applied to the particularly interesting and simple case of cholesteric liquid crystals.

2. Theory

The effective dielectric tensor $\tilde{\varepsilon}$ of the macroscopic model is expressed as a function of the Fourier components $\varepsilon_{\vec{q}}$ of the tensor field $\varepsilon(\vec{r})$:

$$\varepsilon(\vec{r}) = \sum_{\vec{q}} \varepsilon_{\vec{q}} \exp(i\vec{q}\vec{r}). \tag{2}$$

The component of order zero is the space average of $\varepsilon(\vec{r})$, *i.e.* $\varepsilon_{\vec{0}} = \bar{\varepsilon}$, and constitutes a first rough approximation for $\tilde{\varepsilon}$. The other approximations are obtained by adding to $\bar{\varepsilon}$ terms having the general structure:

$$\varepsilon_{\vec{q}_1} G_{-\vec{q}_1} \varepsilon_{\vec{q}_2} G_{-(\vec{q}_1+\vec{q}_2)} \cdots G_{-(\vec{q}_1+\ldots+\vec{q}_{N-1})} \varepsilon_{\vec{q}_N}, \tag{3}$$

where

$$G_{\vec{q}} = \frac{\omega}{c} \left[(\vec{k}+\vec{q})^2 \mathbf{I} - (\vec{k}+\vec{q})(\vec{k}+\vec{q}) - \bar{\varepsilon} \right]^{-1}, \tag{4}$$

$\mathbf{I}$ is the 3×3 identity matrix, $(\vec{k}+\vec{q})(\vec{k}+\vec{q})$ is a dyadic product, and the vectors $\vec{q}_n$ satisfy the following relations:

$$\vec{q}_1 + \ldots + \vec{q}_N = 0, \quad \sum_{n=1}^{N'} \vec{q}_n \neq 0 \quad \forall\, N' < N. \tag{5}$$

The terms given by Eq. (3) can be interpreted as the effect of the multiple scattering within the periodic structure, and the equation (5) states that only the *forward* scattering with multiplicity $N \geq 2$ gives a contribution to $\tilde{\varepsilon}$. The formal expression of $\tilde{\varepsilon}$ can be written as:

$$\tilde{\varepsilon} = \bar{\varepsilon} + \sum_{N=2}^{\infty} \sum_{\vec{q}_1} \cdots \sum_{\vec{q}_{N-1}} \varepsilon_{\vec{q}_1} G_{-\vec{q}_1} \varepsilon_{\vec{q}_2} G_{-(\vec{q}_1+\vec{q}_2)} \cdots G_{-(\vec{q}_1+\ldots+\vec{q}_{N-1})} \varepsilon_{-(\vec{q}_1+\ldots+\vec{q}_{N-1})}. \tag{6}$$

The dependence of $\tilde{\varepsilon}$ on $\vec{k}$ comes from the tensors $G_{\vec{q}}$, as shown by Eq. (4). The dominant contribution to $\tilde{\varepsilon}$ is given in general by the terms with $N = 2$, *i.e.* by the double scattering (two-photon scattering), a fact that allows to greatly simplify Eq. (6). A further simplification is obtained by expanding $G_{\vec{q}}$ in power series of p/λ, where p is an average period of the crystal lattice, since only the first terms of such expansion are expected to give a non-negligible contribution to $\tilde{\varepsilon}(\vec{k})$. This gives

$$\tilde{\varepsilon} = \bar{\varepsilon} + \tilde{\varepsilon}^{(0)} + \left(\frac{p}{\lambda}\right) \tilde{\varepsilon}^{(1)} + \left(\frac{p}{\lambda}\right)^2 \tilde{\varepsilon}^{(2)} + \ldots, \tag{7}$$

For the simple case of crystals periodic in only one direction, say x_3 (1D crystals), the vectors $\vec{q}$ depend on a single index r, and:

$$\vec{q}_r = rq\hat{x}_3, \quad \tilde{\varepsilon}_0^{(m)} = \sum_{r\neq 0} \varepsilon_r G_{-r}^{(m)} \varepsilon_r;$$

where:

$$G_r^{(0)} = -\frac{1}{\varepsilon_{33}} \begin{pmatrix} 0 & 0 & 0 \\ 0 & 0 & 0 \\ 0 & 0 & 1 \end{pmatrix}, \quad G_r^{(1)} = -\frac{1}{r}\frac{1}{\varepsilon_{33}} \begin{pmatrix} 0 & 0 & n_1 \\ 0 & 0 & n_2 \\ n_1 & n_2 & g_{33} \end{pmatrix}, \tag{8}$$

($r = 0, \pm 1, \pm 2, ...$), $q = 2\pi/p$, $\vec{n} = \vec{k}/k_0$, $g_{33} = -\frac{2}{\varepsilon_{33}}(\varepsilon_{13}n_1 + \varepsilon_{23}n_2)$, and only the two-photon scattering has been considered. For chiral structures, the most important term is the one containing $\tilde{\varepsilon}^{(1)}$ and scaling as p/λ, since it is related to the optical activity of the structure. Interestingly, it is identically zero for light propagating along the periodicity axis of 1D crystals, *i.e.* for $\vec{n} = n_3\hat{x}_3$, as clearly shown by the expression of $G_r^{(1)}$, Eq. (8). The higher order terms give in general small corrections to the preceding ones, but in some particular case they can give qualitatively new effects. This actually occurs in cubic crystals (and in particular in the blue phases), because the term scaling as $(p/\lambda)^2$ gives a small anisotropy to the structure. This also occurs along the periodicity axis of 1D crystals, whose optical rotation is related to a term scaling as $(p/\lambda)^3$, since the term scaling as p/λ is zero. In fact, for real $\varepsilon(\vec{r})$ only the terms scaling as $(p/\lambda)^m$ with odd m-values give a contribution to the optical activity.

3. Discussion

(i) The method developed here allows to easily obtain $\tilde{\varepsilon}(\vec{k})$ in all the cases where the function $\varepsilon(\vec{r})$ has only few non-zero Fourier components, a fact that actually occurs in many liquid crystal phases. The simplest and most important one is the choelsteric phase, where only the Fourier components ε_r with $r = 0, \pm 1$ are different from zero. For such crystals:

$$\tilde{\varepsilon}^{(0)} = \begin{pmatrix} \tilde{\varepsilon}_o & 0 & 0 \\ 0 & \tilde{\varepsilon}_o & 0 \\ 0 & 0 & \tilde{\varepsilon}_e \end{pmatrix}, \quad \tilde{\varepsilon}^{(2)} = \varepsilon' \begin{pmatrix} 1 & 0 & 0 \\ 0 & 1 & 0 \\ 0 & 0 & 0 \end{pmatrix}, \quad \tilde{\varepsilon}^{(3)} = \varepsilon'' n_3 \begin{pmatrix} 0 & 1 & 0 \\ -1 & 0 & 0 \\ 0 & 0 & 0 \end{pmatrix}, \tag{9}$$

and $\tilde{\varepsilon}^{(1)} = 0$, where $\tilde{\varepsilon}_o = (\varepsilon_o + \varepsilon_e)/2$, $\tilde{\varepsilon}_e = \varepsilon_e$, $\varepsilon' = (\varepsilon_e - \varepsilon_o)^2(2\varepsilon_o - n_1^2 - n_2^2)/8$ and $\varepsilon'' = i(\varepsilon_e - \varepsilon_o)^2(2\varepsilon_o - n_1^2 - n_2^2)/(4\varepsilon_o)$. The pedices o and e refer to ordinary and extraordinary, respectively. We recall that cholesteric liquid crystals are locally uniaxial, with the optic axis orthogonal to x_3, and that the pitch of their helical structure is equal to $2p$, where p is the lattice period. The Eqs. (9) show that effective medium is still uniaxial, but with the optic axis parallel to x_3. The term scaling as (p/λ) is identically zero for any direction of the light beam: the optical activity of cholesteric is therefore given by the term scaling as $(p/\lambda)^3$. This unusual property constitutes a further demonstration of the unique optical properties of the cholesteric phase.

One may notice that the equations given here can straightforwardly give the expression of $\tilde{\varepsilon}$ up to terms scaling as $(p/\lambda)^3$, whereas the standard effective-medium theories generally only give terms scaling as $(p/\lambda)^0$ and $(p/\lambda)^1$.

(ii) The presence of $\vec{k}$-dependent terms give non-easy problems for the search of plane wave solutions and for the boundary conditions. In fact for any given direction of $\vec{k}$ the dispersion

relation becomes a polynomial that could have, in principle, any number of roots. However, only four solutions, $\pm k_1$ and $\pm k_2$, corresponding to plane waves with different polarization states, have physical meaning. The difficulty for the boundary conditions is due to the fact that the terms of $\tilde{\varepsilon}(\vec{k})$ depending on the m-power of $\vec{k}$ come from the space derivatives of order m of the electric field. The constitutive equations, written in the Landau form, are in fact:

$$\tilde{\varepsilon}_{ij} = \tilde{\varepsilon}_{ij}^{(0)} + \gamma_{ijk}\partial/\partial x_k + \chi_{ijkl}\partial^2/\partial x_k \partial x_l + ...; \qquad \mu = \mu_0.$$

Interestingly, the Bloch wave method gives the actual expression of $\tilde{\varepsilon}(\vec{k})$ without any use of higher order tensors. In the presence of derivative-depending terms, the usual conditions of continuity for the tangential components of $\vec{E}$ and $\vec{H}$ are no more valid. The problem has been at least partially solved only for the simple case of first-order derivatives [5], by writing the constitutive equations in the Post or Tellegen form [6].

(iii) The limits of validity of the macroscopic model have been carefully tested. For achiral crystals, the approximation $\tilde{\varepsilon}(\vec{k}) \approx \tilde{\varepsilon}(\vec{0})$, where all the $\vec{k}$-dependent terms are omitted, is in most cases good enough up to $p/\lambda \approx 0.1$. The full expression of $\tilde{\varepsilon}(\vec{k})$ allows to extend these limits up to $p/\lambda \approx 0.5$, except for the optical properties directly related to the spatial dispersion (as, for instance, the rotatory power). Such properties require a more careful analysis, that has been partially given on the basis of a different approach in Ref. [7]. The limit $p/\lambda \approx 0.5$ is due to the fact that for higher p-values the periodic medium can give Bragg diffraction, where the dispersion curves show forbidden bands. Obviously, homogeneous models are not able to account for the Bragg diffraction bands, even though they could still give approximated expressions for some optical properties at higher p-values.

References

[1] M. Born, *Optik*, 3^d Edition. Berlin: Springer–Verlag, 1985.
[2] M. Born and K. Huang, *Dynamical Theory of Crystal Lattice*. Oxford: Clarendon, 1954.
[3] P. Galatola, "Spatial dispersion and rotatory power of short pitch periodic dielectric media," *Phys. Rev. E*, vol. 55, no. 4, pp. 4338–4344, April 1997.
[4] L.D. Landau, *Elettrodinamica dei Mezzi Continui*, Chap. XII, Sec. 106. Roma: Editori Riuniti, 1986.
[5] G. Peterson, "Comparison of two theories of optical activity," *Am. J. Phys.*, vol. 43, pp. 969, 1975.
[6] J.A. Kong, *Electromagnetic Wave Theory*. New York: Wiley (1990).
[7] P. Hubert, P. Jaegemalm, C. Oldano, and M. Rajteri, "Optic models for short-pitch cholesteric and chiral smectic liquid crystal," *Phys. Rev. E*, vol. 58, pp. 3264-3272, September 1988.

Two-Wave Approximation for Transition Layer of Inhomogeneous Media

N. A. Simonov

Institute for Theoretical and Applied Electrodynamics,
Russian Academy of Sciences,
Izhorskaya 13/19, Moscow, 127412 IVTAN, Russia.
Phone (7-095) 485-8322, Fax (7-095) 484-2644, E-mail: simonov@eldyn.msk.ru

Abstract

We regard the transition layer near the bound of inhomogeneous media on the base of the introduced here concept of the generalized wave modes (GWM). We show in present work that previously described one-dimensional nonlocal model of inhomogeneous media [1] is a two-wave approximation for electrodynamic properties of the medium. The second, evanescent, wave in the model represents a sum of wide spectrum of GWM and can be used for approximate description of the transition layer.

1. Introduction

The transition layer is relatively thin area near the bound of medium, where electrodynamic property cannot be described adequately in terms of ε, μ parameters. Usually, inhomogeneous media, such as composite materials, have a depth of the transition layer approximately the same as a characteristic size a of the structure. But one can expect that in special cases this depth can be considerably larger than a, at least for the materials with sufficiently strong interaction between the inclusions.

Taking into account the presence of the transition layer for inhomogeneous materials, one can provide the general conclusion that the measured effective parameters ε^e, μ^e of them must always differ from those of ε_e, μ_e, which one can calculate for the infinite (boundless) medium.

The most transparent example for this conclusion can be the finely stratified medium (the Rytov solution [2]), which contain dielectric and metal layers. Let us consider only TM modes in it. There exist only one propagating (principal) wave mode in such a structure and all higher order modes are evanescent in the quasi-static case. Acher et al [3] used formulas for the ε_e, μ_e parameters, which correspond to the principal wave in such a structure, for calculation the intrinsic permeability of thin metal films. In the limit of strong skin effect those formulas give the result $\varepsilon_e = \varepsilon, \quad \mu_e = 1$, which is not correct, because do not reflects the diamagnetic properties of such a structure. Our theoretical analysis and the experimental examination permit us to found the correct formulas for the considered case:

$$\varepsilon^e = \varepsilon \frac{l}{d} > \varepsilon, \quad \mu^e = \frac{d}{l} < 1 \qquad \text{(a)}$$

where l is a period of the layers and d is the width of dielectric layers. The difference between the first and the second formulas can be explained by the fact of excitation the wide spectrum of evanescent modes near the plane boundary of this medium. These modes form the transition layer, which depth is close to the skin depth. Therefore, the formulas in [3] are not correct, if the skin effect is noticeable.

2. Determination of the Generalized Wave Modes in Inhomogeneous Medium

Let us consider arbitrary inhomogeneous, but statistically homogeneous and isotropic in **x** and **y** directions medium. It is conveniently to regard the transition layer on the boundary on the base of conception of the generalized wave modes (GWM). Such a mode we determine as a generalized wave process in the medium, when the spatially mean constituents $\mathbf{E}_0$ and $\mathbf{H}_0$ of the electromagnetic field in it spread as a plane wave (factor $\exp(i\omega t)$ is omitted)

$$\mathbf{E}_0(z) = E_0\hat{\mathbf{e}}_0\exp(-ikz), \quad \mathbf{H}_0(z) = H_0\hat{\mathbf{h}}_0\exp(-ikz), \quad \hat{\mathbf{h}}_0 = [\hat{\mathbf{z}}\times\hat{\mathbf{e}}_0] \tag{1}$$

This definition is consistent with the theory of the space dispersion [4] where only spatially means constituents of the field are taken into consideration. In present work we shall take into account the spatially inhomogeneous constituents of the field also. For this purpose we provide decomposition of tangential components of the whole electromagnetic field in arbitrary plane (x, y) in form of finite series of the spatial harmonics (SH). For example, it can be done with help of 2D FFT, but we suppose that each SH is a sum of both elementary plane waves in the (x, y) plane with the same wavenumber. Further we shall apply one-dimension, rather then two-dimensions indexing of SH for the simplicity. Providing transformations of the Maxwell's equations by analogy to the method, have been described in [1], one can obtain the followed system of equations

$$\begin{cases} kE_n = \omega\mu_0\sum\limits_{m=0}^{N-1}\mu_{nm}H_m \\ kH_n = \omega\varepsilon_0\sum\limits_{m=0}^{N-1}\varepsilon_{nm}E_m \end{cases}, \qquad n = 0,\ldots,N-1 \tag{2}$$

Here we use SI system, E_n, H_n are the amplitudes of the spatial harmonics, N – the number of the harmonics, $\varepsilon_{nm}, \mu_{nm}$ are complex parameters, which depend on ε, μ distribution in the (x, y) plane and polarization of the SH only. Naturally, the zero index corresponds to the spatially homogeneous constituents of the field. One can show with help of the Maxwell's equations that for the defined polarization of the $\mathbf{E}_0$, $\mathbf{H}_0$ constituents, polarization of the fields of each SH in the defined (x, y) plane do not depend on the wavenumber k of the mode (1). Hence the same is true for the parameters $\varepsilon_{nm}, \mu_{nm}$. Moreover, it seems natural that those parameters do not depend on z for statistically homogeneous media, although we have no proof of it at present time. Nevertheless, if there are some fluctuations of those parameters in z direction, we always can take the mean values of them.

Therefore, the system (2) is a linear system of equations. It can be rewritten in the equivalent and a more convenient form, as a combination of two matrix equations:

$$\begin{aligned} &\underline{\underline{A}}*\underline{E} = n^2\cdot\underline{E}, \quad \underline{\underline{A}} = [a_{nm}], \quad a_{nm} = \sum_{k=0}^{N-1}\mu_{nk}\cdot\varepsilon_{km}, \quad \underline{E} = (E_0, E_1,\ldots,E_n,\ldots,E_{N-1}) \\ &\underline{\underline{B}}*\underline{H} = n^2\cdot\underline{H}, \quad \underline{\underline{B}} = [b_{nm}], \quad b_{nm} = \sum_{k=0}^{N-1}\varepsilon_{nk}\cdot\mu_{km}, \quad \underline{H} = (H_0, H_1,\ldots,H_n,\ldots,H_{N-1}) \end{aligned} \tag{3}$$

Here $n \equiv k/k_0$ is a refractive index of the GWM, which can be obtained as a solution to the two equivalent dispersion equation

$$\det\left(\underline{\underline{A}} - n^2\underline{\underline{I}}\right) = 0 \Leftrightarrow \det\left(\underline{\underline{B}} - n^2\underline{\underline{I}}\right) = 0 \tag{4}$$

where $\underline{\underline{I}}$ is a unite matrix. It is clearly that the eigenvectors $\underline{E}, \underline{H}$ of the corresponding matrixes $\underline{\underline{A}}, \underline{\underline{B}}$ describe the spatially spectrum of SH for respective GWM. Therefore, in contradistinction to the conventional concept of wave mode, the GWM, travelling trough the inhomogeneous medium, keeps only the spatial spectrum of transversal distribution of the electromagnetic field.

If we pass to the limit of the continuous spatially spectrum, the characteristic polynomial $\det\left(\underline{\underline{A}} - n^2 \underline{\underline{I}}\right)$ transfer to an entire function [5], which have isolated zeros only. Hence the spectrum of GWM for the medium, which is described by the equation (4), is always discreet. It is clear that similar to the finely stratified medium [2], the only principal GWM is usually propagating and all higher order modes are evanescent in quasi-static case. Now we can conclude that by analogy to the Rytov solution, the transition layer is formed by a series of evanescent generalized modes, which are excited by an incident wave.

3. Two-Wave Approach to Description of the Transition Layer

Let us show that one-dimensional nonlocal model of the inhomogeneous medium [1] corresponds to a two-wave approximation for electrodynamic description of the medium. For the uniformity, we rename the 8 constitutive parameters introduced in [1] to $\varepsilon_{km}, \mu_{km}$. Then we can present 4 equations obtained in [1] in the next form

$$\begin{aligned} k \cdot E_0 &= \omega\mu_0(\mu_{00}H_0 + \mu_{01}H_1) & k \cdot H_0 &= \omega\varepsilon_0(\varepsilon_{00}E_0 + \varepsilon_{01}E_1) \\ k \cdot E_1 &= \omega\mu_0(\mu_{10}H_0 + \mu_{11}H_1) & k \cdot H_1 &= \omega\varepsilon_0(\varepsilon_{10}E_0 + \varepsilon_{11}E_1) \end{aligned} \tag{5}$$

Here E_1 and H_1 are the effective complex amplitudes of the spatially inhomogeneous constituents of the tangential components of the field [1]. These amplitudes can be express in the amplitudes of spatial harmonics (2)

$$E_1 = \sqrt{\sum_{m=1}^{N-1} E_m^2}, \quad H_1 = \sqrt{\sum_{m=1}^{N-1} H_m^2} \tag{6}$$

Parameters $\varepsilon_{km}, \mu_{km}$ can be calculated by formulas, which followed from [1], where functions of distribution of the inhomogeneous constituents of the field correspond to the principal wave in the media.

We can rewrite the system (5) in form of two systems by analogy to eq.(3):

$$\begin{cases} a_{00}E_0 + a_{01}E_1 = n^2 \cdot E_0 \\ a_{10}E_0 + a_{11}E_1 = n^2 \cdot E_1 \end{cases} \qquad \begin{cases} b_{00}H_0 + b_{01}H_1 = n^2 \cdot H_0 \\ b_{10}H_0 + b_{11}H_1 = n^2 \cdot H_1 \end{cases} \tag{7}$$

Here coefficients a_{km} and b_{km} are depended on parameters $\varepsilon_{km}, \mu_{km}$ in similar way to (3):

$$\begin{aligned} a_{00} &= \mu_{00}\varepsilon_{00} + \mu_{01}\varepsilon_{10}, & a_{01} &= \mu_{00}\varepsilon_{01} + \mu_{01}\varepsilon_{11} \\ a_{10} &= \mu_{10}\varepsilon_{00} + \mu_{11}\varepsilon_{10}, & a_{11} &= \mu_{10}\varepsilon_{01} + \mu_{11}\varepsilon_{11} \\ b_{00} &= \varepsilon_{00}\mu_{00} + \varepsilon_{01}\mu_{10}, & b_{01} &= \varepsilon_{00}\mu_{01} + \varepsilon_{01}\mu_{11} \\ b_{10} &= \varepsilon_{10}\mu_{00} + \varepsilon_{11}\mu_{10}, & b_{11} &= \varepsilon_{10}\mu_{01} + \varepsilon_{11}\mu_{11} \end{aligned} \tag{8}$$

Solution of Eq.(7) can be obtained by analogy to Eq. (4) through dispersion equations

$$\det\left(\underline{\underline{A}}_2 - n^2 \underline{\underline{I}}_2\right) = 0 \Leftrightarrow \det\left(\underline{\underline{B}}_2 - n^2 \underline{\underline{I}}_2\right) = 0 \qquad (9)$$

where index 2 corresponds to 2x2 matrixes of Eq.(7). Hence the equations (9) have two solutions for the value n^2. Naturally, the first root of (9) must correspond to the principal wave in the medium. The second solution represents an effective GMW, which is a superposition of all higher evanescent generalized modes in it. Therefore one can expect that the second wave of the one-dimensional model can be used for the approximate description of the transition layer of inhomogeneous media. We mean here the case of plane boundary of the medium and plane wave, which normally fall on it.

The model of medium, where two wave modes can be excited, are well-known from theory of the spatial dispersion [4], although only propagating waves was taken into consideration there. The principal point of this problem is to find the additional bound condition, which is necessary for sewing together tangential components of electromagnetic fields on the boundary for incident wave and both modes. The same problem arises, when we consider the transition layer in two-wave approximation. As an additional boundary condition, we can use in this case the continuity of tangential components of the spatial inhomogeneous constituent on the plane boundary. This requirement is equivalent to the introducing of the complex effective characteristic impedance Z_{01} for the spatial inhomogeneous constituent of the field, which spread outside the bound. Then, if the bound lies at $z = 0$, we can write the additional bound condition in the form of $E_1(0)/H_1(0) = Z_{01}$. The value of $Z_{01} = Z_0\sqrt{\mu_{11}/\varepsilon_{11}}$ can be obtained from the formulas in [1], where one must use values $\varepsilon = 1$, $\mu = 1$ for the free space.

We have examined the two-wave approach in particular for the case of the finely stratified medium and get good results. For example, if such a structure contains both dielectric and metal layers, we have the correct result (a) for the limit of strong skin effect in metal layers.

4. Conclusion

The transition layer in inhomogeneous media can be described with help of series of the GWM. But we think that the simple two-wave approach for this problem is quite adequate in many cases. Such an approach is seemed more acceptable, especially in case, when we investigate both theoretically and experimentally the influence of the transition layer on electromagnetic properties of complex composite materials.

Acknowledgement

Author is grateful for A. N. Lagarkov, K. N. Rozanov, and A. P. Vinogradov for the useful discussions. This work was supported by Russian Foundation of Fundamental Investigations Grant no. 99-02-16564-a.

References

[1] N. A. Simonov, "One-dimensional nonlocal model of medium," in *Proc."Bianisotropics'98*, June 1998, Braunschweig, Germany, pp. 281-284.

[2] S. M. Rytov, "Electromagnetic properties of a finely stratified medium," *Sov. Phys. JETP*, vol. 2, pp. 466-475, 1956.

[3] O. Acher *et al.*, "Permeability measurement on ferromagnetic thin films from 50 MHz up to 18 GHz," *Journal of Magnetism and Magnetic Materials*, no. 136, pp. 269 – 278, 1994.

[4] V. M. Agranovich and V. L. Ginzburg, *Spatial Dispersion in Crystal Optics and the Theory of Excitation.* Wiley, New York, 1966.

[5] C. A. Korn and T. M. Korn, *Mathematical Handbook.* New York: McGraw-Hill Book Co., 1968.

Depolarization Dyadics

W. S. Weiglhofer

Department of Mathematics, University of Glasgow
University Gardens, Glasgow G12 8QW, Great Britain
Fax: + 44 – 141 – 330 4111; email: wsw@maths.gla.ac.uk

Abstract

Important ingredients in both exact and approximative treatments that aim to establish the electromagnetic response of an individual scatterer are so–called *depolarization dyadics*. Here, the focus shall be on both the derivation of closed–form expressions for as well as numerical evaluations of the depolarization dyadics. It will be shown how — from the initial approaches to the subject for *isotropic* mediums — important results have been derived for the general *anisotropic* and general *bianisotropic* regime in recent years.

1. Introduction

In order to motivate our approach to the topic of depolarization dyadics, we shall consider an applicational area of electromagnetics in which they play a significant role. That topic is *homogenization*, where two or more component mediums (often envisioned in particulate form) are mixed together to form a composite material. The aim of homogenization theories is then to extract the constitutive parameters of the composite material from a knowledge of the constitutive and geometrical properties of the constituent mediums. The research literature on homogenization is vast. The interested reader will find many important historical works in an anthology [1] and a comprehensive review of new developments in the homogenization of linear bianisotropic materials in a recent book chapter [2].

The first step towards the derivation/estimation of the composite's constitutive properties requires the solution of an electromagnetic scattering problem in which the electromagnetic response of an individual scatterer must be determined. This task can be achieved by adopting *direct* or *indirect scattering approaches*. For a detailed discussion of merits, difficulties and limitations of these approaches, the reader is referred to an up–to–date conceptual review by Lakhtakia [3]. While the direct scattering approach usually consists of numerical implementations, some analytical progress can often be made in the indirect scattering approaches, especially when certain approximations are introduced where appropriate. In particular, in the so–called *Rayleigh estimate*, the complete information about the electromagnetic response is contained in the depolarization dyadics.

In the present review the topic of depolarization dyadics is developed through a complete and exact representation of the electromagnetic field that is applicable even when the field point is contained within the source region. Alternatively, it is shown how the depolarization dyadics of a general, linear bianisotropic medium can be extracted with a Fourier technique in the form of surface integrals. Also, a detailed discussion focusses on the types of mediums for which these integrals can be explicitly evaluated. The basis of this review on depolarization dyadics is a recent review paper on fields in the source region [4] which may be consulted for further details.

2. Theoretical Background

Time–harmonic electromagnetic fields are being considered and a time–dependence of $\exp(-i\omega t)$ of field quantities is assumed throughout and suppressed (ω is the angular frequency). In 6–vector notation, the complex–valued field and source phasors are defined by[1]

$$\underline{\mathbf{F}}(\underline{x}) = \begin{pmatrix} \underline{E}(\underline{x}) \\ \underline{H}(\underline{x}) \end{pmatrix}, \qquad \underline{\mathbf{Q}}(\underline{x}) = \begin{pmatrix} \underline{J}_e(\underline{x}) \\ \underline{J}_m(\underline{x}) \end{pmatrix}, \tag{1}$$

where $\underline{E}(\underline{x})$ and $\underline{H}(\underline{x})$ are standard electric and magnetic field phasors and $\underline{J}_e(\underline{x})$ and $\underline{J}_m(\underline{x})$ are the electric and magnetic current densities, respectively. The most general linear medium, commonly referred to as a *bianisotropic medium*, is described by the frequency–dependent constitutive relations

$$\begin{pmatrix} \underline{D}(\underline{x}) \\ \underline{B}(\underline{x}) \end{pmatrix} = \underline{\underline{\mathbf{K}}} \cdot \underline{\mathbf{F}}(\underline{x}), \qquad \underline{\underline{\mathbf{K}}} = \begin{pmatrix} \underline{\underline{\epsilon}} & \underline{\underline{\xi}} \\ \underline{\underline{\zeta}} & \underline{\underline{\mu}} \end{pmatrix}, \tag{2}$$

where $\underline{D}(\underline{x})$ is the dielectric displacement and $\underline{B}(\underline{x})$ is the magnetic induction. As for the 3×3 constituent dyadics of $\underline{\underline{\mathbf{K}}}$, $\underline{\underline{\epsilon}}$ and $\underline{\underline{\mu}}$ are the well–known permittivity and permeability dyadics, whereas $\underline{\underline{\xi}}$ and $\underline{\underline{\zeta}}$ are the two magnetoelectric dyadics. The medium parameters will normally be complex scalars or pseudoscalars and it will be assumed that they fulfil the general covariance constraint: Trace $\left(\underline{\underline{\xi}} \cdot \underline{\underline{\mu}}^{-1} + \underline{\underline{\mu}}^{-1} \cdot \underline{\underline{\zeta}}\right) = 0$, [5], dictated by the structure of modern electromagnetic theory.

Consequently, the Maxwell equations can be given in the compact form:

$$\left[\underline{\underline{\mathbf{L}}}(\nabla) + i\omega\underline{\underline{\mathbf{K}}}\right] \cdot \underline{\mathbf{F}}(\underline{x}) = \underline{\mathbf{Q}}(\underline{x}), \qquad \underline{\underline{\mathbf{L}}}(\nabla) = \begin{pmatrix} \underline{\underline{0}} & \nabla \times \underline{\underline{I}} \\ -\nabla \times \underline{\underline{I}} & \underline{\underline{0}} \end{pmatrix}, \tag{3}$$

where $\underline{\underline{I}}$ is the 3×3 unit dyadic. Because the differential operator $\underline{\underline{\mathbf{L}}}(\nabla)$ and the constitutive dyadic $\underline{\underline{\mathbf{K}}}$ are both linear, (3) permits a solution representation of the form

$$\underline{\mathbf{F}}(\underline{x}) = \underline{\mathbf{F}}_h(\underline{x}) + \int_{V'} \underline{\underline{\mathbf{G}}}(\underline{x}, \underline{x}') \cdot \underline{\mathbf{Q}}(\underline{x}')\, d^3\underline{x}', \tag{4}$$

wherein V' is a volume such that $\underline{\mathbf{Q}}(\underline{x}) = \underline{\mathbf{0}}$ for $\underline{x} \notin V'$. The field $\underline{\mathbf{F}}_h(\underline{x})$ is a solution of (3) for $\underline{\mathbf{Q}}(\underline{x}) \equiv \underline{\mathbf{0}}$, i.e., mathematically speaking it is the complementary function. The entity $\underline{\underline{\mathbf{G}}}(\underline{x}, \underline{x}')$ is generally called the *dyadic Green function*, abbreviated DGF henceforth. It contains the standard 3×3 DGFs $\underline{\underline{G}}_{ee}$, $\underline{\underline{G}}_{em}$, $\underline{\underline{G}}_{me}$ and $\underline{\underline{G}}_{mm}$. It now follows from (3) and (4) that the DGF fulfils the *dyadic differential equation*

$$\left[\underline{\underline{\mathbf{L}}}(\nabla) + i\omega\underline{\underline{\mathbf{K}}}\right] \cdot \underline{\underline{\mathbf{G}}}(\underline{x}, \underline{x}') = \delta(\underline{x} - \underline{x}')\underline{\underline{\mathbf{I}}}, \tag{5}$$

where $\delta(\underline{x} - \underline{x}')$ is the Dirac delta function and $\underline{\underline{\mathbf{I}}}$ is the unit dyadic.

The field representation (4) holds for all $\underline{x}$. While it can be applied directly in the case $\underline{x} \notin V'$, special care is required when $\underline{x} \in V'$ because of singularities in the integrand. That case is of special interest in this context as it leads to the concept of the depolarization dyadics.

3. Field Representation with the Fikioris Technique

Two broad approaches for dealing with the problem of correctly evaluating the integral in (4) for $\underline{x} \in V'$ have been developed. The first of these was pioneered by Van Bladel [6, 7], and it was

[1] 3–vectors (6–vectors) are in normal (bold) face and underlined whereas 3×3 dyadics (6×6 dyadics) are in normal (bold) face and underlined twice.

later systematically generalized by Yaghjian [8]. Their work and that of others during the 1980s relates to *isotropic dielectric–magnetic mediums* only, i.e., for $\underline{\underline{\epsilon}} = \epsilon \underline{\underline{I}}$, $\underline{\underline{\xi}} = \underline{\underline{0}}$, $\underline{\underline{\zeta}} = \underline{\underline{0}}$, $\underline{\underline{\mu}} = \mu \underline{\underline{I}}$.

More recent work, based upon the principles of electromagnetostatics, reported some progress in the application of that technique to uniaxial [9] and general, homogeneous bianisotropic mediums [10]. The essence of the Van Bladel/Yaghjian technique is that the integral in (4) is treated by excluding a small convex region (often called *exclusion region* or *exclusion volume*) surrounding the source point of the integration region. The integral can then be evaluated and, eventually, the linear dimensions of the exclusion region are shrunk to zero — a procedure that effectively amounts to *principal value integration*.

An alternative approach was developed by Fikioris [11] in which the volume of the exclusion region is not required to be infinitesimally small in size. As a consequence, estimates for the electromagnetic field in the source region thus obtained differ from those arising from the Van Bladel/Yaghjian technique. In particular, the Fikioris technique gives rise to a dependence on the electrical size of the exclusion region in addition to that on its shape; see [12] for further information. Thus, the Fikioris technique amounts to the *regularization* of a divergent integral [13]. It is also worth noting that the Fikioris technique simplifies to the Van Bladel/Yaghjian technique when the exclusion volume is made infinitesimally small.

While these developments concerning the Fikioris technique also related to isotropic mediums only, recent years have seen significant extensions of the method to more complicated, linear homogeneous mediums. Initial application of this approach for a *bi–isotropic medium* [14] was followed by an extension to a *simple uniaxial bianisotropic medium* (i.e., an affinely transformed bi–isotropic medium) [15]. The Fikioris technique was also applied to an *uniaxial dielectric–magnetic medium* [16], an *axially uniaxial bianisotropic medium* (AUBM) [17], a *simple symmetric bianisotropic medium* [18] and an *affinely transformable AUBM* [19]. Results may be extended to mediums related to these by affine or other field transformations [20].

The essence of the Fikioris technique can be outlined in a straightforward way. In order to transform (4) into a suitable format, a volume V'' is defined in such a way that it constitutes a convex region surrounding $\underline{x} = \underline{x}'$. Also, an auxiliary dyadic Green function $\underline{\underline{G}}_P(\underline{x}, \underline{x}')$, called the *Poisson dyadic*, must be introduced. Hence, (4) may be rewritten as

$$\underline{\mathbf{F}}(\underline{x}) = \underline{\mathbf{F}}_h(\underline{x}) + \int_{V'-V''} \underline{\underline{\mathbf{G}}}(\underline{x}, \underline{x}') \cdot \underline{\mathbf{Q}}(\underline{x}')\, d^3\underline{x}' + \int_{V''} \left[\underline{\underline{\mathbf{G}}}(\underline{x}, \underline{x}') \cdot \underline{\mathbf{Q}}(\underline{x}') - \underline{\underline{\mathbf{G}}}_P(\underline{x}, \underline{x}') \cdot \underline{\mathbf{Q}}(\underline{x}) \right] d^3\underline{x}' + \underline{\underline{\mathbf{D}}}(\underline{x}) \cdot \underline{\mathbf{Q}}(\underline{x}) \,. \tag{6}$$

This representation is an exact formula without any simplifications, applicable to a general, linear bianisotropic medium as described by the constitutive dyadic in (2). In connection with the field representation (6) it must be observed that an explicit formula for the infinite–medium DGF $\underline{\underline{G}}(\underline{x}, \underline{x}')$ — and consequently also for the Poisson dyadic $\underline{\underline{G}}_P(\underline{x}, \underline{x}')$ — of a general, linear, homogeneous bianisotropic medium is not available at this time (see [21, 22] for review works on infinite–medium DGFs for complex mediums). This entails then that the dyadic function $\underline{\underline{D}}(\underline{x})$ in (6), which is called the *depolarization dyadic*, and which is given by

$$\underline{\underline{\mathbf{D}}}(\underline{x}) = \int_{V''} \underline{\underline{\mathbf{G}}}_P(\underline{x}, \underline{x}')\, d^3\underline{x}' \,, \tag{7}$$

can also not be derived for a general, linear bianisotropic medium.

While the foregoing developments have fully defined the depolarization dyadic $\underline{\underline{D}}(\underline{x})$, it is in approximations of (6) that its role and significance receives further illumination. One may assume, for example, that V' is itself convex in shape and also *electrically small*, i.e., its maximum chord length is smaller than a tenth of the principal wavelengths in the medium, say. Then, as

the Fikioris technique does not require V'' to be infinitesimally small, one can set $V' = V''$. As a consequence, the representation of the field simplifies to the extent that the integral over the region $V' - V''$ on the right–hand side of (6) vanishes.

If one makes the additional assumption that the current density distribution $\underline{\mathbf{Q}}(\underline{x})$ is uniform inside $V' = V''$, one obtains the *long–wavelength estimate* from the Fikioris technique as

$$\underline{\mathbf{F}}_{lw}(\underline{x}) \cong \underline{\mathbf{F}}_h(\underline{x}) + \left[\underline{\underline{\mathbf{M}}}(\underline{x}) + \underline{\underline{\mathbf{D}}}(\underline{x})\right] \cdot \underline{\mathbf{Q}}(\underline{x}), \tag{8}$$

for $\underline{x} \in V'$, where

$$\underline{\underline{\mathbf{M}}}(\underline{x}) = \int_{V'} \left[\underline{\underline{\mathbf{G}}}(\underline{x}, \underline{x}') - \underline{\underline{\mathbf{G}}}_P(\underline{x}, \underline{x}')\right] d^3\underline{x}'. \tag{9}$$

If, finally, the term involving $\underline{\underline{\mathbf{M}}}(\underline{x})$ is ignored, the *Rayleigh estimate* of the electromagnetic field in the source region arises in the form

$$\underline{\mathbf{F}}_{Ray}(\underline{x}) \cong \underline{\mathbf{F}}_h(\underline{x}) + \underline{\underline{\mathbf{D}}}(\underline{x}) \cdot \underline{\mathbf{Q}}(\underline{x}). \tag{10}$$

In this last relation we can now directly recognize the significance of the depolarization dyadic as a mapping from the source $\underline{\mathbf{Q}}(\underline{x})$ to the scattered field $\underline{\mathbf{F}}_{Ray}(\underline{x}) - \underline{\mathbf{F}}_h(\underline{x})$. Thus, the complete response of the individual scatterer is seen to be contained in the depolarization dyadic $\underline{\underline{\mathbf{D}}}(\underline{x})$.

4. The Depolarization Dyadic

As far as the depolarization dyadic $\underline{\underline{\mathbf{D}}}(\underline{x})$ is concerned, the situation appears now like this: if, for a specific type of medium the dyadic Green function $\underline{\underline{\mathbf{G}}}(\underline{x}, \underline{x}')$ is known, one can obtain the Poisson dyadic $\underline{\underline{\mathbf{G}}}_P(\underline{x}, \underline{x}')$ and thus finds a representation of the depolarization dyadic in terms of a volume integral by virtue of (7). Due to the structure of $\underline{\underline{\mathbf{G}}}_P(\underline{x}, \underline{x}')$, that volume integral can always be transformed into a surface integral with the help of Gauss' theorem.

Consider, for example (see [16] for mathematical details), an *uniaxial, dielectric–magnetic* medium, defined by constitutive dyadics

$$\underline{\underline{\epsilon}} = \epsilon_t \underline{\underline{I}} + (\epsilon_c - \epsilon_t)\, \underline{c}\,\underline{c}, \qquad \underline{\underline{\xi}} = \underline{\underline{0}}, \qquad \underline{\underline{\zeta}} = \underline{\underline{0}}, \qquad \underline{\underline{\mu}} = \mu_t \underline{\underline{I}} + (\mu_c - \mu_t)\, \underline{c}\,\underline{c}, \tag{11}$$

where $\underline{c}$ is a unit vector. After convenient decomposition of $\underline{\underline{\mathbf{D}}}(\underline{x})$ according to

$$\underline{\underline{\mathbf{D}}}(\underline{x}) = \begin{pmatrix} \underline{\underline{D}}_{ee}(\underline{x}) & \underline{\underline{D}}_{em}(\underline{x}) \\ \underline{\underline{D}}_{me}(\underline{x}) & \underline{\underline{D}}_{mm}(\underline{x}) \end{pmatrix}, \tag{12}$$

into 3×3 component dyadics, we find

$$\underline{\underline{D}}_{ee} = \frac{1}{i\omega} q_e \underline{\underline{L}}_e \cdot \underline{\underline{\epsilon}}^{-1}, \qquad \underline{\underline{D}}_{em} = \underline{\underline{0}}, \qquad \underline{\underline{D}}_{me} = \underline{\underline{0}}, \qquad \underline{\underline{D}}_{mm} = \frac{1}{i\omega} q_m \underline{\underline{L}}_m \cdot \underline{\underline{\mu}}^{-1}, \tag{13}$$

where $q_e = \epsilon_c/\epsilon_t$ and $q_m = \mu_c/\mu_t$. The dyadics $\underline{\underline{L}}_{e,m}$ can be explicitly evaluated as

$$\underline{\underline{L}}_{e,m} = \frac{1}{2}\left(\frac{1}{q_{e,m}} + \Lambda(q_{e,m})\right)\left(\underline{\underline{I}} - \underline{c}\,\underline{c}\right) - \Lambda(q_{e,m})\underline{c}\,\underline{c}, \tag{14}$$

$$\Lambda(q) = \frac{1}{1-q}\left(1 - \frac{1}{(q-1)^{1/2}} \tan^{-1}\sqrt{q-1}\right). \tag{15}$$

However, as an alternative to the route taken thus far, it turns out that $\underline{\underline{\mathbf{D}}}(\underline{x})$ may be obtained independently through a Fourier space analysis which does not require a complete knowledge of the infinite–medium DGF of the medium. The procedure was first implemented for a general

anisotropic dielectric medium [23] (for a spherical exclusion volume) and then generalized to the most general, linear, homogeneous bianisotropic medium with constitutive dyadic as given by (2) (for an ellipsoidal exclusion volume) [24]. Following [24], let the surface of an ellipsoidal region V' be parametrized as $\underline{x}_s(\theta,\phi) = \delta\,\underline{\underline{U}} \cdot \hat{\underline{x}}(\theta,\phi)$ where $\hat{\underline{x}}(\theta,\phi)$ is the radial unit vector in a spherical coordinate system (with angular coordinates θ and ϕ) located at the centre of V'; δ is a linear measure of the size of V', and $\underline{\underline{U}}$ is the symmetric shape dyadic ($\underline{\underline{U}} = \underline{\underline{I}}$ when V' is spherical).

Then, the 3×3 depolarization dyadics in (12) are given by

$$\underline{\underline{D}}_{\lambda\lambda'} = \underline{\underline{U}}^{-1} \cdot \tilde{\underline{\underline{D}}}_{\lambda\lambda'} \cdot \underline{\underline{U}}^{-1}, \quad (\lambda,\lambda' = e,m)\,. \tag{16}$$

The 3×3 dyadic $\tilde{\underline{\underline{D}}}_{\lambda\lambda'}$ is calculated as the double integral

$$\tilde{\underline{\underline{D}}}_{\lambda\lambda'} = \frac{1}{4\pi i\omega} \int_{\phi=0}^{2\pi} d\phi \int_{\theta=0}^{\pi} d\theta\, \sin\theta \frac{(\hat{\underline{x}} \cdot \underline{\underline{\tau}}_{\lambda\lambda'} \cdot \hat{\underline{x}})\, \hat{\underline{x}}\,\hat{\underline{x}}}{(\hat{\underline{x}} \cdot \underline{\underline{\epsilon}}' \cdot \hat{\underline{x}})(\hat{\underline{x}} \cdot \underline{\underline{\mu}}' \cdot \hat{\underline{x}}) - (\hat{\underline{x}} \cdot \underline{\underline{\zeta}}' \cdot \hat{\underline{x}})(\hat{\underline{x}} \cdot \underline{\underline{\xi}}' \cdot \hat{\underline{x}})}\,, \tag{17}$$

$$\underline{\underline{\epsilon}}' = \underline{\underline{U}}^{-1} \cdot \underline{\underline{\epsilon}} \cdot \underline{\underline{U}}^{-1}, \quad \underline{\underline{\xi}}' = \underline{\underline{U}}^{-1} \cdot \underline{\underline{\xi}} \cdot \underline{\underline{U}}^{-1}, \quad \underline{\underline{\zeta}}' = \underline{\underline{U}}^{-1} \cdot \underline{\underline{\zeta}} \cdot \underline{\underline{U}}^{-1}, \quad \underline{\underline{\mu}}' = \underline{\underline{U}}^{-1} \cdot \underline{\underline{\mu}} \cdot \underline{\underline{U}}^{-1}, \tag{18}$$

$$\underline{\underline{\tau}}_{ee} = \underline{\underline{\mu}}', \quad \underline{\underline{\tau}}_{em} = -\underline{\underline{\xi}}', \quad \underline{\underline{\tau}}_{me} = -\underline{\underline{\zeta}}', \quad \underline{\underline{\tau}}_{mm} = \underline{\underline{\epsilon}}'. \tag{19}$$

It is clear that in general the double integral in (17) needs to be evaluated numerically. Explicit, closed–form evaluations (for ellipsoidal, spherical, cylindrical and cubical exclusion volumes) exist for the isotropic case: both for achiral isotropic mediums [8] as well as for chiral mediums [14]. For uniaxial dielectric–magnetic and for uniaxial bianisotropic mediums where at least one of the medium dyadics $\underline{\underline{\epsilon}}$, $\underline{\underline{\xi}}$, $\underline{\underline{\zeta}}$, $\underline{\underline{\mu}}$ is of the form $\underline{\underline{a}} = a_c\,\underline{\underline{I}} + a_c\,\underline{c}\,\underline{c}$ ($\underline{c}$ is again a unit vector) explicit expressions (in terms of inverse trigonometric functions) are also available [23], [16], [25]; [17], [26]. The most recently obtained results in closed form relate to a *biaxial dielectric anisotropic medium* with $\underline{\underline{\epsilon}} = \epsilon_x\,\underline{u}_x\,\underline{u}_x + \epsilon_y\,\underline{u}_y\,\underline{u}_y + \epsilon_z\,\underline{u}_z\,\underline{u}_z$, $\underline{\underline{\xi}} = \underline{\underline{0}}$, $\underline{\underline{\zeta}} = \underline{\underline{0}}$, $\underline{\underline{\mu}} = \mu\,\underline{\underline{I}}$, where $\underline{u}_x$, $\underline{u}_y$, $\underline{u}_z$ are the unit vectors of a cartesian coordinate system. The depolarization dyadic $\underline{\underline{\mathbf{D}}}(\underline{x})$ is given in terms of elliptic functions of the first and second kind [27]. Finally, the closed–form results obtained for isotropic/uniaxial/biaxial mediums can be trivially extended to mediums which contain arbitrary skew–symmetric elements in their 3×3 constitutive dyadics, see [24], [27], because any skew–symmetry is filtered out in the integral representation (17).

5. Concluding Remarks

It was shown that depolarization dyadics play an important role in electromagnetic field representations. They arise through regularization procedures which guarantee that the field representations also remain valid when the field point is in the source region. Their significance can be interpreted in a straightforward way, namely that within certain well–defined approximations, particularly the Rayleigh estimate, they provide the complete information about the electromagnetic response of an individual scatterer.

The depolarization dyadics of a general, linear bianisotropic medium can be represented in terms of a two–dimensional integral. There are many special cases for which the integrations can be performed explicitly to yield closed–form expressions. In general, however, these integrals lend themselves easily to numerical treatment that require only small computational resources. Such a numerical approach is also economic because in their most important application, depolarization dyadics are used in homogenization calculations that are necessarily numerical by nature.

Acknowledgement
The author holds a *RSE/SOEID Research Support Fellowship* of the *Royal Society of Edinburgh*.

References

[1] A. Lakhtakia (Ed.), *Selected Papers on Linear Optical Composite Materials*. Bellingham, WA: SPIE Opt. Engg. Press, 1996.

[2] B. Michel, "Recent developments in the homogenization of linear bianisotropic composite materials," in O. N. Singh and A. Lakhtakia (Eds.), *Electromagnetic Fields in Unconventional Materials and Structures*. New York: Wiley, 2000, 39–82.

[3] A. Lakhtakia, "On direct and indirect scattering approaches for homogenization of particulate composites," *Microw. Opt. Technol. Lett.* **25**, 53–56, 2000.

[4] W. S. Weiglhofer, "Electromagnetic field in the source region: a review," *Electromagnetics* **19**, 563–578, 1999.

[5] W. S. Weiglhofer and A. Lakhtakia, "The Post constraint revisited," *Arch. Elektr. Übertr.* **52**, 276–279, 1998.

[6] J. Van Bladel, "Some remarks for Green's dyadic for infinite space," *IRE Trans. Antennas Propagat.* **9**, 563–566, 1961.

[7] J. Van Bladel, *Singular Electromagnetic Fields and Sources*. Oxford: Clarendon Press, 1991.

[8] A. D. Yaghjian, "Electric dyadic Green's functions in the source region," *Proc. IEEE* **68**, 248–263, 1980.

[9] B. Jakoby and F. Olyslager, "Singularity in Green dyadics for uniaxial bianisotropic media," *Electron. Lett.* **31**, 779–781, 1995; errata: **31**, 1396, 1995.

[10] B. Jakoby and F. Olyslager, "Quasistatic asymptotics of dynamic Green dyadics for general bianisotropic media," *Arch. Elektr. Übertr.* **50**, 189–195, 1996.

[11] J. G. Fikioris, "Electromagnetic field inside a current carrying region," *J. Math. Phys.* **6**, 1617–1620, 1965.

[12] J. J. H. Wang, "A unified and consistent view of the singularities of the electric dyadic Green's function in the source region," *IEEE Trans. Antennas Propagat.* **30**, 463–468, 1982.

[13] S.–W. Lee, J. Boersma, C.–L. Law, and G. A. Deschamps, "Singularity in Green's function and its numerical evaluation," *IEEE Trans. Antennas Propagat.* **28**, 311–317, 1980.

[14] A. Lakhtakia and B. Shanker, "Beltrami fields within continuous source regions, volume integral equations, scattering algorithms and the extended Maxwell–Garnett model," *Int. J. Appl. Electromag. Mater.* **4**, 65–82, 1993.

[15] A. Lakhtakia and W. S. Weiglhofer, "Time–harmonic electromagnetic fields in source regions in a simple uniaxial bianisotropic medium," *Int. J. Appl. Electromag. Mater.* **5**, 101–108, 1994.

[16] A. Lakhtakia and W. S. Weiglhofer, "Time–harmonic electromagnetic field in a source region in an uniaxial dielectric–magnetic medium," *Int. J. Appl. Electromag. Mech.* **8**, 167–177, 1997.

[17] W. S. Weiglhofer and A. Lakhtakia, "Source–region electric and magnetic fields in an uniaxial bianisotropic medium," *Electromagnetics* **17**, 387–401, 1997.

[18] A. Lakhtakia and W. S. Weiglhofer, "The Fikioris approach for the source–region electromagnetic field in a simple symmetric bianisotropic medium," *Microw. Opt. Technol. Lett.* **15**, 84–86, 1997.

[19] A. Lakhtakia and W. S. Weiglhofer, "Source–region electromagnetic field in an affinely transformable AUBM," *Int. J. Infrared Millimeter Waves* **19**, 95–106, 1998.

[20] A. Lakhtakia and W. S. Weiglhofer, "On electromagnetic fields in a linear medium with gyrotropic–like magnetoelectric properties," *Microw. Opt. Technol. Lett.* **15**, 168–170, 1997.

[21] W. S. Weiglhofer, "Analytic methods and free–space dyadic Green's functions," *Radio Sci.* **28**, 847–857, 1993.

[22] W. S. Weiglhofer, "Frequency–dependent dyadic Green functions for bianisotropic media," in T.W. Barrett and D.M Grimes (Eds.), *Advanced Electromagnetism: Foundations, Theory, Applications*. Singapore: World Scientific, 1995, 376–389.

[23] B. Michel, "A Fourier space approach to the field singularity of an anisotropic dielectric medium," *Int. J. Appl. Electromag. Mech.* **8**, 219–227, 1997.

[24] B. Michel and W. S. Weiglhofer, "Pointwise singularity of dyadic Green function in a general bianisotropic medium," *Arch. Elektr. Übertr.* **51**, 219–223, 1997; errata **52**, 31, 1998.

[25] W. S. Weiglhofer and A. Lakhtakia, "New expressions for depolarization dyadics in uniaxial dielectric–magnetic media," *Int. J. Infrared Millimeter Waves* **17**, 1365–1376, 1996.

[26] W. S. Weiglhofer, "New expressions for depolarization dyadics in an axially uniaxial bianisotropic medium," *Int. J. Infrared Millimeter Waves* **19**, 993–1005, 1998.

[27] W. S. Weiglhofer, "Electromagnetic depolarization dyadics and elliptic integrals," *J. Phys. A: Math. Gen.* **31**, 7191–7196, 1998.

Author Index